Final Report

Title: Evaluation of Alternative Pozzolanic Materials for Partial Replacement of Portland Cement in Concrete

FDOT Contract Number: BDV31-977-06

Submitted to:

The Florida Department of Transportation Research Center
FDOT Research Center research.center@dot.state.fl.us
605 Suwannee Street, MS 30 Tallahassee, FL 32399

c/o Dr. Harvey DeFord, Ph.D.
Structures Materials Research Specialist
State Materials Office

Submitted by:

Christopher C. Ferraro, Jerry M. Paris, Timothy G. Townsend, Mang Tia

Engineering School of Sustainable Infrastructure and Environment
University of Florida
Gainesville, Florida 32611

February, 2017
Department of Civil Engineering
Engineering School of Sustainable Infrastructure and Environment
College of Engineering
University of Florida
Gainesville, Florida 32611

Disclaimer

The opinions, findings, and conclusions expressed in this publication are those of the authors and not necessarily those of the State of Florida Department of Transportation or the U.S. Department of Transportation.

Prepared in cooperation with the State of Florida Department of Transportation and the U.S. Department of Transportation.

Approximate Conversions to SI Units (from FHWA)

Symbol	When You Know	Multiply By	To Find	Symbol
Length				
in	inches	25.4	millimeters	mm
ft	feet	0.305	meters	m
yd	yards	0.914	meters	m
mi	miles	1.61	kilometers	km
Area				
in^2	square inches	645.2	square millimeters	mm^2
ft^2	square feet	0.093	square meters	m^2
yd^2	square yard	0.836	square meters	m^2
mi^2	square miles	2.59	square kilometers	km^2
Volume				
fl oz	fluid ounces	29.57	milliliters	mL
gal	gallons	3.785	liters	L
ft^3	cubic feet	0.028	cubic meters	m^3
yd^3	cubic yards	0.765	cubic meters	m^3
NOTE: volumes greater than 1000 L shall be shown in m^3				
Mass				
oz	ounces	28.35	grams	g
lb	pounds	0.454	kilograms	kg
Temperature (exact degrees)				
°F	Fahrenheit	5 (F-32)/9 or (F-32)/1.8	Celsius	°C
Illumination				
fc	foot-candles	10.76	lux	lx
fl	foot-Lamberts	3.426	candela/m^2	cd/m^2
Force and Pressure or Stress				
lbf	pound-force	4.45	newtons	N
lbf/in^2	pound-force per square inch	6.89	kilopascals	kPa

1. Report No.	2. Government Accession No.	3. Recipient's Catalog No.
4. Title and Subtitle Evaluation of Alternative Pozzolanic Materials for Partial Replacement of Portland Cement in Concrete		5. Report Date September 2016
		6. Performing Organization Code
7. Author(s) Christopher C. Ferraro, Timothy Townsend, Mang Tia, Jerry Paris		8. Performing Organization Report No.
9. Performing Organization Name and Address Department of Civil and Coastal Engineering Engineering School of Sustainable Infrastructure & Environment University of Florida 365 Weil Hall – P.O. Box 116580 Gainesville, FL 32611-6580		10. Work Unit No.
		11. Contract or Grant No. BDV31-977-06
12. Sponsoring Agency Name and Address Florida Department of Transportation 605 Suwannee Street, MS 30 Tallahassee, FL 32399		13. Type of Report and Period Covered Final Report 7/13-12/16
		14. Sponsoring Agency Code
15. Supplementary Notes None		

16. Abstract

The supply of class F coal fly ash throughout the United States has recently diminished due to supply of natural gas and alternative energy sources as well as environmental restrictions. As a result, the concrete industry in the state of Florida has experienced supply shortages of class F fly ash for construction of FDOT owned structures. To avoid future problems stemming from inevitable fly ash supply shortages in the future, the FDOT chose to explore alternative materials that can be used to replace some or all the fly ash that is currently required in FDOT concrete mixes. Physical and chemical material properties were characterized for nine different replacement candidates. A total of over 60 mortar mixes and 20 concrete mixes were prepared for evaluation of workability, structural adequacy, and durability. Thermal hydration data, plastic properties, mechanical properties, and durability properties were acquired from the mixes to determine ideal replacement proportions for the substitution of class F coal fly ash in portland cement concrete mixes. Since the goal was to find replacements for class F fly ash, performance was compared to that of mortars and concretes containing a 20% replacement of portland cement with class F fly ash.

17. Keywords.	18. Distribution Statement
Concrete; Supplementary Cementitious Materials; Pozzolans; Portland Cement; Fly Ash	No restrictions.

19. Security Classif. (of this report)	20. Security Classif. (of this page)	21. Pages	22. Price
Unclassified	Unclassified	342	

ACKNOWLEDGEMENTS

The Florida Department of Transportation (FDOT) is acknowledged for their funding and other contributions to this study. Special acknowledgement is given to Dr. H.D. DeFord for his guidance and assistance throughout this project. The authors would like to thank Michael Bergin, Shelby Brothers, Richard DeLorenzo and Patrick Carlton for their contributions to this work which included laboratory planning and assistance. The authors would like to thank the donors of material used throughout this research: Florida Rock/Argos, Boral Materials, WR Grace, Burgess Pigments, Separation Technologies, Metaloy, Sioneer, Titan America, Gainesville Renewable Energy Center, and the donor of sugarcane bagasse ash. The following students are acknowledged for their tremendous contributions for conducting laboratory research: Phillipe Holas, Taylor Humbarger, Eric Johnson, Danielle Kennedy, Heather Mariscal, Katherine Maslak, Tyler Mokris, Josias Oeudraogo, Marissa Romero, Tyler Swanson, Caitlin Tibbetts, Paul Thomas, Kiersten Wang, and Benjamin Watts.

EXECUTIVE SUMMARY

Background

The supply of class F coal fly ash throughout the United States has recently diminished due to supply of natural gas and alternative energy sources as well as environmental restrictions. As a result, the concrete industry in the state of Florida has experienced supply shortages of class F fly ash for construction of FDOT owned structures. Reduced availability and increased demand for class F fly ash will continue to pose potential fly ash supply problems, especially in regions that are not close to a source. To avoid future problems stemming from inevitable fly ash supply shortages in the future, the FDOT chose to explore alternative materials that can be used to replace some or all the fly ash that is currently required in FDOT concrete mixes. Thus the primary objective of this research was to evaluate pozzolanic materials that are not currently in use by the FDOT. This research incorporated material characterization with regards to physical and chemical properties, workability characteristics, mechanical properties, and durability characteristics of binary - and ternary-blended mortars and concretes. Since the goal was to find replacements for class F fly ash, performance was compared to that of mortars and concretes containing a 20% replacement of portland cement with class F fly ash.

Research Objectives

The primary objective of this research project was to identify potential alternative pozzolanic materials not currently in use by the FDOT that can be employed to partially or completely replace class F fly ash in FDOT concrete with no significant decrease in performance with respect to plastic, mechanical, and durability properties. Recommendations borne from analysis of the results of this investigation were expected to include revisions of some sections of the FDOT Standard Specifications for Road & Bridge Construction.

Main Findings

The main findings from this study are summarized as follows:

- Portland cement concrete mixtures, which incorporated sugarcane bagasse ash having loss on ignition values exceeding 25%, showed no deleterious effects on the air content of normal concrete.
- Binary mixes incorporating ground glass or class C fly ash in the appropriate proportions performed comparably to concrete containing class F fly ash.
- Ternary mixes incorporating class C fly ash and either Micron^3 ultrafine fly ash, sugarcane bagasse ash, class F fly ash, slag, ground glass, silica fume, or metakaolin in the appropriate proportions performed comparably to concrete containing class F fly ash concrete.
- Class C fly ash can be blended with a highly siliceous material to re-qualify it as a class F fly ash that performs comparably or superior to control concretes in a variety of qualifying metrics.
- The use of ground glass, with an average particle size of less than 20 microns can be used to replace portland cement in concrete at replacement levels of 20% or lower.

- Rice husk ash was found to have a propensity for deleterious reactions based on results from the accelerated alkali silica reactivity test (ASTM C 1260).
- The maturity method and equivalent age-concepts are not appropriate for applying to mortars and cementitious systems containing alternative supplementary materials; the curve-fitting functions do not adequately describe strength-time relationships.
- There are a number of sources of alternative pozzolans in Florida that may be used as a replacement for class F fly ash.

Recommendations

Based upon the findings from this study, the following recommendations are suggested:

- Revise the FDOT Standard Specification for Road and Bridge Construction Section 929 to make allowances for the use of class N fly ash that does not meet ASTM C618 with respect to loss on ignition only.
- Revise the FDOT Standard Specification for Road and Bridge Construction Section 929 to make allowances for the use of class C fly ash that meets ASTM C618, to be used for structures placed in non-aggressive environments.
- Consider revising the FDOT Standard Specification for Road and Bridge Construction Section 929 to make allowances for the use of class C fly ash in ternary systems that contain granulated blast furnace slag, class F fly ash, silica fume or metakaolin for use in structures placed in moderately and extremely aggressive environments.

Recommendations for Future Study

- The research conducted in this study indicates that alternative pozzolans, including sugarcane bagasse ash, rice husk, ground glass, and equilibrium catalyst, should be investigated further to determine their suitability for use in concrete. The experiments performed in this study were limited to unprocessed materials as received from the respective producers. Initial research indicated that the processing of the alternative pozzolans may beneficially affect performance.
- Sulfate and/or chloride exposure tests should be performed prior to qualification of concrete materials containing alternative pozzolans for use in FDOT concrete mixes in all environments.
- Sugarcane bagasse ash and ground glass should be investigated further to determine threshold values for replacement level, particle size, optimum processing (bagasse ash), and long-term chloride and sulfate durability.
- Alternative pozzolans should be tested for alkali-carbonate reaction due to Florida coarse aggregate potentially containing dolomitic limestone.

TABLE OF CONTENTS

Contents Page

List of Tables

List of Figures

1. INTRODUCTION

1.1. Background

The current state of practice for portland cement concretes in Florida is to utilize class F fly ash, a byproduct of coal-fired power plants, as one of the primary accepted materials for partial replacement of portland cement in concrete structures and pavements. Class F (low calcium) fly ash is preferred because it has been readily available as a low-cost byproduct from the coal power plants and traditionally reduces the likelihood of alkali-silica reactivity as compared to class C fly ash. Additionally, benefits such as increased workability, increased late-age strength, and increased resistance to chemical intrusion, amongst others, can be realized from the inclusion of fly ash into portland cement concretes. Fly ash has been used in a number of applications and has proven to be a beneficial mineral admixture for use in concrete structures and pavements. Concrete composed of portland cement as the sole binding agent does not perform as well with regard to durability when compared to concrete containing class F fly ash (or other pozzolans) [1], [2]. Thus, fly ash and other pozzolans have been accepted within the concrete industry as a necessary addition to improve the long-term serviceability of concrete structures [1]–[3].

With recent changes in the generation of electricity in the United States, there has been a significant reduction in the number of coal-generated power utilities. The availability of class F fly ash has therefore diminished, and it is likely that supplies of fly ash will be insufficient to meet demand in the near future; the American Coal Ash Association has reported that in the last decade, the production of coal fly ash has dropped nearly 25% (from 70.15 million tons in 2003 to 53.40 million tons in 2013) [4]. Therefore, it is imperative to find alternative pozzolans for class F fly ash replacement that are commercially available, economically feasible, and suitable for use in concrete in Florida. The goal of this research is to determine a material or materials that are comparable to currently utilized pozzolans in performance, as well as, availability and economic feasibility.

1.2. Research Objectives

The primary objective for this research was to identify one or more materials that could replace class F coal fly ash for FDOT concretes while providing comparable performance in a variety of testing metrics. These metrics included plastic properties, mechanical properties and performance, as well as durability characteristics. Based on the findings of the experimental work, recommendations were made to alleviate the reliance on class F fly ash in FDOT concrete.

1.3. Research Approach

The research approach included a literature review of commonly used pozzolanic materials to determine potential materials for Florida; additionally, this review provided a guideline for desired material properties to aid in the determination of novel materials for use as a portland cement replacement. Following this, materials that were locally abundant were gathered for investigation. The first stage of the investigation into the materials involved the following evaluations:

- Elemental composition analysis by x-ray fluorescence
- Crystalline composition analysis by x-ray diffraction
- Loss on ignition using a muffle furnace
- Particle size distribution by laser light diffraction
- Specific heat capacity by differential scanning calorimetry
- Specific gravity by helium pycnometry
- Material fineness using a Blaine permeameter

After materials characterization, cementitious hydration investigation was on the materials at various mixtures by isothermal conduction calorimetry. After the quantification of the cementitious heat of hydration, mortar was fabricated to evaluate mortars on the following properties:

Workability

- Mortar flow using a flow table (ASTM C1437) [5]
- Time of setting by penetration resistance (ASTM C403) [6]

Structural Adequacy

- Compressive strength of mortar cubes (ASTM C109) [7]
    - Maturity and equivalent age of mortar; 8^{o}C, 23^{o}C, and 38^{o}C (ASTM C1074) [8]
- Direct tensile strength of mortar briquettes (ASTM C307) [9]

Durability

- Length change (ASTM C157) [10]
- Accelerated length change to determine potential for alkali-silica reactivity (ASTM C1260) [11]

After the assessment of mortars for compatibility and comparable performance to the control mortar in the aforementioned evaluations, concrete mixes were fabricated for the top performing mixtures that enabled the highest replacement by percentage. Plastic, mechanical, and durability properties were collected on these concretes based on the experimental program outlined below.

Plastic Properties

- Slump of fresh concrete (ASTM C143) [12]
- Temperature of fresh concrete (ASTM C1064) [13]
- Volumetric air content of fresh concrete (ASTM C173) [14]
- Unit weight of fresh concrete (ASTM C138) [15]
- Time of setting of sieved concrete by penetration resistance (ASTM C403) [6]

Mechanical Properties

- Compressive strength of concrete cylinders (ASTM C39) [16]
- Splitting tensile strength of concrete cylinders (ASTM C496) [17]

- Elastic modulus of concrete cylinders (ASTM C469) [18]
- Flexural strength of concrete beams (ASTM C78) [19]

Durability Properties

- Semi-adiabatic temperature rise of fresh concrete
- Surface resistivity of concrete cylinders (AASHTO TP-95) [20]
- Bulk resistivity of concrete cylinders (AASHTO TP-119) [21]
- Coefficient of thermal expansion of concrete cylinders (AASHTO T336) [22]

A review of the state-of-the-art on the use of alternative supplementary cementitious materials is presented in Chapter 3. The subsequent selection of materials and materials characterization are presented in Chapter 4. Chapter 5 describes the heat of hydration evaluations through isothermal conduction calorimetry. Chapter 6 describes the effects of the alternative supplementary cementitious materials (SCM) on the properties of mortar, while Chapter 7 describes the effects of the SCM on concretes designed to meet FDOT specifications for a Class II (Bridge Deck) concrete according to FDOT Road and Bridge Construction Manual [23].

2. LITERATURE REVIEW

2.1. Introduction

Portland cement concrete is the most widely used material for the construction of the built infrastructure on a global basis. The main binder used in concrete, portland cement (PC), is primarily composed of mined materials which include limestone, sand, and clay that are heated in a kiln and processed for use. The process of producing PC consumes a great deal of energy and results in a release of carbon dioxide. With a worldwide production of approximately four million tons, the replacement of PC with alternative materials has the potential to reduce the negative impacts on the environment [24], [25]. Cement is a material in modern society and reduction in use through alterative materials lessens impacts on air, water, resources, and energy. Alternative materials used to replace portions of PC within portland cement concrete (PCC) are referred to as supplementary cementitious materials (SCM) and are typically waste materials such as coal fly ash and blast furnace slag, generated from the energy and steel industries respectively. There are several benefits of utilizing materials which would normally be waste materials. Firstly, amending structural building materials with waste materials reduces the volume of waste delivered to a landfill. Secondly, the reduction in the use of naturally mined materials reduces the footprint and impact the construction industry has on the natural environment.

This research contribution presents work in which the incorporation of SCM can be used to amend cement and provide multiple benefits on the final PCC product by reducing cost, mitigating the environmental costs of PC, and by improving long-term durability of concrete when used as a partial cement replacement. The novelty of this document that it provides a clear and concise summary of state-of-the–art published research involving SCM that are industrial waste materials. Previously, research has provided information on the benefits of utilizing “main stream” wastes used as SCM such as coal fly ash, granulated blast furnace slag, and silica fume [26]–[39]. Others have provided information on lesser utilized SCM such as sugarcane bagasse ash, rice husk ash, biomass combustion ash and ground glass [40]–[49]. This paper provides a critical review of waste products utilized as SCM, their physical and chemical characteristics, their effect on the plastic and hardened properties of portland cement concrete, as well as information with regard to production and utilization. The purpose of this review is to provide a single document that serves as a reference and potential guide for those who produce industrial waste for comparative analysis of typical waste streams used to replace cement in PCC. Benefits of using SCM in concrete include increased long-term strength, reduced permeability, and mitigation of the potential for deleterious reactions such as alkali-silica reactivity (ASR) or delayed ettringite formation (DEF), both of which are expansive chemical reactions that cause hardened concrete to crack. However, the potential drawbacks of using inappropriate materials to replace PC within PCC can be numerous and harmful to the integrity and serviceability of a structure.

2.2. Background

SCM generally fall into one of two categories: self-cementing or pozzolanic. Self-cementing materials react in a similar manner to PC whereby the resultant mixture hardens during an irreversible hydraulic reaction when combined with water. A pozzolan is a material, primarily

siliceous in composition, which on its own does not have cementitious properties in the presence of water. When a pozzolan is exposed to water and calcium (usually in the form of lime) it hydrates and exhibits cementitious properties [50], [51]. Self-cementing materials show pozzolanic characteristics to some degree, but mainly exhibit hydraulic cementitious characteristics.

Pozzolans can be further classified as either artificial or natural. Natural pozzolans are materials that, with the exception of size reduction or calcination, remain unaltered from their natural mined state [2], [3],[25]. Natural pozzolans include volcanic ash (or crushed pumice), diatomaceous earth, chert, and shale. The use of natural pozzolans is typically cost prohibitive specifically for amendment in concrete as compared to SCM which are products of industrial waste. Their use has been documented in North and South America, Southern Europe and Africa [52]. The worldwide annual production of natural zeolites is approximately three million tons which is less than 0.1% and 0.3% of total cement and coal fly ash production worldwide, respectively [53], [54]. Furthermore, natural pozzolans are not waste products and are not discussed in detail in this document.

Artificial pozzolans are materials that have been produced or altered by an industrial process, and in many cases, such as coal fly ash, are waste products of other industrial processes [55], [56]. Artificial pozzolans include ground granulated blast furnace slag, rice husk ash, sugar cane bagasse ash, silica fume, recycled glass, biomass combustion ash, and coal fly ash. Table 2-1 presents the SCM types and abbreviations used herein, however due to the lack of availability of natural pozzolans as previously mentioned, the term “pozzolan” will be used to describe artificial pozzolans.

Table 2-1. Summary of SCM types and abbreviations

Material	**Type of SCM**
Portland Cement (PCC)	Self-cementing
Class C Fly Ash (FA-C)	Self-cementing
Ground Granulated Blast Furnace Slag (GGBFS)	Self-cementing
Class F Fly Ash (FA-F)	Artificial Pozzolan
Silica Fume (SF)	Artificial Pozzolan
Ground Glass (GG)	Artificial Pozzolan
Rice Husk Ash (RHA)	Artificial Pozzolan
Sugarcane Bagasse Ash (SCA)	Artificial Pozzolan
Biomass Combustion Ash (BCA)	Artificial Pozzolan

2.2.1. Portland Cement Chemistry

Portland cement (PC) is composed of a number of chemical oxides that when written in conventional notation can be cumbersome; therefore, cement chemists often use an alternative nomenclature system (presented in Table 2-2). In PC hydration,$\boldsymbol{C_3S}$ and $\boldsymbol{C_2S}$ react with $\boldsymbol{H}$ to form calcium silicate hydrate ($\boldsymbol{C\text{-}S\text{-}H}$) gels. These gels are the binders in mortars and concretes [2], [50]. Portland cement is primarily composed of four oxides (tricalcium silicate – $\boldsymbol{C_3S}$,

dicalcium silicate – C_2S, tricalcium aluminate – C_3A, and tetracalcium aluminoferrite – C_4AF), the exact composition of which may vary. The reported oxide ranges for PC in the United States, Canada and Europe are: (C_3S, 50-80%), (C_2S, 2-30%), (C_3A, 0-14%), and (C_4AF, 5-15%) [57], [58]. Within the United States, PC is classified as Type I, II, III, IV, or V cement in accordance with ASTM C150 *Standard Specifications for Portland Cement* [59], and the cement types are primarily based on the relative percentages of oxides within the material. European PC grades are determined by EN 197-1 *Composition, Specifications, and Conformity Criteria for Common Cements* [60], which uses different criteria as compared to ASTM C150; the main types of cement are classified by percentage of portland cement and the percentage of SCM that has been blended with it. The requirements per ASTM C150 do not address the blending of cement, whereas requirements for blended cements are specified in ASTM C595 *The Standard Specification for Blended Hydraulic Cements* [61]. Table 2-3 provides the typical range of chemical oxide compositions for portland cement.

Table 2-2. Cement chemist notation for common oxides

Notation	Chemical Formula	Chemical Name (Common Name)
C	CaO	Calcium Oxide (Lime)
S	SiO_2	Silicon Dioxide (Silica)
A	Al_2O_3	Aluminum Oxide (Alumina)
H	H_2O	Water
F	Fe_2O_3	Iron Oxide (Ferrite)
T	TiO_2	Titanium Dioxide (Titania)
M	MgO	Magnesium Oxide (Periclase)
K	K_2O	Potassium Oxide
N	Na_2O	Sodium Oxide
$\bar{S}$	SO_4	Sulfate

Table 2-3. Typical oxide-based chemical compositions of cementitious materials

Chemical Composition	PCC [1]	GGBFS [56]	FA-C [56], [62], [63]
SiO_2	18.7 – 24.4	35 – 40	23.1 – 50.5
Al_2O_3	2.2 – 6.3	10 – 15	13.3 – 21.3
Fe_2O_3	0.2 – 6.1	0.3 – 2.5	3.7 – 22.5
CaO	60.2 – 68.7	30 – 42	11.6 – 29.0
MgO	0.3 – 4.8	8.0 – 9.5	1.5 – 7.5
K_2O	Combined with Na_2O	0.0 – 0.3	0.4 – 1.9
SO_3	1.7 – 4.6	0.0 – 1.3	0.0 – 3.0
TiO_2	–	–	–
Na_2O	0.05 – 1.20	0.0 – 1.4	1.0 – 2.1
Other	~1	0.8 – 8.3	0.2 – 1.1
LOI	~0-3	–	0.3 – 3.5

The hydration reactions of the main oxides within PC are important with regard to making decisions about the potential influences of adding SCMs to a concrete mixture. The initial hydration reactions of C_3S with H (equation 1) and C_3A with gypsum $C\bar{S}H_2$ and H (equation 2) release a significant amount of heat; in the case of C_3S, this takes place generally within the first 15 minutes of hydration [2]. A dormant period of approximately 2-4 hours typically follows the initial reaction, in which very little heat is evolved. After the dormant period, C_3S continues to hydrate, producing the majority of the heat generated during the range of 18-36 hours. C_2S hydrates in a similar manner to C_3S (equation 3), though it is typically at a slower rate as it is less reactive than C_3S [2], [50].

Following the dormant period, C_3A resumes the hydration process for 12-36 hours, depending on the amount of available gypsum. C_4AF hydrates similarly to C_3A (equation 4) but at a reduced rate generating less heat [2]. The hydration of C_3A involves a two-step process; first C_3A reacts with sulfate ions provided by the dissolution of gypsum in water to create $C_6A\bar{S}_3H_{32}$ (ettringite), and this exothermic reaction is then followed by a reaction with excess C_3A and water to form $C_4A\bar{S}H_{12}$. Nevertheless, C_3A and C_4AF are not predominant components in cement and are not major contributors to the strength of concrete;

Cement Hydration Equations [2]

$$2C_3S + 11H \rightarrow C_3S_2H_3 + 3\text{CaOH} \quad (1)$$

$$2C_2S + 9H \rightarrow C_3S_2H_3 + \text{CaOH} \quad (2)$$

$$C_3A + 3C\bar{S}H_2 + 26H \rightarrow C_6A\bar{S}_3H_{32} \quad (3)$$

$$C_4AF + 2\text{CaOH} + 10H \rightarrow C_6AFH_{12} \quad (4)$$

Note: In the above equations the notation of (A,F) means that the either A or F can be present.

2.2.2. Cement Chemistry – Minor Components

In addition to the four main chemical oxides, there are the minor oxides, which are components of cement that can drastically affect the final product of concrete. They too are important to monitor as an excess of any of the minor components can have a profound negative impact on the performance and durability of concrete and mortar. The minor components are gypsum ($CaSO_4 \cdot 2H_2O$ or $C\bar{S}H_2$) and other sulfates as well as alkalis, which include magnesium, potassium and sodium.

Sulfate is introduced into the cement system most often in the form of gypsum. A typical cement composition comprises approximately 4.5% gypsum; it is used to regulate the "set" (hardening) of cement [50], [64], [65], and is limited per the requirements in the *Standard Specification for Portland Cement* [59] to 4.5% sulfate when C_3A is more than 8% of the cement composition. The addition of sulfate is primarily to ameliorate flash set caused by excessive C_3A hydration; however limiting sulfate addition is common to avoid delayed ettringite formation and false set.

When excess soluble sulfates do not react completely, concretes tend to undergo a phenomenon known as "internal sulfate attack" or "delayed ettringite formation" (DEF) in which the unbound sulfates present in the microstructure react to form more voluminous chemical products after the concrete has set. This conversion to higher volume products causes internal stresses in the

concrete to build until cracks are formed, compromising the structure. This reaction tends to only occur when the oversulfation condition is combined with elevated temperatures (70°C and above) during hydration; as the temperature increases beyond 70°C the likelihood of delayed ettringite formation occurring rises dramatically [66]–[68].

Alkalis typically make up an even smaller portion of the chemical composition of cement (typically less than 3%) than sulfates, but can have a consequence just as serious when combined with reactive silica or carbonates the concrete matrix. Thus, the terms alkali-silica reactivity (ASR) and alkali-carbonate reactivity (ACR) are used to describe the deleterious reactions that occur between reactive aggregates and alkalis within PCC. The alkali content for U.S. cements is governed by [59], which limits the "Equivalent alkalis, Na_2O_e" ($Na_2O + 0.658K_2O$) to 0.60% as an optional requirement for "low alkali cements." There is no limitation for alkali content in standard cements; however, cements with an alkali content in excess of 0.9% are considered to have a high alkali content [69], [70]. Aside from portland cement itself, one of the most common sources of alkalis within a PCC mixture is introduced by some pozzolans (such as high calcium coal fly ash, or biomass combustion ash). For 28 different biomass ashes, [71] reported that an average equivalent Na_2O_e of approximately 10%, which is more than ten times what is considered to be high.

Alkali silica reaction initiates in the cement matrix, usually months or years after placement. A reaction between soluble alkalis (potassium oxide and sodium oxide) and silica in the matrix form an expansive gel [72], [73]. The gel behaves in a manner similar to DEF, which is also expansive. Frequently the two problems (ASR and DEF) are confused on a macroscopic level as the symptoms are similar [68]. Mitigation of ASR can be accomplished by reducing the alkali content in the system; some have suggested reducing the amount of alkalis to a level below 0.60%, [74], [75], reducing the water-to-cementitious material ratio (w/cm), avoiding known reactive siliceous aggregates, reducing the available moisture that can carry alkalis, and utilizing low-alkali cement and SCMs. [1], [76, p.], [77]. The addition of most SCMs can accomplish several of the above and can densify the microstructure, making available alkali transport difficult.

Attempting to summarize the overarching and overlapping chemical reactions that occur between sulfates and alkalis, and their integrated roles within the general portland cement chemistry, leads to a vastly oversimplified conclusion: to avoid deleterious expansive reactions, the general consensus is to both balance and limit the alkali and sulfate contents within the cement composition. In addition, limiting the heat generation and adding low-sulfur and low-alkali SCMs should help to mitigate the opportunity for detrimental expansion.

2.2.3. SCM Chemistry

Generally speaking, SCMs, which are mostly siliceous in nature, provide some notable benefits when properly incorporated into a cement mixture. Many of the available SCMs used to replace PC cause a reduction in the heat produced by the hydration of $\boldsymbol{C_3S}$. This is a benefit in areas where concrete is placed in hot weather, or in mass concrete applications, as reducing the heat generated by hydration reduces the cracking potential by reducing stresses caused by thermal gradients between the exterior surfaces of the concrete and the internal portions [78]–[80]. Secondly, the siliceous content of SCMs provide a continued reaction with free calcium (a product of cement hydration) within the microstructure to further produce ***C-S-H*** at later ages;

this is known as the "pozzolanic reaction" [2], [3], [50]. Although the reaction between the free calcium and SCMs is exothermic, the heat produced is typically lower than for the hydration of **C_3S** within PC, and it occurs after the initial hydration of **C_3S** as the primary exothermic reactions are subsiding.

In mature ***C-S-H*** structures formed from ***C_3S*** and ***C_2S***, the calcia-to-silica ratio has been found to be approximately 1.4 – 2.0; this is theorized to be the ideal range [55], [70], [81]. While it is known that cements will have a ***C:S*** of approximately 3.0 [1], the addition of silica in the form of a highly siliceous SCM would result in a lowered ***C:S***, which contributes to a more complete chemical reaction and less unreacted cementitious material.

Typical chemical oxide compositions of the SCMs presented herein are displayed in Table 2-3 and Table 2-4. An index of the published effects of the addition of SCMs to portland cement concrete (PCC) are displayed in Table 2-5. It should be noted that the effects reported are only applicable under the reported mixing conditions, and may vary depending on a number of variables such as the material's chemical composition, physical properties, and application. The effects listed should be taken as generalities and not "rules" governing use.

Table 2-4. Typical chemical compositions of pozzolanic materials

Chemical Composition	**FA-F** [56], [63], [82]	**SF** [56], [83]	**GG** [84]–[86]	**RHA** [56]	**SCBA** [87], [88]	**BCA** [89], [90]
SiO_2	45 – 64.4	85 - 97	50 – 80	87.0 – 87.3	78.0 – 78.4	1.9 – 68.2
Al_2O_3	19.6 – 30.1	0.2 – 0.9	1.0 – 10	0.1 – 0.8	8.6 – 8.9	0.12 – 15.1
Fe_2O_3	3.8 – 23.9	0.4 – 2.0	<1.0	0.1 – 0.8	3.5 – 3.6	0.37 – 9.6
CaO	0.7 – 7.5	0.3 – 0.5	5 – 15	0.5 – 1.4	2.1 – 2.2	5.8 – 83.5
MgO	0.7 – 2.8	0.0 – 1.0	0.6 – 4.0	0.3 – 0.6	0 – 1.7	1.1 – 14.6
K_2O	0.7 – 4.1	0.5 – 1.3	<1.0	2.4 – 3.7	3.4 – 3.5	2.2 – 32.0
SO_3	0 – 0.5	0.0 – 0.4	<1.0	0.0 – 0.3	–	0.36 – 11.7
TiO_2	0.9 – 1.2	–	<1.0	–	–	0.06 – 1.2
Na_2O	0.2 – 0.5	0.1 – 0.4	1 – 15	0.1 – 1.1	0.0 – 0.1	0.22 – 29.8
Other	0.1 – 5.5	0.0 – 1.4	<5.0	1.8 – 5.2	1.2 – 3.0	0.66 – 13.0
LOI	0.2 – 7.2	0.0 – 2.8	<1.0	2.1 – 8.6	0.4	–

Table 2-5. Summary of effects on PC due to partial replacement with specified SCM

Evaluation Method	**Supplementary Cementitious Material**			
	GGBFS [56], [91]–[93]	**FA-C** [56], [94], [95]	**FA-F** [55], [56], [96], [97]	**SF** [98]–[102]
Compressive Strength	↑ (28 days) (30-50%)	↑ (10-50%)	↑ (10-50%) (sand replacement)	↑ (28 days) (5-20%)
Tensile Strength	↑ (30%)	↑ (10-50%)	↑ (10-50%)	↑ (5-30%)
Flexural Strength	↑ (30-60%)	↑ (40-75%)	↑ (40-75%)	↑ (5-25%)
Permeability	↓ (33-50%)	↓ (10-100%)	↓ (10-100%)	↓ (>5%)
Workability	↑ (30-85%)	↑ (10-40%)	↑ (10-40%)	↓ (>5%)
Heat of Hydration	↓	↓	↓	↓ (10%)
Resistance to ASR	↑ (30-60%)	↑ (20-40%)	↑ (20-40%)	↑ (4-20%)
Freeze/Thaw Resistance	↓ (10-60%)	↑ (40-60%)	↑ (40-60%)	↑ (10-20%)
Sulfate/Chloride Resistance	↑ (10-50%)	–	↑ (<50%)	↑ (5-15%)
Resistance to Corrosion	↑ (40%+ GGBFS)	↑ (10-30%)	↑ (10-30%)	↑ (<20% SF)
Setting Time	↑ (10-70%)	↑ or ↓	↑	↑ (5-20%)
Bleeding and Segregation	↑ (40-70%)	↓ (10-40%)	↓ (10-40%)	–

↑ Denotes an "increase" in the metric being reported

↓ Denotes a "decrease" in the metric being reported

\- Denotes either conflicting results (generally due to varied material) or not sufficient reported data to make a conclusion

Note: Values in parentheses represent replacement percentages by weight; for example "GGBFS Compressive strength" as presented below should be understood to mean "There is a general trend of *increasing* compressive strength at 28 days when utilizing 30-50% GGBFS."

Table 2-5. Cont. summary of effects on PC due to partial replacement with specified SCM.

Evaluation Method	Supplementary Cementitious Material			
	RHA [56], [103]–[109]	**SCBA** [110]–[115]	**GG** [85], [86], [116]	**BCA*** [89], [90], [117]
Compressive Strength	↑ (5-30%)	↑ (10-30%)	↓ (10-30%)	↓ (10-40%)
Tensile Strength	↑ (5-30%)	↑ (5-15%)	↓ (10-20%)	↓ (30%)
Flexural Strength	↑ (5-20%)	–	↓ (10-30%)	↓ (10-30%)
Permeability	↓ (7.5-40%)	↓ (10-30%)	-	↓ (10-40%)
Workability	↓ (10-40%)	↓ (10-30%)	↓ (20-30%)	↓ (10-20%)
Heat of Hydration	–	↓ (10-30%)	–	↓ (10-30%)
Resistance to ASR	↑ (4-15%)	–	–	–
Freeze/Thaw Resistance	↑ (10%)	–	–	No Change
Sulfate/Chloride Resistance	↑ (7.5-40%)	↑ (5-30%)	↑ (20-30%)	–
Resistance to Corrosion	↑ (5-30%)	↑ (20%)	–	↑ (10-20%)
Setting Time	↑ Initial (5-30%) ↓ Final (5-35%)	–	–	↑ (5-30%)
Bleeding and Segregation	–	–	–	–

*Due to the high variability of this material, reported results vary widely; these are very generic trends.

2.3. Self-Cementing Materials

2.3.1. Ground Granulated Blast Furnace Slag

The use of ground-granulated blast furnace slag (GGBFS) or granulated blast furnace slag (GBFS) in concrete can be documented circa 1900 where slag was produced as “slag cement.” In the late 19th century and early 20th century, a significant portion of the cement in the United States sold as “portland cement” was actually “slag cement” [118], [119]. Granulated blast furnace slag is a self-cementing material that is a byproduct of the iron production industry [3], [50], [55]. Blast furnace slag is derived from calcia-based fluxes. The resultant calcium silicate-aluminate slag that floats on top of molten iron during the manufacturing process is then skimmed off and rapidly quenched to below 800°C [3], [50], [55]. The quenching process creates a granulated glassy product (GBFS) that can be ground (GGBFS) to a fineness similar to that of PC [80], [120]. The composition of GBFS is approximately 95% non-crystalline calcium-aluminosilicates [56], [70]. The fineness of GGBFS as well as its glass content, calcia-to-silica ratio, and chemical composition have a significant effect on this product when used to replace PC in PCC [121]. Due to its cementitious properties, GGBFS can be utilized as a direct replacement for PC in PCC; however, since the hydration of pure GGBFS is often relatively slow in comparison, the material requires activation with $Ca(OH)_2$, which is found as a product of portland cement hydration [70], [122]. The hydration and curing of pure GGBFS and water is a

slow process that would take many times longer than a pure cement mixture due to slag particles having an impervious outer layer of amorphous silica and alumina. However, when combined with PC, the $Ca(OH)_2$ from the hydrating cement serves as an activating component which accelerates the rate of hydration. The activation process takes place via dissolution of the glassy layers of the slag particles as the pH of solution exceeds 13. Hydrates (including calcium silicate hydrates) precipitate from the saturated pore solution [123].

During the process of manufacturing, GBFS is milled to decrease the particle size for use as an SCM, and the average particle size varies depending the milling process [124]. It has been reported that fineness (particle size) has a contributing effect on the "activity index", a measure of the 28-day compressive strength of a GGBFS cement compared to a control cement [121]. Slags are categorized as Grade 80, 100 or 120 based on respective 28-day compressive strengths of at least 75%, 95%, or 115% of the control. The test method for activity index is described in AASHTO M302 *User Guidelines for Waste and Byproduct Materials in Pavement Construction* and ASTM C989 *Slag Cement for Use in Concrete and Mortars* [125], [126].

It has been well documented that the use of GGBFS as a replacement for PC in concrete increases the resistance to sulfate and chloride attack [1], [2], [93], [127]. Many have attributed this phenomena to a cement matrix that has a lower permeability with the addition of GGBFS as compared to a control [1], [127]. It has been reported by [128] that GGBFS additions to mortar decreased expansion when compared to a PC control mortar. It was hypothesized that the expansion was caused by the ingress of sulfate ions aided by the leaching of portlandite (a product of $\boldsymbol{C_3S}$ hydration). Therefore, removal of $\boldsymbol{C_3S}$ (through replacement of PC with 62% GGBFS, which contains a lower percentage of $\boldsymbol{C_3S}$ than PC) should result in decreased ettringite and gypsum formation when exposed to sulfate, resulting in less expansion of the concrete.

The reduction of alkali-silica reaction (ASR) in GGBFS amended concrete is due to a decrease in the alkalinity of the cement mix, diminished mobility of alkalis, and reduction of free lime [56]. Duchesne and Bérubé [129] examined the effect of the addition of GGBFS on ASR. Concrete samples were made with 0%, 35%, and 50% of GGBFS as a replacement for high alkali content (1.25%) cement. The study revealed that the replacement of PC with GGBFS resulted in lower expansion due to ASR. The results indicated that after a period of 9 years the specimens that incorporated GGBFS expanded approximately 20% less than specimens without slag. The reduction of expansion was due to the mitigation of the availability of free alkalis within the pore water in the cement paste. The alkali concentrations were found to be lower in specimens with GGBFS replacement than in the control concrete [129].

Testing revealed that 40-60% replacement is an optimum percentage as it resulted in 28-day compressive strengths comparable to those of the control [93], [130]. It has been shown with a variety of concrete mix types (using white portland cement, self-consolidating concrete, and ordinary portland cement concretes) that given enough time and appropriate mix conditions, high-volume GGBFS replacement mixes can perform comparably to 100% portland cement mixes [131]–[133].

Current slag production data is limited, but production is estimated to be in the range of 18 to 23 million and 170 to 250 million tons per year for the United States and worldwide, respectively

[24], [134]. It should be noted that these numbers are not solely GGBFS, but include slag used as aggregate.

2.3.2. Coal Fly Ash (CFA)

Coal fly ash (CFA), referred to generically in this report as fly ash (FA) is a byproduct of the coal combustion process; coal combustion residuals (CCRs) are separated into two basic groups: fly ash and bottom ash [3]. Fly ash can be defined as the particulate exiting within the flue gas during coal combustion; the coal production facility's air pollution control devices then capture this material where it is either beneficially used or disposed of as a waste product. In the United States, CFA is separated into two categories (class C and class F) in accordance with ASTM C618 *Standard Specification for Coal Fly Ash and Raw or Calcined Natural Pozzolan for Use in Concrete* based on its chemical composition [135]. In Europe, CFA for use in concrete is regulated by chemical and physical properties of the CFA as prescribed in BS EN 450-1 *Fly Ash for Concrete. Definition, Specifications and Conformity Criteria* [136].

The primary difference between the two U.S. classifications of CFA is total content of silica, alumina, and ferrite in the material of which class F (FA-F) fly ash requires a minimum of 70% and class C (FA-C) fly ash requires 50%. Typically, FA-C has a much higher calcium content than class F fly ash (FA-F); this excess calcium is responsible for the self-cementing nature of FA-C as the principal reactive phases for FA-C are anhydrite ($CaSO_4$) and lime ($Ca(OH)_2$) [70], [137], [138]. However, this high calcium content (as well as elevated concentrations of alkalis, such as potassium and sodium) can lead to deleterious effects when used in concrete mixtures [139], [140].

The variability of the chemical composition of FA-C has been cited as one negative aspect of its use in concrete [141], [142]. The compressive strength of FA-C in concrete and mortars has been reported to be comparable to PC mixes [143]; however, problems with the expansion of concretes and mortars utilizing FA-C has been observed due to the formation of ettringite [142]. The variability of fly ash can be attributed to several factors; the type of coal used (bituminous or sub-bituminous), mineralogical differences in the coal, degree of pulverization of the coal (before it enters the furnace for incineration), type of furnace used to produce energy as well as the oxidizing conditions of the furnace, and the mechanism by which the fly ash is collected (mechanical collection, electrical precipitators, or bag filters) [144]. Furthermore, the manner in which the ash is handled in storage can affect the final product [56]. Colangelo et al. reported that the median particle diameter (D_{50}) can vary by nearly 2.5 times from the sources utilized [145]. Since fly ashes are byproducts of burning coal, their chemical compositions vary from one source to another, as well as from one day to another at the same facility; however, general chemical compositions of different FA-C are presented in Table 2-3.

Since the particle shape of fly ash is spherical, the workability of the fresh concrete is improved as the particle shape provides a lubrication effect [56]. The particle size distribution usually ranges between 0.2-200 μm [146]. The smaller particles fill voids and, combined with a slower rate of hydration, create a lower liquid-to-solid ratio in the concrete matrix. This results in a denser matrix that has a lower permeability, with reduced bleeding (pooling water) and aggregate segregation [56]. FA-C has been shown to decrease permeability (after 3 months) with mix proportions up to 50% replacement [147]. It has been demonstrated that FA-C used as a fine aggregate, rather than a cement replacement, increases compressive strength at 28 days. The

slower pozzolanic reaction also adds to late strength development (beyond 56 days) and increased ultimate strength [95].

Saraswathy et al. [107] found that fly ashes that are "chemically activated," or immersed in a basic solution to initiate the cementing process, achieved higher compressive strength at 10-20% replacement than non-activated fly ash mixes. With respect to durability and corrosion resistance, the activated fly ash performed much better than non-activated fly ash for replacements of up to about 50%. Concrete which contained even modest (10%) replacements of non-activated fly ash exhibited a higher resistance to corrosion that was mainly attributed to the small particles filling interconnected voids and capillaries, which reduced the permeability of the hardened cement paste and retarded the intrusion of corrosive solutions [107].

In 2012, the total production of fly ash in the United States was 52.1 million tons; 11.8 million tons of fly ash were used to produce "concrete/concrete products/grout" as reported by the American Coal Ash Association. An additional 2.3 million tons were used in the production of portland cement. Approximately 45% of fly ash produced in the United States in 2012 was beneficially reused [4]. More than half, or 28.9 million tons, of coal fly ash was landfilled and was not beneficially used. The beneficial use of fly ash, with respect to portland cement, benefits the cement industry (reduces costs) and the environment (consumes a byproduct that otherwise would be landfilled).

2.4. Pozzolans

2.4.1. Class F Coal Fly Ash

Class F fly ash (FA-F) is produced in the same manner as class C fly ash with the primary difference being FA-C is typically produced from subbituminous or lignite coal whereas class F fly ash is produced from bituminous coal [2], [70]. FA-F fly ash has a different chemical composition range due to the differences in coal composition, but it has similar physical characteristics as FA-C. Therefore, many of the effects that are due to physical characteristics (as opposed to chemical reactions) are similar to that of FA-C [3].

Carette and Malhotra investigated the effect of utilizing a 20% FA-F replacement and found that the average compressive strength, relative to the control (no F-FA), of concrete at ages of 7, 28, and 91 days was approximately 75%, 80%, and 92% FA-F, respectively. At an age of one year, the compressive strength of the F-FA concrete was about the same as the control [94].

Utilization of FA-F as a fine aggregate replacement, as opposed to cement replacement, has also shown promise. Siddique reported that FA-F was used to replace fine aggregate in quantities up to 50% replacement. The compressive strength of concrete mixes after one year was approximately 60% higher than the control for mixes which had half of the fine aggregate replaced with FA-F [97]. Similar trends were seen with splitting tensile strength, flexural strength, and modulus of elasticity. The majority of these gains were attributed to the pozzolanic reactions. The control mix had a slump of 100 mm, which was relatively workable, and the 50% replacement had a slump of 20 mm, which was unworkable [97].

One of the primary concerns with respect to the use of class C fly ash in portland cement concrete is that performance, with regard to durability, is variable and inferior to class F fly ash.

Several studies have shown that while FA-F can be used to mitigate alkali-silica reaction, FA-F performs better at lower inclusion rates due to the lowered alkali content [35], [96], [129]. With respect to resistance to external sulfate attack ACI Committee 226 states that, in general, the addition of class F fly ash will raise sulfate resistance, while the addition of some class C fly ash may reduce sulfate resistance [148].

2.4.2. Silica Fume

Silica fume (SF), also referred to as microsilica, condensed silica fume, or volatilized silica, is a byproduct of the silicon and ferrosilicon industry. Quartz reduced at a temperature of 2000°C produces silicon dioxide vapors that condense into spherical particles of amorphous silica, which is collected and used as an SCM in portland cement concrete. The mean particle size of silica fume is typically around 0.1 micron with most (95%) particles under 1 μm [3], [83]. Due to the small particle size and large silica content (>90%) the pozzolanic reaction that takes place is very vigorous. Since silica fume has a relatively large surface-area-to-weight ratio, or "specific surface area" of 15,000 to 30,000 m^2/kg, the reactivity of portland cement that has been partially replaced with silica fume is increased [83]. The increased reactivity typically results in increased heat during hydration of the cement mix as well as higher compressive strength [100], [149]. It has been reported that tensile strength at 28 days increased with the addition of SF up to 15% and is comparable up to about 25%; however, after 28 days the tensile strength of SF blended mixes is lower than that of pure PC mixes [99], [150]. It has been reported that the replacement of PC with modest amounts (5%) of SF dramatically decreased permeability of concrete [101]. Several sources have noted that the inclusion of SF into PC mixes will also increase the resistance to corrosion and sulfate attack, which is mainly due to the reduced permeability [83], [151]. Boddy et al., [98], reported that SF replacement also reduced alkali-silica reactivity to the acceptable 0.10% expansion limit prescribed by ASTM C1260; in which expansion of less than 0.10 % at 16 days after casting is indicative of innocuous behavior in most cases. The inclusion of SF has also been shown to reduce the workability and increase water demand of concrete [152], [153].

2.4.3. Ground Glass

The incorporation of glass into concrete dates back to the 1960's and the topic of study has attracted an abundance of interest as the silica content and brittle physical characteristics of glass are similar to those of concrete [49], [154]. One of the major drawbacks to using glass in concrete is that it is known to cause expansive reactions and cracking when used as an aggregate. However, research has shown that finely ground glass has the tendency to behave like a pozzolan and ultimately contribute to the beneficial aspects of concrete in a manner similar to silica fume [49], [116].

Ground glass (GG), also sometimes referred to as pozzolanic glass powder if the glass has a particle size below 45 μm, is a material made from recycled waste glass. Typically, recycled glass is collected as a combination of clear, green, and brown glass, which then is separated by color [155]. Separated glass is broken into smaller fragments known as cullet, occasionally used as coarse aggregate concrete, but more is likely to be reused to make new consumer products [156]. Cullet can be further broken down by various milling methods to a particle size similar to sand, which is occasionally used as a fine aggregate, or when pulverized, is even finer, and is approximately the size of portland cement [157]. Some researchers have reported that the incorporation of ground glass into concrete has slightly negative effects on the hardened

properties of concrete, which include the reduction of compressive, tensile, and flexural strengths [85], [86]. The main concern regarding the addition of GG (whose main constituent is silica) into concrete is the possibility of creating a concrete that would be more prone to alkali-silica reactivity.

Studies have been conducted that show that alkali-silica reactivity can be minimized when using glass by ensuring that the glass particles are very small. Using the ASTM C1260 test method for determining potential alkali-silica reaction, it has been shown that there is reduced expansion with increasing fineness of glass replacement; this produces a more dispersed silica in the cement matrix [116], [158]. The effect of particle size as well as the mixing condition has been analyzed: mixing the glass with the dry components (with the cement) or mixing it wet (with the water). The resulting expansions from these mixes are shown in Figure 2-1 [116].

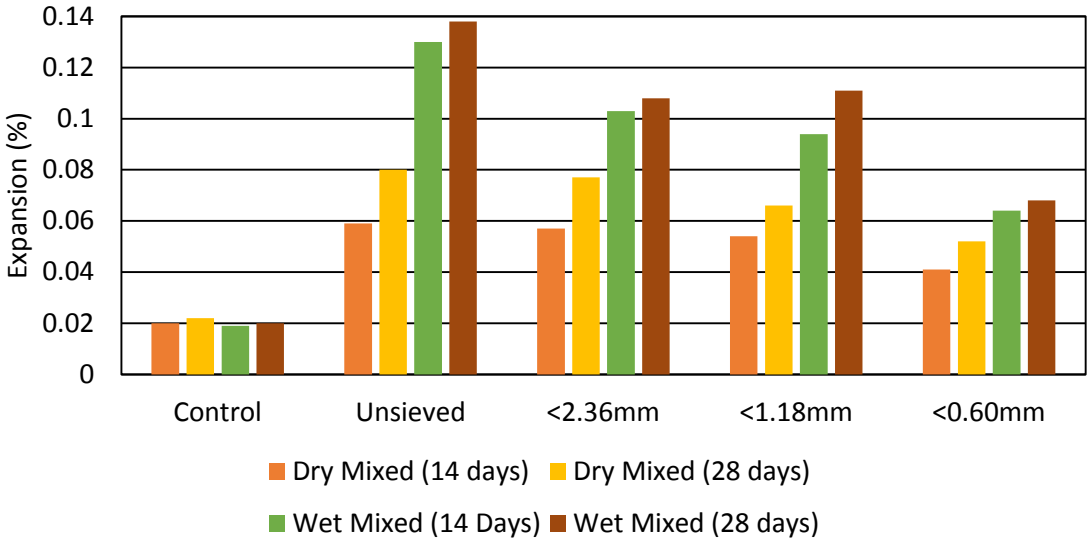

Figure 2-1. ASR expansion in ground glass mortars with varying mix methods and particle size [116]

ASTM has set forth general guidelines for interpreting length change data that state that while using ASTM C1260, for a length change specimen to be considered “non-reactive” (innocuous behavior) after 16 days, the expansion has to be less than 0.10%, “potentially deleterious” is determined to be greater than 0.20% expansion at 16 days, and expansions between 0.10 and 0.20% at 16 days include aggregates that are known to be either innocuous or deleterious [11]. Applying these limits to the data provided by [116], it can be seen that the powdered glasses that are coarser and were mixed “wet” have a higher expansion and can be classified as “potentially reactive”. The powders that are finer tend to have less ASR regardless of mixing method. Furthermore, it was reported that the inclusion of class F fly ash reduced the expansion for replacement additions of 5%, 10% or 20% [116].

According to the United States Environmental Protection Agency, recycled glass in the United States municipal waste stream was in excess of 11.5 million tons in 2011, yet only approximately 28% of the glass generated was recovered and recycled [156]. The majority of recovered glass is not recycled due to the fact that a large amount of colored glass provides an inadequate product to be recycled into new container glass. As a result, 72% of recovered glass is not recycled, and

contributes to approximately 8.3 million tons of material that is landfilled annually. With respect to use as a cementitious replacement, the color of pulverized glass has no bearing on utility, and mixed-color glass can provide a readily accessible supply so long as manufacturing steps are taken to reduce poor performance, such as milling to appropriate particle size and utilizing a replacement percentage that does not negatively affect the final product.

2.4.4. Rice Husk Ash

Rice husk ash (RHA) is a byproduct produced by burning rice grain husks as a fuel source for a boiler, usually to produce energy to power a manufacturing facility. The husks contain approximately 50% cellulose, 25-30% lignin, and 15-20% silica when whole. Subsequent to burning, the ash is primarily composed of amorphous silica with a high specific surface area [159], [160]. It has been reported that incineration temperatures of approximately 900ºC produced amorphous soluble silica [161]; however, when burned at temperatures of 500°C to 700°C the amount of amorphous silica produced tends to be higher[160]. When the ash is pulverized or ground, the surface area is further increased, which aids in the pozzolanic reactivity [159], [162]. Unprocessed ash particle size distribution has been reported to be 1.5 – 2 orders of magnitude larger than pulverized rice husk ash that was milled to be comparable in size to portland cement grains [163].

The addition of RHA to portland cement concrete has been shown to reduce the workability of fresh concrete due to high specific surface area that requires more water to maintain workability [164]. Due to RHA being a biological material, variations in performance are to be expected. Ganesan et al. [102] reported that mixes with a PC replacement of 5-35% RHA resulted in increased initial setting time and decreased final setting time. Khalil et al. [165] reported an increase in both initial and final setting times for mixes with 5-30% replacement of PC with RHA, and Jain [166] reported decreases in both initial and final setting times for mixes which replace PC with 10-30% RHA. These variations in performance can most likely be attributed to a combination of the chemistry of RHA and PC, particle size, available surface area, soluble silica content, and differences in mixture proportions.

Research has shown that, with a proper material (highly siliceous, high specific surface area, and proper water dosage), concretes amended with 5-30% RHA exhibit higher strength than control mixes at early ages and continue to gain strength over the control mixes at later ages due to the highly pozzolanic nature from 5-30% [103], [105], [106], [165]–[167]. With replacements of 10-20% RHA, the chloride ion permeability of portland cement concrete dropped significantly, with a reduction of approximately 80 - 90% compared to control specimens. The chloride ion penetrability of the control mix would be considered to have moderate chloride penetrability, while the 10%, 15%, and 20% RHA mixes, with 81%, 86%, and 89% reduction respectively, would all be considered to have very low chloride ion penetrability according to the specification set forth in ASTM C1202 [108]. This was due to the combined effects of the smaller particles of RHA forming a denser concrete matrix as well as the pozzolanic reaction. It has been reported that concretes amended with RHA perform better with respect to durability tests such as freeze thaw resistance and ASR-related expansion [104], [109].

Presently, the beneficial use of rice husk ash in the United States is very limited and there is no available literature regarding the production of this material. However, estimations based on surveys of crop production and ash production suggest that the rice production in the United

States totaled 9.9 million tons in 2012 [168]. According to [169], approximately 22% of rice paddy is husk, of which 25% is converted to ash and, therefore, approximately 5.5% of the total rice paddy produced is converted to ash. Thus, the United States theoretically would produce approximately 550,000 tons of ash on an annual basis and this material is not currently being reused beneficially. According to [170]], the annual worldwide production of rice was 680 million tons per year based on 2010 data. Assuming 5% of the total rice produced is converted into RHA, the total annual worldwide production of RHA could be approximately 34 million tons which could be a meaningful supply of an alternative replacement to portland cement; this has been realized outside of the United States in places throughout Asia [170], [171].

2.4.5. Sugarcane Bagasse Ash

The process of converting sugarcane to cane sugar involves the cultivation of the entire plant and crushing the stalks to produce the cane juice. The resultant dry, crushed stalks are collectively known as "bagasse" and are often used as a boiler fuel for energy generation by the processing factories. Sugarcane Bagasse Ash (SCBA) is the residual ash from the incineration of bagasse.

Due to limited use of SCBA as a supplementary cementitious material, information with respect to utilization as a replacement of portland cement in concrete is not extensively documented. Nevertheless, the addition of SCBA to PCC has been shown to reduce workability and it has been noted that the use of a water-reducing admixture is typically necessary to achieve a workability that is comparable to PC for mixing and placement [113]. It has been reported that replacements of up to 30% of PC with SCBA increased compressive strength at ages beyond 28 days [111], [113]. Water permeability reduced with addition of SCBA; it was reported that concrete which incorporated 30% replacement of PC with SCBA experienced reductions in permeability of approximately 50% and 70% at ages of 28 and 90 days, respectively [111]. Accordingly, concrete with lower permeability exhibits increased resistance to chloride intrusion and corrosion [110], [112].

Information with respect to the production of sugarcane bagasse ash within the United States is not well documented; however, the production of sugarcane itself is. The USDA reported the total sugarcane yield at 32.5 million tons for 2015, and the rendered ash remainder is reported to vary between 4-18% of the original weight [172], [173]. Therefore, there are is a potential for between 1.3 and 5.9 million tons of bagasse ash available on an annual basis for a partial PC replacement. Currently, this material is not being utilized in the United States or Europe and is being landfilled. It is being utilized in India as a cement replacement and reports indicate that the replacement of PC with SCBA has positive effects on the concrete produced, resulting in higher compressive strengths for replacements up to 35% [114], [115].

2.4.6. Biomass Combustion Ash

Biomass combustion ash (BCA) is produced much in the same way that coal fly ash, sugarcane bagasse ash, and rice husk ash are produced; however, the fuel source is usually municipal wood waste, which may be composed of yard clippings, forestry residues, wood related storm debris, and wood processing residue, amongst other sources. The ash is generated and collected in a similar fashion as coal ash and has been used in a similar manner [102], [174]. Concrete with PC replaced with BCA in percentages between 10 – 20% has been reported to have higher compressive strength and lower permeability. Larger percentages of PC replacement with BCA

(up to 40%) indicate that while early-age strength, prior to 28 days, is sacrificed, late-age strength is superior [89].

The replacement of PC with BCA in mortar systems has relatively little effect on the plastic and elastic behavior of the final product. The compressive strength, tensile strength, flow, and setting time of the control, and the 10% and 20% replacement mixes, respectively, are presented in Figure 2-2. The properties are presented as normalized percentages of those found for the control [89], [90].

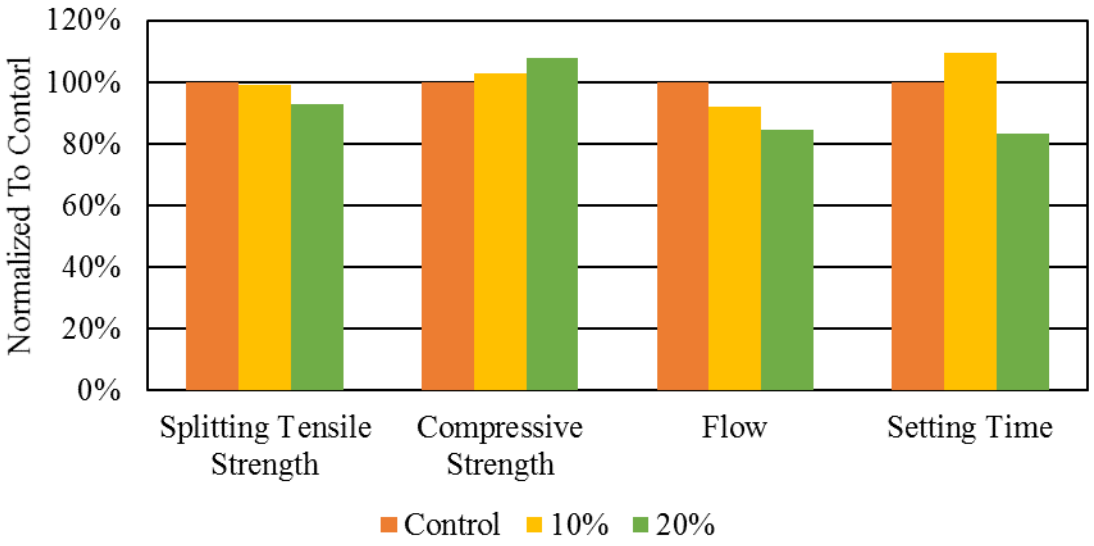

Figure 2-2. Normalized properties of mortars with various BCA replacements [89], [90].

Waste wood ash is considered to be a "carbon neutral" material because the carbon dioxide that is released during the combustion of the wood material would naturally be evolved via decomposition of the wood material in a landfill. Furthermore, when landfilled, the material would release methane gas, which can be much more disruptive to the environment than carbon dioxide. In a biomass facility, any methane produced is combusted to produce more energy [175], [176].

According to the US EPA, approximately 16.4 million tons of wood waste is generated each year, with only 1.6 million tons being recovered and recycled. This amounts to 14.8 million tons of wood that is being landfilled. Assuming a conservative value of 4% ash generated from wood waste, the 14.8 million tons of surplus wood waste would amount to nearly 600,000 tons of ash that could be beneficially used in portland cement concrete in the United States.

2.5. Current State of Research

2.5.1. Ternary and Quaternary Cement Blends

A ternary mix is a cement mix that contains portland cement and two cementitious alternatives, and quaternary mixes utilize three amendments. Due to the variable characteristics and availabilities of SCMs, it can be advantageous to blend several types of SCMs together in a portland cement-based system to achieve desired results. The interaction between the alternative

cementitious materials and the resultant concrete properties are of interest. One of the benefits of utilizing a ternary blend is that a material that is known to have poor performance can be combined with a material that has superior performance, which can reduce cost and deleterious effects. Examples would be portland cement with combinations of alternative materials such as fly ash and activated paper sludge, palm oil ash and fly ash, and rice husk ash blended with fly ash [177]–[181].

The following is another example where the addition of a third cementitious material (ternary blend) to a binary combination of portland cement and an SCM can mitigate an undesirable effect produced by the first SCM. The addition of high volumes of FA-F as a replacement for PC can tend to slow the setting time, as hydration of FA-F is a slow process; however, the addition of small percentages of SF (e.g. 3-6%) FA-creates a product that has superior strength and durability with a more normal setting time [182], [183].

2.5.2. Chemical Balancing

As discussed in Section 2.2., ***C-S-H*** gels in mature hydrated portland cement have a calcia-to-silica ratio of approximately 1.4 – 2.0, with unhydrated portland cement having a ***C:S*** of approximately 3.0. In a pure portland cement system, the conversion to ***C-S-H*** leaves an abundance of calcium products, generally in the form of portlandite ($Ca(OH)_2$). A silica-rich SCM added to the hydrating cement will react with the portlandite to produce more ***C-S-H*** gel with a lower ***C:S*** ratio [184]. Furthermore, some commonly used SCMs, including coal fly ash, metakaolin, blast furnace slag, and sugarcane bagasse ash contain aluminum in greater quantities than contained in portland cement. It has been shown that ***C-S-H*** gels that have a lower ***C:S*** tend to have the added benefit of higher aluminum uptake, creating a ***C-A-S-H*** gel. However, this may result in the formation of "monosulfate" (***AFm***), which in abundance can be deleterious to the hardened portland cement concrete product [184]–[186]. While the ***C:S*** ratio has been studied as a secondary characteristic of hydrated cements, its use has not been established beyond that of a qualitative indicator. Adding to the ambiguity is that different experimental methods will yield a wide range of values for ***C:S*** for the same hydrated paste [185], [187]–[189]. What is of consensus is that the addition of a stable SCM in the correct proportions can chemically balance the system as well as contribute to a myriad of other positive benefits.

2.6. Conclusions

The use of waste materials generated from industrial waste streams have the potential to be beneficial when properly utilized in portland cement concrete. Supplementary cementitious materials that have been historically proven to provide benefit from use include: coal fly ash, blast furnace slag, metakaolin, and silica fume. It is becoming evident that there is a growing need for additional materials that can be used in concert with portland cement. The U.S. Geological Survey estimated the global production of portland cement for 2014 to be more than double the global production in 2003 (4.18 billion tons in 2014 and 2.03 billion tons in 2003) [190]. The ever-growing production of cement, the reduction of coal power plants that provide fly ash, and the increasing push towards more environmentally conscientious materials requires the industry to consider alternative cementitious materials that previously would be deemed waste materials and not be considered viable for use in portland cement concrete. With this pressure on the industry, it is apparent that with regard to the myriad of potential alternatives, the research is lacking when it comes to long-term durability studies on the majority of the less

mainstream materials presented herein, namely sugarcane bagasse ash, rice husk ash, ground glass, wood biomass ash, and ground waste glass. Furthermore, if producers of these materials are to take advantage of this potential market, it is incumbent on them to make a concerted effort to produce a more homogenous product for waste stream materials to be utilized. Some of the shortcomings that are immediately evident with respect to utilizing some of the agricultural ashes is the high level of organics present in the ash due to insufficient and inconsistent incineration. For materials such as wood biomass ash, it may become beneficial to be more selective in the types of fuel used. For example, [71] reported that 28 different wood biomass ashes had widely varying chemical compositions, such as calcium oxide contents ranging between 6 and 84%. Such variations in material composition will only hinder the global acceptance of such materials.

The benefits of SCM additions are not constrained to the physical and chemical effects on the concrete; one of the larger benefits that are realized is the reduction in cost. Many industries that produce these waste stream materials pay to dispose of these materials into landfills or construct their own landfills. Using this material beneficially in concrete reroutes the material away from landfills and safely encapsulates the waste stream materials. This provides a financial gain to the producers and lowered cost to the consumers as compared to portland cement that has been a benefit realized by coal power companies for decades. The cost-benefits of employing SCM in concrete will vary for each application and the materials that are locally available; however, if more waste stream material producers can refine the materials to acceptable levels, the widespread acceptance of more exotic SCMs should become the industry standard.

3. MATERIALS CHARACTERIZATION

This chapter presents the materials selected for this investigation based on the literature review and a survey of locally available materials. Class C coal fly ash was selected as it is a widely available material in the Southeast United States and elsewhere. Pulverized glass was the next material chosen for investigation due to the large amounts of collected glass that is currently being disposed of; three glasses were chosen, two from a manufacturer that specialized in glass for architectural concrete constructions, and a glass from a local start-up company wanted to take recycled glass and process it as a cement replacement. A local utility company that utilizes wood as its primary fuel source provided the ash byproduct of energy production for investigation as a potential SCM. Florida is a leading sugarcane producer in the country, and there is a locally available source of sugarcane bagasse ash; therefore, sugarcane bagasse ash was chosen to be included in this investigation [191]. Additionally, rice is available locally; therefore, rice husk ash was selected for use in this study as well. Expended equilibrium catalyst was provided by a waste materials company and was, consequently, included in the investigation.

With the assumption that some or all of the proposed SCMs would not perform adequately in a binary cementitious mixture [94], SCMs with well documented performance were included and used in ternary blended systems. These SCMs include class F fly ash, blast furnace slag, Micron^3 ultrafine fly ash, silica fume, and metakaolin. Additionally, these materials were used in binary mixes as comparison mixes to the alternative SCMs.

3.1. Chemical Analysis

One of the largest variables in cement chemistry is chemical composition of each cementitious component. There is a myriad of different chemical reactions that can take place during cement hydration and having a knowledge of the potential chemical reactions is a necessity [70]. The chemical composition of a material can be determined in several different ways including flame photometry or various chemical digestions. Typically, though, cement chemical analysis is done by way of x-ray fluorescence spectroscopy (XRF).

3.1.1. Summary of Test Method

X-ray fluorescence consists of subjecting a sample of material to ionizing radiation. This radiation has high enough energy that it can eject inner-shell electrons from an atom causing the atom to be unstable. To resolve the instability, an outer shell electron (which has a higher energy state) drops down to fill the vacancy in the lower-energy shell. To do this, the outer shell electron must lose energy; this is done by ejection of a photon (known as Bremsstrahlung radiation). This photon has a specific energy that is characteristic of the atom from which it is ejected [192]. The energy detected from the photon release is then isolated from the background radiation caused by Rayleigh and Compton scattering (when x-rays scatter but do not eject energy in the form of a photon, or when x-rays scatter and a random amount of energy is released, respectively) [193].

The particular method used for this research was wavelength-dispersive XRF, in which the wavelength of the incident x-rays is varied by applying differing voltages and passing it through different crystals to emit varied ionizing radiation that force the different elements to fluoresce. With repeated analysis on similar materials (for qualification of compliance on cements, for

example) several standard materials were used to calibrate the machine in order to achieve greater accuracy of measurement. For the cases in which the materials being analyzed were not similar to portland cement or blast furnace slag, or a general idea of their composition was unknown, a common analytical method called "standardless" analysis was performed. This analysis utilizes theoretical x-ray intensities calculated from known machine parameters and compares them to the measured intensities [194].

3.1.2. Equipment

For the elemental chemical analysis, the researchers utilized a wavelength-dispersive x-ray fluorescence spectrometer from Panalytical. The analysis method for cement was calibrated using NIST standards. The analyses of all other materials were done using a standardless approach. All of the specimens were analyzed by an outside laboratory (CTL Group). For this research, the analyses were done on pressed powder samples to ensure sulfate content was preserved, rather than by fusing the samples into glass beads at 1000+^{o}C.

3.1.3. Procedure

The procedure used to determine elemental composition was performed in general accordance with ASTM C114 - *Standard Test Methods for Chemical Analysis of Hydraulic Cement* [195]. Specimens were prepared by first drying the raw material in an oven at 105^{o} ± 2^{o}C for 24 hours; mass loss was not recorded prior to this step. Then a portion of the material was set aside for loss on ignition. The material was then carefully weighed out, a liquid binder was mixed into the powder and allowed to dry. The powders were then pressed into specimen 25 mm diameter specimen cups at 20 tons to create pressed pellets which were then placed into the x-ray fluorescence spectrometer for analysis.

3.1.4. Chemical Analysis Testing Results and Discussion

The results from the chemical analysis of the materials investigated during this research are provided in Table 3-1. The portland cement has a relatively high amount of sulfate (SO^3) at 3.27%; ASTM C150 requires the sulfate content to be below 3.0% when the $\boldsymbol{C_3A}$ content is below 8% [59]. The calculated $\boldsymbol{C_3A}$ content was 7%, and the measured $\boldsymbol{C_3A}$ content using XRD (in the next section) was measured to be 4.9%; in either case the sulfate content was too high. However, the remaining requirements within the specification were met with regard to chemical composition and loss on ignition.

All of the standing beneficial use materials (class F fly ash, Micron^3 fly ash, silica fume, slag, and metakaolin) had typical chemical compositions with no abnormalities to note. The totals listed for each material, when listed as 100%, have been normalized; these materials did not have loss on ignition testing done at the time of analysis. Loss on ignition results for each of the materials are presented later in this chapter.

The analysis of the class C fly ash revealed that the equivalent alkalis content was higher than would be allowed for a low-alkali cement. However, blended cements subject to ASTM C595 - *Standard Specification for Blended Hydraulic Cements* are required to have a maximum sulfur trioxide content of 4% unless it is shown that the excess sulfur trioxide will not produce excessive expansion in ASTM C1038 [61]. Sugarcane bagasse ash had an even higher alkali content that needs to be taken into account when reactive aggregates may be used in concretes.

The sulfur trioxide content of SCBA was high, at 3%, but it was lower than the limits for any fly ash as specified in ASTM C618 [135]. Sugarcane bagasse ash would not meet the chemical requirements of ASTM C618 as a class C, F, or N fly ash.

Table 3-1. Chemical composition of materials by x-ray fluorescence.

Chemical Oxide	Portland Cement	Class F Fly Ash	Class C Fly Ash	Ground Blast Furnace Slag	Silica Fume
SiO_2	18.7	57.8	34.7	33.6	90.9
Al_2O_3	5.36	21.4	18.5	14.4	0.39
Fe_2O_3	4.44	11.8	5.66	0.61	2.14
CaO	63.5	1.29	26.4	41.1	0.85
MgO	0.94	1.32	6.36	5.88	0.78
SO_3	3.27	0.24	1.84	2.56	<0.01
Na_2O	0.14	0.90	1.88	0.19	0.20
K_2O	0.40	2.52	0.43	0.34	1.07
TiO_2	0.27	0.99	1.45	0.53	<0.01
P_2O_5	0.64	0.19	0.86	0.02	0.10
Mn_2O_3	0.07	0.04	0.04	0.35	0.19
SrO	0.07	0.05	0.43	0.07	0.01
Cr_2O_3	0.07	0.02	0.01	<0.01	<0.01
ZnO	0.08	0.02	0.01	<0.01	0.07
BaO	-	0.07	0.83	0.06	<0.01
LOI	1.78	0.90	0.23	-	3.76
Total	99.7	99.6	99.5	99.6	100.4
$SiO_2+Al_2O_3+Fe_2O_3$	-	91.0	58.8	-	93.4
$Na_2O + 0.658K_2O$	0.41	2.56	2.17	0.41	0.90

Table 3-1. Continued

Chemical Oxide	Metakaolin	Sugarcane Bagasse Ash	Rice Husk Ash	Equilibrium Catalyst	Wood Ash
SiO_2	51.5	58.7	94.0	38.9	6.96
Al_2O_3	43.7	1.66	0.03	53.2	1.89
Fe_2O_3	0.47	2.52	0.07	1.71	1.09
CaO	<0.01	20.8	0.52	0.57	58.7
MgO	0.14	4.10	0.45	-	5.52
SO_3	0.01	3.00	0.21	0.15	5.84
Na_2O	0.28	0.41	0.08	0.60	3.71
K_2O	0.25	1.86	2.47	0.08	8.57
TiO_2	1.35	0.10	-	1.10	0.21
P_2O_5	0.08	6.72	1.49	0.46	6.12
Mn_2O_3	<0.01	0.16	0.18	-	0.95
SrO	0.02	0.14	-	0.02	0.12
Cr_2O_3	0.01	0.02	-	-	-
ZnO	<0.01	0.07	0.02	0.04	0.11
BaO	0.2	-	-	-	0.08
Cl^-	Not Analyzed	0.01	0.50	0.01	0.01
LOI	1.75				
Total	99.6	100	100	96.8	99.9
$SiO_2+Al_2O_3+Fe_2O_3$	95.7	62.9	94.1	93.8	9.94
$Na_2O + 0.658K_2O$	0.44	1.63	1.71	0.65	9.35

Table 4-1. Continued

Chemical Oxide	CS200 Glass	VCAS160 Glass	Ground Glass	Micron[3] ultrafine fly ash
SiO_2	71.9	61.2	69.6	51.0
Al_2O_3	0.48	14.0	1.93	25.4
Fe_2O_3	0.10	0.28	0.50	4.42
CaO	9.21	17.2	10.4	10.2
MgO	4.11	2.6	0.80	2.15
SO_3	0.20	<0.01	0.09	0.72
Na_2O	12.9	2.64	12.0	0.49
K_2O	0.05	0.05	0.59	1.06
TiO_2	0.01	0.69	0.08	1.45
P_2O_5	<0.01	0.05	0.02	0.37
Mn_2O_3	<0.01	<0.01	0.04	0.08
SrO	0.01	0.07	0.04	0.13
Cr_2O_3	<0.01	0.02	0.06	0.02
ZnO	<0.01	<0.01	0.01	0.04
BaO	<0.01	<0.01	0.05	0.16
LOI	0.42	0.27	2.49	1.48
Total	99.4	99.1	98.7	99.2
$SiO_2+Al_2O_3+Fe_2O_3$	72.5	75.5	72.0	80.8
$Na_2O + 0.658K_2O$	12.97	2.68	12.4	1.19

Rice husk ash had lower equivalent alkalis as compared to sugarcane bagasse ash, as well as lower sulfur trioxide content. This material would meet the chemical composition of a class F fly ash as per ASTM C618. Equilibrium catalyst is not a fly ash nor is it a natural or calcined pozzolan, so applicability to ASTM C618 is not appropriate, but the chemical composition would meet the requirements of the standard.

Wood Ash had the second highest amount of equivalent alkalis at 9.94%, the highest amount of sulfur trioxide at 5.84%, the highest amount of P_2O_5 at 6.12%, and the highest amount of CaO at 58.7% of any of the supplementary cementitious materials. High levels of sulfur trioxide could potentially contribute to internal sulfate attack (delayed ettringite formation) should concrete temperatures rise above approximately 70^{o}C during curing. The high level of deleterious materials indicates a potential for poor performance in mortar and concrete. This material would not meet the chemical requirements specified in ASTM C618.

Each of the three glass materials would meet the chemical requirements of ASTM C618; however, they are not fly ashes or natural pozzolans. The largest area of concern would be the high alkali content of CS200 glass at 13.0%. This could lead to a potential for alkali-silica reactivity issues if reactive aggregate is used in conjunction with this material. The ground glass also contained large amounts of alkalis at 12.4%, again this could prove to be an issue with reactive aggregates.

3.2. Crystallography Analysis

Cement composition is typically reported on an equivalent-oxides basis (elemental composition) as well as crystalline composition (phase composition). The method used to quantify the crystalline composition of powders is known as x-ray diffraction, XRD [also called variants of "x-ray powder diffraction" or "quantitative x-ray diffraction" (QXRD)]. This method involves irradiating a sample and scanning a detector across an angular distance to map the intensities of the diffracted x-rays. The resulting x-ray diffractogram is then compared to patterns of known crystalline materials, and if multiple phases are present, an analysis is done to deconvolute the relative percentages of crystalline materials present. For cement chemistry, the four main phases, $\boldsymbol{C_3S}$, $\boldsymbol{C_2S}$, $\boldsymbol{C_3A}$, and $\boldsymbol{C_4AF}$, are of primary concern. With the SCMs, major crystalline polymorphs of interest include quartz (SiO_2), lime (CaO), gypsum ($\boldsymbol{C\bar{S}H_2}$).

3.2.1. Summary of Test Method

The powder x-ray diffraction method uses x-rays that are produced from an energized x-ray tube and are directed toward the sample. The diffraction geometry is established by the x-ray goniometer, which links the relative positions of the x-ray tube, sample, and x-ray detector A schematic of an x-ray goniometer using Bragg-Brentano focusing geometry is shown in Figure 3-1.

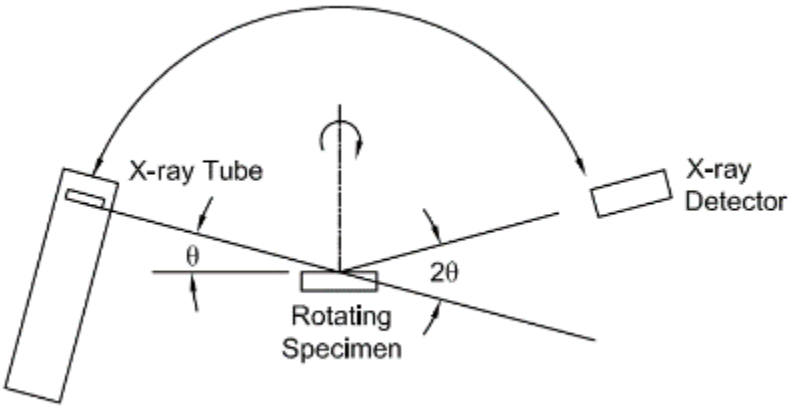

Figure 3-1. X-ray diffraction goniometer showing an x-ray tube, specimen, and x-ray detector.

As the x-ray tube and detector rotate toward each other, the 2θ angle gets larger; the intensity of the x-rays that are detected are then plotted with respect to the 2θ angle. This plot is known as a Bragg diffraction, diffraction pattern, or diffractogram. A typical XRD plot is shown in Figure 3-2.

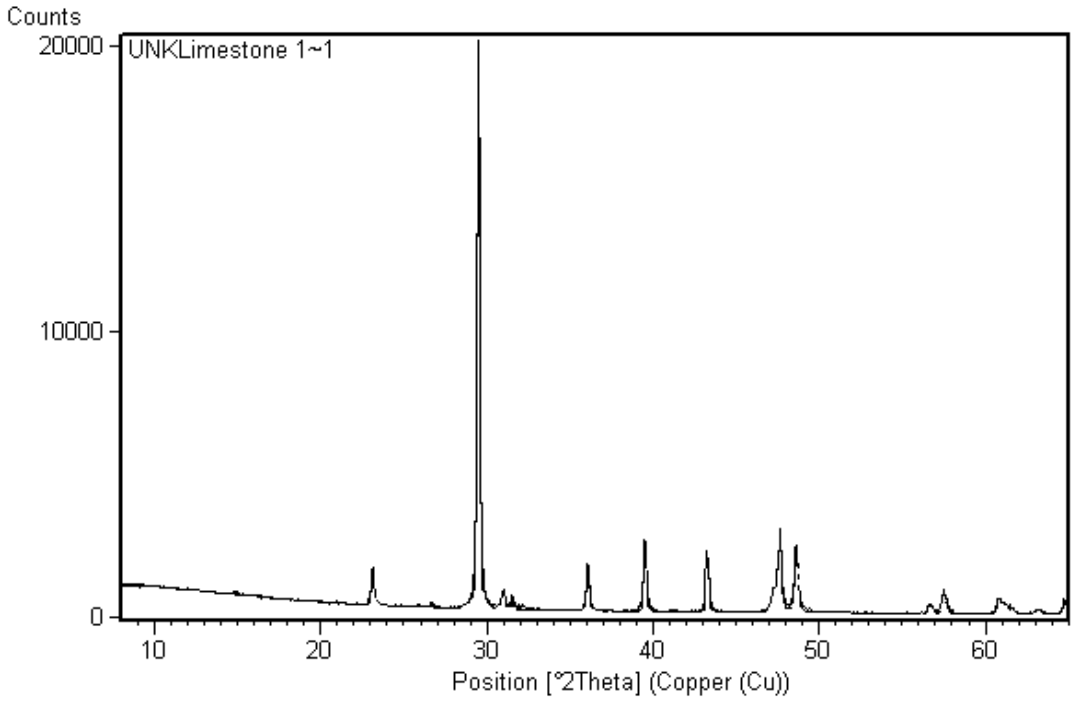

Figure 3-2. X-ray diffraction plot of limestone; x-ray intensity is shown on the y-axis and angle in 2Θ is shown on the x-axis.

From this plot, a set of known crystalline materials' patterns will be compared to the specimen diffractogram. A Rietveld analysis is performed to determine the relative proportions of those patterns present in the sample. In this way, a composition of crystalline material can be identified by the sum of its component crystalline patterns. For instance, a limestone specimen is a mixture of calcium carbonate, quartz, and feldspar, amongst other minerals. The intensities of the "peaks" on the diffractogram are related to physical structure of the crystalline lattice of a material. The highest peaks occur when x-rays are aligned to produce stronger diffractions. Areas of low diffraction occur when the x-rays are aligned with the lattice in such a way that diffracted x-rays destructively interfere as shown in Figure 3-3; incident x-rays are shown in blue, interacting with the crystalline lattice (shown as black dots), scattered x-rays are either destructive (red) or constructive (green). In the constructively interfering condition, the peaks of each x-ray amplitude align with others, creating a larger intensity. In a destructively interfering condition, the peaks of some of the x-ray amplitudes align with the troughs of other x-ray amplitudes, reducing the apparent intensity.

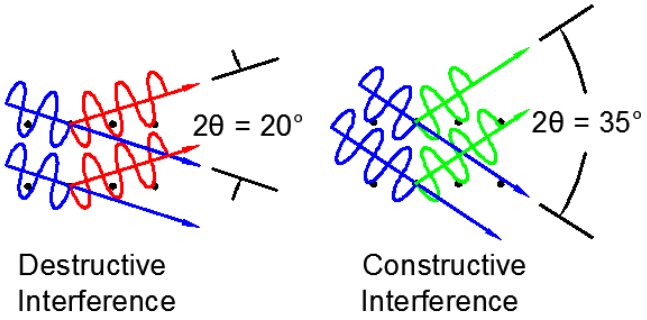

Figure 3-3. Destructive and constructive interference through a lattice due to incident x-rays.

The likelihood of constructive interference (and high intensity) is directly proportional to crystallinity; however, crystallite size will affect the peak intensity and peak width. Non-crystalline, or x-ray amorphous, materials have either poorly formed, irregular lattice structures or short-range ordered lattices and therefore do not have strong diffraction peaks. Thus, phase identification of amorphous components is not possible with XRD. A diffractogram of a completely amorphous material is presented in Figure 3-4.

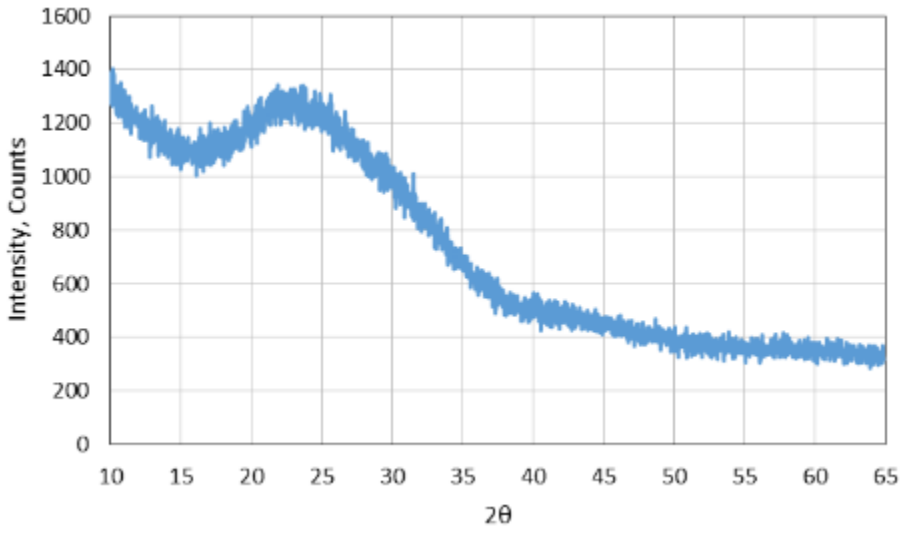

Figure 3-4. Diffractogram of a purely amorphous material.

In the case of most materials of interest, there will be a combination of crystalline and amorphous materials.

The analysis begins with the selection of potential components of the unknown sample. The selection is based on matching the positions and relative intensities of all the significant peaks in the candidate material's published diffraction pattern to peaks contained in the diffractogram of the unknown sample. Once all potential components to be considered have been selected, the corresponding patterns are then scaled up or down until the cumulative profile of the various

component profiles fits the profile of the unknown specimen. The relative intensities between the known patterns are then converted to relative proportions to describe the quantities of phases present in the sample. This type of analysis is known as Rietveld refinement.

3.2.2. Equipment

For this analysis, a Panalytical Cubix Pro powder x-ray diffractometer was used. The analysis was done utilizing Panalytical's Highscore Plus 4.0 software with the ICDD PDF4 database. Each sample was prepared in a backfilled manner with the sample pressed into a stainless steel 38 mm diameter sample holder, Figure 3-5, by hand.

Figure 3-5. X-ray diffraction backfilled sample holder with powder sample.

The Cubix Pro diffractometer was equipped with an X'Celerator detection head with multiple detectors. This configuration allowed for very fast data acquisition, enabling the analysis of cement hydration (0 - 48 hours) using a Kapton-covered wet sample holder. This particular XRD was equipped with incident and divergent optics including automated slits, Soller slits, and masks.

3.2.3. Procedure

A dry powdered sample was loaded into the bottom of a backfilled sample holder and pressed firmly into the sample holder from the back. The sample holder was then closed, and placed right side up into the loading area of the x-ray diffractometer. The software was programmed to run the machine at a predetermined angular speed, total scanning angle, x-ray tube power, and sample spinning rate. For the powder diffraction investigation, the scanning angular range was set to $8^{\circ} - 65^{o}$ 2θ with step sizes of 0.02° and a dwell time of 12 seconds per step; the power of the x-ray tube was set at 45 kW, and current was set to 40 mA.

After the diffractogram was collected, the background (difference between incoherent scattering and zero intensity) was determined, the peaks were identified, and matching patterns were reviewed. When chemical information was known about the sample, the available patterns were first filtered to only include chemistry known to be present in the sample. For instance, a sample of agricultural ashes most likely would not contain heavy elements such as ytterbium, erbium, or

any lanthanides. In this fashion, approximately 70 elements could be removed from the analysis. Once the best-fit patterns were selected, a Rietveld refinement was performed.

The XRD analyses of hydrating samples showed high amorphous contents, as would be expected due to the quantity of aqueous pore solution (water, dissolved solids, and newly-formed C-S-H) present during early-age hydration. This made analysis more involved and crystalline phase identification was possible (by comparing known peak intensities and locations), but quantification was not due to a combination of effects related to the presence (and subsequent transformation) of liquid water; the presence of water produces an imperfect surface (which changes as the sample hydrates and desiccates), the depth of penetration of the x-rays will change as the presence of liquid water lessens, the presence of water causes more buoyant particles to float to the surface causing a more heterogeneous sample, etc. After phase identification was made, the scans were plotted versus time using a Matlab script, and a surface plot was created to show the progression of crystalline growth over the hydration time. An example of this was presented in Figure 3-6 where the peak growth at 9^{o} represents ettringite formation, and the peak growth at approximately 18^{o} is indicative of the formation of portlandite, $Ca(OH)_2$, over time.

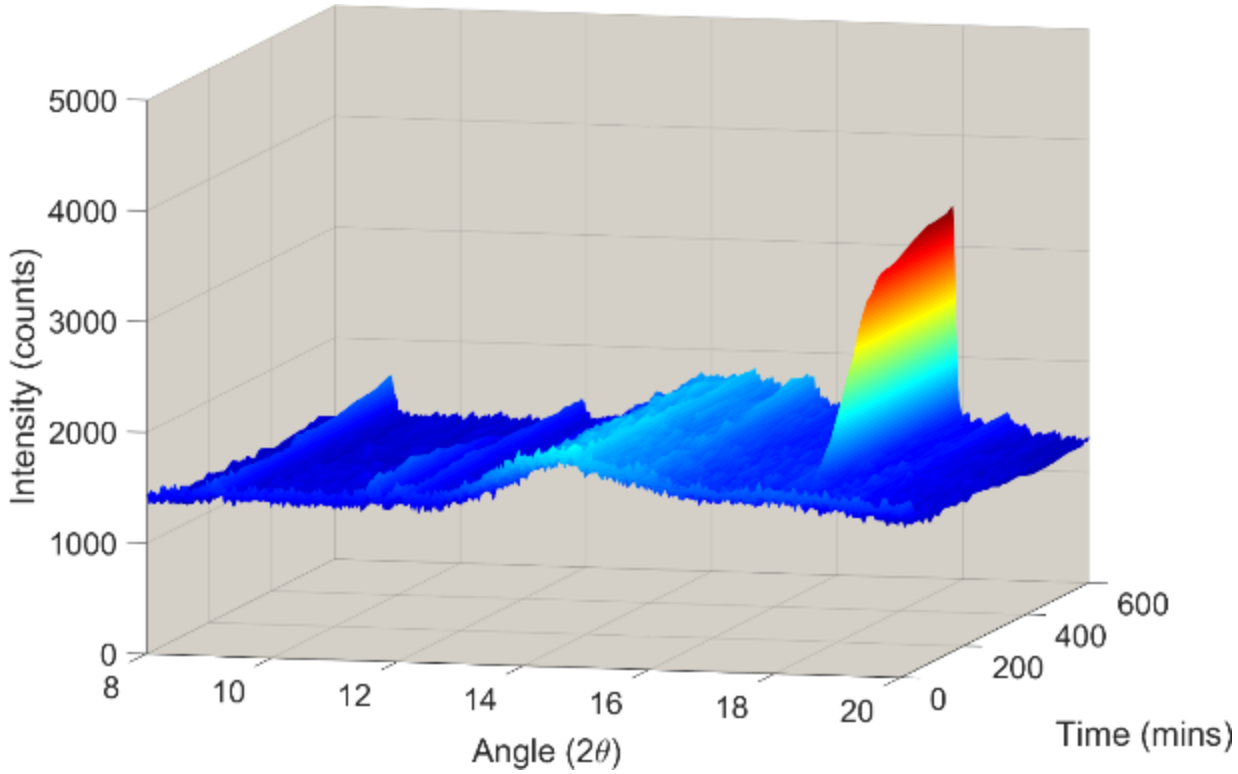

Figure 3-6. In situ hydration XRD plot.

3.2.4. Crystalline Phase Analysis Results

The results of the x-ray powder diffraction are presented in Appendix A.1. It should be noted that with the exception of portland cement and any diffractograms containing only a single

crystalline phase, the percentages of phase proportions shown are not accurate. The Rietveld refinement used for multiphase quantitative analysis produced non-convergent results when analyzing materials with large amorphous background (despite using the determined background in the fitting parameters). This resulted in divergent results when running the refinement multiple times; such a scenario occurred when analyzing the metakaolin samples. This diffractogram resulted in a 67.6% titanium dioxide composition when the original scan showed approximately 5%. The 5% is more likely given that the total titanium dioxide present in the sample is less than 2% as determined by XRF. Therefore, the information presented herein should be taken as qualitative identification rather than quantitative determination. Some of the materials (the glasses and slag) had very little crystalline material which made even qualitative identification impossible.

3.3. Loss On Ignition

The loss on ignition test (LOI) subjects samples of material to high temperatures for extended periods of time to determine the mass loss due to ignition, dehydration, and decomposition of samples containing components such as carbon, hydrates, carbonates, and sulfates. In the context of concrete, loss on ignition is typically performed on cements to determine the amount of prehydration that has occurred prior to use, as any hydrated phased caused by exposure to the environment will be decomposed. ASTM C150 limits the loss on ignition of a cement to 3.0%, with the exception of Type IV cement, which is limited to 2.5% [59]. In regard to fly ash and pozzolans, typically the loss on ignition is an indicator of carbon and/or sulfur compounds that decompose at high temperature; ASTM C618 limits the loss on ignition for fly ashes to 6.0% (type F may have an LOI of up to 12% provided that the user accepts performance or laboratory test results) and natural pozzolans are limited to 10.0% [135].

The largest drawback to having a pozzolan with high LOI is that it is typically indicative of high carbon content. High carbon contents tend to interfere with the adsorption of air-entraining admixtures and water-reducing admixtures; the higher specific surface area of carbon preferentially adsorbs the air-entraining agent rendering it less effective [196], [197]. This can be ameliorated either by the removal of carbon from the material (through calcination) or by pre-treating the material with a sacrificial admixture that is adsorbed by the carbon prior to the addition of air-entraining admixtures.

3.3.1. Summary of Test Method

The standard test method, ASTM D7348, prescribes two methods for evaluation of loss on ignition; one method involves using a furnace, the other method involves a macro-thermogravimetric analyzer, TGA, which combines a furnace with an internal balance to measure mass loss with temperature rise. As the temperature rises, various compounds are decomposed and exit the furnace as gases, and the mass of the sample is reduced. Measuring this mass loss indicates the amount of carbon and/or sulfur in the materials prior to incineration.

3.3.2. Equipment

For this research, the equipment used included crucibles capable of withstanding 950˚C, an analytical balance with a precision of 0.0001 g (0.1 g is required by the standard), crucible tongs, personal protective equipment, and a muffle furnace capable of a maximum temperature of at least 950^{o}C and capable of meeting the temperature ramping requirements set forth in ASTM

C7348 [198]. A NIST-traceable pyrometer capable of accurately measuring temperatures greater than 1000°C was utilized to ensure proper furnace temperature.

3.3.3. Procedure

For the method involving a furnace, a 1-gram sample was measured into a crucible, placed into a furnace, and heated to 500°C in 1 hour. Then the sample temperature is raised to either 750°C or 950°C in one hour. The specimen was held at the final temperature until either a constant mass was achieved, or two hours had elapsed at the final temperature. The method utilizing a macro TGA involves heating the specimen to approximately 107°C while under a dry atmosphere (dry nitrogen, oxygen, or air) to remove moisture. The heating procedure using a TGA is the same as for the furnace method [198].

Once the experiment is complete, the mass of the combusted sample is measured and compared to the initial mass and the loss on ignition is computed based upon Equation (3-1).

$$LOI = \frac{[W - B]}{W} \times 100\% \quad (3\text{-}1)$$

Where:

W = Original mass, g

B = Combusted mass, g

3.3.4. Loss On Ignition Results and Discussion

The results of this evaluation are presented in the form of a percent mass loss as compared to the original mass. A high LOI is considered to be detrimental as it indicates a potential for reduced efficacy of air-entraining agents, as well as reduced workability due to the typically high surface area of carbon. The losses on ignition due to the calcination of the SCMs at a temperature of 950°C are noted in Table 3-2.

The results show that the largest LOI's were attributed to materials that are combustion residues and waste stream materials, namely sugarcane bagasse ash (SCBA), wood ash, and rice husk ash (RHA). This is expected because the most economically efficient energy production involves incomplete combustion of the fuel. Only the sugarcane bagasse ash, and wood ash would not meet the loss on ignition requirement of 10.0% maximum as stated in ASTM C618 [135].

Table 3-2. Loss on ignition results.

Material	Initial Mass (g)	Final Mass (g)	LOI (%)
Portland Cement	2.3076	2.2429	2.80%
RHA – Sieved	2.2163	2.0851	5.92%
RHA	2.5368	2.3960	5.55%
SCBA – Sieved	2.5184	1.4612	41.98%
SCBA	2.8770	1.7530	39.07%
Class C Fly Ash	2.7032	2.6974	0.21%
Class F Fly Ash	2.3161	2.2892	1.16%
GBFS	2.4350	2.4118	0.95%
Wood Ash	2.6555	2.1363	19.55%
ECAT	2.4917	2.4505	1.65%
Micron^3 Fly Ash	2.3701	2.3424	1.17%
VCAS 160	2.3914	2.3833	0.34%
Recycled Glass	2.2081	2.1538	2.46%
CS200	2.2380	2.2289	0.41%
Metakaolin	2.3966	2.3617	1.46%
Silica Fume	2.2409	2.1473	4.18%

3.4. Particle Size Distribution

The particle size distribution of a material is an important parameter that can give an indication of the relative reactivity of a material as cementitious materials tend to be driven by surface chemistry. As the particle size distribution tends to smaller particles, the surface area per unit mass increases; this allows for more available surface for chemical dissolution and reaction. Furthermore, particle size distribution can give an indication of the "particle packing" ability of a material. A denser microstructure can improve durability by reducing the permeability of the cement.

3.4.1. Summary of Test Method

The sieve analysis method for particle size of materials is typically done with a stack of sieves of continuously decreasing opening size. As material passes through the sieves, portions of the material will be retained on sieves with progressively smaller openings. The mass proportion for each sieve is then plotted against the sieve opening size to create a particle size distribution. However, the SCMs being investigated for this research typically have all particles below 0.075 mm (75 μm); therefore, a stack of sieves would be impractical for measuring the particle size distribution.

The particle size distributions, PSDs, for the supplementary cementitious materials in this investigation were measured using a laser light particle analyzer. In this method, a pair of lasers of different wave lengths (red and blue in color) are shone through a column (in which the sample is dispersed) and into light detectors. The angle of light diffusion of the two lasers at different wave lengths can then be used to calculate the particle size causing the light diffusion. To be more specific, the light can be scattered, diffracted, and absorbed by the particles; therefore, optical characteristics of the material are important [199]. Such optical characteristics

include the indices of refraction (both real and imaginary) of both the material as well as the fluid they are dispersed in. This procedure is performed on a representative sample of material and a PSD is produced.

3.4.2. Equipment

For this evaluation, a Horiba LA-950 Laser Particle Analyzer was used. This particular particle analyzer is capable of analysis either in a dry or wet condition. For wet measurements, as cement reacts with water (as are some of the other materials of interest), lab grade 200 proof ethanol was chosen as the dispersion fluid for wet analysis.

3.4.3. Procedure

Initially, a dry procedure was used to analyze the materials. As there is no standard for measuring particle size distribution of cements or pozzolans, ASTM C1709 – *Standard Guide for Evaluation of Alternative Supplementary Cementitious Materials (ASCM) for Use in Concrete* states "*Particle size distribution can be measured by laser diffraction particle size analyzer; or other appropriate test methods*" [200]. Therefore, ASTM B822 - *Standard Test Method for Particle Size Distribution of Metal Powders and Related Compounds by Light Scattering* was employed [201]. In the "dry" method, a sample of material is passed through the measuring chamber via an air stream. The analyzer employed an agglomeration breaker brush that vibrated in the sample hopper and dispersed agglomerates. While this worked well for cement, the vibration of the plastic brush bristles imparted a static charge to some of the other materials which produced erroneous measurements; for instance, a finely divided powder of sugarcane ash showed an average particle size of 2.5 mm (~0.1 in) compared to the average particle size of ethanol dispersed SCBA being ~15 µm.

Therefore, the "wet" procedure was adopted in which a small portion of material (typically less than 0.5 g) was dispersed into 100% pure ethanol and circulated through the measurement chamber. Following the first measurement, an ultrasonic probe was used (35W for one minute) to disturb any agglomerations, the fluid was de-bubbled, and the sample was measured again. This procedure was repeated until the average particle size between successive ultrasonic dispersion changed by less than 1 micron.

With either procedure, the refractive indices of the material and dispersion fluid are required. Each material has two refractive indices: a real index and an imaginary refractive index. The real refractive index describes how light bends when it is transmitted through a material, and the imaginary index describes attenuation of light through the material [202]. The indices of refraction for the materials and dispersion fluid are presented in Table 3-3 and were obtained from the available literature, including documentation provided by the manufacturer of the laser diffractometer.

Table 3-3. Refractive indices of ethanol and the materials investigated (assumed, not measured).

Material	Real Refractive Index	Imaginary Refractive Index	Notes / References
Ethanol	1.36	-	[203], [204]
Portland Cement	1.70	0.10	[205]
RHA	1.60	0.15	The imaginary portion of the refractive index was assumed to be 0.15. This attenuation coefficient was chosen because it is very dark. [206]
SCBA	1.85	1.0	The indices of refraction for this material are not readily available. An index of refraction for carbon black with silica is listed as 1.85. Due to the high carbon and silica content of SCBA, this was chosen, with a 1.0 imaginary component. [207]
Class C Fly Ash	1.65	0.10	The reference material suggested an imaginary component of 1.0. However, the fly ash used for this research did not appear dark in color, and should be spherical in shape; 0.1 was chosen.
Class F Fly Ash	1.56	0.10	[208]
GBFS	1.63	0.15	[208], [209]
Wood Ash			The indices of refraction for this material are not readily available; the real index of refraction was chosen to be the same as RHA. SCBA is darker, so the imaginary index was increased to 0.20.
ECAT	1.66	1.0	The indices of refraction for this material are not readily available. The index of refraction was chosen to be the same as aluminum silicate, due to the chemical composition of this material. [207]
Micron[3] Fly Ash	1.53	0.1	[210]
VCAS 160	1.54	0.1	All glasses were considered to be silicon dioxide and calculated based on measured specific gravity. [211]
Recycled Glass	1.53	0.1	
CS200	1.53	0.1	
Metakaolin	1.60	0.1	[212]
Silica Fume	1.46	0.1	[211], [213]

3.4.4. Particle Size Testing Results and Discussion

There are drawbacks to using this method to determine particle size of powdered materials. The first drawback is that in either a column of air or liquid passing through a laser, the diffraction of

light through the particles will always be interpreted as spherical particles. Therefore, the particle size shown represents the largest particle dimension that was perpendicular to the light beam path at the time of measurement. As such, the software for the particle size analyzer has the capability of calculating surface area of the powder, but it will assume the powder is composed of perfect spheres; as this is not the case for the majority of materials used for cement replacement, this should not be used.

Additionally, the data from air measurements tended to result in higher measured particle size. This is likely due to better dispersion occurring in the wet method. However, care should be taken to insure that the powders are not soluble in the fluid chosen for dispersion.

The results of the particle size distribution analysis are presented in graphical form with the x-axis representing the particle size in μm and the y-axis in cumulative percentage. Each material is shown with the duration of ultrasonic dispersion in the legend, "0 min" relates to an as-received condition, "1 min" denotes one minute of ultrasonic dispersion. The particle size related to 10% passing, 50% passing, and 90% passing sizes for the final particle size are denoted as D_{10}, D_{50}, and D_{90}, respectively, in the lower right corner the charts. This designation denotes that, for instance, 10% of the material is finer than the D_{10} size.

The particle size distribution for all other materials includes the particle size distribution for ordinary portland cement (OPC) as a comparison. The average particle size of cement for this project was 5.6 microns. This value is lower than what is typically reported [1]; however, the majority of researchers use laser diffraction in air. Laser diffraction of cement showed a much higher particle size measured in air than when measured dispersed in ethanol; the size in air was approximately 12 microns, compared to 5.6 in ethanol.

Sugarcane bagasse ash is shown in a sieved condition as that is the condition that the material was used. The "as received" material had some larger particles (such as rocks and unburnt material) as large as 12 mm in diameter. However, in the as received state, the D_{90} was less than approximately 0.1 mm.

The metakaolin particle size distribution had a bimodal shape, that can occur from a manufactured product if the producer blends differing batches of materials.

Silica fume was received in a densified state. The 35-watt ultrasonic probe supplied with the laser particle analyzer was not powerful enough to break up the agglomerations of silica fume. The particle size distribution is presented for conciseness but it is not accurate. It is well known that silica fume, when properly dispersed, has an average particle size of less than one micron [83].

The majority of the materials present particle sizes that are coarser than the cement used in this investigation. This would seem to indicate a reduction in reactivity potential. The materials with the finer particle distributions than cement (metakaolin, Micron^3 fly ash, and silica fume) are known to be highly reactive materials. A summary of the particle sizes for the materials in this research are presented in Table 3-4. The individual particle size distributions for each material are shown in Appendix A.2.

Table 3-4. Summary of material particle sizes.

Material	D_{10}, (μm)	D_{50}, (μm)	D_{90}, (μm)
Portland Cement	2.13	5.56	10.1
RHA	18.5	59.9	101
SCBA - sieved	7.79	14.8	29.9
Class C Fly Ash	1.34	7.10	16.1
Class F Fly Ash	2.51	11.0	29.7
Slag	4.65	9.29	17.0
Wood Ash	8.88	18.7	66.3
ECAT	54.8	75.0	108
Micron[3] Fly Ash	1.51	2.65	4.36
VCAS 160	3.26	11.0	28.3
Recycled Glass	4.43	9.46	16.1
CS200	5.16	16.5	44.3
Metakaolin	0.13	4.43	7.42
Silica Fume[1]	3.66	30.6	80.0

[1] The ultrasonic probe used for agglomeration dispersal was not sufficiently powerful to disturb the densified silica fume. The erroneous data is presented for completeness.

3.5. Specific Heat Capacity

Specific heat capacity (C_{sp}) of a material is defined as "*the heat in calories required to raise the temperature of one gram of a substance one degree Celsius*" [214]. One calorie is equivalent to 4.184 joules (J). The specific heat capacity is a required material property used for thermally balancing isothermal conduction calorimetry specimens.

3.5.1. Summary of Test Method

The Standard *Test Method for Determining Specific Heat Capacity by Differential Scanning Calorimeter* outlines a procedure for measuring the specific heat capacity ,C_{sp}, of a material using a differential scanning calorimeter (DSC) [215]. A differential scanning calorimeter measures the energy required to heat a sample to a known temperature, compared to the energy required to heat a standard material to the same temperature. In this way, one specimen holder has a control sample of a known material (a sapphire disk as per the standard) which has a known C_{sp}. The other specimen holder is empty (a blank) and the energy required to raise the temperature of the sapphire disk is measured and recorded versus temperature. This energy is then corrected according to the known energy required to raise the sapphire to a certain temperature, thus, accounting for any biases in the machine or operator. Then the specimen material can be analyzed in the same way as the control, and the difference in energy recorded is used to determine C_{sp} of the specimen. When plotted, the energy required to raise the empty specimen holder is recorded as the baseline. Then the difference between the baseline and the sapphire standard at any temperature is denoted as D_{st}, while the difference between the baseline and the specimen is denoted as D_s, as shown in Figure 3-7 (adapted from ASTM E1269). The differential distance between the standard and specimen, when accounted for mass, is then used to calculate the specific heat capacity of the specimen.

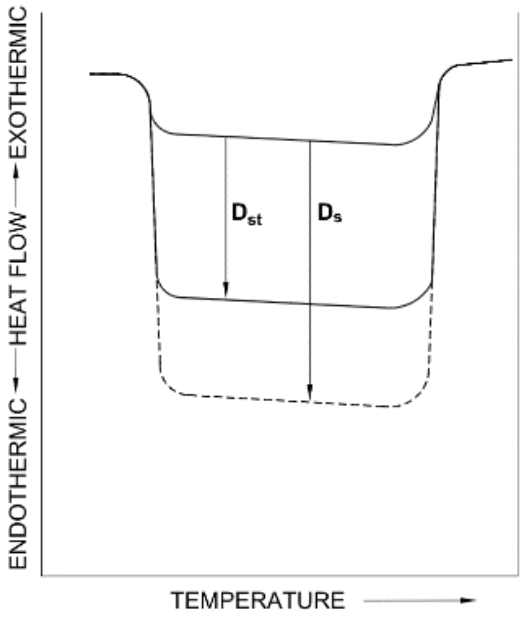

Figure 3-7. Specific heat capacity thermal curves of standard sapphire and unknown specimen, compared to baseline.

3.5.2. Equipment

A TA Instruments Q-20 Differential Scanning Calorimetry and aluminum specimen holders were used for the determination of C_{sp} of the various materials chosen for evaluation. For precise metering of material, a Mettler-Toledo analytical balance with 0.01 mg precision, and equipped with an anti-static module was used. The cooling system for the DSC was an external refrigerator unit (TA Instruments) which provided dry nitrogen as the purging fluid to control temperatures. A sapphire disk standard (α-sapphire, 0.187" diameter x 0.034" height) was obtained from TA Instruments.

3.5.3. Procedure

Each specimen was weighed in an analytical balance to a precision of 0.01 mg. The specific heat capacity at 23°C was the interest of this investigation due to the isothermal calorimetry testing taking place at 23°C. In order to properly evaluate the specific heat capacity at the correct temperature, the samples were allowed to equilibrate at 5°C for five minutes. Then the specimens were heated, at 20°C/min, until reaching a temperature of 60°C. At which point the specimens were allowed to equilibrate for five minutes.

The data acquired from heating the sapphire disk in this method was then corrected to match the specific heat values given in ASTM E1269 (linearly interpolating between values when necessary). The various materials were tested under identical conditions and the specific heat capacities were determined using Equation (4-2).

$$C_p(s) = C_p(st) \cdot \frac{Ds \cdot Wst}{Dst \cdot Ws} \quad (3\text{-}2)$$

Where:

$C_p(s)$ = specific heat capacity of the specimen (J/g-^{o}C)
$C_p(st)$ = specific heat capacity of the sapphire standard (J/g-^{o}C)
D_s = Vertical displacement between the specimen holder and the specimen DSC thermal curve at given temperature (mW)
D_{st} = Vertical displacement between the specimen holder and the sapphire standard DSC thermal curve at given temperature (mW)
W_s = mass of specimen (mg)
W_{st} = mass of sapphire standard (mg)

From this, several plots of specific heat capacities could be prepared to determine the C_{sp} at 23^{o}C. Replicates of each material were evaluated until the spread of C_{sp} values was less than 15% of the mean C_{sp}. The large variance in C_{sp} values was warranted as many of the materials were not homogenized on a milligram scale. This variance can be seen on the less processed materials (such as sugarcane bagasse ash).

3.5.4. Specific Heat Capacity Testing Results

The resulting data from the specific heat capacity evaluations are shown in Appendix A.3. As the temperature of interest for this evaluation was 23^{o}C, the graphs show data between 18^o and 33^{o}C. A summary of the specific heat capacities and the coefficient of variations of each material is presented in Table 3-5.

Table 3-5. Specific heat capacities of material with coefficients of variation for the analyses.

Material	Mean Specific Heat Capacity, (J/g-^{o}C)	Coefficient of Variation, (%)
Ordinary Portland Cement	0.740	0.09
Class C Fly Ash	0.735	0.39
Biomass Ash	0.830	3.99
Recycled Glass	0.687	8.76
Micron^3 Fly Ash	0.743	0.78
Sugarcane Bagasse Ash	0.900	14.2
Metakaolin	0.777	18.2
Equilibrium Catalyst	0.729	16.3
Blast Furnace Slag	0.734	6.84
Diamond	0.453	0.53
VCAS160 Glass	0.700	4.21
CS200 Glass	0.720	2.64
Rice Husk Ash	0.617	7.75
Class F Fly Ash	0.743	2.80
Isothermal Glass Vials	0.682	2.60

3.6. Specific Gravity

Volumetric concrete mix design is a method by which concrete material proportions can be calculated by varying the relative proportions of materials while maintaining a specific volume, typically, one cubic yard. In order to accurately determine the mass and volume of the proportions, the specific gravity of the materials is required. Variability in the specific gravity of materials can lead to concrete yields that differ significantly from one cubic yard.

3.6.1. Summary of Test Method

The test method for determining the specific gravity of the SCMs involves the use of a pycnometer, a device of calibrated volume in which the specimens will be placed, and the displaced volume can be measured. The density of the materials can be determined by dividing the mass by the volume displaced (in g/cm^3 or lb/ft^3). This density is then divided by the density of water (62.4 lb/ft^3 or 1 g/cm^3) to determine the specific gravity in a unitless form. The test method employed for this research was ASTM D5550 – *Standard Test Method for Specific Gravity of Soil Solids by Gas Pycnometer* [216].

3.6.2. Equipment

For the determination of specific gravity of soils, water pycnometry is typically used. In this method, a glass vial of calibrated volume (the pycnometer) is filled with water to the calibrated mark and weighed. The difference in weight between the water-filled pycnometer and the empty pycnometer (in g/cm^3) is the volume in mL or cm^3. Then, a weighed sample of material is placed into the dry pycnometer, and water is added until the water level reaches the calibration mark. The sample is agitated until all of the air has been removed (including de-airing the water) and the sample pycnometer is then weighed. The difference in mass between the pycnometer with the specimen and the water-filled pycnometer is used to calculate the specific gravity.

However, due to the materials investigated, water pycnometry was not utilized, as it was assumed that water would lead to the dissolution of materials; other pycnometry fluids could be used but helium was the most easily available and provides rapid results. Therefore, helium pycnometry was used; the principles of helium pycnometry and water pycnometry are effectively the same. A known mass of material displaces a measured volume of fluid, and this is used to calculate the specific gravity. The helium pycnometry method pumps a known volume of helium into a calibrated container, and the presence of the specimen reduces the effective volume of the container. This reduced volume increases the pressure, and based upon Boyle's law, the volume taken up by the helium can be calculated. This volume is then subtracted from the calibrated volume of the container, and the volume of the specimen is found; this does not take into account any pores that are not open to the surface. Dividing the mass of the specimen by the computed volume gives the specific gravity; an example is shown graphically in Figure 3-8. For this research, a Quantachrome Ultrapyc 1200e helium pycnometer was utilized in combination with a Mettler-Toledo analytical balance (0.01 mg precision).

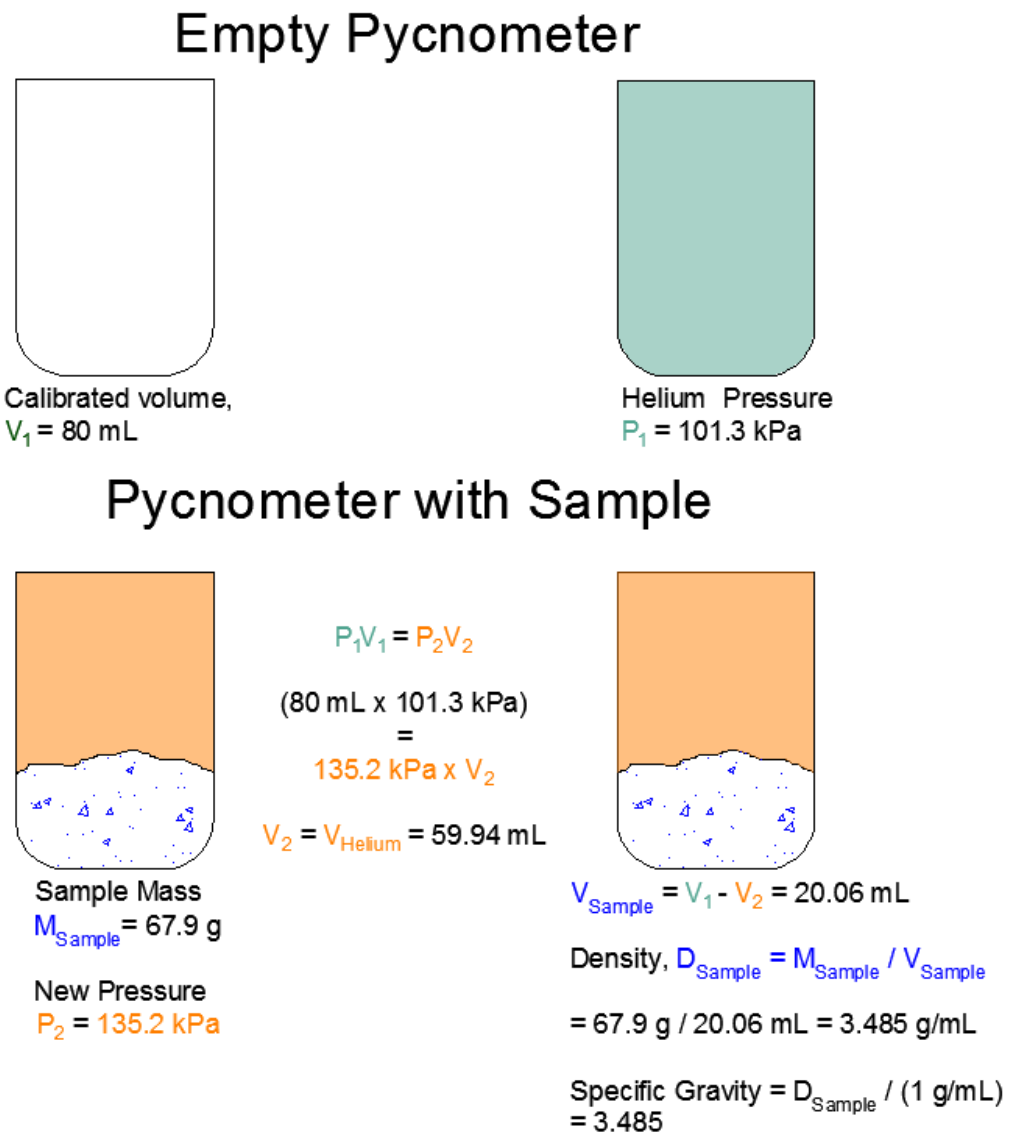

Figure 3-8. Example of specific gravity determination by helium pycnometry.

3.6.3. Procedure

The samples were prepared by oven drying each sample at 105°C for 24 hours to remove moisture; the samples were then stored in a desiccator prior to examination. The pycnometer sample holder was calibrated as per the manufacturer's specifications. Each sample was weighed to the nearest 0.01 mg and placed into the sample holder. The pycnometer metered in a known amount of helium, recorded the pressure in the container, purged the system, and calculated the specific gravity. This was repeated 10 times for each sample. The weight was recorded after the analysis to determine if any material had been purged from the cell. The largest mass discrepancy was 0.0013 g. The mass loss was distributed evenly over the 10 runs to attempt to account for mass differences and the specific gravities were adjusted. With such small mass discrepancies, the specific gravities were not significantly affected.

The data was then evaluated to determine if it was more appropriate to select the average of all 10 runs to determine specific gravity, or to average the last three runs. When looking at the coefficient of variation (the standard deviation divided by the mean) of all 10 runs compared to the coefficient of variation of the last three runs, in almost every scenario, the coefficient of variation of the last 3 runs was much lower. Furthermore, the largest difference in average specific gravity between the 10 runs or three runs was 0.01. Therefore, specific gravities of each material were assumed to be the average of the final three runs.

As a confirmation, Ottawa 20-30 sand was evaluated to have a specific gravity of 2.651, which is in agreement with the technical data sheets provided by U.S. Silica, which state the specific gravity of the sand is 2.65 [217].

3.6.4. Specific Gravity Results and Discussion

The average specific gravities of the SCMs are presented in Table 3-6. Perhaps the most surprising value presented in the results is that of the portland cement. This value is universally taken as 3.15 with variances between 3.10 and 3.25 [1]. When this result of 3.21 was found, it was assumed to be an error; however, the pycnometer was recalibrated with 3 sets of steel spheres (of known mass and volume), as well as a sample of Ottawa sand. The steel sphere calibration was correct, and the value measured for the Ottawa sand was 2.651. The published value for Ottawa sand is 2.65, so this was in agreement as well. As such, the value of 3.21 for portland cement was taken to be correct; it is assumed that limestone inter-grinding during the manufacture of cement may lead to small differences in specific gravity; however, this would not account for the specific gravity of cement being higher than 3.15. The sugarcane bagasse ash had a very low density; this was expected as the material is very light during handling. The three glasses were very similar with respect to specific gravity, whereas the fly ashes were noticeably different; specifically, class F fly ash was much lower than expected.

Table 3-6. Specific gravities of materials investigated.

Material	Average Specific Gravity	Coefficient of Variation, (%)
Portland Cement	3.21	0.07
RHA – Sieved	2.45	0.32
SCBA – Sieved	2.11	0.12
Class C Fly Ash	2.69	0.01
Class F Fly Ash	2.38	0.04
Slag	2.98	0.03
Wood Ash	2.72	0.03
ECAT	2.84	0.04
Micron3 Fly Ash	2.53	0.12
VCAS 160	2.60	0.06
Recycled Glass	2.55	0.17
CS200	2.56	0.10
Metakaolin	2.26	0.22
Silica Fume	2.20	0.10

3.7. Material Fineness

In addition to the particle size distribution of a material, the material fineness drives the hydration reaction rates. Particle size is related to the physical outer dimensions of the particles, whereas the fineness is a measure of the surface area per unit mass of a material. It needs to be stressed that fineness is not the same as surface area. Fineness is normalized to mass; as such smaller particles will tend to have larger fineness, all other variables being equal. When particle morphology changes, surface area per particle will change; to a certain extent, the degree of porosity of particles, if present, will be reflected in a higher fineness. There are multiple methods for determining the surface area of powders; the most frequently used for cementitious materials are the Blaine fineness method, Brunauer-Emmett-Teller (BET) gas adsorption method, and Wagner turbidimeter method. For this research, Blaine fineness was utilized.

3.7.1. Summary of Test Method

In this test method, a mass of material is placed into a volumetrically calibrated cell; a vacuum is then pulled on the sample to pull air through the sample. Based upon the specific gravity, mass of sample, and volume of the cell, the porosity of the sample is calculated. Using the time taken for the vacuum to equilibrate, along with air and temperature correction factors, the fineness of the material is determined by comparison to a material of known fineness using Equation (3-3).

$$S = \frac{S_s \rho_s (b_s - \varepsilon_s)\sqrt{\eta_s}\sqrt{\varepsilon^3}\sqrt{T}}{\rho (b - \varepsilon)\sqrt{\eta}\sqrt{\epsilon_s^3}\sqrt{T_s}} \quad (3\text{-}3)$$

Where:

S = specific surface area, m^2/kg
T = measured time interval of manometer drop, s
η = viscosity of air at temperature of test, μPa·s
ε = porosity of prepared bed
ρ = density of material, kg/m^3
b = constant appropriate for sample
The subscript s refers to the correction factor for the standard sample.

3.7.2. Equipment

Presuming that the evaluations are conducted in an environment with consistent temperature control, the only equipment required for this test method is a scale for measuring material, vacuum grease, a stop watch, and a Blaine permeameter. A typical Blaine permeameter is shown in Figure 3-9.

Figure 3-9. Blaine permeameter.

3.7.3. Procedure

For non-cement materials, the correction factor (b) must be determined by varying the bed porosity and plotting $(\varepsilon^3 T)^{1/2}$ versus the sample porosity and finding the y-intercept of the linear-fit line through the data points. ASTM C204 - *Standard Test Methods for Fineness of Hydraulic Cement by Air-Permeability Apparatus*, specifies that the correlation coefficient for the b correction factor must be 0.9970 or higher [218]. This requirement was removed for two reasons; 1.) Blaine fineness presumes homogenous perfectly spherical particles and 2.) when dealing with heterogeneous materials, the required number of samples to reach this level of correlation would be excessive. Furthermore, several materials did not provide linear relations when plotting $(\varepsilon^3 T)^{1/2}$ versus ε, even when 4 – 5 samples were analyzed.

The mass of the sample is calculated using Equation (3-4). The material is placed into the sample cell, and compacted. The sample cell is placed into the manometer and a vacuum is pulled on the sample. As the manometer fluid begins to drop as air is pulled through the sample, the level of the fluid is monitored and the time that it takes to fall a prescribed distance is recorded.

$$W = \rho V(1 - \varepsilon) \tag{3-4}$$

Where:

W = required sample mass, g
ρ = density of material, kg/m^3
V = volume of cell, cm^3
ε = porosity of prepared bed

3.7.4. Blaine Fineness Results and Discussion

The final results of the Blaine testing are presented in Table 3-7. With standard materials such as cement, class F fly ash, slag, and metakaolin, the fineness measurements provided results with low variation from sample to sample as expected. Some of the other materials provided widely varying results; for instance, equilibrium catalyst had a coefficient of variation of 30.6%. This was largely due to the test for three of the porosities taking less than two seconds to complete (as compared to nearly two minutes for cement). It is presumed that 3,270 cm^2/m is incorrect because it is known that the catalysts have high surface areas.

Table 3-7. Fineness of materials under investigation.

Material	Blaine Fineness, cm^2/g	Coefficient of Variation
Portland Cement	5,860	4.8%
RHA	2,980	21.6%
SCBA – Sieved	7,390	12.1%
Class C Fly Ash	3,550	27.8%
Class F Fly Ash	2,050	5.5%
Slag	3,010	0.4%
Wood Ash	6,520	9.7%
ECAT	3,270	30.6%
VCAS 160	3,370	25.6%
Recycled Glass	3,690	9.7%
CS200	2,620	1.9%
Metakaolin	20,010	3.9%

For the majority of the materials (such as the glasses, or class C fly ash); the results were consistent between specimens. The material fineness should give an indication to reactivity as higher surface area and fineness is related to higher reactivity. The finenesses of the different glasses vary based upon the level of grinding during manufacture.

The sugarcane bagasse ash provided the most divergent results; in a sieved state, the coefficient of variability (CoV), this is the standard deviation divided by the mean, expressed as a percentage) was a relatively low result of 12.1%. However, if one sample is removed from analysis, the fineness changes to 7,960 cm^2/g with a CoV of 4.7% from 7,390 cm^2/g. When sugarcane was analyzed in a raw state (not sieved) the fineness was measured at 25,930 cm^2/g with a coefficient of variation of 304%; the range of fineness was -193,540 to 138,200 cm^2/g. A negative surface area is impossible; therefore, these results were ignored completely. Additionally, there was an anomaly with sugarcane bagasse ash that required the use of a time-lapse camera to record the time. Consistently the samples would take approximately 30 minutes for the manometer fluid to move approximately 1/8”; following this period of time, the manometer fluid would finish moving (approximately 2.125”) in 4 – 10 minutes.

Rice husk ash was similar to sugarcane ash with regards to heterogeneity; when one of the samples was removed from analysis, the fineness (cm^2/g) and coefficient of variation change from 2,980 and 21.6% to 2,650 and 11.7%, respectively. Similarly, removing a sample of the recycled ground glass reduced the coefficient of variability to 4.8% with a fineness of 3,470

cm^2/g; this is similar to the CS200 ground glass powder. With the VCAS glass, all samples were varied from each other and ranged from 2,220 cm^2/g to 4,560 cm^2/g. The class C fly ash also showed a large amount of variability; removing the largest variable sample resulted in a fineness of 2,930 cm^2/g with a coefficient of variation of 11.0%. This is more in line with what is expected based upon the fineness of class F fly ash.

The constant, b, has a very large effect on the final fineness; for instance, changing the b value from 0.52 to 0.53 for as-received sugarcane can change the surface area from 32,870 to 20,780 cm^2/g. As stated previously, determination of the b value on heterogeneous materials is difficult; as such these values are highly erroneous and Blaine fineness is not appropriate for analyzing unrefined materials. Brunauer-Emmett-Teller method is most likely more appropriate for this research; however, the instruments at the University of Florida campus were out of service.

4. ISOTHERMAL CONDUCTION CALORIMETRY

Isothermal conduction calorimetry is an analytical method employed to measure the hydration kinetics of a chemical reaction under isothermal conditions. For the purposes of portland cement hydration, this provides a means to measure the total heat of hydration of a known amount of cementitious mixture (with any SCM or admixture) at a prescribed water-to-cementitious material ratio (w/cm) over time, typically seven days as prescribed in ASTM C1702 [219]. During isothermal conduction calorimetry it is assumed that all heat produced during hydration is removed from the system and the hydrating specimen remains at a constant temperature. The heat evolved is converted to electrical power through heat flow sensors; this electrical power is then integrated over time to produce cumulative heat.

Two other methods that have been utilized to monitor cement hydration are adiabatic calorimetry and semi-adiabatic calorimetry [78], [220]. Adiabatic calorimetry uses a feedback system wherein the temperature of hydrating cement specimen is recorded, and then the same temperature is applied to the hydrating specimen (in theory, no heat is lost). Due to the hydration kinetics of cement being influenced by temperature, adiabatic temperature rise should be higher than isothermal temperature rise. Semi-adiabatic calorimetry involved insulating a hydrating cement specimen and recording the temperature (such that heat loss in the system is prevented, however no heat is applied to the system). The application of these test methods proves to be difficult as minor variances in the temperature control and application can show large variations in results [78].

4.1. Summary of Test Method

During isothermal calorimetry, a cementitious sample of at least 3.0 grams is measured into a glass vial. An amount of water required for a specific water-to-cementitious material ratio is then measured. Any SCMs or admixtures are incorporated into the dry cement specimen or the mixing water, respectively. An inert reference material having an identical thermal mass as the specimen is also prepared. Thermal mass is the product of the mass and specific heat capacity of a material. For the inert reference material, this thermal mass is the cumulative thermal masses of the cement, SCM, and mixing water. The specimen mixture components and inert reference are brought to 23.0^{o}C and are allowed to equilibrate.

ASTM C1702 allows for two mixing methods: internal mixing and external mixing. The internal mixing method involves the specimen and mixing water held separately inside of the calorimeter to equilibrate, then the mixing water is introduced to the powdered sample, and thoroughly mixed [219]. The resulting heat of reaction is captured in whole during this process and is allowed to proceed for a period of time determined by the operator, typically two to seven days. The external mixing method prescribes the materials to be outside of the calorimeter prior to the introduction of mixing water. The materials are equilibrated to temperature (± 0.2^{o}C for the mixing water and ± 1^{o}C for the dry materials), and mixed outside of the calorimeter cell and are then immediately loaded into the calorimeter. Both methods have advantages and disadvantages. Internal mixing utilizes smaller samples (typically below 10 grams), the equilibrium temperature can be controlled to a much higher degree (the calorimeter used for this research can control temperature to within 0.05^{o}C), and the entirety of the heat evolution can be measured. External mixing can be done on larger samples (including concrete samples), can

utilize high shear mixing methods, and has less strict requirements for temperature and mass; therefore, external mixing can have higher variability.

4.2. Equipment

The experiments were conducted on a TAM Air isothermal conduction calorimeter, which is a self-contained device that uses insertable specimen holders to place specimens into a temperature-controlled cell that accurately and precisely measures heat evolution of chemical reactions. The calorimeter used for this research consisted of 8 reacting channels (labelled A1-8) and 8 non-reacting (control) channels (B1-8), Figure 4-1. Each reacting channel had an "admix ampoule" that was comprised of several components as shown in Figure 4-2.

Figure 4-1. Eight-channel isothermal conduction calorimeter.

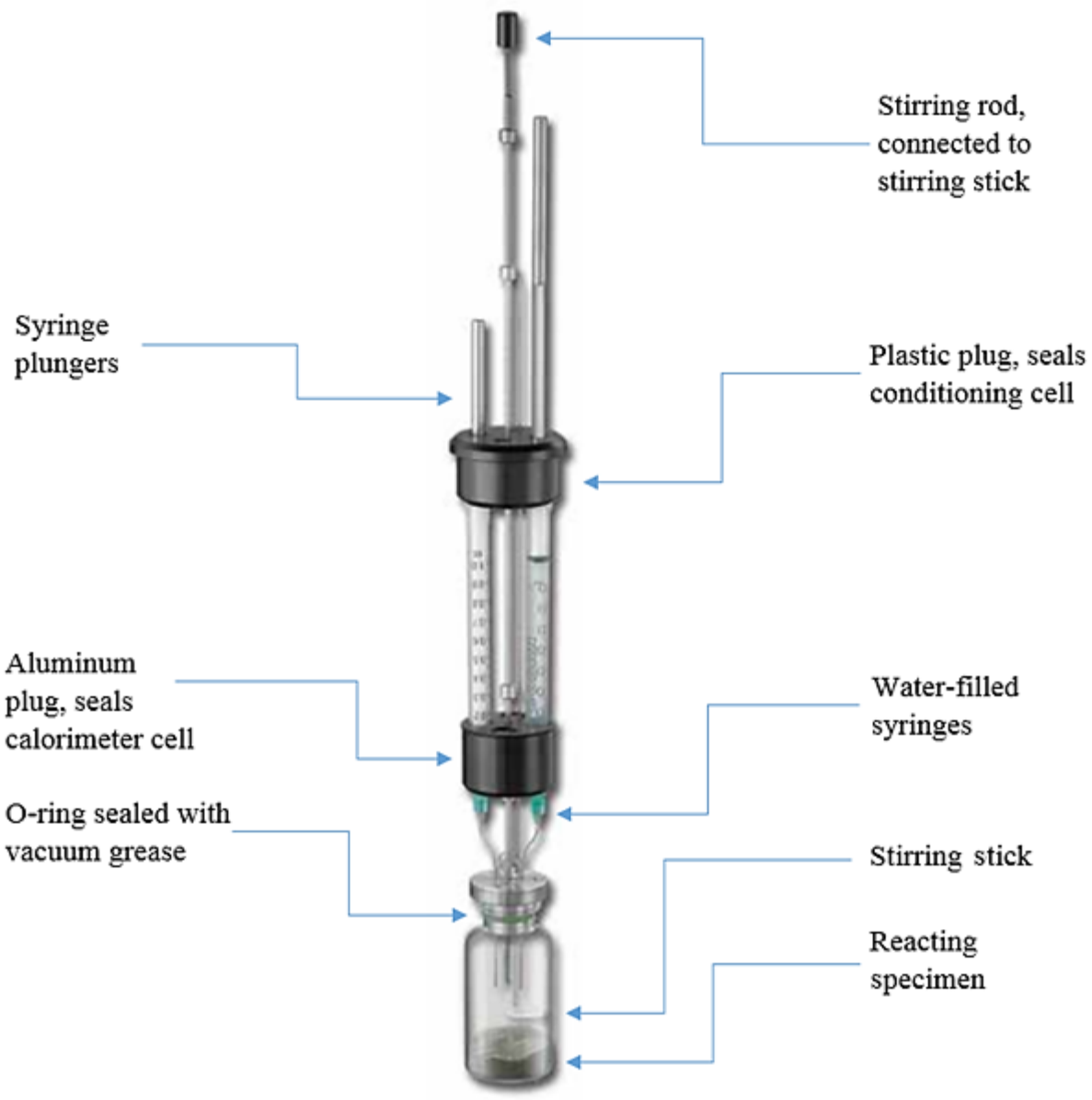

Figure 4-2. Isothermal calorimeter admix ampoule.

The admix ampoule is loaded into the calorimeter and is situated atop a heat flow sensor, which is in contact with the heat sink as shown in Figure 4-3. Heat flow sensors convert thermal energy emitted from the hydration reaction into an electrical signal (voltage) which can be recorded and displayed over time. The non-reacting control specimen is also situated atop a heat flow sensor. Should any external environmental factors cause a temperature change in the non-reacting specimen, the intensity of this output voltage through the heat flow sensor will be deducted from the reacting specimen, effectively negating external thermal effects.

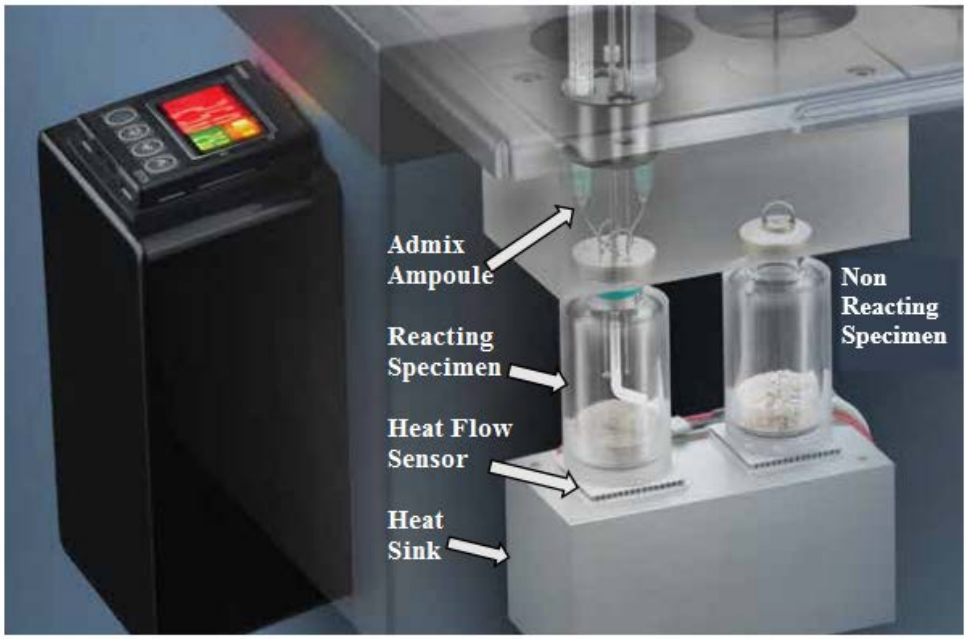

Figure 4-3. Isothermal calorimeter heat sink and thermal sensor arrangement.

4.3. Procedure

This method begins with a thermal mass balancing to ensure that each reacting specimen will have the same thermal mass as the corresponding non-reactive specimen. To do this, the summation of the products of material masses and specific heat capacities for the non-reactive side are determined, then the masses of the reacting specimens are adjusted such that the thermal mass of the reacting side exactly equals that of the non-reacting side using Equation (4-1).

$$\sum_{1}^{n}\left(m_1 \times C_{sp-1}\right) + \left(m_2 \times C_{sp-2}\right) + \cdots + \left(m_n \times C_{sp-n}\right) = \sum\left(m_{nr} \times C_{sp-nr}\right) \quad (4\text{-}1)$$

Where:
m_n = Mass of the n^{th} reacting material, g
$C_{sp\text{-}n}$ = Specific heat capacity of the n^{th} reacting material from ASTM C1702, J/g-K
m_{nr} = Mass of the non-reacting material, g
$C_{sp\text{-}nr}$ = Specific heat capacity of the non-reacting material, J/g-K

Once the mass balance has been done, the materials are dispensed into glass vials at the required mass measured to 0.01g precision. The required water is then measured in the syringes, a stirring stick is attached to the stirring bar, the vial is attached to the end of the admix ampoule, and the entire apparatus is inserted into the calorimeter to equilibrate.

Upon reaching thermal equilibrium, the calorimeter is set to record data, water is dispensed into the dry cementitious materials, and the paste is mixed. The specimen is then left to hydrate for a period of seven days. At the conclusion of the testing period, the calorimeter's data logging function is stopped and the data can be analyzed.

4.4. Procedural Modifications

For the reasons stated in the summary of the method and those reported by Ferraro, [78], researchers opted to utilize internal mixing for isothermal calorimetry. After a thorough review of the standard, several modifications to the standard were established in an effort to reduce variability between specimens. Figure 4-4 shows a flow chart of the ASTM C1702 standard method compared to the modified testing procedure performed for this research with modifications shown in red text.

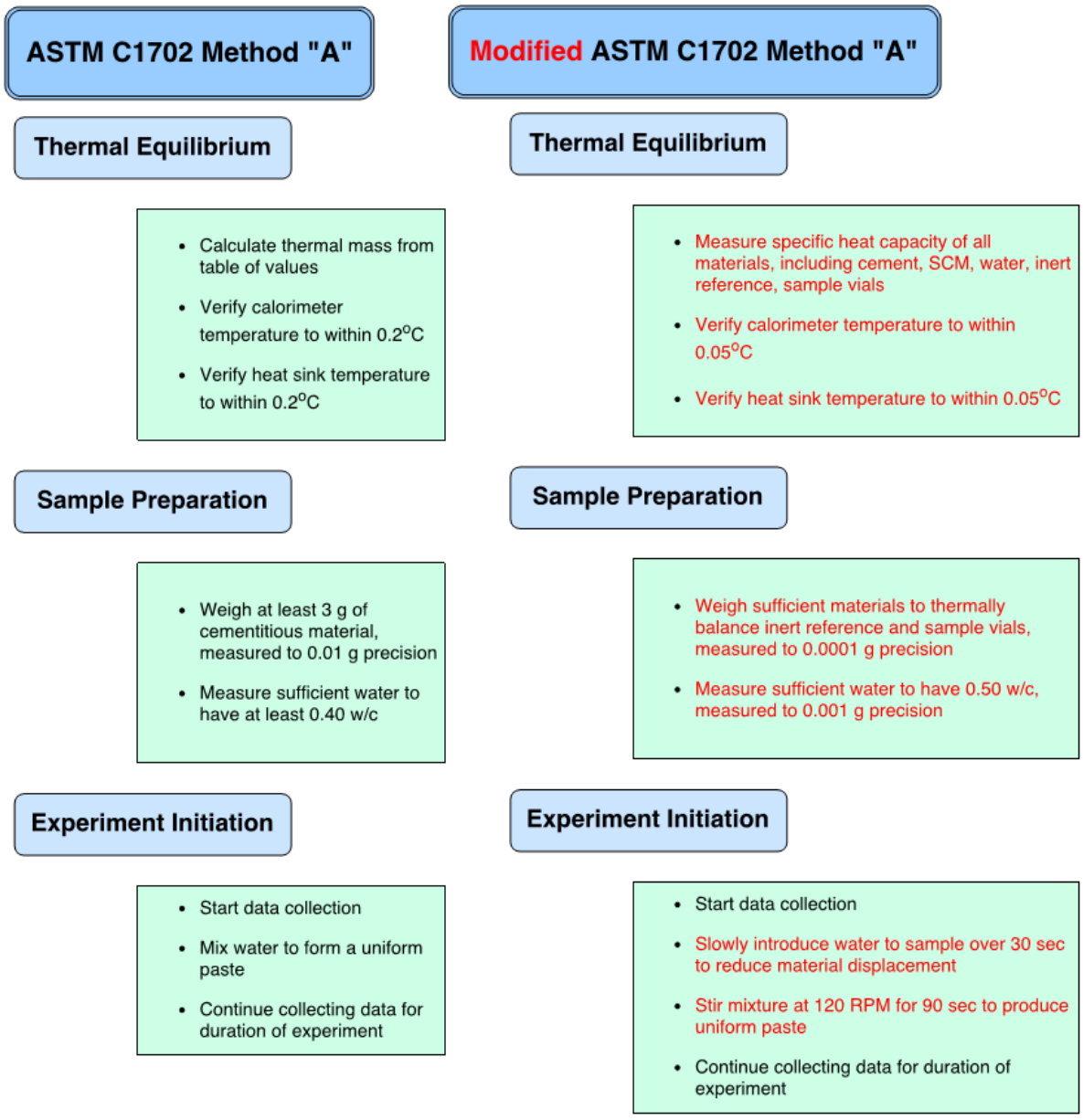

Figure 4-4. Comparison of ASTM C1702 and the Modified method.

The first modification to the method involved measuring the specific heat capacities of the materials of interest as per ASTM E1269 [215]. This was performed as the materials for this research are not addressed in the ASTM C1702 standard. Measuring the specific heat capacities

led to the discovery that the specific heat capacities given in the standard would produce errors because they differed from the measured values. Table 4-1 shows the specific heat capacities given in ASTM C1702 compared to measured values, as well as the relative error that would result from using standard values.

Table 4-1. Comparison of ASTM C1702 specific heat capacities compared to measured values.

Material	Specific heat capacity from ASTM C1702, J/g-K	Measured specific heat capacity, J/g-K	Difference from measured, %
Portland Cement	0.75	0.740	1.4%
Fly Ash	0.80	(Class F) 0.743	7.7%
		(Class C) 0.735	8.8%
Limestone	0.91	0.779	16.8%
Water	4.186	4.186	0.0%
Quartz	0.71	0.743	-4.4%
Slag	0.80	0.734	9.0%

The second modification of the method involved a more accurate temperature validation of the calorimeter and heat sink. The temperature of the calorimeter was verified to be $23^{o} \pm 0.05^{o}C$. This was done to ensure comparable environments between different specimens, as initial temperature conditions highly influence the hydration chemistry of cement. The required measuring precision of the dry materials was modified to 0.0001 g, as that was the precision of the analytical balance available. However, measuring the water to 0.0001 g was difficult as it had to be drawn into a syringe prior to measuring. Therefore, 0.001 g precision was deemed sufficient.

Glass sample vials were found to vary by more than 0.75 g, so the weights of each glass vial were included in the thermal mass balance calculations. The difference in vial volume was concentrated in the thickness of the bottom of the vials, which is the portion in contact with the calorimeter measuring equipment. This difference, when accounting for thermal mass, could represent nearly a 5% difference in total thermal mass difference between the inert reference and reacting specimen. Dispensing the mixing water over 30 seconds time was done to prevent water from aggressively displacing the powdered material, which prevented dry material from depositing on the sides of the vial where it would not be able to hydrate. Mixing of the specimens was done by hand for 90 seconds at about 120 rpm. There was no formal experiment to determine effects of mixing duration and rate; however, one specimen failed to mix properly (plastic stirrer detached) yet the total heat evolution and power curves appeared to be comparable to a replicate that was mixed properly.

The final modification to the method was an alteration to ASTM C1679 - *Measuring Hydration Kinetics of Hydraulic Cementitious Mixtures Using Isothermal Calorimetry*. This method determines the "time to equilibrium" of samples to attain a measured power spread of 0.20 mW/g for all samples [221]. For this evaluation, thermal equilibrium was determined when the following two conditions were met:

- The spread in measured power between all samples was less than 0.040 mW/g, and
- The difference in measured power for any one specimen over a 2-hour period was less than 0.010 mW/g

Following these method modifications, the cement used for this research was evaluated several times over the course of two years, using multiple operators on the same machine and an outside laboratory with another calorimeter and operator. The multi-user (6 users), single laboratory 7-day heat of hydration coefficient of variation was 0.38% compared to the standard 95% confidence interval precision of 6.1% (for one user). The multi-user (7 users), multi-laboratory (two laboratories) 7-day heat of hydration coefficient of variation was 1.1% compared to the standard 95% confidence interval precision of 21.1%. While this was not a round-robin style of evaluation, it does indicate an improvement of the method. A sensitivity analysis of these method modifications was not performed.

4.5. Isothermal Calorimetry Testing Results

All mixes during this evaluation were neat cement pastes (containing only cementitious material and water), without the use of chemical admixtures, at a water-to-cementitious material ratio of 0.50. The isothermal calorimetry results are presented in two fashions: the output voltage versus time, deemed the "power" curve, and the integrated power curve, which shows the cumulative power, known as the "heat generation" curve. From these charts, the relative rates of reactions and heat production can be viewed, on a replacement basis, for each material. Each graph has been normalized by mass of cementitious material. Due to the majority of reactions occurring in the first two days of hydration, the power curves only display the first 48 hours. Additionally, the first reaction is highly exothermic, but it is short lived, so the y-axis is scaled appropriately for the main hydration curve rather than the maximum heat release. The isothermal calorimetry curves for the various cementitious paste mixtures are presented in Appendix B.

The power curve for the 100% portland cement shows typical results; there was an initial heat spike caused by the exothermic wetting of materials, ettringite formation, and aluminate hydration. This initial spike was high in intensity (around 20-30 mW/g depending on mixture), but was short lived, lasting around 30 minutes. Following this is the induction/dormant period in which little exothermic reaction takes place. Following this lull marks an increase in exothermic reaction of calcium silicates and the formation of calcium hydroxide; this period typically results in the maximum heat production, which will be referred to as the "main peak". Subsequent to the main peak are typically one or two shoulders that correspond to lesser exothermic reactions; however, when adding SCMs that have different chemical compositions; these shoulders may be more pronounced than the main hydration peak.

The introduction of ECAT into the cementitious system prompted some introspection on reactivity versus particle size. The larger a particle is in the cementitious system, the less reactive (per unit mass) the particle will tend to be. This is due to the driving forces in hydration reactions being surface and dissolution chemistry; both of which are reduced on a mass basis with larger particles. It was intriguing that the equilibrium catalyst would provide a noticeable reaction; it was suspected that this material would act more as an inert filler due to having a mean particle size of around 75 microns compared to 6 microns for the cement. The reason for

the excess heat in the case of equilibrium is not due to a particle filler effect; but as this material is a catalyst; it has a very high surface area for reactions due to high internal porosity.

With the introduction of increasing amounts of class C fly ash, there was a reduction in the instantaneous heat produced (power), as well as a corresponding reduction in total heat. Also, increasing amounts of C ash not only reduced the power curve intensity, but began to retard the first "peak"; as this peak became less intense, the second peak became more pronounced, which is generally considered to correspond to sulfate phase reactions [2], [70]. Interestingly, with higher additions of class C fly ash, the power reduction from the main hydration stage began to get steeper. This indicates that the exothermic hydration reactants were being exhausted more quickly with the addition of class C fly ash; this can be seen in the heat generation curve, which shows more disparity between the 30% and 40% class C fly ash replacements than the 0%, 10%, and 20% fly ash replacements. This may indicate that there is a threshold level of replacement, above which the class C fly ash addition is more detrimental than beneficial.

The addition of sugarcane bagasse ash showed a drastic reduction in power with cement replacements as small as 5%. This is surprising; typically, a small addition will not have such a marked change on the power curve. SCBA addition also produced the highest power reduction of any material at 20% replacement. The power curve was extended, indicating a less intense but longer lasting exothermic hydration. Consequently, the reduction in cumulative heat generation was not as substantial as one would expect based upon the power reduction. This indicates a potentially beneficial use in hot-weather or mass concrete applications assuming mechanical properties are adequate.

The isothermal curves for ground blast furnace slag show that there was a reduction in power and heat generation. There was also a reduction in the magnitude of the main peak, which decreased more quickly than the first shoulder as the slag replacement percentage increased beyond 20%. Even though the peak power decreased for the slag replacements, by approximately 36 hours, the power measured from the control mixture was lower than that of the slag mixes. The slag continued to produce more power than the control between 1.5 and 5 days of hydration, indicating delayed hydration. This was likely due to the highly insoluble outer layer of slag particles causing hydration to be reduced until sufficient alkalinity was reached to dissolve the other particle layers.

Rice husk ash additions not only presented a reduction in power produced, but also showed a retarding hydration effect with 20% additions, causing a time shift in the peak power of nearly 10 hours. Furthermore, the first shoulder of the power curves was extended; this kept the power production higher than the control for over 24 hours. This indicated a potential for rice husk ash to cause retardation of the setting of mortars or concrete. The reduction in power from one addition of rice husk to another was nearly linear. Lastly, it was noted that the 15% and 20% additions of rice husk ash were very difficult to mix; this was confirmed later during the mortar evaluation, and further rice husk ash mixes were limited to 10% maximum replacement.

The results of the wood ash isothermal calorimetry showed a material that drastically reduced the exothermic heat produced. Additionally, on the heat generation plot, it was evident that the rate of heat production at the end of the test was much higher for the 100% portland cement than for the wood ash mixes. This indicated that the portland cement was still reacting, whereas the

wood ash amended pastes reacted much less vigorously. The 25% addition caused the peak power to be retarded compared to the control, whereas for the 50% addition had the peak power production approximately at the same time as the control. The first power peak was barely visible, but it did appear approximately at the same time as the 50% mixture, but it was overtaken by the shoulder of the power curve. This shoulder was missing from the 50% mix; this could be explained by alternate hydration reactions consuming reactants that would otherwise produce heat, or there may have been an alternate reaction that ceased hydration.

The addition of CS200 ground glass showed a consistent reduction in power as the replacement was increased. There was an extended shoulder on the higher replacements of glass powders, yet the drop off of power happened more subtly, indicating a potential limiting threshold similar to class C fly ash. This discrepancy was evident in the rate of heat generation at the end of the evaluation, between 20% glass and 30% glass content. This further indicated a threshold value of glass content likely occurred between 20% and 30%. As a means of comparing the mixes, a summary table of time-to-peak power, peak power, 7-day heat generation, normalized peak power, and normalized heat generation for each mixture is provided in Table 4-2.

.

Table 4-2. Isothermal peak power and heat generation data summary.

Material	Time to Peak Power, hr	Peak Power, mW/g	7 Day Heat Generation, J/g	Normalized Power, %	Normalized Heat, %
100% OPC	10.3	3.734	346.2	100%	100%
ECAT					
10%	10	3.300	317.5	88%	92%
20%	9.6	2.877	287.9	77%	83%
Class C fly ash					
10%	13.2	3.384	333.0	91%	96%
20%	13.4	3.247	326.9	87%	94%
30%	15.4	3.054	298.5	82%	86%
40%	14.8	2.867	272.1	77%	79%
50%	14.2	2.235	237.2	60%	69%
Class F fly ash					
5%	9.8	3.582	335.6	96%	97%
20%	10.3	3.031	289.8	81%	84%
35%	10.8	2.484	240.6	67%	69%
50%	10.5	1.906	192.4	51%	56%
SCBA					
5%	11.6	3.212	331.1	86%	96%
10%	12.5	2.903	320.1	78%	92%
15%	14.0	2.522	298.1	68%	86%
20%	13.9	2.187	277.3	59%	80%
Slag					
5%	10.2	3.574	342.4	96%	99%
20%	9.9	3.054	323.3	82%	93%
35%	12.8	2.678	295.4	72%	85%
50%	14.4	2.381	272.4	64%	79%
RHA					
5%	12.4	3.446	337.2	92%	97%
10%	14.1	3.188	325.8	85%	94%
15%	16.5	2.873	316.9	77%	92%
20%	18.3	2.425	300.5	65%	87%
Wood Ash					
5%	11.4	3.762	345.2	101%	100%
20%	13.2	3.485	308.7	93%	89%
35%	11.6	2.774	256.2	74%	74%
50%	10.9	1.977	189.8	53%	55%
CS200 Glass					
5%	10	3.560	332.2	95%	96%
10%	9.7	3.390	318.2	91%	92%
20%	10.9	2.697	275.1	72%	79%
30%	12	2.072	213.2	55%	62%
Ground Glass					
5%	10.3	3.608	335.3	97%	97%
20%	10.4	3.077	292.6	82%	85%

Table 4-2. Continued

Material	Time to Peak Power, hr	Peak Power, mW/g	7 Day Heat Generation, J/g	Normalized Power, %	Normalized Heat, %
Metakaolin					
5%	8.9	3.7780	358.0	102%	103%
10%	7.7	3.6159	350.6	97%	101%
Silica Fume					
5%	11.4	3.5458	339.0	95%	98%
10%	10.8	3.3481	329.8	90%	95%

5. CEMENTITIOUS MORTAR TESTING

5.1. Mortar Mix Selection

Prior to evaluating SCM performance in concrete, mortar tests were performed to determine threshold replacement values where performance was limited based on portland cement addition rates. As mortar mixes and specimens were much smaller than concrete, more test mixes could be analyzed prior to doing full-scale concrete evaluations. The addition rates of the various SCMs were determined from the available literature presented in Chapter 2. Following binary blends, a series of ternary-blended mixes were designed to maximize the inclusion of class C fly ash while utilizing a smaller portion of another SCM to determine if ternary-blended class C fly ash mixes would perform adequately in durability mixes. Class C fly ash was chosen as the main ternary-blended material as it presents the most likely candidate for replacement for class F fly ash; the particle sizes and shapes are comparable, and the only underlying issue is the chemical composition. A table of binary mortar mixes are presented in Table 5-1; it should be noted that the proportions for each mortar varied with the testing method. The ternary mixes included 20 - 40% class C fly ash with 4 - 20% other SCMs.

Table 5-1. Binary mortar mixes by replacement material.

Material	Approximate Binary Replacement Level
Class C fly ash	10-50% (20% increments)
Class F fly ash	20-40% (20% increments)
Blast Furnace Slag	10-50% (20% increments)
Rice husk ash	5-10% (5% increments)
Sugarcane bagasse ash	10-30% (10% increments)
Ground glass (all varieties)	5-20% (5% increments)
Waste wood ash	25-50% (25% increments)
Metakaolin	5-10% (5% increments)
Silica Fume	4-8% (4% increments)

5.2. Evaluation of Structural Adequacy

5.2.1. Compressive Strength of Mortar

The compressive strength of mortar test was used herein as a means to qualify which cementitious blends of alternative supplementary cementitious materials had a net positive, comparable, or negative affect on the cementitious system with regard to structural and mechanical properties. The compressive strength of concrete is the most widely used quality assurance test used in industry to determine conformance to building construction documents. This method is similar but removes the variability of coarse aggregate. Although; the compressive strengths of mortars and concretes will differ from each other, this method is not being used as quality control but rather a litmus test for the alternative materials.

Summary of Test Method

The compressive strength of mortar is determined by following the steps outlined in ASTM C109 - *Standard Test Method for Compressive Strength of Hydraulic Cement Mortars (Using 2-*

in. or [50-mm] Cube Specimens) [7]. This method involves creating cubical mortar specimens of nominal 2 inches, which are then tested to ultimate failure at various testing ages. This test method can be used to qualify materials such as in the coal fly ash specification [135] or to quantify the activity index for a slag as per ASTM C989 [126].

Equipment

The test method requires a suite of equipment used for mixing mortar; this equipment was used for each of the mortar assessments. The method requires a variable speed mixer with specific beater, non-absorptive molds for casting specimens that are 2 inches or 50 mm, a tamping device, trowel, calipers, and a compression frame. Additionally, a scale for measuring out materials, storage containers, and temperature-controlled rooms were used for this method.

Procedure

The test method requires the design of a mortar mixture with appropriate proportions for the desired structural performance. Per ASTM C109, the prescribed mixture proportions have a ratio of 2.75:1.0:0.485 for the sand, cementitious material, and water, respectively [7]. This was modified slightly to have a 0.5 water/cementitious ratio to be consistent with the isothermal calorimetry testing and the length change testing. The material was then placed into the mixing bowl, and mixed in general accordance with ASTM C305, with the exception that the mixing procedure used for all mortars, consisted of mixing half of the sand with the cementitious materials on high for 30 seconds (with an enclosure on the mixer to prevent material loss) [222]. Then the water was added over a period of 30 seconds (with the mixer on low). Following the addition of the water, the remaining sand was dispensed into the bowl and the mixer continued for a total of 3 minutes. The mixer was then turned off for a 2-minute resting period, during which time the bottom of the bowl was quickly scraped to dislodge any materials that were not mixing. Following this, the mixer was turned on again for 3 minutes. The method was modified because the introduction of sand per the method resulted in a stall/malfunction of the mixer.

The fresh mortar was then placed into 2-inch cube molds in two lifts; after each lift, a series of 32 tamping motions was performed as per ASTM C109 to remove entrapped air. The specimens were then troweled flat, and stored in a temperature- and humidity-controlled room for 24 hours. The specimens were then removed from the molds and placed into containers with saturated lime water. Each group of specimens was stored in separate containers to avoid leaching of materials from one mix and affecting another mix. The containers chosen for this were plastic 6” x 12” cylindrical concrete molds which allowed for storage of up to 24 specimens per container. The specimens were stored in limewater until the time of testing (with the exception of the 1-day test, which occurred immediately after removal from the molds).

Prior to testing the specimens in the compression machine, the sides of each specimen to be tested were measured to the nearest 0.001” and recorded. These values were used to calculate the area over which the load was applied. The specimens were then loaded into a compression frame, which was programmed to test the specimens at a load rate of 75 psi/sec until the ultimate load dropped by 50%, thus, indicating failure. The ultimate load, along with the specimen dimensions, was then used in Equation (5-1) to calculate the ultimate compressive stress; this value was then averaged over three specimens for each testing age. The testing ages were 1, 3, 7, 14, 28, and 56 days.

$$fm = \frac{P}{LW} \quad (5\text{-}1)$$

Where:

fm = Compressive strength, psi
P = Total maximum load, lbf
L = Length of face of specimen to be loaded, in
W = Width of face of specimen to be loaded, in

Compressive Strength of Mortars Results and Discussion

The compressive strength of the various mortars are presented in Appendix C.1, and a summary table of compressive strength values is presented in Table 5-2. Based upon the literature review, it was expected that the slag (at high replacements), silica fume, and metakaolin would outperform the control with respect to compressive strength; the results presented herein show the expected behavior. The addition of class F fly ash was expected to produce lower compressive strength than controls, with higher addition rates causing even lower strengths. This behavior was observed during the investigation. Typically, class F fly ash mixes gain strength at later ages due to the pozzolanic reactivity; however, the addition of 40% class F fly ash appeared to be excessive and detrimental to the performance of the mortar with respect to compressive strength.

Table 5-2. Summary of compressive strengths of mortars.

Mix Design	Testing Age, psi					
	1	3	7	14	28	56
Control						
	2898	4907	6137	7119	7105	8272
Class C Fly Ash						
10%	2127	3298	4105	5039	5775	6208
20%	1618	3688	4597	4932	5597	6766
30%	1160	2991	4193	4738	4969	5812
50%	953	2462	3705	4761	4915	6170
Class F Fly Ash						
20%	2128	3894	4223	5765	6465	7527
40%	1169	2272	2910	3609	4725	5585
Rice husk Ash						
5%	3071	5517	6799	7825	6520	8373
10%	2501	5332	6386	8072	8518	9566
Sugarcane Bagasse Ash						
10%	2260	4384	5343	6167	7554	6817
20%	2281	4681	6484	8118	6800	8898
VCAS160 Glass						
20%	2227	4109	5218	5395	7949	8718
CS200 Glass						
20%	1846	4190	5245	5938	7685	8341
Ground Glass						
10%	2303	4644	5871	6485	7429	8402
20%	2038	3971	4797	6241	6809	8874
Ground Blast Furnace Slag						
10%	2453	4003	5271	6305	6330	7394
30%	1502	3144	4211	5276	6763	8463
50%	1213	2759	4171	5351	6905	9665
Equilibrium Catalyst						
10%	2417	4299	5344	5815	7064	7698
20%	2046	3807	4530	5951	6238	7821
Wood Ash						
25%	2702	4047	4534	5134	5125	6271
50%	1709	2487	2595	2898	3556	3613
Silica Fume						
4%	3998	7374	9100	10830	12265	12006
8%	2767	5627	8393	10031	9313	9612

Table 5-2. Continued.

Mix Design	Testing Age, psi					
	1	3	7	14	28	56
Metakaolin						
5%	2964	5547	7926	9212	10378	9157
10%	3094	5939	7638	9904	10851	8953
20% Class C Fly Ash and						
5% RHA	1734	4047	5166	5088	6374	7780
5% Slag	1865	3710	5231	6206	7661	8567
10% Slag	1879	4056	6402	7982	9526	10512
5% Class F Fly Ash	1805	3305	4506	5808	6810	7783
10% Class F Fly Ash	2503	3640	5158	7023	6560	8971
10% CS200 Glass	2020	4433	5278	6365	8866	9515
10% Ground Glass	1654	3625	5017	6579	7432	8665
5% Sugarcane Bagasse Ash	1727	4196	4655	5879	7165	8692
10% Sugarcane Bagasse Ash	1880	4289	6329	6080	7907	9684
5% Micron[3]	1968	4266	5341	6984	8030	9400
10% Micron[3]	1852	4781	6471	7940	9794	8653
4% Silica Fume	2138	4954	6713	8613	9635	10460
5% Metakaolin	1769	3997	6533	8728	6650	8849
30% Class C Fly Ash and						
5% Metakaolin	1276	4292	6211	6751	7887	7468
10% Metakaolin	1150	3580	5197	7424	8399	8016
20% Ground Glass	1089	2384	3078	3783	4319	5465
10% Slag	1488	2516	4001	4522	5198	7490
5% Class F Fly Ash	1156	3683	5726	6471	8679	8614
10% Class F Fly Ash	1438	3414	4903	6751	7055	8230
5% Sugarcane Bagasse Ash	1548	3540	5118	5669	6439	8904
4% Silica Fume	1198	4137	5374	7531	8283	7112
8% Silica Fume	1643	3472	4731	5247	6603	8318
40% Class C Fly Ash and						
10% Rice Husk Ash	811	2381	2987	3361	3995	6020
5% Class F Fly Ash	969	2753	4786	5618	5722	7808
4% Silica Fume	900	3092	4358	4962	5763	8136
8% Silica Fume	1267	2415	3109	3680	5006	6329
10% Ground Blast Furnace Slag	688	2669	3687	4685	6119	7004
20% Ground Blast Furnace Slag	2281	4681	6484	8118	6800	8898
5% Metakaolin	751	2887	4289	5082	6370	6329
10% Metakaolin	709	2307	3856	4999	5628	6675
50% Class C Fly Ash and						
10% Ground Blast Furnace Slag	339	1690	2768	3688	5102	6208
20% Ground Blast Furnace Slag	173	1063	2176	3049	4442	6248

The binary class C ash mixtures show that the mixes were not comparable to the control mix in a binary system. When replacing cement with either 5% - 10% rice husk ash or 20% sugarcane bagasse ash, the mixes outperformed the control mixture at any age past three days. Glass replacements at a level of 20% showed comparable performance to the control past 28 days, indicating pozzolanic activity. The equilibrium catalyst performed comparably to the control at 20% replacements, but was inferior to the control at 10% replacement. Wood ash seemed to provide a detrimental effect on the compressive strength of mortars at high replacement levels; the wood ash at 25% replacement was only comparable to control at 1 day.

All of the ternary mortars utilized at least 24% replacement of cement and contained up to 70% of alternative SCM. At a replacement of 30% or less, all of the mixes were comparable or better performing than the control mix at 56 days; the mix with the lowest compressive strength in this group was 20% class C fly ash and 5% class F fly ash. The best performers were 20% C ash with either 4% silica fume, or 10% slag at 126% and 127% of the control, respectively. The average normalized compressive strength was 109% of the control.

Ternary mixes that utilized 30% class C fly ash showed overall lower compressive strength than the previous group, with an average normalized strength of 94%. The lowest compressive strength was found for the 30% class C fly ash with 20% ground glass (66% normalized strength). If this mix is ignored, the average normalized strength of the group was 97%; with the second lowest performing mix being 30% C ash and 5% F ash. The highest performing mix included 30% C ash and 10% sugarcane ash at 108% of the control strength. This was due to the high surface area and amorphous silica content. A material with similar properties, silica fume, was the second highest performing mix in this group at 104% of the control strength.

Of the ternary mixes that utilized 40% or more class C fly ash, only the 4% silica fume, 5% class F fly ash, and 20% slag mixes were comparable or superior to the control at 56 days. These 40% C fly ash mixes show a potential for replacement at a relatively high level with minimal amounts of well-established SCMs in order to make the mixes perform adequately with regards to compressive strength.

5.2.2. Direct Tensile Strength of Mortar

Tensile strength of concrete is typically determined indirectly under splitting compression forces [1], [223]. However, with mortar, specimens can be tested under direct axial tension by casting "dog bone"-shaped specimens known as briquettes. In order to determine if there was a detrimental effect on tensile strength with the addition of the various alternative cementitious materials, the tensile strength test was performed on the mortar briquettes.

Summary of Test Method

This test method follows ASTM C307 - *Standard Test Method for Tensile Strength of Chemical-Resistant Mortar, Grouts, and Monolithic Surfacings* [9]. The evaluation involved casting mortar specimens and storing the specimens in saturated limewater held at 23^{o}C until the time of testing, at ages 7, 28, and 56 days, respectively. The test involves the placement of specimens into a universal testing machine, and loaded axially until the specimen ruptures. The cross-sectional area of the ruptured specimen is then measured to determine ultimate tensile stress. Two replicate specimens were tested in the same fashion and the tensile stresses of each specimen were averaged to determine the tensile strength at the given testing age.

Equipment

The only equipment used for this evaluation that differed from the mortar cube equipment was brass tensile briquette molds, a universal testing machine capable of loading a specimen under axial tension, and a set of specimen grips to hold the specimen as shown in Figure 5-1.

Figure 5-1. Tensile briquette in grips during testing [224].

Procedure

The mortar used for this evaluation was obtained from the same batch as the mortar cubes used for compression. The mortar was placed in two approximately equal layers into each mold and tamped with a rubber tamper to remove entrapped air. After 24 hours of curing in a temperature -controlled room, the specimens were removed from the molds and stored in the same containers as the mortar cubes until the testing. The specimens were placed into the tensile grips and loaded by moving the crosshead of the machine at a constant rate of 0.25 inches/min as per the standard. When the samples ruptured, the ruptured face was measured to determine the cross-sectional area of the failure plane. The ultimate load on the testing machine was divided by the cross-sectional area of the sample to determine the tensile stress at failure.

Direct Tensile Strength of Mortar Results and Discussion

The tensile strength charts are displayed in Appendix C.2 with a summary table of values and normalized values presented in Table 5-3. With the exception of seven mixes, all of the tensile strength results at 56 days were at least 90% of the control tensile strength, with the worst performing mix being 40% class C fly ash and 8% silica fume at 76% of normalized strength. This evaluation showed no clear indication that any of the additions resulted in significantly lower strengths than the control. Additionally, the large variation in strengths of individual specimens lead the researchers to conclude that this test method did not provide sufficient evidence to exclude a particular mix based upon tensile strength performance alone. These results in combination with compressive strength performance were used to remove mixes from consideration.

Table 5-3. Summary table of tensile and normalized tensile strength of mortars.

Mix Design	Testing Age	Tensile Strength, psi 7	28	56	Normalized, % 7	28	56
Control							
		537	574	515	100	100	100
Class C Fly Ash							
10%		442	517	462	82	90	90
20%		536	507	589	100	88	114
30%		398	415	439	74	72	85
50%		399	458	431	74	80	84
Class F Fly Ash							
20%		401	562	475	75	98	92
40%		273	412	427	51	72	83
Rice husk Ash							
5%		502	482	599	93	84	116
10%		435	546	597	81	95	116
Sugarcane Bagasse Ash							
10%		443	485	553	82	84	107
20%		502	617	617	93	107	120
VCAS160 Glass							
20%		394	549	477	73	96	93
CS200 Glass							
20%		401	498	509	75	87	99
Ground Glass							
10%		420	488	574	78	85	111
20%		396	505	567	74	88	110
Ground Blast Furnace Slag							
10%		495	512	598	92	89	116
30%		436	544	632	81	95	123
50%		353	448	529	66	78	103
Equilibrium Catalyst							
10%		528	515	587	98	90	114
20%		457	442	504	85	77	98
Wood Ash							
25%		447	476	515	83	83	100
50%		304	397	397	57	69	77
Silica Fume							
4%		603	729	741	112	127	144
8%		481	669	663	90	117	129

Table 5-3. Continued.

Mix Design	Testing Age, psi					
	1	3	7	14	28	56
Metakaolin						
5%	528	502	580	98	87	113
10%	589	670	660	110	117	128
20% Class C Fly Ash and						
5% RHA	374	464	482	70	81	94
5% Slag	429	541	507	80	94	98
10% Slag	368	600	622	69	105	121
5% Class F Fly Ash	462	521	539	86	91	105
10% Class F Fly Ash	436	604	539	81	105	105
10% CS200 Glass	440	551	480	82	96	93
10% Ground Glass	472	512	635	88	89	123
5% Sugarcane Bagasse Ash	411	451	483	77	79	94
10% Sugarcane Bagasse Ash	448	577	556	83	101	108
5% Micron[3]	420	528	496	78	92	96
10% Micron[3]	462	568	663	86	99	129
4% Silica Fume	445	534	483	83	93	94
5% Metakaolin	520	636	575	97	111	112
30% Class C Fly Ash and						
5% Metakaolin	429	454	634	80	79	123
10% Metakaolin	429	461	523	80	80	102
20% Ground Glass	314	484	583	58	84	113
10% Slag	395	426	502	74	74	97
5% Class F Fly Ash	442	557	622	82	97	121
10% Class F Fly Ash	427	449	575	80	78	112
5% Sugarcane Bagasse Ash	441	497	546	82	87	106
4% Silica Fume	424	505	581	79	88	113
8% Silica Fume	455	432	507	85	75	98
40% Class C Fly Ash and						
10% Rice Husk Ash	374	391	409	70	68	79
5% Class F Fly Ash	400	462	529	74	80	103
4% Silica Fume	384	442	466	72	77	90
8% Silica Fume	286	313	390	53	55	76
10% Ground Blast Furnace Slag	358	495	507	67	86	98
20% Ground Blast Furnace Slag	230	470	487	43	82	95
5% Metakaolin	385	455	476	72	79	92
10% Metakaolin	367	441	608	68	77	118
50% Class C Fly Ash and						
10% Ground Blast Furnace Slag	196	345	430	36	60	83
20% Ground Blast Furnace Slag	184	328	461	34	57	90

5.2.3. Activation Energy and Maturity of Mortars

The concept of activation energy and maturity of cementitious mixtures is that the chemical reactions that occur require a specific energy input into the system prior to strength gain. The energy input can be in the form of chemical energy (from hydration reactions), thermal energy or mechanical energy. Changing the thermal energy (in the form of environmental effects) will result in varying strength gains of concrete at different temperatures. The development of strength with regards to temperature is known as maturity. Therefore, it is accepted that by creating specimens to be tested at varying temperatures, a strength-maturity relationship is developed to predict strength based on temperature history during curing.

Beyond determining an activation energy or maturity index for a particular mix, this testing regimen gives insight into mortar mixtures (and presumably concrete mixtures) that perform less than adequately either at high (38^{o}C) temperatures, or at low (8^{o}C) temperatures. This evaluation is very valuable for the state of Florida as the temperatures throughout the state annually can fluctuate outside of the testing range.

Previous research has gone into determining the best methods to evaluate the relationship between strength gain, time, and temperature of concretes; this research has resulted in several equations and methods. One of the adopted methods in ASTM C1074 is the Nurse-Saul approach in which a datum temperature is determined (below which, chemical reactions are assumed to cease) and a temperature-time versus strength curve is developed. A temperature-time factor is determined by finding the cumulative area under a time-temperature history curve of the curing (where the temperature is the difference in temperature from the datum temperature). In this manner, concretes with the same temperature-time factor (or maturity index) are assumed to have comparable strength; this temperature-time history curve can be seen in Figure 5-2.

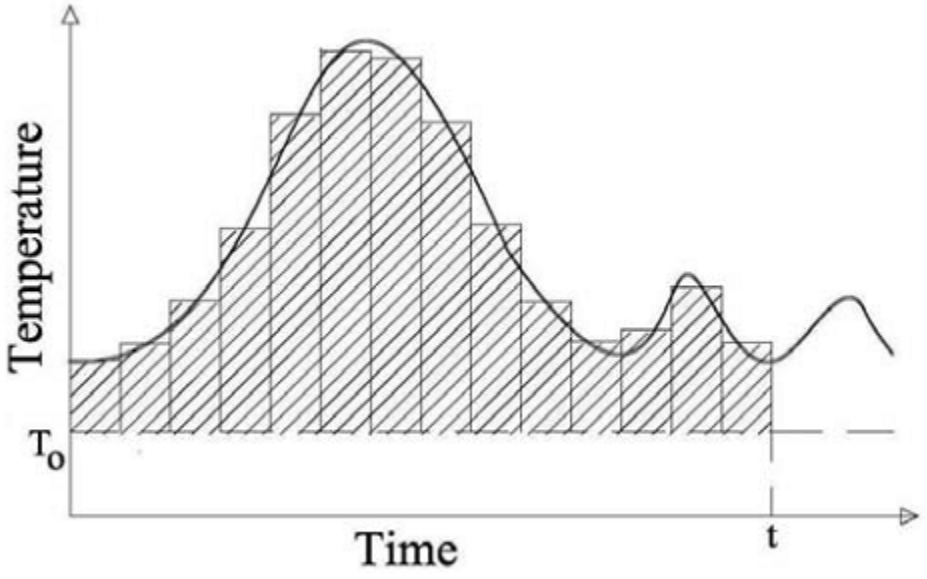

Figure 5-2. Nurse-Saul maturity function [225].

The other ASTM C1074 accepted method for determining the strength gain relationship with temperature variation is the equivalent age concept. This method involves determining the apparent activation energy from the negative slope of a linear best-fit line through the natural log of the rate constant versus the inverse of temperature for the three experimental temperatures. The rate constant for strength development of a particular concrete mixture is "the initial slope of the relative strength –versus-age curve at constant temperature curing" [226]. Along with the rate constant, k, the datum time, t_0, (time when strength is assumed to begin) and limiting strength, S_u, (maximum strength assuming infinite curing time) are varied a curve-fitting equation (5-3)to fit the measured values. With the apparent activation energy, the "Arrhenius equation" is used to determine the equivalent age of concretes or mortars cured at different temperatures and ages.

Summary of Test Method

This method employs two different test methods to accomplish the task of predicting concrete strength. The first method, known as the "maturity method", computes a "temperature-time" factor, which is the area under a time-temperature curve compiled during curing using Equation (5-2) from *ASTM C1074 - Standard Practice for Estimating Concrete Strength by the Maturity Method* [8].

$$M(t) = \sum (T_a - T_0)\Delta t \tag{5-2}$$

Where

M(t) = the time temperature factor at *t*, °C-days or °C-hours
Δt = time interval, days or hours
T_a = average concrete temperature during time interval *t*, °C
T_0 = datum temperature, °C

Specimens are tested at various temperature-time factors to create a relationship between strength and temperature-time factor. When field concrete is placed, maturity monitors are used to record the temperature-time factor so that in-place strength can be estimated from the curve. The alternate method, which was the method chosen for this investigation, involves casting specimens at three temperatures, and testing the specimens at different ages. The strengths for each temperature are determined and plotted using the maturity function described in Equation (5-3). In this method, S_u, t_0, and k are varied to find the best fit for the equation to the test data.

$$S = S_u \frac{k(t - t_0)}{1 + k(t - t_0)} \tag{5-3}$$

Where

S = average mortar cube compressive strength at age *t*, MPa or psi
t = test age, days or hours
S_u = limiting strength, MPa or psi
t_0 = age when strength development is assumed to begin, hours or days
k = the rate constant

Following this, the negative slope of the linear best-fit of ln(k) versus 1/T gives the Q value. This Q value is then multiplied by the universal gas constant (8.314 J/mol) to obtain the apparent activation energy. This activation energy is used in the Arrhenius equation, which is modified in ASTM C1074 as shown as Equation (5-4).

$$t_e = \sum_{0}^{t} e^{-Q\left(\frac{1}{273+T_a}-\frac{1}{273+T_s}\right)} \Delta t \quad (5\text{-}4)$$

Where

t_e = equivalent age at a specified temperature, T_s, days or hours
Q = activation energy divided by the universal gas constant
T_a = average temperature of the concrete during time interval Δt, ^oC
T_s = specified temperature, typically 23^{o}C/298K

Equipment

In addition to the standard equipment used for making mortar cubes, water baths at differing temperatures were used to store the specimens. Typically mixes are all stored in the same limewater container (such as a 150 gallon tank of limewater); however, due to the varied chemistry of the different mixes, each mix was stored in a separate container (1.5 gallon).

Procedure

The mixing and proportioning of the materials for this method was the same as for the mortar cube method. The only difference was that the mixes which were to be stored at either 8^{o}C or 38^{o}C would have the mixing water and dry ingredients brought to those respective temperatures prior to mixing. The brass molds were also stored at temperature, prior to mixing, for 24 hours. Additionally, the mixing bowl and beater were brought to the correct temperature prior to mixing.

After mixing, the molds were moved into the controlled environments to cure. The 23^{o}C molds were moved to a standard curing room to cure for 24 hours prior to demolding. The 38^{o}C molds were placed on a shelf inside the hot water bath for approximately 12 hours before demolding. The 8^{o}C molds with moist coverings were placed into a refrigerator for approximately 48 hours before demolding.

The room temperature mixes were broken on a standard schedule of 1, 3, 7, 14, 28, and 56 days. The hot mixes were broken at approximately one half of the standard times, and the cold were broken at approximately twice the standard times. The data was then compiled and each set of temperature data was fitted to Equation (5-3), using Matlab software, while constraining the t_0 and k to positive values. Based upon these values, additional calculations were carried out according to ASTM C1074, and activation energies were determined for each mixture.

Shortcomings of the Method

This method has many shortcomings due to the complexity of attempting to predict strength at a given temperature from curing history. The first shortcoming of this method is due to the curing method prescribed, which specifies that cube specimens in the molds must immediately be

submerged into water baths. This method not only changes the water-to-cementitious material ratio of the plastic mix, but does not accurately describe the curing conditions in the field. It is known that the availability of water during curing will affect the strength of concretes and mortars [227], [228].

During data analysis, it became apparent that using the curve fitting method on non-traditional SCMs would lead to the best fit occurring when t_0 was less than 0. As t_0 is the time when strength is assumed to begin, this value cannot be before the cementitious mixture was mixed; therefore, this value needs to be constrained to positive values. This can be avoided by two methods: firstly, as denoted in the specification, time of set can be run at all three temperatures. While this is possible for a small number of mixes, this was not feasible when attempting 60 maturity mixes. A secondary method is to use the time of set values of the ambient cured mix and use a multiplier for the cold and hot mixes. This method was not utilized, as there is no standard method to determine what these multipliers might be.

A further issue exists for the curve fitting equations [225]. These methods have principally been used to model the strength-time relationship of concretes containing portland cement only, or portland cement and fly ash. When attempting to add other materials, such as slag, or metakaolin, the curve fitting functions break down; this was seen by Ferraro [78]. Slag mortar mixes, in particular, seem to react opposite of what is expected from portland cement or portland cement and fly ash mixes. Tank [229] has shown that a 50% slag mortar at 0.45 w/cm will produce higher ultimate strengths for hot mixes than the room temperature or cold mortars. This was seen by Ferraro [78] as well; typical portland cement mixtures will show hot mixtures having a higher *rate of strength gain* but will have reduced ultimate strength. Additionally, a mix with a specific temperature-time factor can have strengths that are higher or lower than those obtained at ambient conditions, dependent on the material that it is amended with. For instance, a 25% wood ash or 30% class C fly ash mix, at 23^{o}C will have strengths of approximately 5,400 psi at 28 days. However, at an elevated temperature (and therefore higher temperature-time factors), the strengths are 5,200 psi and 8,600 psi, respectively at 26 days; this amounts to 4% lower or 160% higher than ambient strength with higher temperature-time factors. This means that the prediction of strength cannot be done simply based upon temperature-time factors alone; it is also dependent on the material being used. When a mix performs worse at high temperatures than at ambient conditions, the use of a temperature-time factor will produce non-conservative, underestimations of strength.

Some of the mixtures do not have the same strength profile that a standard portland cement mixture has; typically, a portland cement strength gain profile begins with a large early-age strength gain, followed by plateauing strength gain. However, some of the alternative SCM mixes have a high pozzolanic activity and cause the plateauing phase to increase nearly linearly; albeit at a lower rate. Additionally, some mixtures show a tendency to reach a maximum strength, and further curing results in reduced compressive strength. This tendency to have reduced later-age strength is seen most readily in the metakaolin mixes. It is obvious that the metakaolin mixes behave differently, but a particular mechanism that reduces the later-age strength, presumably by altering the microstructure, is not apparent. However, metakaolin has the second highest alumina content of any of the materials investigated (44%). Yet the highest alumina-bearing material, the equilibrium catalyst (53%), does not exhibit this behavior. If the alumina content is a factor, the fact that the equilibrium catalyst did not exhibit the strength

reduction at later ages could be attributed to the occurrence of the detrimental reactions within the high-surface-area pore structure within the catalyst.

These anomalies in typical strength profiles cause the curve fitting equations to produce erroneous variable values, with either ultimate strengths being lower than the highest strength seen during investigation, or t_0 being below 0. This can be ameliorated by 1) reducing the number of specimen testing ages and 2) beginning the testing regimen earlier, with a smaller curing range. Alternatively, different curve fitting functions could be developed to more accurately describe these materials.

Activation Energy and Equivalent-Age Results

The results of this investigation are presented in Appendix C.3. For each mix, the strength-age data for each temperature is presented in a table along with the variables, activation energy, and equivalent ages for each temperature. Additionally, two figures show the strength data for each temperature as a function of time, and the strength data as a function of computed equivalent age. Convergent strength curves indicate a better correlation with the activation energy method. Mixes where the equivalent-age curves were divergent indicate that the method did not appropriately describe the behavior with temperature.

For the majority of the mixes, the equivalent-age method produced graphs in which the three temperature mixes overlaid on top of each other. This indicates that a good correlation existed between temperature and strength for those mixes. This was not the case for binary metakaolin mixes; this method produced divergent results for this particular mixture. Additionally, low doses of RHA and SCBA (5% and 10%, respectively) produced desirable results, but higher addition rates did not. Slag, when added at replacement levels of 30% and below, showed good correlation to temperature. The ternary blended mixture of 30% class C fly ash and 20% ground glass produced a negative value for the activation energy. Not only was this result unexpected, it does not make physical sense; this is due to the decreasing values of k as temperature increases. The rate constant, k, is the "initial slope of the relative strength-versus-age curve at constant temperature curing" [226]; this value decreases with temperature rise, despite ultimate strength increasing with temperature. This error was likely due to the poor strength performance and subsequent outlier removal during data processing. If only the first three test values are taken for the cold tests, the activation energy becomes positive; as expected.

When the ternary mixes were tested, an unexpected behavior emerged wherein two materials, that in a binary mixture had adequate correlation to temperature, produced divergent results when combined in a ternary mix. The most notable combination was class C fly ash and silica fume; nearly every ternary blend of these materials produced unfavorable results. Additionally, slag replacements, when combined with class C ash at 40% or more, did not produce viable results. The largest discrepancy noted was that of 40% class C fly ash and 10% slag; at approximately 20 days of equivalent age, the cold strength was 2,900 psi and the hot was 7,600 psi.

Based upon the shortcoming mentioned previously along with the data scatter shown in the results, the second minor hypothesis "the maturity and equivalent age concept is not appropriate for application to mortars and concretes using non-conventional SCM materials" was shown to be correct. The method cannot be applied to each of the aforementioned materials to produce

satisfactory results. It also appears that the results were not solely based on the materials, since combining two materials that performed well separately, did not perform well in combination.

5.3. Evaluation of Workability

5.3.1. Mortar Flow

Two of the largest costs associated with concrete installations are labor and chemical admixture costs. The placement of concrete by skilled laborers can be hindered due to stiff concrete mixes, or "unworkable" mixes. In an effort to ameliorate unworkable mixes, chemical admixtures in the form of water reducers or plasticizers are used to reduce the required water in the mixture to attain a certain flowability. In order to ascertain the impact of the SCMs on the concrete/mortar workability in the absence of chemical admixtures, the flow of mortar was measured using *ASTM C1437 – Standard Test Method for Flow of Hydraulic Cement Mortar* [5].

Summary of Test Method

The test method outlines a procedure for measuring the flowability of a cement mortar using a flow table. The mortar is placed into a cone mold on a brass table, the mold is lifted and the table is picked up and dropped by either machine or hand crank a specified number of times. The distance that the mortar spreads over the table is measured and compared to the original diameter of the bottom of the mold, and presented as a percentage of the original diameter. Mortars are evaluated to determine the necessary water required to achieve comparable flow characteristics or a specified flow; alternatively, mortar can be evaluated for efficacy of admixtures. For this research, the flow table was used to compare the effects of the SCMs at various replacement percentages. As an example, Figure 5-3 shows the progression from the control mortar (0% replacement) to 30% replacement of sugarcane bagasse ash.

Figure 5-3. Mortar flow table mixes. From left to right: control, 10%, SCBA, 20% SCBA, and 30% SCBA.

Equipment

The materials were proportioned using a Mettler-Toledo PB3002-S scale having a precision of 0.5g. The mixer and consolidating tamper utilized were the same as used for the mortar cubes. Researchers used a 12" NIST-traceable pair of calipers, capable of measuring to a precision of 0.0005 inches, to measure the mortar flow. The brass flow table used for this research utilized a motorized lifting mechanism that controlled the number of drops as well as the rate (in drops per minute) as shown in Figure 5-4.

Figure 5-4. Upper left: scale, caliper, trowel and scoop. Bottom Left: flow table with removable brass cone mold. Right: twelve-quart stand mixer with stainless steel paddle and bowl.

Procedure

The test method does not prescribe a specific mix design for mortars; therefore, the mortars evaluated had a sand:cementitious:water ratio of 2.25:1:0.5. These mortars were then used to fabricate mortar bars for expansion testing. The mortar was placed into the brass mold (after it was centered on the dry flow table) in two approximately equal lifts. After each lift, using a rubber or wooden tamper, the mortar was consolidated with 20 strokes. Once the second lift was completed and tamped, any excess mortar was struck off the mold such that the mortar was flush with the top of the mold. Immediately afterward, the mold was removed and the table dropped 25 times in 15 seconds. Researchers found it necessary to amend this portion of the specification to reduce the number of drops to 10 over 6 seconds (both versions have a drop rate of 100 drops/min). This was necessary as the higher replacement fly ash mixtures would fall off the table around 12-15 drops; making measurement impossible.

Immediately after the completion of the dropping, the mortar spread was measured diametrically along the scribed lines in the table. The flow was then calculated using Equation (5-5).

$$Mortar\ Flow = \frac{A - D}{D}\ x100\% \qquad (5\text{-}5)$$

Where:

A = Average spread diameter, in

D = Original inside base diameter, in

Mortar Flow Testing Results and Discussion

The mortar flow for each mixture was plotted on a graph of mortar flow versus replacement percentage; these graphs are presented in Appendix C.4 with a summary presented in Table 5-4. The 0% replacement mortar flow was the same for all mixtures; it represents the control 100% OPC mix. A summary of mortar flow table values is presented below along with the mixture designs for the mixes. The mix design values are adjusted for the specific gravities of the materials, as well as the absorption of the fine aggregate. The mixture proportions are presented in terms of pounds and the sand:cementitious and water:cementitious ratios are unitless.

Based on the findings presented herein, researchers found it necessary to limit the investigation of some of the materials due to the workability issues that presented with high addition rates. Namely, rice husk ash was not investigated at replacement rates higher than 10%, sugarcane bagasse ash use was limited to 20% replacement, and equilibrium catalyst was restricted to 20% replacement. These findings were not wholly unexpected; the sugarcane and rice husk ashes are known from literature to have high specific surface area due to the structure of the plants [230]. The equilibrium catalyst also was expected to reduce the workability as most catalysts require high surface areas to drive chemical reactions.

Table 5-4. Mortar mix designs for length change and flow table results.

Mix Design	Sand	Cement	Water	Ash 1	Ash 2	Flow (%)	S:C	W:C
Control	5.84	2.61	1.33	-	-	64.9%	2.24	0.51
Class C fly ash								
10%	5.82	2.34	1.32	0.26	-	95.4%	2.24	0.51
20%	5.80	2.07	1.32	0.52	-	95.0%	2.24	0.51
30%	5.78	1.81	1.31	0.77	-	107%	2.24	0.51
40%	5.76	1.54	1.31	1.03	-	114%	2.24	0.51
50%	5.75	1.28	1.31	1.28	-	121%	2.24	0.51
60%	5.73	1.02	1.30	1.53	-	133%	2.24	0.51
Class F fly ash								
10%	5.79	2.33	1.32	0.26	-	93.4%	2.24	0.51
20%	5.75	2.05	1.31	0.51	-	96.4%	2.24	0.51
30%	5.70	1.78	1.30	0.76	-	103%	2.24	0.51
40%	5.66	1.52	1.29	1.01	-	117%	2.24	0.51
50%	5.62	1.25	1.28	1.25	-	125%	2.24	0.51
Ground Blast Furnace Slag								
10%	5.86	2.35	1.33	0.26	-	90.6%	2.24	0.51
20%	5.85	2.09	1.33	0.52	-	92.1%	2.24	0.51
30%	5.84	1.82	1.33	0.78	-	94.5%	2.24	0.51
40%	5.83	1.56	1.33	1.04	-	97.6%	2.24	0.51
Rice Husk Ash								
5%	5.82	2.47	1.32	0.13	-	61.1%	2.24	0.51
10%	5.80	2.33	1.32	0.26	-	28.1%	2.24	0.51
Sugarcane Bagasse Ash								
10%	5.81	2.33	1.32	0.26	-	74.0%	2.24	0.51
20%	5.78	2.06	1.31	0.52	-	59.2%	2.24	0.51
30%	5.75	1.80	1.31	0.77	-	0.00%	2.24	0.51
Equilibrium Catalyst								
10%	5.83	2.34	1.33	0.26	-	84.5%	2.24	0.51
20%	5.82	2.08	1.32	0.52	-	62.0%	2.24	0.51
30%	5.80	1.81	1.32	0.78	-	22.9%	2.24	0.51
Wood Ash								
10%	5.81	2.33	1.32	0.26	-	86.2%	2.24	0.51
20%	5.78	2.07	1.32	0.52	-	85.0%	2.24	0.51
30%	5.76	1.80	1.31	0.77	-	89.1%	2.24	0.51
40%	5.73	1.53	1.30	1.02	-	70.3%	2.24	0.51

Table 5-4. Continued.

Mix Design	Sand	Cement	Water	Ash 1	Ash 2	Flow (%)	S:C	W:C
50%	5.70	1.27	1.30	1.27	-	52.6%	2.24	0.51
60%	5.68	1.01	1.29	1.52	-	58.5%	2.24	0.51
70%	5.65	0.76	1.29	1.77	-	54.0%	2.24	0.51
CS200 Glass								
10%	5.81	2.34	1.32	0.26	-	98.9%	2.24	0.51
20%	5.79	2.07	1.32	0.52	-	102%	2.24	0.51
30%	5.76	1.80	1.31	0.77	-	105%	2.24	0.51
40%	5.74	1.54	1.31	1.02	-	104%	2.24	0.51
VCAS 160 Glass								
5%	5.83	2.47	1.32	0.13	-	87.3%	2.24	0.51
10%	5.82	2.34	1.32	0.26	-	91.1%	2.24	0.51
15%	5.80	2.20	1.32	0.39	-	92.6%	2.24	0.51
20%	5.79	2.07	1.32	0.52	-	93.7%	2.24	0.51
25%	5.78	1.94	1.31	0.65	-	91.2%	2.24	0.51
30%	5.77	1.80	1.31	0.77	-	95.0%	2.24	0.51
35%	5.76	1.67	1.31	0.90	-	95.5%	2.24	0.51
40%	5.75	1.54	1.31	1.03	-	93.8%	2.24	0.51
Ground Glass								
5%	5.82	2.47	1.32	0.13	-	89.6%	2.24	0.51
10%	5.81	2.33	1.32	0.26	-	93.8%	2.24	0.51
15%	5.80	2.20	1.32	0.39	-	91.0%	2.24	0.51
20%	5.79	2.07	1.32	0.52	-	87.7%	2.24	0.51
25%	5.80	1.94	1.32	0.65	-	79.5%	2.24	0.51
30%	5.78	1.81	1.31	0.77	-	80.4%	2.24	0.51
35%	5.77	1.67	1.31	0.90	-	77.1%	2.24	0.51
40%	5.75	1.54	1.31	1.03	-	73.2%	2.24	0.51
Ternary blends containing 20% Class C fly ash								
20% C + 5% F	5.78	1.94	1.32	0.52	0.13	107%	2.24	0.51
20% C + 5% Slag	4.99	1.66	1.11	0.44	0.11	109%	2.25	0.50
20% C + 5% RHA	4.97	1.66	1.11	0.44	0.11	90.4%	2.25	0.50
20% C + 5% Wood	4.96	1.32	1.10	0.66	0.22	103%	2.25	0.50
Ternary blends containing 30% Class C fly ash								
30% C + 5% Micron[3]	6.69	1.93	1.49	0.89	0.15	110%	2.25	0.50
30% C + 10% F	4.95	1.32	1.10	0.66	0.22	119%	2.25	0.50
30% C + 10% Slag	4.98	1.44	1.11	0.66	0.11	115%	2.25	0.50
30% C + 10% RHA	4.96	1.43	1.10	0.66	0.11	77%	2.25	0.50

Table 5-4. Continued.

Mix Design	Sand	Cement	Water	Ash 1	Ash 2	Flow (%)	S:C	W:C
30% C + 10% Wood	4.95	1.10	1.10	0.88	0.22	110%	2.25	0.50
Ternary blends containing 40% Class C fly ash								
40% C + 5% F	4.95	1.21	1.10	0.88	0.11	115%	2.25	0.50
40% C + 10% F	4.93	1.10	1.10	0.88	0.22	117%	2.25	0.50
40% C + 10% Micron[3]	6.66	1.48	1.48	1.18	0.30	127%	2.25	0.50
40% C + 10% Slag	4.96	1.10	1.10	0.88	0.22	124%	2.25	0.50
40% C + 10% Wood	4.95	1.10	1.10	0.66	0.44	103%	2.25	0.50
Ternary blends containing 50% Class C fly ash								
50% C + 10% Micron[3]	6.64	1.18	1.47	1.47	0.29	139%	2.25	0.50
50% C + 10% Slag	4.94	0.88	1.10	1.10	0.22	131%	2.25	0.50
50% C + 10% RHA	4.91	0.87	1.09	1.09	0.22	53%	2.25	0.50
50% C + 10% Wood	4.93	0.88	1.10	0.88	0.44	105%	2.25	0.50

5.3.2. Time of Setting

One aspect of concrete workability and placement is the time for the concrete to reach its final "set"; for this test method, the time of set is defined as the time required to reach 4000 psi penetrative resistance. This parameter dictates when the concrete finishing, form removal, and joint cutting can take place. As concrete takes longer to set, the removal of forms is delayed and contractor times will increase, thereby increasing overall cost. For special applications, such as roadway repair, the time of set will control when a traffic lane can reopen for servicing traffic.

Typically, this test method is used to determine the contribution to set retardation or acceleration caused by the addition of chemical admixtures or mixture proportion adjustments. The goal of this task is to identify, if any, the acceleration or retardation of a standard mortar mix caused by the inclusion of the SCMs of interest.

Summary of Test Method

The test method prescribed in *ASTM C403 – Standard Test Method for Time of Setting of Concrete Mixtures by Penetration Resistance* outlines a method for sampling, placing, and testing of sieved mortars from concrete [6]. In this method, a mortar is typically obtained by sieving a concrete, then placed into a mold and monitored over time by penetrating the surface of the mortar with different sized needles. The needles range in size from 1 in^2 cross section down to 1/40 in^2. The needles are part of a large mechanism that is instrumented with a gauge that can read force between 20 lbf and 200 lbf. In this way, a penetrative resistance pressure can be read as low as 20 psi (the lowest gauge reading with the largest needle size) up to 8000 psi (the 1/40 in^2 needle up to 200 lb of force). The test method defines two setting times: initial set and final set, which are defined to be the times at which the penetrative resistance is 500 psi and 4000 psi, respectively. In order to attain these times, the mortar is penetrated several times over the course of several hours (for a typical mortar), with the needle size decreasing as the mortar gains strength. This test method was amended as the mortar specimens did not come from sieved concrete, but rather were fabricated alongside the mortar cube specimens.

Equipment

The mortars analyzed for this testing method were manufactured in conjunction with the mortar cubes. Therefore, all equipment utilized for the preparation of mortar is the same as described in compressive strength of mortar section. The molds for this research were required to have a minimum dimension of 6 inches; as such, 6 inch cube molds were filled with mortar and tested, as shown with a specimen in Figure 5-5. The penetrative resistance device is also shown in this figure, with the dial gauge on top, and the needle is advanced by using the lever arms on the right hand side of dial gauge on top.

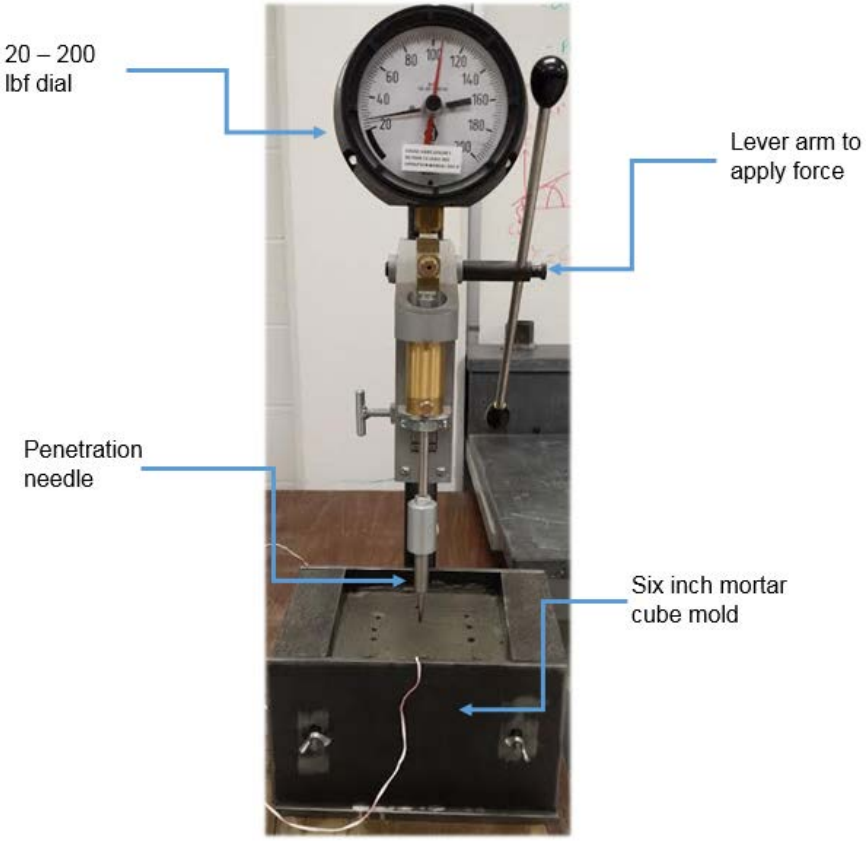

Figure 5-5. Six-inch cube mold containing mortar, along with a penetrative resistance measuring device.

Not shown in Figure 5-5 is a glass pane that was used on top of the specimen mold to prevent moisture loss between measurements. As an additional measurement, temperature was logged using an embedded thermocouple. The thermocouple was placed at approximately mid depth in the middle of the reacting specimen.

Procedure

The procedure for measuring the time of set for this research began with the assembly of the cube molds, using high vacuum grease to ensure water-tightness. Once the molds were ready and the mortar was mixed, mortar was placed into the molds in two lifts, consolidating the mixture by a combination of vibration and rodding. The specimens were then troweled flat and immediately covered with a pane of glass. Beginning with the ¼ in^2 needle, penetrative measurements were made beginning at approximately 2 hours after the water and cement were mixed, and readings were continued with progressively smaller needles approximately every 45

minutes after an initial reading (at least 80 psi) was reached, until the conclusion of the experiment. As the specimens began to approach final set, the readings were taken at shorter durations to avoid missing the target resistance by a large time margin.

Time of Setting Results

The time of set information was plotted as the penetration resistance versus time after mixing. Where available, the thermocouple temperature data was plotted on a secondary axis along with the ambient temperature as recorded from the logger; the graphs are presented in Appendix C.5. Occasionally, data from the logger would be corrupt and the hand-recorded temperature data (taken during measurements) was reported.

5.4. Evaluation of Durability

5.4.1. Length Change – Dimensional Stability

Concrete dimensional stability is of primary concern as expansion or contraction of structural members can lead to undue stress, which can cause premature failure. The expansion or contraction of concrete can be due to external variables such as chemical intrusion and temperature fluctuations, or internal chemical reactions such as internal sulfate attack (delayed ettringite formation). The investigation of the length change of mortars evaluated the susceptibility of a mortar to expand or contract due to internal variables; thus, identifying potential stability incompatibilities.

Summary of Test Method

The test method prescribed in *ASTM C157 – Standard Test Method for Length Change of Hardened Hydraulic-Cement Mortar and Concrete* outlines a method for mixing, curing, storing, and measuring mortar prisms of either 1 inch square cross section or 3 inch square cross section [10]. The samples are prepared by weighing the raw materials, mixing for a prescribed amount of time, placing into molds where they are consolidated and left to cure. The specimens are then demolded and cured, followed by a period of storage during which the specimens are measured, at specific ages, to the nearest 0.0001 inch to determine changes in length.

Equipment

The materials were proportioned using a Mettler-Toledo PB3002-S scale having a precision of 0.5g. The mixing equipment was the same that was used to create mortar cubes. The specimens were cast into steel 1” x 1” x 10” double-gang molds. For curing and storage, researchers created specimen storage containers that allowed limewater-saturated and air-stored specimens to be stored together by affixing an expanded metal shelf to the top of a plastic container as shown in Figure 5-6.

For the measurement of the specimens, a length change comparator with a digital dial gauge capable of 0.0001” accuracy was used to measure length, and an 11.625” invar steel reference bar was used to zero the dial gauge.

Figure 5-6. Length change specimen storage container.

Procedure

The mixes prepared for length change had a sand:cementitious:water ratio of 2.25:1:0.5. Each cement replacement was calculated as a percentage replacement by mass of the total cementitious content. The adopted mixing procedure for this method was the same mixing method utilized for mortar cubes [7]. Once mixing ceased, the mortar was placed into the molds in two equal layers. Each layer was tamped to remove voids, taking care to tamp the mortar into the corners of the molds and around the gauge studs. Any excess mortar was struck off of the mold; the molds were then left to cure for 24 hours. After a period of 24 ± ½ hours, the specimens were removed from their molds and immediately labeled, and the curing procedure outlined in ASTM C157 [10] was followed. Periodically, the specimens were measured to chart changes in length. Researchers did not have access to the tool required to set the lengths between gauge studs at 250 ± 2.5 mm; as such, the gauge length of each specimen was calculated by measuring the distance between gauge studs and subtracting twice the length of a gauge stud. This calculated gauge length was used for the determination of percentage length change for each specimen.

Length Change Testing Results and Discussion

The results of the length change evaluation are presented as a graph of the percentage length change over time for both water-stored and air-stored specimens. This particular method does not prescribe limits for pass or failure; therefore, the results are qualitative and comparative in nature. The results of the length change mixes compared to the control mix are presented in Appendix C.6.

The mortar mixes containing class F fly ash showed less drying shrinkage than the control specimens. In general, the larger the replacement of cement with class F fly ash, the less shrinkage occurred. The length change of the water-cured specimens was not significantly different from the control mixture. The trend of class F fly ash to reduce the drying shrinkage and produce a more dimensionally stable mortar was expected and is well documented in the literature [56], [96], [97]. For this reason, many of the proposed ternary mixtures included moderate (5 – 10%) inclusions of class F fly ash as a means to temper any instability caused by other additions.

Class C fly ash is typically avoided as an SCM due to a history of stability issues caused by the inclusion of it into portland cement concretes (typically seen with highly amorphous siliceous aggregates). However, the results obtained for this research show that the particular class C fly ash received did not produce unfavorable expansion or shrinkage. The results obtained closely

match those of class F fly ash with large replacements (30% or more) providing a more dimensionally stable mortar. With high replacements of the class C fly ash, some expansion was measured in the water-cured specimens; nevertheless, the resultant expansion was minimal.

The addition of ground blast furnace slag into the mortar produced mortars that had higher drying shrinkage over time, as well as higher expansion when stored in a moist condition. The tendency for slag to decrease dimensional stability, however minor, meant that the slag would only be used to increase strength in ternary blends with materials that are known to have reduced shrinkage and expansion over time.

Due to issues with workability, rice husk ash additions were limited to 5% and 10%. The two mixtures performed slightly better than the control with regards to drying shrinkage, but not as well as a 20% class F fly ash addition. It appears that increasing the level of addition of RHA beyond this would further reduce the shrinkage; however, doing so would require the use of plasticizing or water-reducing admixtures. As the effect of admixtures on mortars was not evaluated, the use of the admixtures was not employed for this test method. The water-cured specimens showed no appreciable difference from the control mixtures. The inclusion of sugarcane bagasse ash into portland cement mortars produced a material with less dimensional stability, with the 30% replacement providing the most shrinkage. Larger replacements were not investigated, as the workability, much like the rice husk ash, was made much worse with increasing amounts of SCBA. However, the 10% and 20% additions of SCBA were comparable in shrinkage to the control while performing slightly better with respect to expansion. This result, coupled with the workability results, lead researchers to limit the inclusion of sugarcane bagasse ash to no more than 20%.

The addition of wood ash to portland cement mortars produced increasing amounts of shrinkage with increasing addition rates from 10% to 60%. The shrinkage experienced by the addition of 60% wood ash was nearly twice the shrinkage experienced by the control specimens. Furthermore, as the replacement percentage increased past 50%, the water-cured specimens began to experience expansion amounting to approximately 0.075%, over three times the expansion measured on the control specimens. Both the shrinkage and expansion of the high volume wood ash mortars were the largest dimensional instabilities measured in this research.

When VCAS160 ground glass powder was added to portland cement mortars, the shrinkage was comparable to the control with replacements less than 20%; each addition from 5% to 20% decreased the measured shrinkage. Shrinkage was reduced further with larger additions up to 40% glass. The water-cured specimens performed similar to the control mix. The ground glass mortars performed comparably to the other two glasses (CS200 and VCAS160) with shrinkage being reduced with larger addition rates and slightly higher expansion measurements.

Summary of Results

A summary of the length change evaluations is presented in Table 5-5. The total shrinkage and expansion of the air- and water-cured specimens are presented. This data is also compared to the control mix and presented as a percentage change from the control. Therefore, a mixture that has lower shrinkage and lower expansion than control will show percentages below 100% for each category; these mixes are considered to be more dimensionally stable than the control mixture under these testing conditions.

Table 5-5. Summary of length-change mixes.

	64 Week Shrinkage	64 Week Expansion	Normalized Shrinkage	Normalized Expansion
Control	-0.119%	0.018%	100%	100%
Class F Fly Ash				
10%	-0.103%	0.015%	87%	84%
20%	-0.102%	0.016%	86%	88%
30%	-0.093%	0.014%	78%	78%
40%	-0.077%	0.020%	65%	113%
50%	-0.079%	0.022%	66%	127%
Class C				
10%	-0.106%	0.013%	89%	75%
20%	-0.102%	0.012%	85%	68%
30%	-0.099%	0.022%	75%	122%
40%	-0.080%	0.019%	67%	109%
50%	-0.086%	0.027%	72%	150%
Slag				
10%	-0.123%	0.015%	103%	82%
20%	-0.129%	0.019%	108%	105%
30%	-0.122%	0.022%	102%	122%
40%	-0.131%	0.031%	110%	177%
Rice Husk Ash				
5%	-0.113%	0.019%	95%	106%
10%	-0.107%	0.015%	89%	85%
Sugarcane Bagasse Ash				
10%	-0.128%	0.008%	107%	45%
20%	-0.125%	0.011%	105%	61%
30%	-0.140%	0.022%	117%	125%
Equilibrium Catalyst				
20%	-0.108%	0.016%	91%	89%
30%	-0.104%	0.022%	87%	122%
Wood Ash				
10%	-0.123%	0.014%	103%	80%
20%	-0.135%	0.024%	113%	136%
30%	-0.146%	0.019%	122%	108%
40%	-0.181%	0.019%	151%	107%
50%	-0.216%	0.077%	181%	436%
60%	-0.207%	0.080%	173%	453%
CS200				
10%	-0.116%	0.013%	98%	72%
20%	-0.113%	0.017%	95%	94%
40%	-0.093%	0.029%	78%	116%

Table 5-5. Continued.

	64 Week Shrinkage	64 Week Expansion	Normalized Shrinkage	Normalized Expansion
VCAS160				
5%	-0.118%	0.016%	99%	89%
10%	-0.113%	0.017%	95%	98%
15%	-0.108%	0.019%	91%	106%
20%	-0.104%	0.019%	87%	109%
25%	-0.108%	0.020%	90%	112%
30%	-0.097%	0.023%	81%	131%
35%	-0.092%	0.021%	77%	121%
40%	-0.085%	0.018%	71%	101%
Ground Glass				
5%	-0.118%	0.014%	99%	77%
10%	-0.119%	0.026%	100%	148%
15%	-0.115%	0.018%	96%	103%
20%	-0.106%	0.020%	88%	112%
25%	-0.099%	0.017%	83%	98%
30%	-0.101%	0.020%	84%	114%
35%	-0.094%	0.024%	79%	134%
40%	-0.093%	0.024%	78%	135%

The worst performing materials as a whole were the wood ash binary mixes, with performance decreasing as the addition rate increased. The slag mixtures and the sugarcane bagasse ash mixes performed slightly worse than the control mix, but were not substantially detrimental. All other mixes performed either comparably or better than the control.

5.4.2. Accelerated Length Change – Alkali-Silica Reactivity

A less common but very destructive condition can occur in concretes in which alkalis present either in the cementitious paste, or the environment in which the concrete is placed, can cause a reaction with silica present in the aggregate of concrete. This deleterious reaction is known as alkali-silica reaction, or ASR, and is typically seen with highly siliceous aggregates. Although the standard method involves the evaluation of the aggregates tendency to react with alkalis, researchers were interested in the affect that the SCMs would have on the mortars exposed to high-alkaline environments.

Summary of Test Method

In *ASTM C1260 – Standard Test Method for Potential Alkali Reactivity of Aggregates (Mortar-Bar Method)*, a set of mortar bars are cast in the same manner as for the standard length change method as described in in the previous section [11]. Once the bars are removed from the molds, they are placed into water and the temperature is increased to 80^{o}C over 24 hours. The bars are then placed into a highly alkaline solution for 14 days at the elevated temperature. The lengths of the bars are monitored over the course of the 14 days to determine any expansion. The test

method has a limit of 0.10% expansion for innocuous performance. Mixtures that expand more than 0.20% are susceptible to "potentially deleterious expansion" and bars that expand between 0.10% and 0.20% show a mix of innocuous and deleterious in field performance.

Equipment

The materials were proportioned using a Mettler-Toledo PB3002-S scale having a precision of 0.5g. The mixer and consolidating tamper utilized were the same as used for the mortar cubes. The specimens were cast into steel 1" x 1" x 10" double-gang molds. For curing and storage, researchers created specimen storage containers consisting of a cylindrical container having a diameter of approximately 5 inches and a height of approximately 12 inches, with a "stage" made of perforated stainless steel inside the container. This allowed the bars to be stored vertically, with the gage studs protruding through the perforations in the steel stage, no force was applied to the gage studs, as per the standard; Figure 5-7.

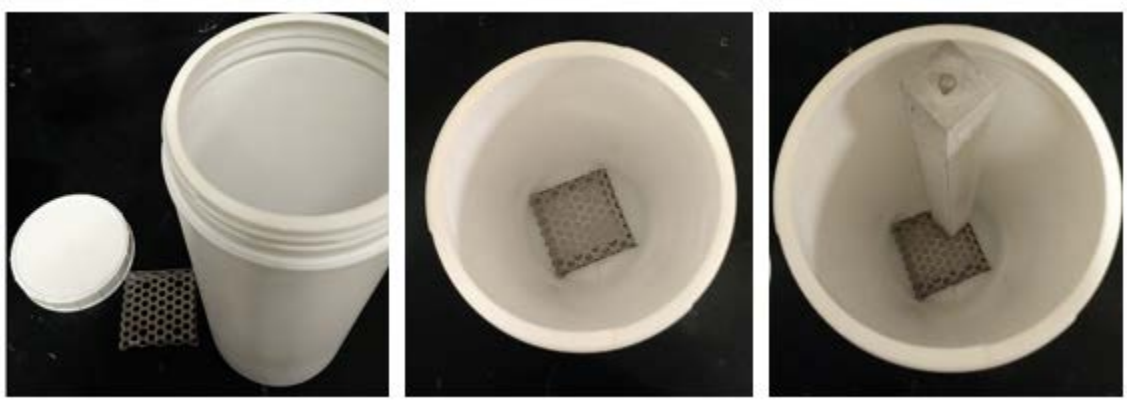

Figure 5-7. Accelerated length change specimen storage container with stainless steel stage.

For the measurement of the specimens, a length change comparator with a digital dial gauge capable of 0.0001" accuracy was used to measure length, and an 11.625" invar steel reference bar was used to tare the dial gauge. For sample conditioning, a laboratory oven with a 1^{o} F digital thermostat was used to keep the specimens at 176^{o} F (80^{o} C).

Procedure

The mixes prepared for length change were comprised of a sand:cementitious:water ratio of 2.25:1:0.5, and the method prescribes a w/cm of 0.47. Each cement replacement was calculated as a percentage replacement by mass of the total cementitious content. The adopted mixing procedure for this method was the same mixing method utilized for mortar cubes.

Once mixing ceased, the mortar was placed into the molds in two equal layers. Each layer was tamped to remove voids, taking care to tamp the mortar into the corners of the molds and around the gauge studs. Any excess mortar was struck off of the mold; the molds were then left to cure for 24 hours.

After a period of 24 ± ½ hours, the specimens were removed from their molds and immediately labeled and the curing procedure outlined in ASTM C1260 was followed. Periodically, the specimens were measured to observe changes in length.

Accelerated Length Change Testing Results and Discussion

As discussed previously, the goal of the method is to determine the potential reactivity of aggregates; however, the expectation was to determine if changing the cementitious components would have a noticeable effect on the potential for expansion while keeping the aggregates the same. The results of the accelerated length change evaluation are presented as a graph of the percentage length change over time for each set of specimens. The results of the length change mixes compared to the control mix are presented in Appendix C.7. The dotted and dashed-dotted lines represent the innocuous and potentially deleterious limits prescribed in the method, respectively. The data is presented on a graph of percent length change against time of curing. As the test method involved two days of curing prior to immersion in the alkaline solution followed by 14 days of submersion, the measurements begin two days after molding, and continued for 14 days (16 days after curing).

With the exception of Figure C-195, all of the graphs represent the average of the 3-4 specimens created for each mixture. There was noticeable expansion with the inclusion of class F fly ash, particularly in the 40% replacement; however, this expansion was still well below the innocuous limit.

Class C fly additions showed a similar trend to class F fly ash, with the larger additions providing larger expansion, but still well below the innocuous limit. Ground blast furnace slag also showed a tendency to increase expansion; still at an acceptable level. The addition of rice husk ash, even at 5% addition rate, expanded well beyond the "potentially deleterious" zone. The addition of 10% rice husk ash produced expansion that was over 10 times the acceptable innocuous limit. This behavior was unexpected as the chemical composition of the rice husk ash did not seem to contain deleterious mineral phases. It has been noted by [231] that this particular method of evaluation can produce failing results with aggregate combinations that show adequate performance under field conditions. The preferred method for evaluation of ASR is *ASTM C1293 – Standard Test Method for Determination of Length Change of Concrete Due to Alkali-Silica Reaction* [232]. This method was not investigated, as it requires the fabrication of large specimens stored at an elevated temperature for 12 months. The researchers did not have the equipment to store the specimens, nor the temperature conditioned space to store 60 mixes for this evaluation for 12 months.

The addition of sugarcane bagasse ash to mortar specimens increased expansion, particularly with the 30% addition. The expansions that were observed were well within the innocuous zone. Equilibrium catalyst additions produced comparable expansion to the control and class F fly ash mixtures. This was expected, as the silica content of the material was low compared to the other materials. Wood ash at large replacements of 25% and 50% produced little reactivity, which is on par with the control and class F fly ash mixes. The addition of glass at 10% and 20% produced little expansion. It is noted in research that expansion due to the inclusion of glass is more frequently encountered when the particle sizes are large, for instance, when used as fine aggregate [86]. The addition of metakaolin produced comparable expansion to the control.

The addition of silica fume produced expansion at 8% replacement; while this was well below the innocuous limit, it was not the expected result. Silica fume is frequently added to concrete to reduce ASR expansion. This expansion at 8% replacement could indicate that the densified silica fume was not properly dispersed in the mortar. Large agglomerations of silica could react

The only mixtures that would not be considered innocuous were those including rice husk ash. While the average expansion of the 40% C ash and 10% rice husk ash mixture would technically be considered "potentially deleterious," having a 14-day expansion of 0.20%, two of the four specimens were over the 0.20% limit, and therefore the entire mix should be considered to have failed.

Summary of Results

The results of this test method, although not designed to evaluate the alkali-silica reactivity of cementitious paste, proved to be an effective means to remove one of the materials, RHA, from further consideration as an SCM due to substantial expansion, even at 5% replacement rates. However, further exploration of the material was conducted to contribute additional information to the engineering knowledge base. It is posited that the primary mechanism for failure is due to the very large particles of RHA; grinding and milling the RHA could potential alleviate this issue. A summary of the accelerated length change evaluations is presented in Table 5-6. The data presented is the total expansion of the specimens. The second worst performing mixture was a ternary-blended mixture of 30% class C fly ash and 10% wood ash; however, even this mixture had less than half of the maximum expansion.

Table 5-6. Summary of accelerated length change mixes, gage length is 10.0 inches.

Mix Design	Average Initial Comparator Reading, in	14 Day Average Comparator Reading, in	Percent Length Change
Control	0.0843	0.0844	0.001%
Class F			
10%	-0.1123	-0.1123	0.000%
20%	-0.1169	-0.1155	0.014%
40%	-0.0958	-0.0928	0.030%
Class C			
10%	0.1666	0.1661	-0.005%
20%	0.1345	0.1330	-0.015%
30%	-0.1229	-0.1214	0.015%
40%	-0.1109	-0.1082	0.027%
50%	0.0758	0.0779	0.021%
Ground Blast Furnace Slag			
10%	-0.1165	-0.1157	0.008%
30%	-0.1262	-0.1236	0.026%
50%	-0.1110	-0.1095	0.015%
Rice Husk Ash			
5%	-0.1185	-0.0927	0.261%
10%	-0.1260	-0.0161	1.113%
Sugarcane Bagasse Ash			
10%	-0.1258	-0.1233	0.025%
20%	-0.1197	-0.1152	0.046%
30%	-0.0918	-0.0848	0.071%
Equilibrium Catalyst			
10%	-0.1441	-0.1431	0.010%
20%	-0.0386	-0.0371	0.015%
Wood Ash			
25%	-0.1121	-0.1102	0.019%
50%	-0.1053	-0.1041	0.012%
CS200			
20%	-0.1196	-0.1188	0.008%
VCAS160			
20%	-0.1351	-0.1340	0.011%
Ground Glass			
10%	-0.0721	-0.0699	0.022%
20%	-0.1122	-0.1115	0.007%
Metakaolin			
5%	0.1218	0.1218	0.000%
10%	0.1253	0.1261	0.008%

Table 5-6. Continued.

Mix Design	Average Initial Comparator Reading, in	14 Day Average Comparator Reading, in	Percent Length Change
Silica Fume			
4%	-0.1100	-0.1095	0.005%
8%	-0.1192	-0.1164	0.028%
20% C Ash and 5%			
Class F fly ash	-0.0646	-0.0633	0.013%
Slag	-0.1084	-0.1058	0.026%
RHA	-0.1271	-0.0899	0.377%
SCBA	-0.1239	-0.1212	0.027%
Micron[3]	-0.0963	-0.0953	0.010%
Metakaolin	0.1202	0.1212	0.010%
20% C Ash and 10%			
Class F fly ash	-0.1169	-0.1155	0.014%
Slag	-0.1086	-0.1074	0.012%
CS200	-0.0675	-0.0678	-0.003%
SCBA	-0.1045	-0.1024	0.021%
Ground Glass	-0.0930	-0.0921	0.009%
30% C Ash and			
5% Class F fly ash	-0.1380	-0.1354	0.026%
5% Slag	-0.1517	-0.1502	0.015%
5% Metakaolin	0.1239	0.1258	0.019%
4% Silica Fume	-0.1269	-0.1251	0.018%
8% Silica Fume	-0.0890	-0.0866	0.024%
10% Class F fly ash	-0.0840	-0.0820	0.020%
10% Slag	-0.1038	-0.1022	0.016%
10% SCBA	-0.1101	-0.1082	0.019%
10% Wood Ash	-0.1157	-0.1111	0.047%
20% Wood Ash	-0.0759	-0.0726	0.033%
40% C Ash and			
5% Class F fly ash	-0.1046	-0.1022	0.024%
5% Slag	-0.1192	-0.1173	0.019%
4% Silica Fume	-0.1140	-0.1108	0.032%
8% Silica Fume	-0.1165	-0.1138	0.027%
10% Wood Ash	-0.1373	-0.1339	0.034%
10% Slag	-0.0882	-0.0852	0.030%
10% RHA	-0.1012	-0.0811	0.203%
20% Wood Ash	-0.1139	-0.1105	0.034%
50% C Ash and			
10% Slag	-0.0866	-0.0851	0.015%
20% Slag	-0.1263	-0.1245	0.018%

6. CONCRETE TESTING

Plastic property evaluation of each mix included slump, volumetric air content, temperature, unit weight, and time of setting. To investigate structural adequacy, the concretes were exposed to uniaxial unconfined compression, splitting tension, and flexural forces to determine ultimate strengths as well as static compressive modulus. The evaluation of concrete durability involved measuring the heat production of the concrete under semi-adiabatic conditions for one week, measuring the bulk and surface electrical resistivity of the concrete over time, and analyzing the ionic concentrations within the pore fluid by extracting the fluid under compressive loading.

The curing ages were chosen based on assumed variation with time; that is to say, properties that were expected to vary widely over time (such as compressive strength) were tested more frequently than those which were not expected to change as much (such as flexural strength). This reduction in testing ages minimized the concrete batch sizes, testing overlaps, concrete storage requirements, and labor required to perform the investigations.

The planned tests, testing ages, and number of specimens required are presented in Table 6-1. With the exception of flexural strength and pore water expression, all specimens were 4" diameter by 8" tall cylindrical concrete specimens. The flexural specimens were 4" x 4" x 14" concrete beams, and the pore water specimens were 2" diameter by 4" tall sieved mortar. Also included in the batch size was additional concrete that was to be used for destructive plastic property testing (air content) and for sieving to describe the time of setting of each concrete.

Table 6-1. Test type, age, and number of specimens for concrete assessment.

Test Method	Testing Ages			
	7 days	28 days	56 days	91 days
Compressive Strength [16]	4" x 8" (3)	4" x 8" (3)	4" x 8" (3)	4" x 8" (3)
Splitting Tensile Strength [17]		4" x 8" (3)		4" x 8" (3)
Modulus of Elasticity [18]		4" x 8" (3)		4" x 8" (3)
Flexural Strength [19]		4" x 14" (3)		4" x 14" (3)
Pore Water Expression	2" x 4" (1)	2" x 4" (1)		2" x 4" (2)
Bulk/Surface Resistivity [20], [21]	4" x 8" (3)	4" x 8" (3)	4" x 8" (3)	4" x 8" (3)

6.1. Concrete Mixture Design

Concrete mix design is the process by which the proportions of a concrete mixture are varied in order to attain a certain set of characteristics. These characteristics include target workability/slump, target air content, compressive strength (typically evaluated at 28 days), aggregate types, aggregate ratios, water-to-cementitious content ratios, amongst other aspects. As this research focused on mixtures for FDOT usage, a typical concrete mixture fitting general requirements was designed. The decision to avoid using an excessively high strength concrete or other high performance mixtures was that the effects of the cement replacements would be more easily scrutinized with weaker mixes, as any detrimental effects would not be concealed.

The design of the baseline concrete mix was influenced by the Florida Department of Transportation Standard Specifications for Road and Bridge Construction, which outlines the requirements for concrete mixtures approved for use on FDOT projects [23]. This research was

to generally apply to structural concrete, and therefore Section 346 – Portland Cement Concrete was followed during the design phase. This particular section states that "Fly ash or slag materials are required in all classes of concrete" with varying amounts of SCM required for the different concrete applications. The various applications as well as the required amounts of SCMs are presented in Table 6-2. The prescribed dosages for each material are not mandatory, rather at least one material replacement is required at the prescribed dosage.

Table 6-2. General prescribed cement replacements of SCM in Florida concretes.

Application	Fly Ash	Blast Furnace Slag	Metakaolin	Silica Fume
Mass Concrete	18 – 50%	50 – 70%	8 – 12%	3 – 9%
Drilled Shafts	33 – 37%	58 – 62%		
Precast Concrete	25% max.	70% max.		
Other Concrete	18 – 30%	25 – 70%		

The FDOT Road and Bridge Construction specifications also list the acceptable SCMs in Section 929 Pozzolans and Slag. The accepted materials include class F and Class C fly ash (including ultra-fine), blast furnace slag, coke or bark ash (class F), metakaolin, and silica fume. The majority of materials investigated for this research do not meet the qualifications prescribed in ASTM C618 [135], which considers only coal fly ashes and natural pozzolans. Section 346 classifies FDOT concrete as shown in Table 6-3.

Table 6-3. Florida Department of Transportation concrete cementitious content requirements.

Class of Concrete	Specified Minimum Strength (28 days), psi	Target Slump, in	Minimum Cementitious, lb/yd3	Maximum water-to-cementitious
I	3,000	3	470	0.53
I (Pavement)	3,000	2	470	0.50
II	3,400	3	470	0.53
II (Bridge Deck)	4,500	3	611	0.44
III	5,000	3	611	0.44
III (Seal)	3,000	8	611	0.53
IV	5,500	3	658	0.41
IV (Drilled Shaft)	4,000	8.5	658	0.41
V (Special)	6,000	3	752	0.37
V	6,500	3	752	0.37
VI	8,500	3	752	0.37

In order to design a mix that was based closely to a mid-range FDOT structural concrete class, but would not require excessive admixtures, a w/cm of 0.42 was chosen. This was so that the mixes would qualify for classes I-III and be similar to a class IV but without the excess cementitious material. This led to a final design of a mix with 615 lb/yd^3 of cementitious material, with a w/cm of 0.42, target slump of 3" (with 1" to 6" of slump being acceptable) and a target air content of 3% with the maximum air content being 6% as per FDOT 346 [233].

The mix designs utilized a Florida sand for the fine aggregate. Florida sands typically have low fineness modulus and the sand chosen was representative of a typical Florida sand. The coarse aggregate chosen was a #57 Florida limerock. The measured aggregate properties are presented in Table 6-4.

Table 6-4. Properties of aggregates used in concrete mixes.

Aggregate Property			
Coarse Aggregate Properties			
Specific Gravity	2.45		
Absorption, %	5.37		
Fine Aggregate Properties			
Specific Gravity	2.64		
Absorption, %	0.37		
Sieve Analysis			
Sieve Size	Mass Retained, (g)	Retained, %	Cum. Retained, %
4	2.7	0.22	0.22
8	19.2	1.59	1.82
16	102.1	8.48	10.3
30	294.3	24.5	34.7
50	489.5	40.7	75.4
100	261.7	21.7	97.1
Pan	32.8	2.72	99.9
Fineness Modulus	2.20		

After speaking with Dr. DeFord at the FDOT, it was decided to utilize an aggregate ratio of 0.400 as this is a standard metric utilized for Florida concretes. This is the volume ratio of fine aggregate to total aggregate. Using the information herein, the control concrete mixture was designed; Table 6-5 contains the general mix design (without correction for water contents or batch size).

Table 6-5. Concrete mixture design for the control concrete mix.

Material	Measured Specific Gravity	Weight, lb/yd^3	
Portland cement	3.22	615	
Water	1.00	257	
Fine Aggregate	2.64	1251	
Coarse Aggregate	2.45	1740	
Calculated Unit Weight		143	lb/ft^3

6.2. Concrete Mixture Selection

The ultimate goal of this research was to find an acceptable replacements for class F fly ash, at replacement levels of at least 20%, to supplement portland cement in Florida concretes. Investigation of the concretes involved evaluating the structural adequacy of concrete;

specifically, the compressive, splitting tensile and flexural strengths, and the modulus of elasticity. Furthermore, the evaluation of the concrete under semi-adiabatic conditions during curing, surface and bulk resistivity, and as-extracted pore fluid analysis was expected to give an indication of the relative durability characteristics of the concretes with changing paste content.

The performance of the different mortars were scrutinized based on strengths, durability testing, and workability, and any mixes that proved to provide severely negative results in any test were removed from consideration. The bases for disqualification included failure of the accelerated length change test, high shrinkage or expansion in the length change test, a flow below 65% on the flow table, or a compressive strength below 60% of control in any of the 7-, 28-, and 56-day tests at room temperature.

The rice husk ash was removed from consideration as an acceptable replacement for fly ash due to failure of the accelerated length change test, but the 10% rice husk ash mix was retained for further investigation for purely academic purposes, as this material is not scrutinized heavily in the literature.

Wood ash replacements higher than 40% were removed as they had a significant amount of drying shrinkage as well as high wet-cured expansion in the length change test. The mixes that were removed due to poor workability were the 30% SCBA, 20% ECAT, and 30% ECAT mixes. Recycled glass was removed from investigation as the company that originally donated the material shut their facility down; thus the only glass material investigated was a manufactured product. The mixes listed in Table 6-6 were removed due to poor performance with respect to compressive strength.

Table 6-6. Mixes removed from consideration due to compressive strength performance.

Mix Design	Normalized Compressive Strength	Age (days)
40% F Ash	47%	7
50% Wood	42 – 49%	7, 28, 56
40% C / 10% RHA	49 – 53%	7, 28
40% C / 20% Slag	51%	7
50% C / 10% Slag	56%	7
50% C / 20% Slag	35 – 58%	7, 28
30% C / 20% GG	50%	7
40% C / 8% SF	51%	7

Consequently, the mortar mixes that performed adequately totaled over 50 mixes. As this number of mixes was still too large to investigate, the number of mixes was reduced to 22 based on the following. The initial mixes would be used as comparison mixes; these included the control, 20% class F fly ash, 20% class C fly ash, 30% class C fly ash, 5% metakaolin, 4% silica fume, and 50% slag. Following this, the mixes were compared on a basis of compressive strength. Mixes that outperformed control at 28 days were organized by compressive strength, followed by mixes that outperformed control at 56 days. Any mixes that seemed semi-redundant were removed. For instance, 30% C / 4% silica fume and 30% C / 8% silica fume out performed control at either 28 or 56 days; however, silica fume is an expensive additive, and it is known to be effective in small additions. Therefore, the performance of 4% silica fume with 30% class C

fly ash was deemed to be sufficient, and the 8% silica fume ternary mix was discarded. Furthermore, when an SCM that was less expensive than cement performed sufficiently, the highest effective replacement level was chosen to investigate, and the other replacement levels were eliminated. Table 6-7 presents all of the mixes that performed better than control at either 28 or 56 days; this narrowed the number of competent mixes from over 60 to 39 mixes. The remaining mixes were narrowed to 22 total mixes; the reasons why certain mixes were removed are described in Table 6-7.

The final mix designs selected are shown in Table 6-8 components are listed in lb/yd^3, unless otherwise specified. This table also includes the amounts and type of chemical admixtures that were required to attained a target air content of 1 – 6% and a target slump of 1 – 6 inches.

Table 6-7. Normalized compressive strength of mortar mixes that are comparable to control.

Mix	Mix Design	28 day	56 day	Notes
1	10% Recycled Glass	95%	113%	Removed, product is no longer available,
2	20% Recycled Glass	90%	119%	and performs similar to other glasses
3	10% ECAT	92%	110%	Removed due to workability concerns and
4	20% ECAT	85%	105%	marginal performance
5	20% F Ash	86%	101%	
6	5% Metakaolin	128%	123%	
7	10% Metakaolin	140%	128%	Removed, 5% Metakaolin is sufficient
8	5% RHA	90%	113%	Removed for consideration as a viable
9	10% RHA	106%	129%	alternative due to ASR testing results, but 10% investigated for research purposes
10	20% SCBA	115%	120%	
11	4% SF	149%	161%	
12	8% SF	119%	129%	Removed, 4% SF is sufficient
13	30% Slag	86%	114%	Removed, 50% slag is sufficient
14	50% Slag	88%	130%	
15	20% VCAS	98%	105%	Removed, worse performance than CS200
16	20% C / 5% F	87%	105%	Removed, 30C/5F performed better
17	20% C / 10% F	89%	121%	
18	30% C / 5% F	110%	116%	
19	30% C / 10% F	92%	111%	
20	40% C / 5% F	79%	105%	Removed, poor early performance
21	20% C / 5% Micron^3	103%	126%	Removed, Micron^3 is expensive and its
22	20% C / 10% Micron^3	128%	116%	effects are well documented
23	20% C / 5% RHA	81%	105%	Removed due to ASR testing results
24	20% C / 5% SCBA	81%	117%	Removed, 20C/10SCBA performed better
25	20% C / 10% SCBA	100%	130%	
26	30% C / 10% SCBA	85%	120%	
27	20% C / 5% Slag	95%	115%	
28	20% C / 10% Slag	120%	141%	
29	30% C / 10% Slag	78%	101%	Removed, 20C/10Slag performed better
30	20% C / 10% GG	92%	116%	Removed, product no longer available
31	20% C / 4% SF	123%	141%	

Table 6-7. Continued.

Mix	Mix Design	28 day	56 day	Notes
32	30% C / 4% SF	100%	96%	
33	30% C / 8% SF	83%	112%	Removed, 30C4SF is sufficient
34	40% C / 4% SF	67%	109%	Removed, poor early age performance
35	20% C / 10% CS	107%	128%	
36	20% CS200	93%	112%	
37	20% C / 5% Meta	101%	119%	Removed, 30C5Meta performed adequately
38	30% C / 5% Meta	103%	100%	
39	30% C / 10% Meta	104%	108%	Removed, 30C5Meta performed adequately

Table 6-8. Concrete mix design legend. Weights are in lb/yd^3 unless otherwise noted.

Mix	Portland Cement	Replacement #1		Replacement #2		Water	Fine Agg.	Coarse Agg.	AEA (oz./cwt)	Type D (oz./cwt)	Type F (oz./cwt)
1	615	-	-	-	-	257	1251	1740	0.375	6.0	-
2	492	C Ash	123	-	-	257	1243	1729	0.375	4.0	-
3	492	CS200	123	-	-	257	1242	1727	0.375	8.0	-
4	308	Slag	308	-	-	257	1244	1730	0.375	8.0	4.0
5	431	C Ash	185	-	-	257	1241	1726	0.375	-	-
6	461	C Ash	123	Micron^3	31	257	1242	1728	0.375	4.0	-
7	369	C Ash	185	SCBA	62	257	1260	1710	0.375	8.0	6.5
8	431	C Ash	123	SCBA	62	257	1235	1718	0.375	3.0	6.0
9	400	C Ash	185	F Ash	31	257	1237	1720	0.375	-	-
10	431	C Ash	123	F Ash	62	257	1237	1720	0.375	4.0	-
11	461	C Ash	123	Slag	31	257	1244	1729	0.375	4.0	-
12	554	RHA	62	-	-	257	1244	1729	0.375	-	9.0
13	431	C Ash	123	CS200	62	257	1239	1723	0.375	-	-
14	431	C Ash	123	Slag	62	257	1243	1728	0.375	2.0	-
15	369	C Ash	185	F Ash	62	257	1235	1717	0.375	-	-
16	590	Silica Fume	25	-	-	257	1250	1740	0.375	2.0	4.0
17	584	Metakaolin	31	-	-	257	1250	1738	0.375	4.0	6.0
18	467	C Ash	123	Silica Fume	25	257	1242	1727	0.375	-	2.0
19	406	C Ash	185	Silica Fume	25	257	1237	1720	0.375	-	3.0
20	400	C Ash	185	Metakaolin	31	257	1238	1721	0.375	-	3.0
21	492	SCBA	123	-	-	257	1229	1709	0.375	4.0	10.0
22	492	F Ash	123	-	-	257	1240	1724	0.375	-	2

6.3. Compressive Strength of Concrete

The most frequently performed qualitative evaluation of concretes is the compressive strength test. This test method is used to qualify structural members in the field as well as for use in the laboratory for performance comparison to alternate concrete mixtures. Concrete is a heterogeneous mixture of aggregates, cement, supplemental cementitious materials, and water. Any variance in the materials or the material proportions can affect nearly every aspect of the resultant concrete; as such, the impact of the various SCMs on the properties of concrete is of the utmost importance.

6.3.1. Summary of Test Method

The compressive strength test is performed by preparing specimens that are representative of the concrete that is to be placed in the field (typically 4" diameter x 8" tall cylinders), then at appropriate ages they are loaded until failure in axial compression as shown in Figure 6-1 in accordance with *ASTM C39, Standard Test Method for Compressive Strength of Cylindrical Concrete Specimens* [16]. This test method allows researchers to compare strength development over time between various mix designs. The strength of concretes can then be compared to evaluate the impact of the various SCMs on the structural adequacy of concrete.

Figure 6-1. Concrete specimen loaded in compression to failure.

6.3.2. Equipment

The specimens were prepared by grinding the ends of the cylinders on a Kyowa concrete cylinder end grinder to meet the specifications outlined in ASTM C39 [16]. The specimens were measured using Mitutoyo 12" calipers. Then the specimens were tested on an automatically controlled 600 kip Forney compression frame.

6.3.3. Procedure

The procedure for evaluating the compressive strength of concrete specimens began with proper fabrication and curing methods. The concrete for this research was prepared in compliance with ASTM C31 - *Standard Practice for Making and Curing Concrete Test Specimens in the Field* [234]. The plastic properties of each mixture were recorded, including slump [12], air content [14], temperature [13], unit weight [15], and time of setting [6]. The specimens were demolded

within 24±0.5 hr after mixing, and placed directly into storage tanks filled with lime water and kept in a temperature-controlled room, as shown in Figure 6-2.

Figure 6-2. Concrete specimen storage.

Prior to testing, the concrete cylinders had the ends ground flat and plane in a Kyowa concrete cylinder grinder; during this time, the specimens constantly had free water on the surface so as to not desiccate. The specimens were then measured to determine length (for any corrections) and diameter (for cross-sectional area) as per ASTM C39 [16]. Following the cylinder preparation and curing, the specimens were transported to the Florida Department of Transportation State Materials Office for compressive testing on an automated 600-kip Forney loading frame. The specimens were loaded at a rate of 35 psi/s until the sustained load fell by 50% indicating failure of the specimen. The ultimate load was recorded and divided by the cross-sectional area to determine the ultimate stress. None of the cylinders tested required corrections due to the length.

6.3.4. Compressive Strength of Concrete Testing Results and Discussion

The results of the plastic properties of the concrete mixtures are presented in Table 6-9. The compressive strength results are presented in a series of charts in Appendix D.1; a summary is provided in Table 6-10. The charts present the compressive strength in units of lb/in^2 on the left axis and are normalized to the control mix on the right.

After comparing the results at seven days, eight mixes did not reach 90% of the control strength. At 28 days there were only two concrete mixes (20% class F fly ash and 20% CS200) that did reach 90% of the control strength at 28 days. By 91 days of curing, only the 20% class F ash mix was less than 90% of the control strength; this mix had 84% normalized strength. This result showed that, for compressive strength, all of the mixes outperformed 20% class F fly ash mixes.

Table 6-9. Concrete plastic properties.

Mix	Mix Type	Slump (in)	Air, (%)	Density (pcf)	Temp. (^{o}F)	Time of Set	
						Initial (hr : min)	Final (hr : min)
1	Control	4	5.50	140.1	79	5:33	7:24
2	20% C Ash	6.25	5.00	140.8	80	6:15	8:07
3	20% CS200	2.5	5.75	139.2	80	8:22	10:19
4	50% Slag	3.25	5.00	141.2	79	7:05	9:45
5	30% C Ash	3.25	2.75	142.8	79	5:43	7:50
6	20% C Ash / 5% Micron[3]	2.25	3.00	142.8	82	6:32	8:24
7	30% C Ash / 10% SCBA	2.25	5.00	140.6	83	8:58	11:26
8	20% C Ash / 10% SCBA	2.25	3.75	143.4	76	7:46	10:18
9	30% C Ash / 5% F Ash	2.5	2.75	143.8	82	6:19	8:10
10	20% C Ash / 10% F Ash	3.5	3.75	141.2	80	7:15	9:32
11	20% C Ash / 5% Slag	2.25	3.75	143.6	80	6:21	8:21
12	10% RHA	2.25	3.50	143.2	79	7:37	10:49
13	20% C Ash / 10% CS200	3.25	2.75	143.4	74	6:23	8:07
14	20% C Ash / 10% Slag	8.5	2.50	142.4	78	6:16	8:37
15	30% C Ash / 10% F Ash	3.0	2.00	144.8	78	6:32	8:38
16	4% Silica Fume	4.5	4.50	143.6	76	5:34	7:25
17	5% Metakaolin	5.0	3.25	143.0	76	6:28	8:51
18	20% C Ash / 4% Silica Fume	2.0	3.25	142.2	75	6:10	8:13
19	30% C Ash / 4% Silica Fume	4.25	4.25	140.6	80	5:53	8:01
20	30% C Ash / 5% Metakaolin	2.50	2.75	144.2	80	5:38	7:56
21	20% SCBA	4.0	3.0	140.0	77	7:39	9:53
22	20% F Ash	8.75[1]	5.75	137.8	73	5:51	7:51

[1] The initial slump of Mix 22 was approximately 2.25 inches; 2 oz./cwt of ADVA120 was added as WRDA60 is known to be a retarder and 20% F Ash was anticipated to have a long time until setting. The slump was not anticipated to increase as drastically as it did from a modest addition.

Table 6-10. Summary of compressive strengths of concretes.

Mix	Mix Design	Compressive Strength				Normalized Strength			
		7 Day	28 Day	56 Day	91 Day	7 Day	28 Day	56 Day	91 Day
1	Control	5763	6773	7350	7658	100	100	100	100
2	20% C Ash	5166	6588	7088	7320	90	97	96	96
3	20% CS200	4498	5919	6576	6959	78	87	89	91
4	50% Slag	5862	8032	8789	9189	102	119	120	120
5	30% C Ash	5247	7031	7622	7939	91	104	104	104
6	20% C 5% Micron[3]	5986	7397	8126	8407	104	109	111	110
7	30% C 10% SCBA	4518	6309	6930	7241	78	93	94	95
8	20% C 10% SCBA	5873	7544	7912	8058	102	111	108	105
9	30% C 5% F	5159	6771	7555	7572	90	100	103	99
10	20% C 10% F	5024	6687	7177	7683	87	99	98	100
11	20% C 5% Slag	5958	7499	8242	8227	103	111	112	107
12	10% RHA	5501	6815	7445	7417	95	101	101	97
13	20% C 10% CS200	5004	6886	7505	8000	87	102	102	104
14	20% C 10% Slag	4276	6343	7302	7736	74	94	99	101
15	30% C 10% F	5226	6747	7605	8283	91	100	103	108
16	4% Silica Fume	6052	7469	8260	8500	105	110	112	111
17	5% Metakaolin	7231	8580	8894	8840	125	127	121	115
18	20% C 4% Silica Fume	5869	7557	8236	8752	102	112	112	114
19	30% C 4% Silica Fume	4965	6426	6987	7566	86	95	95	99
20	30% C 5% Metakaolin	5550	7168	7695	7669	96	106	105	100
21	20% SCBA	5106	6635	6819	7309	89	98	93	95
22	20% F Ash	3921	5251	6023	6447	68	78	82	84

6.4. Concrete Compressive Modulus of Elasticity

The reaction to loading a material takes place in two ranges: elastic and plastic. The elastic range is where the loading of the material will temporarily deform a material, but will return to the original dimensions when the load is removed. The plastic range is where a material is permanently deformed due to loading. For ductile materials such as aluminum or steel, the plastic deformation results in bends, dents, or folds. For brittle materials such as glass or concrete, the plastic deformation results in cracked, or broken pieces. While materials such as glass or concrete will fail in a brittle nature, they still can behave elastically if the stress levels are low enough. The amount of stress divided by the measured, while in the elastic range, is known as the Young's modulus, or modulus of elasticity. This describes the elastic strain response during loading, where strain, ε, is the deformation, typically noted in either units of strain (inches of deformation divided by inches of original length) or micro strain, μ_s, (millionths of inches of deformation divided by inches of original length). This concept of strain is shown in Figure 6-3.

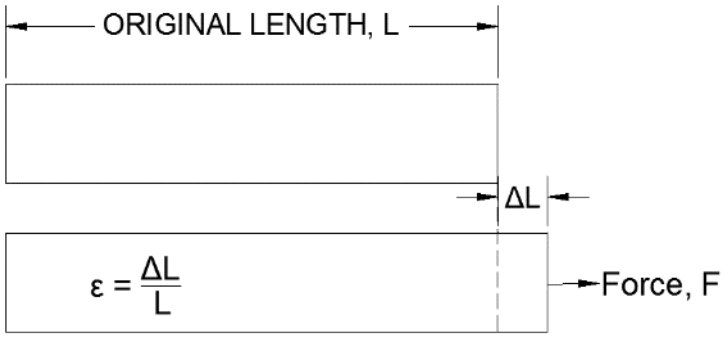

Figure 6-3. Strain depicted in terms of force, original length, and differential length.

The strain observed in the elastic range is linearly correlated to the load that is applied; that is to say that doubling the force/load/stress will double the strain. The elastic modulus is described as the stress (load divided by area) divided by the strain. Therefore, when comparing moduli of materials, the larger the modulus relates to a material that deforms less under a given load.

6.4.1. Summary of Test Method

The test method described in ASTM C469 - *Standard Test Method for Static Modulus of Elasticity and Poisson's Ratio of Concrete in Compression* includes attaching a strain measurement device to cylindrical concrete specimens during loading [18]. This device measures the strain of the specimens as a function of the concrete loading. The cylinders are taken to 40% of their ultimate capacity (to stay within the elastic range) and the average of three cycles of loading is taken as the elastic modulus. This standard also describes the measurement of Poisson's ratio of the concrete specimens; however, this parameter was not investigated.

6.4.2. Equipment

The equipment used for this investigation included all of the equipment required for the compressive strength of concrete. Additionally, an Epsilon Tech modulus frame was used to measure the strain induced by the compressive load. Software was used to find the best linear fit through the data points (stress and strain), the slope of this line is the elastic modulus (in units of lb/in^2).

6.4.3. Procedure

The first step in measuring the elastic modulus was to determine the compressive strength of the specimens to be evaluated. This was done by performing compressive strength testing on cylindrical specimens that were created and stored along with the modulus specimens. Then, 40% of the ultimate load was computed. The specimens were then placed into a modulus frame that was equipped with devices to measure displacements below 0.0001".

The specimens were then loaded to the pre-determined 40% of ultimate load at a rate of 35 psi/sec, and then unloaded at the same rate. This loading procedure was repeated a total of four times on each specimen. The first loading cycling was discarded due to equipment settling. The modulus was calculated using the load, specimen dimensions, and measured displacements. The average of the final three moduli was taken as the final value.

6.4.4. Summary and Discussion of Modulus of Elasticity Results

The results of the elastic modulus testing for both 28 and 91 days of curing are presented in Table 6-11. For the majority of concrete mixtures, the moduli of elasticity of the different mixes were similar to the control (within 10%) with the mix having the lowest 28- and 91-day moduli being the 20% sugarcane bagasse ash mix (91% and 94%, respectively), and the highest moduli at 28 and 91 days being the 5% metakaolin mix (120% and 116%, respectively).

Table 6-11. Compressive modulus of elasticity for concrete mixtures.

Mix	Mix Design	28 Day Modulus (psi)	Normalized 28 Day Modulus	91 Day Modulus (psi)	Normalized 91 Day Modulus
1	Control	4,564,081	100%	4,745,081	100%
2	20% C Ash	4,547,378	100%	4,811,946	101%
3	20% CS200	4,457,543	98%	4,821,011	102%
4	50% Slag	4,966,647	109%	5,497,365	116%
5	30% C Ash	4,962,605	109%	5,193,252	109%
6	20% C 5% Micron[3]	4,964,352	109%	5,424,255	114%
7	30% C 10% SCBA	4,568,472	100%	5,049,318	106%
8	20% C 10% SCBA	5,028,667	110%	5,139,725	108%
9	30% C 5% F	4,954,509	109%	4,827,337	102%
10	20% C 10% F	4,648,105	102%	4,889,730	103%
11	20% C 5% Slag	5,083,726	111%	4,998,891	105%
12	10% RHA	5,006,163	110%	4,856,372	102%
13	20% C 10% CS200	5,022,991	110%	4,951,203	104%
14	20% C 10% Slag	4,599,171	101%	4,921,459	104%
15	30% C 10% F	5,003,659	110%	5,259,484	111%
16	4% Silica Fume	5,245,300	115%	5,288,471	111%
17	5% Metakaolin	5,474,285	120%	5,486,507	116%
18	20% C 4% Silica Fume	4,705,991	103%	5,204,900	110%
19	30% C 4% Silica Fume	4,525,659	99%	4,993,808	105%
20	30% C 5% Metakaolin	4,823,692	106%	4,891,750	103%
21	20% SCBA	4,133,115	91%	4,444,693	94%
22	20% F Ash	4,262,183	93%	4,459,982	94%

From these results, it can be seen that only two concrete mixes (20% class F fly ash, and 20% sugarcane bagasse ash) did not reach 95% of the control modulus (both reached 94% of control at 91 days). This indicates that all of the mixes are either comparable to or better than the control at both 28 and 91 days, with the average moduli at 28 and 91 days being 105% and 106% respectively. These results are interesting in that with up to 40% replacement in some instances, the performance of the concrete was improved with regards to modulus of elasticity. It should be noted that for a two-week period during testing, there was an issue that caused the data to be recorded using the wrong calibration factor for the testing frame (this led to largely erroneous data in the raw data files). The calibration factor that was erroneously used was 74% of the correct calibration factor; therefore, the data collected during that time period was divided by 0.74 to account for the difference. As a consequence, there are five mixes that were tested for

91-day modulus during that time period, four of those five mixes (9, 11, 12, and 13) showed a 91-day modulus slightly lower than the 28-day modulus. This is most likely an error, but the data cannot be corrected further; as such, the data for these mixes and dates should be taken with the assumption that the 91-day data is conservatively low.

6.5. Splitting Tensile Strength of Concrete

The largest controlling factor in crack prevention of concrete is the tensile strength [223]. There have been several test methods developed to indirectly measure tensile strength, such as splitting tensile strength and flexural strength; direct tension of concrete cylinders is not done due to the difficulty in gripping the ends of a cylinder without causing stress concentrations around the grips. One method for direct axial tension of cylindrical specimens (rock cores) involves epoxying platens to the ends of the cylinders and pulling on the platens [235]. This method is inconvenient as it requires the purchasing of epoxy, reusable platens, and additional time for the epoxy to cure (for concrete, this would have to be done while in a moist environment). The most common method for determining the tensile strength of concrete is the splitting tensile test, ASTM C496 - *Standard Test Method for Splitting Tensile Strength of Cylindrical Concrete Specimens* [17].

6.5.1. Summary of Test Method

The evaluation of tensile strength of concrete involves placing a concrete cylinder on its side and compressing it diametrically. This compressive pressure causes a tensile stress gradient that is perpendicular to the loading direction causing the cylinder to split from the center. This failure plane can be seen in the failed specimen in Figure 6-4. The load required to fail the specimen is then used to calculate the tensile strength based upon the size of the cylinder. Three replicates are tested and averaged for each testing age; for this investigation, it was not expected that the tensile strength would change much beyond 28 days; therefore, specimens were only tested at 28 and 91 days.

Figure 6-4. Fracture plane visible through the end of a failed splitting tensile specimen.

6.5.2. Equipment

The required equipment for this test method is a compression frame with a capacity high enough to ensure failure of the specimens (for this investigation, 45,000 lb was sufficient). Additionally, a splitting tensile frame was utilized, as well as sacrificial wood strips that comply with ASTM C496. The splitting tensile frame shown in Figure 6-5 allows for the convenient alignment of cylindrical specimens, but is not mandatory.

Figure 6-5. Splitting tensile frame with cylinder.

6.5.3. Procedure

The specimens were first stored in limewater for either 28 or 91 days. The ends of the cylinders were ground flat for measuring the length accurately. The diameters of the specimens were measured as well. The specimens were loaded into the splitting tensile frame with a wood strip between the top and bottom bearing faces of the cylinder to distribute the compressive force. The frame was then positioned into the compression frame directly under the tensile splitting head, and was loaded until failure at a rate of 130 lb/sec of compressive load, which amounts to approximately 155 psi/min of tensile stress. The prescribed loading rate is 100 – 200 psi/min of tensile stress. The ultimate compressive load was then used along with the cylinder dimensions to calculate the tensile stress at failure using Equation (6-1).

$$T = \frac{2P}{\pi L d} \tag{6-1}$$

Where:

T = Splitting tensile strength, psi
P = maximum applied load indicated by the compression frame, lb
L = length, in
d = diameter, in

6.5.4. Splitting Tensile Strength of Concrete Results and Discussion

In an ideal scenario, a split tension specimen will be completely free of air voids; with specimens using limestone, this generally ends with a fracture plane splitting the specimen through the aggregate as shown in Figure 6-6. Typically, concretes with much harder and less porous aggregate, such as granite or marble, would exhibit intergranular fractures where the fracture planes go around the aggregate-paste interface rather than through the aggregate.

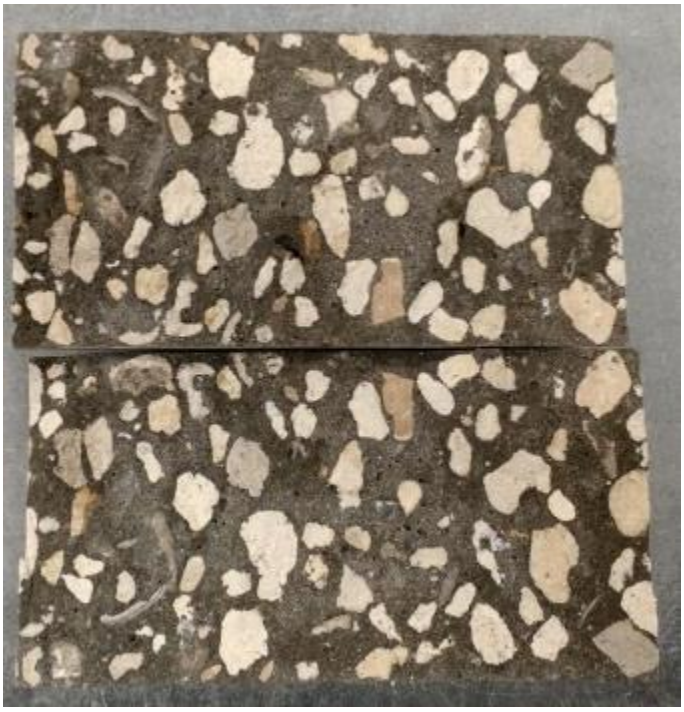

Figure 6-6. Tensile specimen with transgranular fractures.

The results presented in Table 6-12 represent the splitting tensile strength at 28 and 91 days of curing. Any test values that were 85% less than the average of the three replicates were removed, and the average tensile strength was recalculated; *these values were shown with an asterisk to indicate only two replicate specimens were used to determine strength*. The normalized percentages were compared to the control concrete mix.

Only four of the concrete mixes had a tensile strength that was more than 10% below the control at 28 days; with the majority of mixes (11) outperforming the control at 28 days. At 91 days, all mixes had normalized strengths of 90% or more; 15 of the mixes outperformed the control mix at 91 days with 6 mixes having normalized strengths over 110% of control. This shows that the replacement materials at 91 days of curing had comparable performance to control concretes, and in many cases, superior performance. This increased tensile strength indicates a potential to have less cracking of concrete members, which has implications for increased durability. The two mixes with the highest tensile strength, 20% C and 5% Micron^3 and 30% C ash, both performed worse than the control at 28 days, indicating a high degree of pozzolanic activity.

Table 6-12. Splitting tensile strength of concrete results.

		Splitting Tensile Strength (psi)			
Mix	Mix Design	28 days	91 days	Normalized 28 day	Normalized 91 day
1	Control	* 613	695	100%	100%
2	20% C Ash	* 579	687	94%	99%
3	20% CS200	609	718	99%	103%
4	50% Slag	616	784	101%	113%
5	30% C Ash	* 520	847	77%	122%
6	20% C 5% Micron[3]	574	868	94%	125%
7	30% C 10% SCBA	* 618	704	94%	101%
8	20% C 10% SCBA	712	704	116%	101%
9	30% C 5% F	611	773	100%	111%
10	20% C 10% F	545	667	89%	96%
11	20% C 5% Slag	553	718	90%	103%
12	10% RHA	513	717	84%	103%
13	20% C 10% CS200	682	677	111%	97%
14	20% C 10% Slag	633	772	103%	111%
15	30% C 10% F	719	756	117%	109%
16	4% Silica Fume	696	755	114%	109%
17	5% Metakaolin	* 722	743	118%	107%
18	20% C 4% Silica Fume	* 703	784	115%	113%
19	30% C 4% Silica Fume	583	642	95%	92%
20	30% C 5% Metakaolin	663	715	108%	103%
21	20% SCBA	663	675	108%	97%
22	20% F Ash	542	631	88%	91%

* Indicates only two specimens were used to calculate average

6.6. Flexural Strength of Concrete

Splitting tensile strength gives an indication of tensile strength for members undergoing shear failure such as members under compression. The flexural strength of a concrete gives an indication of the strength for members undergoing bending forces such as beams or pavements [223].

6.6.1. Summary of Test Method

Two methods for determining flexural strength are commonly used: third-point and center-point loading. The center-point loading procedure involves loading a simply supported beam using a single loading point in the center of the beam; this method can produce moments in the beam that require additional calculation to determine the modulus of rupture at failure. The second method, ASTM C78 - *Standard Test Method for Flexural Strength of Concrete (Using Simple Beam with Third-Point Loading)* involves loading the top portion of the beam with two loading points, ensuring a constant loading moment between the loading points [19]. The failure is considered valid if it occurs between the loading points. This geometry results in much easier

calculations [19]. In this method, a beam is placed into a frame that supports the bottom of the beam on two semi-cylindrical supports, the beam is then compressed with two semi-cylindrical loading blocks in such a way that the distance between contact points on the beam is equivalent to one-third of the length of the beam span as shown in Figure 6-7. For this investigation, beams of 4” x 4” x 14” were created to ensure that the depth was 1/3 the bottom span length and had 1 inch of overhang on either side of the support blocks.

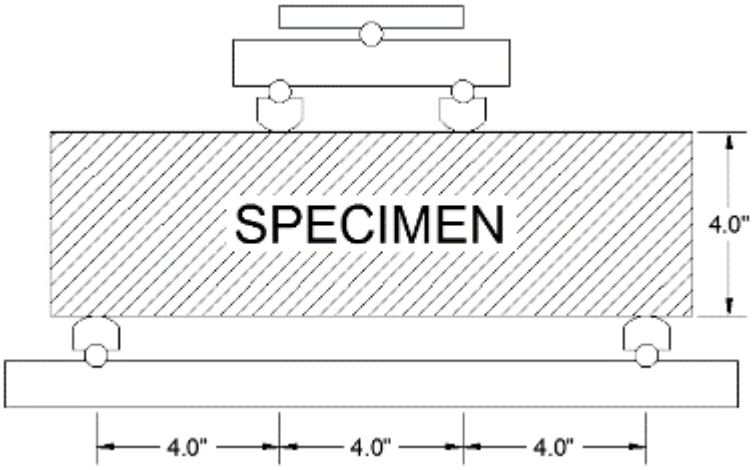

Figure 6-7. Flexural strength testing schematic of 4" x 4" x 14" beam.

6.6.2. Equipment

The required equipment for this test method is a compression frame with a capacity high enough to ensure failure of the specimens (for this investigation, 6,000 lb would be necessary). A frame that could simply support a concrete beam of 4 inches, and a loading head with spherical seated loading blocks. Additionally, the standard calls for the use of ¼” thick leather strips to be used on all bearing faces of the beam should there exist gaps over 0.004”. A pair of calipers is required to measure the failure face of the beam to accurately calculate the flexural strength.

6.6.3. Procedure

The specimens were first stored in limewater for either 28 or 91 days. The specimens were removed from the water storage and had lines drawn on the sides to ensure that the loading surfaces were positioned correctly on the beam. Prior to this investigation, the bottom bearing blocks and top loading blocks were aligned to guarantee proper spacing. The specimens were then loaded onto the bottom bearing block and the top loading blocks were positioned on top of the previously drawn lines. The specimens were then loaded at a rate such that the surface under tension was loaded at a rate of 150 psi/min. The specimens were loaded until failure, at which point the ultimate load on the machine was recorded, and the failure surface was measured for average width and depth. These values were used in Equation (6-2) to determine flexural strength when failure occurred within the loading blocks. Failure outside of the loading blocks did not occur, so alternate equations were not necessary as per ASTM C78 [19]. A typical failed specimen can be seen in Figure 6-8.

$$R = \frac{PL}{bd^2} \quad (6\text{-}2)$$

Where:

R = Modulus of Rupture, psi
P = Maximum applied load indicated by the compression frame, lbf
L = Span length between outermost supports, in
b = Average width of specimen at the fracture, in
d = Average depth of specimen at the fracture, in

Figure 6-8. Typical flexure beam with failure through aggregates.

6.6.4. Flexural Strength of Concrete Results and Discussion

The flexural strength results for all 22 concrete mixes are presented in Table 6-13. None of the measurements were removed as outliers. The only concrete mixes that were less than 95% of the control at 28 days were the 30% C ash and 4% silica fume mixture, and the 20% F Ash mix, which performed at 92% and 94% of the control, respectively. At 91 days, only the 20% C ash mixture performed lower than 95% of the control at 91%. The remainder of the mixes performed comparably or outperformed the control at 91 days. This further shows that even alternative SCM replacements of up to 40% (in the case of 30% C and 10% F ash) can outperform the control at 28 and 91 days. The most surprising performance was that of 20% C ash which showed effectively no strength gain. It should be noted that the 28-day maximum strength of the three flexural specimens for the 20% C ash mix was lower than the maximum strength of the three specimens at 91 days; ultimately, there is no statistical difference between the two ages.

Table 6-13. Flexural strength of concrete results.

Mix	Mix Design	Flexural Strength 28 Days	91 Days	Normalized 28 Days	Normalized 91 Days
1	Control	749	800	100%	100%
2	20% C Ash	733	732	98%	91%
3	20% CS200	737	791	98%	99%
4	50% Slag	831	875	110%	109%
5	30% C Ash	736	785	98%	98%
6	20% C 5% Micron[3]	811	815	108%	102%
7	30% C 10% SCBA	719	793	96%	99%
8	20% C 10% SCBA	805	888	107%	111%
9	30% C 5% F	754	825	101%	103%
10	20% C 10% F	727	770	97%	96%
11	20% C 5% Slag	863	847	115%	106%
12	10% RHA	765	863	102%	108%
13	20% C 10% CS200	820	832	109%	104%
14	20% C 10% Slag	741	846	99%	106%
15	30% C 10% F	763	855	102%	107%
16	4% Silica Fume	864	831	115%	104%
17	5% Metakaolin	887	872	118%	109%
18	20% C 4% Silica Fume	839	887	112%	111%
19	30% C 4% Silica Fume	690	771	92%	96%
20	30% C 5% Metakaolin	763	837	102%	105%
21	20% SCBA	790	800	105%	100%
22	20% F Ash	702	798	94%	100%

6.7. Semi-Adiabatic Calorimetry of Concrete

Temperature rise of concrete has been a concern to the industry for decades with the ever-increasing utilization of mass concrete placements. Temperature rise of concretes and mortars can be evaluated by three main methods: isothermal calorimetry, semi-adiabatic calorimetry, and adiabatic calorimetry. The three different methods provide different hydration conditions; the hydration reaction rates and magnitudes are directly related to the hydration conditions. As explained in Chapter 4, an ideal isothermal calorimeter will remove heat from the hydrating sample instantaneously and maintain a specific temperature throughout the duration of the experiment. A perfect adiabatic calorimeter involves insulating the reacting specimens in a way such that no heat from the specimen is lost to the environment and there is no contribution (addition or subtraction of heat) from the environment. This typically involves high amounts of insulation in conjunction with a closed-loop heating system that monitors the heat evolved from the specimen to maintain (and typically contribute) additional heat such that heat lost to the environment is exactly equivalent to heat input into the system. A semi-adiabatic calorimeter is a device that employs insulation to maintain heat during hydration; however, heat is lost or

gained from the environment without any compensation. For this investigation, the use of an "off-the-shelf" semi-adiabatic calorimeter was used to replicate "field conditions" of concrete more closely than isothermal calorimetry. Buying or constructing an adiabatic calorimeter was outside the scope of the project and would be economically unviable.

6.7.1. Summary of Test Method

Currently there is no ASTM specification regarding the use of a semi-adiabatic calorimeter. The experimental program for this test method involved creating two concrete cylindrical specimens (4" x 8") and placing them into the semi-adiabatic calorimeter that was equipped with thermocouple temperature sensors in the base of the specimen cavity. These thermocouples were connected to a data logger. In order to make results comparable to isothermal paste experiments, the semi-adiabatic calorimeter experiments were performed for the same duration: 7 days.

6.7.2. Equipment

The only equipment required for this experimentation method outside of the equipment required for making the specimens was a Calmetrix™ FA-Fl 4000 – 4-Channel semi-adiabatic calorimeter and a laptop equipped with CalCommander data reading software as shown in Figure 6-9.

Figure 6-9. FA-Fl 4000 Semi-adiabatic calorimeter with laptop running CalCommander software.

6.7.3. Procedure

The procedure involved creating concrete specimens and immediately placing them into the semi-adiabatic calorimeter for a period of seven days. Two replicate specimens were created for each semi-adiabatic experiment, with the remaining two calorimeter channels being left open as "ambient" channels. The information regarding the mix, such as plastic properties and amounts of admixtures, was entered into the CalCommander software. At the conclusion of seven days, the specimens were removed from the calorimeter and the data was downloaded. The average of the heat rise from the cylinders was subtracted from the average of the "ambient" channels to produce a curve of heat rise in degrees Celsius above ambient as a function of time.

6.7.4. Semi-Adiabatic Calorimetry Results and Discussion

The charts of the seven-day semi-adiabatic testing are presented in Appendix D.2. A summary of the average ambient temperature and peak semi-adiabatic temperature rise for each mix is presented in The only exceptions are for 20% C ash, 20% CS200, and 20%C10%SCBA concrete mixes. The data for the 20% C ash and 20% CS200 ground glass mixes were corrupted prior to ending the experiments; the calorimeter has passive monitoring so there is no way to determine if there is a problem before or during the experiment. The data for the 20%C 10%SCBA concrete was never recorded; the software occasionally loses the license number and subsequently runs in "Demo Mode" where it appears to function properly, but will not record data or show any errors.

Every concrete mixture released less heat than the control mixture. The two mixes that produced similar heat rise to the control were the 4% silica fume and 5% metakaolin mixes. Silica fume and metakaolin are both known to vigorously react in a cementitious environment, and the heat rise associated with the inclusion of these materials was expected.

The concrete mixture that produced the least amount of heat was the 30%C 10%SCBA mix, closely followed by the 50% slag mixture, having normalized maximum heat rises of approximately 55% and 63%, respectively. The lowered maximum heat flow of the 30%C 10%SCBA mix was accompanied by a period of extended heat release for several days; this is a similar trend to that seen under isothermal conditions for pastes containing sugarcane bagasse ash. On average, the reduction in maximum heat rise from control is 3.8^{o} C or 28%; this reduction was expected considering that the majority of the mixes replaces cement at over 20%.

Table 6-14. Summary of semi-adiabatic temperature rise results.

Mix	Mix Design	Ambient Temp, °C	Temperature Rise, °C	Time to Peak Temp., hr
1	Control	23.4	13.6	11.5
2	20% C Ash	-	-	-
3	20% CS200	-	-	-
4	50% Slag	22.8	8.0	11.4
5	30% C Ash	23.0	10.2	10.3
6	20% C 5% Micron3	23.1	11.2	10.5
7	30% C 10% SCBA	23.1	7.8	13.8
8	20% C 10% SCBA	-	-	-
9	30% C 5% F	22.8	9.4	10.7
10	20% C 10% F	23.0	9.3	12.6
11	20% C 5% Slag	23.1	10.5	12.1
12	10% RHA	22.9	11.5	18.2
r13	20% C 10% CS200	22.9	9.0	13.1
14	20% C 10% Slag	22.7	9.7	12.3
15	30% C 10% F	22.7	8.5	12.3
16	4% Silica Fume	22.6	12.0	14.3
17	5% Metakaolin	22.5	12.6	15.5
18	20% C 4% Silica Fume	21.4	11.4	14.9
19	30% C 4% Silica Fume	22.4	9.5	11.0
20	30% C 5% Metakaolin	22.5	9.0	10.1
21	20% SCBA	21.9	10.3	14.7
22	20% F Ash	22.0	9.8	10.1

6.8. Surface Resistivity of Concrete

Concrete durability is a topic of great interest as concrete becomes used in a wider array of environments. Concrete durability partly pertains to the ability to resist degradation under environmental factors such as temperature or chemical exposure. Several test methods have been developed to give an indication of the ability of a concrete to withstand certain exposure conditions (deicing salt exposure, freeze-thaw cycles, chloride penetration, and air or water permeability tests, amongst others). These tests can last for several hours in the case of rapid chloride permeability, or several years with different exposure tests. As a means to attempt to indicate durability of concretes, electrical resistance tests have been developed to track the resistance of electricity through the concrete. For this particular investigation, surface resistivity has been chosen as one method to evaluate potential durability, as it has been shown to correlate well to rapid chloride permeability [236].

6.8.1. Summary of Test Method

This test method, AASHTO TP-95 - *Standard Method of Test For Surface Resistivity Indication of Concrete's Ability To Resist Chloride Ion Penetration,* utilizes a 4-pronged Wenner probe that measures concrete resistivity on the surface of a cylindrical specimen [20]. The probes pass

current from one probe to the next, the voltage drop across the tips is then used to calculate a resistance across the probe. This test method essentially shows the evolution of the densification of the concrete microstructure. If one were to compare two concretes, as shown in Figure 6-10, one with a less dense microstructure (more porosity, gel space) and one with denser microstructure (less porosity), the electrical currents must travel further, shown as curved arrows, through the sparser pores to find a pathway from one probe tip to another. This longer travel path results in a higher resistance, which produces a higher voltage drop.

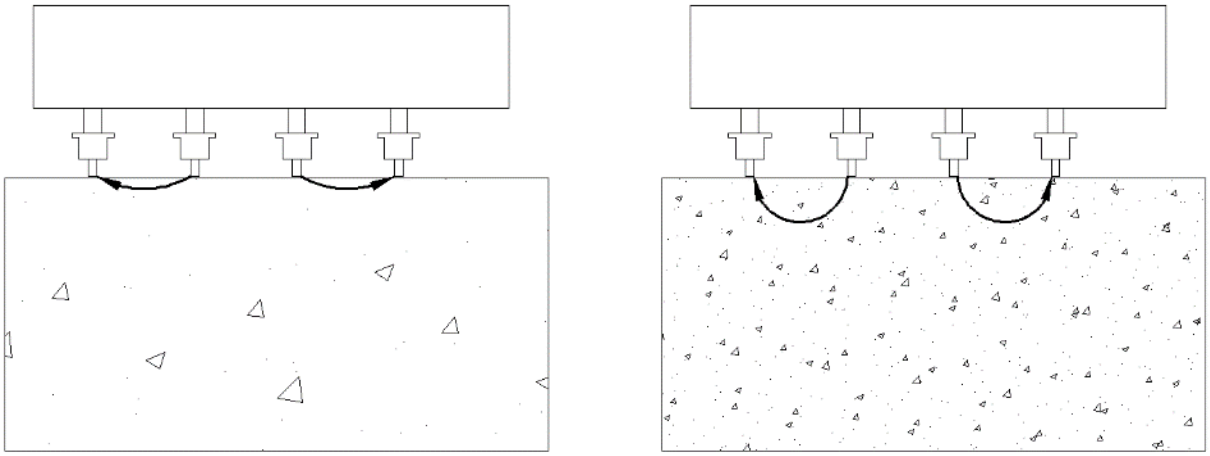

Figure 6-10. Surface resistivity of less dense concrete (left) compared to denser concrete (right).

6.8.2. Equipment

The only equipment required for this evaluation is a surface resistivity meter, shown in Figure 6-11.

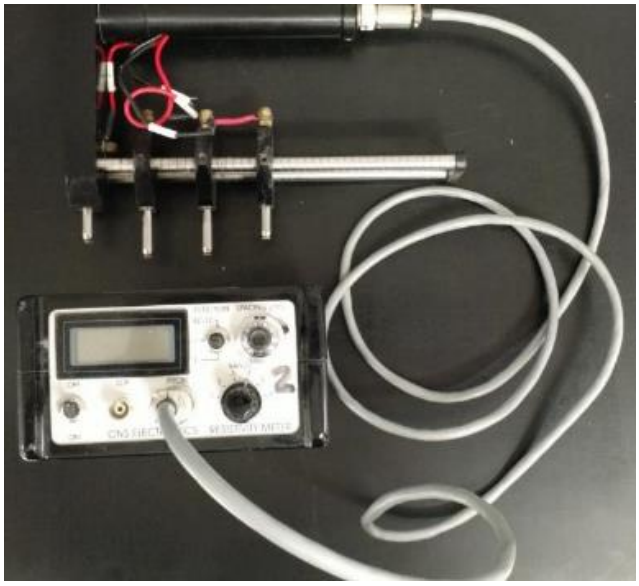

Figure 6-11. CNS Farnell™ surface resistivity probe.

6.8.3. Procedure

Three moist-cured specimens for each concrete mixture were selected to be evaluated for the duration of the experimental program (91 days). These cylinders were removed from storage on day 7 and had 4 lines marked on one face (to indicate quadrants of the cylinder). The cylinder was then laid on its side and 8 measurements were taken around the circumference of the cylinders on the quadrant lines (2 measurements per marking). The cylinders were saturated, with the surface damp but without pooled water, when measured. This test is extremely sensitive to moisture content; thus having a dry specimen will greatly over-estimate resistance. The probe spacing was set at 38 mm. After the measurements are taken, they are averaged for that cylinder, these steps are repeated for the other two cylinders, the three average readings are averaged to get an average reading for the concrete mix at that age. The cylinders are then placed back into curing tanks until the next test age at which point the same cylinders are tested again.

6.8.4. Surface Resistivity Results and Discussion

The results of the surface resistivity of each concrete mix are presented in Appendix D.3, each chart contains the data for the mix of interest as well as the resistivity readings for the control mix as a comparison. The results of the concrete surface resistivity testing revealed that every concrete mix outperformed the control at 28 days and beyond, except for 20% class C fly ash and 20% CS200 glass mixes, which had normalized surface resistivity values of 97% and 98%, respectively. This illustrates that every concrete mixture is at least comparable to the control with respect to surface resistivity, indicating that each blend most likely improved the durability characteristics of the concrete. At seven days, only six mixes outperformed the control; however, the measurements for two mixes (mix 18 and 21) were overlooked at seven days.

Fifteen mixes outperformed the 20% class F fly ash mix in this surface resistivity evaluation. As class F fly ash is considered a highly beneficial material for concrete durability, this would indicate that there are many materials that may match or exceed its impact on concrete durability. A table of the surface resistivity values, as well as normalized resistance values are presented below in Table 6-15.

Table 6-15. Surface resistivity and normalized surface resistivity values of concrete mixes.

		Surface Resistivity, kΩ-cm				Normalized Resistivity, %			
Mix	Mix Design	7	28	56	91	7	28	56	91
1	Control	4.9	6.0	6.9	7.7	100	100	100	100
2	20% C Ash	4.2	5.8	7.5	9.0	86	97	109	118
3	20% CS200	4.3	5.9	9.3	14.0	86	98	135	183
4	50% Slag	6.7	14.2	19.3	24.7	136	237	279	322
5	30% C Ash	4.3	6.6	9.0	11.6[1]	87	110	130	152[1]
6	20% C 5% Micron[3]	4.4	8.1	13.1	17.8[2]	89	135	189	233[2]
7	30% C 10% SCBA	4.6	7.5	10.8	14.3	92	125	157	187
8	20% C 10% SCBA	5.0	8.1	10.6	13.8	102	135	153	181
9	30% C 5% F	4.5	8.1	12.3	15.4	92	134	178	201
10	20% C 10% F	4.4	7.2	-	14.9	89	119	-	195
11	20% C 5% Slag	4.8	8.2	11.0	12.9	97	137	160	168
12	10% RHA	5.0	7.4	10.8	13.7	102	123	156	179
13	20% C 10% CS200	4.4	6.9	11.8	14.6	89	115	171	190
14	20% C 10% Slag	4.5	7.4	10.4	12.6	90	124	151	164
15	30% C 10% F	4.5	8.3	12.5	16.5	91	139	181	216
16	4% Silica Fume	6.3	11.6	16.6	20.8	127	193	240	272
17	5% Metakaolin	7.9	15.0	16.7	19.3	161	251	241	252
18	20% C 4% Silica Fume	-	10.6	17.5[3]	21.4	-	177	253[3]	280
19	30% C 4% Silica Fume	4.1	7.8	11.4	15.5	82	130	165	203
20	30% C 5% Metakaolin	5.0	11.3	13.6	13.7	101	188	197	179
21	20% SCBA	-	6.2	7.7[3]	8.4	-	103	112[3]	110
22	20% F Ash	4.7	6.7[4]	7.3	13.8[5]	94	112[4]	106	179[5]

[1] This measurement took place at 107 days, rather than 91 days.
[2] This measurement took place at 105 days, rather than 91 days.
[3] This measurement took place at 61 days, rather than 56 days.
[4] This measurement took place at 33 days, rather than 28 days.
[5] This measurement took place at 94 days, rather than 91 days.

6.9. Bulk Resistivity of Concrete

In addition to surface resistivity, bulk resistivity of concrete is gaining acceptance as a method of concrete durability assessment. The most apparent shortcoming of the surface resistivity test is that location of measurement will appreciably change the results. With bulk resistivity, the electrical current is passed through the entire specimen from end to end; in this way, the most electrically conductive path through the bulk of the specimen will be measured consistently. This method is sensitive to moisture changes just as the surface resistivity test is, but can be run even faster than the surface resistivity test (seconds compared to minutes).

6.9.1. Summary of Test Method

The bulk resistivity method, proposed by Spragg et al., [221], uses the same 4-tipped Wenner probe as surface resistivity. In this method, the probe tips are connected to stainless steel plates

that are placed on the ends of the cylinders to have the electrical current passed through the entire specimen as shown in Figure 6-12. In between the plates and the concrete specimen are saturated sponges. As the current flows from one end of the specimen to the other, the electricity follows the path of least resistance and gives a value of resistance for the bulk specimen. This measure of resistance is then normalized for the size of the specimen using Equation (6-3).

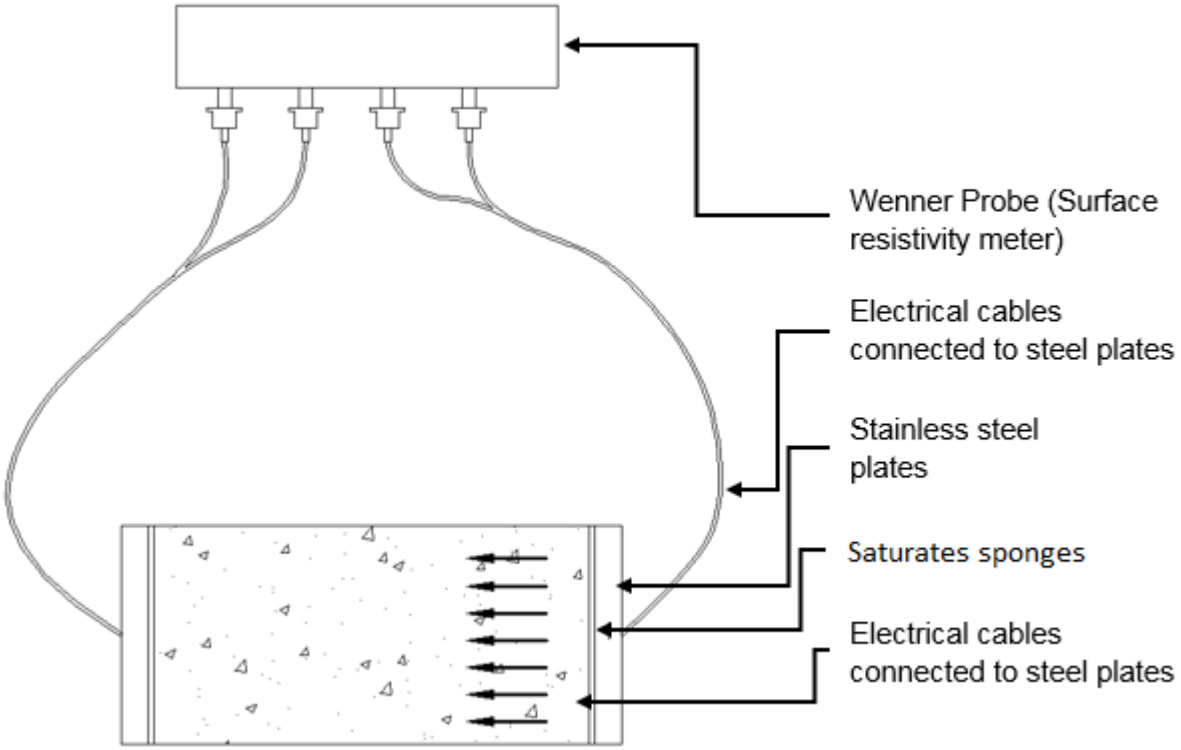

Figure 6-12. Bulk resistivity apparatus.

$$\rho = \frac{R_b \cdot A}{L} \tag{6-3}$$

Where:

ρ = Bulk resistivity, kΩ-cm
R_b = Total resistance measured by Wenner Probe (with sponge resistance removed), kΩ
A = Cross sectional area of specimen, cm^2
L = Length of specimen, cm

6.9.2. Equipment

The equipment required for this evaluation is a surface resistivity meter, stainless steel plates slightly larger than the cross sectional area of the specimen, calipers, sponges, and electrical leads to attach the plates to the probe shown in Figure 6-13.

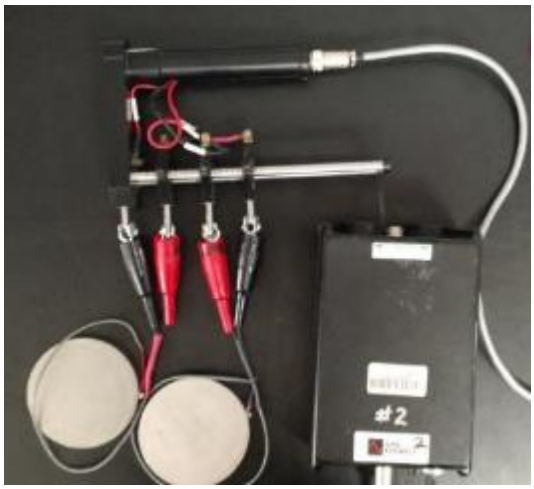

Figure 6-13. CNS Farnell™ surface resistivity probe, with electrical leads connecting the probe to the steel plates.

6.9.3. Procedure

This test method requires the same curing procedure as the surface resistivity test. Additionally, the specimens should have ground or saw cut ends free of voids. The sponges must be saturated prior to beginning this test method. Measuring the resistance is easiest in a vertical manner. To calibrate the sponges, the top sponge is placed between the steel plates and the resistance is recorded. After removing the top sponge, the bottom sponge is then placed between the steel plates, and a cylinder is placed on top of the steel plated (to replicate the amount of force on the bottom plate during measurement). The bottom sponge resistance is then recorded. The bottom sponge is placed on the bottom plate, followed by the specimen, then top sponge, and then the top plate. The meter function is switched from ρ, the default kΩ-cm setting, to Rc/10 for total resistance (the range was set to 3 to increase precision) on the meter control box as shown in Figure 6-14. This resistance is then multiplied by 10 and recorded as R. The resistance of the sponges is then subtracted from the total resistance, R, and is recorded as R_b. The bulk resistance, ρ, is then calculated using the specimen dimensions and Equation (6-3).

Figure 6-14. Resistivity meter controls.

6.9.4. Bulk Resistivity Results and Discussion

The results of the bulk resistivity of each concrete mix are presented in Appendix D.4, each chart contains the data for the mix of interest as well as the resistivity readings for the control mix as a comparison. The results of this investigation showed few differences compared to surface resistivity, with the same general trends appearing for both test methods; this indicated a general agreement of the methods. The measured bulk resistance and normalized bulk resistance measurements are presented in Table 6-16. The measured nominal resistances for the majority of the mixes were higher than the control.

Table 6-16. Bulk resistivity and normalized surface resistivity values of concrete mixes.

		Bulk Resistivity, kΩ-cm				Normalized Resistivity, %			
Mix	Mix Design	7	28	56	91	7	28	56	91
1	Control	2.5	3.3	3.7	4.3	100	100	100	100
2	20% C Ash	2.1	3.0	4.0	5.0	82	90	108	117
3	20% CS200	1.7	3.2	5.8	8.1	68	97	156	190
4	50% Slag	3.4	8.1	10.5	13.5[1]	135	241	284	316[1]
5	30% C Ash	2.2	3.8	5.4	8.1[2]	86	113	144	190[2]
6	20% C 5% Micron[3]	2.4	4.1	7.5	10.7	92	124	202	250
7	30% C 10% SCBA	2.6	4.1	6.4	8.1	100	124	172	190
8	20% C 10% SCBA	2.4	4.1	5.9	9.0	95	121	159	211
9	30% C 5% F	3.1	4.5	7.2	9.5	120	135	194	224
10	20% C 10% F	2.2	4.3	-	9.4	85	130	-	222
11	20% C 5% Slag	2.5	4.3	5.9	7.8	99	130	158	184
12	10% RHA	2.6	4.1	6.2	9.7	103	123	166	228
13	20% C 10% CS200	2.3	4.6	7.4	9.5	89	136	198	224
14	20% C 10% Slag	2.2	4.6	6.9	8.5	88	136	185	199
15	30% C 10% F	2.4	4.5	7.2	9.5	93	136	193	224
16	4% Silica Fume	3.4	6.2	9.4	12.4	133	186	253	292
17	5% Metakaolin	4.0	8.2	8.9	11.4	157	246	239	268
18	20% C 4% Silica Fume	-	5.8	9.8[3]	13.3	-	172	265[3]	311
19	30% C 4% Silica Fume	2.1	4.2	6.5	9.0	83	126	175	211
20	30% C 5% Metakaolin	2.7	6.3	7.9	8.4	107	189	213[3]	197
21	20% SCBA	-	3.3	4.8[3]	5.9	-	98	129	138
22	20% F Ash	2.7	4.3[4]	-	10.9[5]	104	124[4]	-	253[5]

[1] This measurement took place at 107 days, rather than 91 days.
[2] This measurement took place at 105 days, rather than 91 days.
[3] This measurement took place at 61 days, rather than 56 days.
[4] This measurement took place at 33 days, rather than 28 days.
[5] This measurement took place at 108 days, rather than 91 days.

Spragg et al. showed a correlation between bulk/direct resistance and surface resistance, with surface resistance being 1.86 times higher than bulk resistance [237]. A similar trend was seen with the data collected during this investigation; however, the difference between bulk and surface resistance was a factor of 1.69 instead of 1.86, as presented in Figure 6-15.

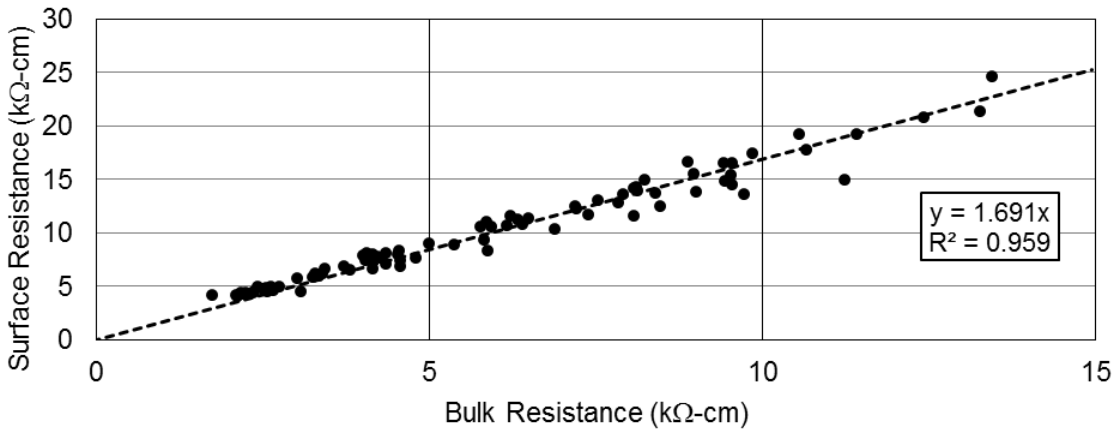

Figure 6-15. Bulk resistance compared to surface resistance of concrete cylinders.

6.10. Coefficient of Thermal Expansion of Concrete

The coefficient of thermal expansion is the expansion of a material, per unit length, per degree as described by Equation (6-4). For concrete materials, the coefficient of thermal expansion, CTE, is typically measured in millionths (of inches per inch or millionths of meters per meter) per degree and is typically around 10 millionths per degree Celsius, or 5.5 millionths per degree Fahrenheit [1]. This unit can also be expressed as microstrain per degree (με/°F or με/°C). This value is critical for long, uninterrupted span lengths (such as traffic lanes, or bridge decks) as the temperature variation over a day could be as high as 20°C in Florida. Over a distance of 100 ft. of concrete, this could amount to over ¼" of length change. As the concrete in traffic lanes or bridge decks is constrained longitudinally by adjacent concrete, this could present a buckling problem. This CTE value is used to space expansion joints in long members for this reason. As such, identifying changes in the CTE of concrete caused by varying the cementitious materials is of importance, especially for transportation engineering.

$$CTE = \frac{\left(\frac{\Delta L}{L}\right)}{\Delta T} \tag{6-4}$$

Where:

ΔL = Change in length due thermal changes, in or mm
L = Original length, in or mm
ΔT = Change in temperature, °F or °C

6.10.1. Summary of Test Method

The evaluation of coefficient of thermal expansion involves taking concrete specimens that are saturated and placing them into a CTE frame that is typically made of metal that has a known coefficient of thermal expansion. Atop this frame is a linear variable differential transformer, or LVDT. This LVDT converts axial motion into an electrical signal that can be converted into distance. The entire frame is placed into a temperature-controlled water bath. The bath is set to 10°C for equilibrium, then ramps to 50°C and waits for equilibrium. The LVDT that rests atop the cylinder measures the distance travelled throughout the temperature ramp. The known

expansion of the frame is subtracted from the LVDT measurement, and the resulting corrected cylinder expansion is divided by the length of the cylinder. This result is then averaged with the corrected CTE value measured during ramping from 50°C to 10°C. The coefficient of thermal expansion testing setup can be seen in Figure 6-16.

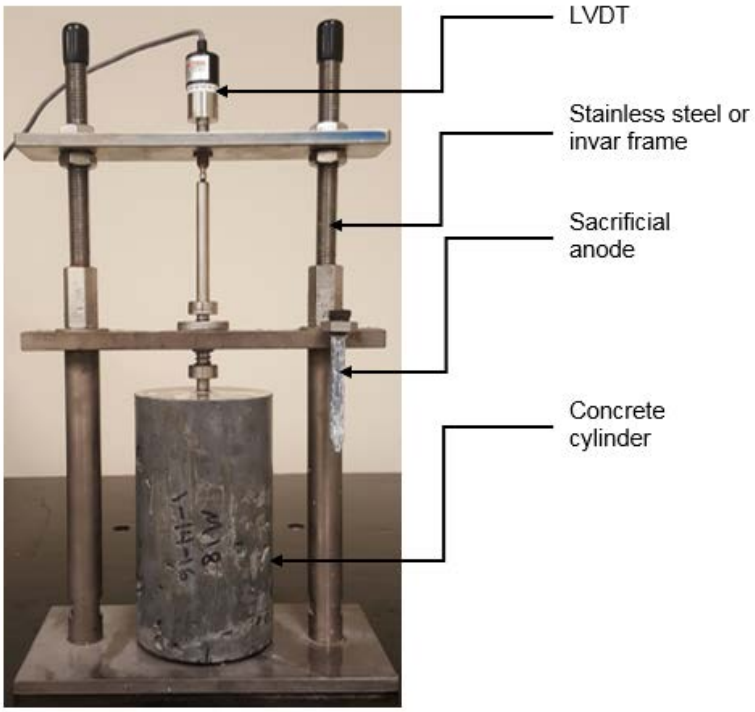

Figure 6-16. Coefficient of thermal expansion frame.

6.10.2. Equipment

The equipment required for this evaluation method includes a temperature-controlled water bath capable of circulating water between 10°C and 50°C and holding temperatures to within 0.1°C, calipers with a precision of 0.1 mm, a rigid frame, temperature measuring devices (thermocouples, thermistors, or resistance temperature detectors), LVDT with a minimum resolution of 0.00001 in, and any calibration equipment to ensure the equipment meets the specifications in the AASHTO T 336-15 Designation – Standard Method of Test for Coefficient of Thermal Expansion of Hydraulic Cement Concrete [22].

6.10.3. Procedure

Preparing the specimen for this evaluation included curing the specimens in limewater for 91 days. The specimens were ground until the length of the specimens were 7 ± 0.01 inches. The specimens were then placed into the frame, assuring that the LVDT was touching the top of the cylinder and the bottom of the cylinder was resting on the support buttons. The frame and cylinder were loaded into the water bath at 20°C. The water bath was set to 10°C and held constant until three successive LVDT readings varied by less than 0.00001 inches over a period of 30 minutes. At this point, the first LVDT reading was taken. The bath was then ramped up to 50°C and held constant until three successive LVDT readings varied by less than 0.00001 inches over a period of 30 minutes. The second LVDT reading was taken; following this the bath was

ramped back down to 10°C and held until the LVDT readings were constant and a final reading was taken. The CTE from 10°C – 50°C was then averaged with the CTE from 50°C – 10°C. The CTE investigations were carried out at Florida Department of Transportation State Materials Office. In order to have more robust results, two cylinders for each mixture were evaluated at a time.

6.10.4. Coefficient of Thermal Expansion of Concrete Results and Discussion

The results of this evaluation, presented in Table 6-17, show relatively little variation with all values falling within approximately 5% of the CTE of the control mix (8.4 microstrain/°C). The mix having the highest coefficient of thermal expansion was the 20% class C fly ash mix at 8.9 µs/°C. This increase would lead to approximately 6% more expansion joints required for large span concrete members when the joint spacing is dependent on thermal expansion. The mixes with the least amount of thermal strain at 8.0 µs/°C were the 20% C ash with 10% sugarcane bagasse ash mix and the 10% rice husk ash mix. The results of this investigation show that none of the materials would prove to be particularly detrimental from an expansion point of view; in fact, some of the mixes exhibited less thermal expansion than the control.

Table 6-17. Results of the coefficient of thermal expansion of concrete testing.

		Coefficient of Thermal Expansion, µs/°C		
Mix	Mix Design	Cylinder 1	Cylinder 2	Average
1	Control	8.6	8.2	8.4
2	20% C Ash	9.2	8.6	8.9
3	20% CS200	8.9	8.6	8.8
4	50% Slag	8.7	8.5	8.6
5	30% C Ash	8.7	8.4	8.5
6	20% C 5% Micron[3]	8.7	8.4	8.5
7	30% C 10% SCBA	8.2	8.5	8.3
8	20% C 10% SCBA	8.0	8.0	8.0
9	30% C 5% F	8.6	8.0	8.3
10	20% C 10% F	8.2	8.5	8.3
11	20% C 5% Slag	8.5	8.5	8.5
12	10% RHA	8.3	7.6	8.0
13	20% C 10% CS200	8.9	8.2	8.5
14	20% C 10% Slag	8.3	8.5	8.4
15	30% C 10% F	8.7	8.8	8.7
16	4% Silica Fume	8.3	8.5	8.4
17	5% Metakaolin	8.8	8.8	8.8
18	20% C 4% Silica Fume	8.5	8.4	8.5
19	30% C 4% Silica Fume	8.9	8.2	8.5
20	30% C 5% Metakaolin	8.6	8.4	8.5
21	20% SCBA	8.5	7.7	8.1
22	20% F Ash	8.3	8.1	8.2

6.11. Summary of Findings for Concrete

The results of the mechanical evaluations are compiled into Table 6-18, which utilizes a color map where yellow color designates comparable performance to the control, red coloring denotes poorer performance, and green denotes superior performance. The numbers provided in the results table are normalized to the control; numbers presented in boldface text are the results that were over 100% of the control. It is immediately evident that several mixes performed much better than the control, notably the mixtures containing the highly reactive pozzolans (Micron[3], silica fume, and metakaolin) and slag. The performance of class F fly ash achieved strength gain at the slowest rate; this was not surprising as the rate of strength gain for class F fly ash amended mixes is known to be reduced at early ages, yet will be satisfactory with respect to control mixes in long term testing [2],[55]. These materials provide proof that less desirable materials such as class C fly ash can be amended with small amounts of well-established SCMs to provide superior performance in concrete.

Table 6-18. Summary of normalized mechanical properties. Values in bold represent performance over 100% of control.

		Compression				Tension		Modulus		Flexure	
Mix	Design	7	28	56	91	28	91	28	91	28	91
1	Control	**100**	**100**	**100**	**100**	**100**	**100**	**100**	**100**	**100**	**100**
2	20% C Ash	90	97	96	96	94	99	99	98	98	91
3	20% CS200	78	87	89	91	99	**103**	93	95	98	99
4	50% Slag	**102**	**119**	**120**	**120**	**101**	**113**	**109**	**110**	**110**	**109**
5	30% C Ash	91	**104**	**104**	**104**	77	**122**	**102**	**102**	98	98
6	20% C 5% Micron[3]	**104**	**109**	**111**	**110**	94	**125**	**105**	**105**	**108**	**102**
7	30% C 10% SCBA	78	93	94	95	94	**101**	97	97	96	99
8	20% C 10% SCBA	**102**	**111**	**108**	**105**	**116**	**101**	**106**	**103**	**107**	**111**
9	30% C 5% F	90	**100**	**103**	99	**100**	**111**	**100**	99	**101**	**103**
10	20% C 10% F	87	99	98	**100**	89	96	99	**100**	97	96
11	20% C 5% Slag	**103**	**111**	**112**	**107**	90	**103**	**105**	**104**	**115**	**106**
12	10% RHA	95	**101**	**101**	97	84	**103**	**100**	98	**102**	**108**
13	20% C 10% CS200	87	**102**	**102**	**104**	**111**	97	**101**	**102**	**109**	**104**
14	20% C 10% Slag	74	94	99	**101**	**103**	**111**	97	**101**	99	**106**
15	30% C 10% F	91	**100**	**103**	**108**	**117**	**109**	**100**	**104**	**102**	**107**
16	4% Silica Fume	**105**	**110**	**112**	**111**	**114**	**109**	**105**	**105**	**115**	**104**
17	5% Metakaolin	**125**	**127**	**121**	**115**	**118**	**107**	**113**	**107**	**118**	**109**
18	20% C 4% Silica Fume	**102**	**112**	**112**	**114**	**115**	**113**	**106**	**107**	**112**	**111**
19	30% C 4% Silica Fume	86	95	95	99	95	92	97	99	92	96
20	30% C 5% Metakaolin	96	**106**	**105**	**100**	**108**	**103**	**103**	**100**	**102**	**105**
21	20% SCBA	89	98	93	95	**108**	97	99	98	**105**	**100**
22	20% F Ash	68	78	82	84	88	91	88	92	94	**100**

What is surprising is that the remaining mixes were at least comparable to the control mixes for nearly every mechanical test. Even the 20% CS200 glass mixture, at 28 days, was almost within

10% of the control. Additionally, sugarcane at 20% and class C fly ash at 20% were comparable to the control, yet when combined they seem to react synergistically in the case of 20% class C fly ash and 10% SCBA. This same synergistic effect was seen when class C fly ash was mixed with ground glass.

Compiling the results of the electrical resistivity data on the concretes in Table 6-19 (using the same color and typeface scheme) provides an insight into the relative performance of the concrete specimens as it pertains to apparently durability. It was expected that 20% class F fly ash would perform better in this suite of tests compared to the mechanical properties; this proved to be the case. It was unexpected that the majority of the mixes would outperform the control mix as well as the class F fly ash mixture. Once again, the highest performance came from materials that are well known in the concrete industry. However, the ternary mixes involving alternative SCMs fared extremely well in both electrical resistivity evaluations leading one to assert that the concrete mixes, as a whole, performed comparable to a class F fly ash mix.

Table 6-19. Summary of normalized resistivity data. Values that are bolded represent performance over 100% of control.

		Surface Res				Bulk Res			
Mix	Design	7	28	56	91	7	28	56	91
1	Control	**100**	**100**	**100**	**100**	**100**	**100**	**100**	**100**
2	20% C Ash	86	97	**109**	**118**	82	90	**108**	**117**
3	20% CS200	86	98	**135**	**183**	68	97	**156**	**190**
4	50% Slag	**136**	**237**	**279**	**322**	**135**	**241**	**284**	**316**
5	30% C Ash	87	**110**	**130**	**152**	86	**113**	**144**	**190**
6	20% C 5% Micron[3]	89	**135**	**189**	**233**	92	**124**	**202**	**250**
7	30% C 10% SCBA	92	**125**	**157**	**187**	**100**	**124**	**172**	**190**
8	20% C 10% SCBA	**102**	**135**	**153**	**181**	95	**121**	**159**	**211**
9	30% C 5% F	92	**134**	**178**	**201**	**120**	**135**	**194**	**224**
10	20% C 10% F	89	**119**	-	**195**	85	**130**	-	**222**
11	20% C 5% Slag	97	**137**	**160**	**168**	99	**130**	**158**	**184**
12	10% RHA	**102**	**123**	**156**	**179**	**103**	**123**	**166**	**228**
13	20% C 10% CS200	89	**115**	**171**	**190**	89	**136**	**198**	**224**
14	20% C 10% Slag	90	**124**	**151**	**164**	88	**136**	**185**	**199**
15	30% C 10% F	91	**139**	**181**	**216**	93	**136**	**193**	**224**
16	4% Silica Fume	**127**	**193**	**240**	**272**	**133**	**186**	**253**	**292**
17	5% Metakaolin	**161**	**251**	**241**	**252**	**157**	**246**	**239**	**268**
18	20% C 4% Silica Fume	-	**177**	**253**	**280**	-	**172**	**265**	**311**
19	30% C 4% Silica Fume	82	**130**	**165**	**203**	83	**126**	**175**	**211**
20	30% C 5% Metakaolin	**101**	**188**	**197**	**179**	**107**	**189**	**213**	**197**
21	20% SCBA	-	**103**	**112**	**110**	-	98	**129**	**138**
22	20% F Ash	94	**112**	**106**	**179**	**104**	**124**	-	**253**

With regards to the main hypothesis of this study, “Waste stream materials can be utilized as cement additions at replacement levels of 20% or more to create Florida concretes that are comparable to 20% class F fly ash concrete with respect to plastic properties, structural adequacy, and durability,” the plastic properties, mechanical properties and durability properties can be normalized to the 20% class F fly ash mixture to easily compare performance.

Based upon the plastic properties reported in Table 6-9, the use of the proper dosages of admixtures, any of the concrete mixtures proposed can provide satisfactory slump, air content, and setting time. With respect to mechanical properties, taking the information that is presented in Table 6-18 and normalizing to the 20% class F fly ash performance, colored coding such that any mixture not performing to at least 90% of the 20% F ash mixture is red, and all others are green, it can be seen that every mix was at least comparable (within 10%) at 91 days with any test method; this information is presented in Table 6-20. Similarly, the electrical resistivity data is presented the in the same fashion. The resistivity data collected from surface and bulk resistivity was converted to equivalent classes of chloride ion permeability based upon the work performed by Ardani, [238], and Spragg et al., [237]; the classes are “high permeability” (red), “moderate permeability” (yellow), and “low permeability” (green). The resistance requirements for each of the chloride permeability classifications are presented in Table 6-21. The information presented in Table 6-22 shows that the majority of concrete mixtures would be in the same or better class as the 20% class F fly ash mix with regards to chloride ion permeability. In summary, it has been shown that there are pozzolanic materials not currently in use by the FDOT that can be used to replace class F fly ash in concrete, resulting in comparable performance.

Table 6-20. Mechanical properties normalized to the 20% class F fly ash performance.

		Compression				Tension		Modulus		Flexure	
Mix	Design	7	28	56	91	28	91	28	91	28	91
1	Control	147	129	122	119	113	110	114	109	107	100
2	20% C Ash	132	125	118	114	107	109	112	107	104	92
3	20% CS200	115	113	109	108	112	114	106	104	105	99
4	50% Slag	150	153	146	143	114	124	124	119	117	110
5	30% C Ash	134	134	127	123	87	134	116	111	105	98
6	20% C 5% Micron[3]	153	141	135	130	106	138	119	114	116	102
7	30% C 10% SCBA	115	120	115	112	107	112	110	106	102	99
8	20% C 10% SCBA	150	144	131	125	131	112	120	112	115	111
9	30% C 5% F	132	129	125	117	113	123	114	108	107	103
10	20% C 10% F	128	127	119	119	101	106	113	109	104	96
11	20% C 5% Slag	152	143	137	128	102	114	120	113	123	106
12	10% RHA	140	130	124	115	95	114	114	107	109	108
13	20% C 10% CS200	128	131	125	124	126	107	115	111	117	104
14	20% C 10% Slag	109	121	121	120	117	122	110	110	106	106
15	30% C 10% F	133	128	126	128	133	120	113	113	109	107
16	4% Silica Fume	154	142	137	132	128	120	119	115	123	104
17	5% Metakaolin	184	163	148	137	133	118	128	117	126	109
18	20% C 4% Silica Fume	150	144	137	136	130	124	120	117	120	111
19	30% C 4% Silica Fume	127	122	116	117	108	102	111	108	98	97
20	30% C 5% Metakaolin	142	137	128	119	122	113	117	109	109	105
21	20% SCBA	130	126	113	113	122	107	112	106	113	100
22	20% F Ash	100	100	100	100	100	100	100	100	100	100

Table 6-21. Chloride ion permeability classification based upon electrical resistivity.

ASTM C1202 Chloride Permeability	Surface Resistivity, kΩ-cm (Ardani, 2012)	Bulk Resistivity, kΩ-cm (Spragg et al., 2010)
High	< 9.7	< 5.2
Moderate	9.7 - 19.3	5.2 - 10.4
Low	19.3 - 38.6	10.4 - 20.8

Table 6-22. Electrical resistivity data with chloride ion permeability class denoted by color.

		Surface Res				Bulk Res			
Mix	Design	7	28	56	91	7	28	56	91
1	Control	4.9	6.0	6.9	7.7	2.6	3.3	3.7	4.3
2	20% C Ash	4.2	5.8	7.5	9.0	2.1	3.0	4.0	5.0
3	20% CS200	4.3	5.9	9.3	14.0	1.7	3.2	5.8	8.1
4	50% Slag	6.7	14.2	19.3	24.7	3.4	8.1	10.6	13.5
5	30% C Ash	4.3	6.6	9.0	11.6	2.2	3.8	5.4	8.1
6	20% C 5% Micron[3]	4.4	8.1	13.1	17.8	2.4	4.1	7.5	10.7
7	30% C 10% SCBA	4.6	7.5	10.8	14.3	2.6	4.1	6.4	8.1
8	20% C 10% SCBA	5.0	8.1	10.6	13.8	2.4	4.1	5.9	9.0
9	30% C 5% F	4.5	8.1	12.3	15.4	3.1	4.5	7.2	9.5
10	20% C 10% F	4.4	7.2	-	14.9	2.2	4.3	-	9.4
11	20% C 5% Slag	4.8	8.2	11.0	12.9	2.5	4.3	5.9	7.8
12	10% RHA	5.0	7.4	10.8	13.7	2.6	4.1	6.2	9.7
13	20% C 10% CS200	4.4	6.9	11.8	14.6	2.3	4.6	7.4	9.5
14	20% C 10% Slag	4.5	7.4	10.4	12.6	2.2	4.6	6.9	8.5
15	30% C 10% F	4.5	8.3	12.5	16.5	2.4	4.5	7.2	9.5
16	4% Silica Fume	6.3	11.6	16.6	20.8	3.4	6.2	9.4	12.4
17	5% Metakaolin	7.9	15.0	16.7	19.3	4.0	8.2	8.9	11.4
18	20% C 4% Silica Fume	-	10.6	17.5	21.4	-	5.8	9.8	13.3
19	30% C 4% Silica Fume	4.1	7.8	11.4	15.5	2.1	4.2	6.5	9.0
20	30% C 5% Metakaolin	5.0	11.3	13.6	13.7	2.7	6.3	7.9	8.4
21	20% SCBA	-	6.2	7.7	8.4	-	3.3	4.8	5.9
22	20% F Ash	4.7	6.7	7.3	13.8	2.7	4.3	-	10.9

Note:
Colors represent penetration classes as given by Table 6-21.
Red: High Penetration
Yellow: Moderate Penetration
Green: Low Penetration

7. CONCLUSONS, OBSERVATIONS, AND RECOMMENDATIONS FOR FUTURE WORK

7.1. Background

Reduced availability and increased demand for class F fly ash will continue to pose potential fly ash supply problems, especially in regions that are not close to a source. To avoid future problems stemming from inevitable fly ash supply shortages in the future, the FDOT chose to explore alternative materials that can be used to replace some or all the fly ash that is currently required in FDOT concrete mixes. Thus the primary objective of this research was to evaluate pozzolanic materials that are not currently in use by the FDOT . This research incorporated material characterization with regards to physical and chemical properties, workability characteristics, mechanical properties, and durability characteristics of binary- and ternary-blended mortars and concretes. Since the goal was to find replacements for class F fly ash, performance was compared to that of mortars and concretes containing a 20% replacement of portland cement with class F fly ash.

7.2. Research Objectives

The primary objective of this research project was to identify potential alternative pozzolanic materials not currently in use by the FDOT that can be employed to partially or completely replace class F fly ash in FDOT concrete with no significant decrease in performance with respect to plastic, mechanical, and durability properties. Recommendations borne from analysis of the results of this investigation were expected to include revisions of some sections of the FDOT Standard Specifications for Road & Bridge Construction.

7.3. Conclusions

The following conclusions were drawn from this study as follows:

- Supplementary cementitious materials investigated in this study were used to replace class F fly ash in portland cement concrete in binary and ternary mixtures. Binary mixes incorporating ground glass or class C fly ash in the appropriate proportions performed comparably to class F fly ash concrete. While Class C fly ash replacement is not a permanent solution it can be used to limit the use of Class F fly ash mixes in ternary mixes by incorporating class C fly ash and either micron^3 ultrafine fly ash, sugarcane bagasse ash, class F fly ash, slag, ground glass, silica fume or metakaolin. In the appropriate proportions, such mixes are expected to perform comparably (and in some cases better) to class F fly ash concrete.
- The class C fly ash received for this research project did not show deleterious characteristics that are commonly reported in the literature. Class C fly ash can be blended with a highly siliceous material to re-qualify it as a class F fly ash that performs comparably or superior to control concretes based on a variety of qualifying metrics.
- Portland cement concrete mixtures, which incorporated sugarcane bagasse ash having loss on ignition values exceeding 25%, showed no deleterious effects on the air content of normal concrete. However, further study of concrete and mortar which contains

sugarcane bagasse ash with loss on ignition values within the limits of ASTM C618 should be evaluated.
- Binary mixes incorporating ground glass or class C fly ash in the appropriate proportions performed comparably to concrete containing class F fly ash.
- Ternary mixes incorporating class C fly ash and either Micron^3 ultrafine fly ash, sugarcane bagasse ash, class F fly ash, slag, ground glass, silica fume, or metakaolin in the appropriate proportions performed comparably to concrete with class F fly ash.
- The use of ground glass, with an average particle size of less than 20 microns, can be used to replace portland cement in concrete at replacement levels of 20% or lower.
- Rice husk ash was found to have a propensity for deleterious reactions based on results from the accelerated alkali silica reactivity test (ASTM C 1260).
- There are a number of sources of alternative pozzolans in Florida that may be used as a replacement for Class F fly ash.
- The maturity method and equivalent-age concepts are not appropriate for applying to mortars containing alternative supplementary materials; the curve-fitting functions do not adequately describe strength-time relationships.

7.4. Observations

- Binary concrete mixes containing ground blast furnace slag, silica fume, or metakaolin were tested to show baseline performance prior to ternary blending. These mixes performed similar to what is reported in the
- For the determination of carbon content versus sulfur content, thermogravimetric analysis should be utilized rather than loss on ignition.
- Concretes using high LOI materials showed no difference in air contents than those made from low LOI materials, although high entrained air contents were not attempted.
- The use of a laser particle analyzer provides different results depending upon the dispersion method. The measurement of particle size in an air column resulted in a larger reported particle size compared to a fluid suspension.
- With the exception of class C coal fly ash, none of the alternative materials qualify as a slag, silica fume, or class C, F, or N fly ash per ASTM specifications C1240, C989, or C618.
- The Blaine fineness test, ASTM C204, is inappropriate for evaluating alternative supplementary cementitious materials. The Brunauer-Emmett-Teller, BET, method is more applicable for determination of material specific surface area.
- The direct tensile strength of mortars was not able to show significant differences between the SCMs evaluated.
- The bulk resistivity method is less variable than the surface resistivity method as an indicator of durability. Ultimately, this method is more conservative as it relies on the path of least resistance through the specimen.
- The coefficient of thermal expansion of concretes was largely unaffected by the additions of SCMs.

7.5. Recommendations for FDOT Specification Revision

Based upon the findings from this study, the following recommendations are suggested:

- Revise the FDOT Standard Specification for Road and Bridge Construction Section 929 to make allowances for the use of Class N fly ash that does not meet ASTM C618 with respect to loss on ignition only.
- Revise the FDOT Standard Specification for Road and Bridge Construction Section 929 to make allowances for the use of Class C fly ash that meets ASTM C618, to be used for structures placed in non-aggressive environments.
- Consider revising the FDOT Standard Specification for Road and Bridge Construction Section 929 to make allowances for the use of Class C fly ash in ternary systems that contain granulated blast furnace slag, Class F fly ash, silica fume, or metakaolin for use in structures placed in moderately and extremely aggressive environments.

7.6. Recommendations for Future Work

The following recommendations are based on the conclusions and observations of this study:

- The research conducted in this study indicates that alternative pozzolans including sugarcane bagasse ash, rice husk, ground glass, and equilibrium catalyst should be investigated further to determine their suitability for use in concrete. The experiments performed in this study were limited to unprocessed materials as received from the respective producers. Initial research indicated that the processing of the alternative pozzolans may beneficially affect performance.
- Sulfate and/or chloride exposure tests should be performed prior to qualification of concrete materials containing alternative pozzolans for use in FDOT concrete mixes in all environments.
- Sugarcane bagasse ash and ground glass should be investigated further to determine threshold values for replacement level, particle size, optimum processing (bagasse ash), and long-term chloride and sulfate durability.
- Alternative pozzolans should be tested for alkali-carbonate reaction due to Florida coarse aggregate potentially containing dolomitic limestone.

REFERENCES

[1] S. Kosmatka and B. Wilson, *Design and Control of Concrete Mixtures*, 16th ed. Skokie, Il: Portland Cement Association, 2016.

[2] S. Mindess, F. Young, and D. Darwin, *Concrete*. Upper Saddle River, NJ: Prentice-Hall, Inc., 2003.

[3] V. Malhotra and P. K. Mehta, *Pozzolanic and Cementitious Materials*, vol. 1. United Kingdom: Gordon and Breach Publishers, 1996.

[4] ACAA, "2012 Coal Combustion Product (CCP) Production and Use Survey Report." American Coal Ash Association, 2013.

[5] ASTM C1437, "Standard Test Method for Flow of Hydraulic Cement Mortar," ASTM International, West Conshohocken, PA, 2013.

[6] ASTM C403, "Standard Test Method for Time of Setting of Concrete Mixtures by Penetration Resistance," ASTM International, West Conshohocken, PA, 2008.

[7] ASTM C109, "Standard Test Method for Compressive Strength of Hydraulic Cement Mortars (Using 2-in. or [50-mm] Cube Specimens)," ASTM International, West Conshohocken, PA, 2013.

[8] ASTM C1074, "Standard Practice for Estimating Concrete Strength by the Maturity Method," ASTM International, West Conshohocken, PA, 2011.

[9] ASTM C307, "Standard Test Method for Tensile Strength of Chemical-Resistant Mortar, Grouts, and Monolithic Surfacings," ASTM International, West Conshohocken, PA, 2012.

[10] ASTM C157/157M, "Standard Test Method for Length Change of Hardened Hydraulic-Cement Mortar and Concrete," ASTM International, West Conshohocken, PA, 2008.

[11] ASTM C1260, "Standard Test Method for Potential Alkali Reactivity of Aggregates (Mortar-Bar Method)," ASTM International, 100 Barr Harbor Drive, PO Box C700, West Conshohocken, PA, 19428-2959, 2014.

[12] ASTM C143/143M, "Standard Test Method for Slump of Hydraulic-Cement Concrete," ASTM International, West Conshohocken, PA, 2012.

[13] ASTM C1064/1064M, "Standard Test Method for Temperature of Freshly Mixed Hydraulic-Cement Concrete," ASTM International, West Conshohocken, PA, 2013.

[14] ASTM C173, "Standard Test Method for Air Content of Freshly Mixed Concrete by the Volumetric Method," ASTM International, West Conshohocken, PA, 2016.

[15] ASTM C138/138M, "Standard Test Method for Density (Unit Weight), Yield, and Air Content (Gravimetric) of Concrete," ASTM International, West Conshohocken, PA, 2013.

[16] ASTM C39, “Standard Test Method for Compressive Strength of Cylindrical Concrete Specimens,” ASTM International, West Conshohocken, PA, 2016.

[17] ASTM C496, “Standard Test Method for Splitting Tensile Strength of Cylindrical Concrete Specimens,” ASTM International, West Conshohocken, PA, 2011.

[18] ASTM C469, “Standard Test Method for Static Modulus of Elasticity and Poisson’s Ratio of Concrete in Compression,” ASTM International, West Conshohocken, PA, 2014.

[19] ASTM C78/78M, “Standard Test Method for Flexural Strength of Concrete (Using Simple Beam with Third-Point Loading),” ASTM International, West Conshohocken, PA, 2010.

[20] AASHTO TP-95, “Standard Method of Test For Surface Resistivity Indication of Concrete’s Ability To Resist Chloride Ion Penetration.” AASHTO, 2014.

[21] AASHTO TP-119, “Standard Method of Test for Electrical Resistivity of a Concrete Cylinder Tested in a Uniaxial Resistance Test.” AASHTO, 2015.

[22] AASHTO T-336, “Standard Method of Test for Coefficient of Thermal Expansion of Hydraulic Cement Concrete.” AASHTO, 2011.

[23] FDOT, “Standard Specification for Road and Bridge Construction.” Florida Department of Transportation, 2015.

[24] H. van Oss, “U.S. Geological Survey, Mineral Commodity Summaries,” USGS, 2014.

[25] S. Seraj *et al.*, “Evaluating the Performance of Alternative Supplementary Cementing Material in Concrete,” University of Texas at Austin, Austin, TX, Technical Report FHWA/TX-14/0-6717-1, Oct. 2014.

[26] M. Boháč, M. Palou, R. Novotný, J. Másilko, D. Všianský, and T. Staněk, “Investigation on early hydration of ternary Portland cement-blast-furnace slag–metakaolin blends,” *Constr. Build. Mater.*, vol. 64, pp. 333–341, Aug. 2014.

[27] K. Celik, C. Meral, A. Petek Gursel, P. K. Mehta, A. Horvath, and P. J. M. Monteiro, “Mechanical properties, durability, and life-cycle assessment of self-consolidating concrete mixtures made with blended portland cements containing fly ash and limestone powder,” *Cem. Concr. Compos.*, vol. 56, pp. 59–72, Feb. 2015.

[28] Y. Kocak and S. Nas, “The effect of using fly ash on the strength and hydration characteristics of blended cements,” *Constr. Build. Mater.*, vol. 73, pp. 25–32, Dec. 2014.

[29] K. Kuder, D. Lehman, J. Berman, G. Hannesson, and R. Shogren, “Mechanical properties of self consolidating concrete blended with high volumes of fly ash and slag,” *Constr. Build. Mater.*, vol. 34, pp. 285–295, Sep. 2012.

[30] N. M. Piatak, M. B. Parsons, and R. R. Seal II, “Characteristics and environmental aspects of slag: a review,” *Appl. Geochem.*, vol. 57, pp. 236–266, 2015.

[31] F. Sanchez and K. Sobolev, “Nanotechnology in concrete – A review,” *Constr. Build. Mater.*, vol. 24, no. 11, pp. 2060–2071, Nov. 2010.

[32] M. E.-S. I. Saraya, “Study physico-chemical properties of blended cements containing fixed amount of silica fume, blast furnace slag, basalt and limestone, a comparative study,” *Constr. Build. Mater.*, vol. 72, pp. 104–112, Dec. 2014.

[33] M. Schneider, M. Romer, M. Tschudin, and H. Bolio, “Sustainable cement production—present and future,” *Cem. Concr. Res.*, vol. 41, no. 7, pp. 642–650, Jul. 2011.

[34] C. Shi and J. Qian, “High performance cementing materials from industrial slags — a review,” *Resour. Conserv. Recycl.*, vol. 29, no. 3, pp. 195–207, Jun. 2000.

[35] M. Thomas, “The effect of supplementary cementing materials on alkali-silica reaction: A review,” *Cem. Concr. Res.*, vol. 41, no. 12, pp. 1224–1231, Dec. 2011.

[36] P. E. Tsakiridis, G. D. Papadimitriou, S. Tsivilis, and C. Koroneos, “Utilization of steel slag for Portland cement clinker production,” *J. Hazard. Mater.*, vol. 152, no. 2, pp. 805–811, Apr. 2008.

[37] Q. Wang, J. Feng, and P. Yan, “The microstructure of 4-year-old hardened cement-fly ash paste,” *Constr. Build. Mater.*, vol. 29, pp. 114–119, Apr. 2012.

[38] Z. T. Yao *et al.*, “A comprehensive review on the applications of coal fly ash,” *Earth-Sci. Rev.*, vol. 141, pp. 105–121, Feb. 2015.

[39] J. Zhu, Q. Zhong, G. Chen, and D. Li, “Effect of particle size of blast furnace slag on properties of portland cement,” *Procedia Eng.*, vol. 27, pp. 231–236, Jan. 2012.

[40] E. Aprianti, P. Shafigh, S. Bahri, and J. N. Farahani, “Supplementary cementitious materials origin from agricultural wastes – A review,” *Constr. Build. Mater.*, vol. 74, pp. 176–187, Jan. 2015.

[41] M. Berra, T. Mangialardi, and A. E. Paolini, “Reuse of woody biomass fly ash in cement-based materials,” *Constr. Build. Mater.*, vol. 76, pp. 286–296, Feb. 2015.

[42] B. Carrasco, N. Cruz, J. Terrados, F. A. Corpas, and L. Pérez, “An evaluation of bottom ash from plant biomass as a replacement for cement in building blocks,” *Fuel*, vol. 118, pp. 272–280, Feb. 2014.

[43] M. Carsana, M. Frassoni, and L. Bertolini, “Comparison of ground waste glass with other supplementary cementitious materials,” *Cem. Concr. Compos.*, vol. 45, pp. 39–45, Jan. 2014.

[44] W. Chalee, T. Sasakul, P. Suwanmaneechot, and C. Jaturapitakkul, “Utilization of rice husk–bark ash to improve the corrosion resistance of concrete under 5-year exposure in a marine environment,” *Cem. Concr. Compos.*, vol. 37, pp. 47–53, Mar. 2013.

[45] G. C. Cordeiro, R. D. Toledo Filho, L. M. Tavares, and E. M. R. Fairbairn, “Pozzolanic Activity and Filler Effect of Sugar Cane Bagasse Ash in Portland Cement and Lime Mortars,” *Cem. Concr. Compos.*, vol. 30, no. 5, pp. 410–418, May 2008.

[46] R. Madandoust and R. Ghavidel, “Mechanical properties of concrete containing waste glass powder and rice husk ash,” *Biosyst. Eng.*, vol. 116, no. 2, pp. 113–119, Oct. 2013.

[47] A. M. Matos and J. Sousa-Coutinho, “Durability of mortar using waste glass powder as cement replacement,” *Constr. Build. Mater.*, vol. 36, pp. 205–215, Nov. 2012.

[48] A. Sales and S. A. Lima, “Use of Brazilian sugarcane bagasse ash in concrete as sand replacement,” *Waste Manag.*, vol. 30, no. 6, pp. 1114–1122, Jun. 2010.

[49] C. Shi and K. Zheng, “A review on the use of waste glasses in the production of cement and concrete,” *Resour. Conserv. Recycl.*, vol. 52, no. 2, pp. 234–247, Dec. 2007.

[50] P. Hewlett, *Lea’s Chemistry of Cement and Concrete*, 4th ed. Elsevier Ltd, 2006.

[51] H. LeChatlier, *Experimental Researches on the Constitution of Hydraulic Mortars*. New York: McGraw, New York., 1905.

[52] G. K. Hoffman, “Pozzolans and Supplementary Cementitious Materials,” in *Industrial Minerals and Rocks*, Society for Mining, Metallurgy, and Exploration, 2006, pp. 1161–1172.

[53] V. Malhotra, “Role of Fly Ash in Reducing Greenhouse Gas Emissions During the Manufacturing of Portland Cement Clinker,” in *Advances in concrete technologies in the Middle East*, 2008, pp. 19–20.

[54] R. L. Virta, “Minerals Commodity Summaries 2015,” United States Geological Society, Jan. 2015.

[55] A. Neville, *Properties of Concrete*. Prentice Hall, 2011.

[56] R. Siddique and M. I. Khan, *Supplementary Cementing Materials*. Springer, 2011.

[57] C. Pedrajas, V. Rahhal, and R. Talero, “Determination of Characteristic Rheological Parameters in Portland Cement Pastes,” *Constr. Build. Mater.*, vol. 51, pp. 484–491, Jan. 2014.

[58] H. van Oss, “Background Facts and Issues Concerning Cement and Cement Data,” US Department of the Interior & USGS, Open-File Report 1152, 2005.

[59] ASTM C150, “Standard Specification for Portland Cement,” ASTM International, 100 Barr Harbor Drive, PO Box C700, West Conshohocken, PA, 19428-2959, 2016.

[60] CEN, “BS EN 197-1: 2011 Cement Composition, Specification and Conformity Criteria for Common Cements.” British Standards Institute, 2011.

[61] ASTM C595, “Standard Specification for Blended Hydraulic Cements,” ASTM International, West Conshohocken, PA, 2016.

[62] X. Guo, H. Shi, L. Chen, and W. A. Dick, “Alkali-Activated Complex Binders from Class C Fly Ash and Ca-Containing Admixtures,” *J. Hazard. Mater.*, vol. 173, no. 1–3, pp. 480–486, Jan. 2010.

[63] M. Sumer, “Compressive Strength and Sulfate Resistance Properties of Concretes Containing Class F and Class C Fly Ashes,” *Constr. Build. Mater.*, vol. 34, pp. 531–536, Sep. 2012.

[64] G. Camarini and J. A. De Milito, “Gypsum hemihydrate–cement blends to improve renderings durability,” *Constr. Build. Mater.*, vol. 25, no. 11, pp. 4121–4125, Nov. 2011.

[65] L. Fei and L. M. Zhang, “Effects of Gypsum on Cementitious Systems with Different Mineral Mixtures,” *Key Eng. Mater.*, vol. 509, pp. 20–25, 2012.

[66] C. Famy, K. L. Scrivener, and A. R. Brough, “Role of Microstructural Characterisation in Understanding the Mechanism of Expansion Due to Delayed Ettringite Formation,” in *Internal Sulfate Attack and Delayed Ettringite Formation*, Switzerland: RILEM Publications S.A.R.L., 2002, pp. 167–172.

[67] J. Skalny, J. Marchand, and I. Odler, *Sulfate Attack on Concrete*. Spon Press, 2002.

[68] M. Thomas and T. Ramlochan, “Field cases of delayed ettringite formation,” *Int. RILEM TC*, pp. 85–97, 2002.

[69] P. Wedding and L. Spellman, “Some Opportunities to Offset Poor Quality Characteristics of High-Alkali Cement,” *Cem. Concr. Aggreg.*, vol. 5, no. 1, p. 73, 1983.

[70] H. Taylor, *Cement Chemistry*, 2nd ed. London: Thomas Telford Publishing, 2004.

[71] S. V. Vassilev, D. Baxter, L. K. Andersen, and C. G. Vassileva, “An overview of the chemical composition of biomass,” *Fuel*, vol. 89, no. 5, pp. 913–933, May 2010.

[72] T. Ichikawa and M. Miura, “Modified model of alkali-silica reaction,” *Cem. Concr. Res.*, vol. 37, no. 9, pp. 1291–1297, Sep. 2007.

[73] Z. Xu and R. D. Hooton, “Migration of alkali ions in mortar due to several mechanisms,” *Cem. Concr. Res.*, vol. 23, no. 4, pp. 951–961, Jul. 1993.

[74] R. F. Blanks, “Effect of Alkalis in Portland Cement on the Durability of Concretes,” *ASTM Bull. 142*, 1946.

[75] E. D. Hill, “Alkali Limits for Prevention of Alkali-Silica Reaction: A Brief Review of their Development,” *Cem. Concr. Aggreg.*, vol. 18, no. 1.

[76] ACI Committee 221, “State-of-the-Art Report on Alkali-Aggregate Reactivity,” Federal Highway Administration and American Concrete Institute International, 31, 2003.

[77] R. Lane and J. Best, “Properties of Fly Ash in Portland Cement Concrete,” 1982.

[78] C. Ferraro, “Determination of Test Methods for the Prediction of the Behavior of Mass Concrete,” Dissertation, University of Florida, Gainesville, FL, 2009.

[79] P. K. Mehta and D. Pritz, “Use of Rice Hull Ash to Reduce Temperature in High-Strength Mass Concrete.,” *ACI J.*, vol. 4, 1978.

[80] X.-Y. Wang, H.-K. Cho, and H.-S. Lee, “Prediction of temperature distribution in concrete incorporating fly ash or slag using a hydration model,” *Compos. Part B Eng.*, vol. 42, no. 1, pp. 27–40, Jan. 2011.

[81] J. I. Escalante-Garcia, G. Mendoza, and J. H. Sharp, “Indirect determination of the Ca/Si ratio of the C-S-H gel in Portland cements,” *Cem. Concr. Res.*, vol. 29, no. 12, pp. 1999–2003, Dec. 1999.

[82] I. Acar and M. Atalay, “Characterization of Sintered Class F fly Ashes,” *Fuel*, vol. 106, pp. 195–203, Apr. 2003.

[83] Silica Fume Association, “Silica Fume User’s Manual.” Silica fume Association, 2005.

[84] R. U. D. Nassar and P. Soroushian, “Strength and Durability of Recycled Aggregate Concrete Containing Milled Glass as Partial Replacement for Cement,” *Constr. Build. Mater.*, vol. 29, pp. 368–377, Apr. 2012.

[85] A. Shayan and A. Xu, “Performance of Glass Powder as a Pozzolanic Material in Concrete: A Field Trial on Concrete Slabs,” *Cem. Concr. Res.*, vol. 36, no. 3, pp. 457–468, Mar. 2006.

[86] B. Taha and G. Nounu, “Properties of Concrete Contains Mixed Colour Waste Recycled Glass as Sand and Cement Replacement,” *Constr. Build. Mater.*, vol. 22, no. 5, pp. 713–720, May 2008.

[87] G. C. Cordeiro, R. D. Toledo Filho, L. M. Tavares, and E. de M. R. Fairbairn, “Ultrafine Grinding of Sugar Cane Bagasse Ash for Application as Pozzolanic Admixture in Concrete,” *Cem. Concr. Res.*, vol. 39, no. 2, pp. 110–115, Feb. 2009.

[88] G. C. Cordeiro, R. D. Toledo Filho, L. M. Tavares, and E. M. R. Fairbairn, “Experimental Characterization of Binary and Ternary Blended-Cement Concretes Containing Ultrafine Residual Rice Husk and Sugar Cane Bagasse Ashes,” *Constr. Build. Mater.*, vol. 29, pp. 641–646, Apr. 2012.

[89] C. B. Cheah and M. Ramli, “The Implementation of Wood Waste Ash as a Partial Cement Replacement Material in the Production of Structural Grade Concrete and Mortar: An Overview,” *Resour. Conserv. Recycl.*, vol. 55, no. 7, pp. 669–685, May 2011.

[90] R. Rajamma, R. J. Ball, L. A. C. Tarelho, G. C. Allen, J. A. Labrincha, and V. M. Ferreira, “Characterisation and Use of Biomass Fly Ash in Cement-Based Materials,” *J. Hazard. Mater.*, vol. 172, no. 2–3, pp. 1049–1060, Dec. 2009.

[91] E. Gruyaert, P. Van den Heede, M. Maes, and N. De Belie, “Investigation of the Influence of Blast-Furnace Slag on the Resistance of Concrete Against Organic Acid or Sulphate Attack by Means of Accelerated Degradation Tests,” *Cem. Concr. Res.*, vol. 42, no. 1, pp. 173–185, Jan. 2012.

[92] A. Hadjsadok, S. Kenai, L. Courard, F. Michel, and J. Khatib, “Durability of Mortar and Concretes Containing Slag with Low Hydraulic Activity,” *Cem. Concr. Compos.*, vol. 34, no. 5, pp. 671–677, May 2012.

[93] V. Malagavelli, “High Performance Concrete with GGBS and ROBO Sand,” *Int. J. Eng. Sci. Technol.*, vol. 2, no. 10, pp. 5107–5113, 2010.

[94] G. G. Carette and V. M. Malhotra, “Characterization of Canadian Fly Ashes and Their Relative Performance in Concrete,” *Can. J. Civ. Eng.*, vol. 14, no. 5, pp. 667–682, Oct. 1987.

[95] F. Raba, S. Smith, and M. Mearing, “Sub Bituminous Fly Ash Utilization in Concrete,” presented at the Symposium on Fly Ash Incorporation on Hydrated Cement Systems, Boston, MA, 1981.

[96] S. M. H. Shafaatian, A. Akhavan, H. Maraghechi, and F. Rajabipour, “How Does Fly Ash Mitigate Alkali–Silica Reaction (ASR) in Accelerated Mortar Bar Test (ASTM C1567)?,” *Cem. Concr. Compos.*, vol. 37, pp. 143–153, Mar. 2013.

[97] R. Siddique, “Effect of fine aggregate replacement with Class F fly ash on the mechanical properties of concrete,” *Cem. Concr. Res.*, vol. 33, no. 4, pp. 539–547, Apr. 2003.

[98] A. M. Boddy, R. D. Hooton, and M. D. A. Thomas, “The Effect of the Silica Content of Silica Fume on Its Ability to Control Alkali–Silica Reaction,” *Cem. Concr. Res.*, vol. 33, no. 8, pp. 1263–1268, Aug. 2003.

[99] R. Hooton, “Influence of Silica Fume Replacement of Cement Physical Properties and Resistance to Sulfate Attack, Freezing and Thawing, and Alkali-Silica Reactivity,” *ACI Mater. J.*, vol. 90, no. 2, pp. 143–152, 1993.

[100] W. Kurdowski and W. Nocuń-Wczelik, “The Tricalcium Silicate Hydration in the Presence of Active Silica,” *Cem. Concr. Res.*, vol. 13, no. 3, pp. 341–348, May 1983.

[101] D. Perraton, P. Aitcin, and D. Vezina, “Permeabilities of Silica Fume Concrete,” *Am. Concr. Inst. Spec. Publ.*, vol. 108, pp. 63–84, 1988.

[102] R. Siddique, “Utilization of wood ash in concrete manufacturing,” *Resour. Conserv. Recycl.*, vol. 67, pp. 27–33, Oct. 2012.

[103] K. Ganesan, K. Rajagopal, and K. Thangavel, “Rice Husk Ash Blended Cement: Assessment of Optimal Level of Replacement for Strength and Permeability Properties of Concrete,” *Constr. Build. Mater.*, vol. 22, no. 8, pp. 1675–1683, Aug. 2008.

[104] N. Hasparyk, P. Monteiro, and H. Carasek, “Effect of Silica Fume and Rice Husk Ash on Alkali-Silica Reaction,” *ACI Mater. J.*, vol. 97, no. 4, pp. 486–492, 2000.

[105] M. Jamil, A. B. M. A. Kaish, S. N. Raman, and M. F. M. Zain, “Pozzolanic Contribution of Rice Husk Ash in Cementitious System,” *Constr. Build. Mater.*, vol. 47, pp. 588–593, Oct. 2013.

[106] T. M. Mauro and C. A. R. Silva, “Influence of Rice Husk Ash in Mechanical Characteristics of Concrete,” presented at the IV International ACI/CANMET Conference on Quality of Concrete Structures and Recent Advances in Concrete Materials and Testing, Pernambuco, Brazil, 2005.

[107] V. Saraswathy, S. Muralidharan, K. Thangavel, and S. Srinivasan, “Influence of Activated Fly Ash on Corrosion-Resistance and Strength of Concrete,” *Cem. Concr. Compos.*, vol. 25, no. 7, pp. 673–680, Oct. 2003.

[108] J. Sousa Coutinho, “The combined benefits of CPF and RHA in improving the durability of concrete structures,” *Cem. Concr. Compos.*, vol. 25, no. 1, pp. 51–59, Jan. 2003.

[109] M. Zhang and V. Malhotra, “High-Performance Concrete Incorporating Rice Husk Ash as a Supplementary Cementing Material,” *Am. Concr. Inst.*, vol. 93, no. 6, pp. 629–636, 1996.

[110] N. Amin, “Use of Bagasse Ash in Concrete and Its Impact on the Strength and Chloride Resistivity,” *ACI J. Mater. Civ. Eng.*, vol. 23, no. 5, pp. 717–720, 2011.

[111] N. Chusilp, C. Jaturapitakkul, and K. Kiattikomol, “Utilization of Bagasse Ash as a Pozzolanic Material in Concrete,” *Constr. Build. Mater.*, vol. 23, no. 11, pp. 3352–3358, Nov. 2009.

[112] R. Núñez-Jaquez, J. Buelna-Rodríguez, C. Barrios-Durstewitz, C. Gaona-Tiburcio, and J. E. Almeraya-Calderón, “Corrosion of Modified Concrete with Sugar Cane Bagasse Ash,” *Int. J. Corros.*, vol. 2012, Aug. 2012.

[113] S. Rukzon and P. Chindaprasirt, “Utilization of bagasse ash in high-strength concrete,” *Mater. Des.*, vol. 34, pp. 45–50, Feb. 2012.

[114] G. Sireesha, M. Kanta Rao, and P. Kanta Rao, “An Experimental Study on Strength Properties of Concrete When Cement Is Partially Replaced With Sugar-Cane Bagasse Ash,” *IOSR J. Mech. Civ. Eng.*, vol. 9, no. 3, pp. 35–38, Oct. 2013.

[115] M. Yashwanth, “An Experimental Study on Bagasse Ash As Replacement for Cement in Lightweight Concrete,” *Int. J. Latest Trends Eng. Technol.*, vol. 3, no. 3, pp. 253–260, Jan. 2014.

[116] G. Lee, T. C. Ling, Y. L. Wong, and C. S. Poon, “Effects of Crushed Glass Cullet Sizes, Casting Methods and Pozzolanic Materials on ASR of Concrete Blocks,” *Constr. Build. Mater.*, vol. 25, no. 5, pp. 2611–2618, May 2011.

[117] T. C. Esteves, R. Rajamma, D. Soares, A. S. Silva, V. M. Ferreira, and J. A. Labrincha, “Use of Biomass Fly Ash for Mitigation of Alkali-Silica Reaction of Cement Mortars,” *Constr. Build. Mater.*, vol. 26, no. 1, pp. 687–693, Jan. 2012.

[118] E. C. Eckel, *Cements, Limes, and Plasters : Their Materials, Manufacture, and Properties*. New York : J. Wiley & Sons, 1905.

[119] E. C. Eckel, “Summaries of the Literature of Structural Materials,” vol. 10, no. 5, pp. 542–550, 1902.

[120] S. Grzeszczyk and E. Janowska-Renkas, “The Influence of Small Particle on the Fluidity of Blast Furnace Slag Cement Paste Containing Superplasticizers,” *Constr. Build. Mater.*, vol. 26, no. 1, pp. 411–415, Jan. 2012.

[121] S. C. Pal, A. Mukherjee, and S. R. Pathak, “Investigation of hydraulic activity of ground granulated blast furnace slag in concrete,” *Cem. Concr. Res.*, vol. 33, no. 9, pp. 1481–1486, Sep. 2003.

[122] R. Andersson, H. E. Gram, and J. Deja, “Alkali-Activated Slag.” CBI Research.

[123] F. Bellmann and J. Stark, “Activation of blast furnace slag by a new method,” *Cem. Concr. Res.*, vol. 39, no. 8, pp. 644–650, Aug. 2009.

[124] H. Wan, Z. Shui, and Z. Lin, “Analysis of Geometric Characteristics of GGBS Particles and Their Influences on Cement Properties,” *Cem. Concr. Res.*, vol. 34, no. 1, pp. 133–137, Jan. 2004.

[125] AASHTO, “M302-11, Standard Specification for Ground Granulated Blast-Furnace Slag for Use in Concrete and Mortars.” American Association of State Highway and Transportation Officials, 2011.

[126] ASTM C989, “Standard Specification for Slag Cement for Use in Concrete and Mortars,” ASTM International, West Conshohocken, PA, 2013.

[127] P. Brown, R. D. Hooton, and C. Boyd, “Microstructural changes in concretes with sulfate exposure,” *Cem. Concr. Compos.*, vol. 26, no. 8, pp. 993–999, Nov. 2004.

[128] E. Rozière, A. Loukili, R. El Hachem, and F. Grondin, “Durability of concrete exposed to leaching and external sulphate attacks,” *Cem. Concr. Res.*, vol. 39, no. 12, pp. 1188–1198, Dec. 2009.

[129] J. Duchesne and M.-A. Bérubé, “Long-term effectiveness of supplementary cementing materials against alkali–silica reaction,” *Cem. Concr. Res.*, vol. 31, no. 7, pp. 1057–1063, Jul. 2001.

[130] P. J. Wainwright and N. Rey, “The Influence of Ground Granulated Blastfurnace Slag (GGBS) Additions and Time Delay on the Bleeding of Concrete,” *Cem. Concr. Compos.*, vol. 22, no. 4, pp. 253–257, 2000.

[131] G. Hannesson, K. Kuder, R. Shogren, and D. Lehman, “The influence of high volume of fly ash and slag on the compressive strength of self-consolidating concrete,” *Constr. Build. Mater.*, vol. 30, pp. 161–168, May 2012.

[132] A. Lübeck, A. L. G. Gastaldini, D. S. Barin, and H. C. Siqueira, “Compressive strength and electrical properties of concrete with white Portland cement and blast-furnace slag,” *Cem. Concr. Compos.*, vol. 34, no. 3, pp. 392–399, Mar. 2012.

[133] G. Menéndez, V. Bonavetti, and E. F. Irassar, “Strength development of ternary blended cement with limestone filler and blast-furnace slag,” *Cem. Concr. Compos.*, vol. 25, no. 1, pp. 61–67, Jan. 2003.

[134] IEA, “Cement Technology Roadmap 2009.” International Energy Agency, 2009.

[135] ASTM C618, “Standard Specification for Coal Fly Ash and Raw or Calcined Natural Pozzolan for Use in Concrete,” ASTM International, West Conshohocken, PA, 2015.

[136] CEN, “BS EN 450-1:2012 Fly Ash for Concrete. Definition, Specifications and Conformity Criteria.” British Standards Institute, 2012.

[137] G. J. McCarthy, K. D. Swanson, L. P. Keller, and W. C. Blatter, “Mineralogy of western fly ash,” *Cem. Concr. Res.*, vol. 14, no. 4, pp. 471–478, Jul. 1984.

[138] D. M. Roy, “Hydration of Blended Cements Containing Slag, Fly Ash, or Silica Fume,” *Proc Meet. Inst. Concr. Technol.*, vol. 29, 1987.

[139] K. Mather, “Factors Affecting Sulfate Resistance of Mortars,” in *Seventh International Congress on the Chemistry of Cement*, Paris, France, 1981, pp. 580–585.

[140] W. H. Price, “Pozzolans - A Review,” *ACI J.*, vol. 72, no. 5, pp. 225–232, 1975.

[141] T. Ponikiewski and J. Gołaszewski, “The effect of high-calcium fly ash on selected properties of self-compacting concrete,” *Arch. Civ. Mech. Eng.*, vol. 14, no. 3, pp. 455–465, May 2014.

[142] Z. Yamei, S. Wei, and S. Lianfei, “Mechanical Properties of High Performance Concrete Made with High Calcium High Sulfate Fly Ash,” *Cem. Concr. Res.*, vol. 27, no. 7, pp. 1093–1098, Jul. 1997.

[143] V. G. Papadakis, “Effect of fly ash on Portland cement systems: Part II. High-calcium fly ash,” *Cem. Concr. Res.*, vol. 30, no. 10, pp. 1647–1654, Oct. 2000.

[144] D. C. Adriano, A. L. Page, A. A. Elseewi, A. C. Chang, and I. Straughan, “Utilization and Disposal of Fly Ash and Other Coal Residues in Terrestrial Ecosystems: A Review1,” *J. Environ. Qual.*, vol. 9, no. 3, p. 333, 1980.

[145] F. Colangelo, R. Cioffi, F. Montagnaro, and L. Santoro, “Soluble Salt Removal from MSWI Fly Ash and its Stabilization for Safer Disposal and Recovery as Road Basement Material,” *Waste Manag.*, vol. 32, no. 6, pp. 1179–1185, Jun. 2012.

[146] W. Bumrongjaroen, I. Muller, and I. Pegg, “Characterization of Glassy Phase in Fly Ash From Iowa State University,” The Catholic University of America, Vitreous State Laboratory, Technical Report VSL-07R520x-1, Dec. 2007.

[147] T. R. Naik, S. S. Singh, and M. M. Hossain, “Permeability of Concrete Containing Large Amounts of Fly Ash,” *Cem. Concr. Res.*, vol. 24, no. 5, pp. 913–922, 1994.

[148] ACI Committee 226, “Use of Fly Ash in Concrete,” American Concrete Institute, 29, 1987.

[149] M. Mazloom, A. A. Ramezanianpour, and J. J. Brooks, “Effect of Silica Fume on Mechanical Properties of High-Strength Concrete,” *Cem. Concr. Compos.*, vol. 26, no. 4, pp. 347–357, May 2004.

[150] H. A. Toutanji, L. Liu, and T. El-Korchi, “The role of silica fume in the direct tensile strength of cement-based materials,” *Mater. Struct.*, vol. 32, no. 3, pp. 203–209.

[151] J. G. Cabrera and P. A. Claisse, “Measurement of chloride penetration into silica fume concrete,” *Cem. Concr. Compos.*, vol. 12, no. 3, pp. 157–161, Jan. 1990.

[152] M. Jalal, E. Mansouri, M. Sharifipour, and A. R. Pouladkhan, “Mechanical, rheological, durability and microstructural properties of high performance self-compacting concrete containing SiO2 micro and nanoparticles,” *Mater. Des.*, vol. 34, pp. 389–400, Feb. 2012.

[153] H. S. Wong and H. Abdul Razak, “Efficiency of calcined kaolin and silica fume as cement replacement material for strength performance,” *Cem. Concr. Res.*, vol. 35, no. 4, pp. 696–702, Apr. 2005.

[154] T. J. Hirsch, “Modulus of Elasticity of Concrete Affected by Elastic Moduli of Cement Paste Matrix and Aggregate,” *ACI J. Proc.*, vol. 59, no. 3, 1962.

[155] Glass Packing Institute, “Glass Recycling Facts,” 2013. [Online]. Available: www.gpi.org/recycling/glass-recycling-facts.

[156] EPA, “Common Wastes & Materials - Glass,” Feb-2014. [Online]. Available: http://www.epa.gov/osw/conserve/materials/glass.htm.

[157] C. Shi, Y. Wu, C. Riefler, and H. Wang, “Characteristics and pozzolanic reactivity of glass powders,” *Cem. Concr. Res.*, vol. 35, no. 5, pp. 987–993, May 2005.

[158] Y. Shao, T. Lefort, S. Moras, and D. Rodriguez, “Studies on concrete containing ground waste glass,” *Cem. Concr. Res.*, vol. 30, no. 1, pp. 91–100, Jan. 2000.

[159] D. G. Nair, A. Fraaij, A. A. K. Klaassen, and A. P. M. Kentgens, “A structural investigation relating to the pozzolanic activity of rice husk ashes,” *Cem. Concr. Res.*, vol. 38, no. 6, pp. 861–869, Jun. 2008.

[160] N. Yalçin and V. Sevinç, “Studies on silica obtained from rice husk,” *Ceram. Int.*, vol. 27, no. 2, pp. 219–224, 2001.

[161] M. Nehdi, J. Duquette, and A. El Damatty, “Performance of rice husk ash produced using a new technology as a mineral admixture in concrete,” *Cem. Concr. Res.*, vol. 33, no. 8, pp. 1203–1210, Aug. 2003.

[162] Q. Feng, H. Yamamichi, M. Shoya, and S. Sugita, “Study on the pozzolanic properties of rice husk ash by hydrochloric acid pretreatment,” *Cem. Concr. Res.*, vol. 34, no. 3, pp. 521–526, Mar. 2004.

[163] B. Chatveera and P. Lertwattanaruk, “Evaluation of Sulfate Resistance of Cement Mortars Containing Black Rice Husk Ash,” *J. Environ. Manage.*, vol. 90, no. 3, pp. 1435–1441, Mar. 2009.

[164] S. K. Antiohos, V. G. Papadakis, and S. Tsimas, “Rice husk ash (RHA) effectiveness in cement and concrete as a function of reactive silica and fineness,” *Cem. Concr. Res.*, vol. 61–62, pp. 20–27, Jul. 2014.

[165] N. M. Khalil, E. M. Hassan, M. M. E. Shakdofa, and M. Farahat, “Beneficiation of the huge waste quantities of barley and rice husks as well as coal fly ashes as additives for Portland cement,” *J. Ind. Eng. Chem.*, vol. 20, no. 5, pp. 2998–3008, Sep. 2014.

[166] N. Jain, “Effect of nonpozzolanic and pozzolanic mineral admixtures on the hydration behavior of ordinary Portland cement,” *Constr. Build. Mater.*, vol. 27, no. 1, pp. 39–44, Feb. 2012.

[167] D. D. Bui, J. Hu, and P. Stroeven, “Particle size effect on the strength of rice husk ash blended gap-graded Portland cement concrete,” *Cem. Concr. Compos.*, vol. 27, no. 3, pp. 357–366, Mar. 2005.

[168] United States Department of Agriculture, “Crop Production 2012 Summary,” ISSN: 1057-7823, Jan. 2013.

[169] N. Singhania, “Adding to the Mix,” *Institute of Civil Engineers and Surveyors*, 2004.

[170] R. Khan, A. Jabbar, I. Ahmad, W. Khan, A. N. Khan, and J. Mirza, “Reduction in environmental problems using rice-husk ash in concrete,” *Constr. Build. Mater.*, vol. 30, pp. 360–365, May 2012.

[171] M. R. Gidde and A. P. Jivani, “Waste to Wealth - Potential of Rice Husk in India a Literature Review,” in *Proceedings of the International Conference on Cleaner Technology and Environmental Management*, PEC, Pondicherry, India, 2007, pp. 586–590.

[172] United States Department of Agriculture, “Crop Production 2015 Summary,” ISSN: 1057-7823, 2016.

[173] T. Adams, G. Whitehouse, and D. Maples, “Properties and Operating Experience with Bagasse as a Boiler Fuel,” presented at the National Waste Processing Conference, 1978, pp. 101–106.

[174] T. Ramos, A. M. Matos, and J. Sousa-Coutinho, “Mortar with wood waste ash: Mechanical strength carbonation resistance and ASR expansion,” *Constr. Build. Mater.*, vol. 49, pp. 343–351, Dec. 2013.

[175] EPA, “Municipal Solid Waste Generation, Recycling, and Disposal in the United States: Facts and Figures for 2011,” Environmental Protection Agency, May 2013.

[176] Gainesville Renewable Energy Center, “Local, Sustainable Fuel,” *Gainesville Renewable Energy Center*, 2013. [Online]. Available: http://gainesvillebiomass.com/clean-fuel/. [Accessed: 08-Jan-2014].

[177] S. Goñi, M. Frias, R. Vigil de la Villa, and R. García, “Sodium chloride effect on durability of ternary blended cement. Microstructural characterization and strength,” *Compos. Part B Eng.*, vol. 54, pp. 163–168, Nov. 2013.

[178] I. Vegas, J. J. Gaitero, J. Urreta, R. García, and M. Frías, “Aging and durability of ternary cements containing fly ash and activated paper sludge,” *Constr. Build. Mater.*, vol. 52, pp. 253–260, Feb. 2014.

[179] P. Chindaprasirt, S. Rukzon, and V. Sirivivatnanon, “Resistance to chloride penetration of blended Portland cement mortar containing palm oil fuel ash, rice husk ash and fly ash,” *Constr. Build. Mater.*, vol. 22, no. 5, pp. 932–938, May 2008.

[180] S. H. Sathawane, V. S. Vairagade, and K. S. Kene, “Combine Effect of Rice Husk Ash and Fly Ash on Concrete by 30% Cement Replacement,” *Procedia Eng.*, vol. 51, pp. 35–44, 2013.

[181] N. Ranjbar, M. Mehrali, U. J. Alengaram, H. S. C. Metselaar, and M. Z. Jumaat, “Compressive strength and microstructural analysis of fly ash/palm oil fuel ash based geopolymer mortar under elevated temperatures,” *Constr. Build. Mater.*, vol. 65, pp. 114–121, Aug. 2014.

[182] M. D. A. Thomas, M. H. Shehata, S. G. Shashiprakash, D. S. Hopkins, and K. Cail, “Use of ternary cementitious systems containing silica fume and fly ash in concrete,” *Cem. Concr. Res.*, vol. 29, no. 8, pp. 1207–1214, Aug. 1999.

[183] T. Nochaiya, W. Wongkeo, and A. Chaipanich, “Utilization of fly ash with silica fume and properties of Portland cement–fly ash–silica fume concrete,” *Fuel*, vol. 89, no. 3, pp. 768–774, Mar. 2010.

[184] B. Lothenbach, K. Scrivener, and R. D. Hooton, “Supplementary cementitious materials,” *Cem. Concr. Res.*, vol. 41, no. 12, pp. 1244–1256, Dec. 2011.

[185] C. Li, H. Sun, and L. Li, “A review: The comparison between alkali-activated slag (Si + Ca) and metakaolin (Si + Al) cements,” *Cem. Concr. Res.*, vol. 40, no. 9, pp. 1341–1349, Sep. 2010.

[186] I. G. Richardson and G. W. Groves, “The incorporation of minor and trace elements into calcium silicate hydrate (C [illegible] C-S-H) gel in hardened cement pastes,” *Cem. Concr. Res.*, vol. 23, no. 1, pp. 131–138, Jan. 1993.

[187] J. J. Chen, J. J. Thomas, H. F. W. Taylor, and H. M. Jennings, “Solubility and structure of calcium silicate hydrate,” *Cem. Concr. Res.*, vol. 34, no. 9, pp. 1499–1519, Sep. 2004.

[188] S.-Y. Hong and F. P. Glasser, “Alkali binding in cement pastes: Part I. The C-S-H phase,” *Cem. Concr. Res.*, vol. 29, no. 12, pp. 1893–1903, Dec. 1999.

[189] A. Kar, I. Ray, A. Unnikrishnan, and J. F. Davalos, “Estimation of C–S-H and calcium hydroxide for cement pastes containing slag and silica fume,” *Constr. Build. Mater.*, vol. 30, pp. 505–515, May 2012.

[190] H. van Oss, “Mineral Industry Surveys,” USGS, Reston, VA, 2, 2015.

[191] M. McConnell, “Sugar and Sweeteners Outlook.” USDA, 2016.

[192] R. Jenkins, *X-Ray Fluorescence Spectrometry*. John Wiley & Sons, Inc., 1988.

[193] J. A. Anzelmo and J. R. Lindsay, *J. Chem. Educ.*, vol. 64, no. 8, pp. A181–A185, 1987.

[194] Y. Kataoka, “Standardless X-ray Fluorescence Spectrometry (Fundamental Parameter Method using Sensitivity Library),” *Rigaku J.*, vol. 6, no. 1, pp. 33–40, 1989.

[195] ASTM C114, “Standard Test Methods for Chemical Analysis of Hydraulic Cement,” ASTM International, West Conshohocken, PA, 2013.

[196] C. Jolicoeur, T. Cong To, É. Benoît, R. Hill, Z. Zhang, and M. Pagé, “Fly Ash-Carbon Effects on Concrete Air Entrainment: Fundamental Studies on their Origin and Chemical Mitigation,” presented at the 2009 World of Coal Ash Conference, Lexington, KY, USA, 2009, p. 23.

[197] C. Jolicoeur, T. Cong To, T. Soan Nyguen, R. Hill, and M. Pagé, “Mode of Action of Anionic Surfactants for Air Entrainment in Cement Pastes w-w/o Fly Ash,” presented at the 2009 World of Coal Ash Conference, Lexington, KY, USA, 2009, p. 19.

[198] ASTM D7348, “Standard Test Methods for Loss on Ignition (LOI) of Solid Combustion Residues,” ASTM International, West Conshohocken, PA, 2013.

[199] C. F. Bohren and D. R. Huffman, *Absorption and Scattering of Light by Small Particles*. New York: Wiley and Sons, 1983.

[200] ASTM C1709, “Standard Guide for Evaluation of Alternative Supplementary Cementitious Materials (ASCM) for Use in Concrete,” ASTM International, West Conshohocken, PA, 2011.

[201] ASTM B822, “Standard Test Method for Particle Size Distribution of Metal Powders and Related Compounds by Light Scattering.” ASTM B822, 2010.

[202] R. Xu, *Particle Characterization: Light Scatting Methods*. Gluwer Academic Publisher, 2002.

[203] T. M. Aminabhavi and V. B. Patil, “Density, viscosity, and speed of sound in binary mixtures of 1-chloronaphthalene with methanol, ethanol, propan-1-ol, butan-1-ol, pentan-1-ol, and hexan-1-ol in the temperature range (298.15-308.15) K,” *J. Chem. Eng. Data*, vol. 43, no. 4, pp. 504–508, 1998.

[204] A. K. Nain, P. Droliya, R. K. Manchanda, A. Khurana, and D. Nayak, “Physicochemical studies of homoeopathic formulations (extremely diluted solutions) of acidum salicylicum in ethanol by using volumetric, acoustic, viscometric and refractive index measurements at 298.15, 308.15 and 318.15 K,” *J. Mol. Liq.*, vol. 215, pp. 680–690, Mar. 2016.

[205] V. A. Hackley, L.-S. Lum, V. Gintautas, and C. F. Ferraris, “Particle Size Analysis by Laser Diffraction Spectrometry: Application to Cementitious Powders.” NIST, 2004.

[206] I. J. Fernandes *et al.*, “Characterization of rice husk ash produced using different biomass combustion techniques for energy,” *Fuel*, vol. 165, pp. 351–359, Feb. 2016.

[207] Horiba Instruments, “Refractive Index Tables.” Horiba Instruments, 2005.

[208] R. B. Jewell and R. F. Rathbone, “Optical Properties of Coal Combustion Byproducts for Particle-Size Analysis by Laser Diffraction,” *Coal Combust. Gasif. Prod.*, vol. 1, pp. 1–7, 2009.

[209] G. Goswami and P. K. Panigrahy, “A Discussion of the Paper ‘Blast Furnace Cement Mortars Manufactured with Fresh Granulated and Weathered Slags: Influence of Gypsum Content and Ageing on Carbonation Depth and Strength Development’ by G. Frigione and R. Sersale,” *Cem. Concr. Res.*, vol. 20, no. 5, pp. 1117–1120, 1995.

[210] E. M. van der Merwe, L. C. Prinsloo, C. L. Mathebula, H. C. Swart, E. Coetsee, and F. J. Doucet, “Surface and bulk characterization of an ultrafine South African coal fly ash with reference to polymer applications,” *Appl. Surf. Sci.*, vol. 317, pp. 73–83, Oct. 2014.

[211] B. J. Skinner and D. E. Appleman, “Melanophlogite, A Cubic Polymorph of Silica,” *Am. Mineral.*, vol. 48, pp. 854–867, 1963.

[212] M. Hancock and R. N. Rothon, “Principal Types of Particulate Fillers,” in *Particulate-Filled Polymer Composites*, 2nd ed., United Kingdom: Rapra Technology Limited, 2003, p. 67.

[213] “Silica, Amorphous [MAK Value Determination],” in *The MAK Collection for Occupational Health and Safety*, vol. 2, Wiley-VCH Verlag GmbH & Co., 1991, pp. 158–179.

[214] “Specific heat,” *Merriam-Webster.com*, 2016. .

[215] ASTM E1269, “Standard Test Method for Determining Specific Heat Capacity by Differential Scanning Calorimetry,” ASTM International, West Conshohocken, PA, 2011.

[216] ASTM D5550, “Standard Test Method for Specific Gravity of Soil Solids by Gas Pycnometer,” ASTM International, West Conshohocken, PA, 2014.

[217] J. Hoffman, “Product Data Sheets,” 2014.

[218] ASTM C204, “Standard Test Methods for Fineness of Hydraulic Cement by Air-Permeability Apparatus,” ASTM International, West Conshohocken, PA, 2011.

[219] ASTM C1702, “Standard Test Method for Measurement of Heat of Hydration of Hydraulic Cementitious Materials Using Isothermal Conduction Calorimetry,” ASTM International, West Conshohocken, PA, 2014.

[220] A. Zayed *et al.*, “Long-Life Slab Replacement Concrete,” Mar. 2015.

[221] ASTM C1679, “Standard Practice for Measuring Hydration Kinetics of Hydraulic Cementitious Mixtures Using Isothermal Calorimetry,” ASTM International, West Conshohocken, PA, 2014.

[222] ACI 305, “Specification for Hot Weather Concreting.” American Concrete Institute, 2014.

[223] ASTM, *Significance of Tests and Properties of Concrete and Concrete-Making Materials*. ASTM International, 2006.

[224] FHWA, “Cementitious Materials - Petrographic Methods of Examining Hardened Concrete: A Petrographic Manual Chapter 11.” 2006.

[225] N. J. Carino, *The Maturity Method*, 2nd ed. New York: CRC Press, 2004.

[226] R. Tank and N. Carino, “Rate constant functions for strength development of concrete,” *ACI Mater. J.*, vol. 88-M11, pp. 74–83, 1991.

[227] F. López Gayarre, C. López-Colina Pérez, M. A. Serrano López, and A. Domingo Cabo, “The effect of curing conditions on the compressive strength of recycled aggregate concrete,” *Constr. Build. Mater.*, vol. 53, pp. 260–266, Feb. 2014.

[228] A. A. Ramezanianpour and V. M. Malhotra, “Effect of curing on the compressive strength, resistance to chloride-ion penetration and porosity of concretes incorporating slag, fly ash or silica fume,” *Cem. Concr. Compos.*, vol. 17, no. 2, pp. 125–133, Jan. 1995.

[229] R. Tank, “The Rate Constant Model for Strength Development of Concrete,” Ph.D. Dissertation, Polytechnic University, Michigan, 1988.

[230] F. F. Ataie and K. A. Riding, “Use of bioethanol byproduct for supplementary cementitious material production,” *Constr. Build. Mater.*, vol. 51, pp. 89–96, Jan. 2014.

[231] M. D. A. Thomas, B. Fournier, K. J. Folliard, M. H. Shehata, J. H. Ideker, and C. Rogers, “Performance Limits for Evaluating Supplementary Cementing Materials Using Accelerated Mortar Bar Test,” *Mater. J.*, vol. 104, no. 2, pp. 115–122, Mar. 2007.

[232] ASTM C1293, “Standard Test Method for Determination of Length Change of Concrete Due to Alkali-Silica Reaction,” ASTM International, West Conshohocken, PA, 2008.

[233] FDOT, “FDOT 346-2 Portland Cement Concrete Materials.” Florida Department of Transportation, 2013.

[234] ASTM C31, “Standard Practice for Making and Curing Concrete Test Specimens in the Field,” ASTM International, West Conshohocken, PA, 2015.

[235] ASTM D2936, “Standard Test Method for Direct Tensile Strength of Intact Rock Core Specimens,” ASTM International, West Conshohocken, PA, 2012.

[236] A. Chini, L. Muszynski, and J. Hicks, “Determination of Acceptance Permeability Characteristics for Performance-Related Specifications for Portland Cement Concrete,” University of Florida, Gainesville, FL, Final Report BC 354-41, 2003.

[237] R. P. Spragg, J. Castro, T. Nantung, M. Paredes, and W. J. Weiss, “Variability Analysis of the Bulk Resistivity Measured Using Concrete Cylinders,” Indiana Department of Transportation & Purdue University, Indiana, USA, SPR-3509, 2011.

[238] A. Ardani, “Surface Resistivity Test Evaluation as an Indicator of the Chloride Permeability of Concrete.” FHWA, 2012.

A. APPENDIX A – MATERIALS CHARACTERIZATION

A.1. X-ray Diffraction Results

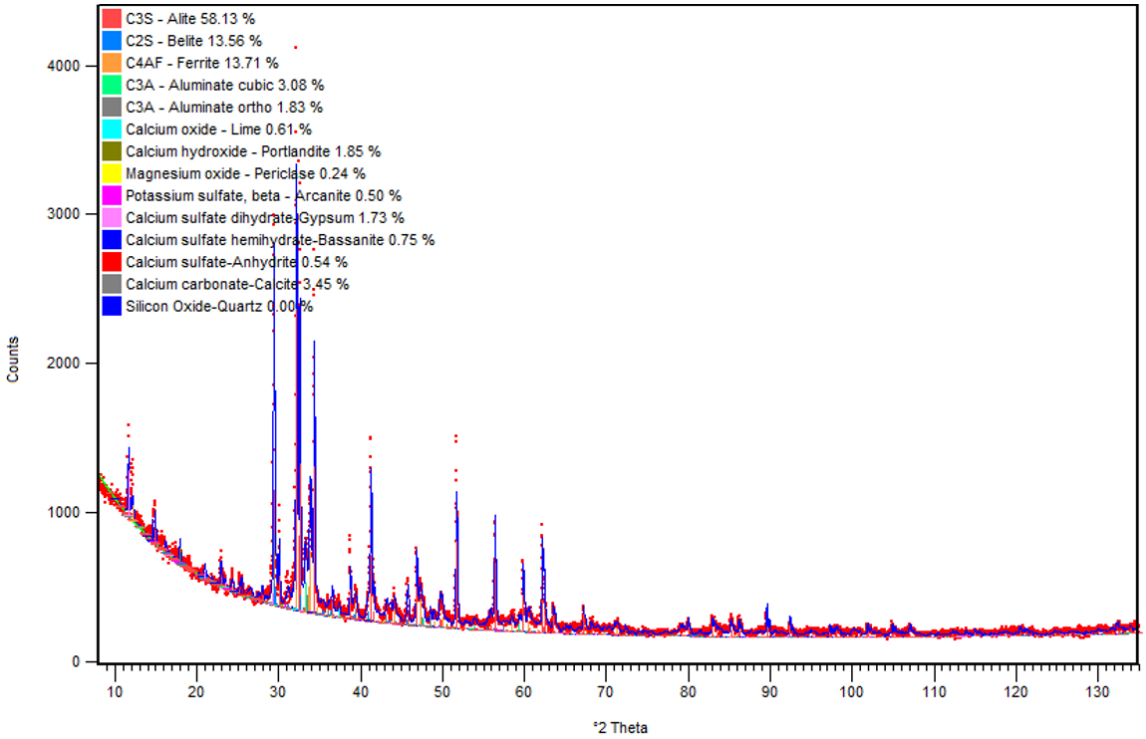

Figure A-1. X-ray diffractogram of portland cement.

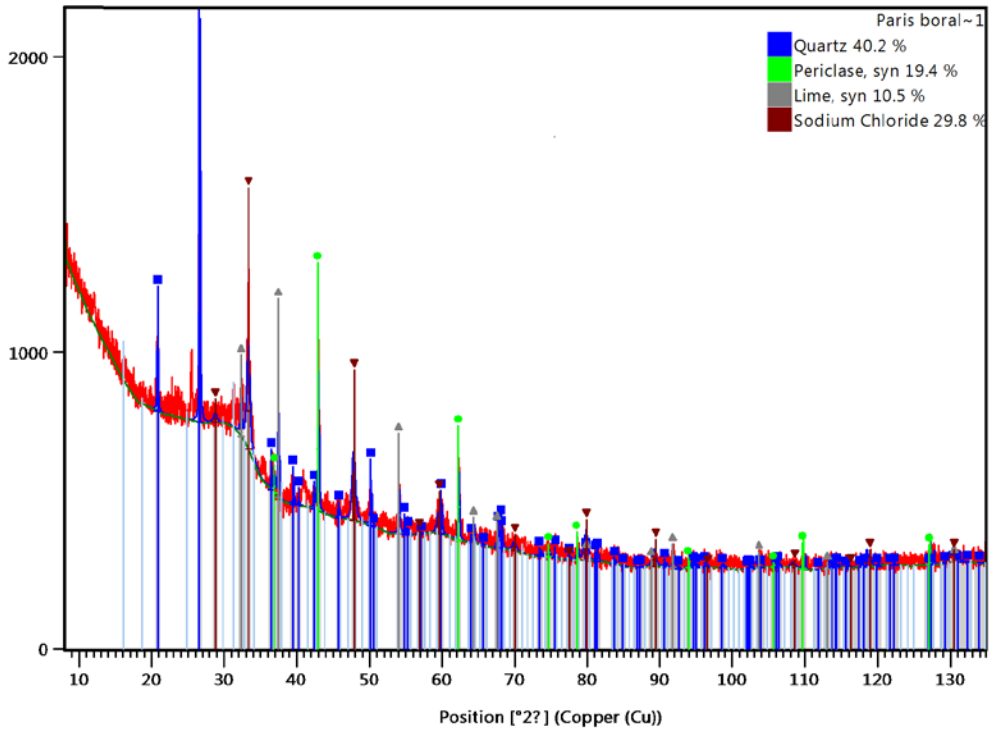

Figure A-2. X-ray diffractogram of class C fly ash.

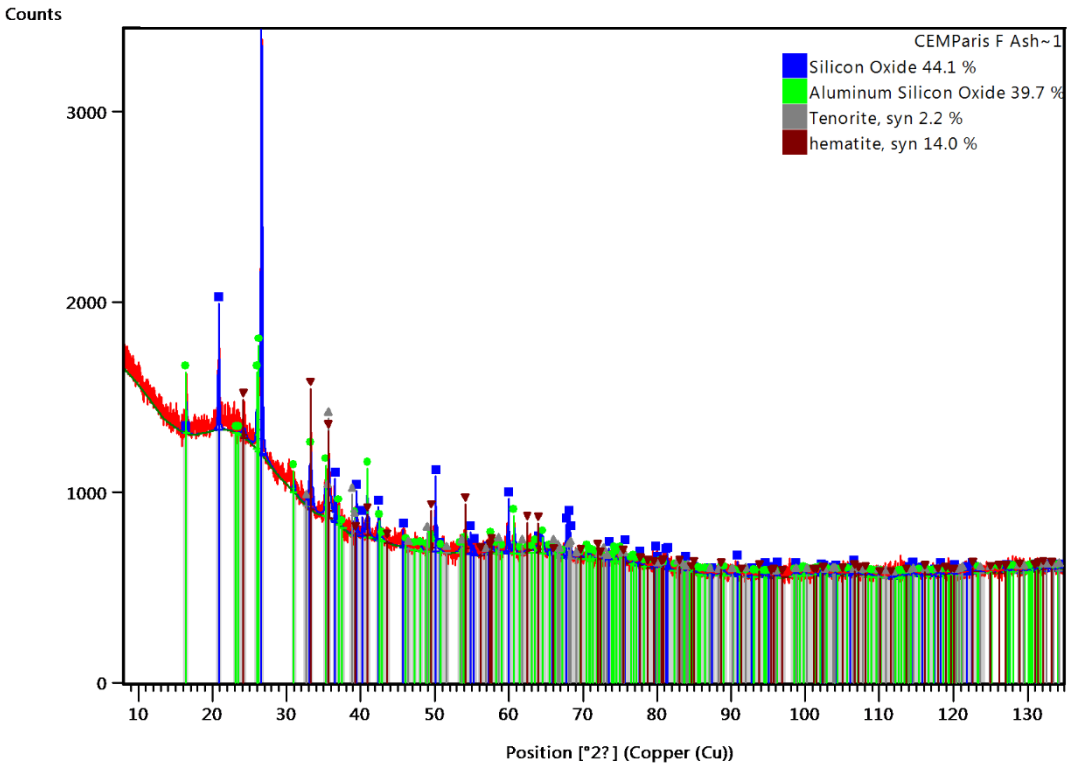

Figure A-3. X-ray diffractogram of class F fly ash.

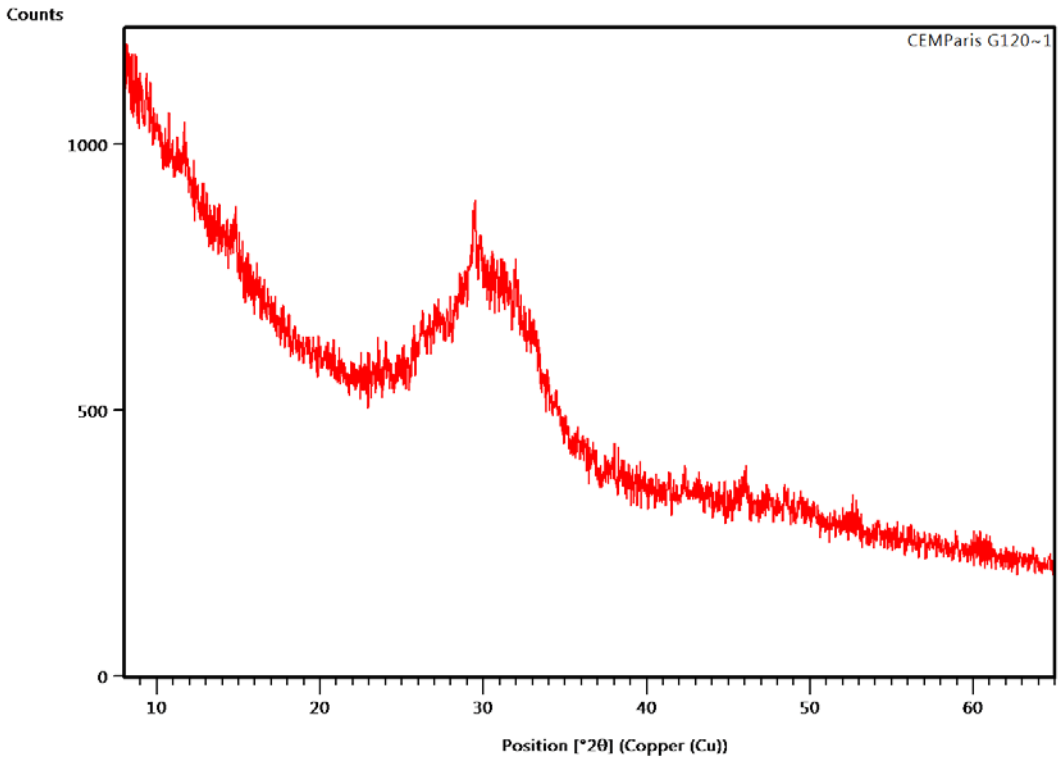

Figure A-4. X-ray diffractogram for blast furnace slag.

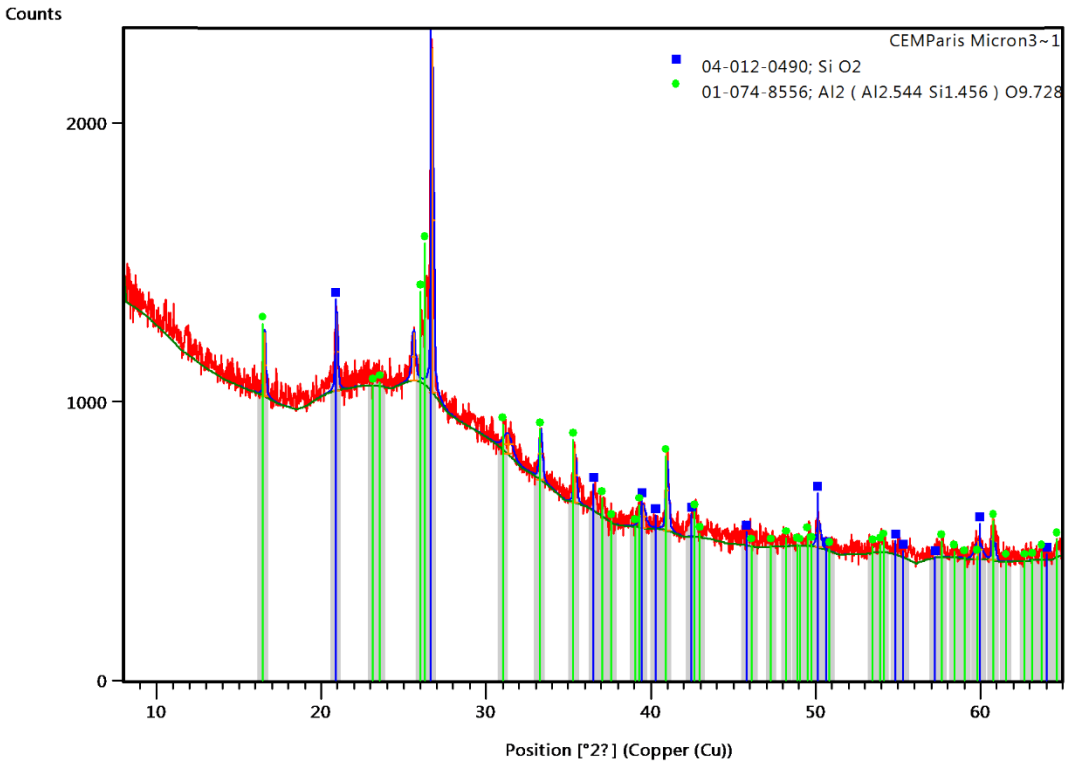

Figure A-5. X-ray diffractogram for Micron[3] ultrafine fly ash.

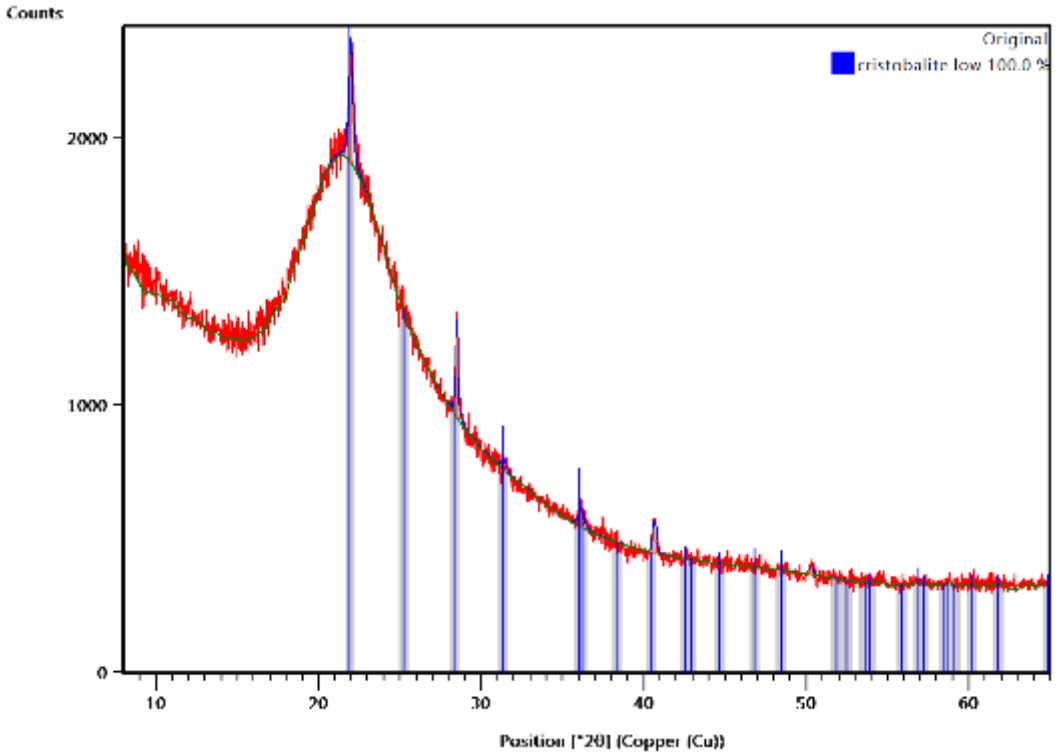

Figure A-6. X-ray diffractogram of RHA.

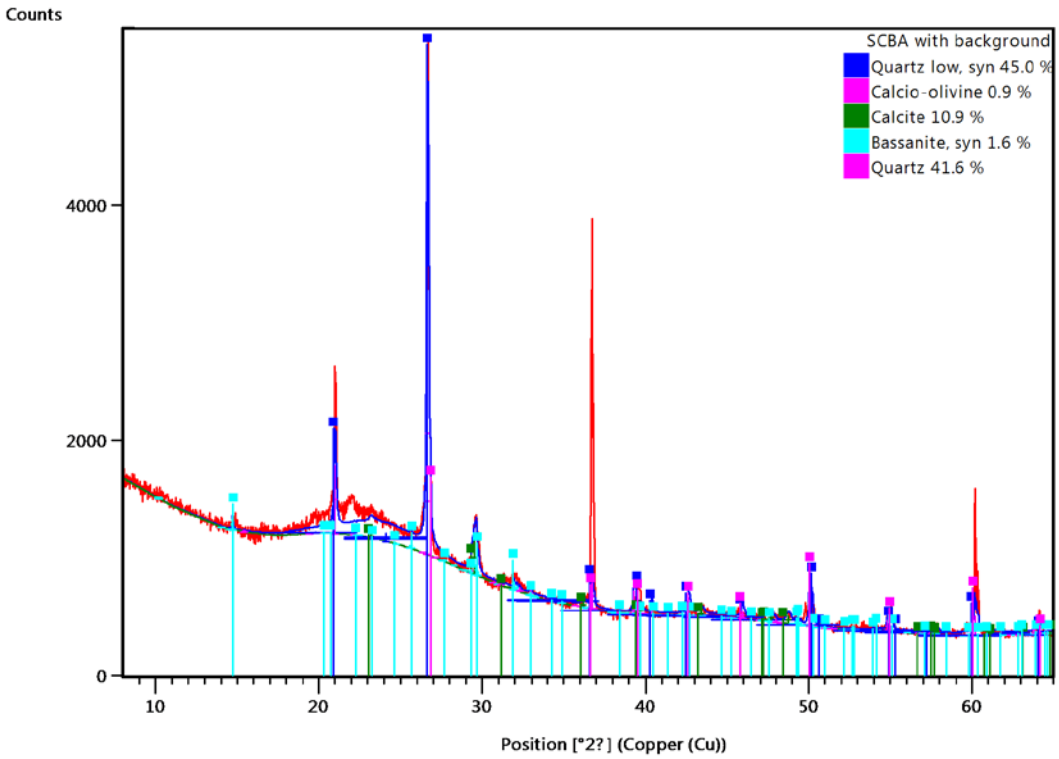

Figure A-7. X-ray diffractogram of SCBA.

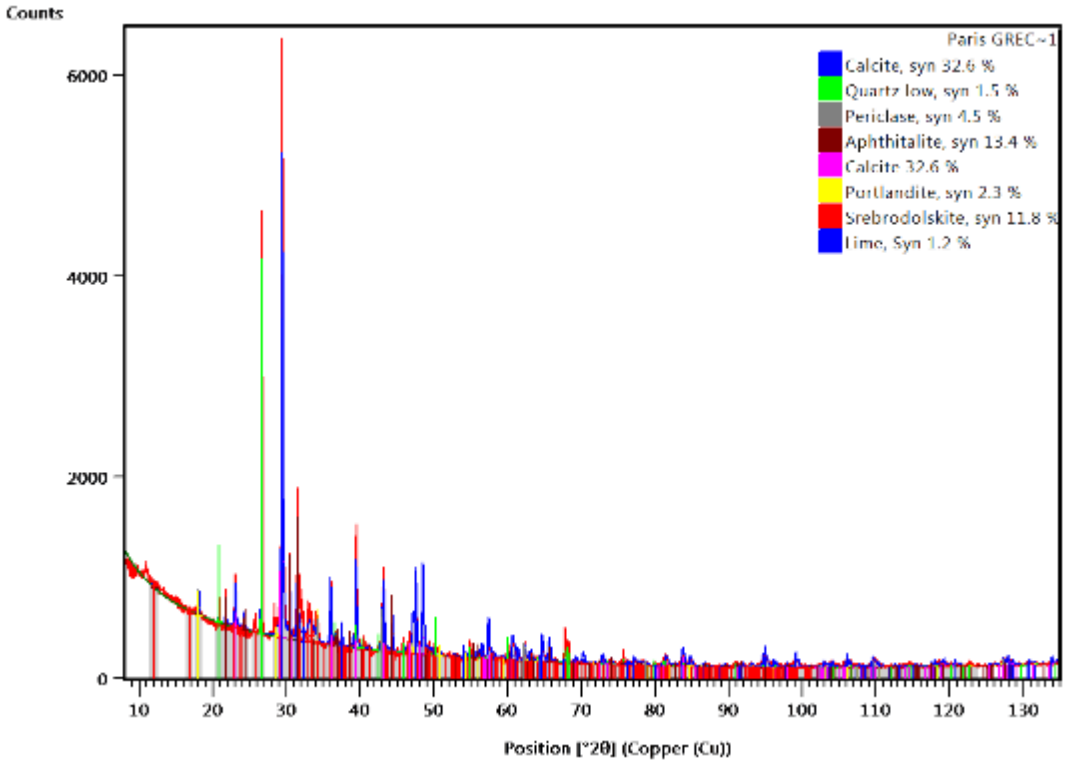

Figure A-8. X-ray diffractogram of wood ash.

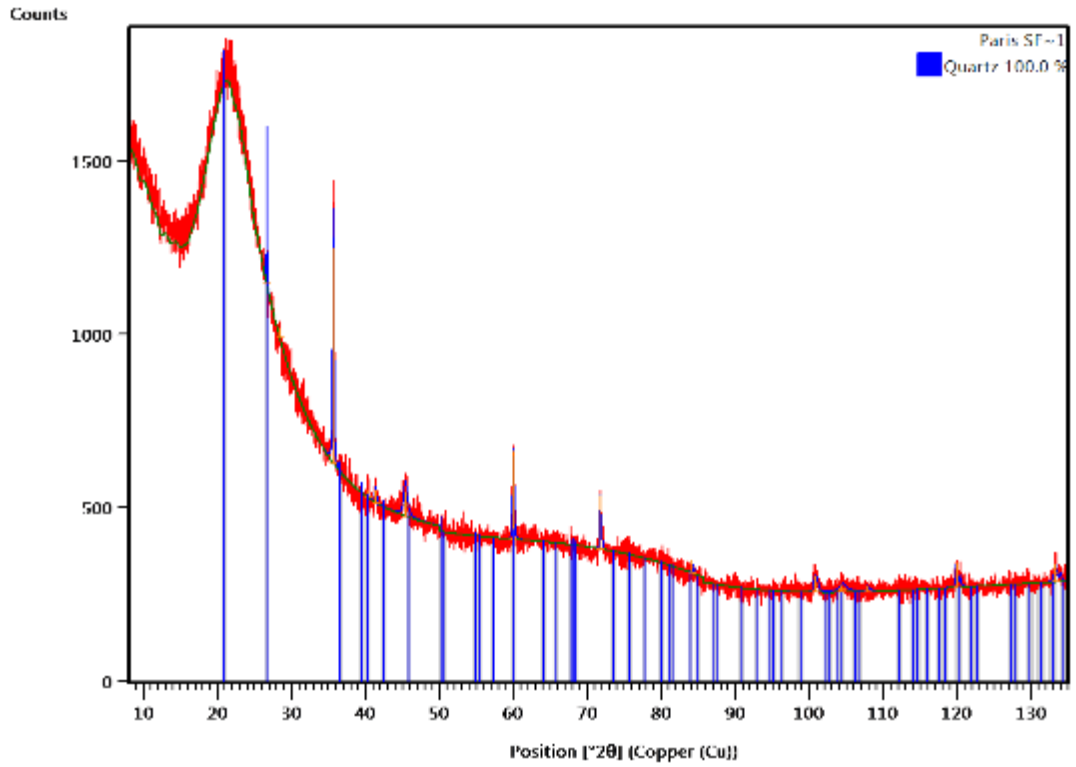

Figure A-9. X-ray diffractogram of silica fume.

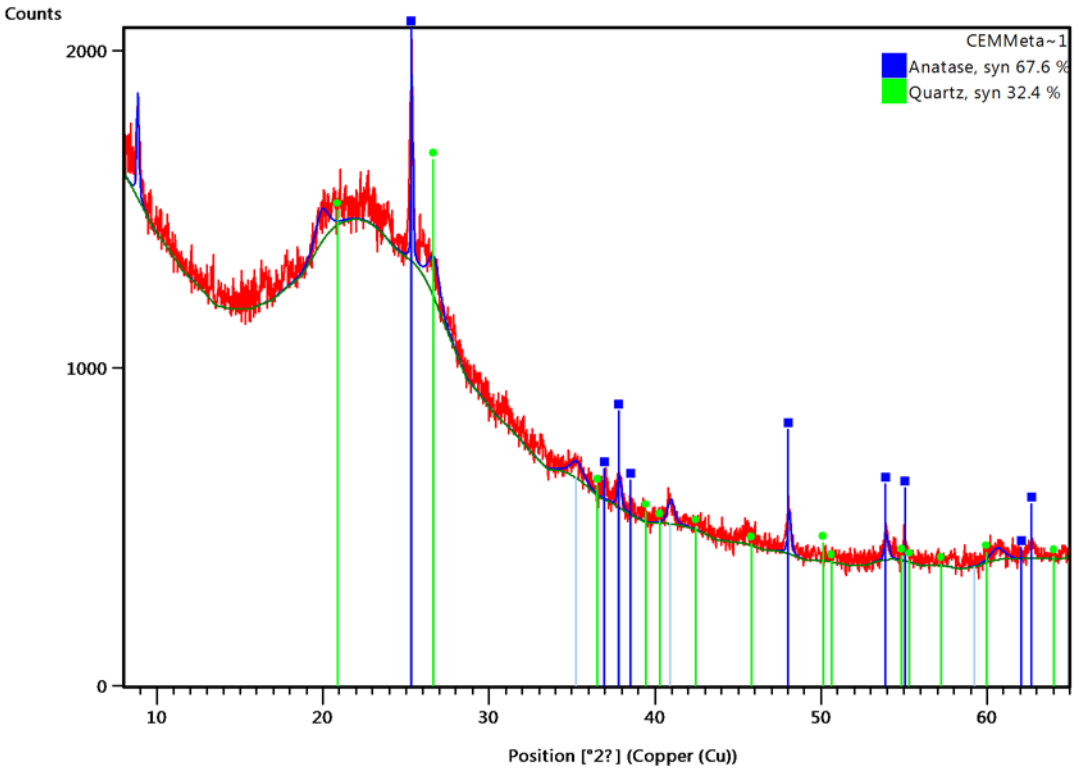

Figure A-10. X-ray diffractogram of metakaolin.

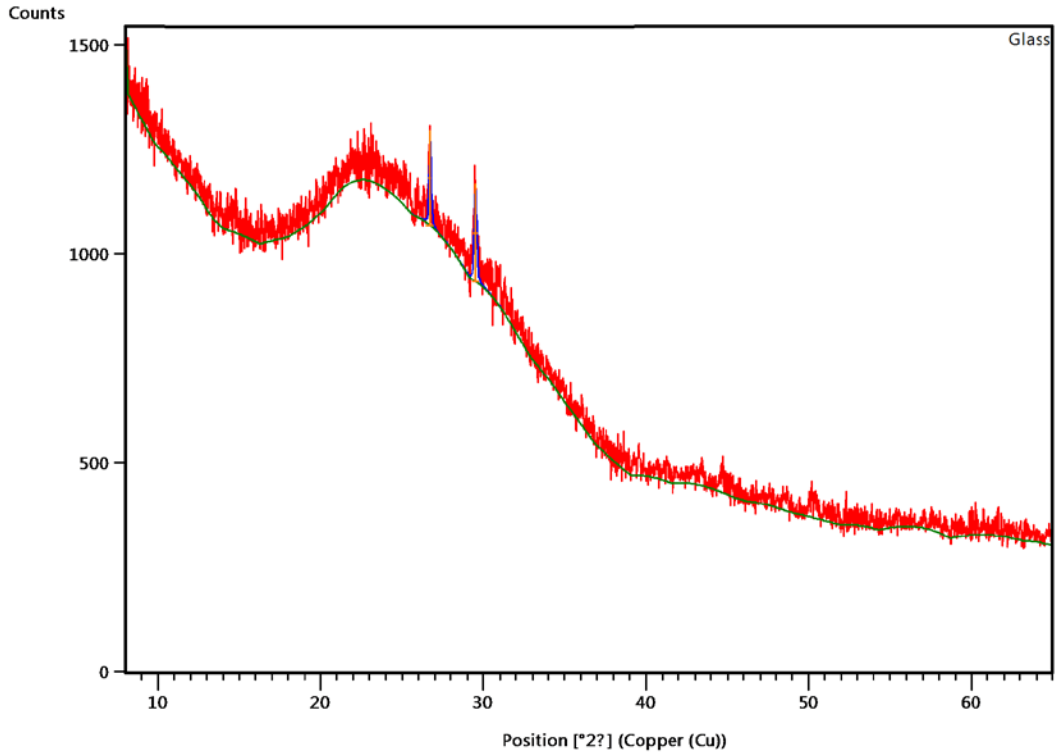

Figure A-11. X-ray diffractogram for recycled glass.

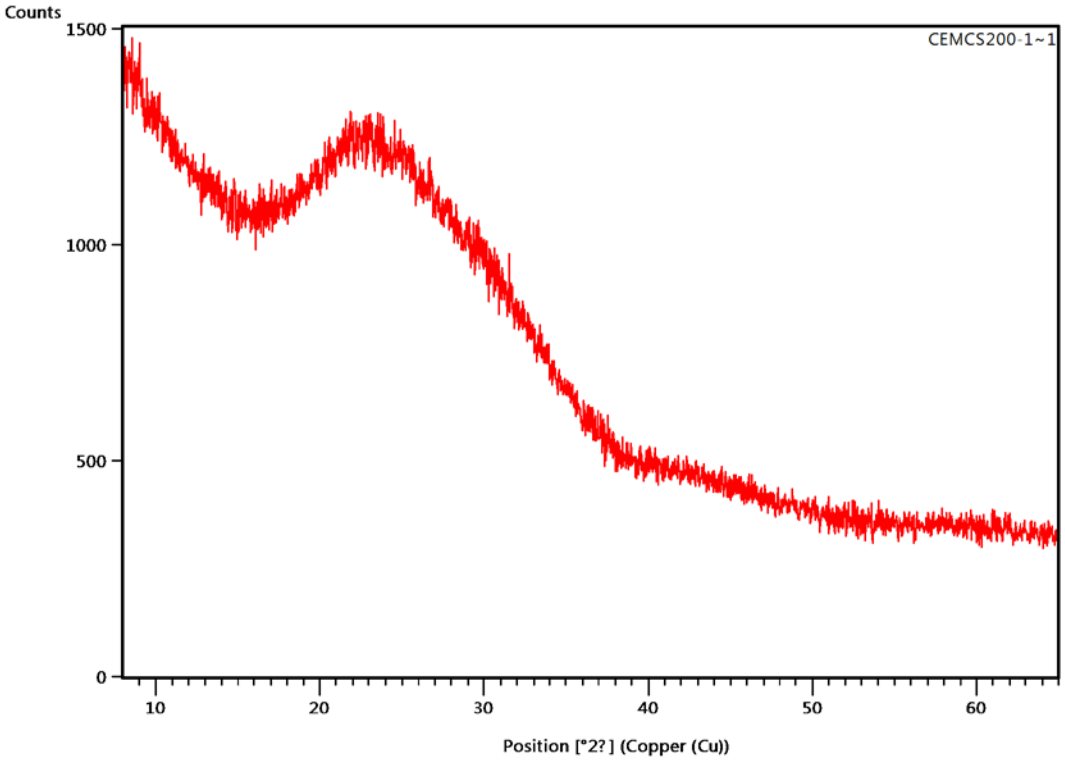

Figure A-12. X-ray diffractogram for CS200 ground glass.

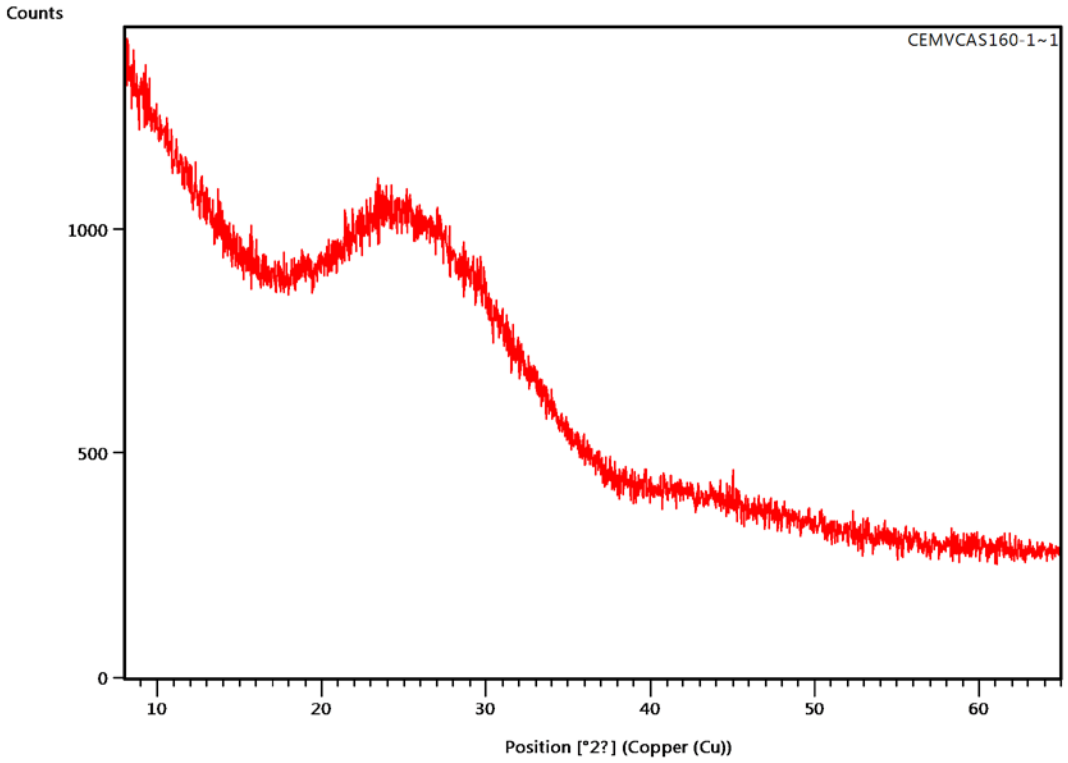

Figure A-13. X-ray diffractogram for VCAS 160 ground glass.

A.2. Laser Particle Analysis Results

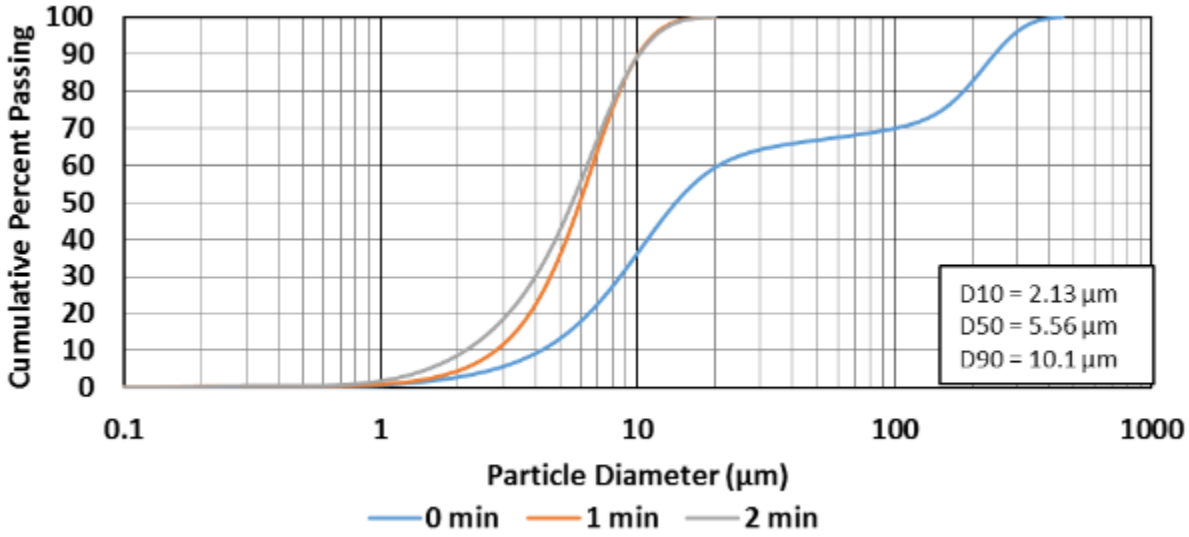

Figure A-14. Particle size distribution for portland cement.

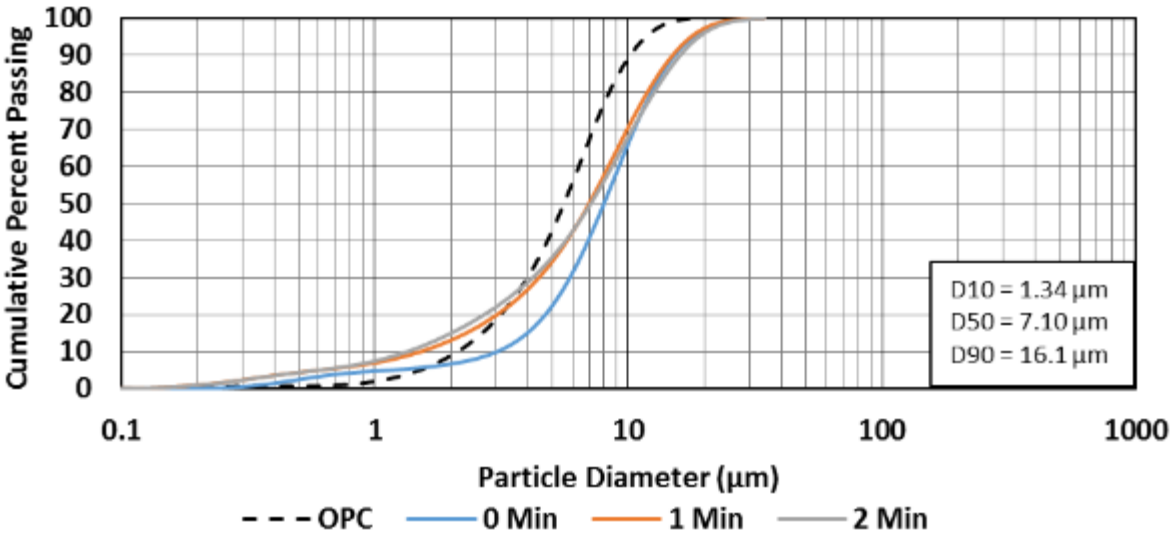

Figure A-15. Particle size distribution for class C fly ash.

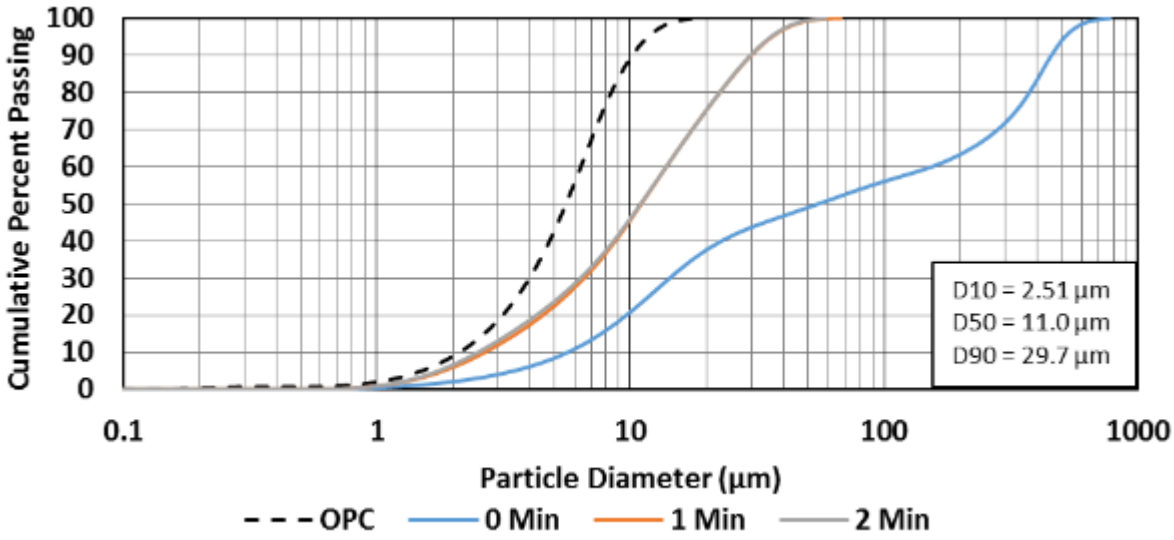

Figure A-16. Particle size distribution for class F fly ash.

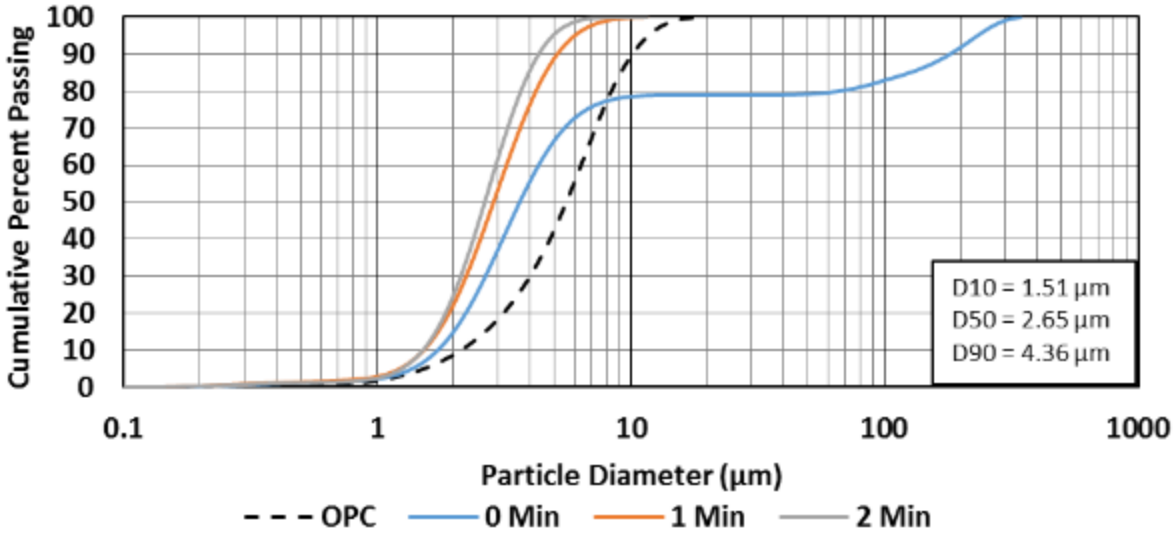

Figure A-17. Particle size distribution for Micron[3].

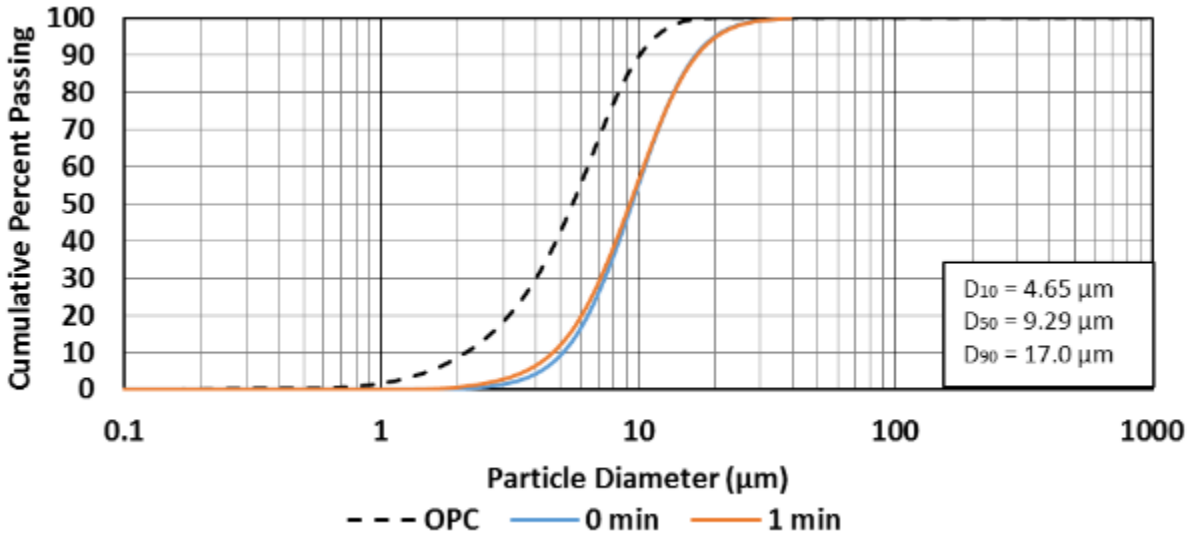

Figure A-18. Particle size distribution for ground blast furnace slag.

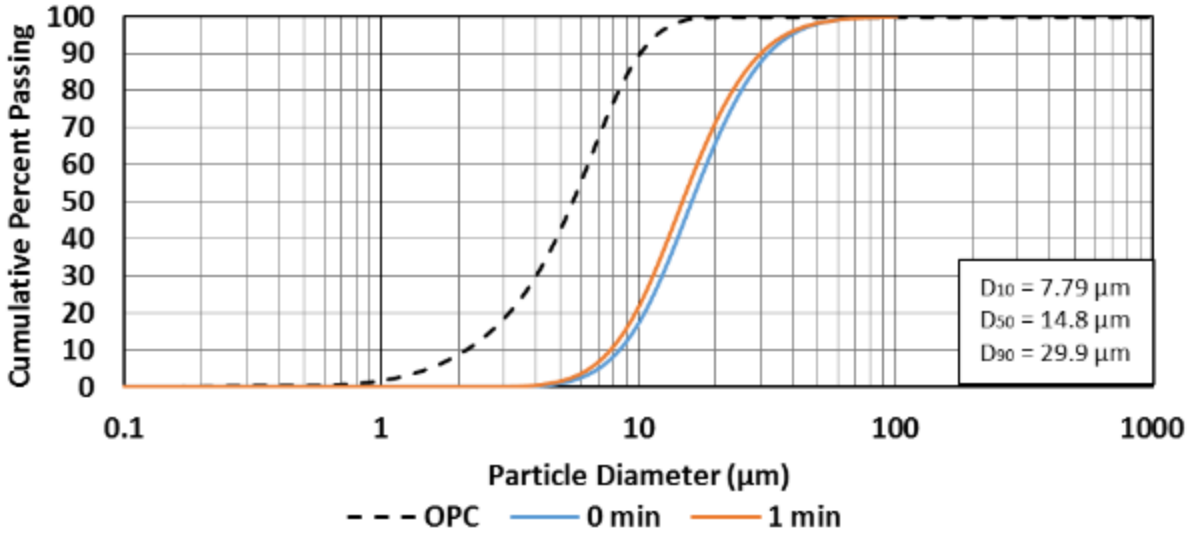

Figure A-19. Particle size distribution for sieved SCBA (below 75 µm).

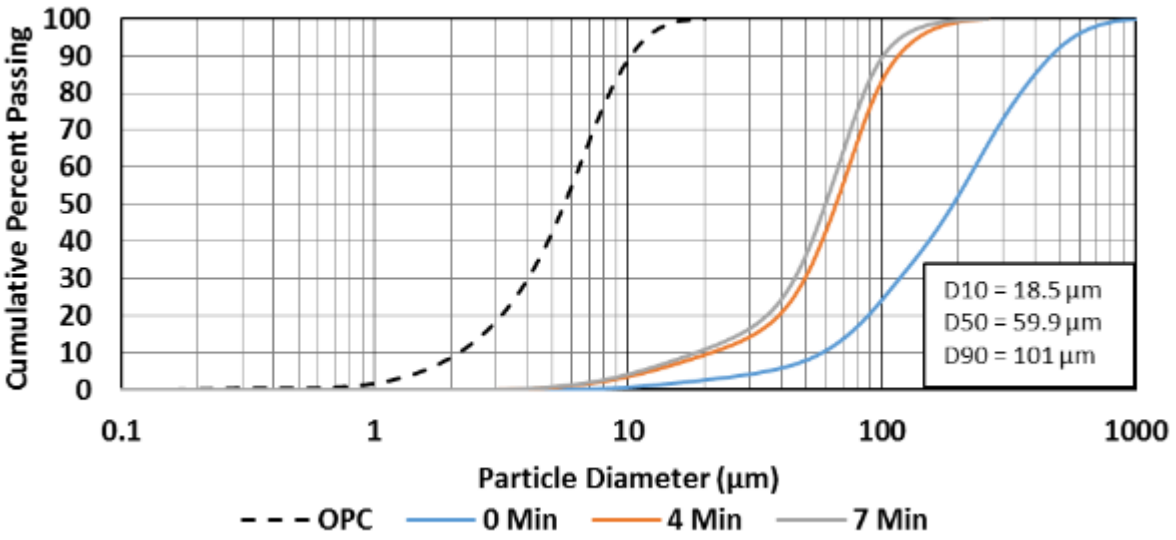

Figure A-20. Particle size distribution for rice husk ash.

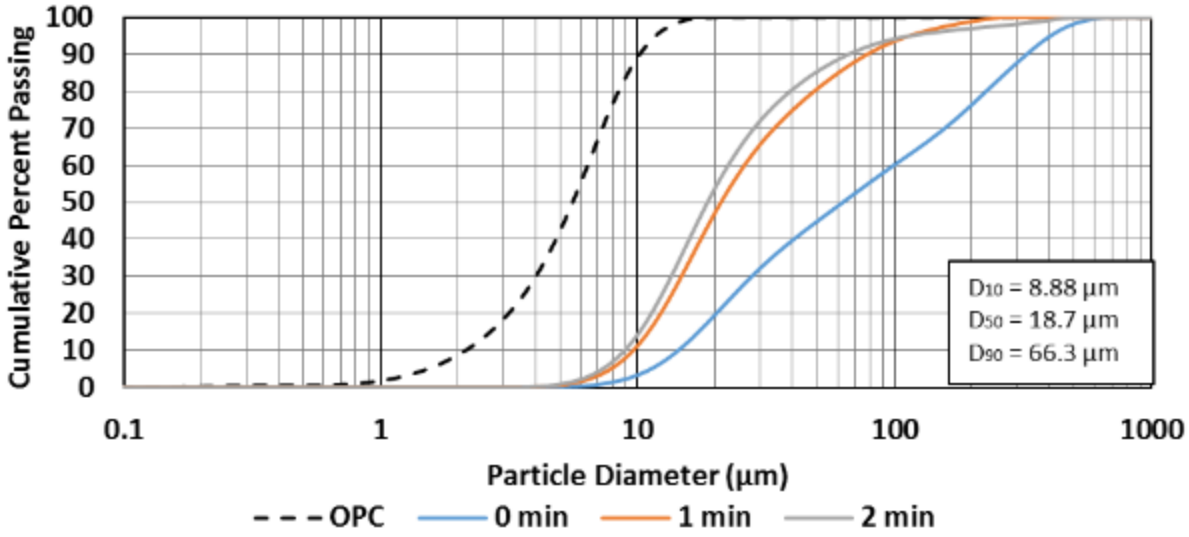

Figure A-21. Particle size distribution for wood ash.

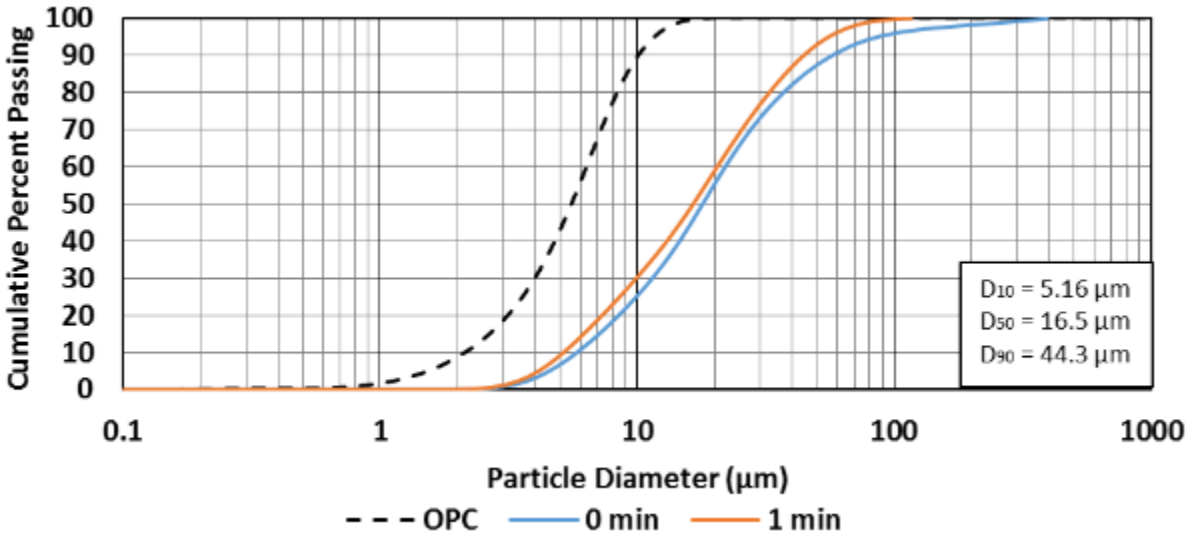

Figure A-22. Particle size distribution for CS200 ground glass.

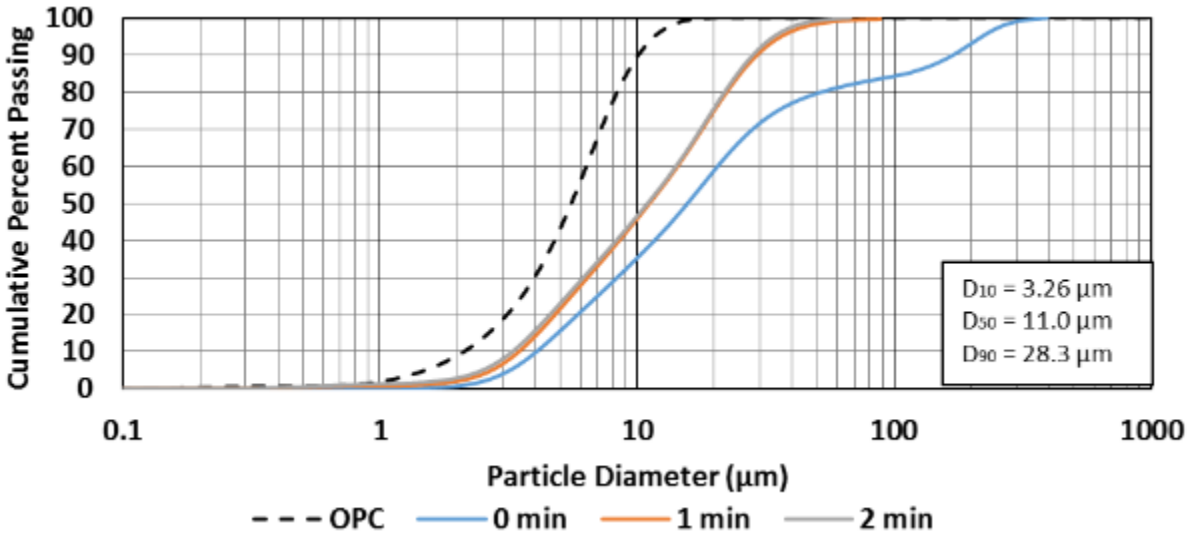

Figure A-23. Particle size distribution for VCAS160 ground glass.

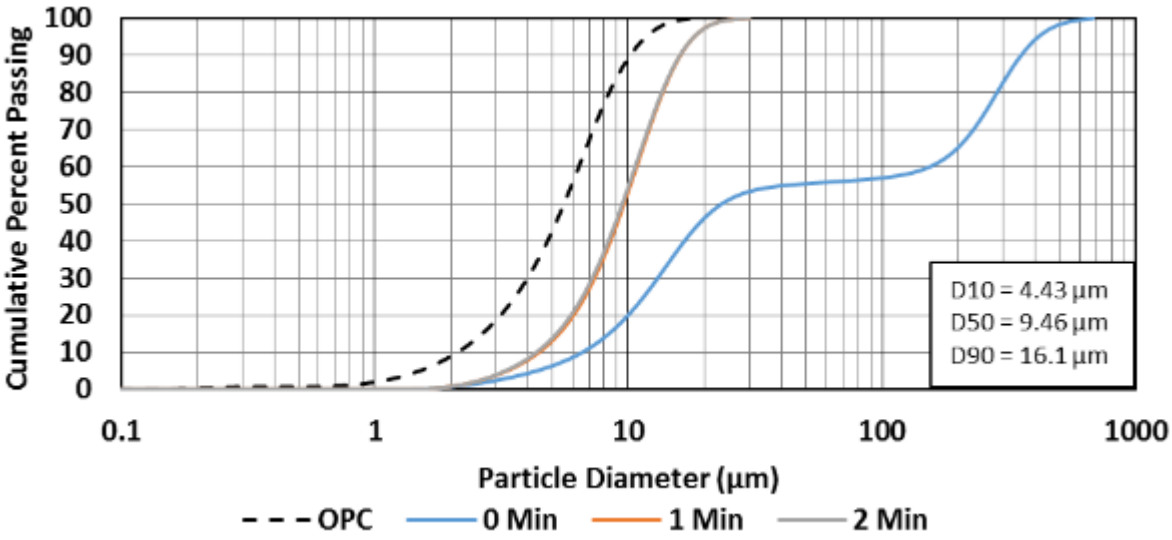

Figure A-24. Particle size distribution for ground glass.

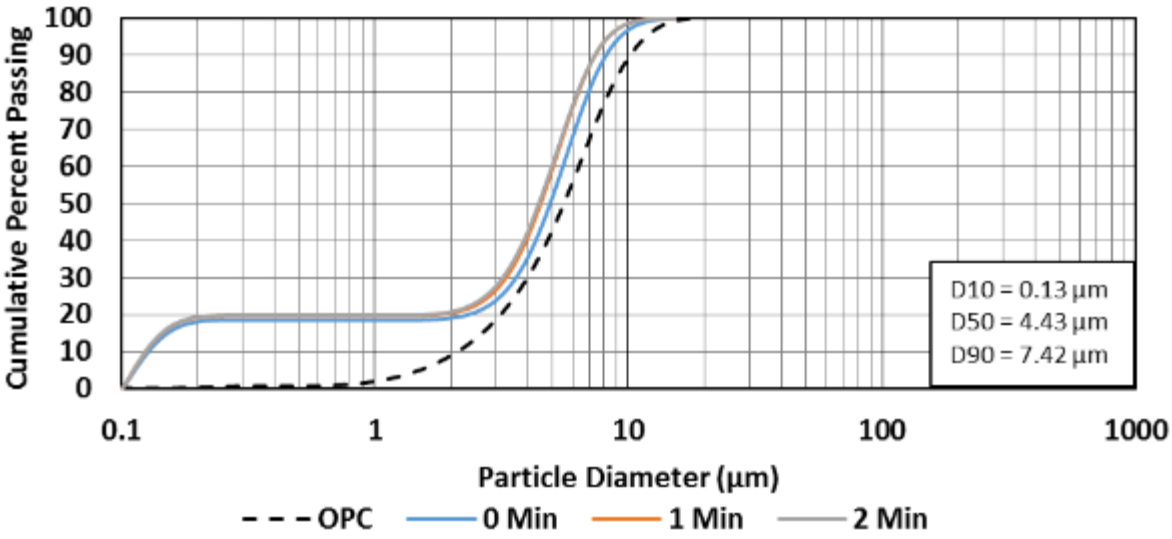

Figure A-25. Particle size distribution for metakaolin.

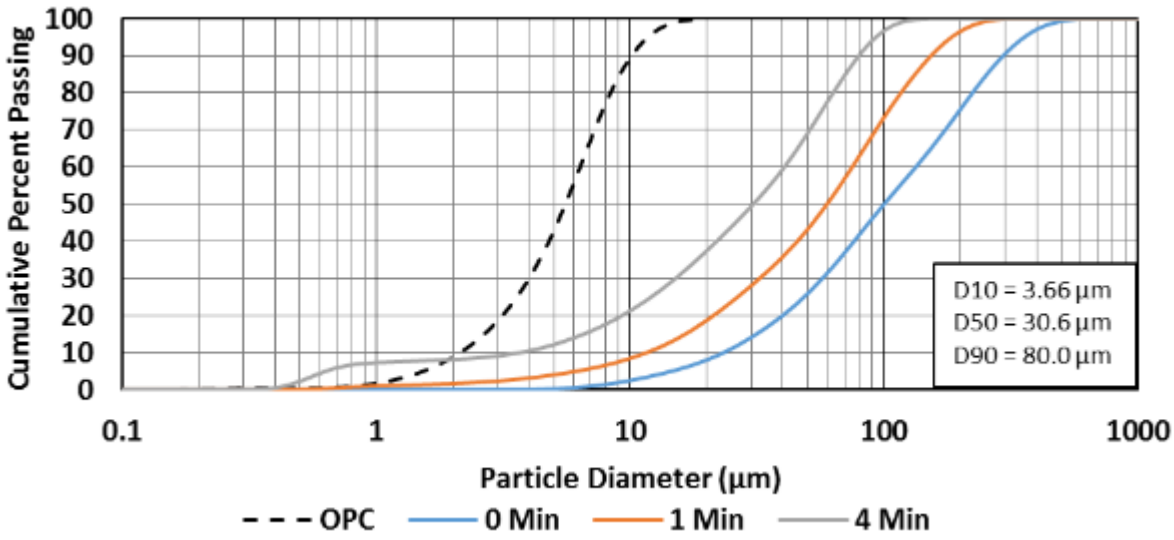

Figure A-26. Particle size distribution for silica fume.

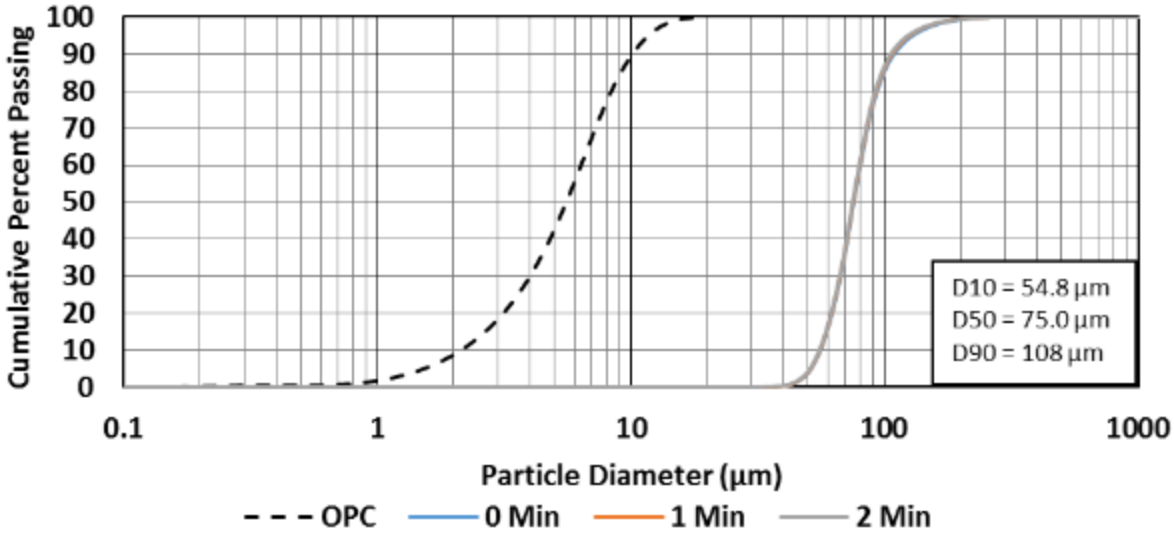

Figure A-27. Particle size distribution for equilibrium catalyst.

A.3. Specific Heat Capacity Results

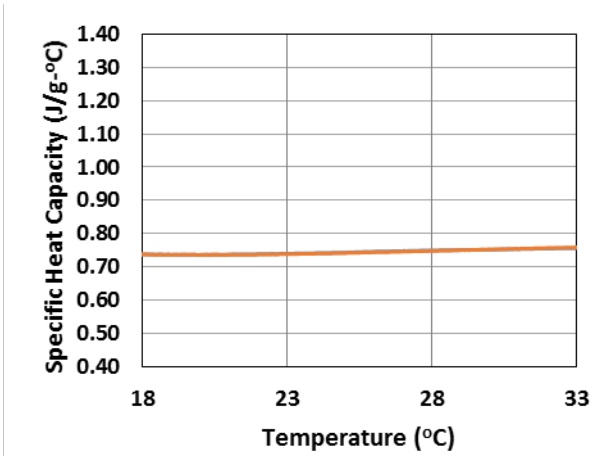

Figure A-28. Specific heat capacity of OPC.

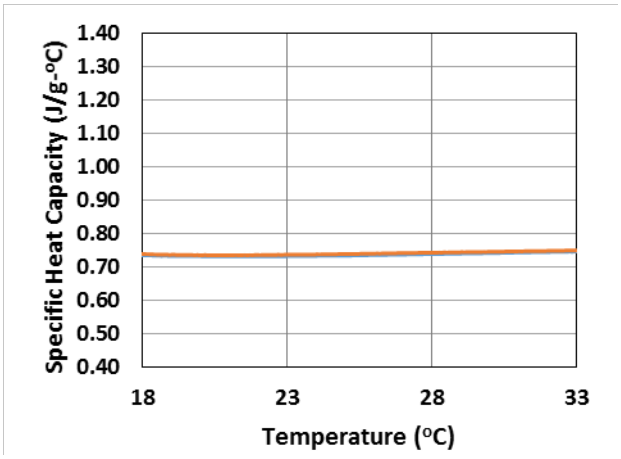

Figure A-29. Specific heat capacity of Class C ash

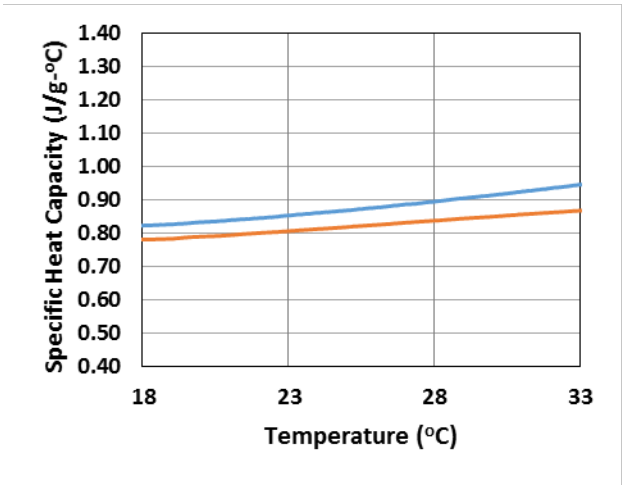

Figure A-30. Specific heat capacity of biomass ash.

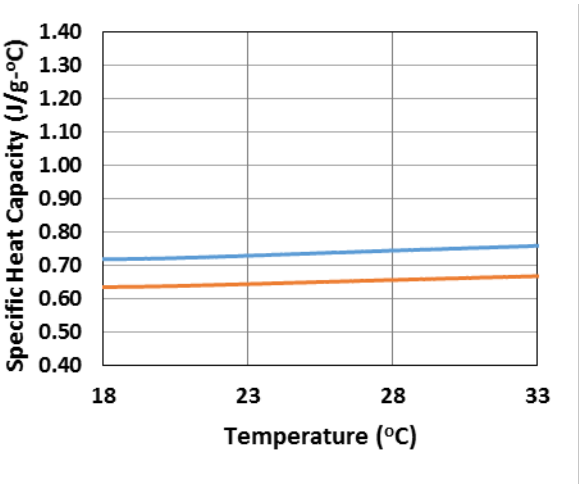

Figure A-31. Specific heat capacity of glass.

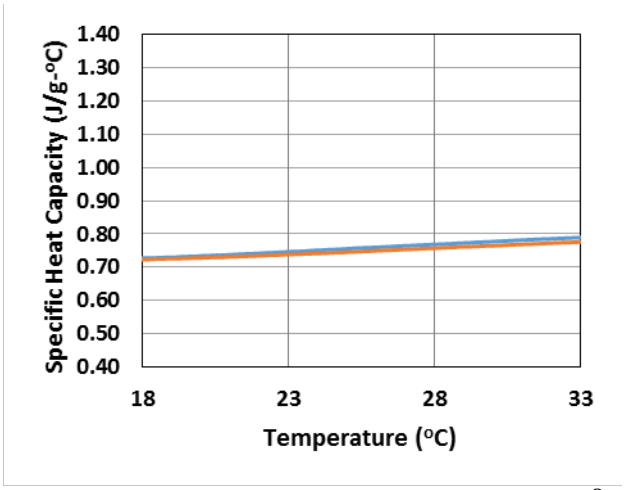

Figure A-32. Specific heat capacity of Micron[3].

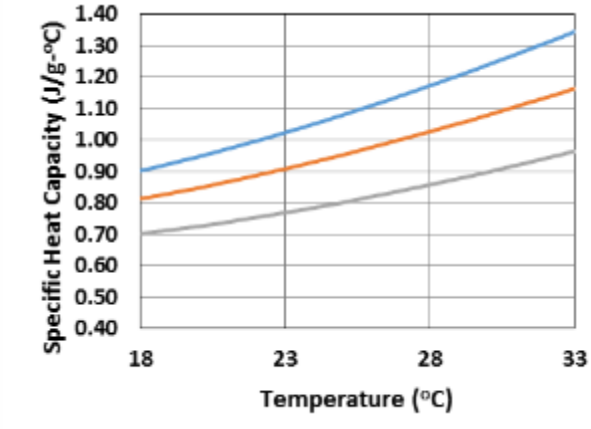

Figure A-33. Specific heat capacity of SCBA.

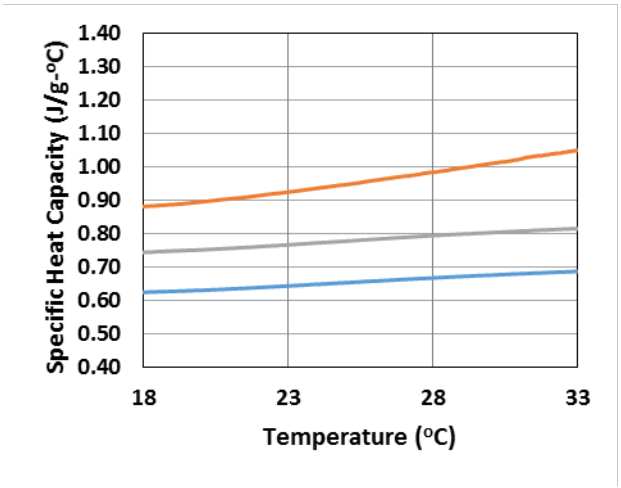

Figure A-34. Specific heat capacity of metakaolin.

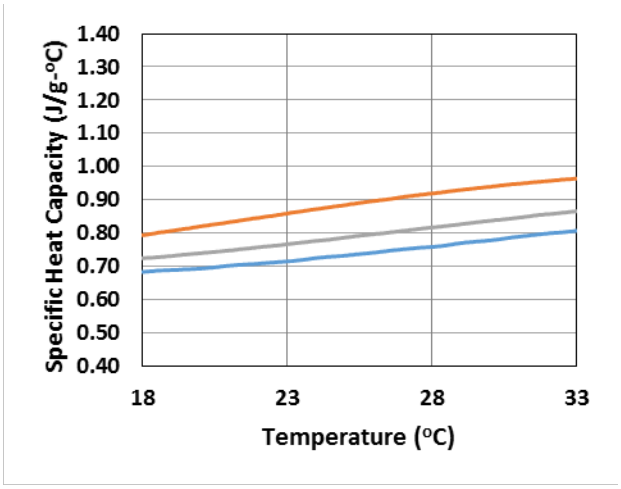

Figure A-35. Specific heat capacity of ECAT.

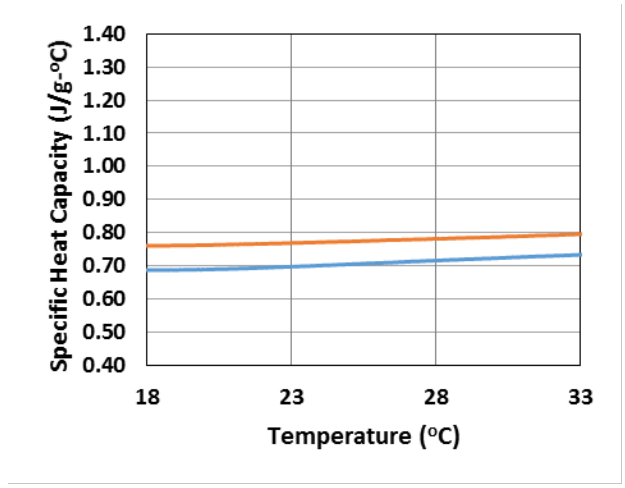

Figure A-36. Specific heat capacity of slag.

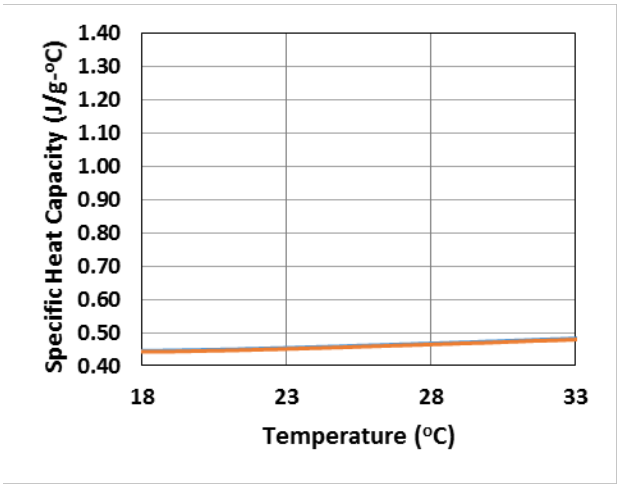

Figure A-37. Specific heat capacity of diamond.

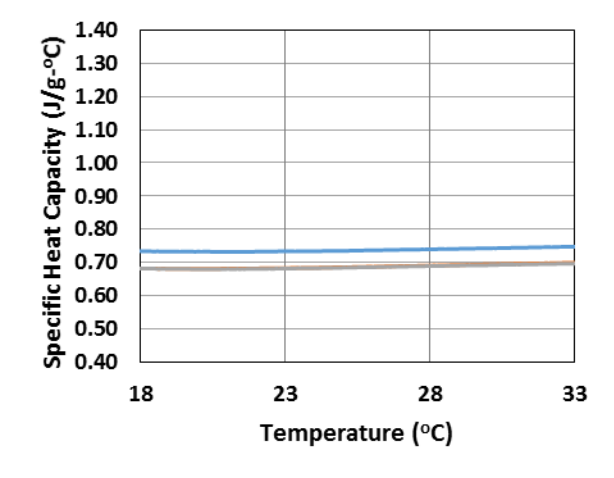

Figure A-38. Specific heat capacity of VCAS 160.

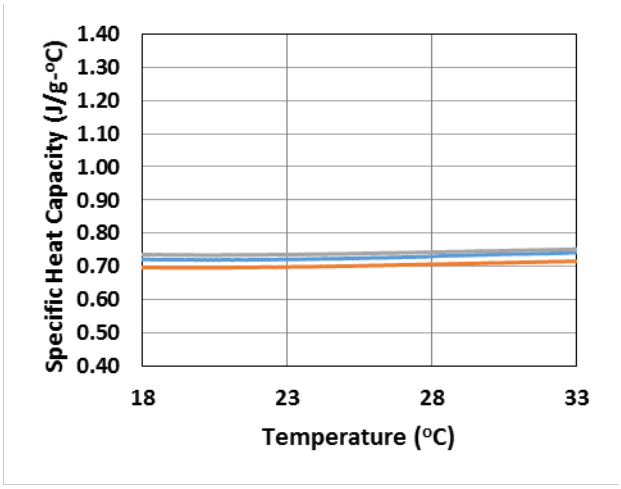

Figure A-39. Specific heat capacity of CS200.

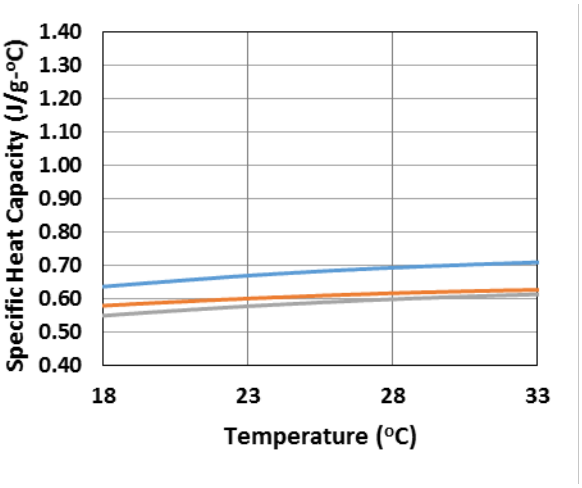

Figure A-40. Specific heat capacity of rice ash.

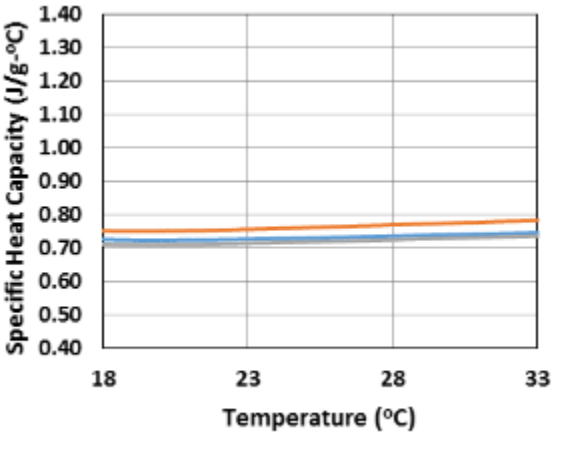

Figure A-41. Specific heat capacity of F ash.

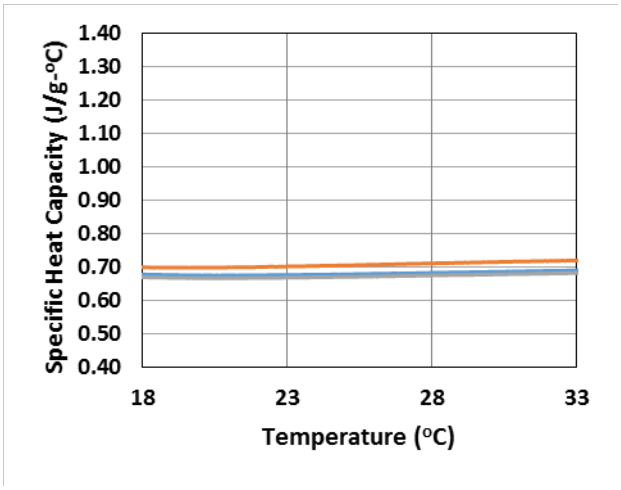

Figure A-42. Specific heat capacity of isothermal glass vials.

B. APPENDIX B – ISOTHERMAL CALORIMETRY RESULTS

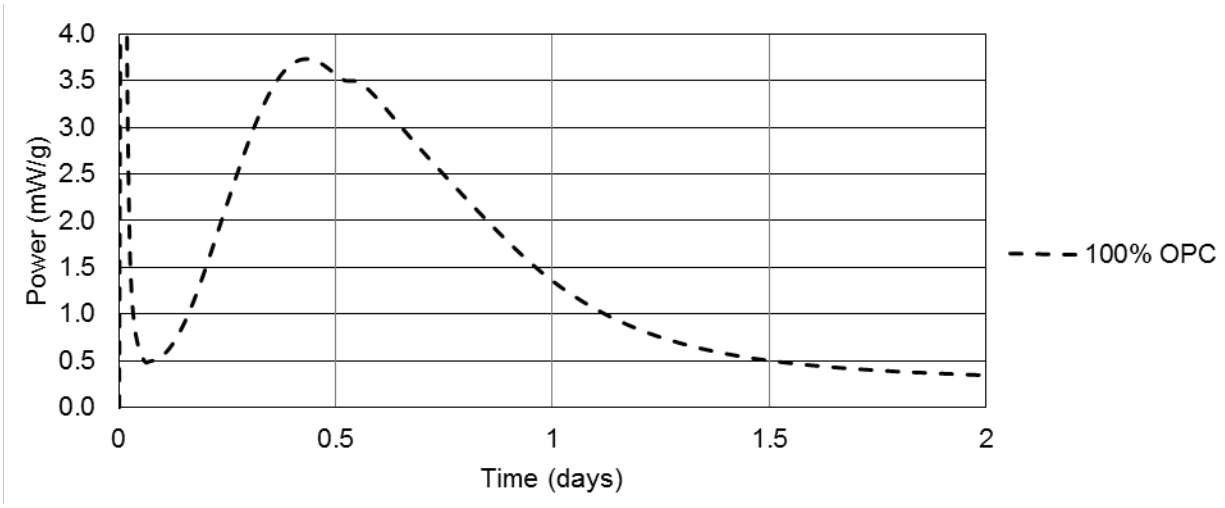

Figure B-1. Isothermal calorimetry power curve for 100% portland cement.

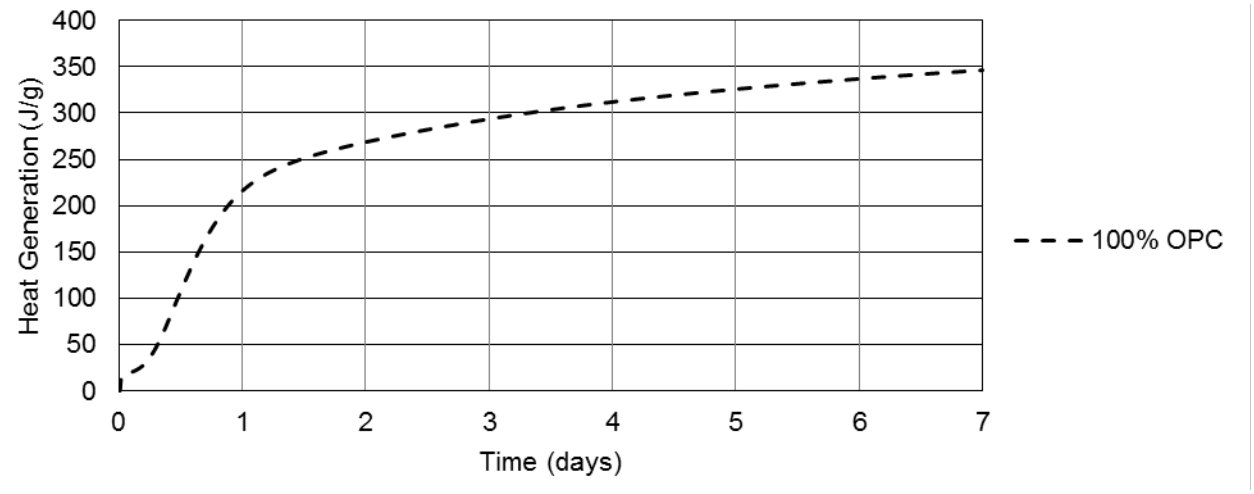

Figure B-2. Isothermal calorimetry heat generation curve for 100% portland cement.

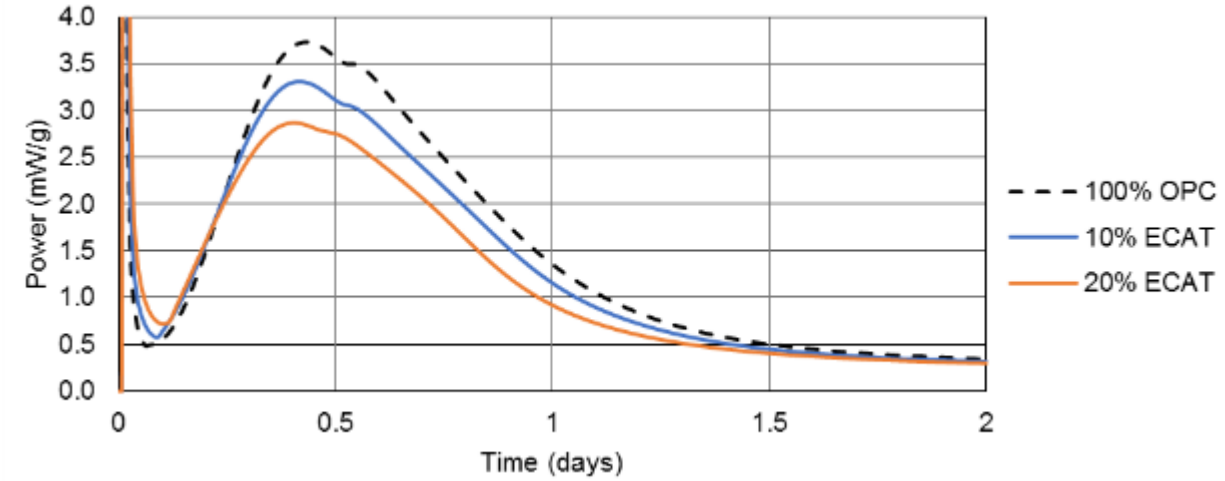

Figure B-3. Isothermal calorimetry power curve for equilibrium catalyst.

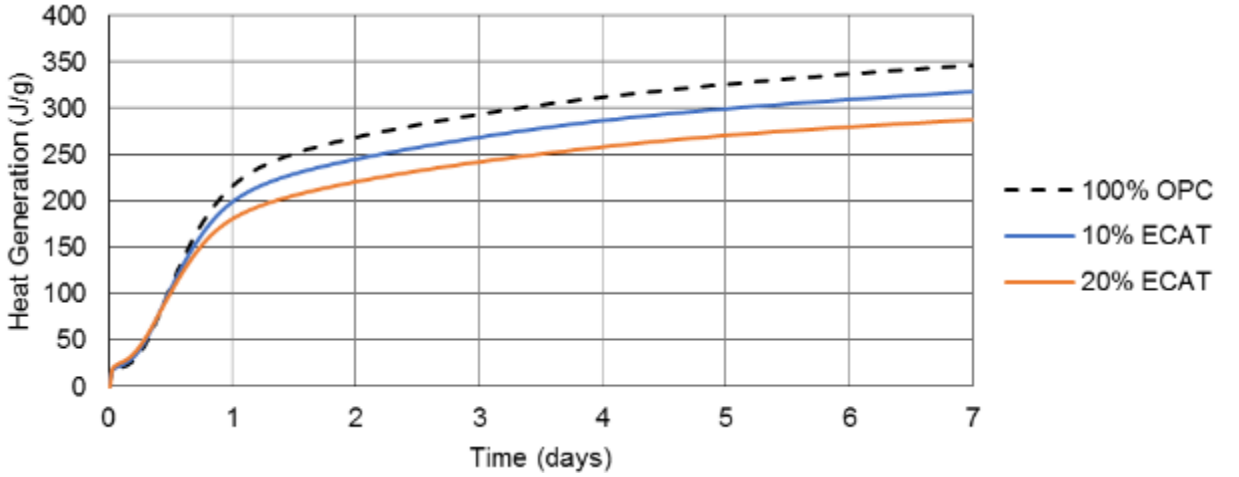

Figure B-4. Isothermal calorimetry heat generation curve for equilibrium catalyst.

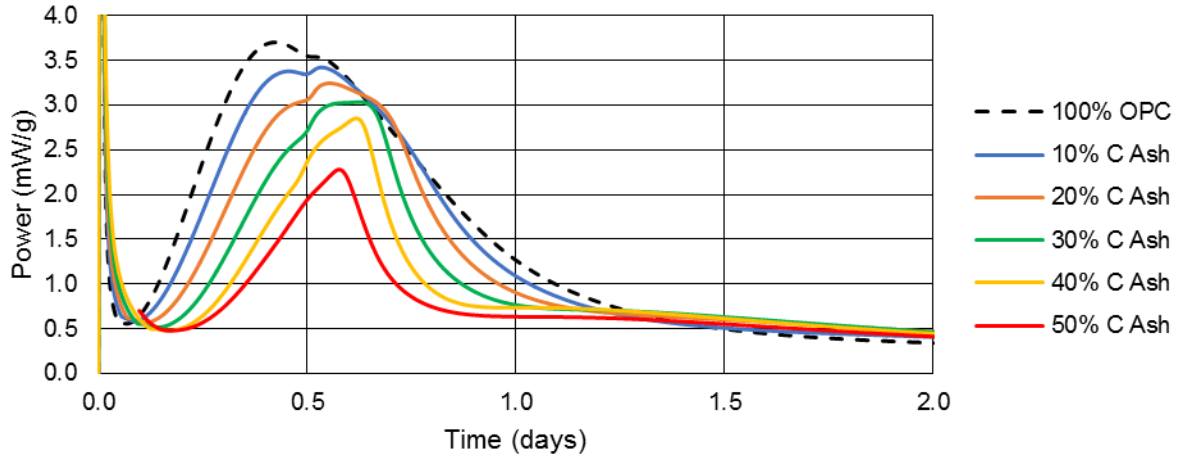

Figure B-5. Isothermal calorimetry power curve for class C fly ash.

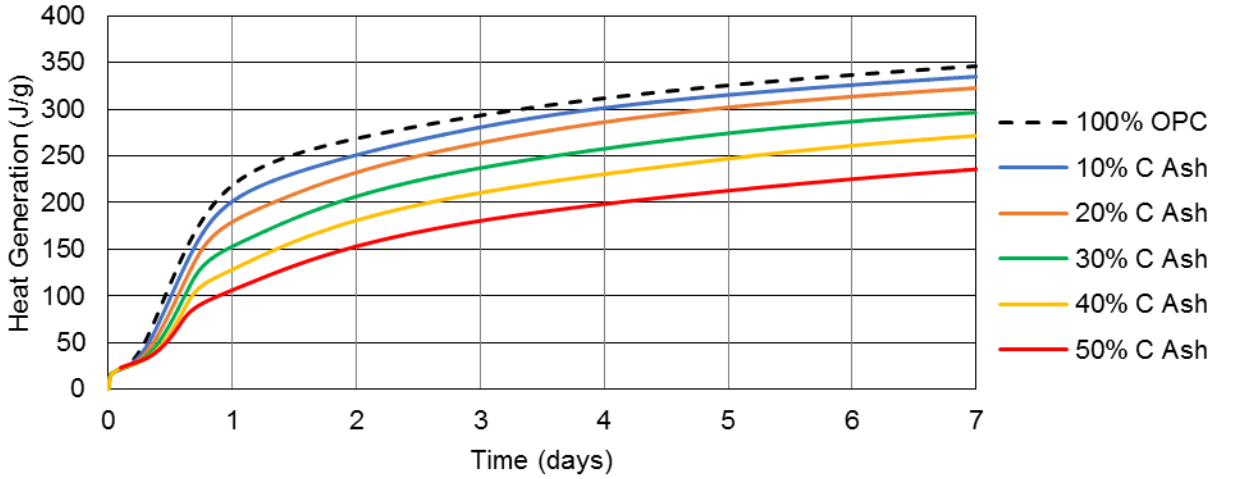

Figure B-6. Isothermal calorimetry heat generation curve for class C fly ash.

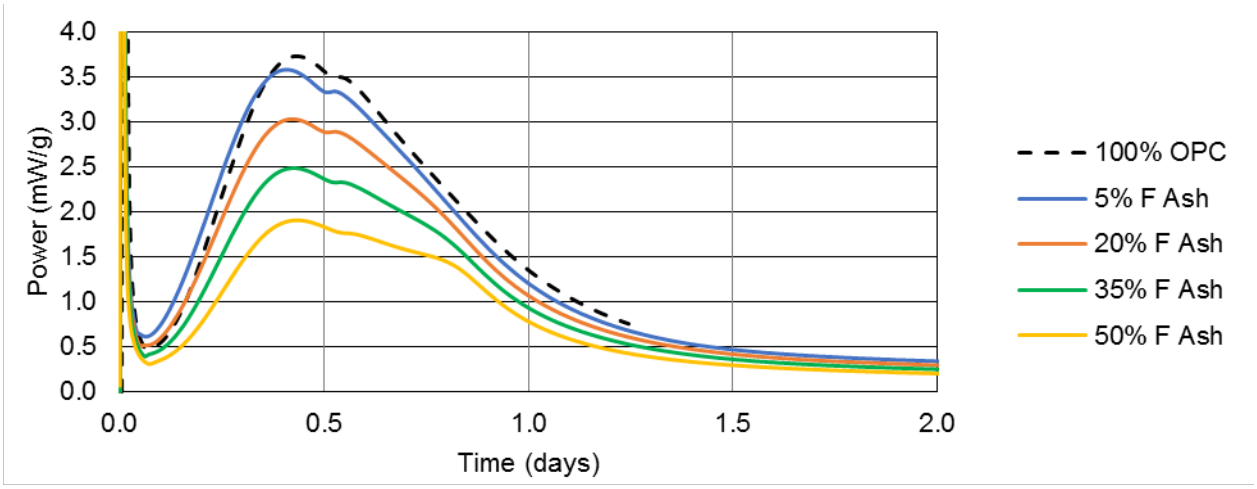

Figure B-7. Isothermal calorimetry power curve for class F fly ash.

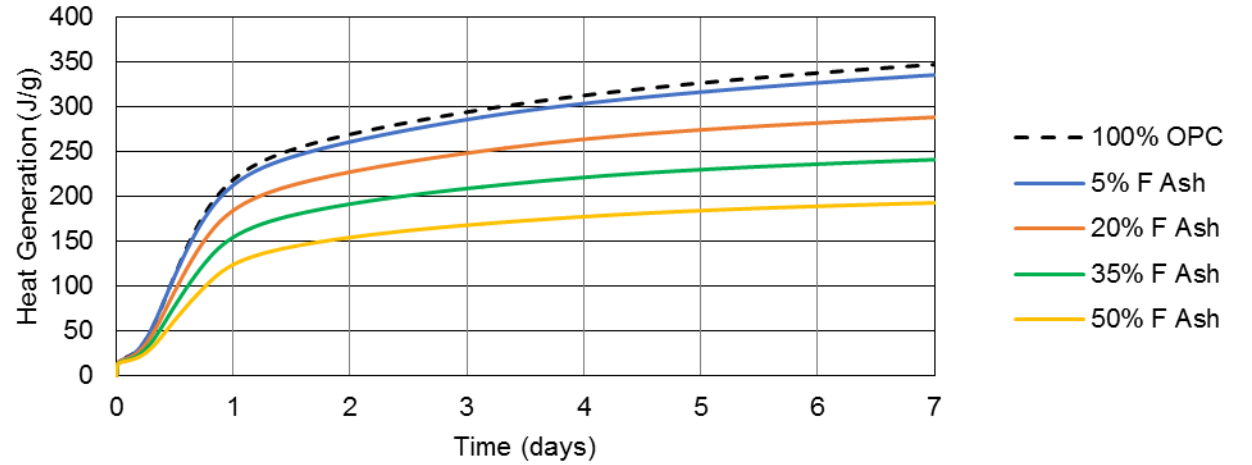

Figure B-8. Isothermal calorimetry heat generation curve for class F fly ash.

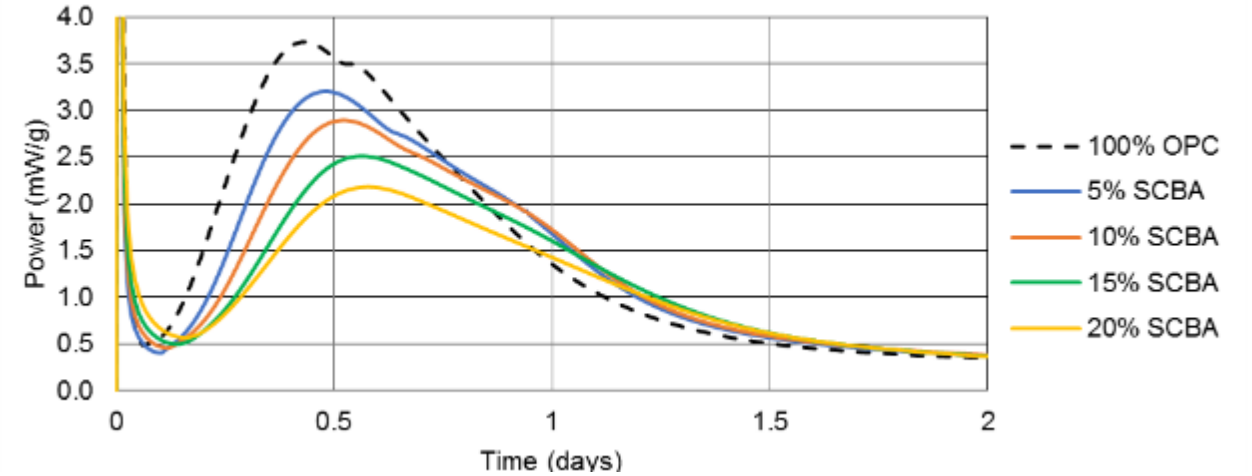

Figure B-9. Isothermal calorimetry power curve for sugarcane bagasse ash.

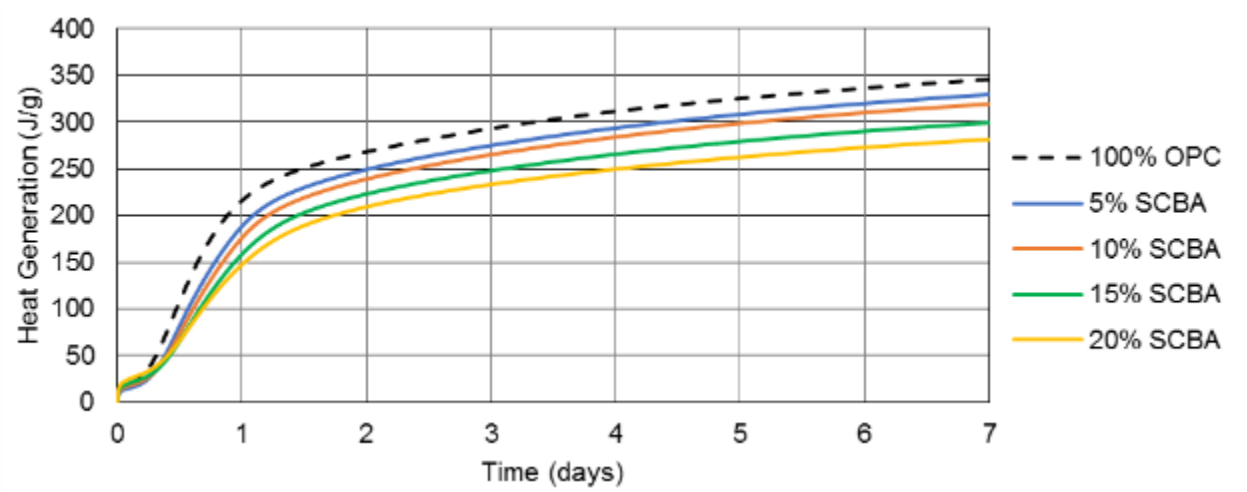

Figure B-10. Isothermal calorimetry heat generation curve for sugarcane bagasse ash.

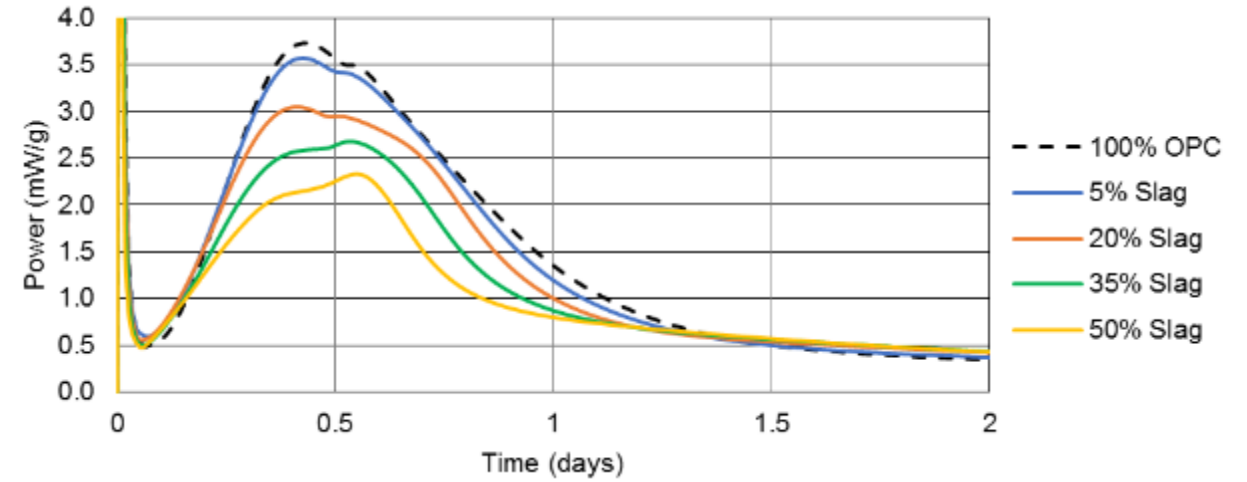

Figure B-11. Isothermal calorimetry power curve for ground blast furnace slag.

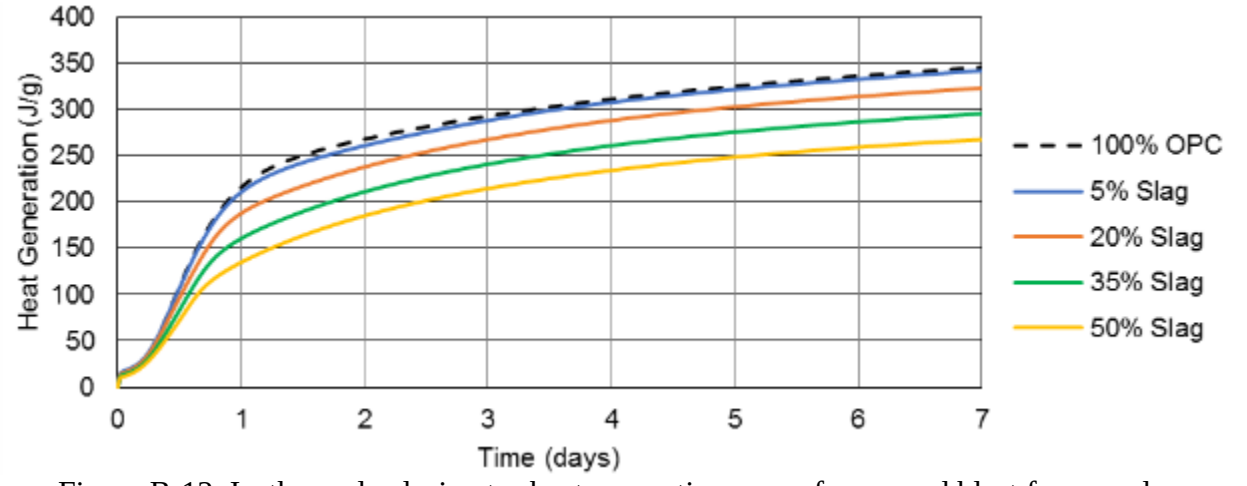

Figure B-12. Isothermal calorimetry heat generation curve for ground blast furnace slag.

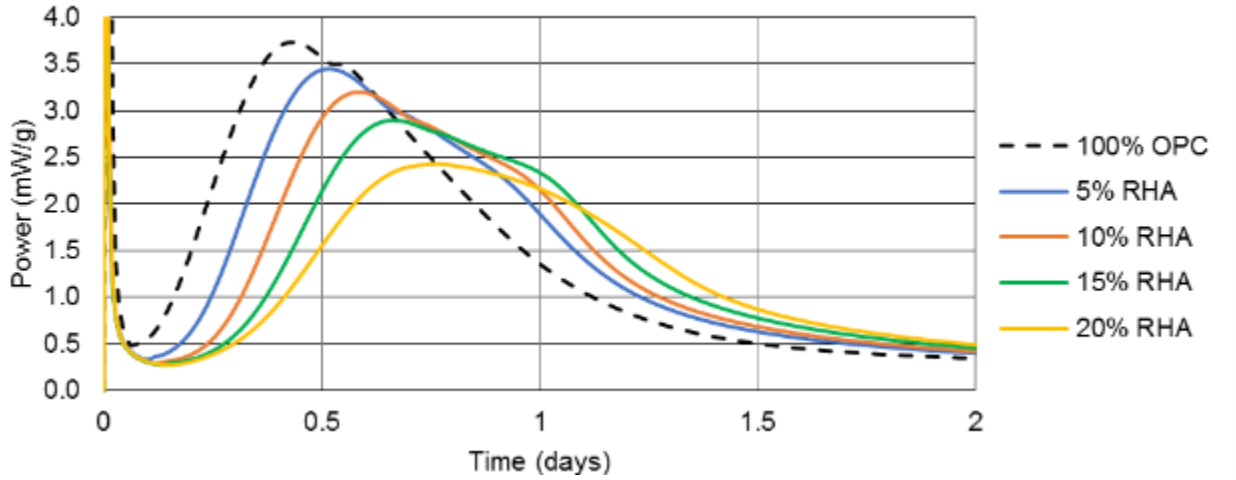

Figure B-13. Isothermal calorimetry power curve for rice husk ash.

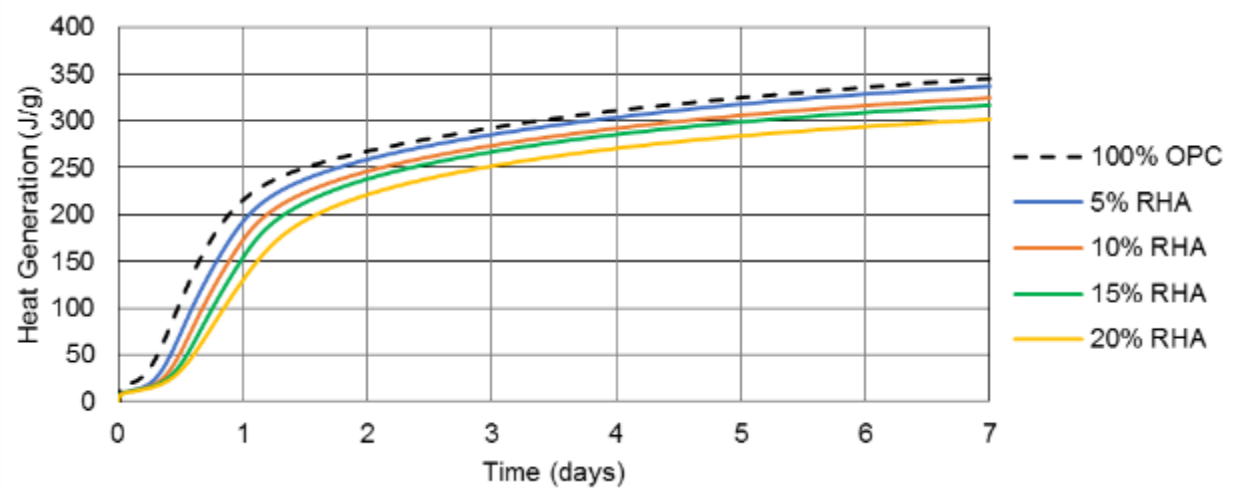

Figure B-14. Isothermal calorimetry heat generation curve for rice husk ash.

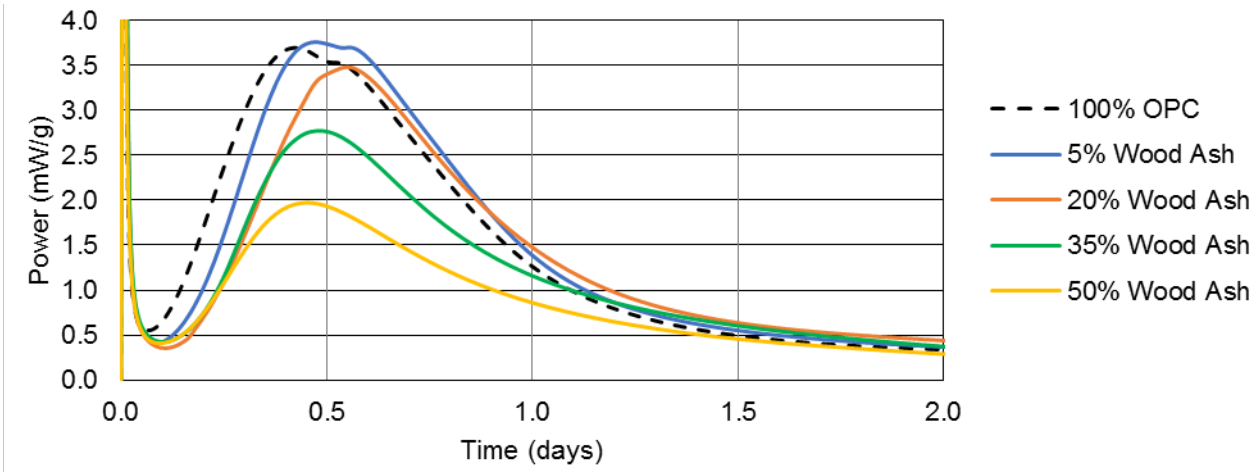

Figure B-15. Isothermal calorimetry power curve for wood ash.

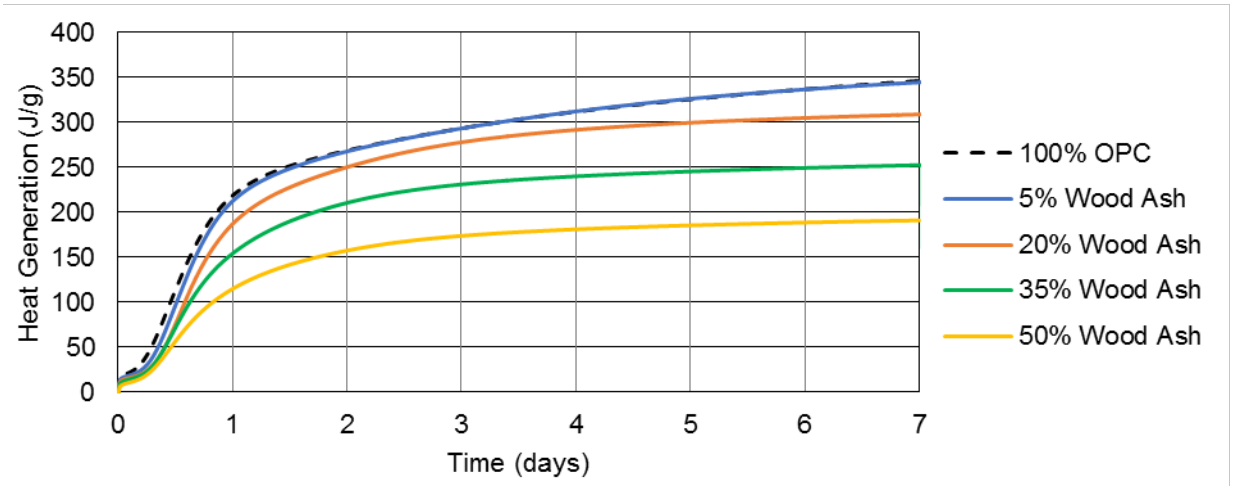

Figure B-16. Isothermal calorimetry heat generation curve for wood ash.

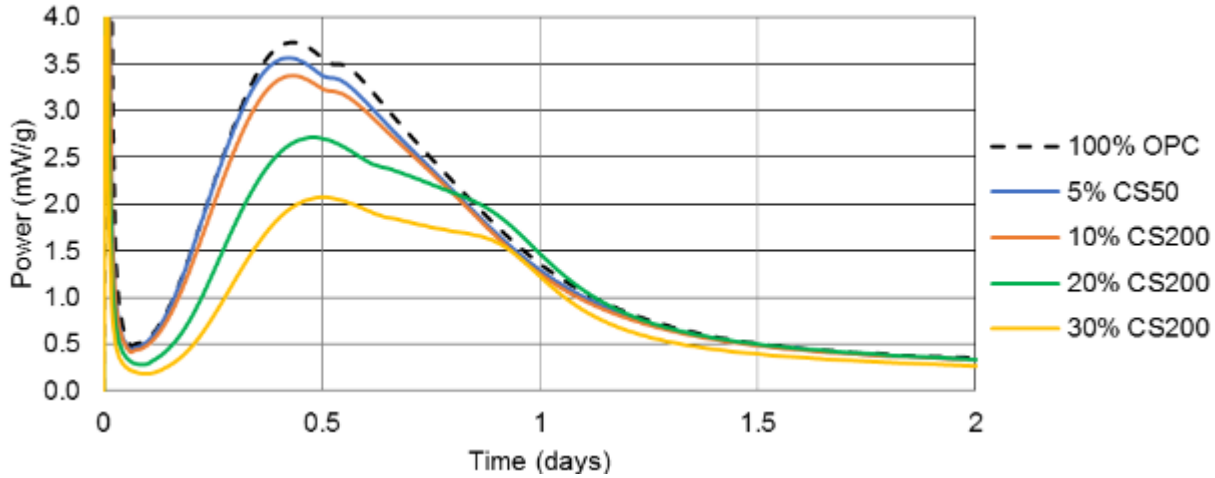

Figure B-17. Isothermal calorimetry power curve for CS200 ground glass.

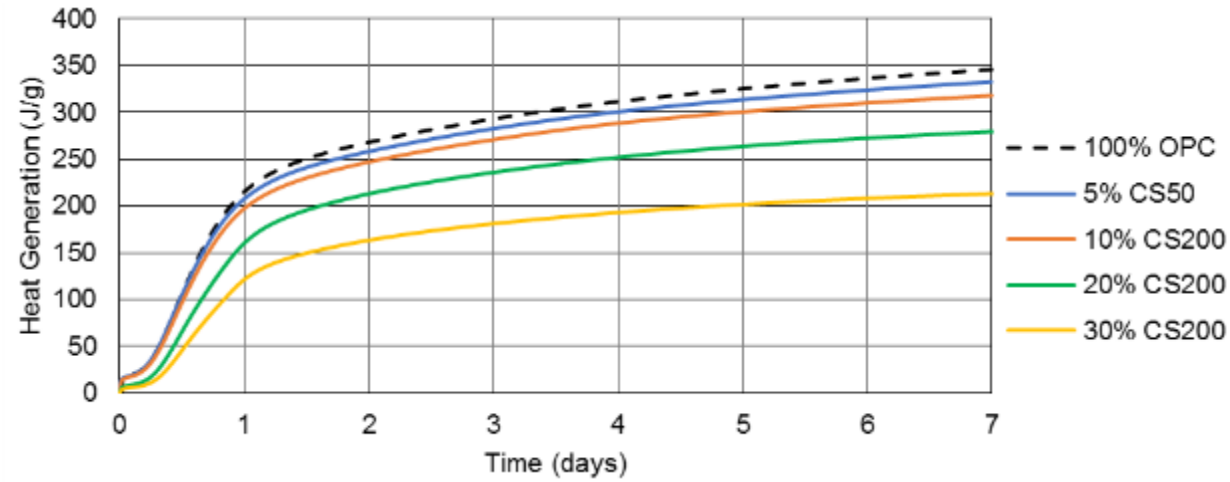

Figure B-18. Isothermal calorimetry heat generation curve for CS200 ground glass.

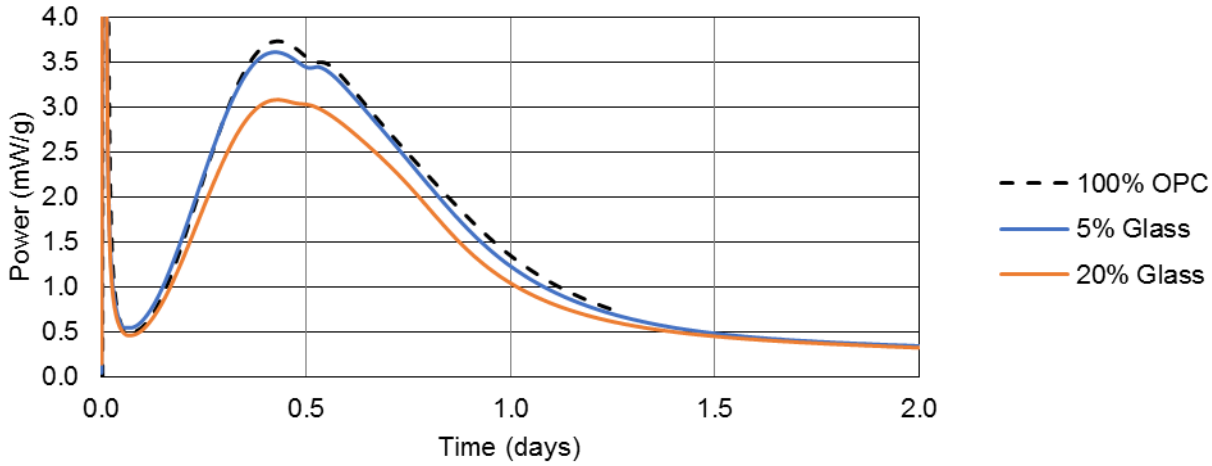

Figure B-19. Isothermal calorimetry power curve for ground glass.

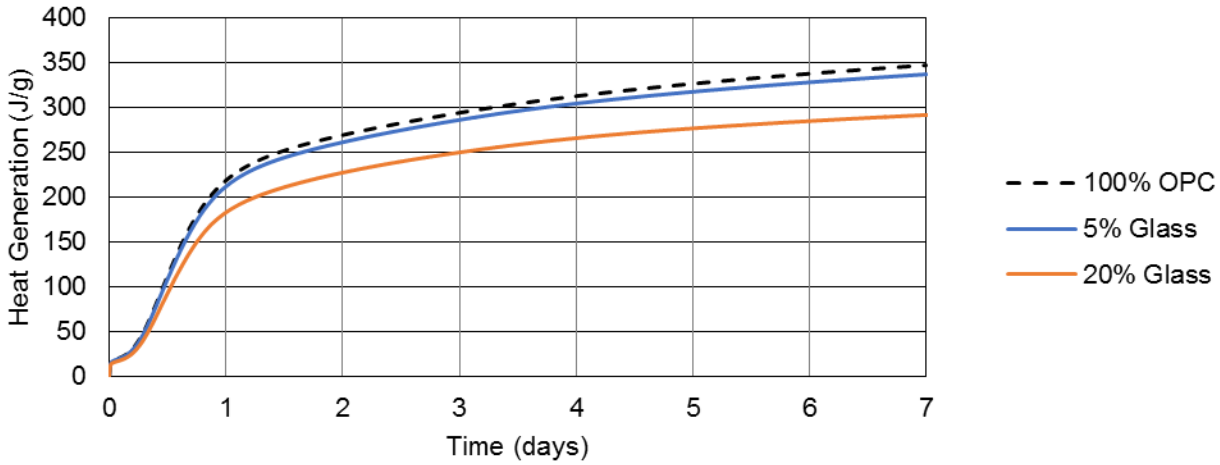

Figure B-20. Isothermal calorimetry heat generation curve for ground glass.

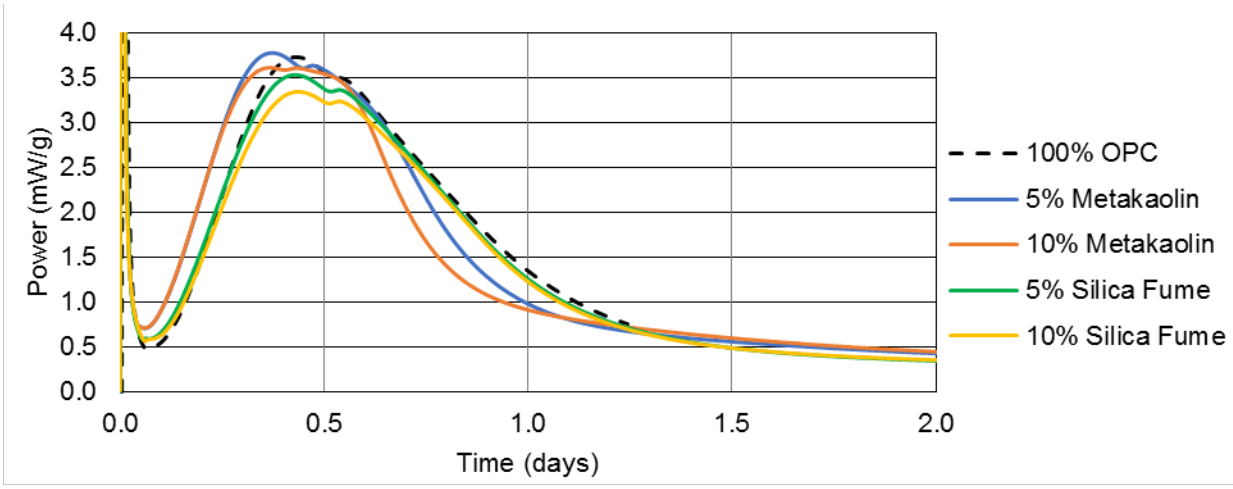

Figure B-21. Isothermal calorimetry power curve for metakaolin and silica fume.

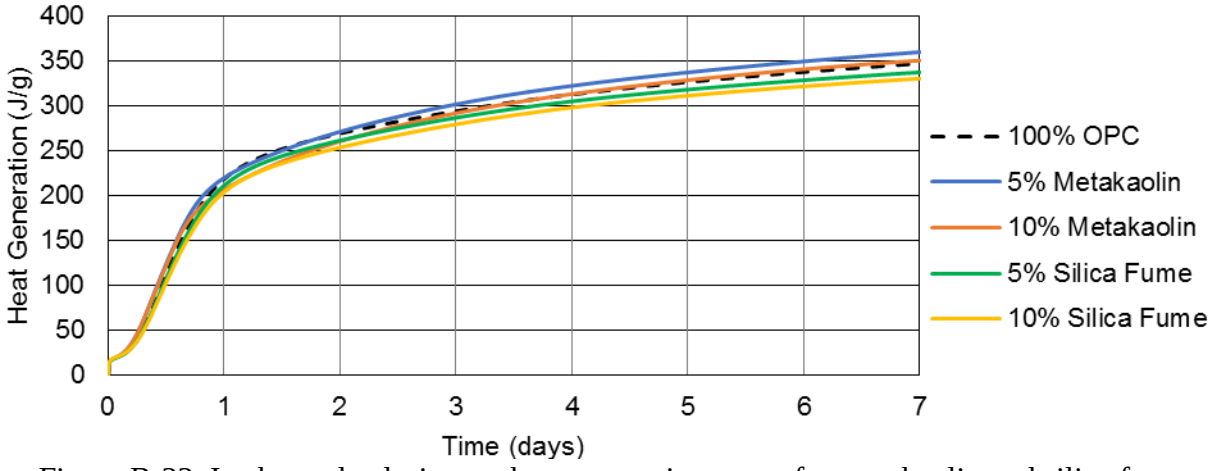

Figure B-22. Isothermal calorimetry heat generation curve for metakaolin and silica fume.

C. APPENDIX C – CEMENTITIOUS MORTAR RESULTS

C.1. Compressive Strength of Mortar Results

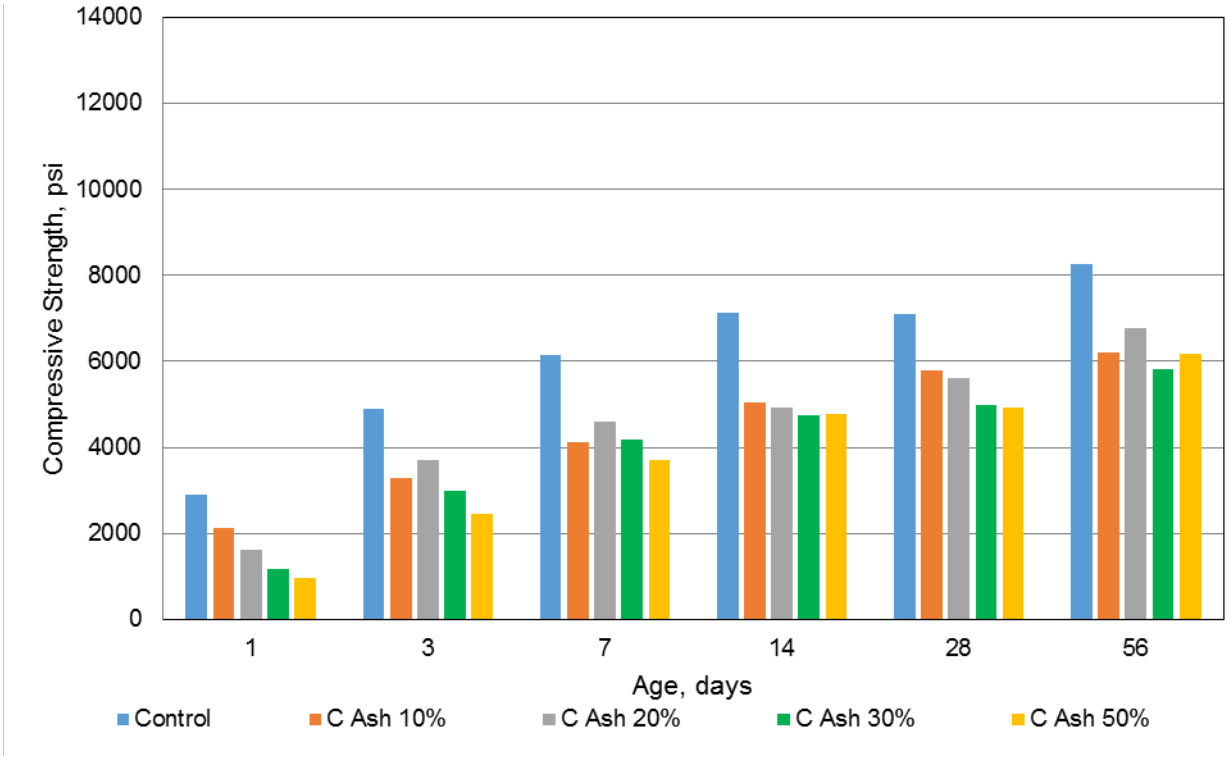

Figure C-1. Compressive strength of mortars containing class C fly ash.

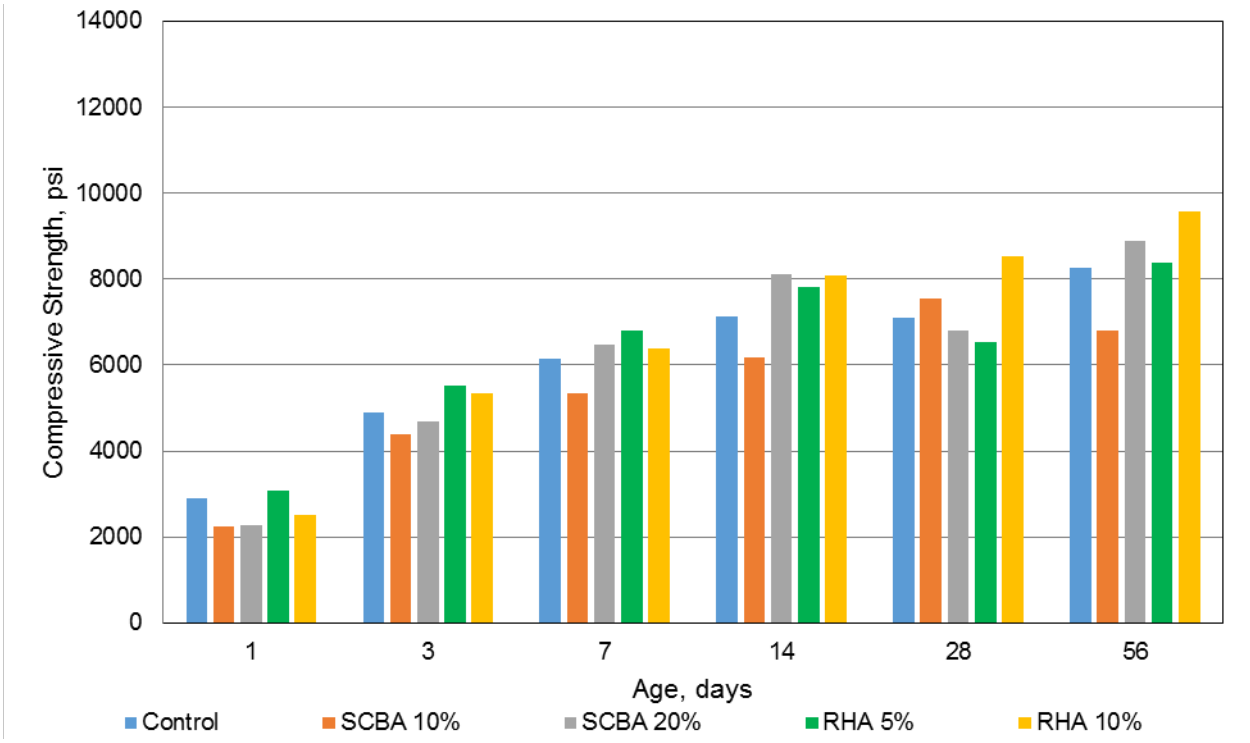

Figure C-2. Compressive strength of mortars containing rice husk or sugarcane bagasse ash.

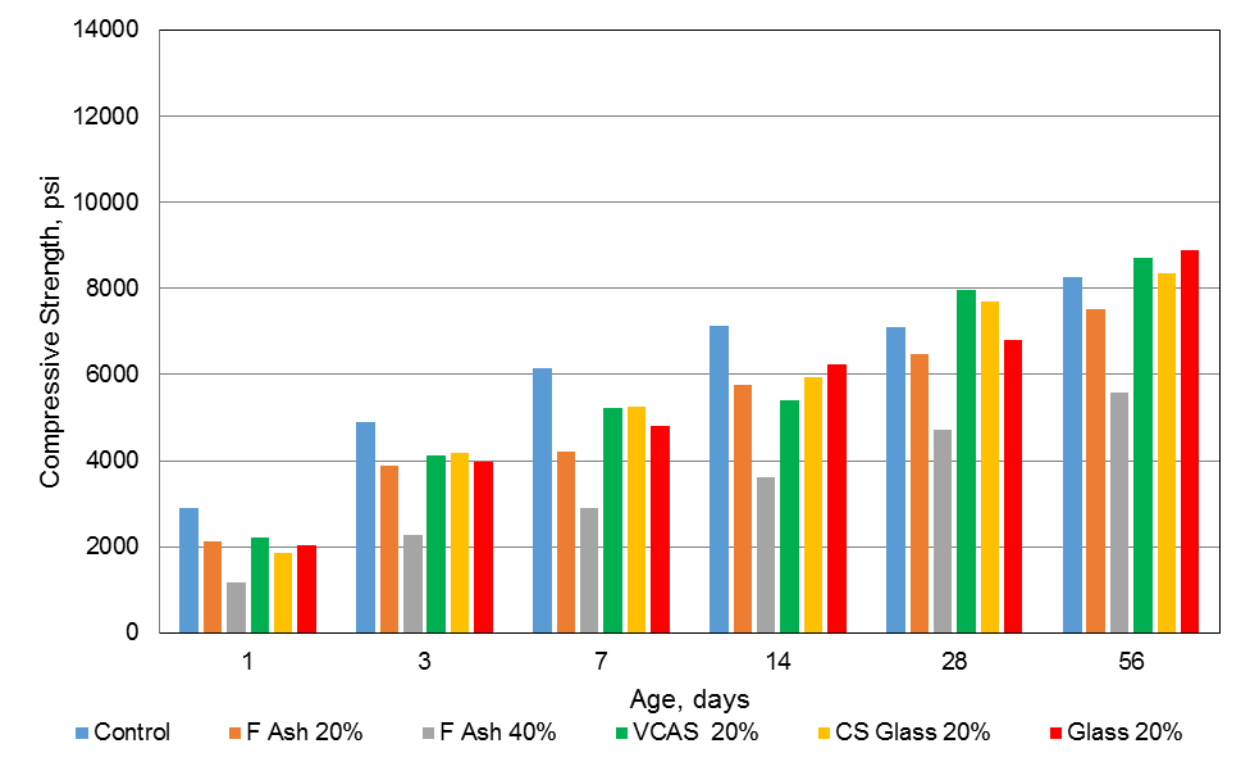

Figure C-3. Compressive strength of mortars containing class F fly ash or glass.

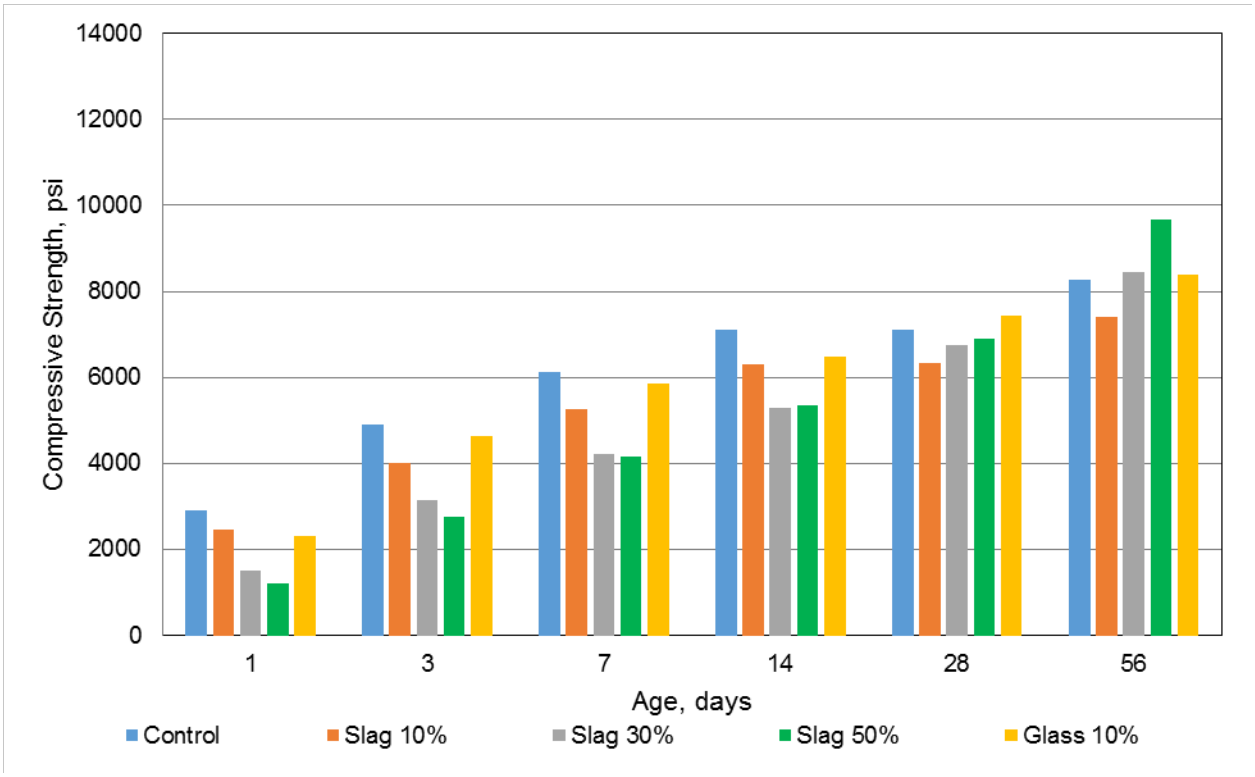

Figure C-4. Compressive strength of mortars containing slag or glass.

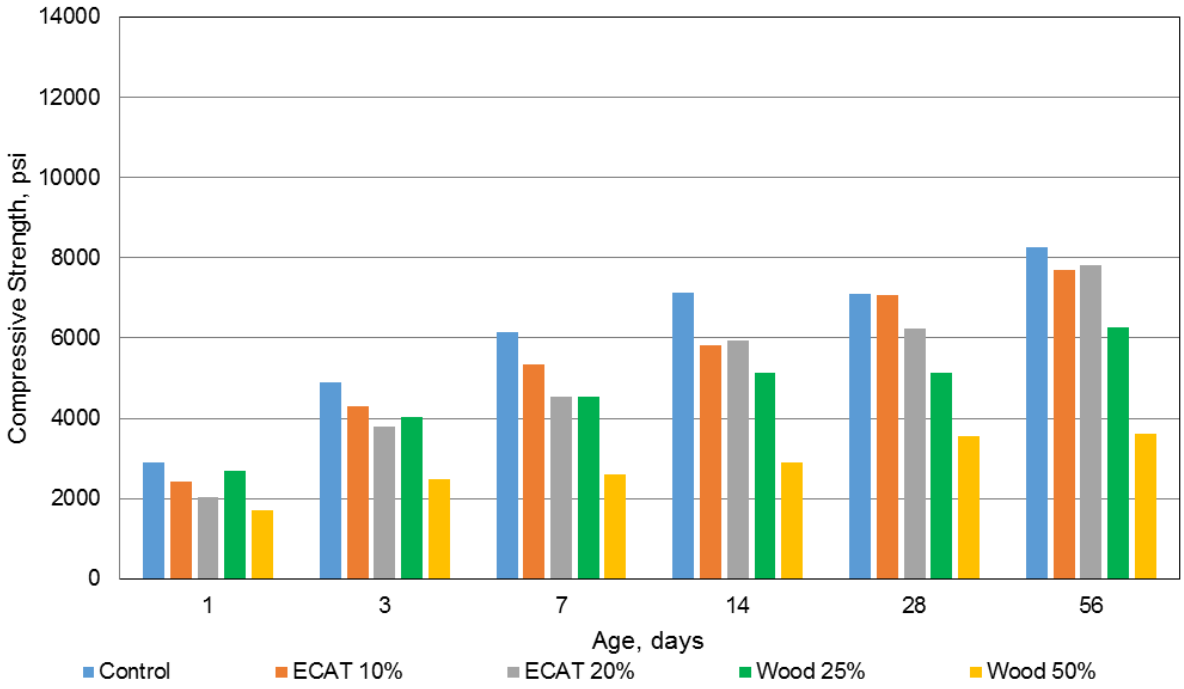

Figure C-5. Compressive strength of mortars containing equilibrium catalyst or wood ash.

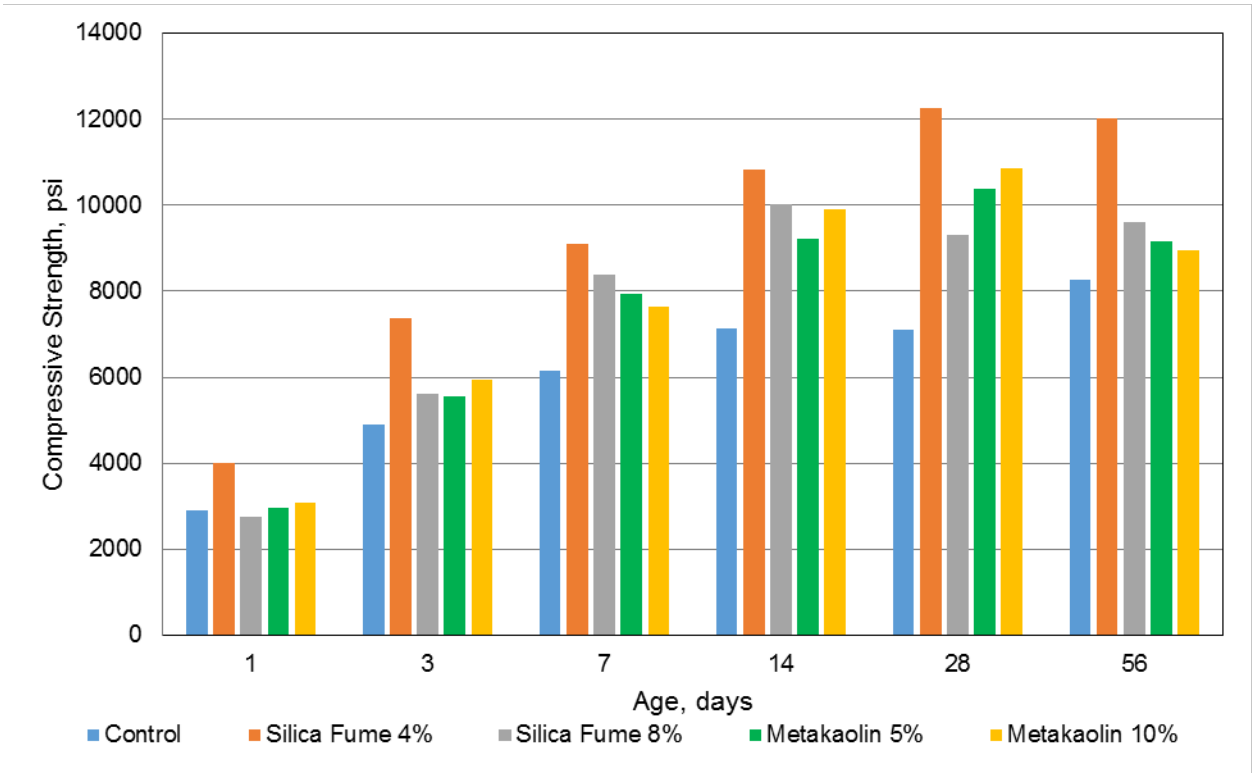

Figure C-6. Compressive strength of mortars containing silica fume or metakaolin.

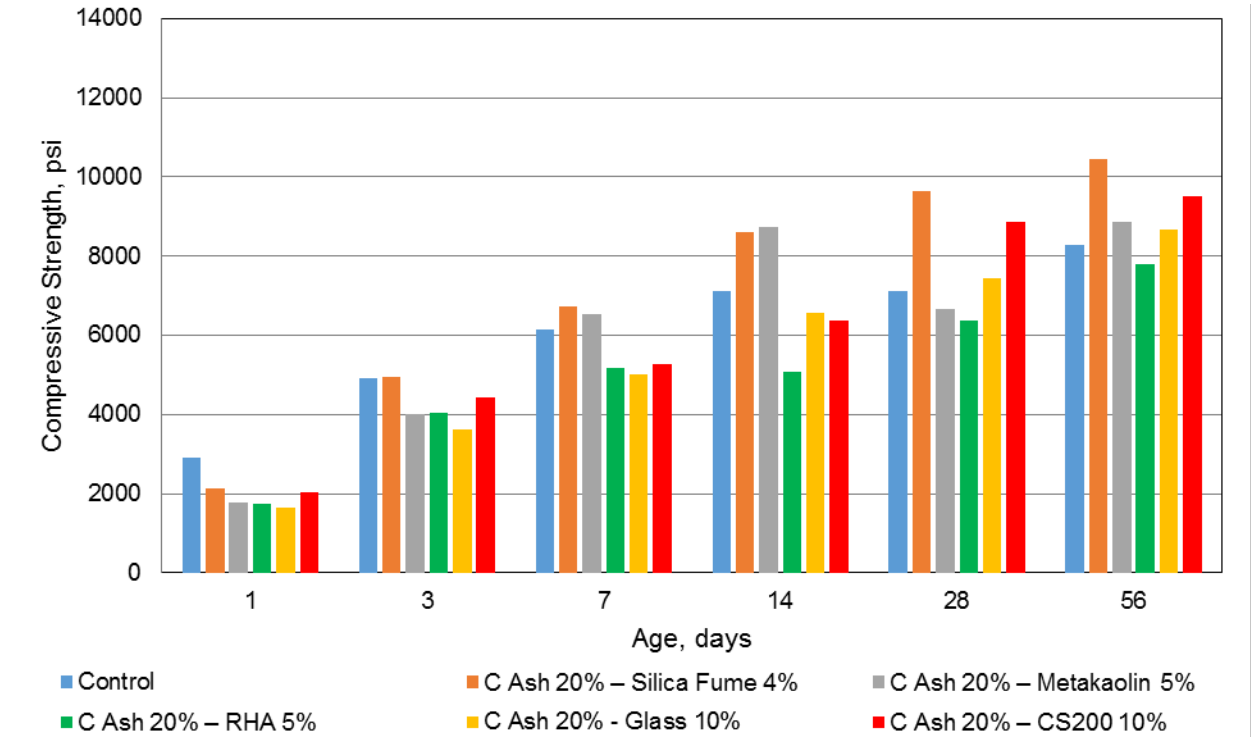

Figure C-7. Compressive strength of ternary mortars containing 20% class C fly ash and either silica fume, metakaolin, rice husk ash, or glass.

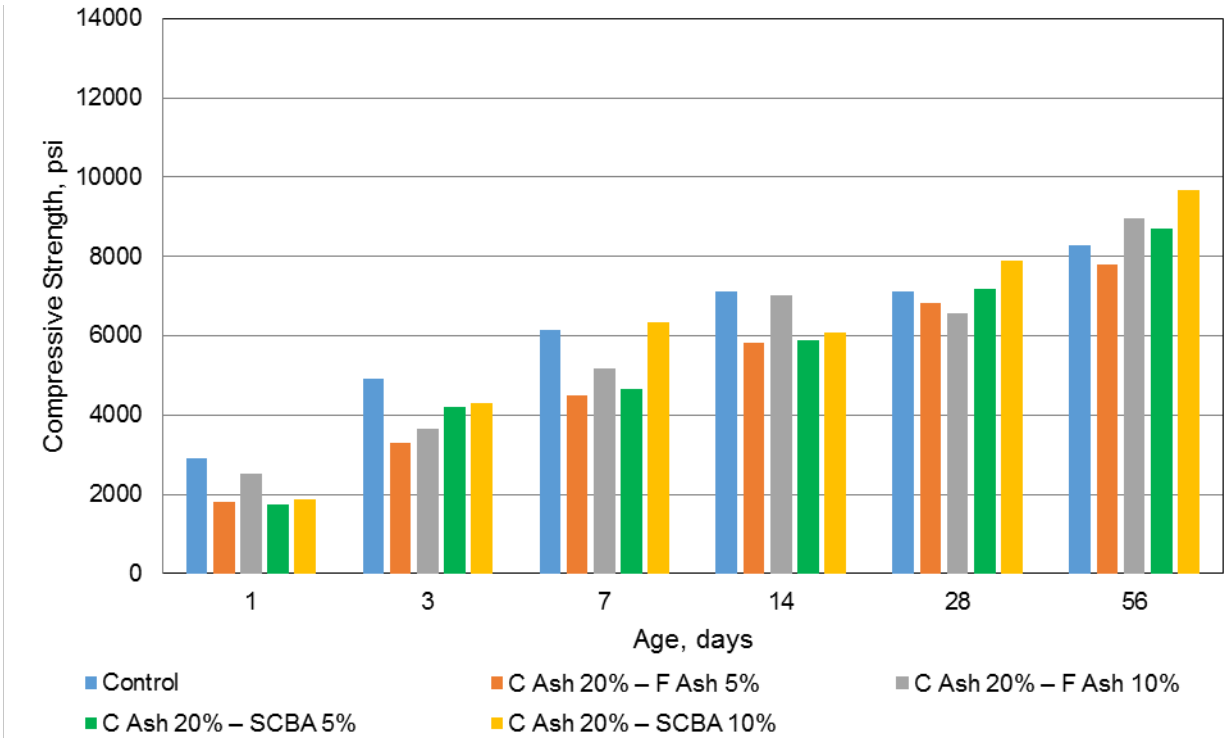

Figure C-8. Compressive strength of ternary mortars containing 20% class C fly ash and either class F fly ash, or sugarcane bagasse ash.

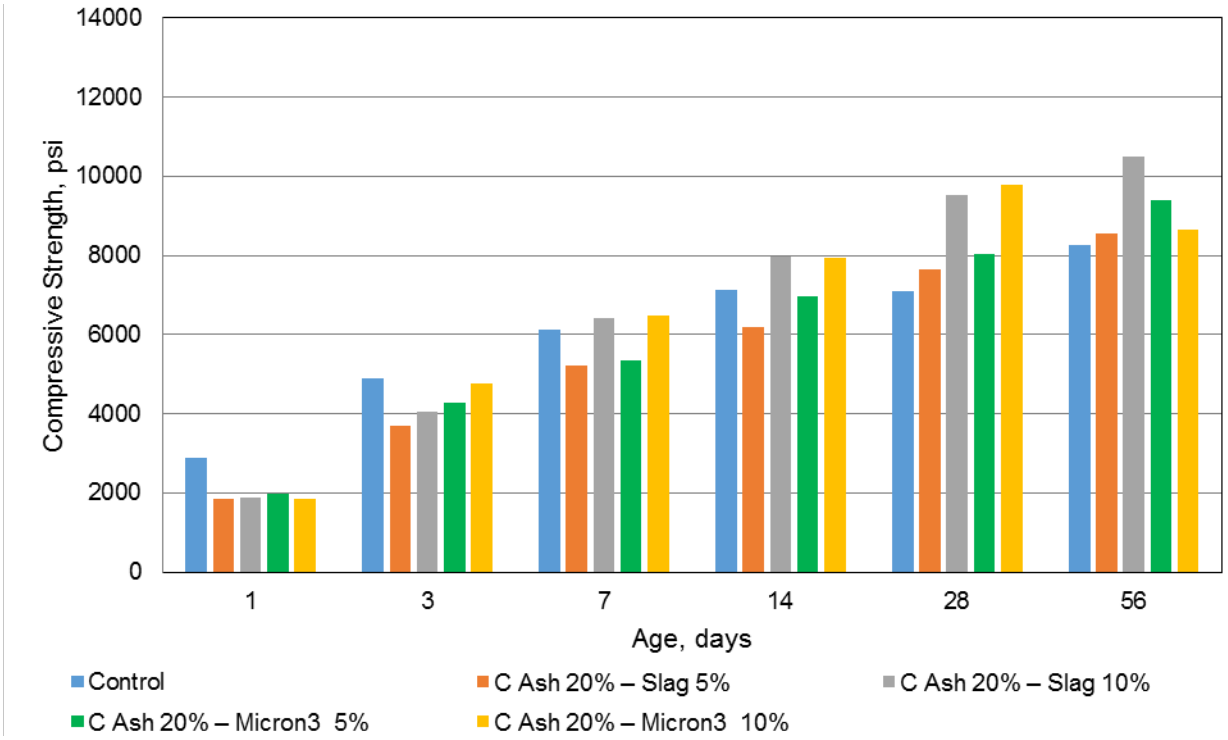

Figure C-9. Compressive strength of ternary mortars containing 20% class C fly ash and either slag or Micron^3.

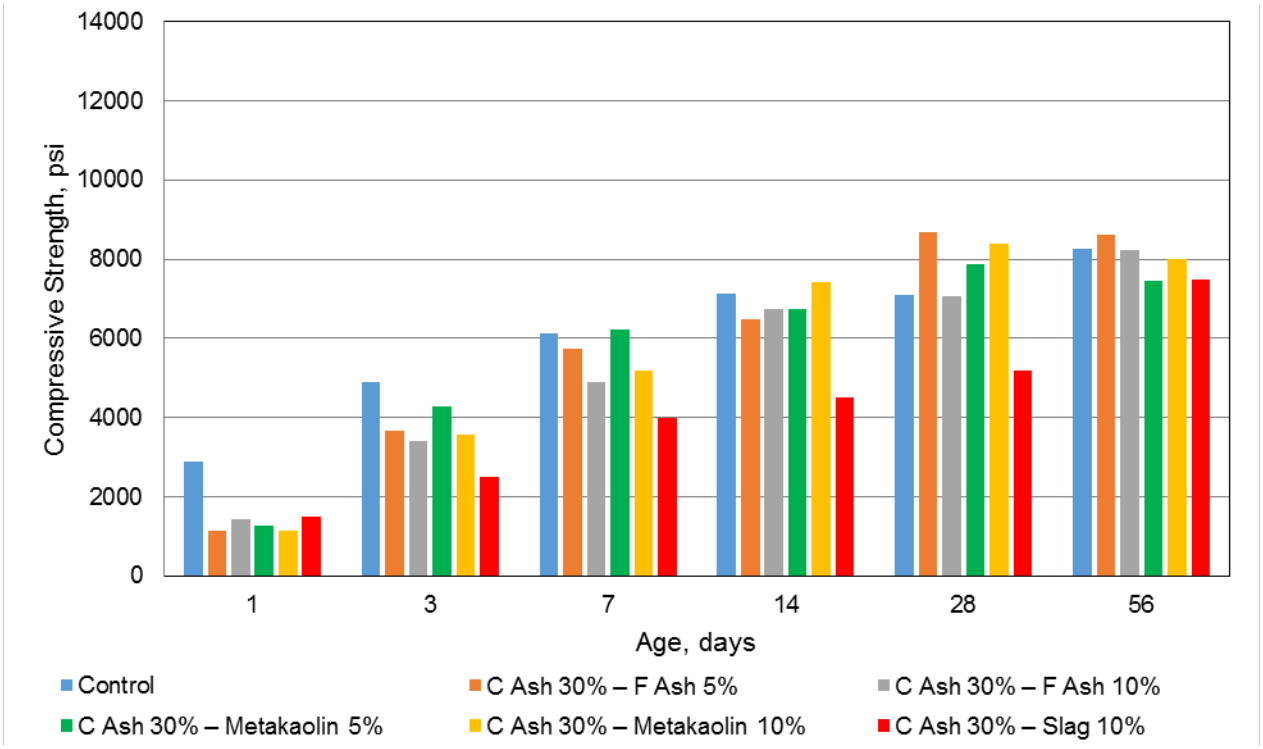

Figure C-10. Compressive strength of ternary mortars containing 30% class C fly ash and either class F fly ash, metakaolin, or slag.

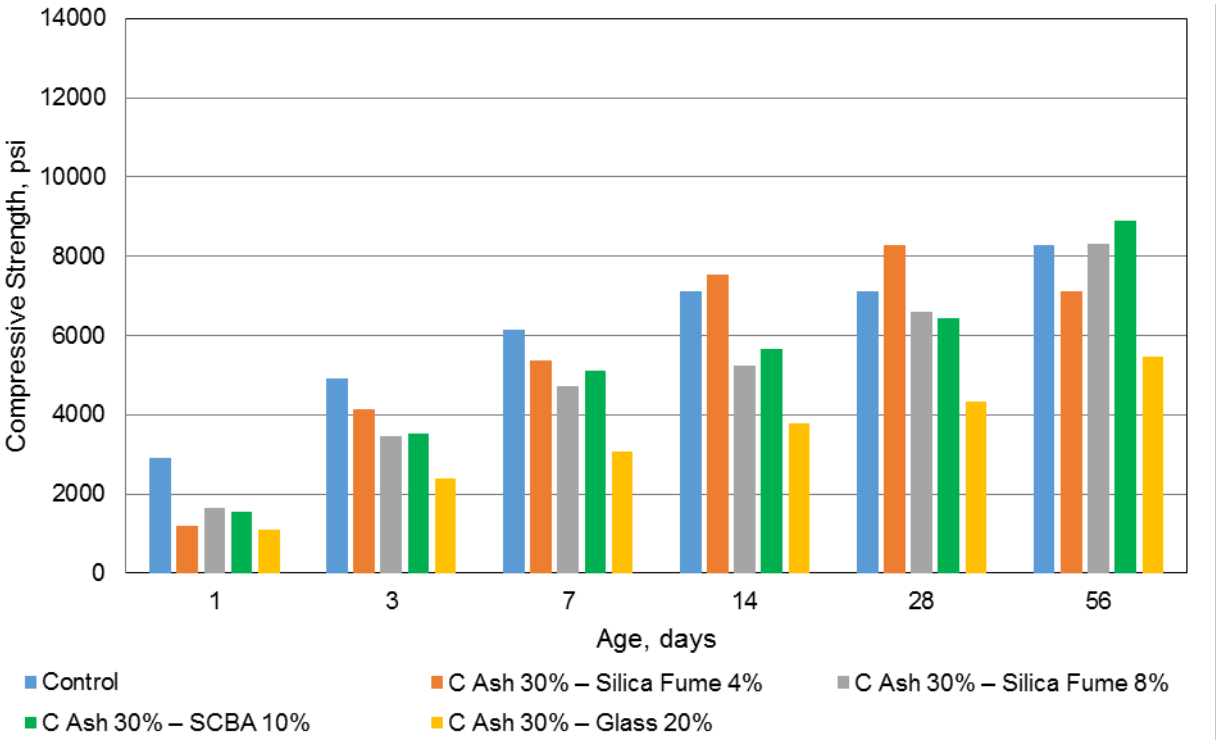

Figure C-11. Compressive strength of ternary mortars containing 30% class C fly ash and either silica fume, sugarcane bagasse ash, or glass.

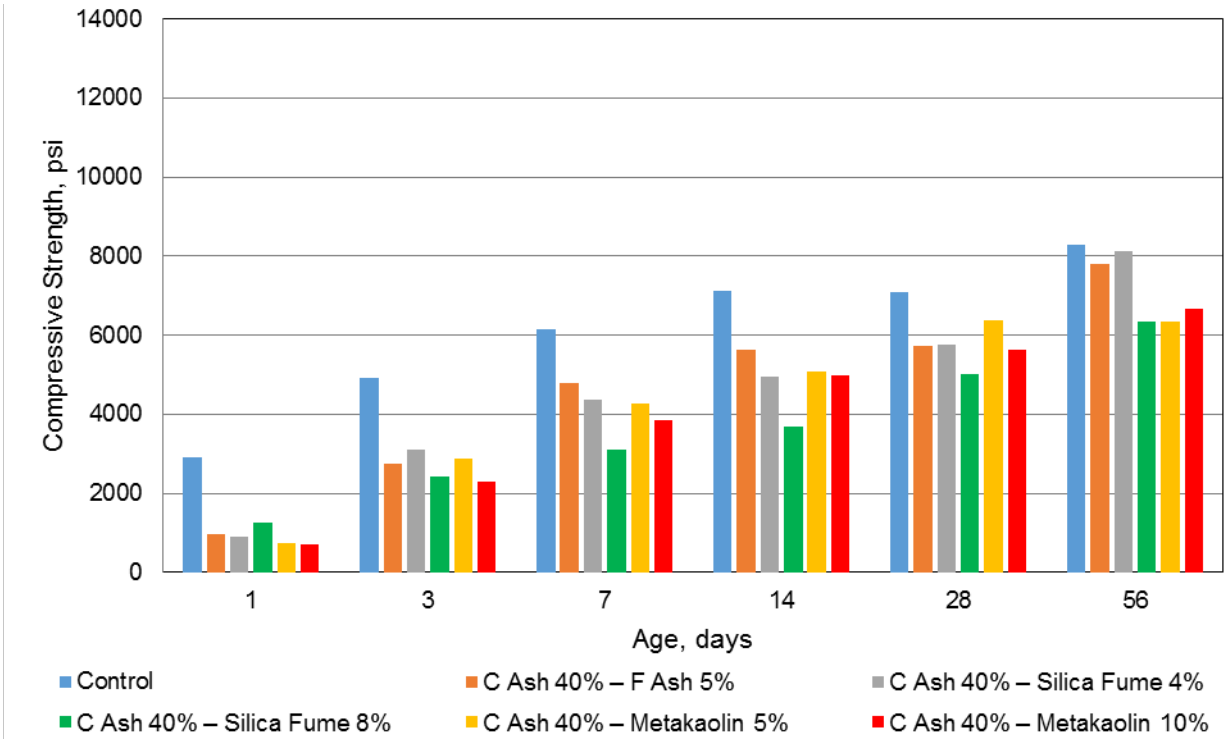

Figure C-12. Compressive strength of ternary mortars containing 40% class C fly ash and either class F fly ash, silica fume, or metakaolin.

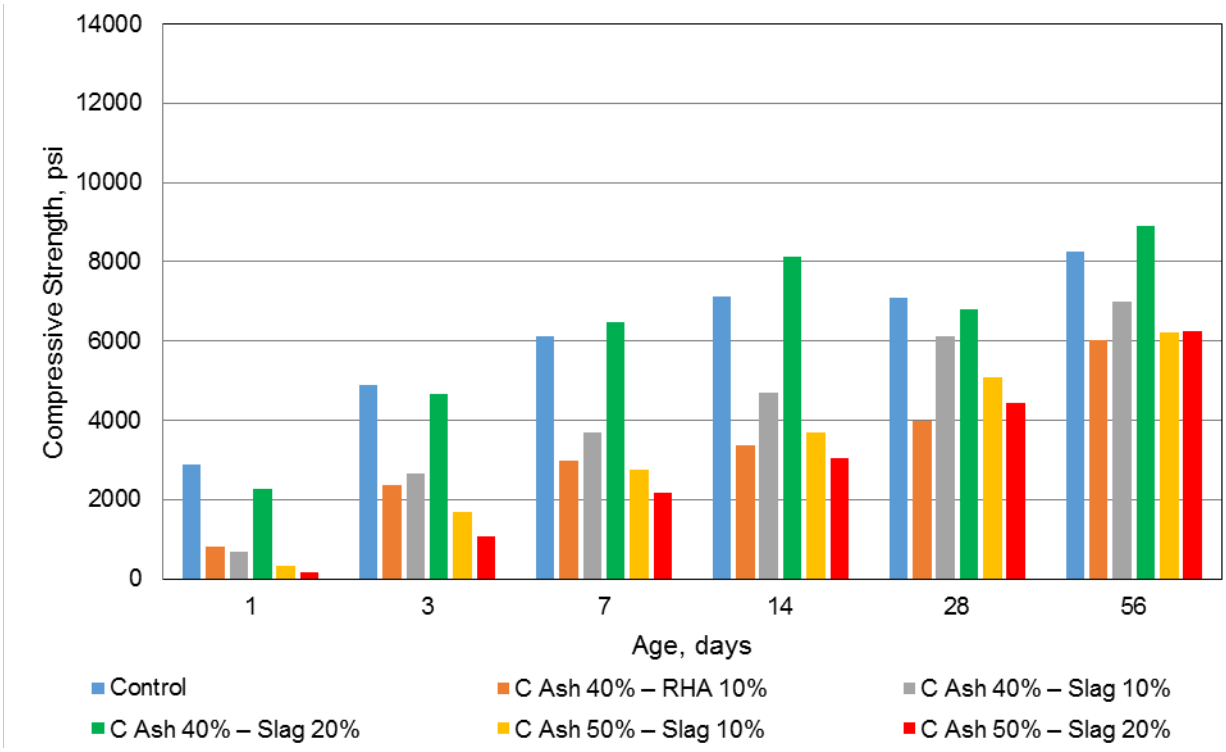

Figure C-13. Compressive strength of ternary mortars containing 50% class C fly ash and either rice husk ash or slag.

C.2. Tensile Strength of Mortar Result

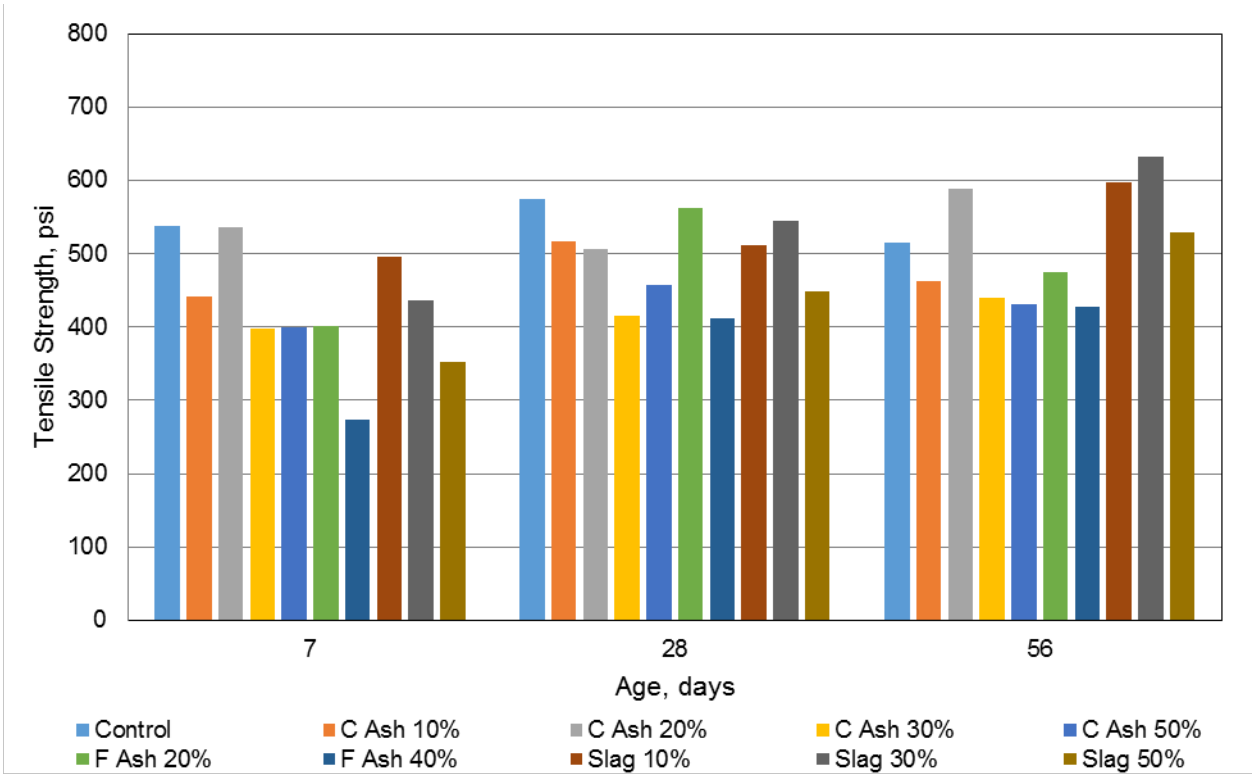

Figure C-14. Tensile strength of binary mortars.

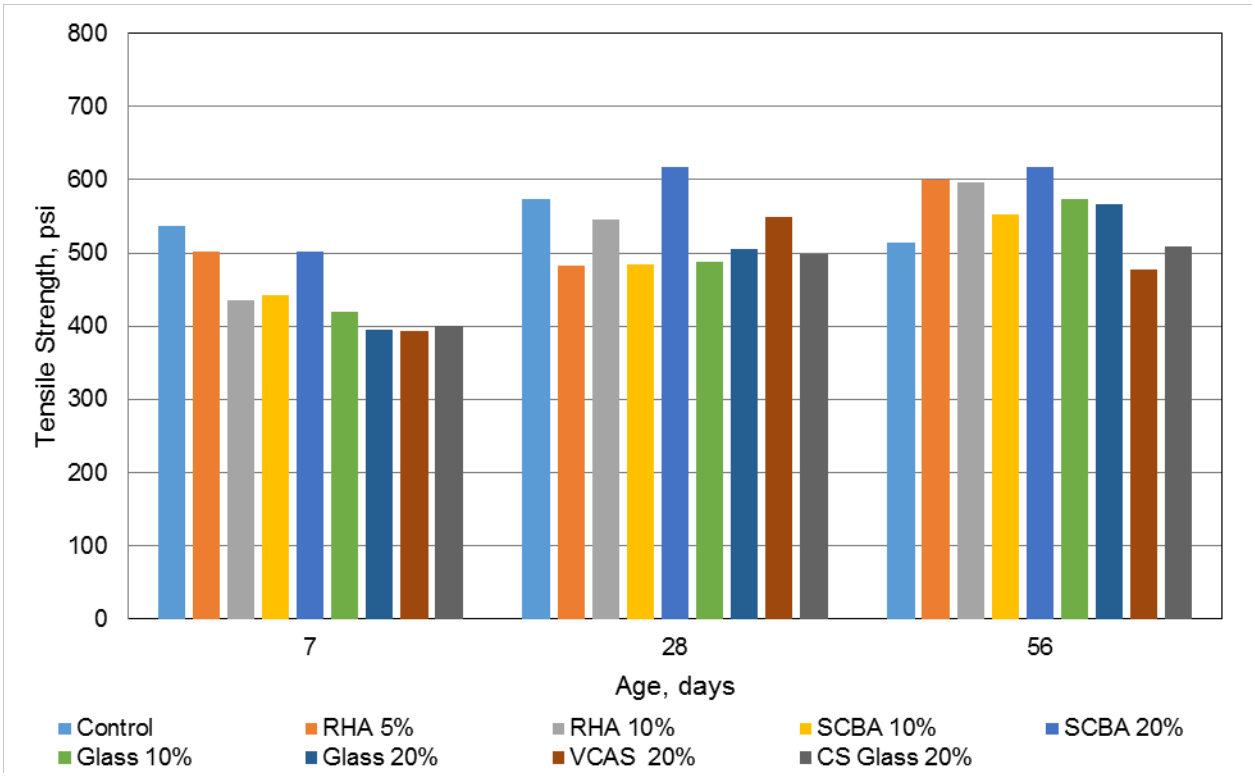

Figure C-15. Tensile strength of binary mortars.

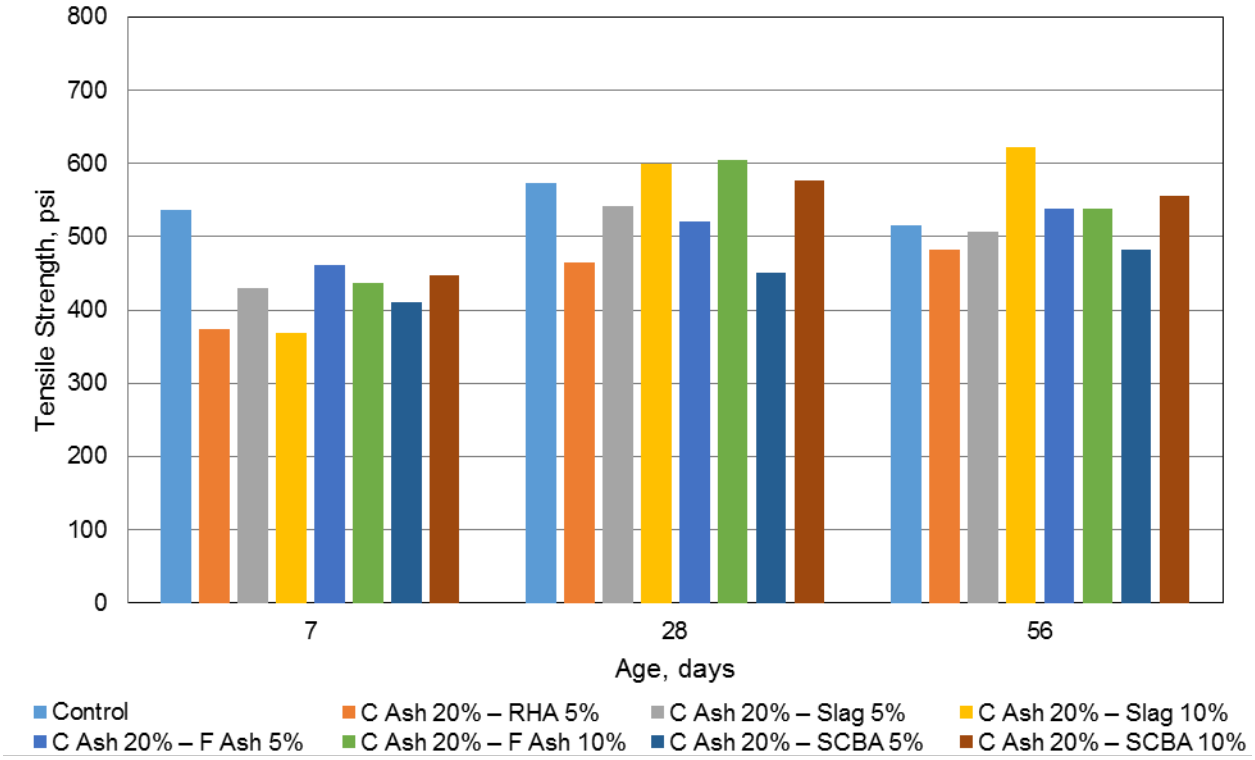

Figure C-16. Tensile strength of ternary mortars containing 20% class C fly ash.

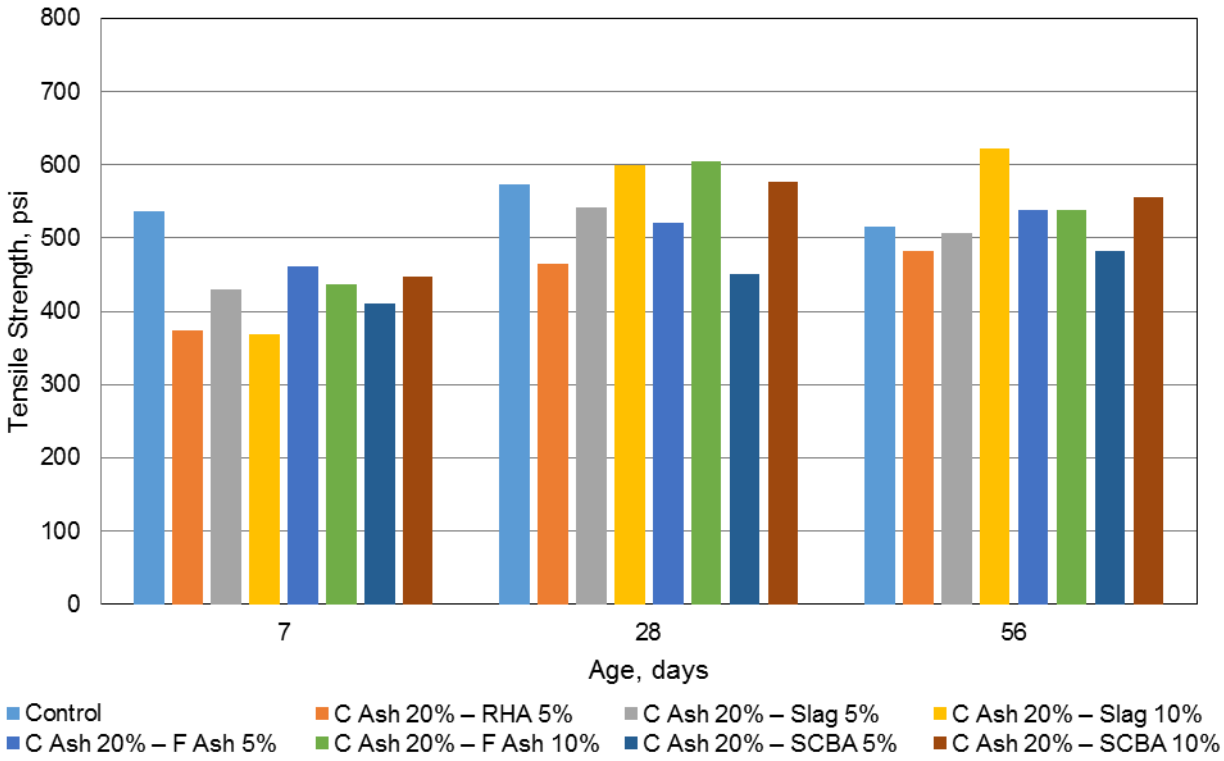

Figure C-17. Tensile strength of ternary mortars containing 20% class C fly ash.

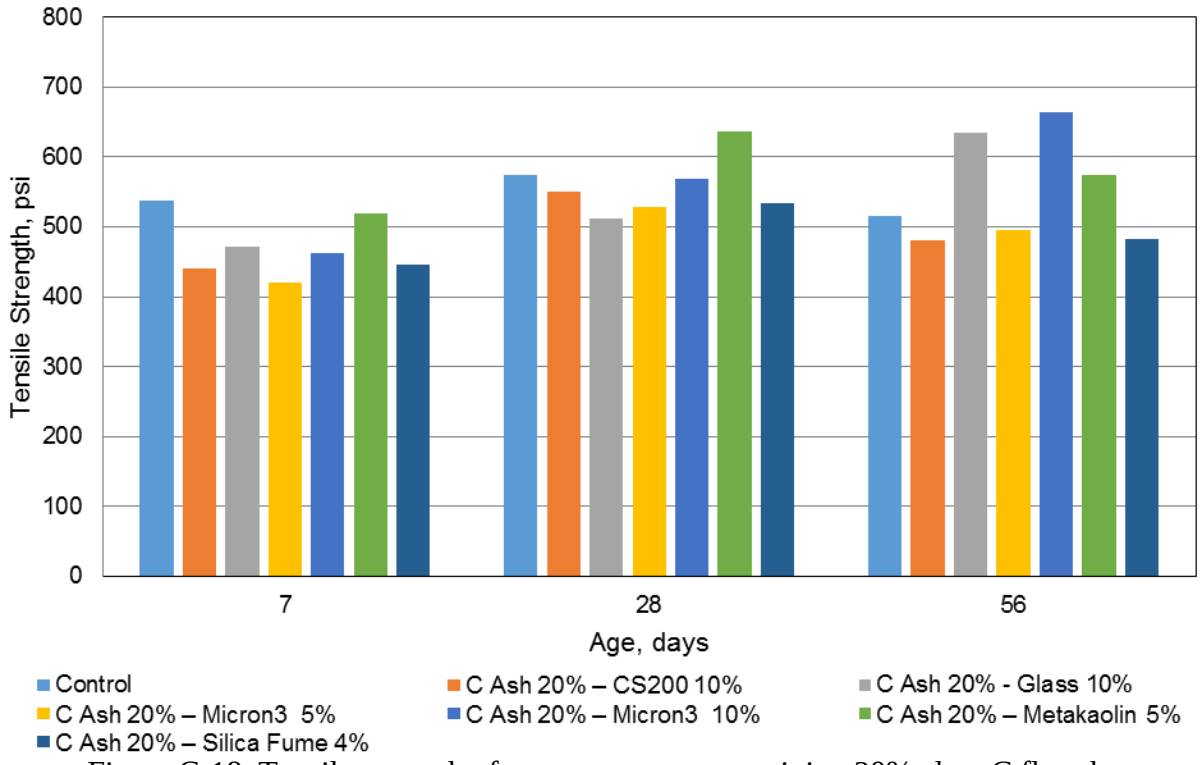

Figure C-18. Tensile strength of ternary mortars containing 20% class C fly ash.

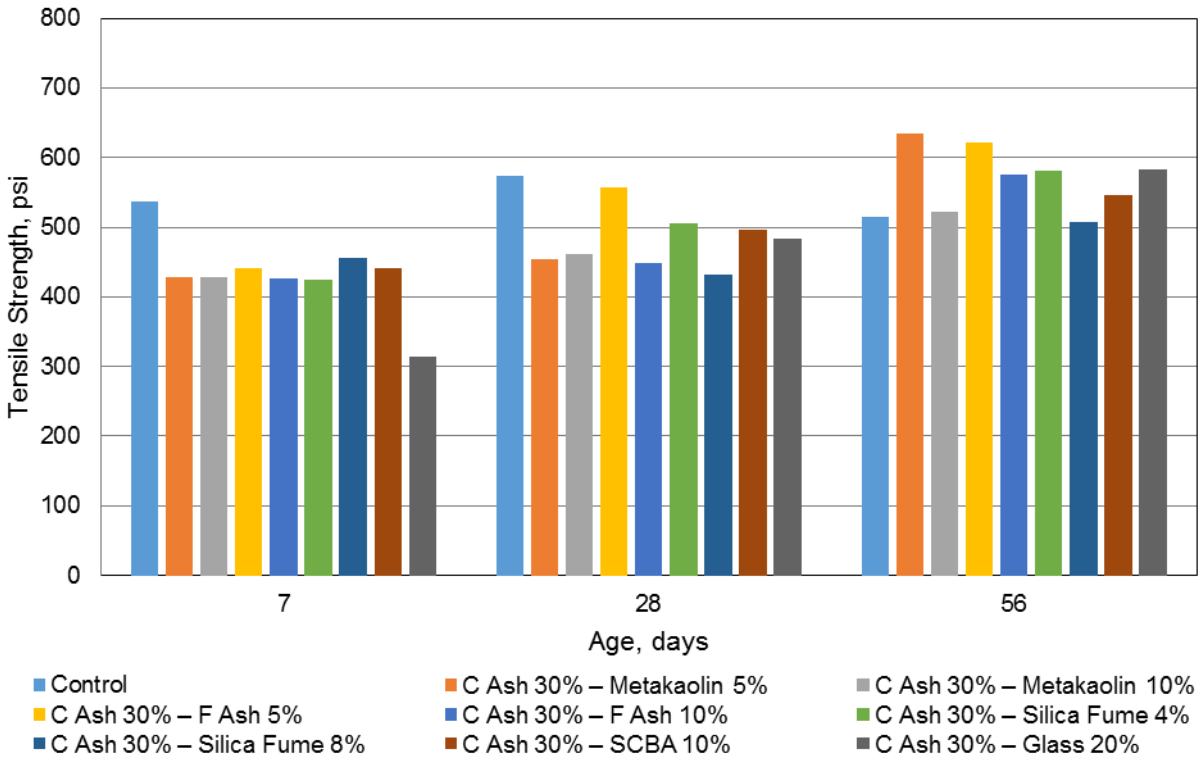

Figure C-19. Tensile strength of ternary mortars containing 30% class C fly ash.

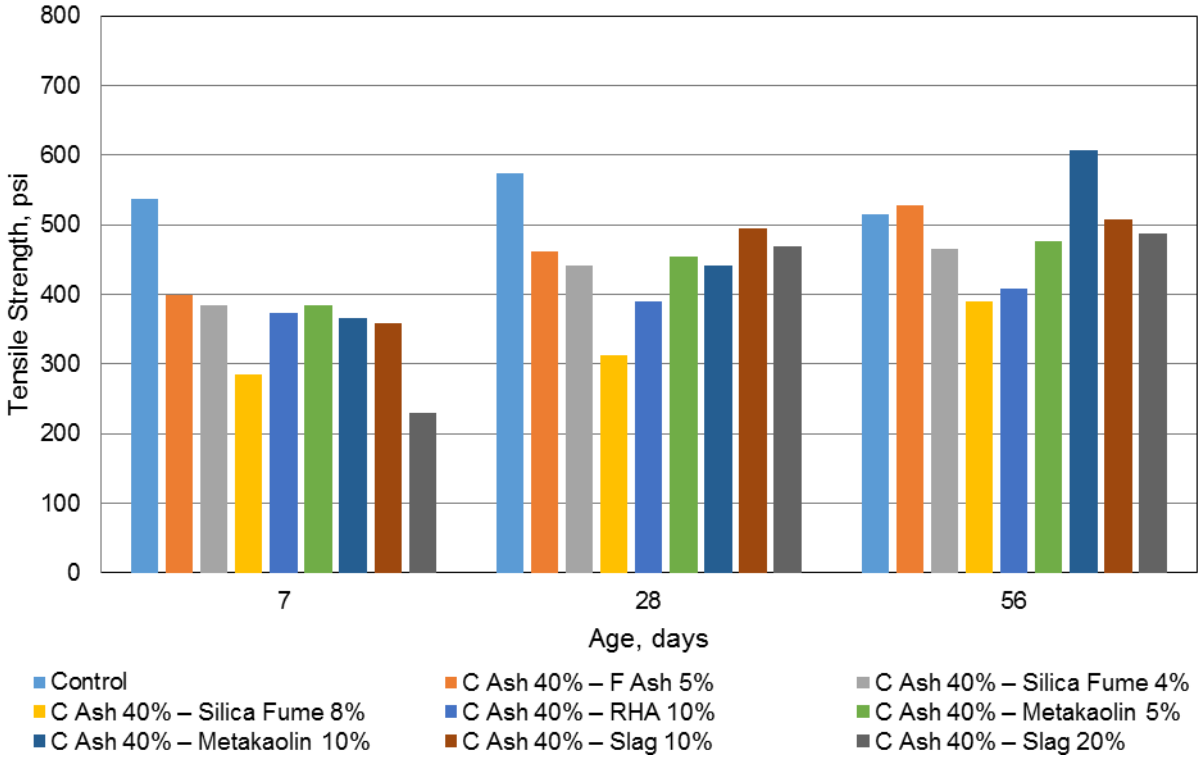

Figure C-20. Tensile strength of ternary mortars containing 40% class C fly ash.

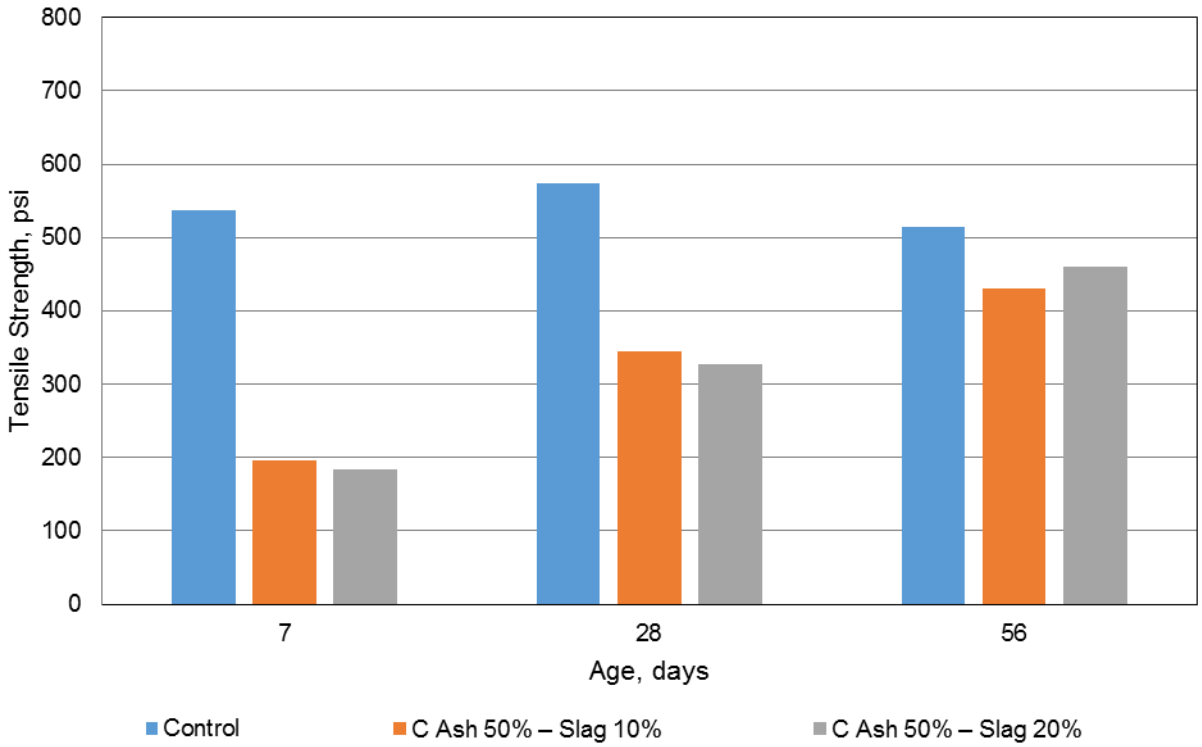

Figure C-21. Tensile strength of ternary mortars containing 50% class C fly ash.

C.3. Activation Energy and Equivalent Age of Mortar Results

Table C-1. Strength-age data for mortars containing 100% portland cement.

Temp, °C	Age, days	Strength, psi	Su, psi	k	t_o	E_a, J/mol	Equiv. Age, days
8	2.31	1733	6510	0.159	0.008		0.94
	7.15	3458					2.90
	16.4	4801					6.66
	33.4	5241					13.5
	66.5	6166					27.0
	133	6151					54.1
23	1.01	2898	8474	0.412	0.000	41,600	1.01
	3.09	4907					3.09
	7.01	6137					7.01
	14.1	7119					14.1
	28.1	7778					28.1
	56.3	8272					56.3
38	0.46	2614	7458	0.884	0.000		1.03
	1.37	4238					3.09
	3.20	5249					7.22
	6.40	6391					14.5
	12.6	6946					28.4
	25.6	7110					57.8

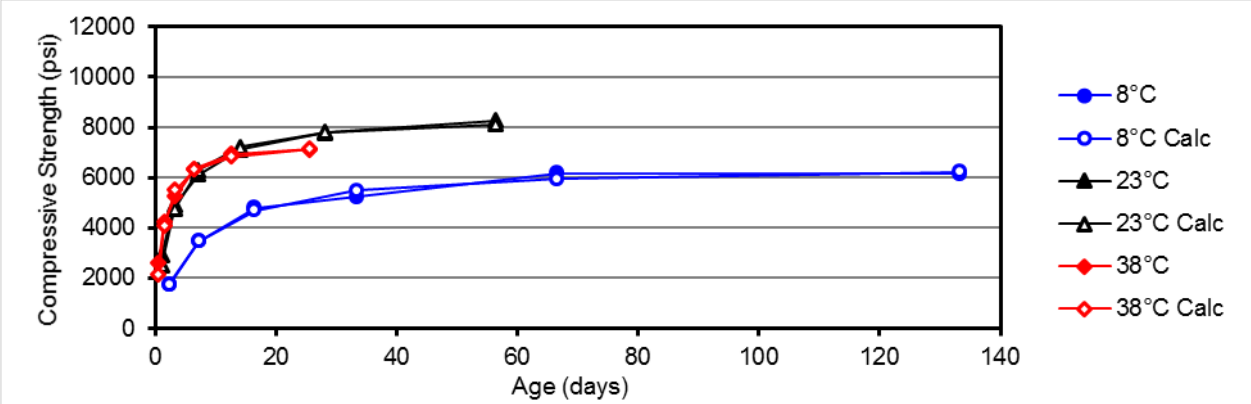

Figure C-22. Strength data for mortar containing 100% portland cement.

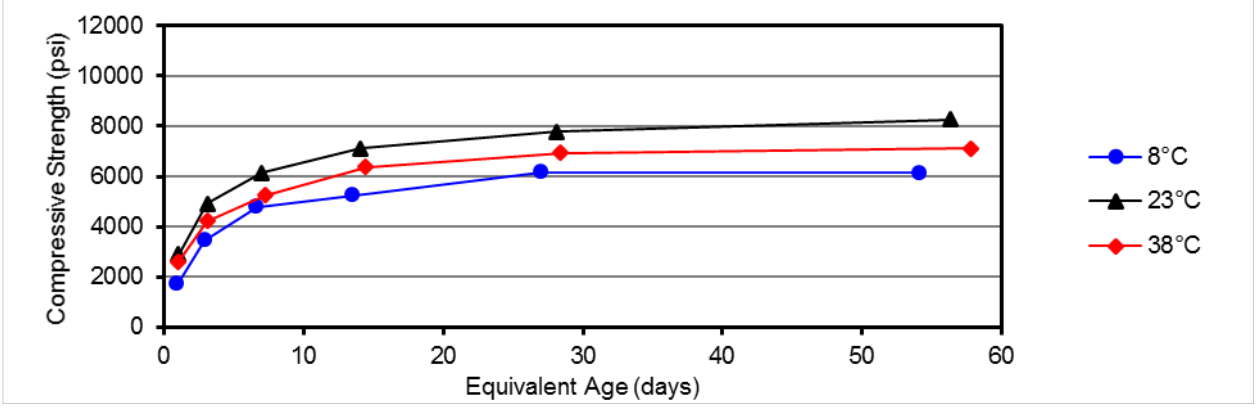

Figure C-23. Equivalent age data for mortar containing 100% portland cement.

Table C-2. Strength-age data for mortars containing 10% class C fly ash.

Temp, °C	Age, days	Strength, psi	Su	k	t_o	E_a, J/mol	Equiv. Age, days
8	2.39	1386	8365	0.078	0.000		0.76
	7.19	3785					2.28
	16.5	4794					5.24
	33.4	5265					10.6
	66.4	6212					21.0
	133	8364					42.3
23	1.00	2127	6386	0.300	0.000	53,000	1.00
	3.04	3298					3.04
	7.00	4105					7.00
	14.0	5039					14.0
	28.0	5663					28.0
	56.1	6208					56.1
38	0.46	2021	7067	0.692	0.000		1.30
	1.37	3618					3.86
	3.21	4261					9.08
	6.39	5918					18.1
	12.5	5713					35.4
	25.6	6822					72.2

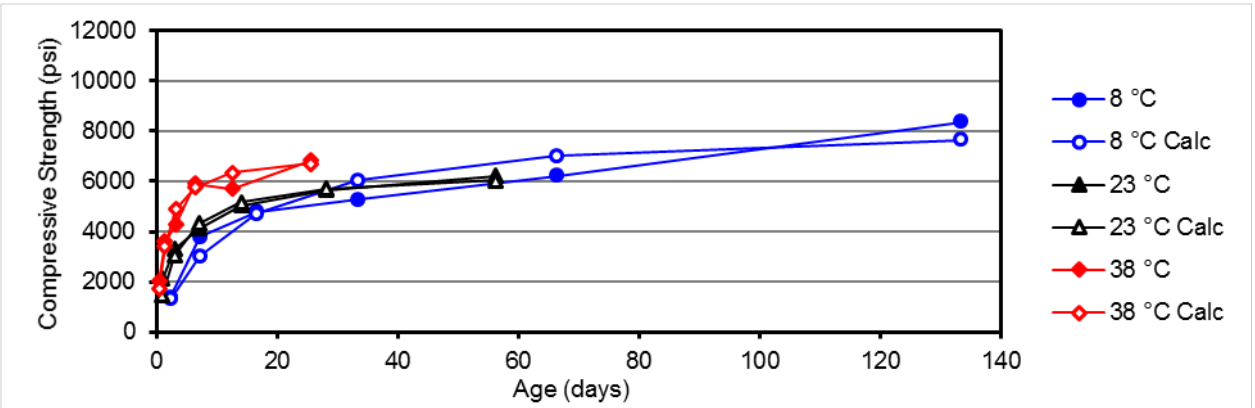

Figure C-24. Strength data for mortar containing 10% class C fly ash.

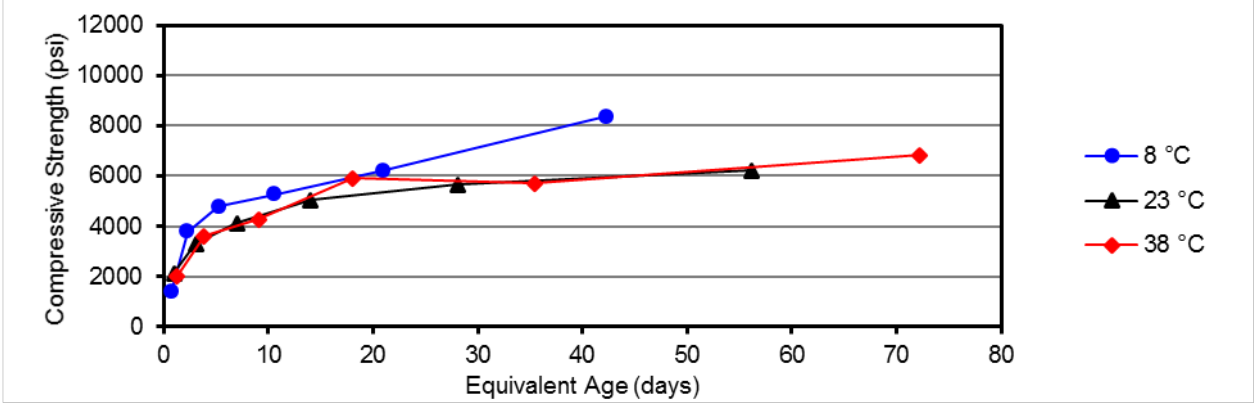

Figure C-25. Equivalent age data for mortar containing 10% class C fly ash.

Table C-3. Strength-age data for mortars containing 20% class C fly ash.

Temp, °C	Age, days	Strength, psi	Su	k	t_o	E_a, J/mol	Equiv. Age, days
8	2.36	1101					0.95
	7.15	3370					2.89
	16.8	5134	7994	0.111	0.856		6.78
	33.3	6072					13.5
	66.8	6992					27.0
	134	7609					54.1
23	1.02	1618					1.02
	3.02	3688					3.02
	7.04	4597	6767	0.307	0.000	41,800	7.04
	14.2	4932					14.2
	28.0	5700					28.0
	56.3	6766					56.3
38	0.46	1506					1.03
	1.35	3166					3.06
	3.21	4465	6825	0.618	0.000		7.29
	6.40	5494					14.5
	12.5	5901					28.3
	25.5	6530					57.8

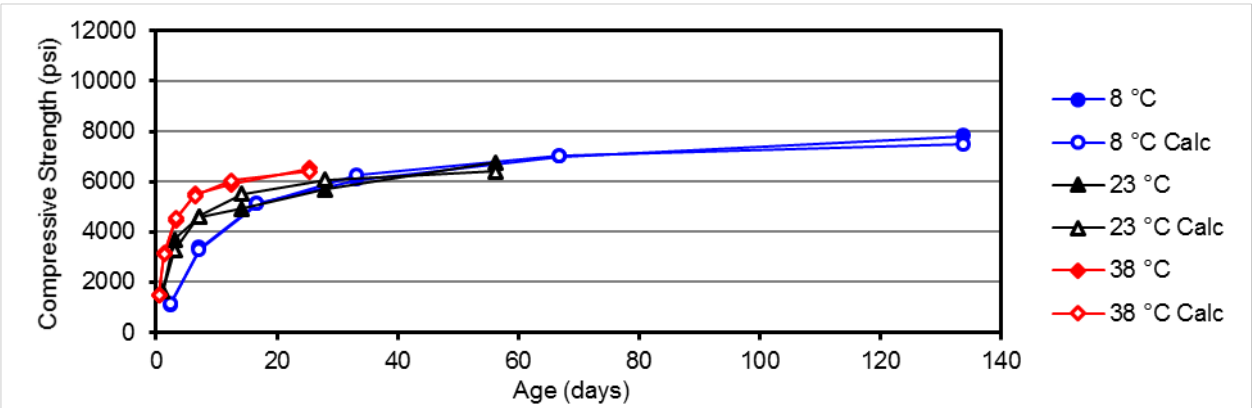

Figure C-26. Strength data for mortar containing 20% class C fly ash.

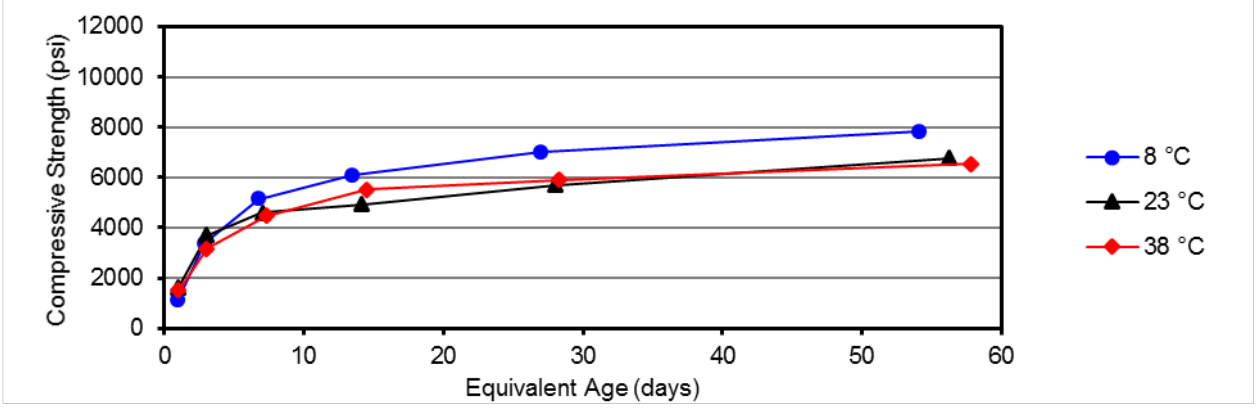

Figure C-27. Equivalent age data for mortar containing 20% class C fly ash

Table C-4. Strength-age data for mortars containing 30% class C fly ash.

Temp, °C	Age, days	Strength, psi	Su	k	t_o	E_a, J/mol	Equiv. Age, days
8	2.36	1142	9267	0.048	0.000		0.79
	7.15	2699					2.01
	16.8	4419					4.71
	33.3	5451					9.53
	66.8	6330					18.7
	134	8644					37.3
23	1.02	1160	5982	0.340	0.267	58,800	1.00
	3.02	2991					3.02
	7.04	4193					7.06
	14.2	4738					14.0
	28.0	5389					28.0
	56.3	5812					56.8
38	0.46	1057	6743	0.532	0.095		1.46
	1.35	2790					4.26
	3.21	4229					10.1
	6.40	4937					20.2
	12.5	6032					39.7
	25.5	6265					80.6

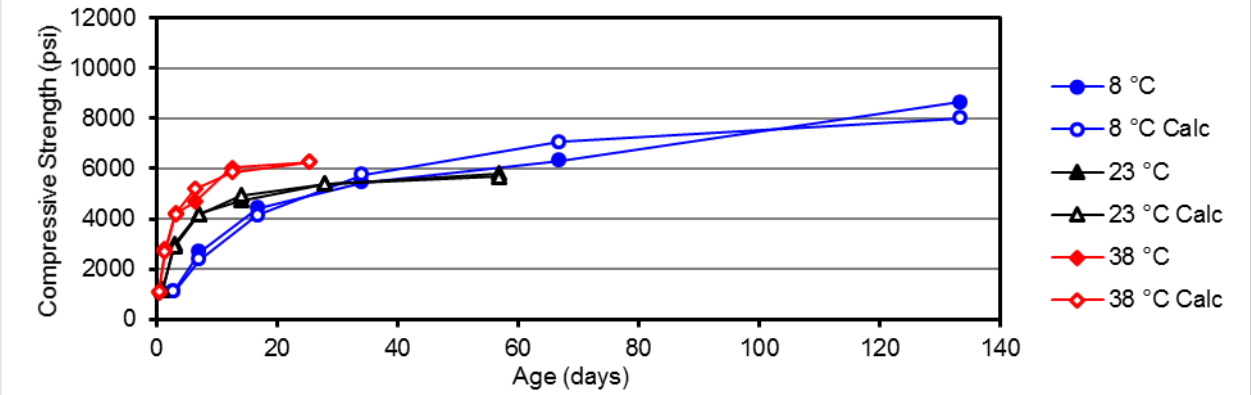

Figure C-28. Strength data for mortar containing 30% class C fly ash.

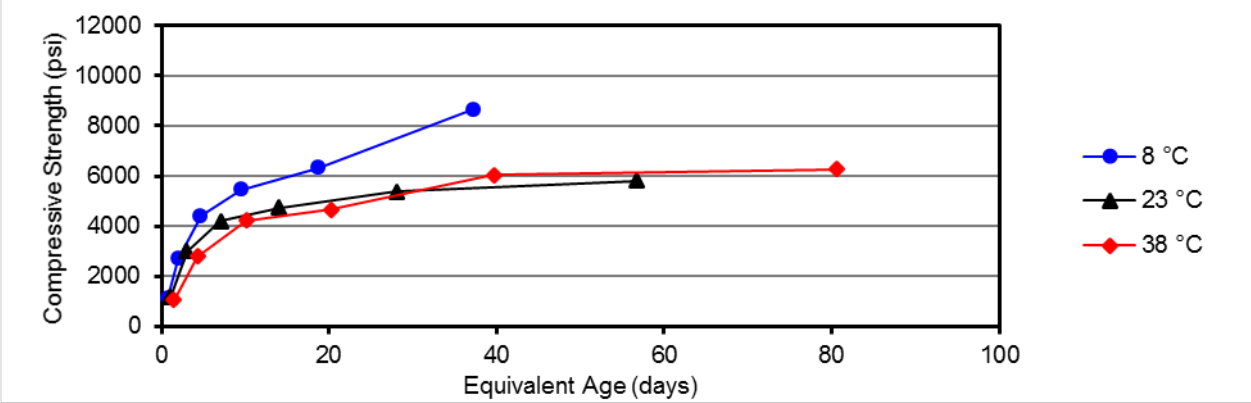

Figure C-29. Equivalent age data for mortar containing 30% class C fly ash.

Table C-5. Strength-age data for mortars containing 50% class C fly ash.

Temp, °C	Age, days	Strength, psi	Su	k	t_o	E_a, J/mol	Equiv. Age, days
8	2.32	498	6222	0.051	0.592		0.93
	7.04	1513					2.84
	17.1	3010					6.88
	33.0	3693					13.3
	67.0	4848					27.0
	202	5685					81.5
23	1.03	953	6589	0.183	0.047	41,900	1.03
	3.11	2462					3.11
	7.15	3705					7.15
	14.2	4761					14.2
	28.0	5293					28.0
	56.0	6170					56.0
38	0.46	897	7812	0.285	0.000		1.05
	1.39	2409					3.16
	3.16	3590					7.18
	6.37	4663					14.5
	13.0	6832					29.6
	26.1	6591					59.2

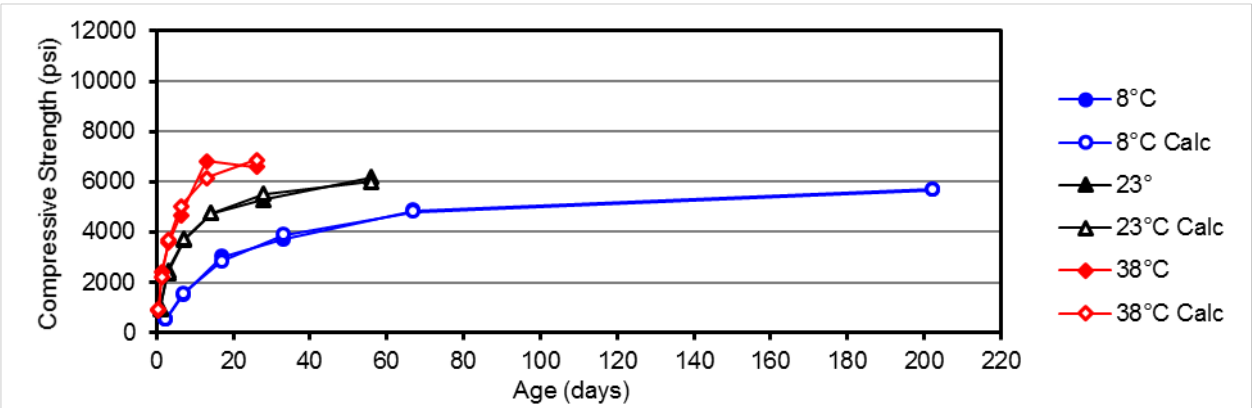

Figure C-30. Strength data for mortar containing 50% class C fly ash.

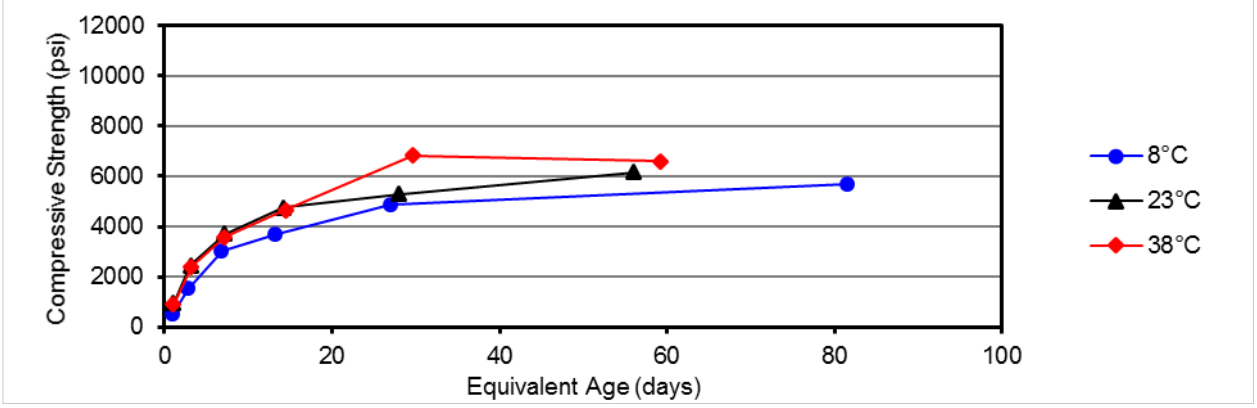

Figure C-31. Equivalent age data for mortar containing 50% class C fly ash.

Table C-6. Strength-age data for mortars containing 20% class F fly ash.

Temp, °C	Age, days	Strength, psi	Su	k	t_o	E_a, J/mol	Equiv. Age, days
8	2.39	1687					1.12
	7.16	4093					3.36
	16.5	5436	7994	0.135	0.272		7.76
	33.4	6348					15.7
	67.4	6907					31.7
	133	7964					62.6
23	1.00	2128					1.00
	3.35	3894					3.35
	7.03	4223	7744	0.236	0.000	34,700	7.03
	14.1	5765					14.1
	28.3	6687					28.3
	56.1	7527					56.1
38	0.45	1834					0.89
	1.47	3848					2.90
	3.25	4761	7682	0.570	0.000		6.43
	6.40	5401					12.7
	12.6	6801					25.0
	25.6	7593					50.6

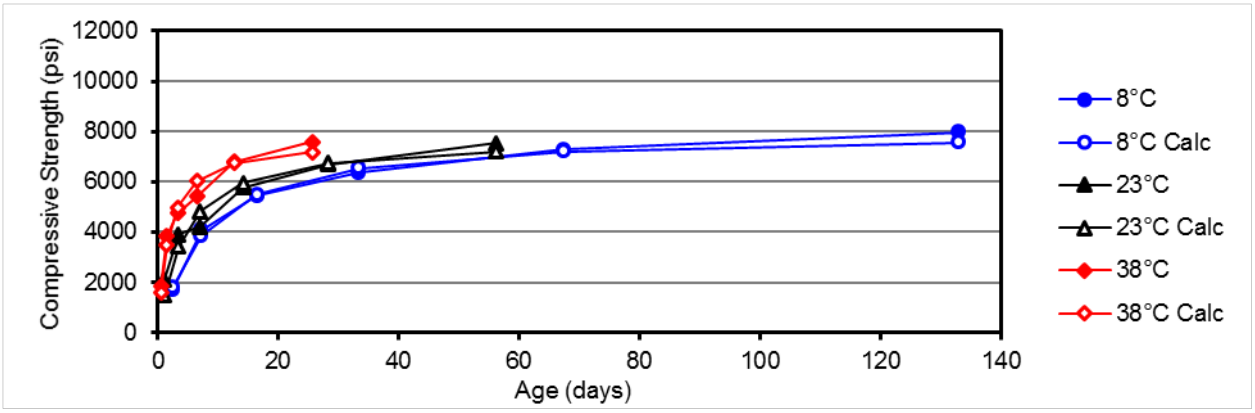

Figure C-32. Strength data for mortar containing 20% class F fly ash.

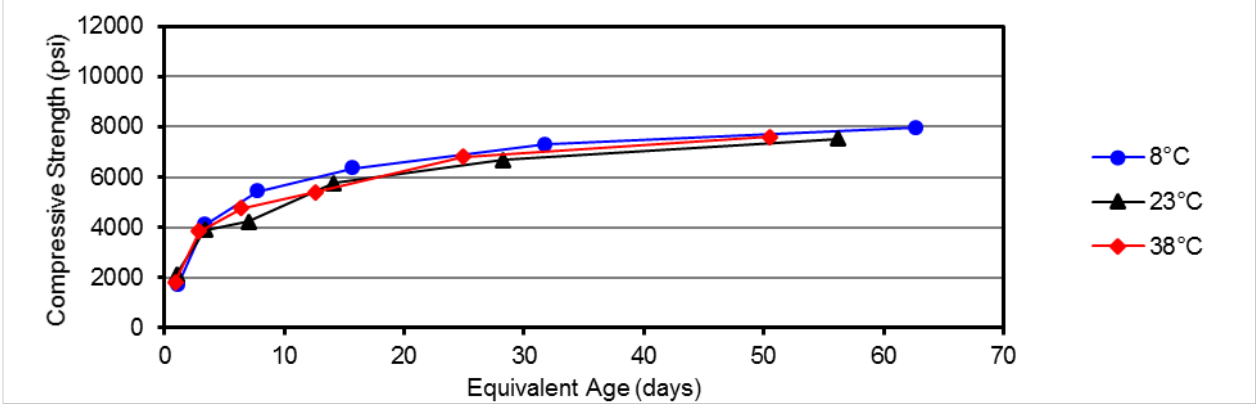

Figure C-33. Equivalent age data for mortar containing 20% class F fly ash.

Table C-7. Strength-age data for mortars containing 40% class F fly ash.

Temp, °C	Age, days	Strength, psi	Su	k	t_o	E_a, J/mol	Equiv. Age, days
8	2.40	1025					1.27
	7.19	2364					3.82
	16.5	2906	5881	0.066	0.000		8.77
	33.4	3698					17.7
	66.9	4388					35.5
	133	5856					70.7
23	1.01	1169					1.01
	3.05	2272					3.05
	7.04	2910	5604	0.172	0.000	29,200	7.04
	14.2	3609					14.2
	28.1	4342					28.1
	56.5	5585					56.5
38	0.46	1002					0.81
	1.39	2127					2.46
	3.21	2918	7338	0.218	0.000		5.68
	6.44	3910					11.4
	12.6	5310					22.4
	26.1	6453					46.2

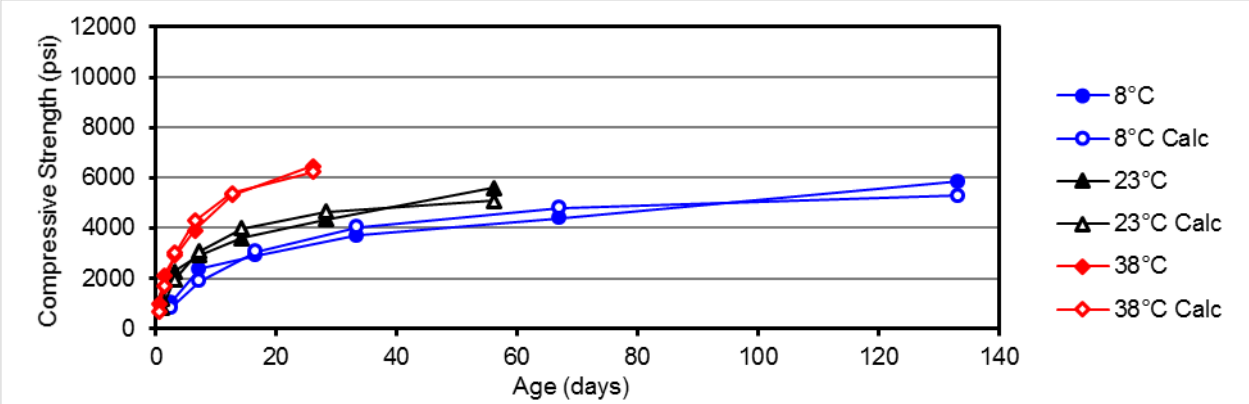

Figure C-34. Strength data for mortar containing 40% class F fly ash.

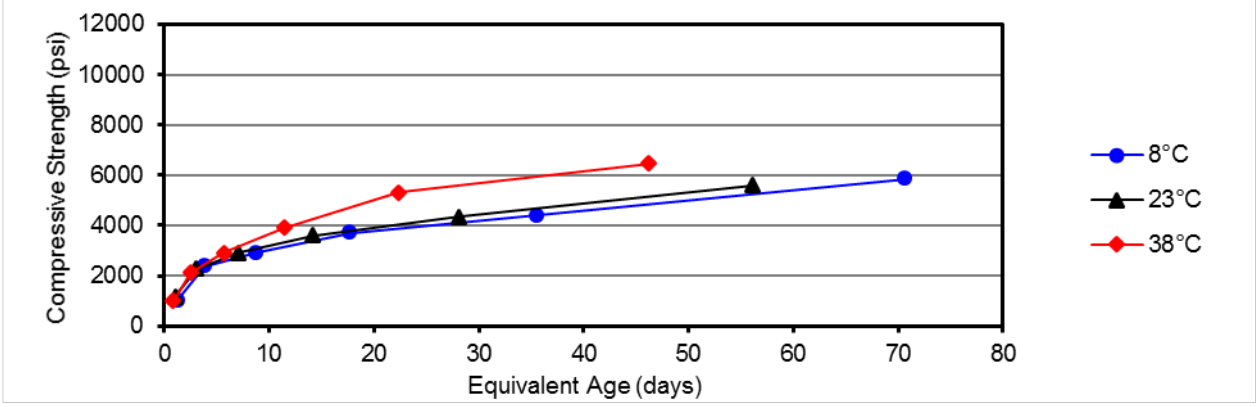

Figure C-35. Equivalent age data for mortar containing 40% class F fly ash.

Table C-8. Strength-age data for mortars containing 5% rice husk ash.

Temp, °C	Age, days	Strength, psi	Su	k	t_o	E_a, J/mol	Equiv. Age, days
8	1.90	1572					0.60
	7.11	4107					2.24
	16.9	5445	8688	0.109	0.000		5.32
	32.9	6436					10.4
	67.2	7055					21.2
	133	8687					41.9
23	1.02	3071					1.02
	3.06	5517					3.06
	7.23	6799	8374	0.654	0.123	53,300	7.23
	14.1	7825					14.1
	28.1	6983					28.1
	56.1	8373					56.1
38	0.43	2015					1.23
	1.39	4572					3.94
	3.43	5790	7791	0.932	0.042		9.74
	6.39	6230					18.2
	12.5	7605					35.5
	25.4	7432					72.2

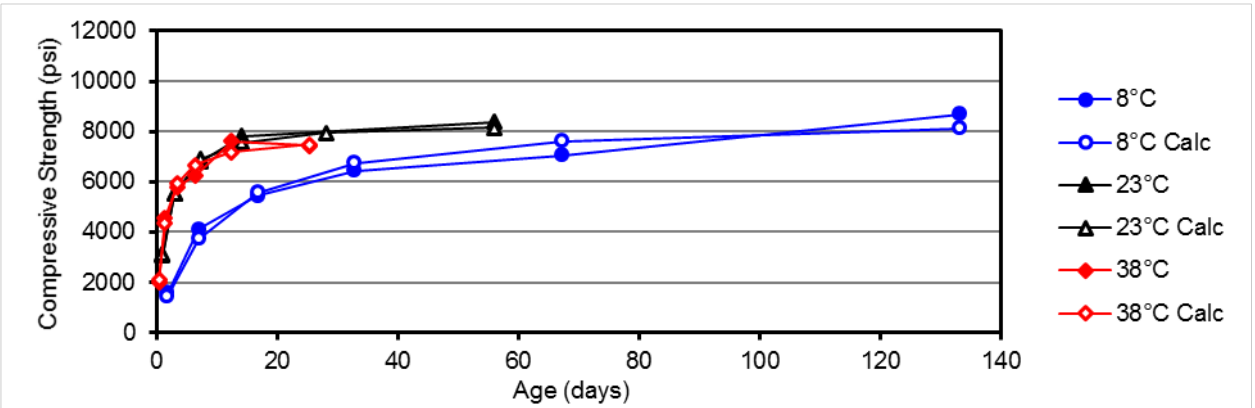

Figure C-36. Strength data for mortar containing 5% rice husk ash.

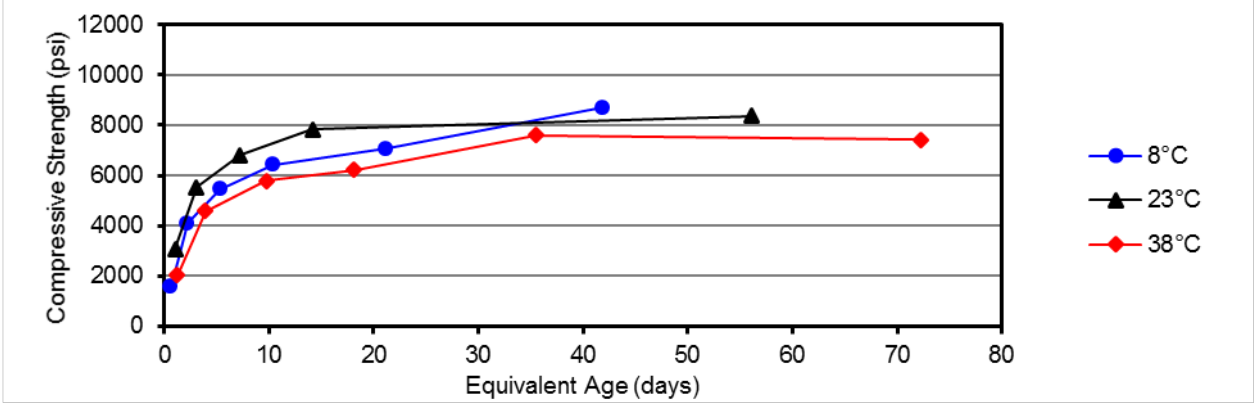

Figure C-37. Equivalent age data for mortar containing 5% rice husk ash.

Table C-9. Strength-age data for mortars containing 10% rice husk ash.

Temp, °C	Age, days	Strength, psi	Su	k	t_o	E_a, J/mol	Equiv. Age, days
8	2.33	1193					1.12
	7.06	4013					3.41
	17.0	5164	7547	0.144	0.828		8.25
	33.3	5555					16.1
	66.2	7024					32.0
	133	7431					64.4
23	1.01	2501					1.01
	3.48	5332					3.48
	7.12	6386	9625	0.327	0.000	33,500	7.12
	14.3	8072					14.3
	28.1	8208					28.1
	56.1	9566					56.1
38	0.45	2140					0.87
	1.23	3615					2.36
	3.08	4607	7992	0.5735	0.000		5.94
	7.18	6130					13.8
	13.3	7138					25.6
	25.4	7781					49.0

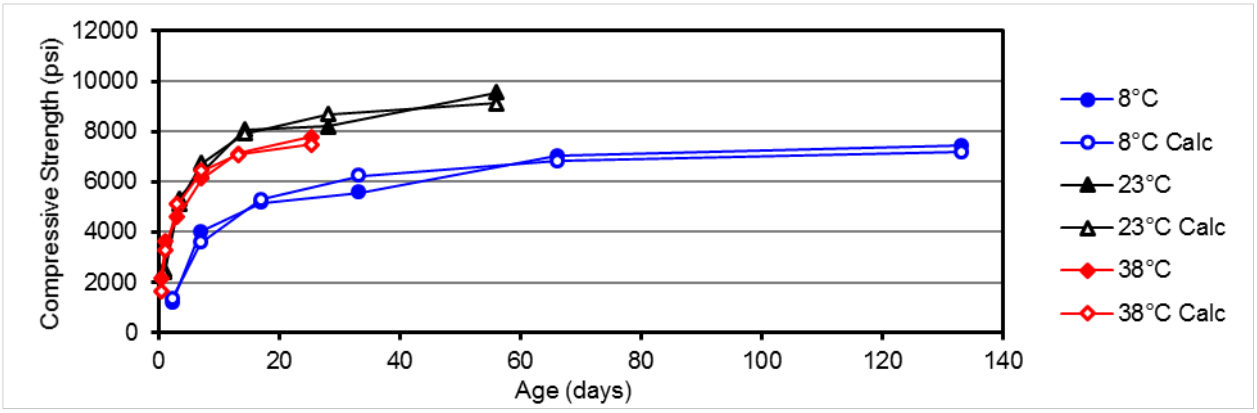

Figure C-38. Strength data for mortar containing 10% rice husk ash.

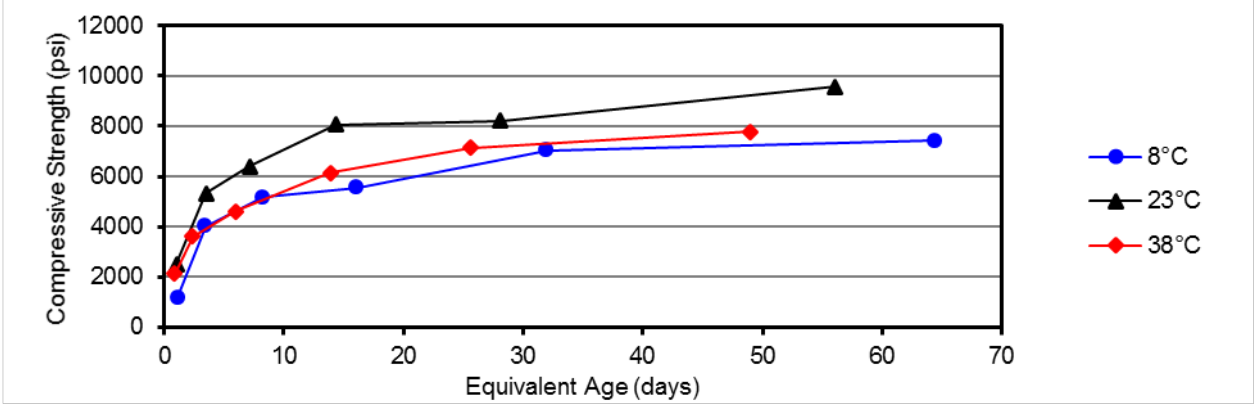

Figure C-39. Equivalent age data for mortar containing 10% rice husk ash.

Table C-10. Strength-age data for mortars containing 10% sugarcane bagasse ash.

Temp, °C	Age, days	Strength, psi	Su	k	t_o	E_a, J/mol	Equiv. Age, days
8	2.41	1835					0.86
	7.16	4172					2.55
	16.5	5501	8778	0.103	0.000		5.90
	33.3	6243					11.9
	65.5	7135					23.4
	133	8777					47.6
23	0.94	2260					0.94
	3.01	4384					3.01
	7.06	5343	7368	0.452	0.000	47,500	7.06
	14.1	6167					14.1
	28.2	7368					28.2
	56.3	6817					56.3
38	0.46	2294					1.16
	1.38	3808					3.49
	3.21	5597	8146	0.720	0.159		8.13
	6.40	6632					16.2
	12.6	7392					31.9
	25.6	7689					64.9

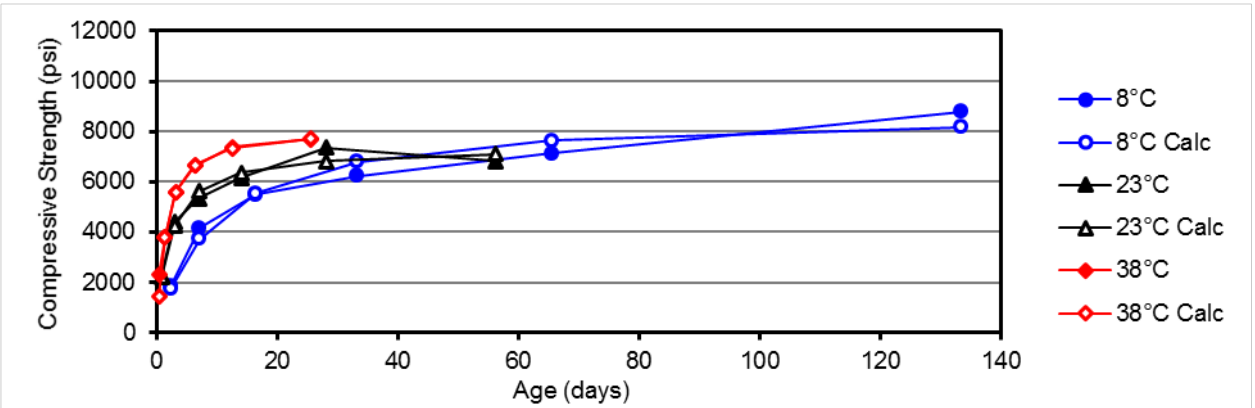

Figure C-40. Strength data for mortar containing 10% sugarcane bagasse ash.

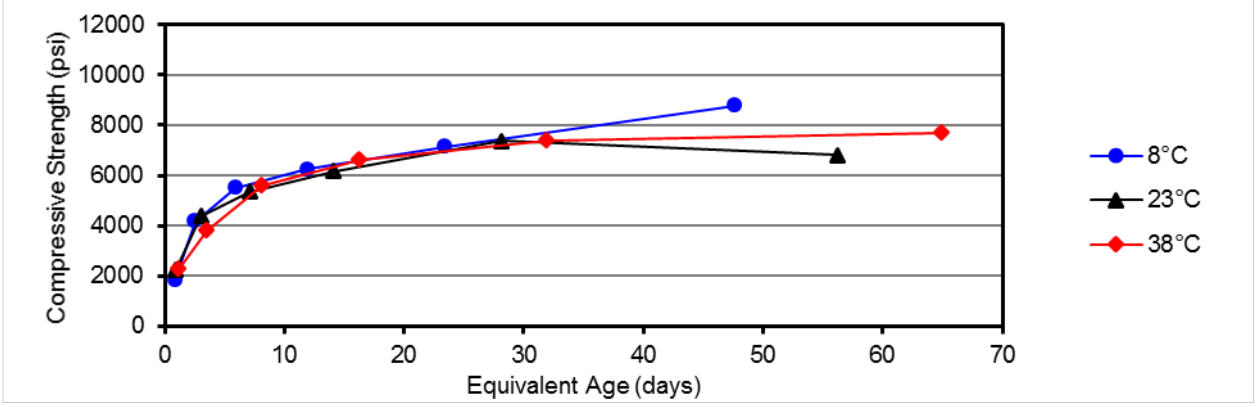

Figure C-41. Equivalent age data for mortar containing 10% sugarcane bagasse ash.

Table C-11. Strength-age data for mortars containing 20% sugarcane bagasse ash.

Temp, °C	Age, days	Strength, psi	Su	k	t_o	E_a, J/mol	Equiv. Age, days
8	2.44	1397					1.20
	7.03	2875					3.44
	17.0	3427	6634	0.085	0.000		8.33
	33.0	4687					16.1
	66.9	5753					32.8
	120	6195					58.8
23	1.03	2281					1.03
	3.08	4681					3.08
	7.01	6484	9696	0.313	0.055	32,900	7.01
	14.3	8118					14.3
	28.1	8912					28.1
	55.9	8898					55.9
38	0.46	1619					0.87
	1.43	2556					2.72
	3.11	3743	7657	0.323	0.000		5.92
	6.22	4978					11.9
	13.1	5835					25.0
	25.9	7232					49.3

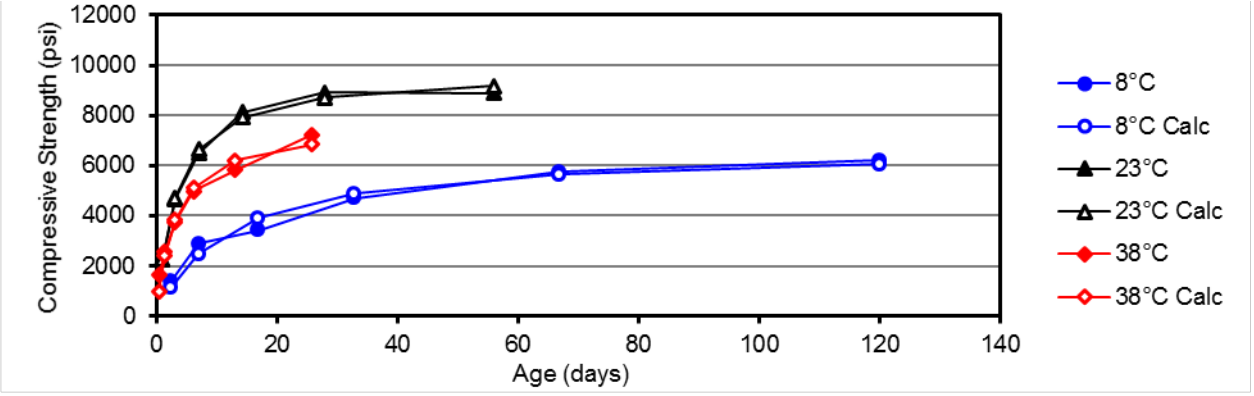

Figure C-42. Strength data for mortar containing 20% sugarcane bagasse ash.

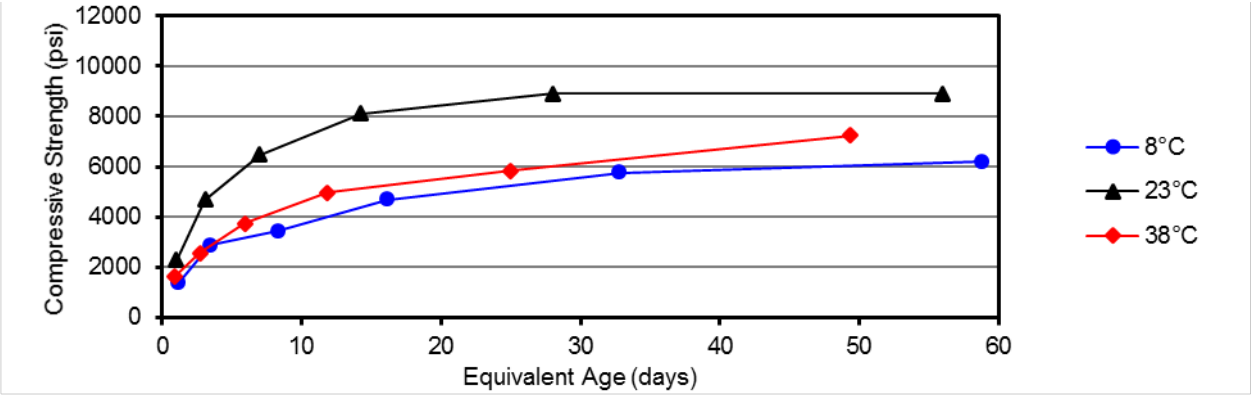

Figure C-43. Equivalent age data for mortar containing 20% sugarcane bagasse ash.

Table C-12. Strength-age data for mortars containing 10% blast furnace slag.

Temp, °C	Age, days	Strength, psi	Su	k	t_o	E_a, J/mol	Equiv. Age, days
8	2.71	1838					0.90
	7.15	4178					2.36
	16.5	5611	9262	0.096	0.000		5.44
	33.4	6792					11.0
	66.9	7599					22.0
	133	9155					43.9
23	1.02	2453					1.02
	3.06	4003					3.06
	6.96	5271	7593	0.347	0.000	51,100	6.96
	14.0	6305					14.0
	31.2	6789					31.2
	55.9	7394					55.9
38	0.44	1928					1.19
	1.37	3488					3.73
	3.20	5239	7438	0.789	0.2454		8.70
	12.4	6633					33.8
	25.6	7159					69.5

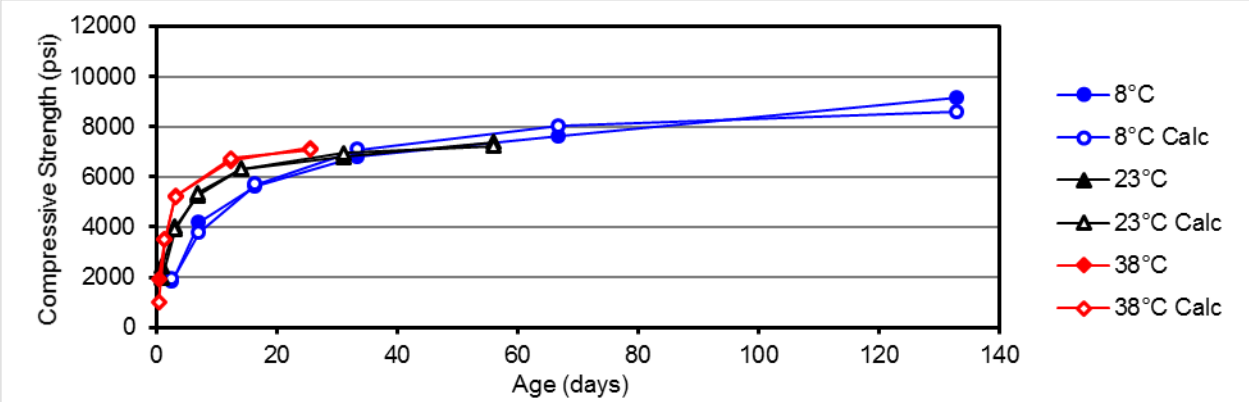

Figure C-44. Strength data for mortar containing 10% blast furnace slag.

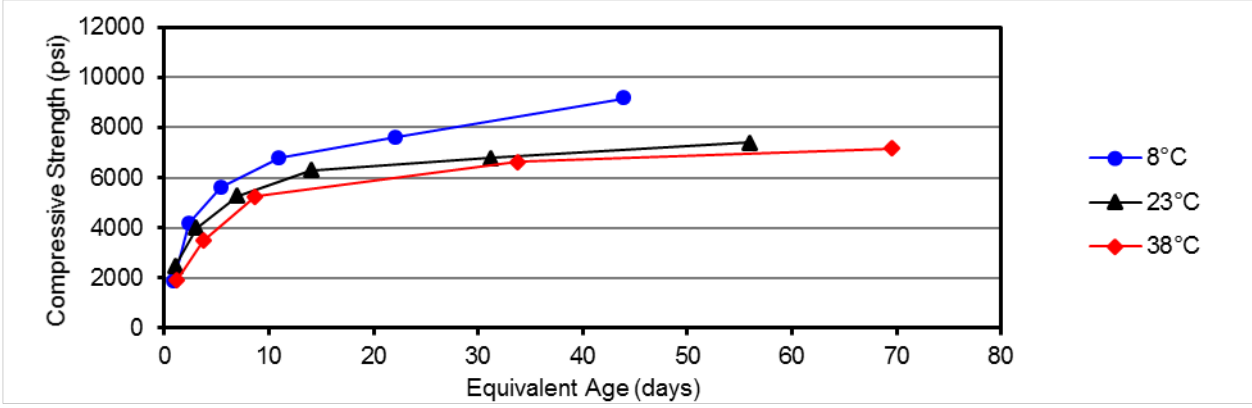

Figure C-45. Equivalent age data for mortar containing 10% blast furnace slag.

Table C-13. Strength-age data for mortars containing 30% blast furnace slag.

Temp, °C	Age, days	Strength, psi	Su	k	t_o	E_a, J/mol	Equiv. Age, days
8	2.28	990					0.82
	7.17	3240					2.57
	16.4	4250	7729	0.078	0.000		5.89
	33.4	5406					12.0
	66.5	5988					23.8
	133	7569					47.8
23	1.00	1502					1.00
	3.01	3144					3.01
	6.14	4211	8750	0.149	0.000	47,300	6.14
	14.0	5276					14.0
	28.2	6676					28.2
	56.1	8463					56.1
38	0.45	1366					1.15
	1.37	3070					3.47
	3.20	4634	7520	0.556	0.073		8.08
	6.41	6074					16.2
	13.0	6865					32.9
	25.5	6696					64.5

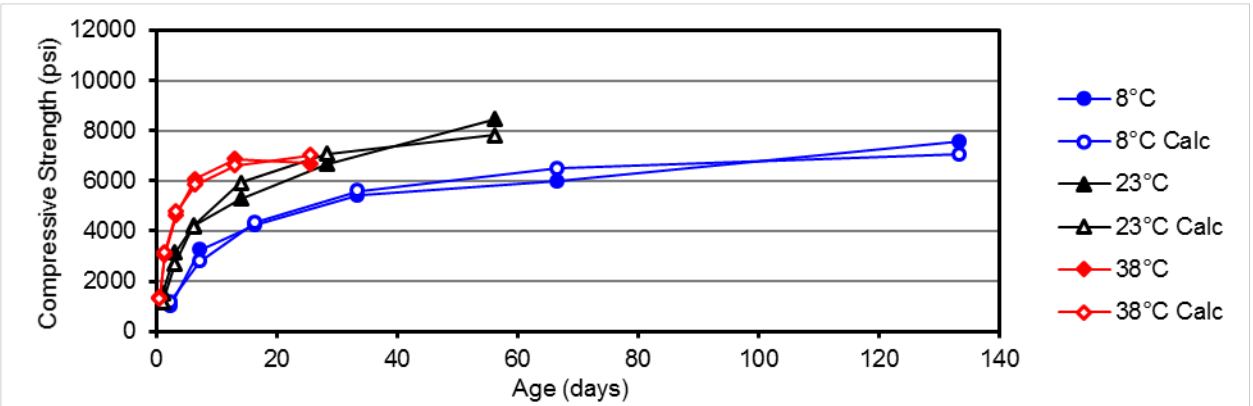

Figure C-46. Strength data for mortar containing 30% blast furnace slag.

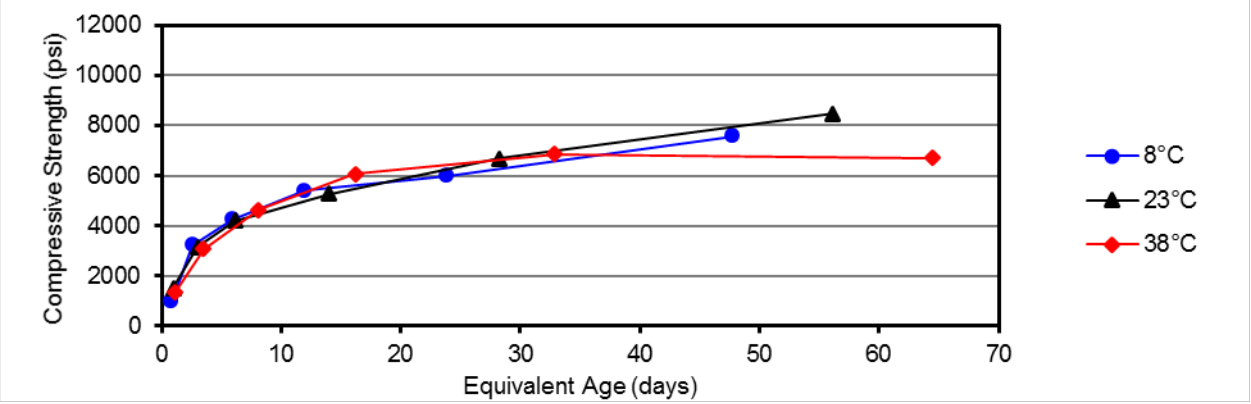

Figure C-47. Equivalent age data for mortar containing 30% blast furnace slag.

Table C-14. Strength-age data for mortars containing 50% blast furnace slag.

Temp, °C	Age, days	Strength, psi	Su	k	t_o	E_a, J/mol	Equiv. Age, days
8	2.37	588					0.80
	7.13	1736					2.39
	16.5	2975	8674	0.034	0.081		5.54
	33.4	4721					11.2
	67.1	5865					22.5
	133	7141					44.6
23	1.01	1213					1.01
	2.86	2759					2.86
	7.16	4171	10,920	0.081	0.000	50,400	7.16
	14.0	5351					14.0
	28.0	6811					28.0
	56.1	9665					56.1
38	0.45	1144					1.20
	1.37	3252					3.68
	3.20	5248	12,380	0.271	0.093		8.58
	6.48	7755					17.4
	12.5	10,544					33.7
	25.5	10,183					68.4

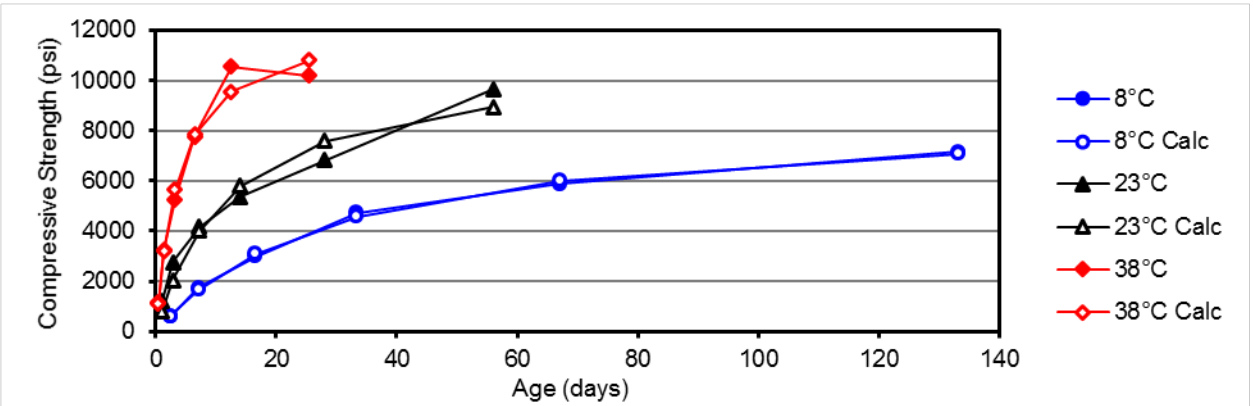

Figure C-48. Strength data for mortar containing 50% blast furnace slag.

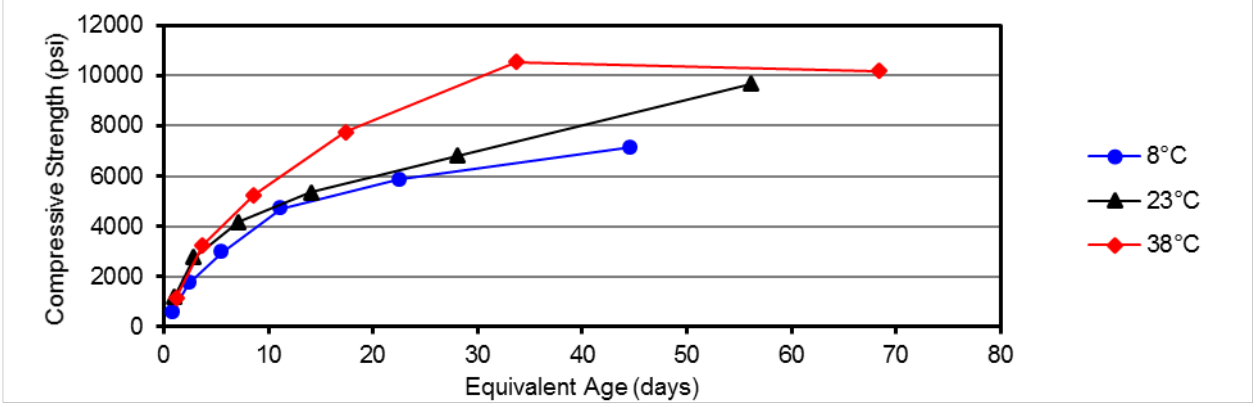

Figure C-49. Equivalent age data for mortar containing 50% blast furnace slag.

Table C-15. Strength-age data for mortars containing 5% metakaolin.

Temp, °C	Age, days	Strength, psi	Su	k	t_o	E_a, J/mol	Equiv. Age, days
8	2.68	2653	9679	0.266	1.316		1.37
	6.98	5409					3.56
	16.8	8013					8.55
	33.8	9678					17.2
	67.0	8911					34.2
	133	7823					67.8
23	1.02	2964	10,240	0.470	0.189	31,000	1.02
	3.05	5547					3.05
	7.15	7926					7.15
	14.1	9212					14.1
	28.2	9986					28.3
	56.0	9157					56.0
38	0.46	2668	10450	0.959	0.116		0.85
	1.37	5423					2.52
	3.11	8075					5.72
	6.54	Removed, 7052					12.0
	13.3	Removed, 8565					24.4
	25.1	9921					46.1

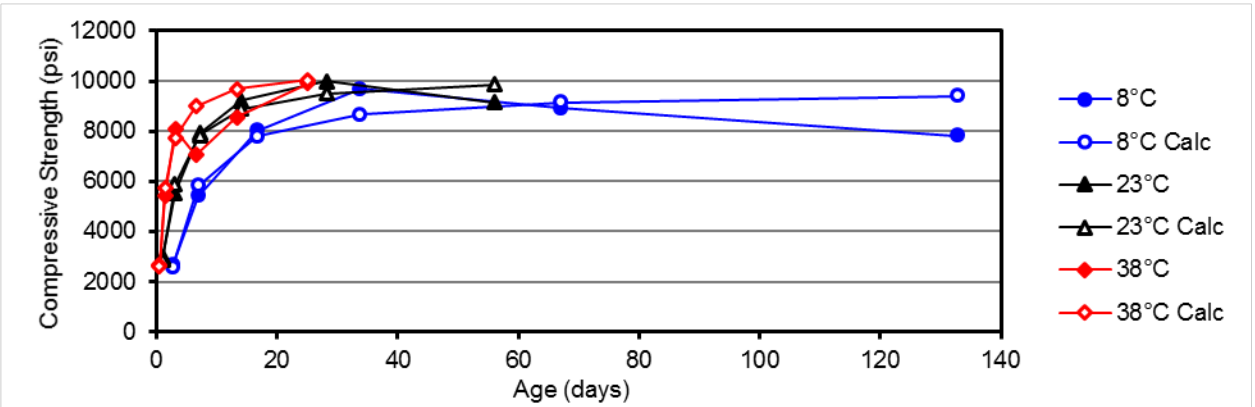

Figure C-50. Strength data for mortar containing 5% metakaolin.

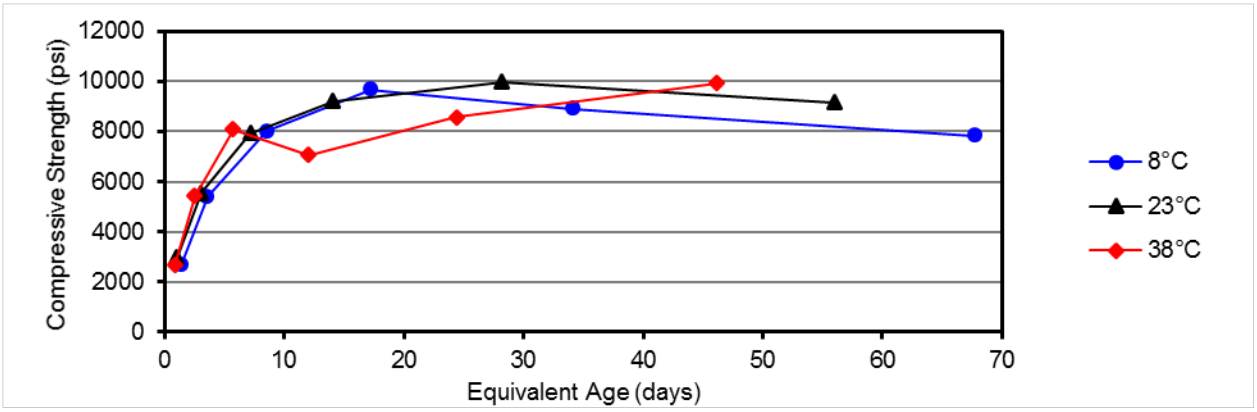

Figure C-51. Equivalent age data for mortar containing 5% metakaolin.

Table C-16. Strength-age data for mortars containing 10% metakaolin.

Temp, °C	Age, days	Strength, psi	Su	k	t_o	E_a, J/mol	Equiv. Age, days
8	2.42	2204					1.43
	7.14	5544					4.21
	17.1	6614	8812	0.274	1.20		10.1
	34.2	8811					20.2
	67.9	8750					40.0
	133	6662					78.4
23	0.92	3028					0.92
	2.93	5903					2.93
	6.93	7320	10,950	0.398	0.000	24,400	6.93
	13.9	9967					13.9
	26.9	10,869					26.9
	55.0	9522					55.0
38	0.46	2822					0.73
	1.34	5841					2.17
	3.31	8675	11,375	0.753	0.000		5.34
	6.33	8997					10.2
	13.1	9010					21.1
	25.4	11,374					41.0

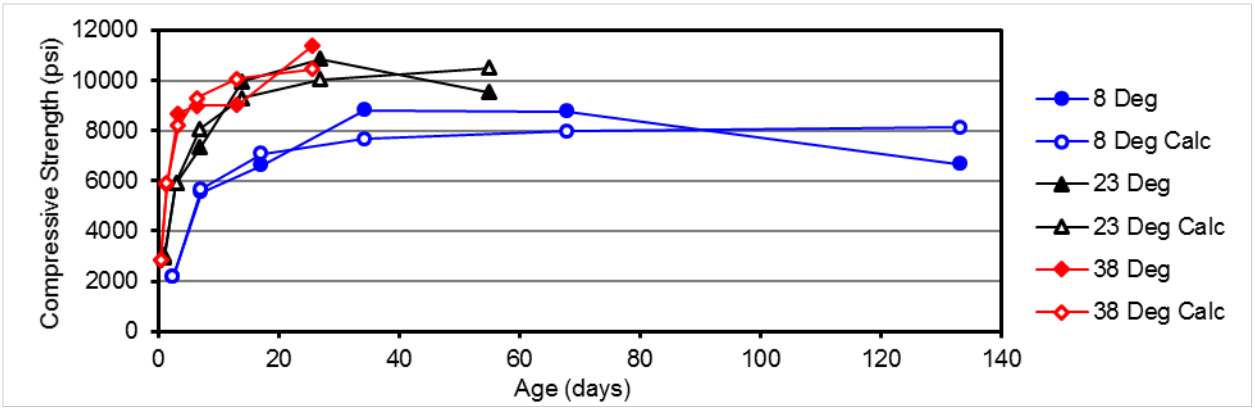

Figure C-52. Strength data for mortar containing 10% metakaolin.

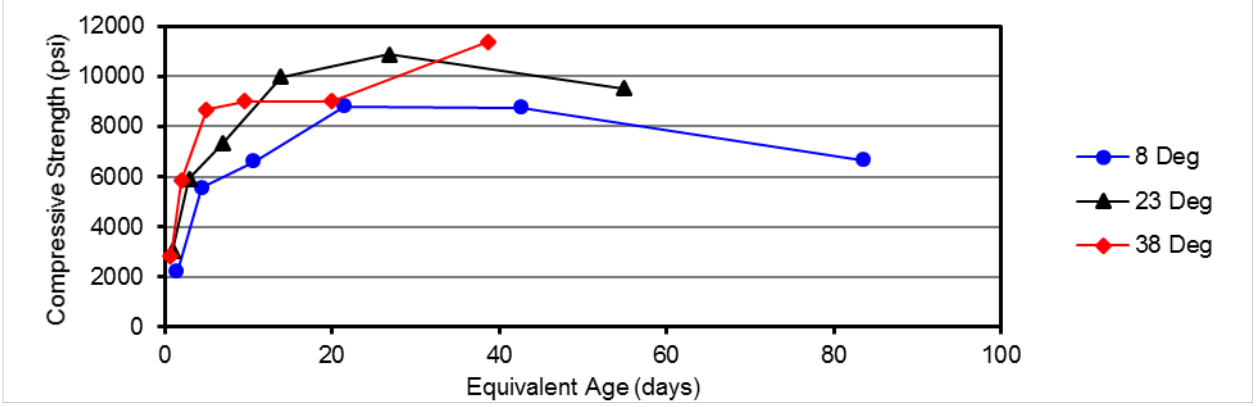

Figure C-53. Equivalent age data for mortar containing 10% metakaolin.

Table C-17. Strength-age data for mortars containing 4% silica fume.

Temp, °C	Age, days	Strength, psi	Su	k	t_o	E_a, J/mol	Equiv. Age, days
8	2.38	2078					1.25
	7.06	5209					3.71
	17.1	7843	10,400	0.213	1.21		8.96
	33.1	9245					17.4
	66.91	9380					35.1
	133	9199					69.9
23	1.02	3998					1.02
	3.01	7374					3.01
	6.90	9100	12,460	0.464	0.000	29,700	6.90
	13.9	10,830					13.9
	28.1	11,587					28.1
	55.2	12,006					55.2
38	0.46	2671					0.82
	1.39	5199					2.49
	3.19	6420	9228	0.722	0.000		5.70
	6.27	6424					11.2
	12.9	7570					23.1
	25.9	9228					46.3

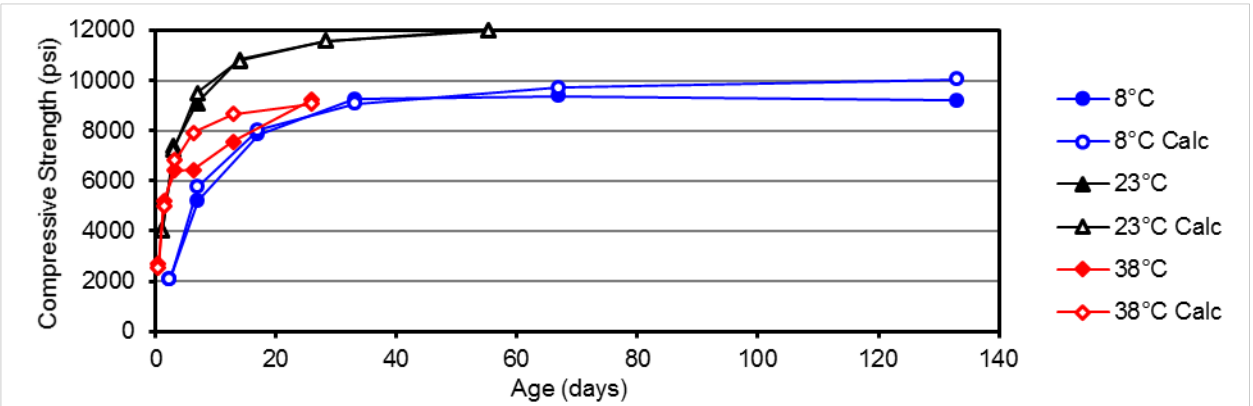

Figure C-54. Strength data for mortar containing 4% silica fume.

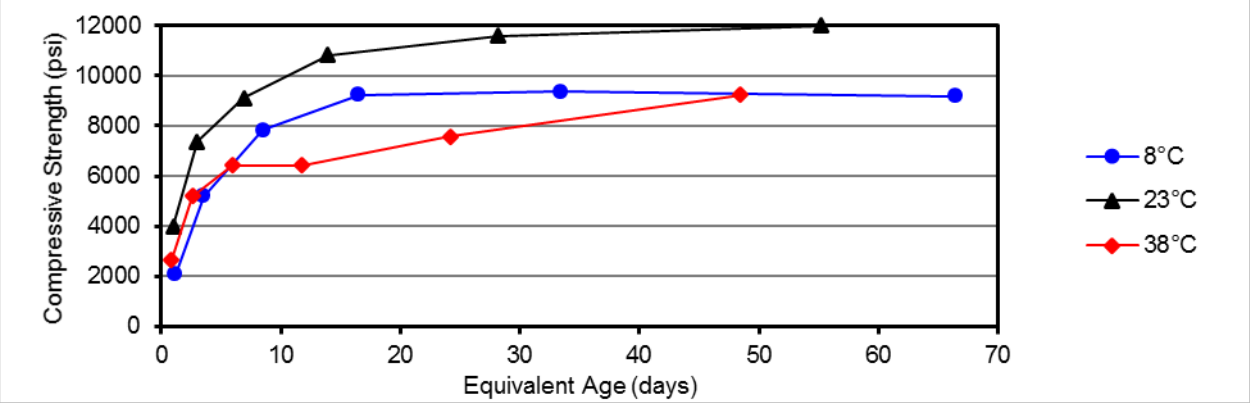

Figure C-55. Equivalent age data for mortar containing 4% silica fume.

Table C-18. Strength-age data for mortars containing 8% silica fume.

Temp, °C	Age, days	Strength, psi	Su	k	t_o	E_a, J/mol	Equiv. Age, days
8	2.37	1817					1.11
	7.11	4798					3.34
	16.4	6126	10,400	0.097	0.000		7.72
	33.0	7702					15.5
	67.2	8839					31.6
	132	10,005					62.0
23	1.52	2767					1.52
	3.13	5627					3.13
	7.03	8393	10,200	0.677	0.994	34,800	7.03
	14.3	10,031					14.3
	28.0	9294					28.0
	55.9	9612					55.9
38	0.45	2200					0.90
	1.37	4431					2.71
	3.21	5460	10,930	0.393	0.000		6.35
	6.22	7291					12.3
	13.1	9394					25.9
	25.1	10,118					49.7

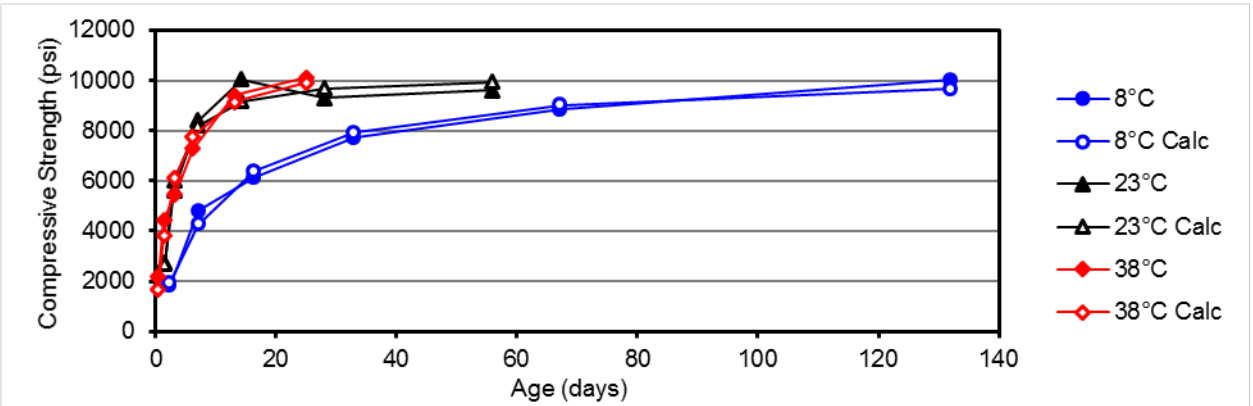

Figure C-56. Strength data for mortar containing 8% silica fume.

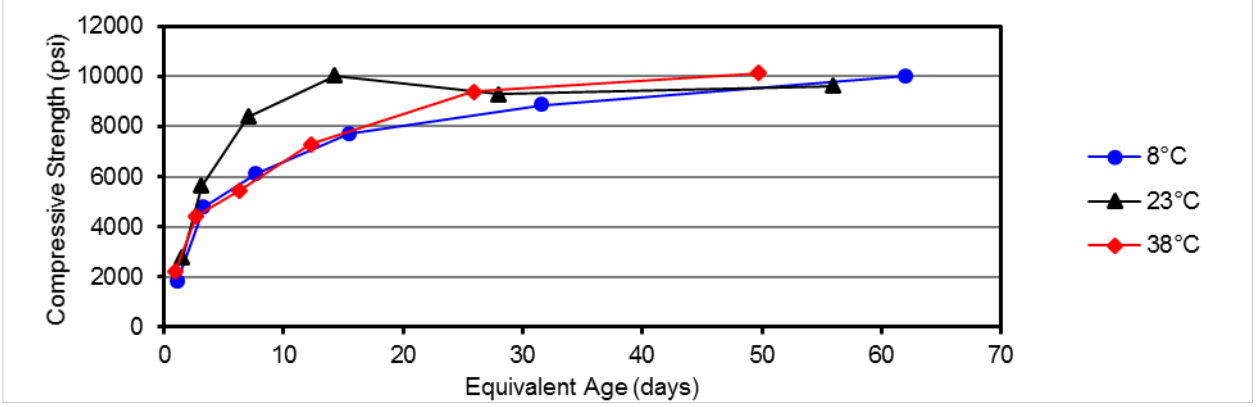

Figure C-57. Equivalent age data for mortar containing 8% silica fume.

Table C-19. Strength-age data for mortars containing 10% ground glass.

Temp, °C	Age, days	Strength, psi	Su	k	t_o	E_a, J/mol	Equiv. Age, days
8	2.39	2082					0.81
	7.29	3971					2.47
	17.2	5533					5.82
	33.5	6323	8657	0.108	0.000		11.3
	67.3	7777					22.8
	133	8264					45.0
23	1.01	2303					1.01
	2.99	4644					2.99
	7.01	5871					7.01
	14.0	6485	8403	0.354	0.000	50,000	14.0
	28.1	7358					28.1
	56.1	8402					56.1
38	0.45	2559					1.21
	1.37	4632					3.65
	3.31	5804					8.82
	6.41	6635	8239	0.850	0.000		17.1
	13.2	7641					35.1
	25.5	8147					67.8

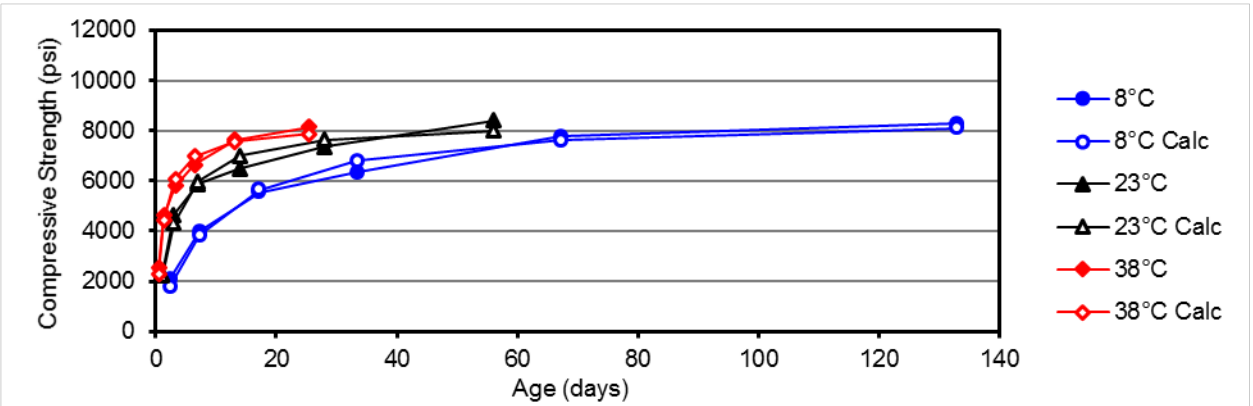

Figure C-58. Strength data for mortar containing 10% ground glass.

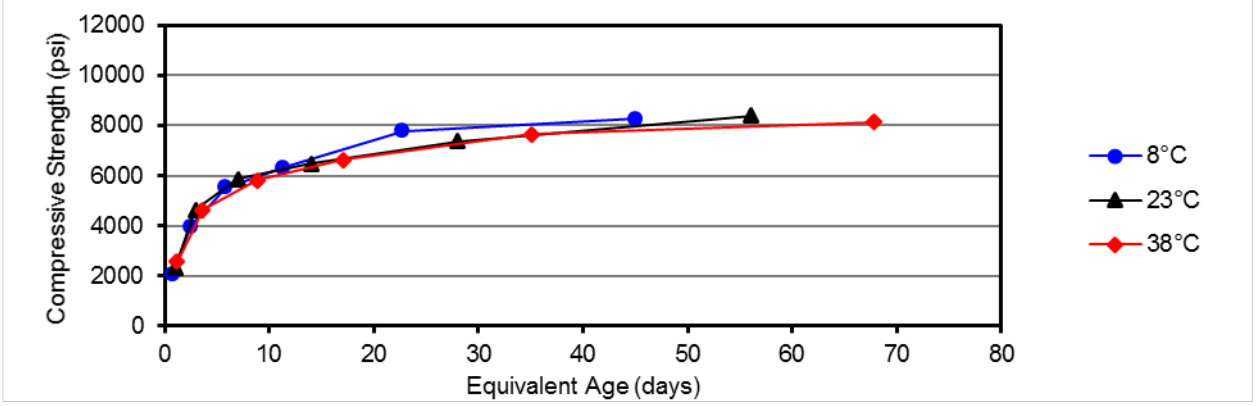

Figure C-59. Equivalent age data for mortar containing 10% ground glass.

Table C-20. Strength-age data for mortars containing 20% ground glass.

Temp, °C	Age, days	Strength, psi	Su	k	t_o	E_a, J/mol	Equiv. Age, days
8	2.44	1525					1.00
	7.27	3542					2.97
	16.4	4484	6734	0.123	0.000		6.72
	33.4	4582					13.7
	66.1	6187					27.0
	133	6611					54.4
23	0.98	2038					0.98
	3.16	3971					3.16
	7.09	4797	8875	0.203	0.000	41,200	7.09
	14.0	6241					14.0
	28.2	7039					28.2
	56.2	8874					56.2
38	0.42	1947					0.93
	1.07	4097					2.39
	3.03	4555	8098	0.685	0.000		6.79
	6.22	6369					14.0
	13.3	7356					29.9
	25.6	8025					57.3

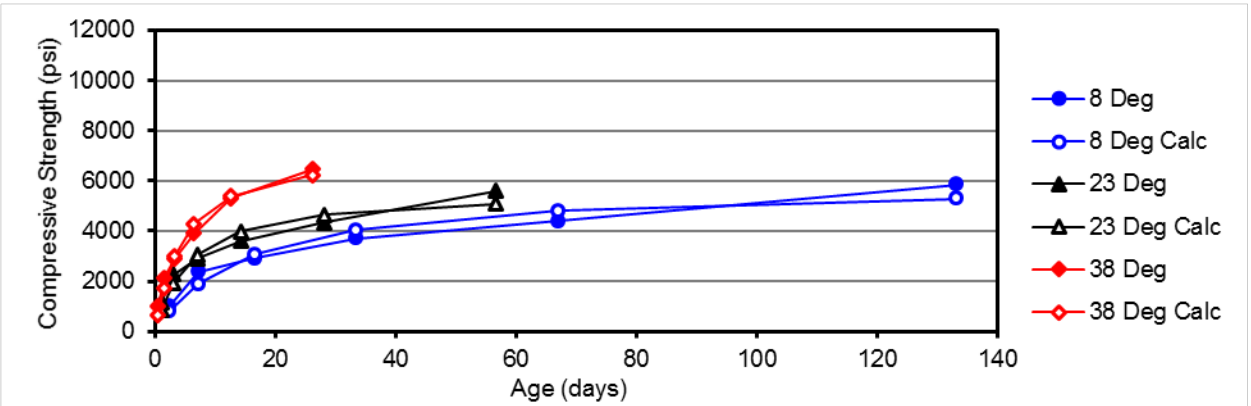

Figure C-60. Strength data for mortar containing 20% ground glass.

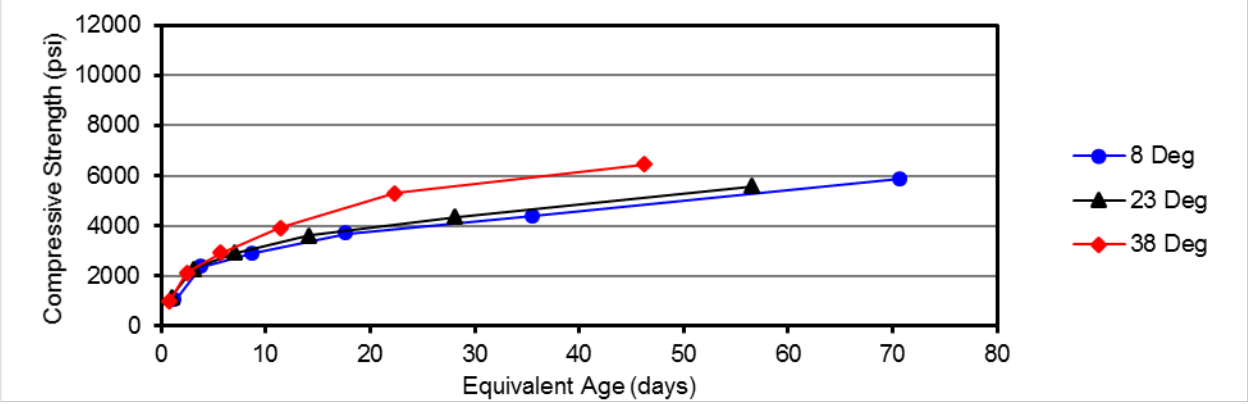

Figure C-61. Equivalent age data for mortar containing 20% ground glass.

Table C-21. Strength-age data for mortars containing 10% equilibrium catalyst.

Temp, °C	Age, days	Strength, psi	Su	k	t_o	E_a, J/mol	Equiv. Age, days
8	2.38	1559					0.69
	7.88	3806					2.30
	17.1	5333	9971	0.0679	0.000		4.98
	33.3	6616					9.71
	66.4	7654					19.4
	133	9592					38.8
23	1.00	2417					1.00
	3.09	4299					3.09
	7.11	5344	7930	0.356	0.000	56,900	7.11
	14.1	5815					14.1
	28.1	7190					28.1
	56.0	7698					55.9
38	0.46	2051					1.39
	1.37	3979					4.19
	3.18	5370	7896	0.700	0.000		9.70
	6.37	6132					19.4
	12.6	7155					38.3
	25.5	7655					77.6

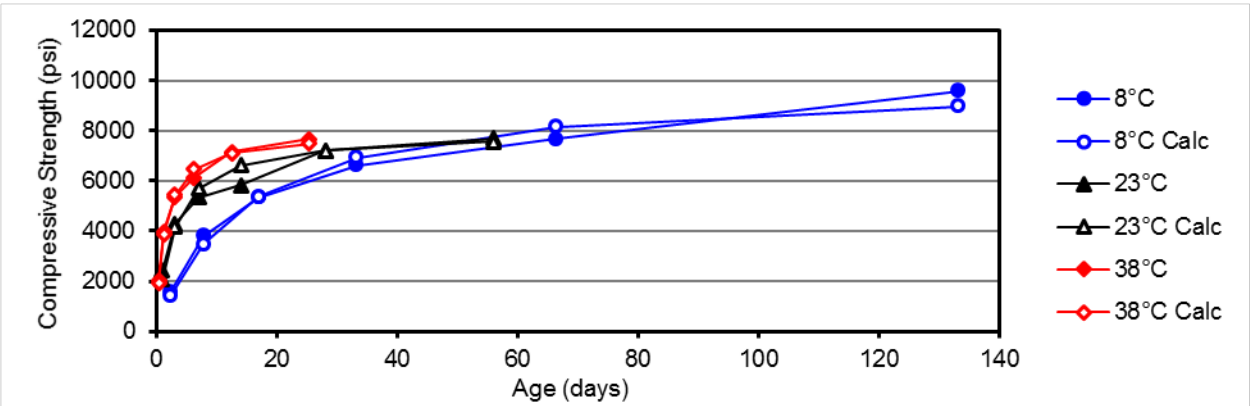

Figure C-62. Strength data for mortar containing 10% equilibrium catalyst.

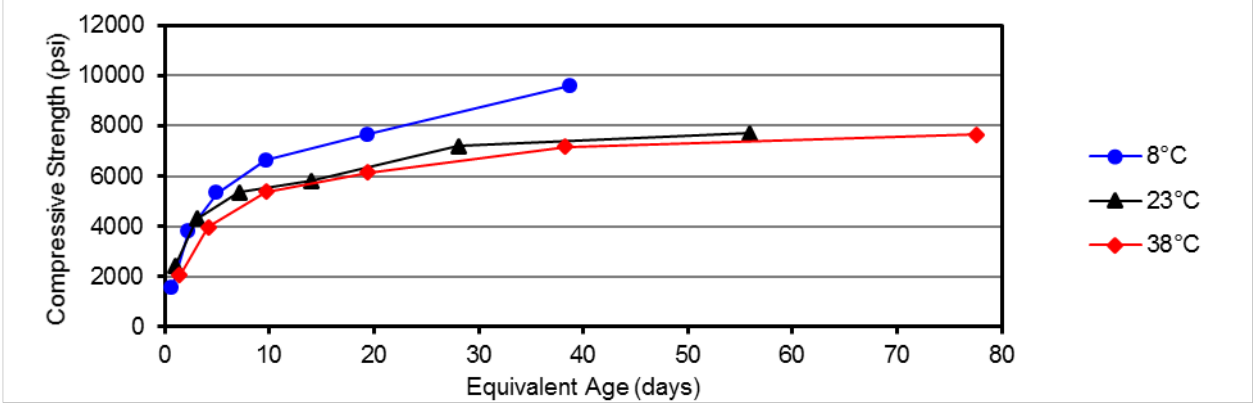

Figure C-63. Equivalent age data for mortar containing 10% equilibrium catalyst.

Table C-22. Strength-age data for mortars containing 20% equilibrium catalyst.

Temp, °C	Age, days	Strength, psi	Su	k	t_o	E_a, J/mol	Equiv. Age, days
8	2.37	1323					0.81
	7.26	3555					2.46
	16.9	4733	8004	0.0881	0.000		5.74
	34.5	5435					11.7
	67.0	6900					22.8
	133	7652					45.2
23	1.03	2046					1.03
	3.24	3807					3.24
	7.16	4530	7882	0.243	0.000	49,800	7.16
	14.1	5951					14.1
	28.0	6615					28.0
	56.4	7821					56.4
38	0.44	1670					1.16
	1.37	3522					3.65
	3.27	4336	6662	0.691	0.000		8.69
	6.34	5008					16.8
	12.5	6229					33.2
	25.0	6434					66.5

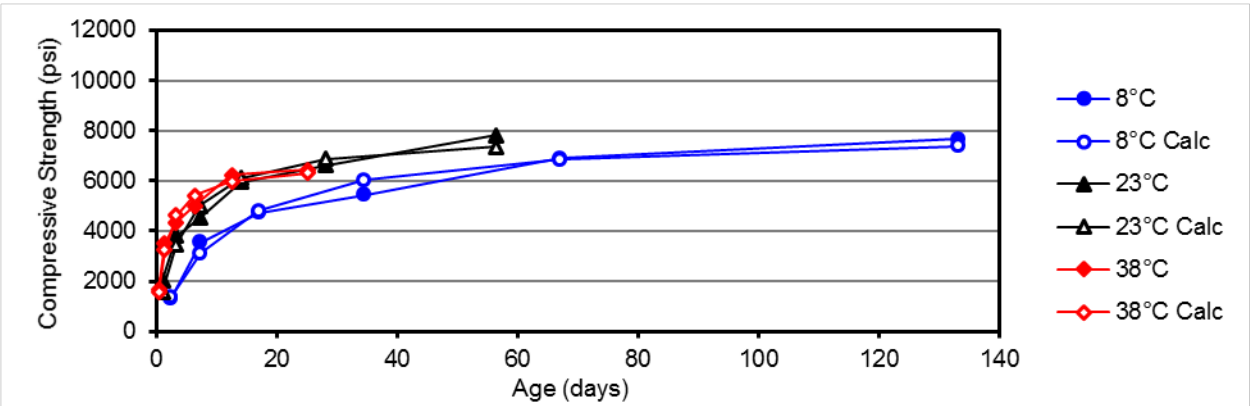

Figure C-64. Strength data for mortar containing 20% equilibrium catalyst.

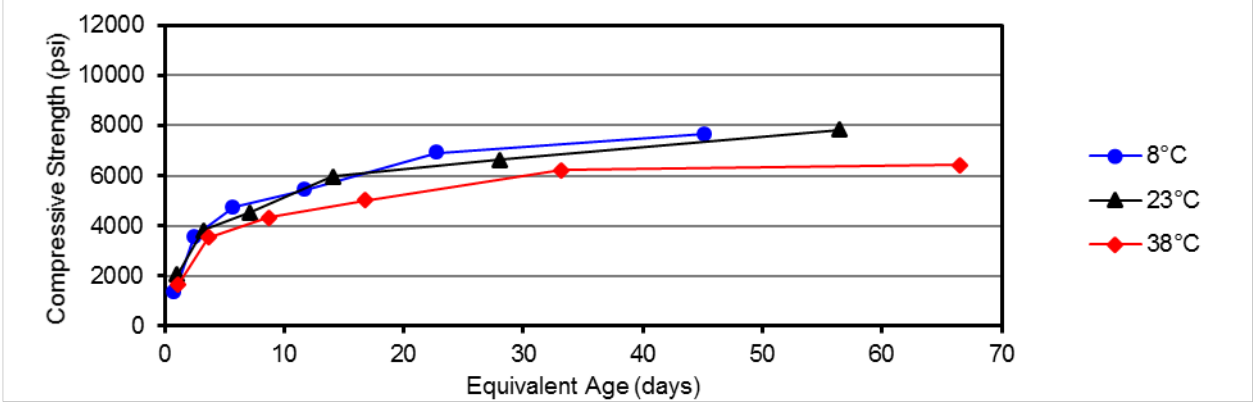

Figure C-65. Equivalent age data for mortar containing 20% equilibrium catalyst.

Table C-23. Strength-age data for mortars containing 25% wood ash.

Temp, °C	Age, days	Strength, psi	Su	k	t_o	E_a, J/mol	Equiv. Age, days
8	2.40	378					0.95
	7.16	3797					2.85
	17.0	4163	5678	0.280	2.09		6.75
	33.4	4470					13.3
	67.3	5416					26.8
	132	6160					52.6
23	1.00	2702					1.00
	3.17	4047					3.17
	7.03	4534	6272	0.446	0.000	42,500	7.03
	14.0	5134					14.0
	28.1	5474					28.1
	56.0	6271					56.0
38	0.45	1926					1.03
	1.38	3708					3.18
	4.21	4555	5251	1.64	0.090		9.68
	6.39	4348					14.7
	13.0	5243					30.0
	25.5	5216					58.7

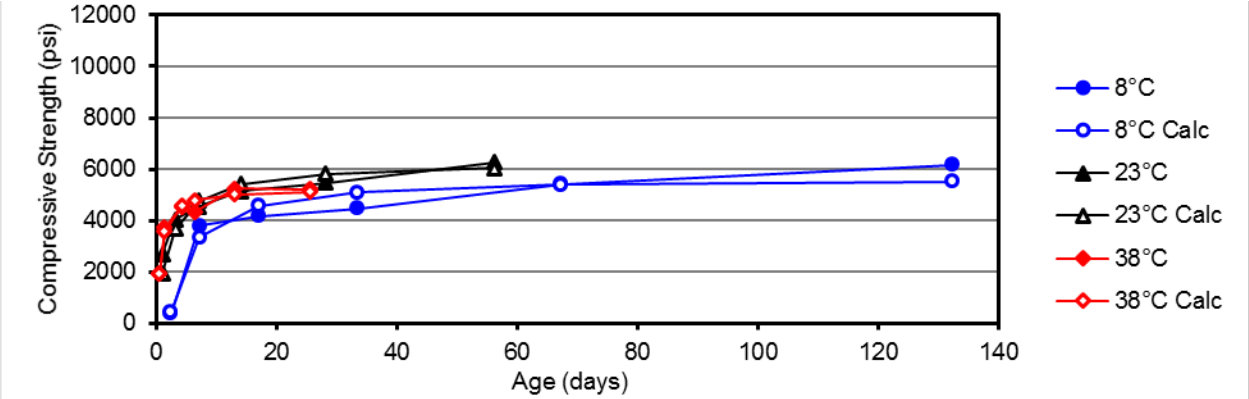

Figure C-66. Strength data for mortar containing 25% wood ash.

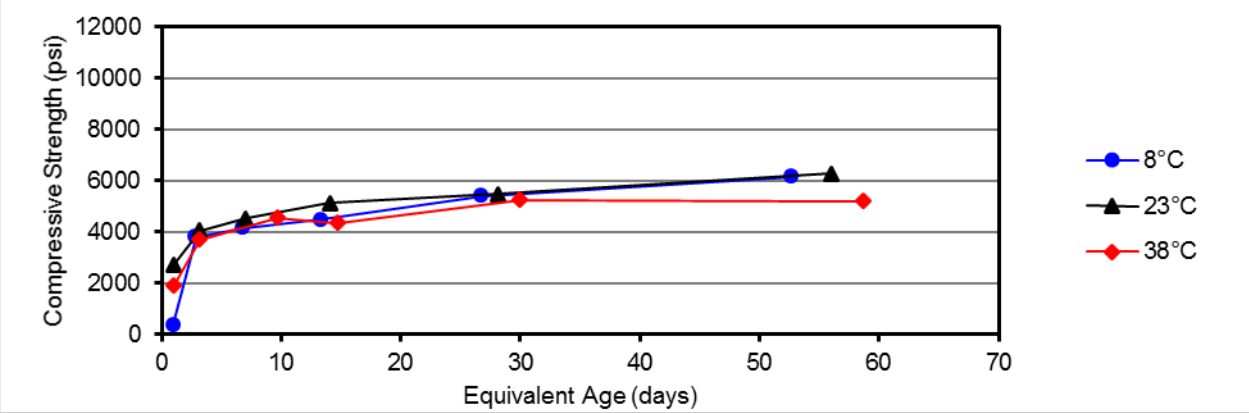

Figure C-67. Equivalent age data for mortar containing 25% wood ash.

Table C-24. Strength-age data for mortars containing 50% wood ash.

Temp, °C	Age, days	Strength, psi	Su	k	t_o	E_a, J/mol	Equiv. Age, days
8	1.98	1704					0.55
	7.03	2250					1.94
	17.0	2762					4.69
	34.4	3148	3870	0.170	0.000		9.46
	67.0	3578					18.5
	133	3833					36.6
23	0.99	1709					0.99
	2.06	2487					2.06
	7.14	2595					7.14
	14.1	2898	3372	1.03	0.000	59,400	14.1
	27.9	3393					27.9
	56.0	3613					56.1
38	0.45	1467					1.45
	1.35	2069					4.33
	2.11	2431					6.76
	6.45	2609	2896	1.94	0.000		20.7
	13.2	2589					42.2
	24.4	2895					78.2

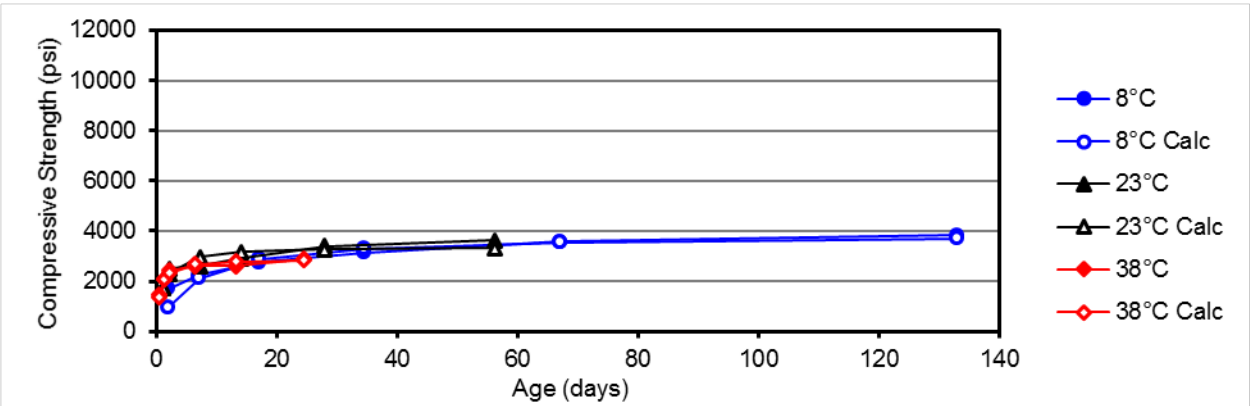

Figure C-68. Strength data for mortar containing 50% wood ash.

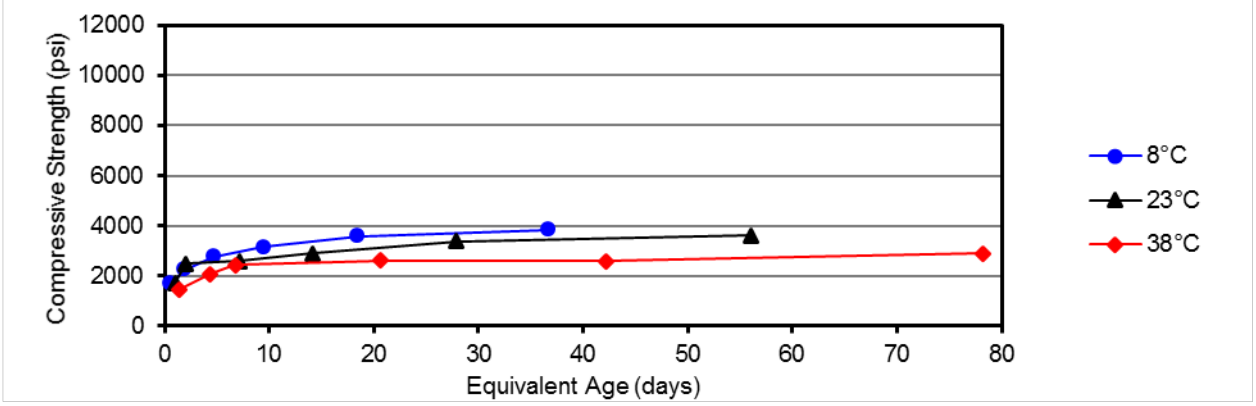

Figure C-69. Equivalent age data for mortar containing 50% wood ash.

Table C-25. Strength-age data for mortars containing 20% VCAS160 glass.

Temp, °C	Age, days	Strength, psi	Su, psi	k	t_o, days	E_a, J/mol	Equiv. Age, days
8	2.39	1428					0.98
	7.14	3668					2.93
	17.0	4956	8886	0.079	0.000		6.97
	33.4	6092					13.7
	66.5	7199					27.3
	133	8581					54.8
23	1.01	2227					1.01
	3.01	4109					3.01
	7.00	5218	8960	0.252	0.000	41,000	7.00
	14.0	Removed, 5395					14.0
	28.1	7639					28.1
	56.1	8718					56.1
38	0.46	1998					1.02
	1.38	4037					3.08
	3.23	5447	9902	0.426	0.000		7.21
	6.40	6915					14.3
	12.6	8074					28.1
	25.5	9576					56.9

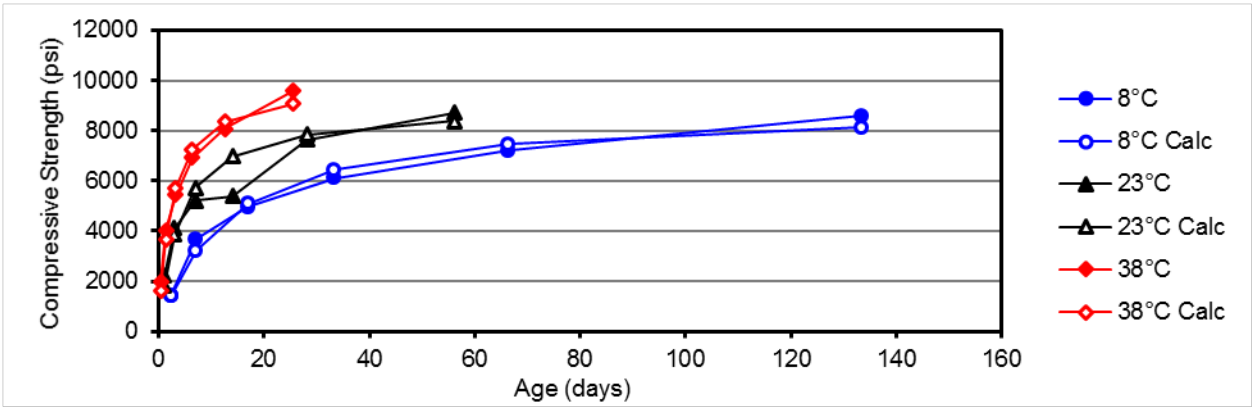

Figure C-70. Strength data for mortar containing 20% VCAS160 glass.

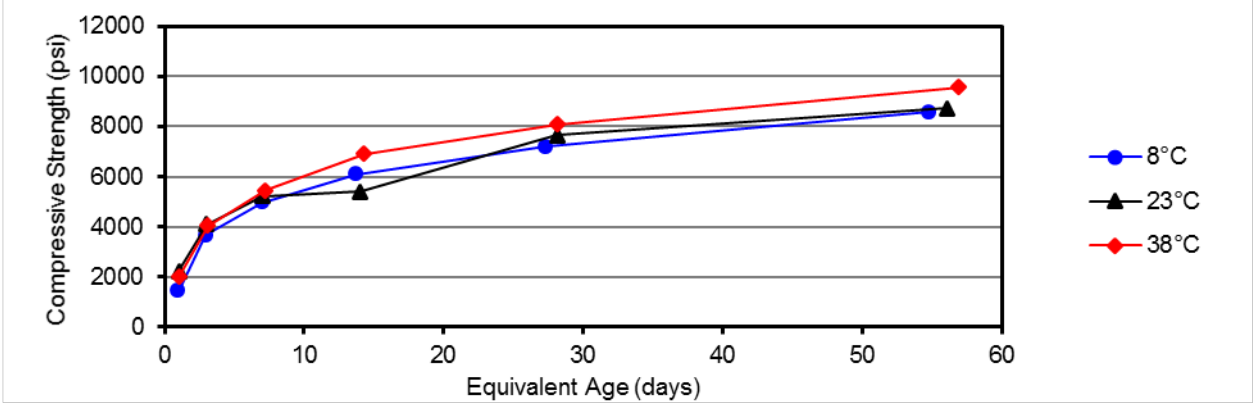

Figure C-71. Equivalent age data for mortar containing 20% VCAS160 glass.

Table C-26. Strength-age data for mortars containing 20% CS200 glass.

Temp, °C	Age, days	Strength, psi	Su, psi	k	t_o, days	E_a, J/mol	Equiv. Age, days
8	2.37	1418	9116	0.088	0.000		0.89
	7.13	3800					2.68
	17.0	5570					6.37
	33.3	6245					12.5
	67.00	7812					25.1
	134	8614					50.2
23	0.99	1846	8342	0.265	0.000	45,200	0.99
	3.08	4190					3.08
	7.08	5245					7.08
	14.1	5938					14.1
	28.2	7270					28.2
	56.3	8341					56.3
38	0.46	1979	8437	0.563	0.000		1.12
	1.37	3849					3.32
	3.22	5136					7.80
	6.44	Removed, 5286					15.6
	12.9	7111					31.2
	25.4	8257					61.6

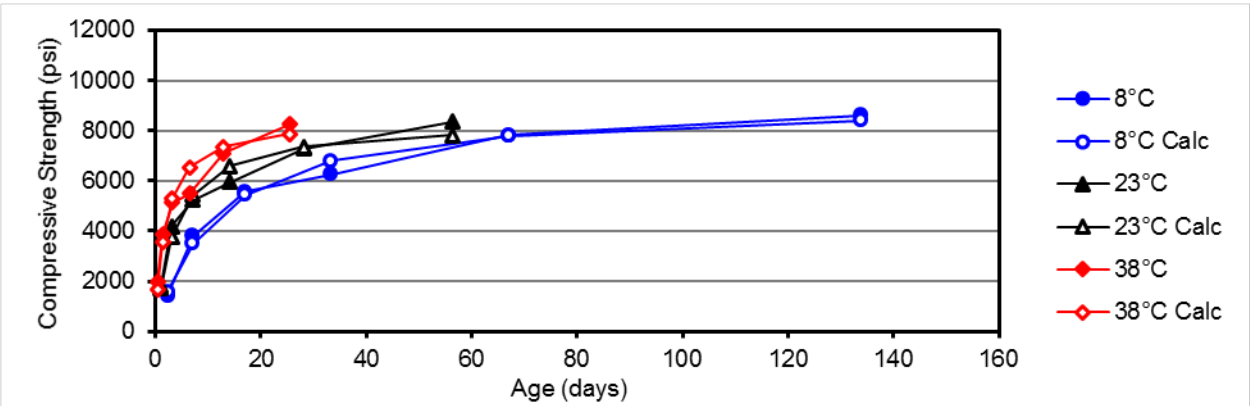

Figure C-72. Strength data for mortar containing 20% CS200 glass.

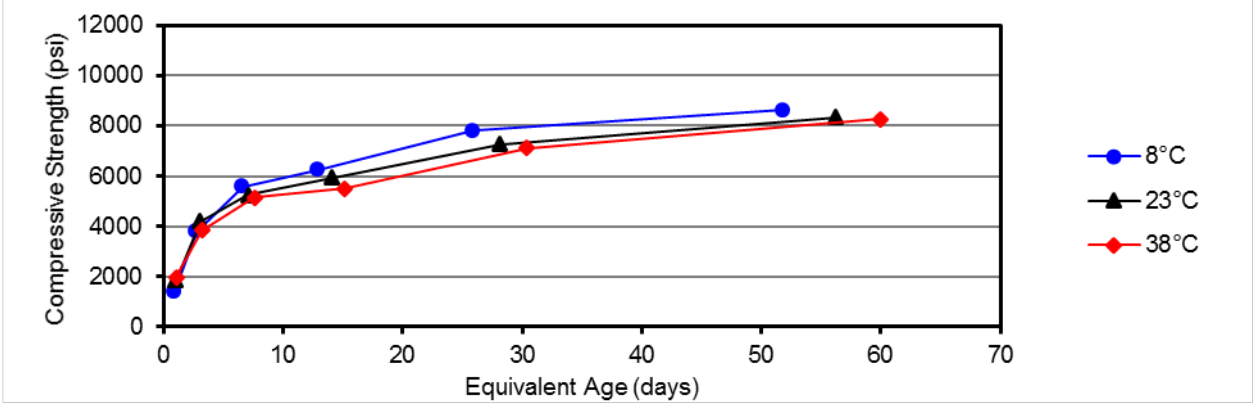

Figure C-73. Equivalent age data for mortar containing 20% CS200 glass.

Table C-27. Strength-age data for mortars containing 20% C ash and 5% RHA.

Temp, °C	Age, days	Strength, psi	Su, psi	k	t_o, days	E_a, J/mol	Equiv. Age, days
8	2.39	1197	8708	0.082	0.000		1.07
	7.26	3782					3.24
	17.5	5039					7.80
	33.2	6165					14.8
	67.1	6811					29.9
	133	8571					59.4
23	1.00	1734	7116	0.406	0.000	37,200	1.00
	2.07	4047					2.07
	7.14	5166					7.14
	14.2	5088					14.2
	28.6	6300					28.6
	56.2	7780					56.2
38	1.48	1873	8029	0.371	0.000		3.07
	1.32	3542					2.73
	3.19	4600					6.62
	6.42	5511					13.3
	13.6	6524					28.2
	25.2	7428					52.3

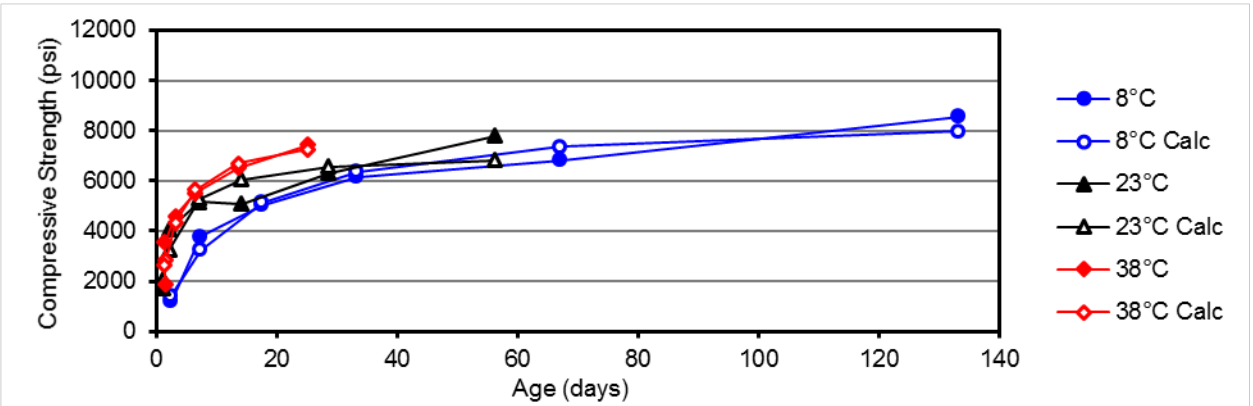

Figure C-74. Strength data for mortar containing 20% C ash and 5% RHA.

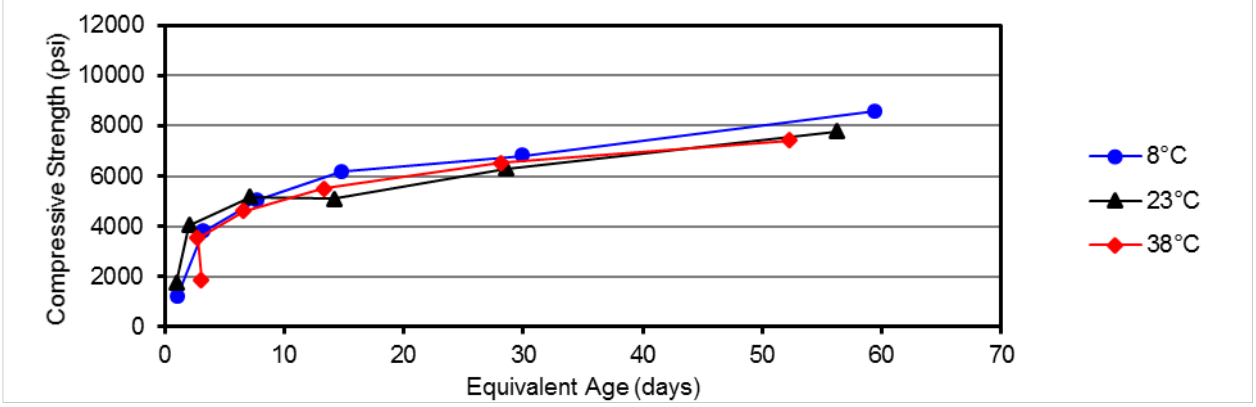

Figure C-75. Equivalent age data for mortar containing 20% and 5% RHA.

Table C-28. Strength-age data for mortars containing 20% C ash and 5% slag.

Temp, °C	Age, days	Strength, psi	Su, psi	k	t_o, days	E_a, J/mol	Equiv. Age, days
8	2.41	1120	7685	0.122	0.965		0.99
	7.20	3380					2.96
	16.4	5090					6.74
	33.3	5889					13.7
	66.5	6839					27.3
	133	7331					54.6
23	1.01	1865	8808	0.215	0.000	41,000	1.01
	3.01	3710					3.01
	7.24	5231					7.24
	14.0	6206					14.0
	28.1	7389					28.1
	56.2	8567					56.2
38	0.47	1542	7411	0.672	0.069		1.05
	1.41	3716					3.16
	3.28	4388					7.33
	6.40	6559					14.3
	12.5	6826					28.0
	25.1	6679					0.99

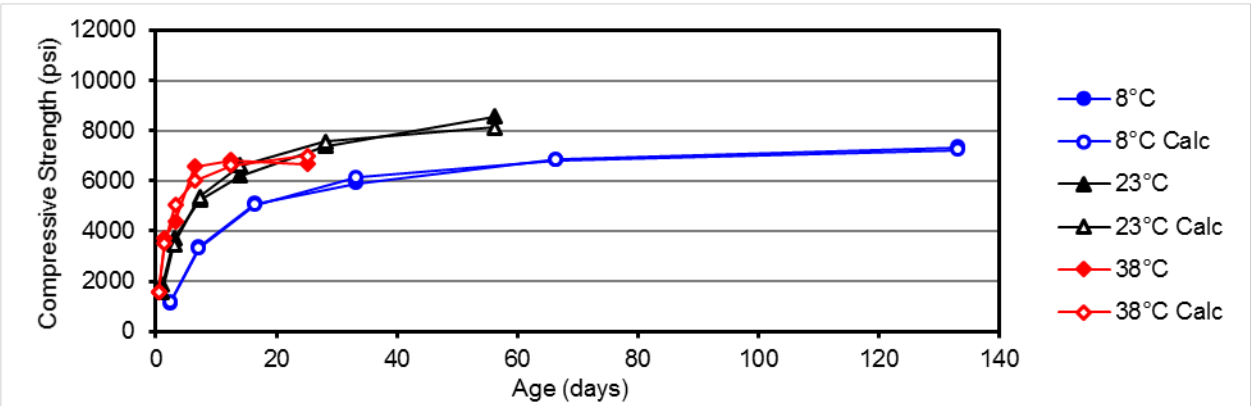

Figure C-76. Strength data for mortar containing 20% C ash and 5% slag.

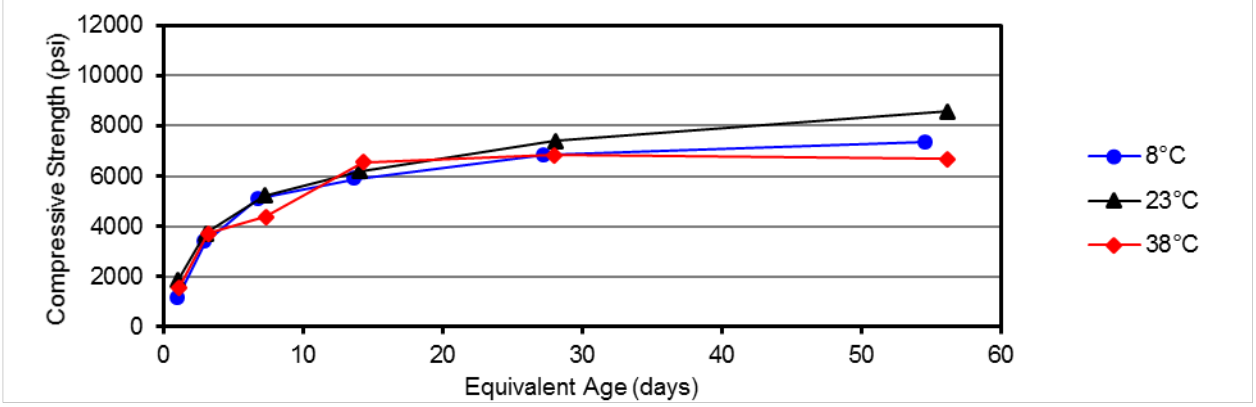

Figure C-77. Equivalent age data for mortar containing 20% C ash and 5% slag.

Table C-29. Strength-age data for mortars containing 20% C ash and 10% slag.

Temp, °C	Age, days	Strength, psi	Su, psi	k	t_o, days	E_a, J/mol	Equiv. Age, days
8	2.37	1308	8694	0.066	0.000		0.81
	7.09	2617					2.43
	16.9	4724					5.79
	33.4	5541					11.4
	66.8	7900					22.9
	133	7398					45.5
23	1.00	1879	11330	0.182	0.000	49,400	1.00
	2.98	4056					2.98
	7.14	6402					7.14
	14.1	7982					14.1
	28.1	9372					28.1
	56.9	10,512					56.9
38	0.45	1676	9978	0.508	0.065		1.19
	1.33	3921					3.51
	3.17	5645					8.35
	6.13	8140					16.1
	13.2	8756					34.7
	26.0	9017					68.5

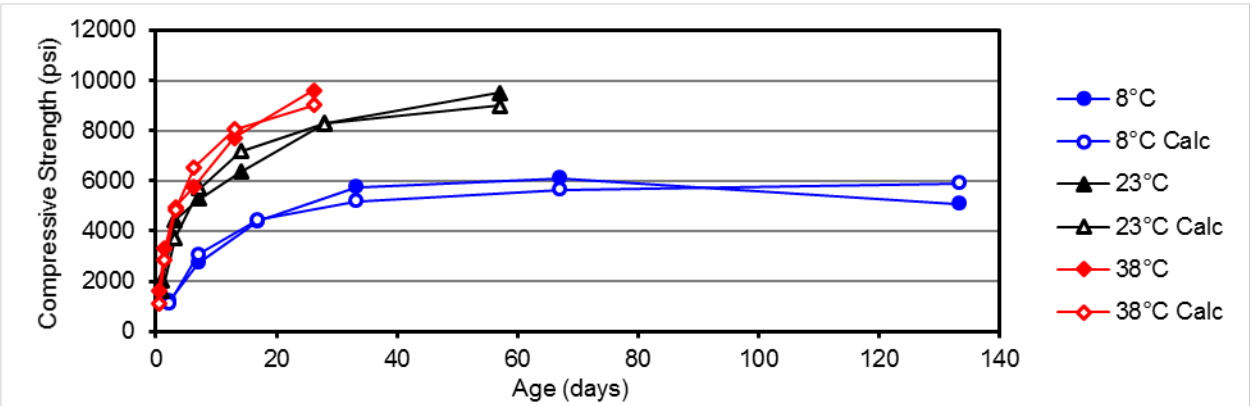

Figure C-78. Strength data for mortar containing 20% C ash and 10% slag.

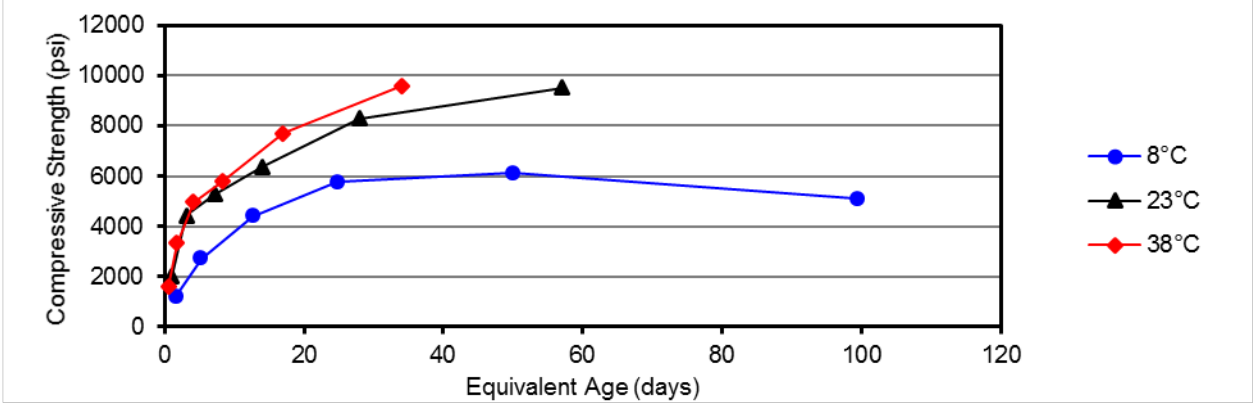

Figure C-79. Equivalent age data for mortar containing 20% C ash and 10% slag.

Table C-30. Strength-age data for mortars containing 20% C ash and 5% F ash.

Temp, °C	Age, days	Strength, psi	Su, psi	k	t_o, days	E_a, J/mol	Equiv. Age, days
8	2.39	1053					0.93
	7.28	3601					2.85
	16.5	5080					6.46
	34.3	Removed, 5243	8708	0.082	0.000		13.4
	66.4	Removed, 6284					26.0
	133	8009					52.1
23	1.03	1805					1.03
	3.04	3305					3.04
	7.12	4506					7.12
	14.3	5808	8144	0.197	0.000	43,200	14.3
	28.3	6772					28.3
	56.4	7783					56.4
38	0.45	1601					1.05
	1.33	3431					3.10
	3.20	4468					7.47
	6.41	5901	7949	0.489	0.000		15.0
	12.5	6921					29.1
	26.0	7477					60.7

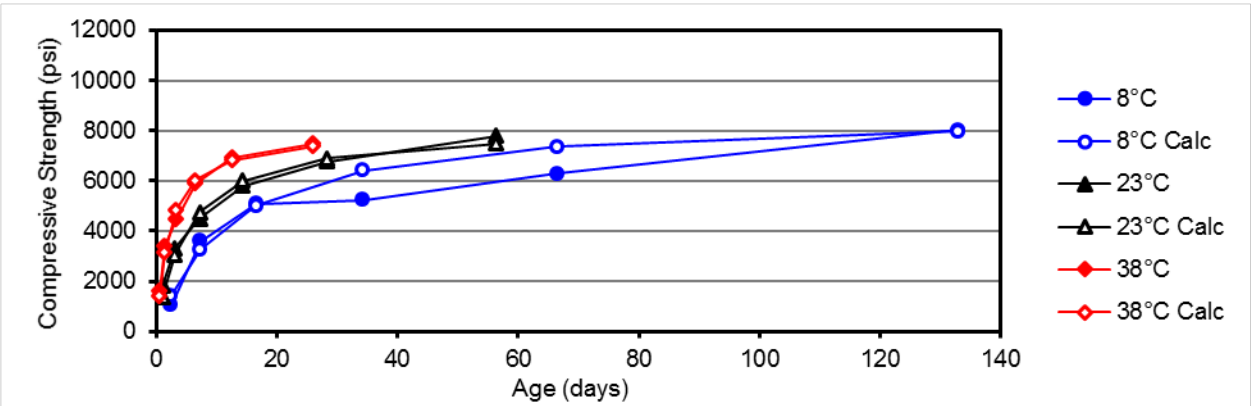

Figure C-80. Strength data for mortar containing 20% C ash and 5% F ash.

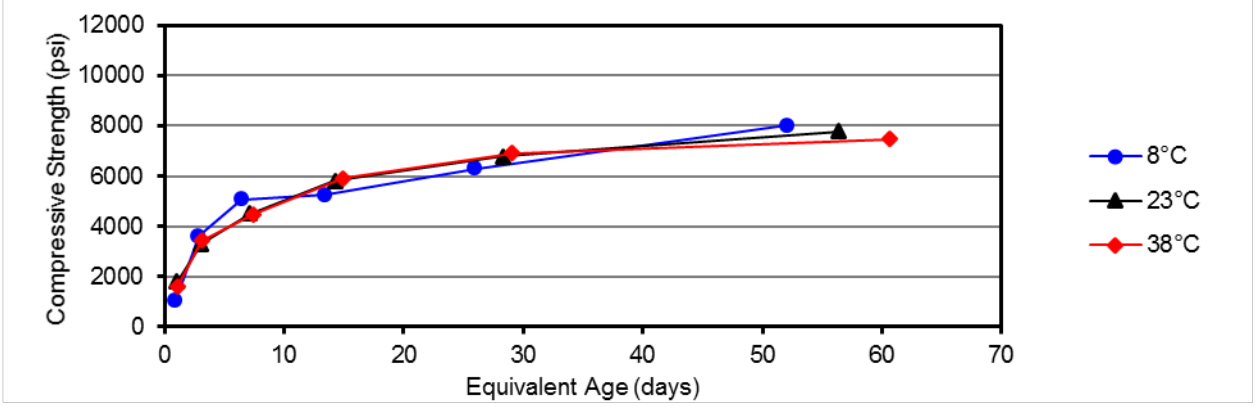

Figure C-81. Equivalent age data for mortar containing 20% C ash and 5% F ash.

Table C-31. Strength-age data for mortars containing 20% C ash and 10% F ash.

Temp, °C	Age, days	Strength, psi	Su, psi	k	t_o, days	E_a, J/mol	Equiv. Age, days
8	2.35	1404	8511	0.079	0.000		1.10
	7.13	2911					3.33
	17.1	5153					8.01
	33.2	5942					15.5
	67.0	7138					31.4
	133.0	7829					62.1
23	1.01	2503	8991	0.221	0.000	35,000	1.01
	3.08	3640					3.08
	7.01	5158					7.01
	14.2	7023					14.2
	28.0	6944					28.0
	55.9	8971					55.9
38	0.44	1272	7730	0.331	0.000		0.88
	1.36	2708					2.69
	3.31	3797					6.57
	6.39	4903					12.7
	13.0	6491					25.8
	26.1	6973					51.8

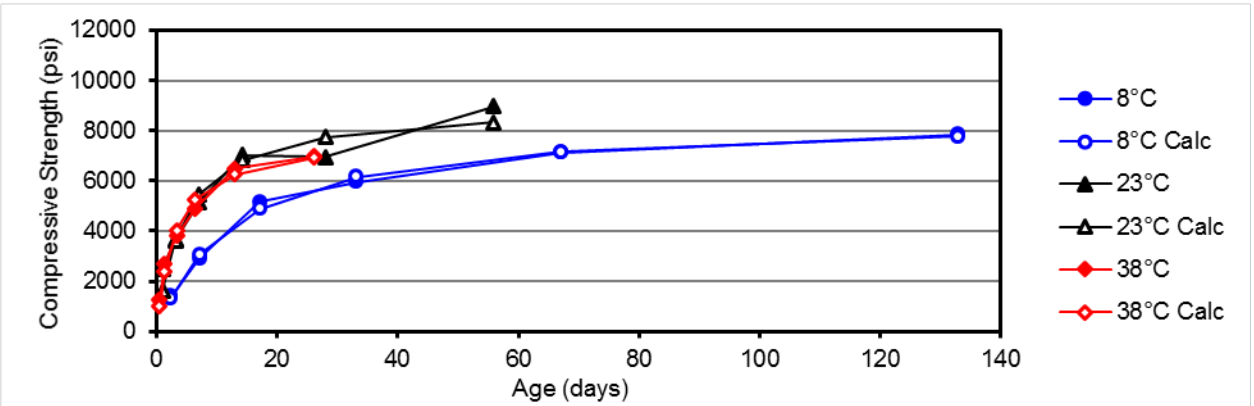

Figure C-82. Strength data for mortar containing 20% C ash and 10% F ash.

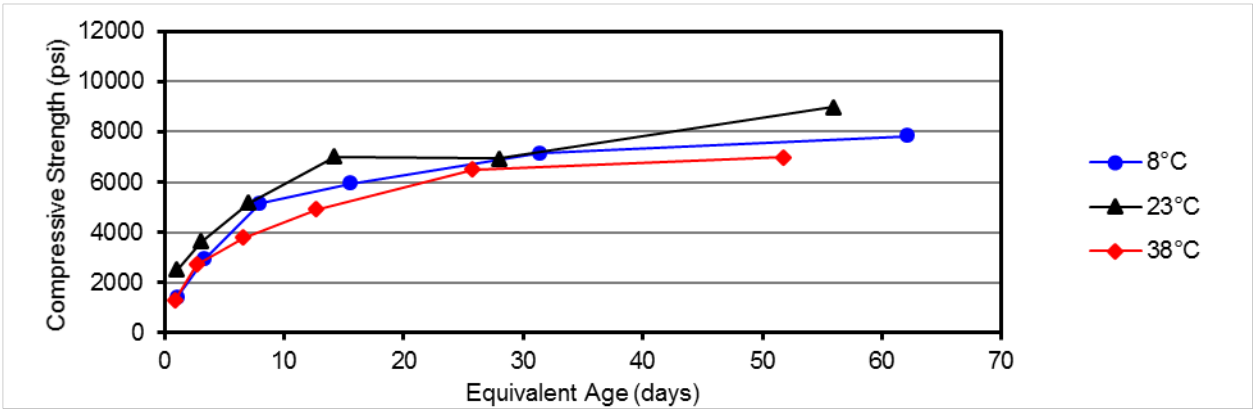

Figure C-83. Equivalent age data for mortar containing 20% C ash and 10% F ash.

Table C-32. Strength-age data for mortars containing 20% C ash and 10% CS200 glass.

Temp, °C	Age, days	Strength, psi	Su, psi	k	t_o, days	E_a, J/mol	Equiv. Age, days
8	2.19	1196	6182	0.159	0.855		1.40
	7.06	2728					4.52
	17.0	4396					10.9
	33.2	5755					21.3
	67.1	6105					42.9
	133	5091					85.4
23	1.00	2020	9792	0.195	0.000	13,500	1.00
	3.16	4433					3.16
	7.15	5278					7.15
	14.1	6365					14.1
	28.0	8300					28.0
	57.1	9515					57.1
38	0.44	1602	10240	0.279	0.000		0.66
	1.39	3320					2.08
	3.20	4957					4.78
	6.33	5773					9.47
	13.1	7705					19.5
	26.2	9597					39.2

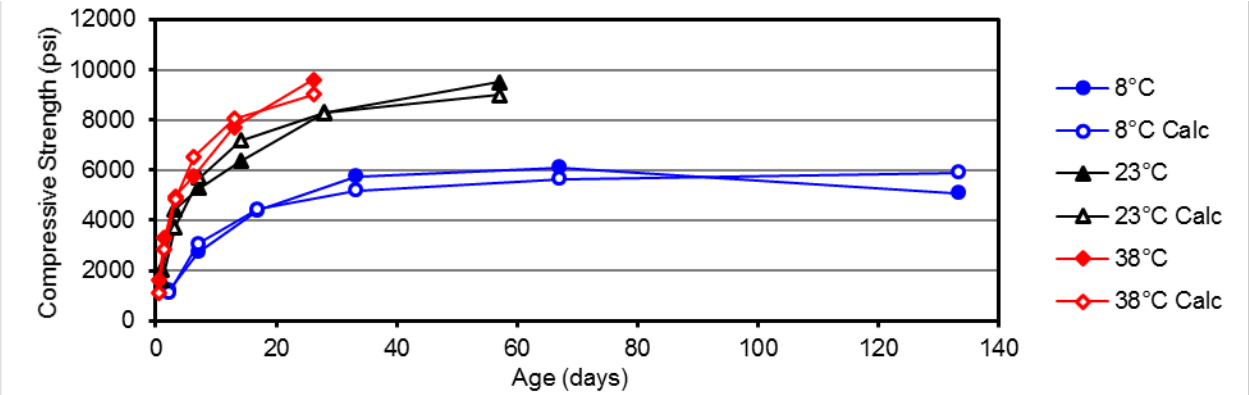

Figure C-84. Strength data for mortar containing 20% C ash and 10% CS200 glass.

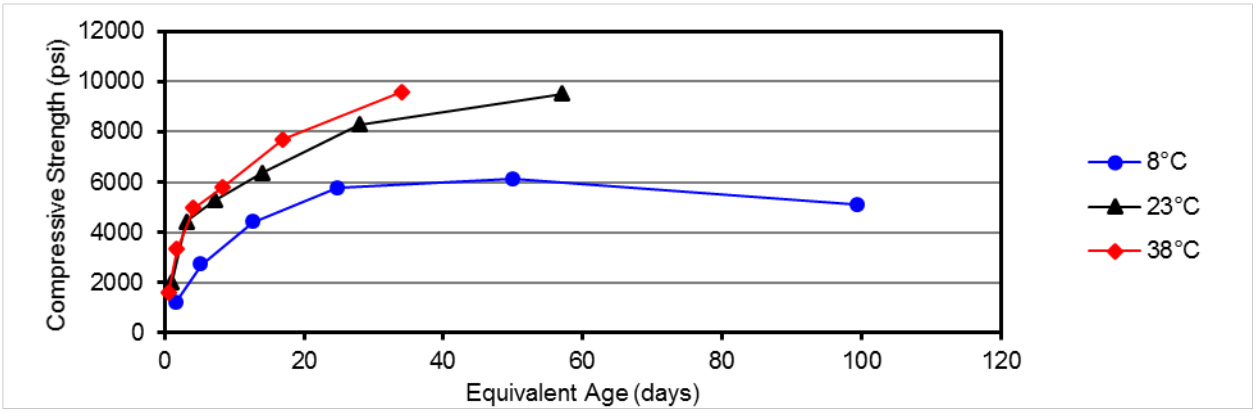

Figure C-85. Equivalent age data for mortar containing 20% C ash and 10% CS200 glass.

Table C-33. Strength-age data for mortars containing 20% C ash and 5% SCBA.

Temp, °C	Age, days	Strength, psi	Su, psi	k	t_o, days	E_a, J/mol	Equiv. Age, days
8	2.33	1255	8672	0.068	0.000		0.85
	7.19	3334					2.62
	17.0	4796					6.20
	33.1	5324					12.1
	67.0	6633					24.4
	76.1	8562					48.5
23	0.97	1727	8843	0.205	0.000	46,500	0.97
	3.03	4196					3.03
	7.01	4655					7.01
	14.0	5879					14.0
	28.1	Removed, 6303					28.1
	56.3	8692					56.3
38	0.47	1572	7557	0.463	0.000		1.16
	1.36	3500					3.38
	3.26	4026					8.13
	6.38	5175					15.9
	13.0	6707					32.5
	26.1	7196					64.9

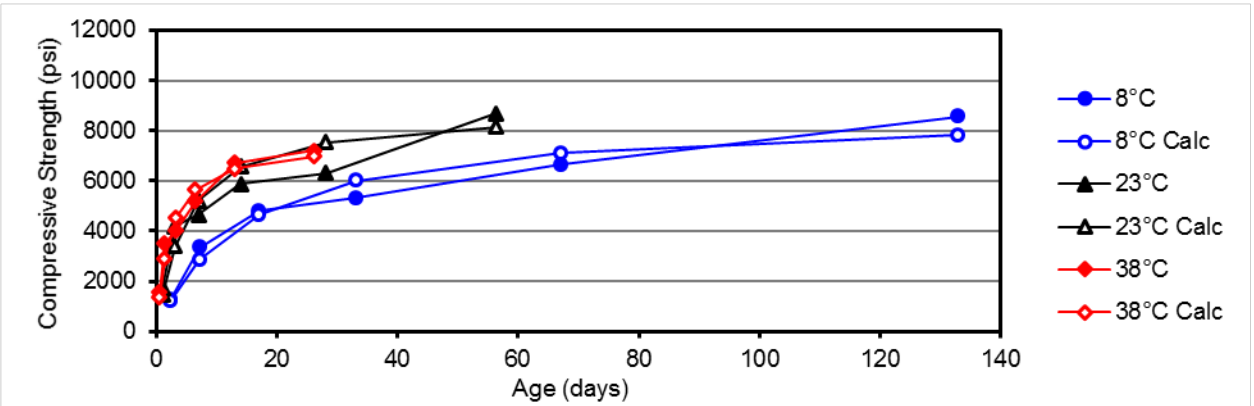

Figure C-86. Strength data for mortar containing 20% C ash and 5% SCBA.

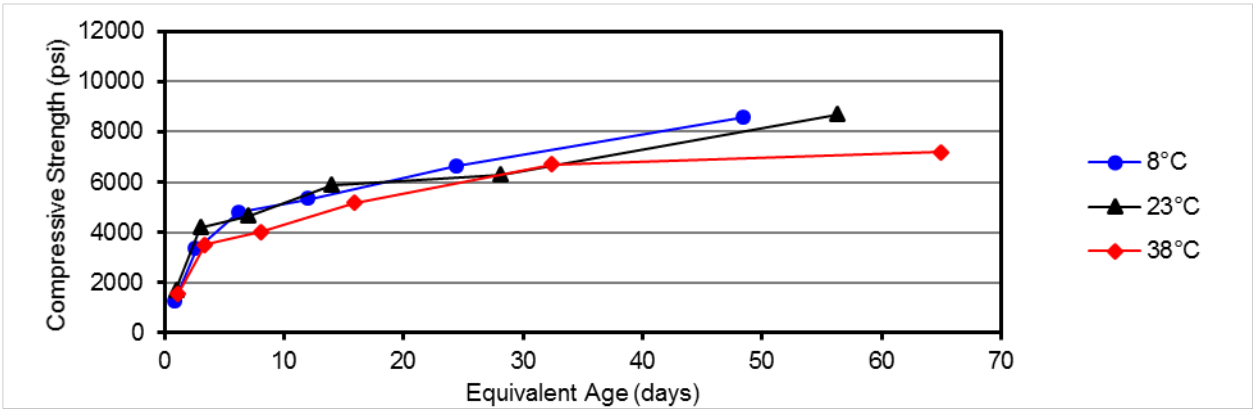

Figure C-87. Equivalent age data for mortar containing 20% C ash and 5% SCBA.

Table C-34. Strength-age data for mortars containing 20% C ash and 10% SCBA.

Temp, °C	Age, days	Strength, psi	Su, psi	k	t_o, days	E_a, J/mol	Equiv. Age, days
8	2.32	1435	7757	0.081	0.000		0.87
	7.11	2979					2.67
	16.9	4430					6.34
	33.3	5822					12.5
	66.9	5698					25.1
	133.0	7737					50.0
23	1.02	1880	9773	0.244	0.000	45,100	1.02
	3.07	4289					3.07
	7.14	6329					7.14
	14.1	Removed, 6080					14.1
	28.3	7790					28.3
	56.0	9684					56.0
38	0.46	1545	8196	0.523	0.086		1.11
	1.36	2819					3.29
	3.35	5119					8.13
	6.40	6710					15.5
	13.1	7686					31.8
	26.1	6931					63.2

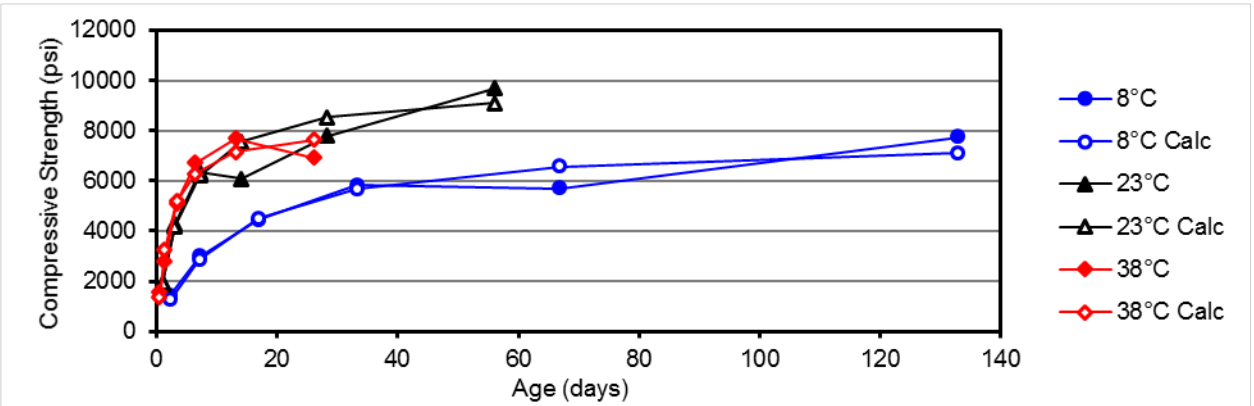

Figure C-88. Strength data for mortar containing 20% C ash and 10% SCBA.

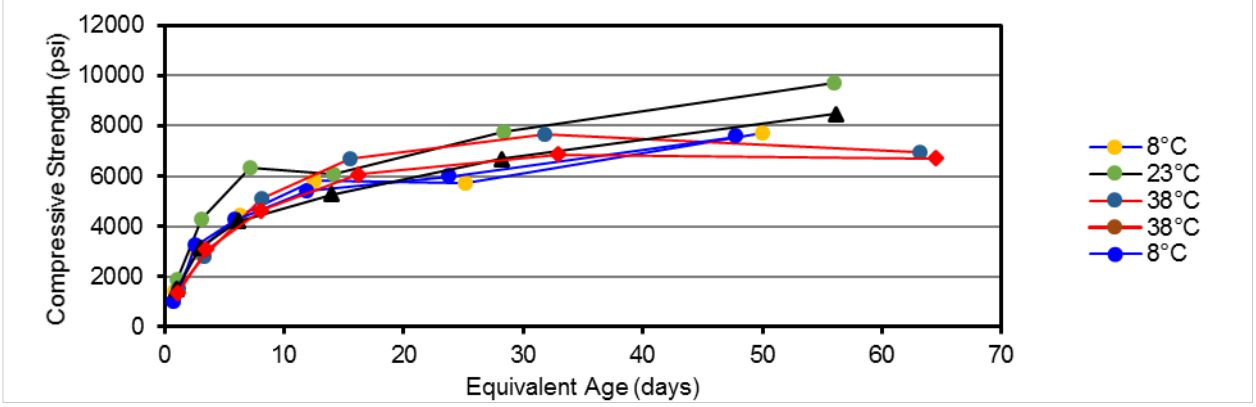

Figure C-89. Equivalent age data for mortar containing 20% C ash and 10% SCBA.

Table C-35. Strength-age data for mortars containing 20% C ash and 5% Micron[3].

Temp, °C	Age, days	Strength, psi	Su, psi	k	t_o, days	E_a, J/mol	Equiv. Age, days
8	2.33	1227	10220	0.063	0.000		0.68
	7.21	3520					2.11
	17.0	5600					4.98
	34.4	6412					10.1
	67.0	7748					19.7
	134.0	9806					39.3
23	0.99	1968	10080	0.165	0.000	56,600	0.99
	4.06	4266					4.06
	7.12	5341					7.12
	14.1	6984					14.1
	28.2	7983					28.2
	56.0	9400					56.0
38	0.48	1864	8339	0.656	0.036		1.44
	1.34	3951					4.06
	3.21	5494					9.72
	6.40	6912					19.4
	13.3	Removed, 6692					40.2
	26.1	7904					79.1

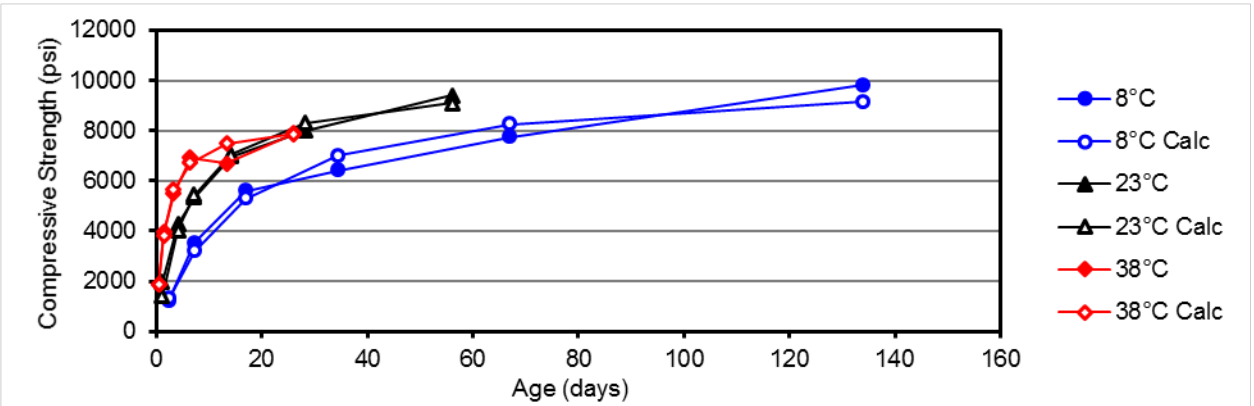

Figure C-90. Strength data for mortar containing 20% C ash and 5% Micron[3].

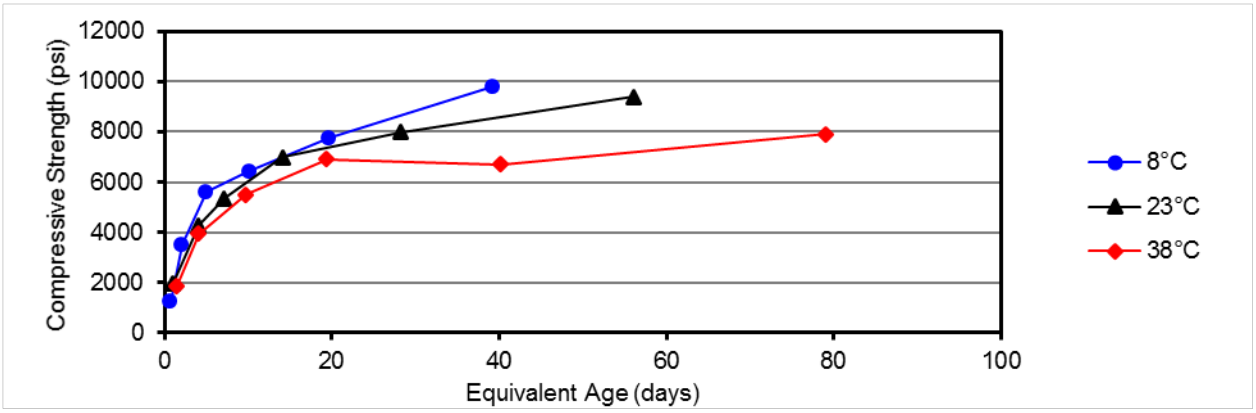

Figure C-91. Equivalent age data for mortar containing 20% C ash and 5% Micron[3].

Table C-36. Strength-age data for mortars containing 20% C ash and 10% Micron[3].

Temp, °C	Age, days	Strength, psi	Su, psi	k	t_o, days	E_a, J/mol	Equiv. Age, days
8	2.27	1223					1.60
	7.12	3812					5.02
	16.9	6522	9080	0.143	1.27		11.9
	34.2	7526					24.1
	66.9	8502					47.1
	132.8	8245					93.6
23	0.99	1852					0.99
	3.09	4781					3.09
	6.93	6471	11,200	0.210	0.000	16,200	6.93
	14.2	7940					14.2
	27.9	9922					27.9
	56.0	Removed, 8653					56.0
38	0.44	1676					0.61
	1.36	3219					1.87
	3.12	6253	12840	0.278	0.000		4.28
	6.42	8121					8.81
	13.1	9906					17.9
	26.1	11,410					35.9

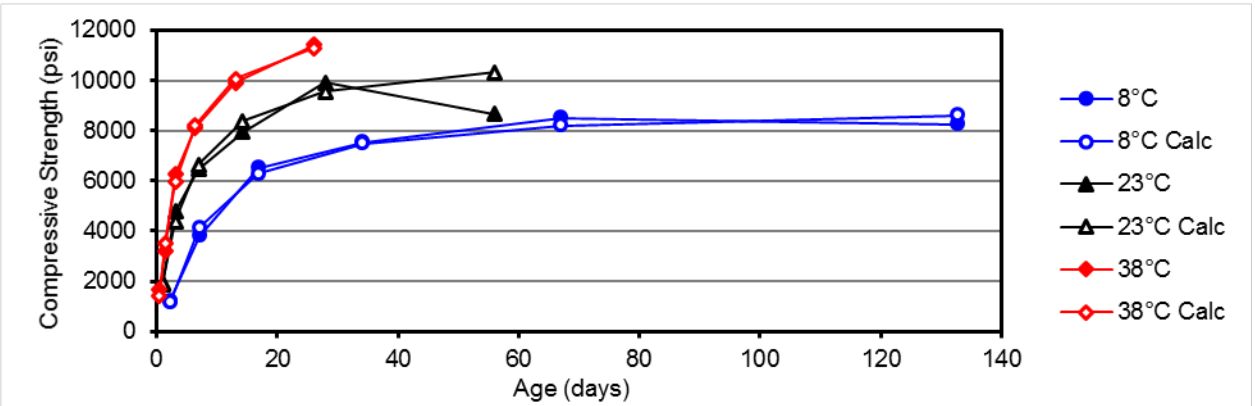

Figure C-92. Strength data for mortar containing 20% C ash and 10% Micron[3].

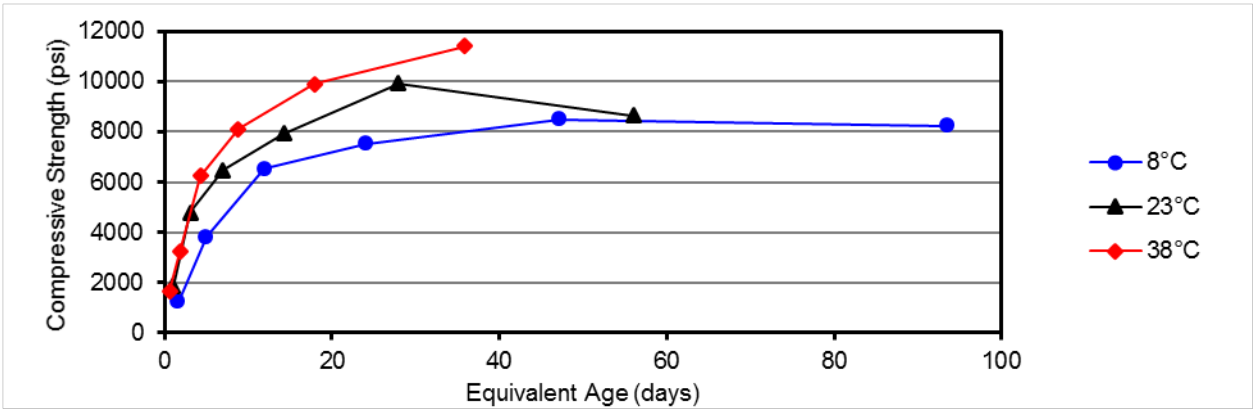

Figure C-93. Equivalent age data for mortar containing 20% C ash and 10% Micron[3].

Table C-37. Strength-age data for mortars containing 20% C ash and 4% silica fume.

Temp, °C	Age, days	Strength, psi	Su, psi	k	t_o, days	E_a, J/mol	Equiv. Age, days
8	2.41	1584					2.00
	7.19	3973					5.98
	17.2	5251					14.3
	33.2	Removed, 6811	6358	0.291	1.28		27.6
	67.3	6311					56.0
	133	5945					110
23	1.01	2138					1.01
	3.09	4954					3.09
	7.17	6713					7.17
	14.2	8613	11110	0.237	0.000	8,500	14.2
	28.2	9599					28.2
	57.3	10460					57.3
38	0.45	1915					0.53
	1.44	4099					1.70
	3.18	5946					3.76
	6.43	7648	10640	0.419	0.000		7.59
	13.3	9145					15.7
	2.41	1584					2.00

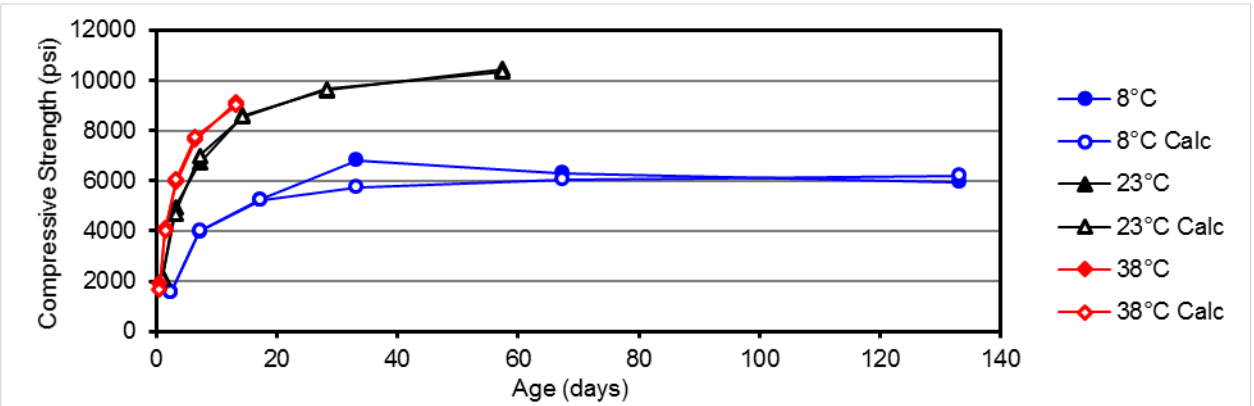

Figure C-94. Strength data for mortar containing 20% C ash and 4% silica fume.

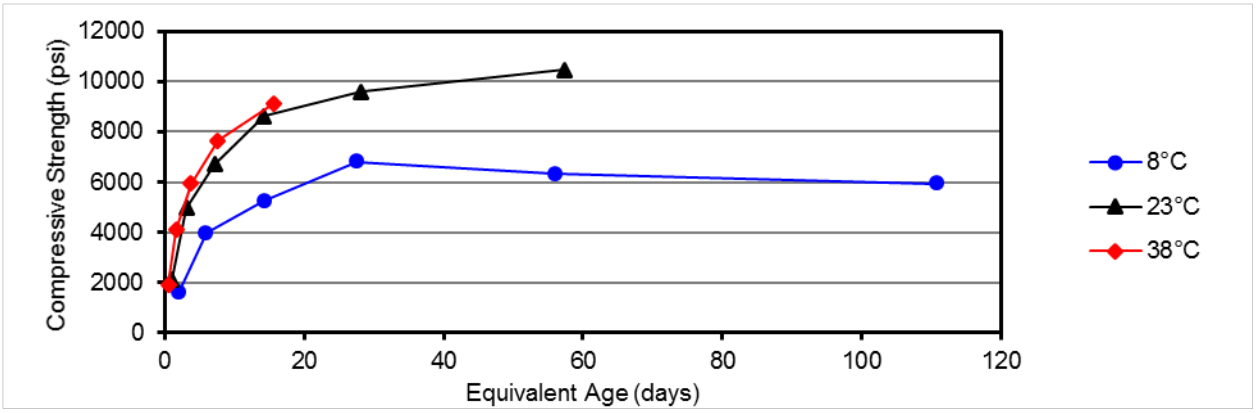

Figure C-95. Equivalent age data for mortar containing 20% C ash and 4% silica fume.

Table C-38. Strength-age data for mortars containing 20% C ash and 5% metakaolin.

Temp, °C	Age, days	Strength, psi	Su, psi	k	t_o, days	E_a, J/mol	Equiv. Age, days
8	2.35	1064	8271	0.188	1.628		1.25
	7.17	3915					3.80
	16.9	6248					8.94
	32.9	7425					17.5
	67.3	7992					35.7
	130.0	7307					69.0
23	1.01	1769	9400	0.339	0.395	29,200	1.01
	3.03	3997					3.03
	7.00	6533					7.00
	14.0	8728					14.0
	27.9	7893					27.9
	56.2	8849					56.2
38	0.45	1477	9624	0.630	0.163		0.80
	1.36	4163					2.42
	3.09	6225					5.48
	6.12	7552					10.9
	13.0	8739					23.0
	24.9	8947					44.2

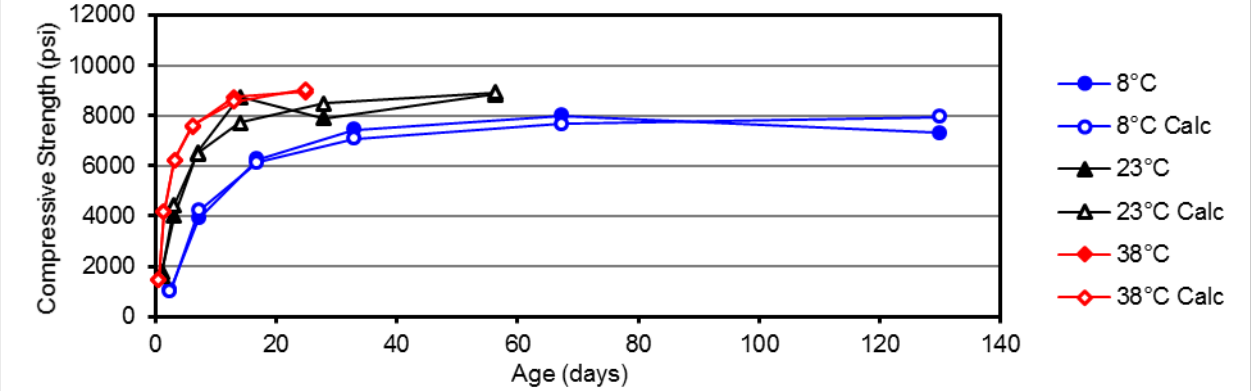

Figure C-96. Strength data for mortar containing 20% C ash and 5% metakaolin.

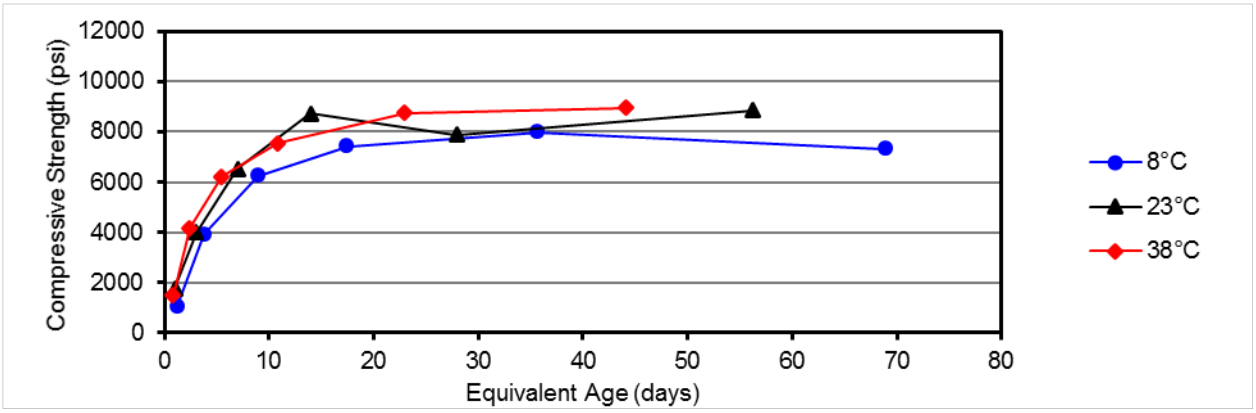

Figure C-97. Equivalent age data for mortar containing 20% C ash and 5% metakaolin.

Table C-39. Strength-age data for mortars containing 20% C ash and 10% ground glass.

Temp, °C	Age, days	Strength, psi	Su, psi	k	t_o, days	E_a, J/mol	Equiv. Age, days
8	2.38	984	8461	0.114	1.048		1.25
	7.02	3814					3.69
	17.0	5251					8.96
	33.1	6410					17.4
	67.0	7489					35.3
	131.4	8104					69.2
23	0.99	1654	8953	0.200	0.000	29,600	0.99
	3.01	3625					3.01
	7.10	5017					7.10
	14.1	6579					14.1
	28.0	7174					28.0
	55.9	8665					55.9
38	0.48	1617	9252	0.388	0.000		0.85
	1.35	3097					2.41
	3.22	4915					5.75
	6.37	6825					11.4
	13.2	7836					23.5
	26.0	8271					46.4

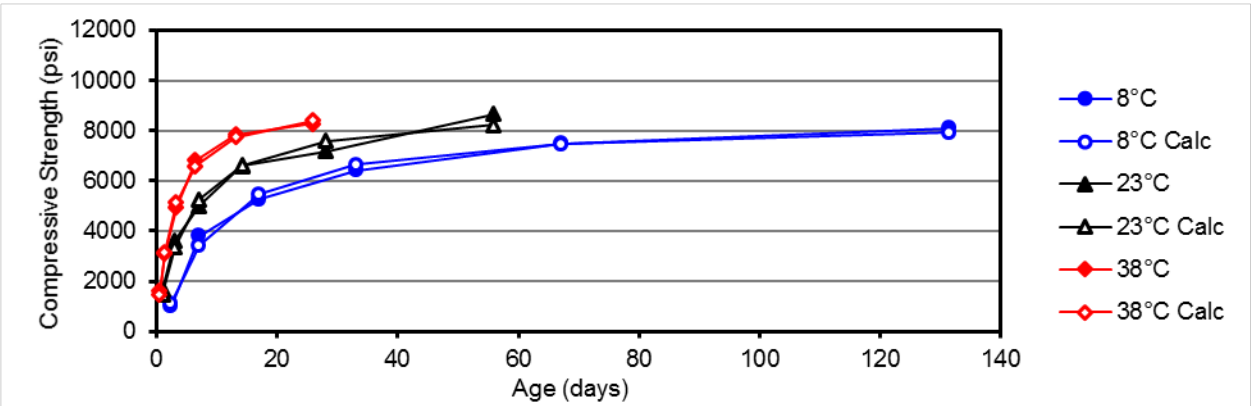

Figure C-98. Strength data for mortar containing 20% C ash and 10% ground glass.

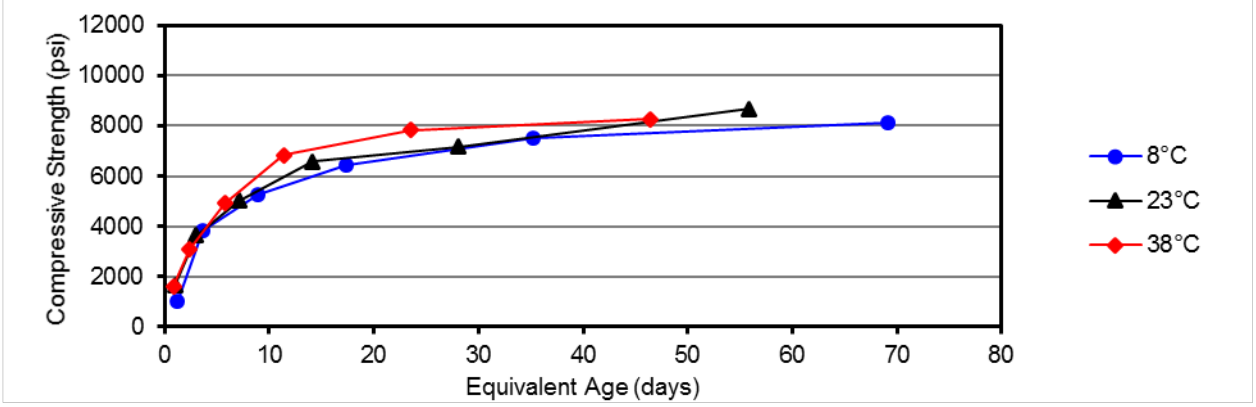

Figure C-99. Equivalent age data for mortar containing 20% C ash and 10% ground glass.

Table C-40. Strength-age data for mortars containing 30% C ash and 5% metakaolin.

Temp, °C	Age, days	Strength, psi	Su, psi	k	t_o, days	E_a, J/mol	Equiv. Age, days
8	2.38	760	8769	0.089	1.074		0.80
	7.12	2918					2.41
	17.0	5118					5.75
	34.3	6025					11.6
	70.1	7239					23.7
	135.3	8285					45.7
23	1.01	1276	8041	0.491	0.626	50,000	1.01
	3.02	4292					3.02
	7.11	6211					7.11
	14.0	6751					14.0
	28.0	7991					28.0
	56.2	7468					56.2
38	0.46	1420	9274	0.690	0.199		1.22
	1.36	4027					3.62
	3.10	6414					8.26
	6.40	7006					17.1
	13.1	9109					35.0
	25.4	8400					67.7

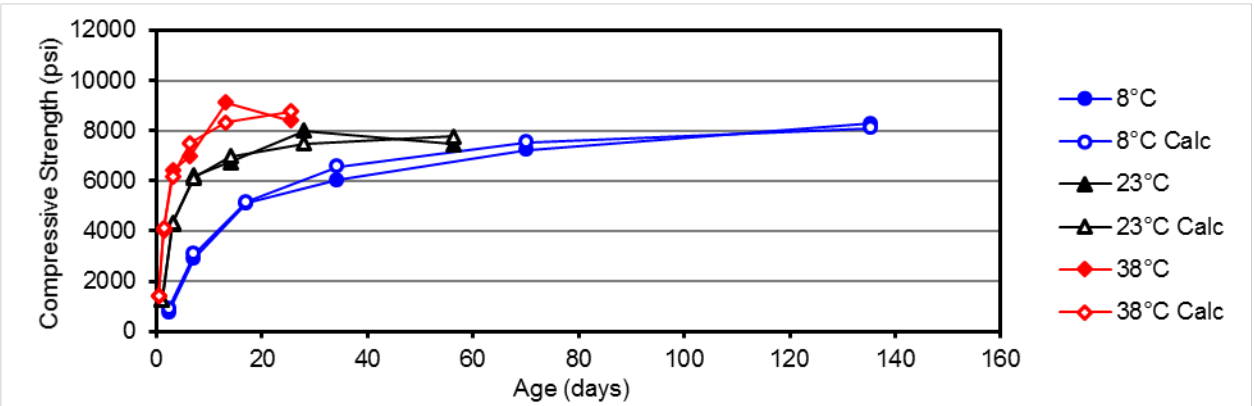

Figure C-100. Strength data for mortar containing 30% C ash and 5% metakaolin.

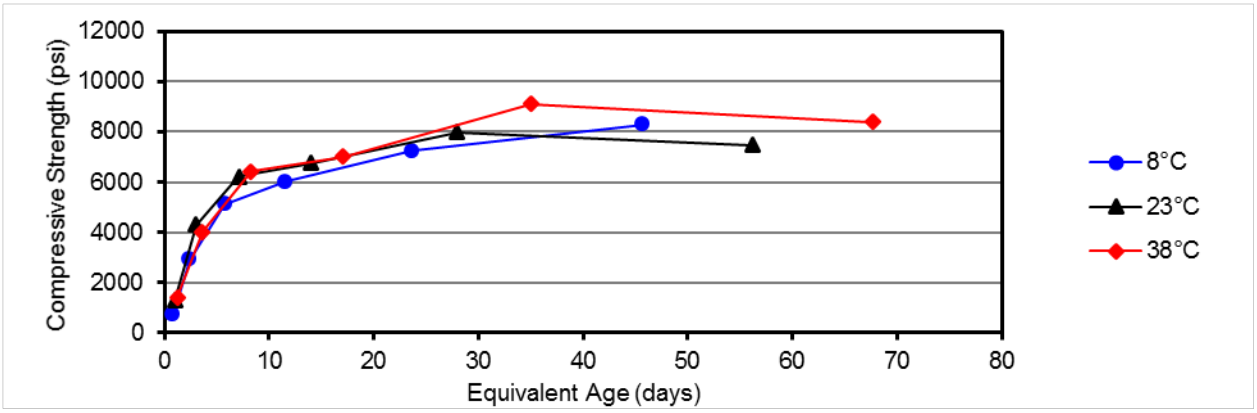

Figure C-101. Equivalent age data for mortar containing 30% C ash and 5% metakaolin.

Table C-41. Strength-age data for mortars containing 30% C ash and 10% metakaolin.

Temp, °C	Age, days	Strength, psi	Su, psi	k	t_o, days	E_a, J/mol	Equiv. Age, days
8	2.39	716	8520	0.070	0.938	57,400	0.69
	7.08	2685					2.04
	17.0	4564					4.89
	33.1	5664					9.52
	67.2	7050					19.32
	134.0	7751					38.55
23	0.99	1150	8961	0.253	0.426		0.99
	3.01	3580					3.01
	7.01	5197					7.01
	14.2	7424					14.16
	29.2	8098					29.18
	55.9	8016					55.89
38	0.44	1049	7783	0.748	0.261		1.36
	1.52	3321					4.68
	3.20	5448					9.85
	6.42	7094					19.80
	13.2	7065					40.71
	25.1	6923					77.18

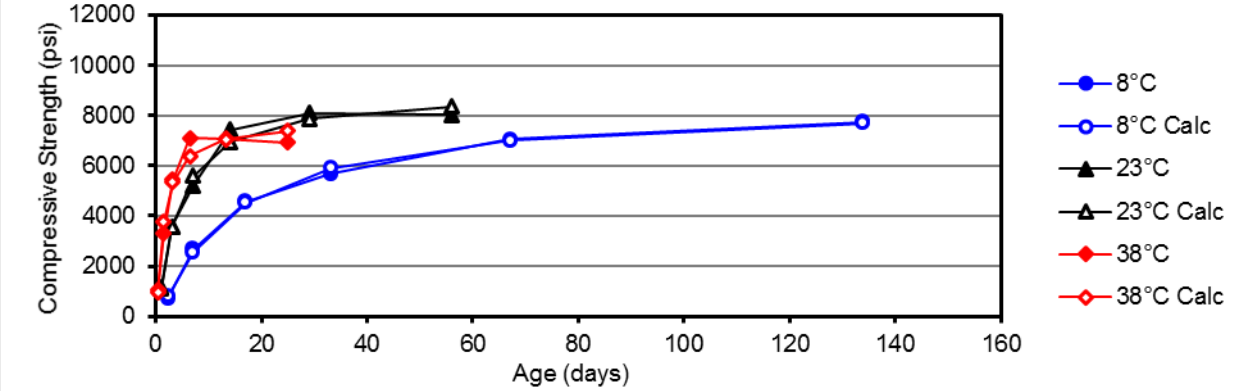

Figure C-102. Strength data for mortar containing 30% C ash and 10% metakaolin.

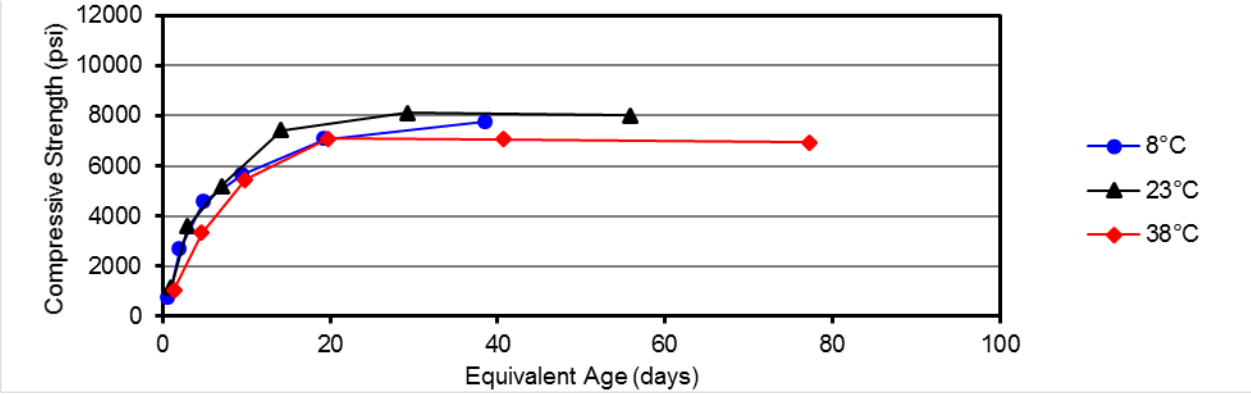

Figure C-103. Equivalent age data for mortar containing 30% C ash and 10% metakaolin.

Table C-42. Strength-age data for mortars containing 30% C ash and 10% slag.

Temp, °C	Age, days	Strength, psi	Su, psi	k	t_o, days	E_a, J/mol	Equiv. Age, days
8	2.37	1049	7326	0.061	0.000		0.91
	7.04	2411					2.71
	17.4	3624					6.71
	33.4	4824					12.9
	67.0	5850					25.8
	133.2	6639					51.2
23	0.99	1488	7994	0.130	0.000	44,000	0.99
	3.10	2516					3.10
	7.10	4001					7.10
	14.2	4522					14.2
	28.1	6056					28.1
	56.0	7490					56.0
38	0.45	1369	9072	0.379	0.000		1.06
	1.38	2885					3.27
	3.14	4358					7.44
	6.33	5936					15.0
	13.2	7596					31.3
	26.2	8011					62.0

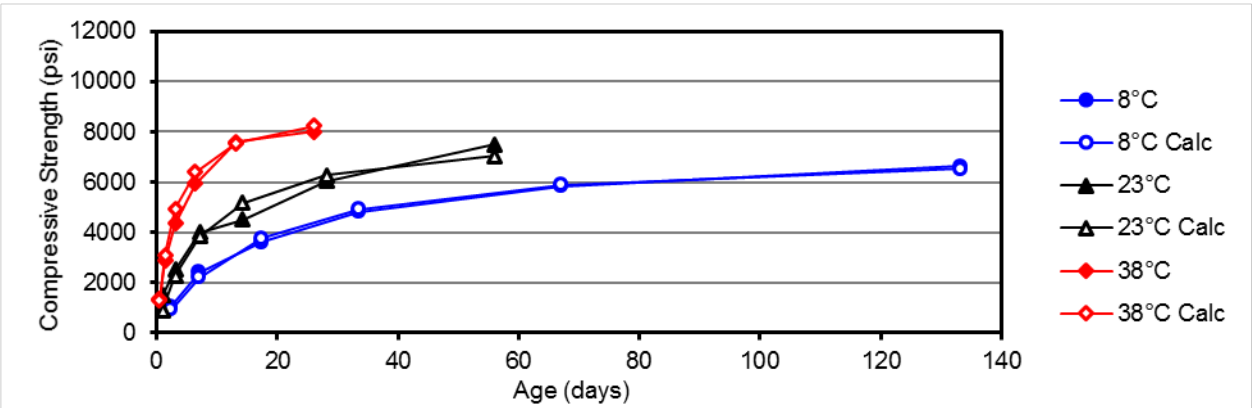

Figure C-104. Strength data for mortar containing 30% C ash and 10% slag.

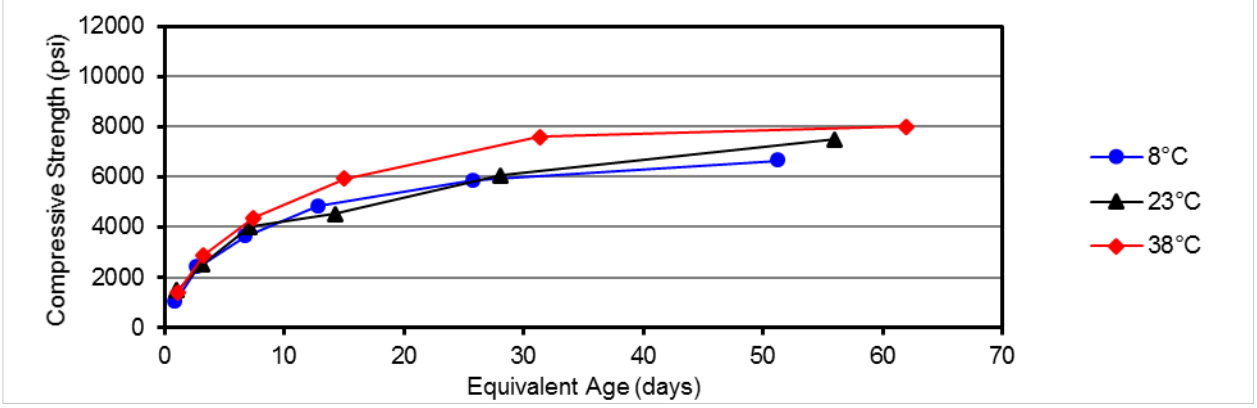

Figure C-105. Equivalent age data for mortar containing 30% C ash and 10% slag.

Table C-43. Strength-age data for mortars containing 30% C ash and 5% F ash.

Temp, °C	Age, days	Strength, psi	Su, psi	k	t_o, days	E_a, J/mol	Equiv. Age, days
8	2.42	792					1.27
	7.17	2790					3.76
	17.	4528	7938	0.089	1.166		8.95
	33.2	6027					17.4
	67.3	6719					35.4
	133.3	5531					70.0
23	1.02	1156					1.02
	3.03	3683					3.03
	7.11	5726	9408	0.220	0.330	29,700	7.11
	14.0	6471					14.0
	28.0	8519					28.0
	55.1	8614					55.1
38	0.46	1187					0.82
	1.37	3366					2.45
	3.20	5376	10920	0.300	0.012		5.73
	6.15	6705					11.0
	13.3	9063					23.7
	25.1	9544					45.0

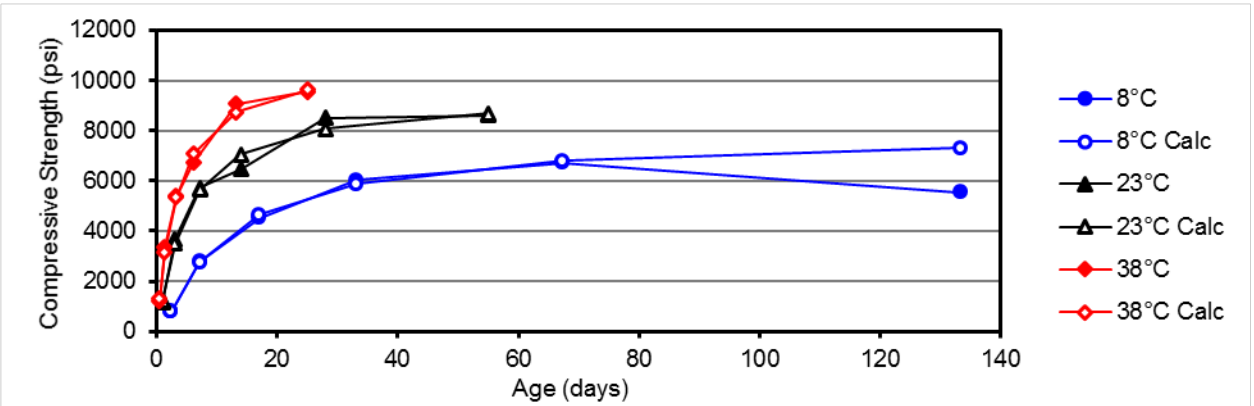

Figure C-106. Strength data for mortar containing 30% C ash and 5% F ash.

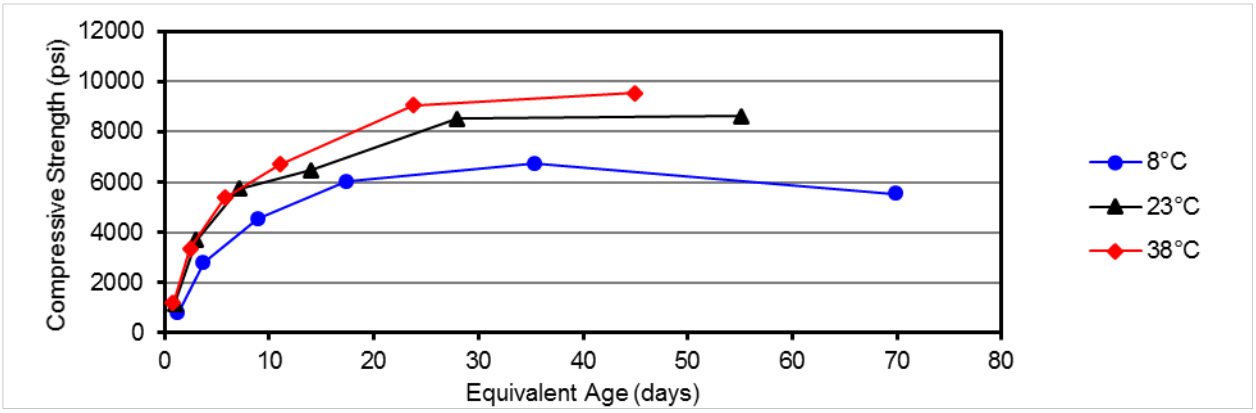

Figure C-107. Equivalent age data for mortar containing 30% C ash and 5% F ash.

Table C-44. Strength-age data for mortars containing 30% C ash and 10% F ash.

Temp, °C	Age, days	Strength, psi	Su, psi	k	t_o, days	E_a, J/mol	Equiv. Age, days
8	1.87	896	6421	0.065	0.000		0.70
	7.05	2009					2.64
	16.8	3280					6.29
	33.0	4452					12.3
	66.8	5312					25.0
	133.9	5685					50.1
23	0.99	1438	8746	0.193	0.000	45,300	0.99
	3.00	3414					3.00
	7.13	4903					7.13
	14.0	6751					14.0
	28.1	7172					28.1
	56.1	8230					56.1
38	0.45	1220	8136	0.424	0.051		1.09
	1.39	2899					3.38
	3.19	4411					7.74
	5.93	6024					14.4
	13.0	7173					31.5
	26.0	7154					53.9

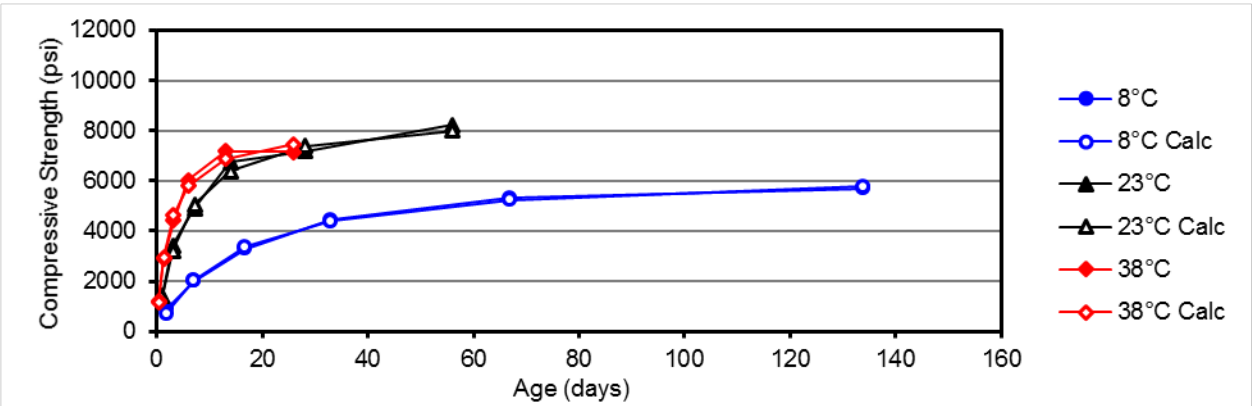

Figure C-108. Strength data for mortar containing 30% C ash and 10% F ash.

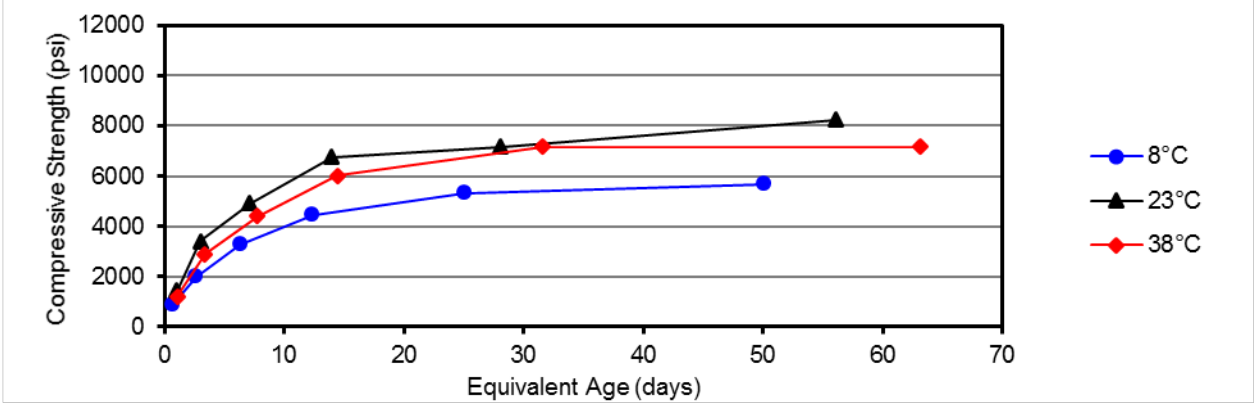

Figure C-109. Equivalent age data for mortar containing 30% C ash and 10% F ash.

Table C-45. Strength-age data for mortars containing 30% C ash and 10% SCBA.

Temp, °C	Age, days	Strength, psi	Su, psi	k	t_o, days	E_a, J/mol	Equiv. Age, days
8	2.40	1537	4873	0.107	0.000		1.37
	7.17	2161					4.09
	17.0	3116					9.67
	33.1	3845					18.9
	66.9	4035					38.2
	131.9	4728					75.3
23	1.00	1548	8694	0.188	0.000	25,900	1.00
	3.03	3540					3.03
	7.19	5118					7.19
	13.9	5669					13.9
	27.9	6639					27.9
	55.9	8904					55.9
38	0.45	1278	9170	0.311	0.000		0.74
	1.36	2772					2.26
	3.21	4408					5.33
	6.38	6278					10.6
	13.1	7154					21.7
	26.1	8276					43.3

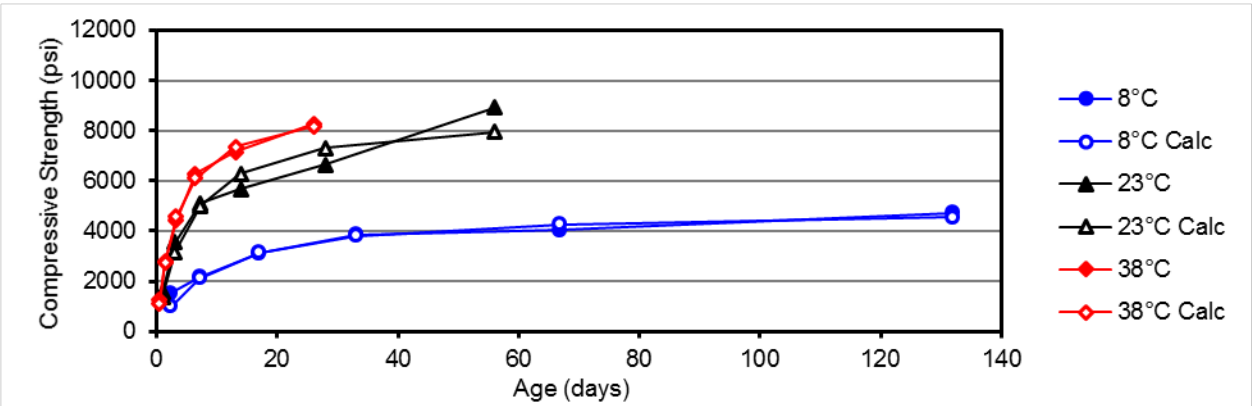

Figure C-110. Strength data for mortar containing 30% C ash and 10% SCBA.

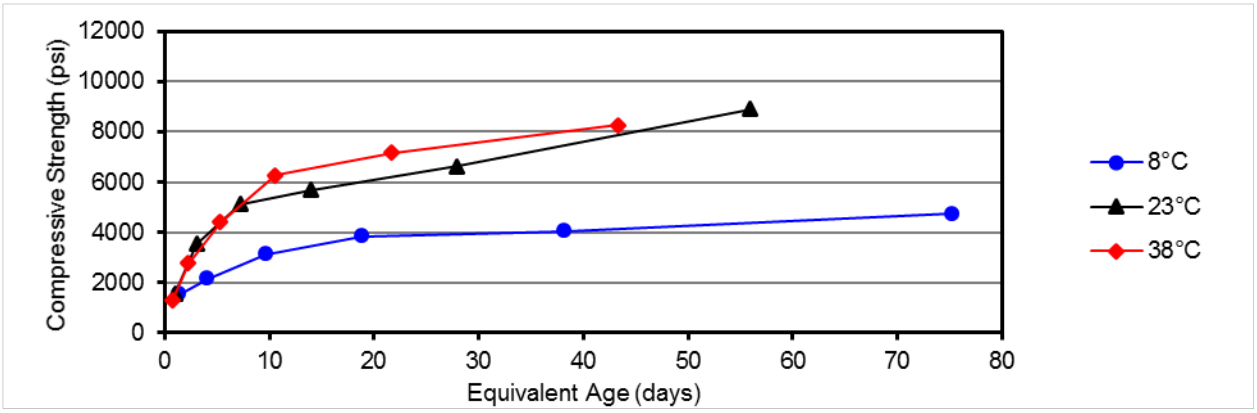

Figure C-111. Equivalent age data for mortar containing 30% C ash and 10% SCBA.

Table C-46. Strength-age data for mortars containing 30% C ash and 4% silica fume.

Temp, °C	Age, days	Strength, psi	Su, psi	k	t_o, days	E_a, J/mol	Equiv. Age, days
8	2.39	768	6798	0.126	1.493		1.27
	7.14	2597					3.81
	16.3	4417					8.70
	33.0	5751					17.6
	67.1	6195					35.8
	133.0	6092					71.0
23	0.99	1198	8068	0.412	0.572	29,000	0.99
	3.11	4137					3.11
	7.10	5374					7.10
	14.0	7531					14.0
	28.0	7790					28.0
	56.2	7112					56.2
38	0.45	1271	11040	0.408	0.155		0.79
	1.38	3648					2.44
	3.19	5525					5.62
	6.15	8348					10.9
	13.0	9935					23.0
	25.1	9363					44.4

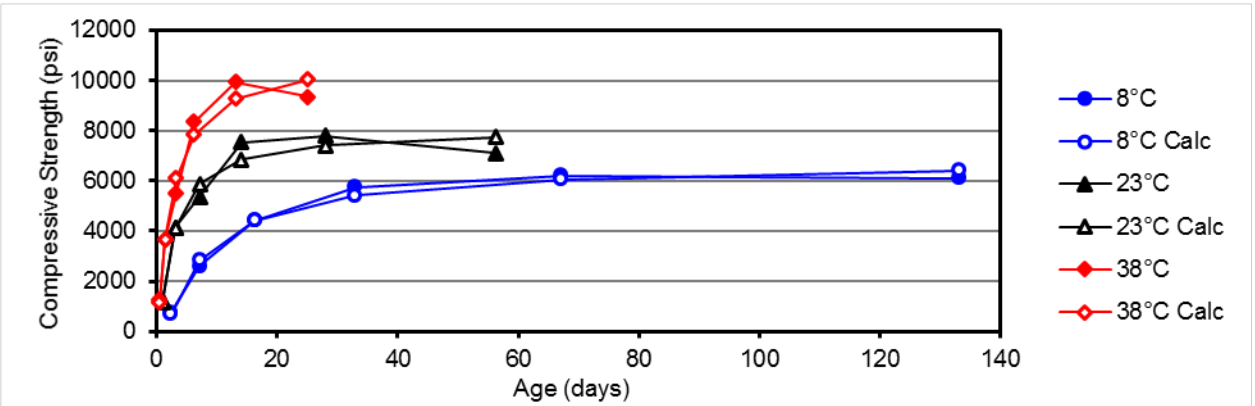

Figure C-112. Strength data for mortar containing 30% C ash and 4% silica fume.

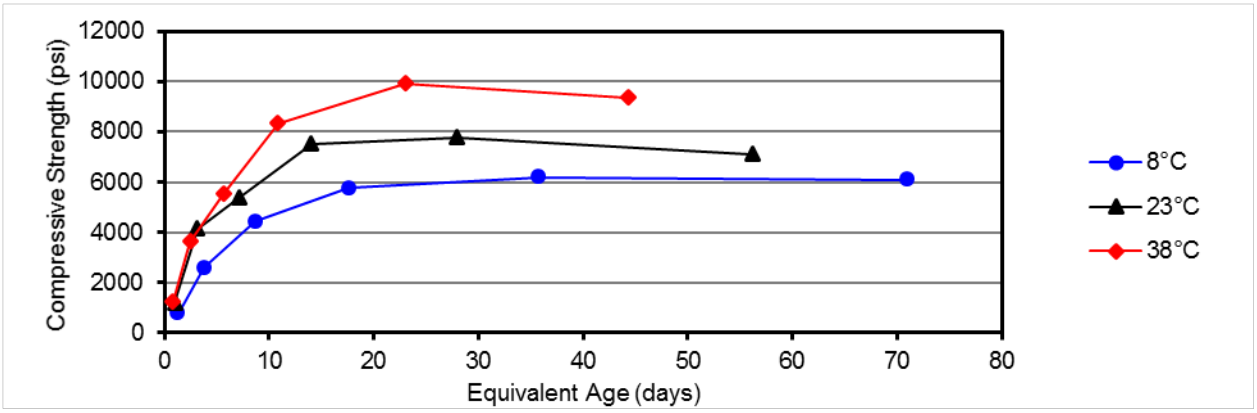

Figure C-113. Equivalent age data for mortar containing 30% C ash and 4% silica fume.

Table C-47. Strength-age data for mortars containing 30% C ash and 8% silica fume.

Temp, °C	Age, days	Strength, psi	Su, psi	k	t_o, days	E_a, J/mol	Equiv. Age, days
8	2.39	1026	6226	0.106	0.598		1.41
	7.16	2459					4.23
	17.2	4021					10.2
	33.1	5034					19.6
	67.0	5066					39.6
	133.2	5964					78.7
23	1.03	1643	8635	0.177	0.000	24,200	1.03
	3.03	3472					3.03
	6.94	4731					6.94
	13.6	5247					13.6
	28.0	Removed, 6418					28.0
	55.9	8318					55.9
38	0.46	1559	10410	0.289	0.000		0.74
	1.32	3092					2.13
	3.27	4864					5.25
	6.06	6462					9.75
	13.3	Removed, 6752					21.3
	25.3	9279					40.7

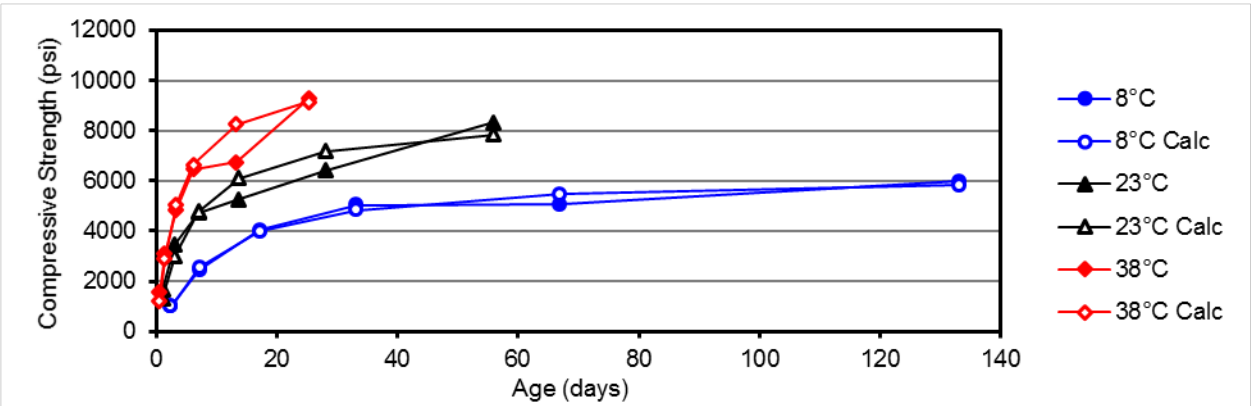

Figure C-114. Strength data for mortar containing 30% C ash and 8% silica fume.

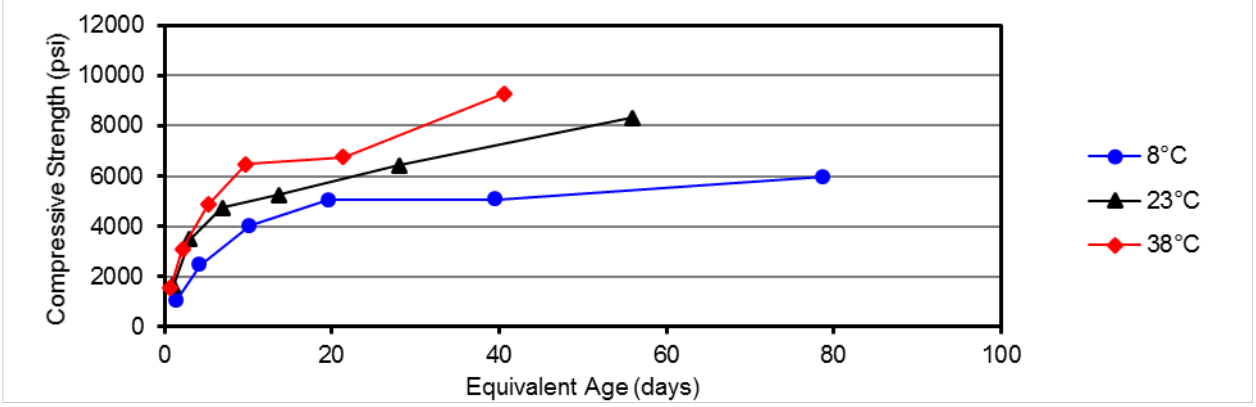

Figure C-115. Equivalent age data for mortar containing 30% C ash and 8% silica fume.

Table C-48. Strength-age data for mortars containing 30% C ash and 20% glass.

Temp, °C	Age, days	Strength, psi	Su, psi	k	t_o, days	E_a, J/mol	Equiv. Age, days
8	2.37	824					2.83
	7.00	1928					8.35
	17.1	2885					20.4
	33.4	Removed, 2450	3389	0.259	1.170		39.8
	67.0	Removed, 2878					79.9
	133.8	3226					159.6
23	1.00	1089					1.00
	3.03	2384					3.03
	7.09	3078					7.09
	14.1	3783	5627	0.193	0.000	- 8,100	14.1
	28.4	4659					28.4
	56.0	5465					56.0
38	0.45	928					0.38
	1.38	2163					1.17
	3.23	2806					2.75
	6.39	4307	8337	0.186	0.000		5.45
	13.1	6084					11.1
	26.2	6914					22.3

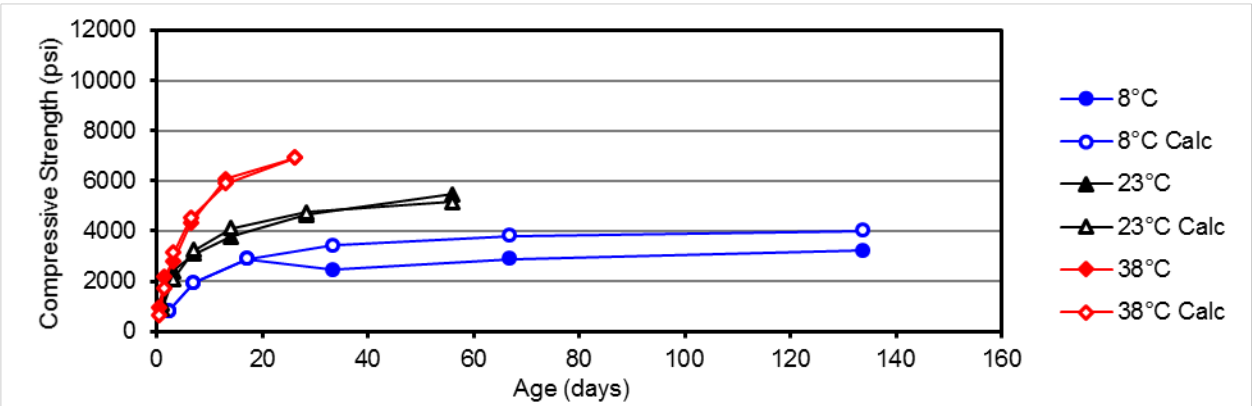

Figure C-116. Strength data for mortar containing 30% C ash and 20% glass.

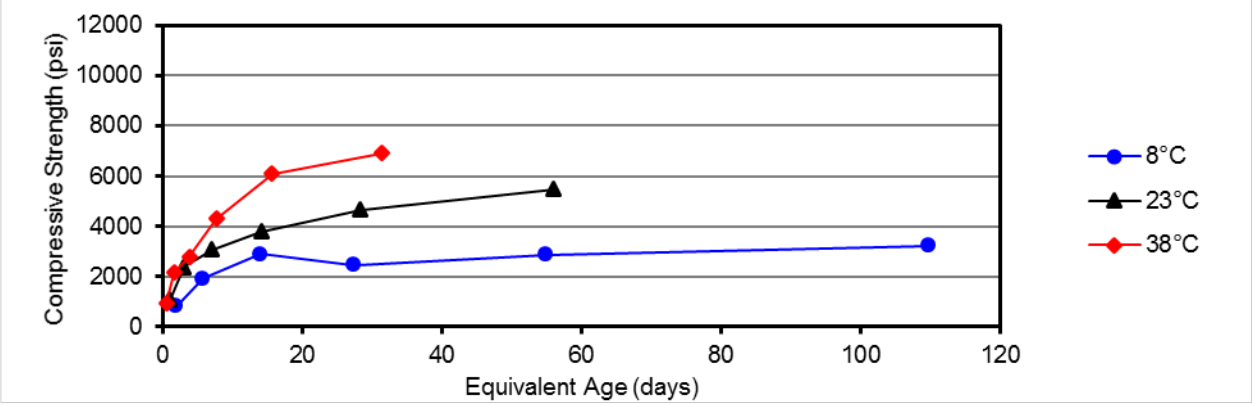

Figure C-117. Equivalent age data for mortar containing 30% C ash and 20% glass.

Table C-49. Strength-age data for mortars containing 40% C ash and 10% RHA.

Temp, °C	Age, days	Strength, psi	Su, psi	k	t_o, days	E_a, J/mol	Equiv. Age, days
8	2.39	737					1.63
	7.15	1791					4.88
	16.00	2381	3829	0.104	0.000		10.92
	32.94	2763					22.48
	66.88	3312					45.65
	134.12	3722					91.54
23	1.02	811					1.02
	3.01	2381					3.01
	6.97	2987	6508	0.121	0.000	17,600	6.97
	14.18	3361					14.18
	28.12	Removed, 4159					28.12
	55.99	6020					55.99
38	0.46	484					0.64
	1.37	2099					1.93
	3.25	2894	7239	0.218	0.000		4.59
	6.36	4208					8.98
	16.47	5020					23.25
	26.16	6697					36.94

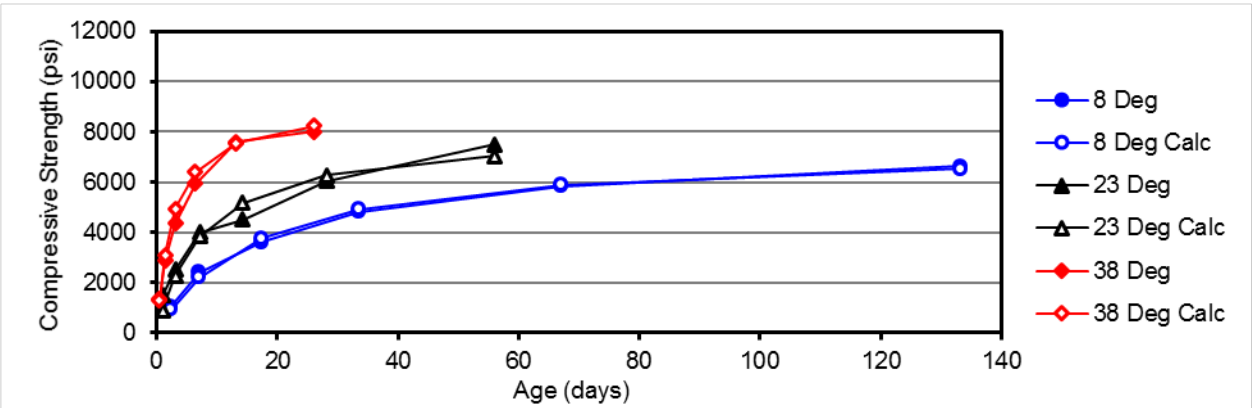

Figure C-118. Strength data for mortar containing 40% C ash and 10% RHA.

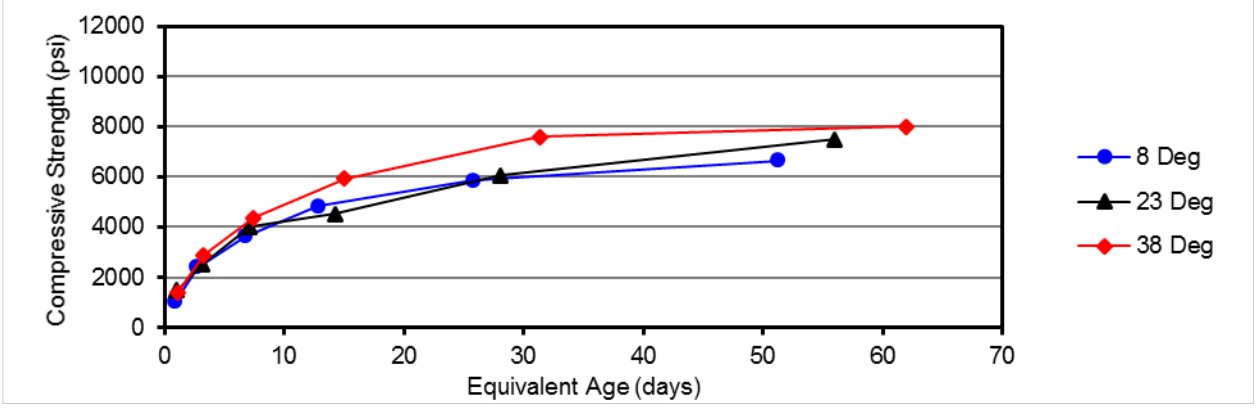

Figure C-119. Equivalent age data for mortar containing 40% C ash and 10% RHA.

Table C-50. Strength-age data for mortars containing 40% C ash and 4% silica fume.

Temp, °C	Age, days	Strength, psi	Su, psi	k	t_o, days	E_a, J/mol	Equiv. Age, days
8	2.38	379					0.95
	7.22	1690					2.88
	16.9	3202	6201	0.071	1.587		6.74
	34.1	4298					13.6
	66.9	5466					26.7
	132.3	5334					52.8
23	1.00	900					1.00
	2.99	3092					2.99
	6.98	4358	8880	0.130	0.000	42,300	6.98
	14.0	4962					14.0
	28.0	Removed, 5231					28.0
	56.1	8136					56.1
38	0.46	746					1.06
	1.37	2465					3.13
	3.12	4149	8184	0.412	0.252		7.15
	6.12	6179					14.0
	13.1	7175					30.0
	24.2	7034					55.5

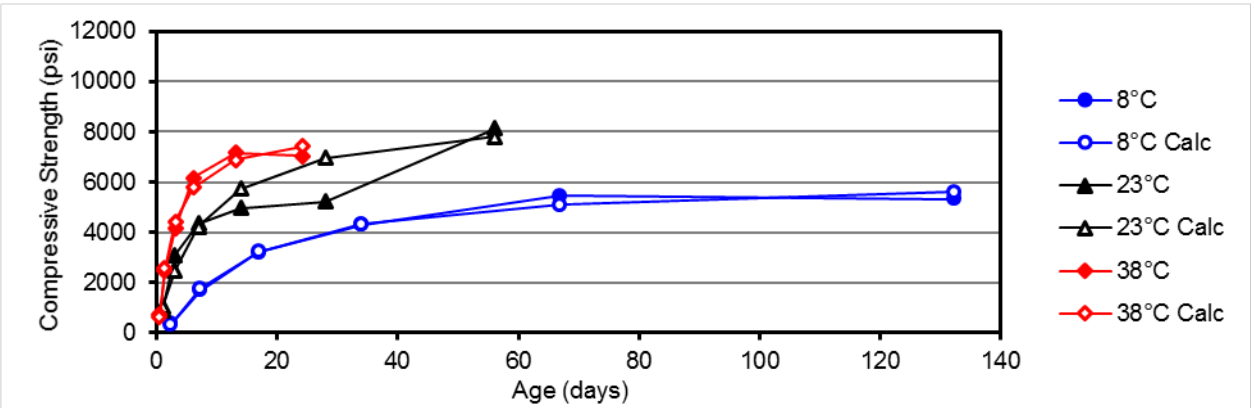

Figure C-120. Strength data for mortar containing 40% C ash and 4% silica fume.

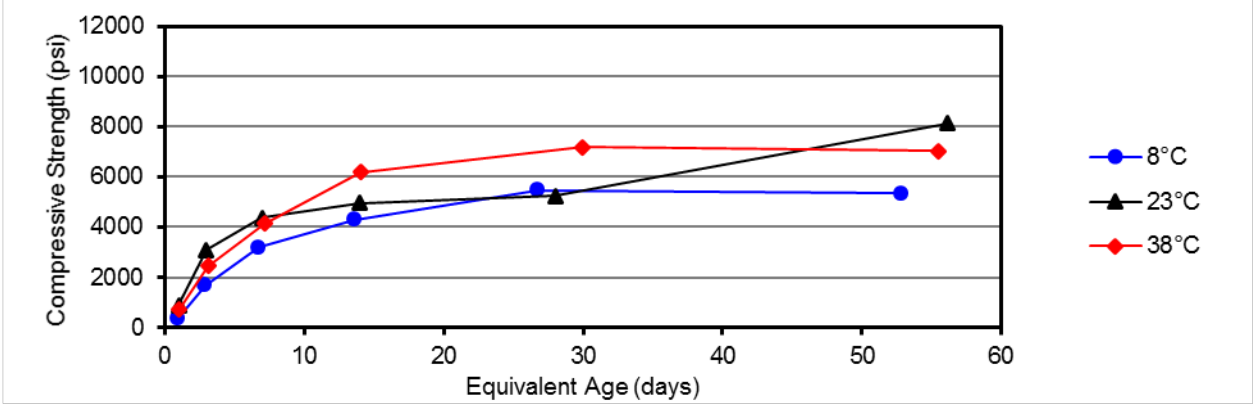

Figure C-121. Equivalent age data for mortar containing 40% C ash and 4% silica fume.

Table C-51. Strength-age data for mortars containing 40% C ash and 8% silica fume.

Temp, °C	Age, days	Strength, psi	Su, psi	k	t_o, days	E_a, J/mol	Equiv. Age, days
8	2.39	707	4574	0.083	0.027		1.31
	7.01	1769					3.83
	17.1	2607					9.35
	33.1	3403					18.1
	67.1	3720					36.7
	133.2	4301					72.9
23	1.00	1267	6451	0.137	0.000	27,800	1.00
	3.12	2415					3.12
	7.09	3109					7.09
	14.0	3680					14.0
	28.1	4723					28.1
	56.0	6329					56.0
38	0.47	1248	8523	0.261	0.000		0.81
	1.41	2466					2.43
	3.27	3648					5.64
	6.21	5330					10.7
	13.1	6494					22.5
	25.5	7510					44.0

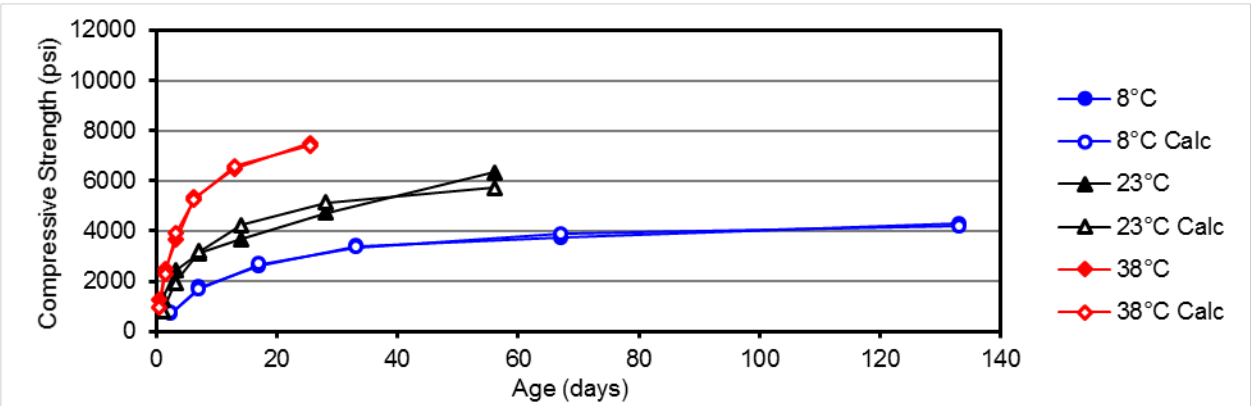

Figure C-122. Strength data for mortar containing 40% C ash and 8% silica fume.

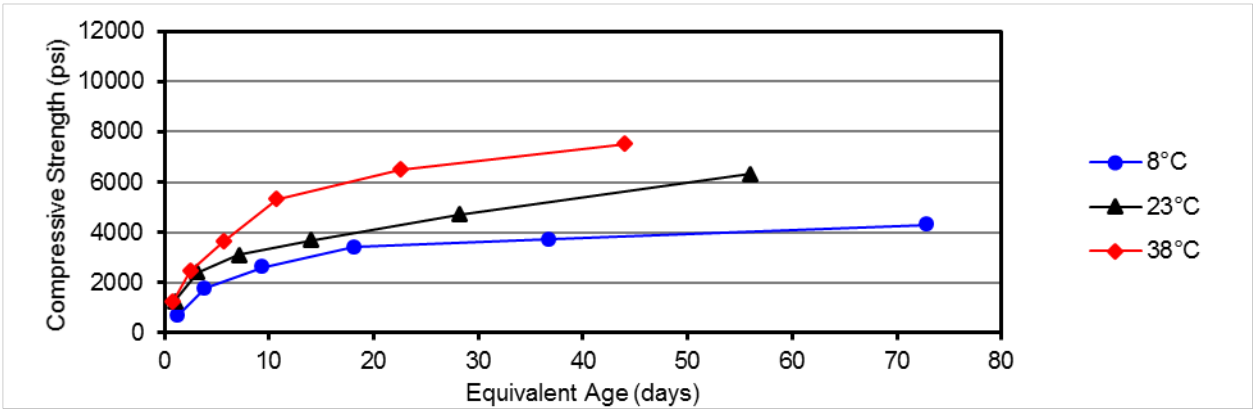

Figure C-123. Equivalent age data for mortar containing 40% C ash and 8% silica fume.

Table C-52. Strength-age data for mortars containing 40% C ash and 5% F ash.

Temp, °C	Age, days	Strength, psi	Su, psi	k	t_o, days	E_a, J/mol	Equiv. Age, days
8	2.39	431	6970	0.083	1.705		0.92
	7.05	1999					2.70
	17.0	3962					6.51
	33.0	5070					12.6
	68.0	5971					26.0
	131.0	6275					50.2
23	1.08	969	8019	0.188	0.301	44,200	1.08
	3.06	2753					3.06
	7.03	4786					7.03
	14.0	5618					14.0
	28.0	6150					28.0
	56.2	7808					56.2
38	0.43	690	7687	0.518	0.233		1.02
	1.37	2949					3.27
	3.18	4562					7.57
	5.16	5350					12.3
	13.0	7211					31.0
	25.1	6836					59.8

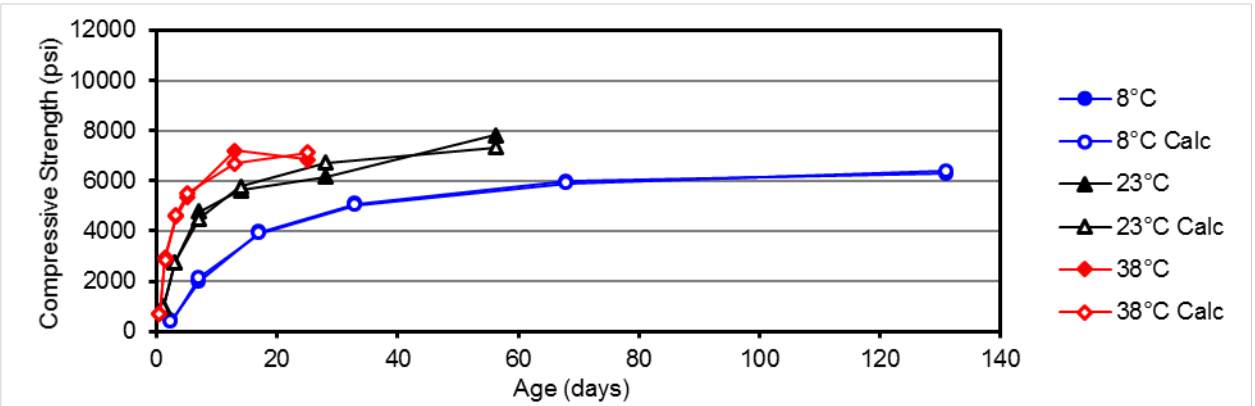

Figure C-124. Strength data for mortar containing 40% C ash and 5% F ash.

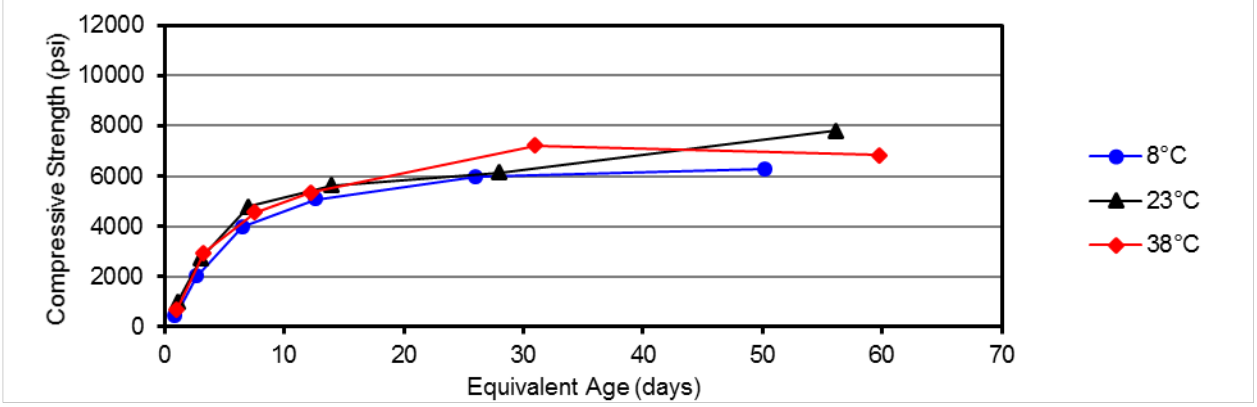

Figure C-125. Equivalent age data for mortar containing 40% C ash and 5% F ash.

Table C-53. Strength-age data for mortars containing 40% C ash and 5% metakaolin.

Temp, °C	Age, days	Strength, psi	Su, psi	k	t_o, days	E_a, J/mol	Equiv. Age, days
8	2.38	411	7885	0.068	1.528		0.74
	7.25	2194					2.27
	17.1	4200					5.34
	33.0	5310					10.3
	68.0	6153					21.3
	133.3	7327					41.7
23	1.01	751	6879	0.258	0.504	53,600	1.01
	3.10	2887					3.10
	7.11	4289					7.11
	14.00	5082					14.0
	28.0	6373					28.0
	56.0	6329					56.0
38	0.45	847	7689	0.616	0.266		1.29
	1.38	2965					3.93
	3.12	4922					8.92
	6.39	6241					18.3
	13.3	6963					38.1
	26.1	7015					74.5

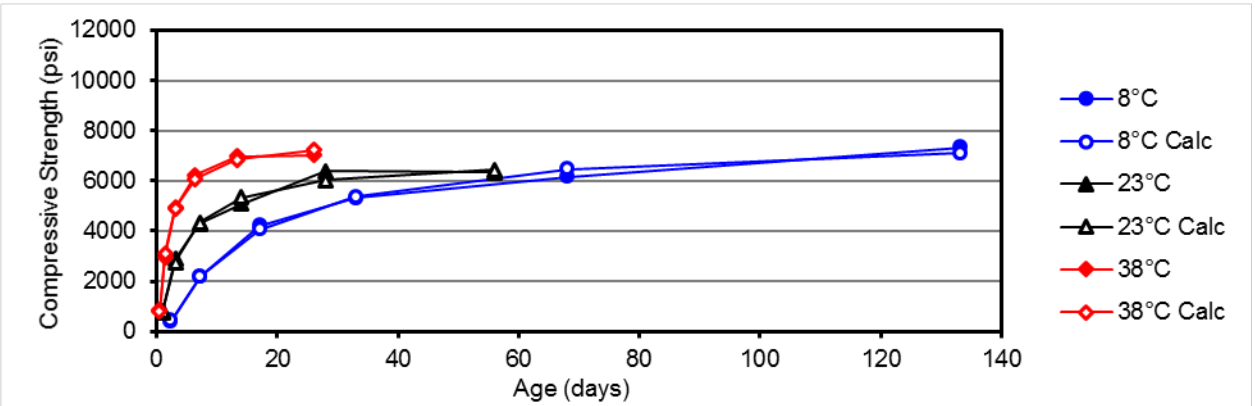

Figure C-126. Strength data for mortar containing 40% C ash and 5% metakaolin.

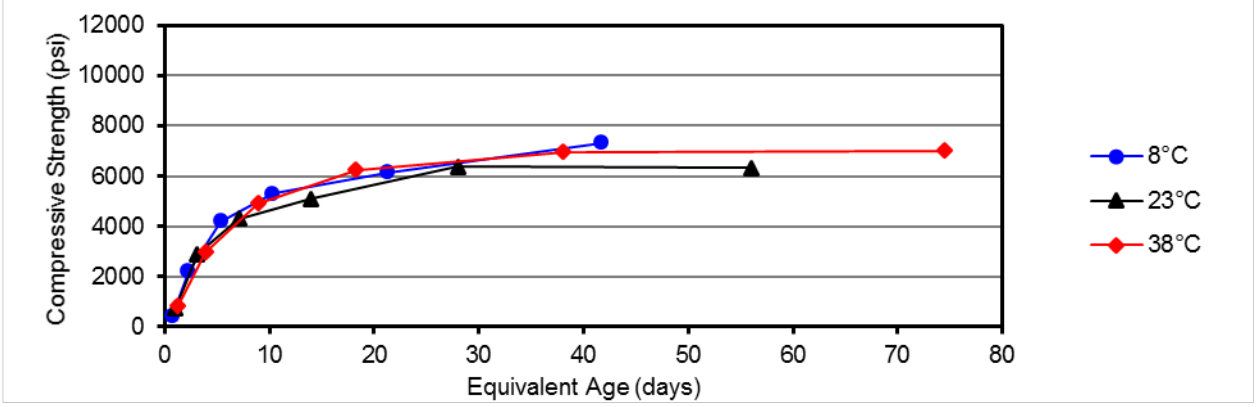

Figure C-127. Equivalent age data for mortar containing 40% C ash and 5% metakaolin.

Table C-54. Strength-age data for mortars containing 40% C ash and 10% metakaolin.

Temp, °C	Age, days	Strength, psi	Su, psi	k	t_o, days	E_a, J/mol	Equiv. Age, days
8	2.39	371	6813	0.058	1.209		0.73
	7.12	1833					2.18
	17.0	3406					5.21
	34.1	4149					10.5
	67.0	5447					20.6
	135.0	6106					41.4
23	1.01	709	7587	0.154	0.314	54,500	1.01
	3.03	2307					3.03
	7.12	3856					7.12
	14.2	4999					14.2
	28.0	6432					28.0
	56.0	6675					56.0
38	0.46	807	7667	0.557	0.263		1.34
	1.37	2742					3.99
	3.20	5041					9.31
	7.39	6135					21.5
	13.2	6296					38.4
	25.0	7417					72.9

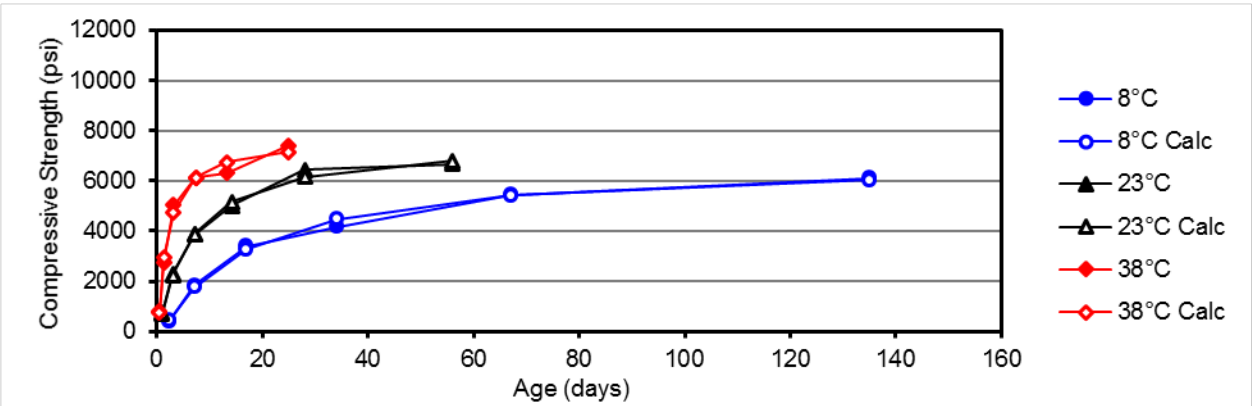

Figure C-128. Strength data for mortar containing 40% C ash and 10% metakaolin.

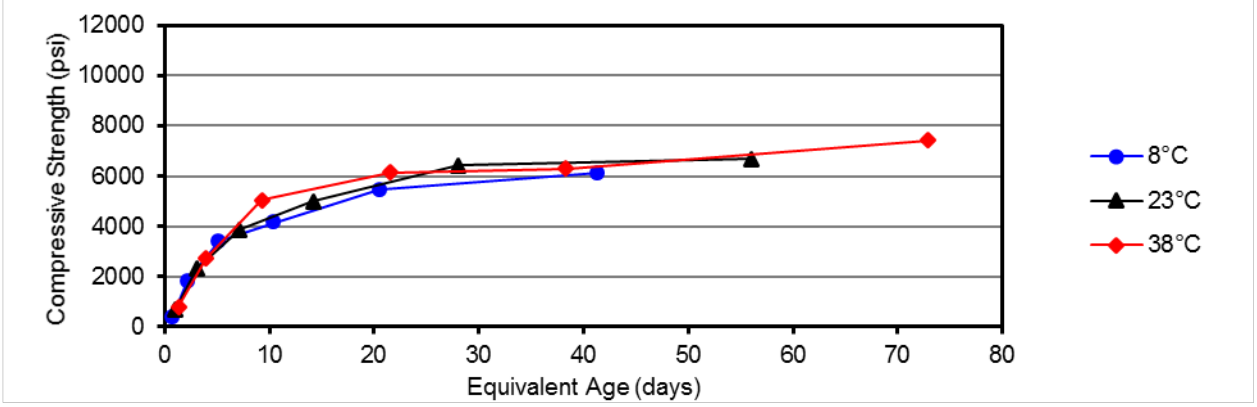

Figure C-129. Equivalent age data for mortar containing 40% C ash and 10% metakaolin.

Table C-55. Strength-age data for mortars containing 40% C ash and 10% slag.

Temp, °C	Age, days	Strength, psi	Su, psi	k	t_o, days	E_a, J/mol	Equiv. Age, days
8	2.40	328	4898	0.091	1.722		1.23
	7.12	1474					3.64
	17.1	2967					8.75
	33.3	3803					17.0
	67.3	3795					34.4
	131.0	4669					66.9
23	1.01	688	7744	0.128	0.000	31,00	1.01
	3.28	2669					3.28
	7.06	3687					7.06
	14.0	4685					14.0
	28.1	5926					28.1
	56.0	7004					56.0
38	0.46	638	7002	0.331	0.177		0.85
	1.51	2096					2.77
	3.30	3507					6.06
	6.39	4695					11.7
	12.3	5885					22.5
	25.5	6065					46.7

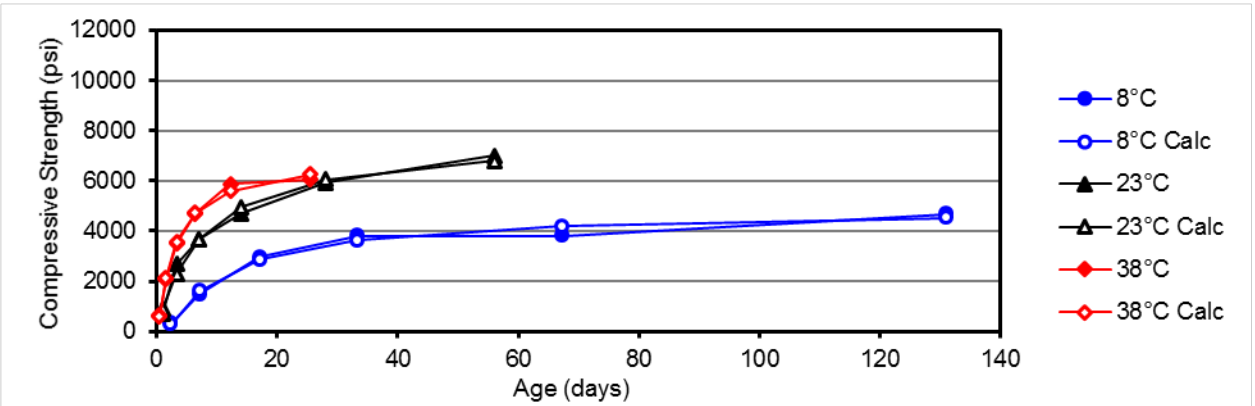

Figure C-130. Strength data for mortar containing 40% C ash and 10% slag.

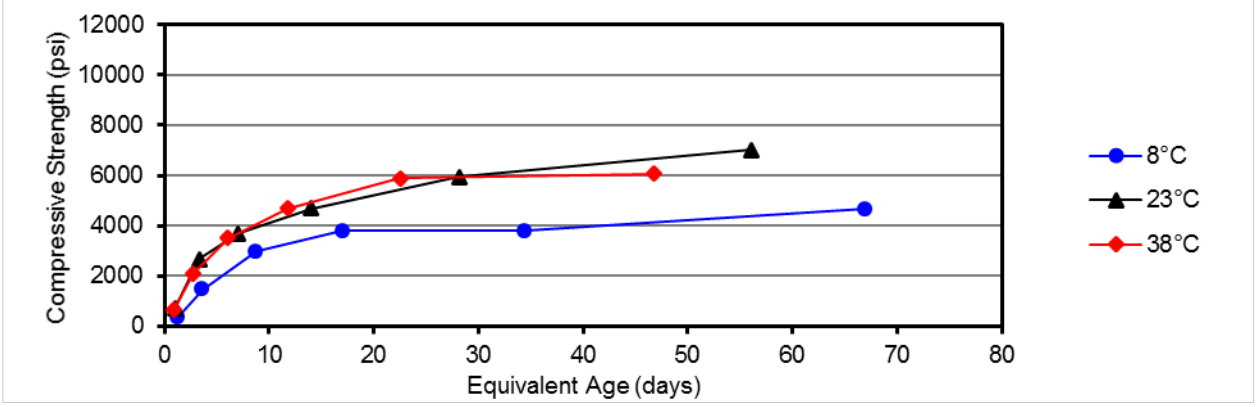

Figure C-131. Equivalent age data for mortar containing 40% C ash and 10% slag.

Table C-56. Strength-age data for mortars containing 40% C ash and 20% slag.

Temp, °C	Age, days	Strength, psi	Su, psi	k	t_o, days	E_a, J/mol	Equiv. Age, days
8	2.39	224	4368	0.065	1.687		1.62
	7.16	1098					4.85
	17.0	2159					11.5
	32.3	2872					21.9
	67.0	3818					45.3
	133.2	3720					90.1
23	1.02	351	8802	0.064	0.000	18,000	1.02
	3.03	1911					3.03
	7.20	3101					7.20
	14.2	3848					14.2
	28.2	5238					28.2
	56.0	7246					56.0
38	0.54	572	11510	0.139	0.090		0.76
	1.39	1903					1.97
	3.21	3518					4.57
	6.45	5222					9.18
	13.5	7609					19.3
	25.1	8909					35.8

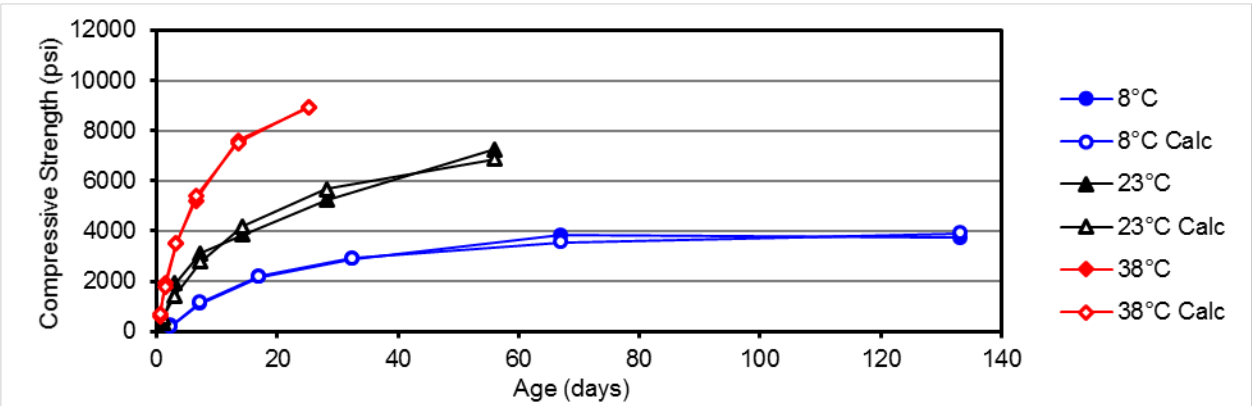

Figure C-132. Strength data for mortar containing 40% C ash and 20% slag.

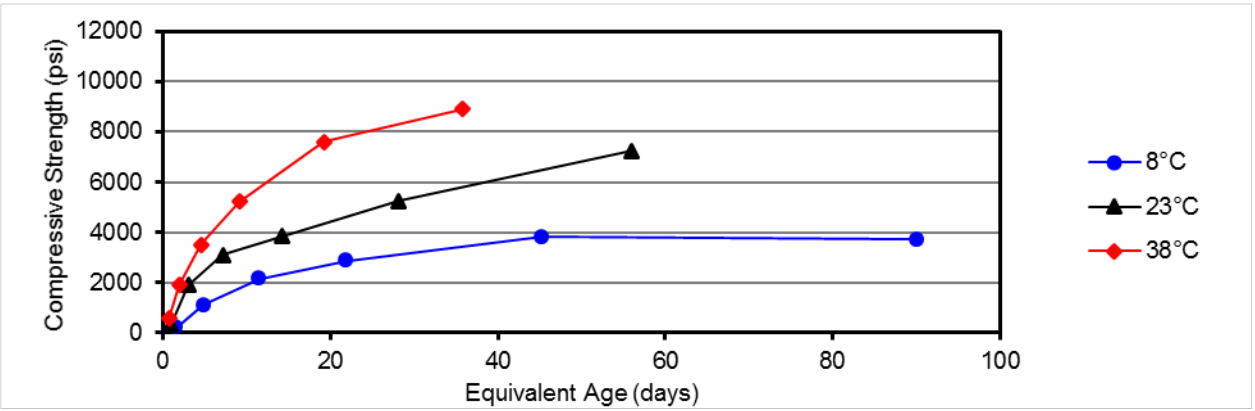

Figure C-133. Equivalent age data for mortar containing 40% C ash and 20% slag.

Table C-57. Strength-age data for mortars containing 50% C ash and 10% slag.

Temp, °C	Age, days	Strength, psi	Su, psi	k	t_o, days	E_a, J/mol	Equiv. Age, days
8	2.42	193	4385	0.062	1.810		1.36
	7.11	1011					4.01
	17.1	2108					9.65
	33.2	3081					18.7
	67.0	3335					37.8
	133.0	3954					75.0
23	1.00	339	7348	0.079	0.000	26,400	1.00
	2.98	1690					2.98
	6.95	2768					6.95
	14.2	3688					14.2
	28.0	4823					28.0
	55.9	6208					55.9
38	0.44	355	8357	0.186	0.156		0.74
	1.32	1610					2.22
	3.17	2986					5.32
	6.26	4379					10.5
	13.1	5930					22.0
	25.0	6879					42.0

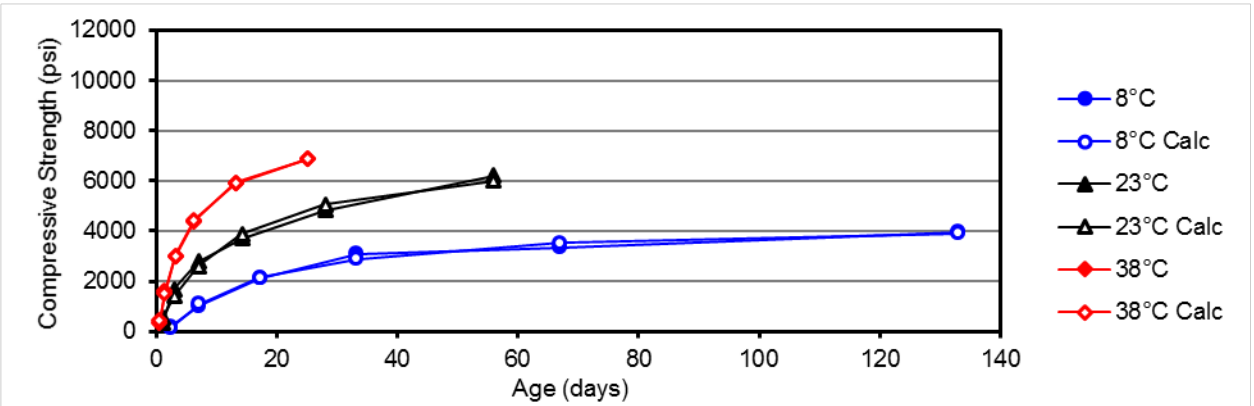

Figure C-134. Strength data for mortar containing 50% C ash and 10% slag.

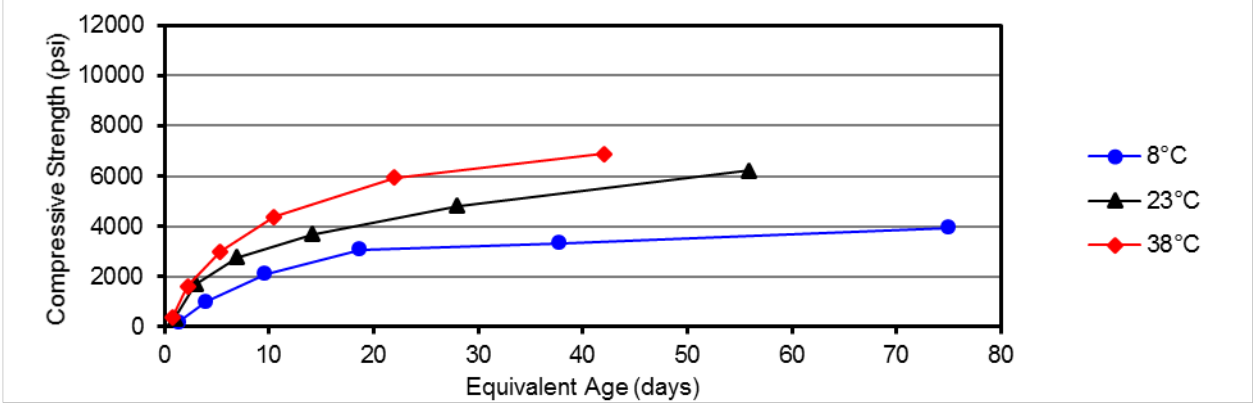

Figure C-135. Equivalent age data for mortar containing 50% C ash and 10% slag.

Table C-58. Strength-age data for mortars containing 50% C ash and 20% slag.

Temp, °C	Age, days	Strength, psi	Su, psi	k	t_o, days	E_a, J/mol	Equiv. Age, days
8	2.37	89	6295	0.017	1.623		0.74
	6.99	489					2.17
	17.0	1408					5.27
	33.0	2056					10.2
	67.0	3404					20.8
	131.4	4310					40.7
23	1.01	173	9008	0.038	0.000	54,000	1.01
	3.14	1063					3.14
	7.03	2176					7.03
	14.1	3049					14.1
	28.1	4517					28.1
	56.0	6248					56.0
38	0.44	186	8787	0.161	0.340		1.26
	1.40	1239					4.05
	3.35	2744					9.65
	6.38	4522					18.4
	13.2	5868					38.0
	25.4	7030					73.2

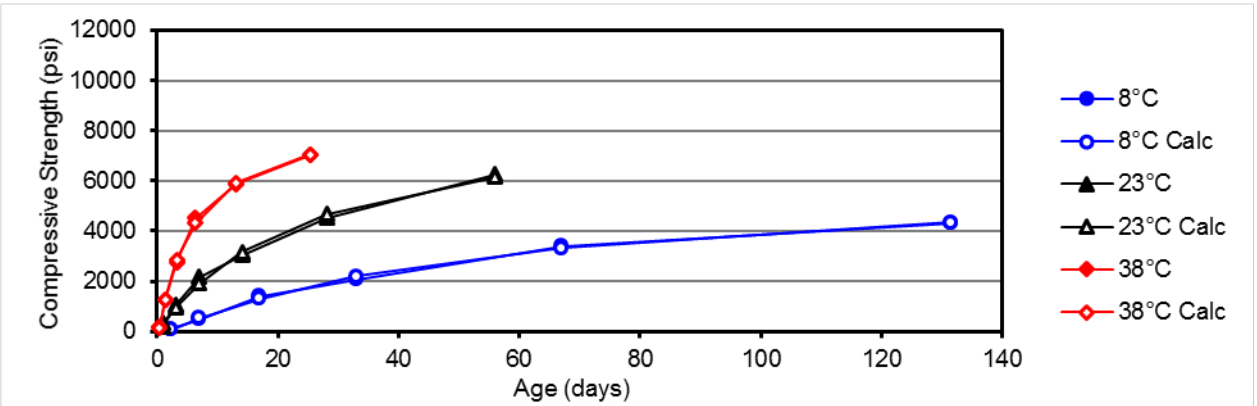

Figure C-136. Strength data for mortar containing 50% C ash and 20% slag.

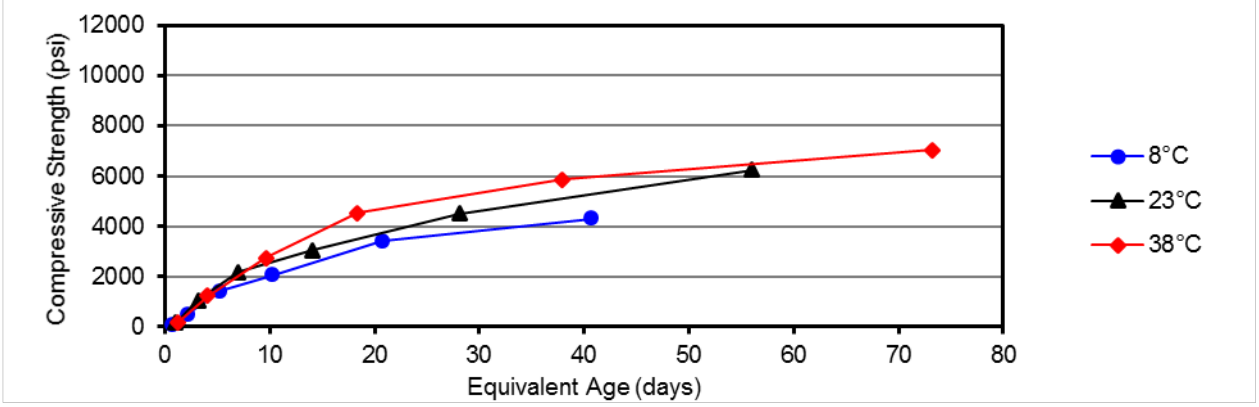

Figure C-137. Equivalent age data for mortar containing 50% C ash and 20% slag.

C.4. Mortar Flow Table Results

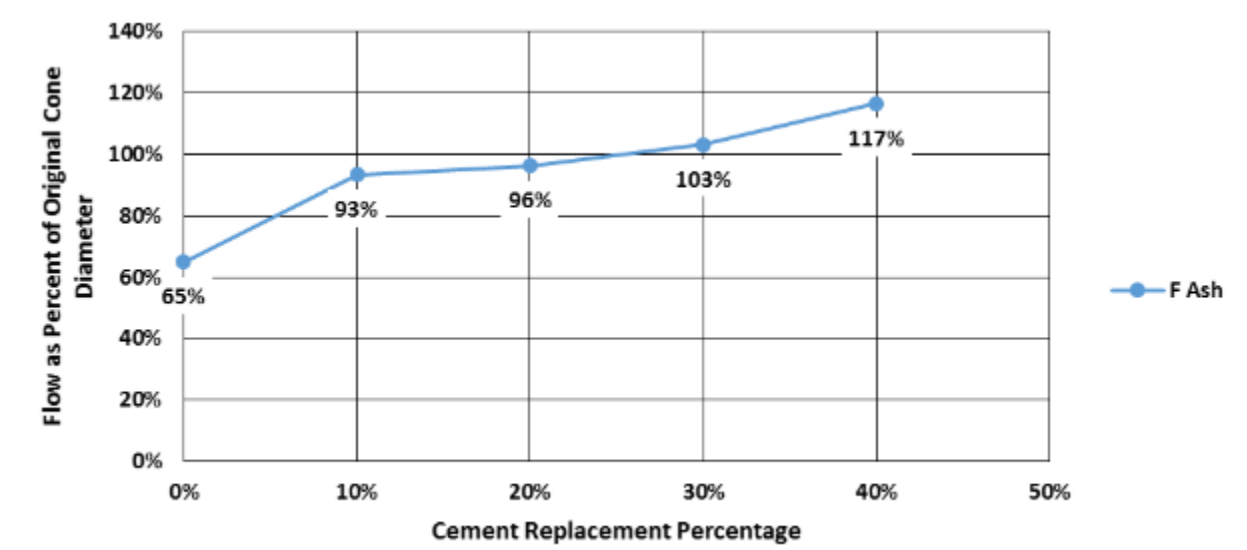

Figure C-138. Mortar flow table results for mortars containing 10% - 40% class F fly ash.

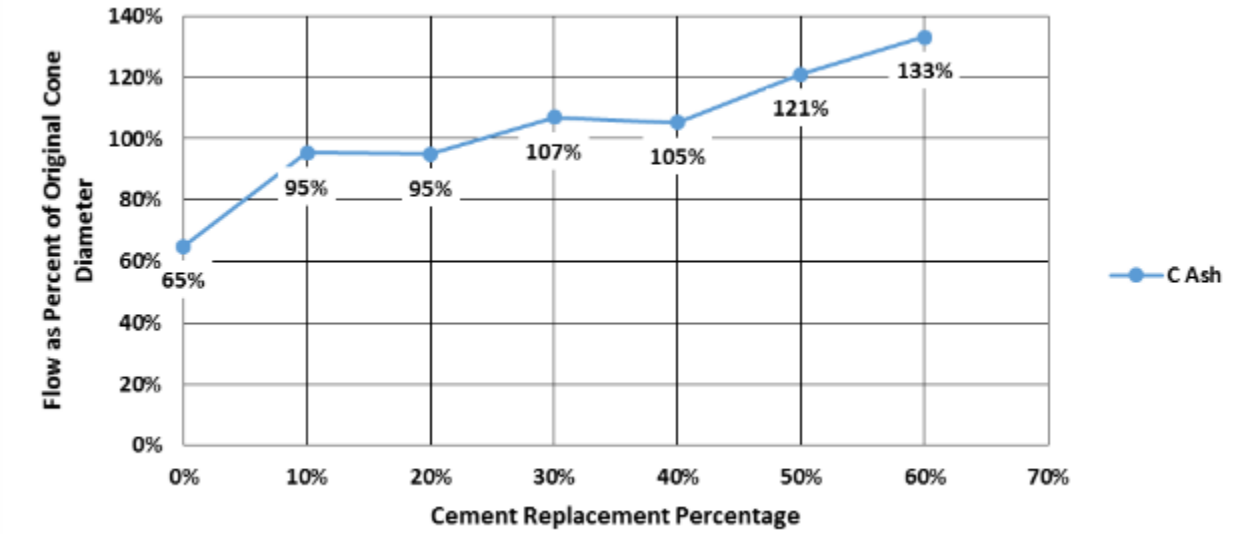

Figure C-139. Mortar flow table results for mortars containing 10% - 60% class C fly ash.

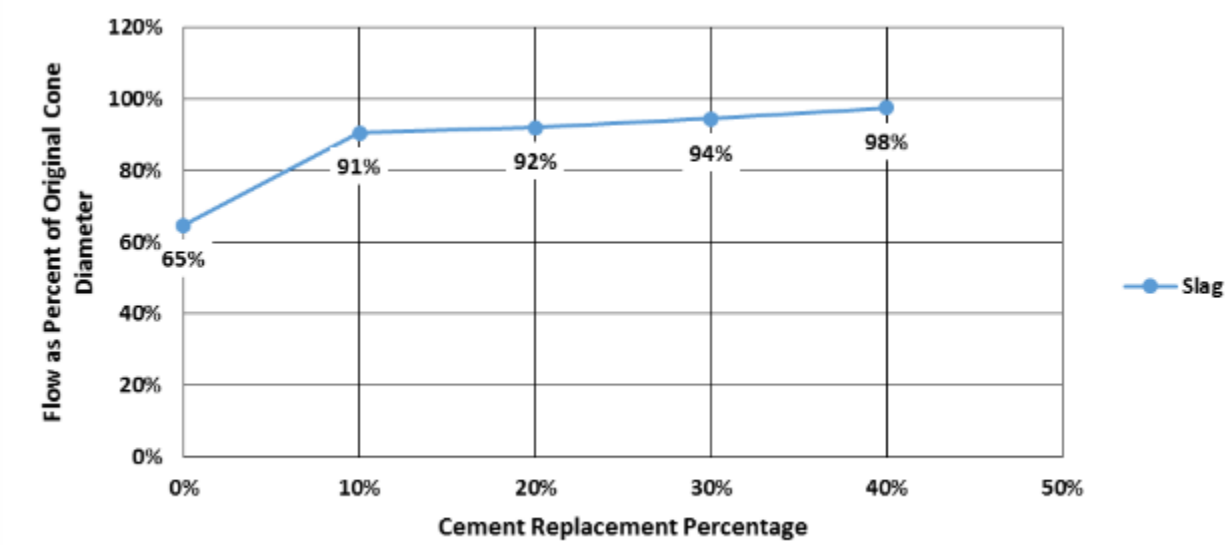

Figure C-140. Mortar flow table results for mortars containing 10% - 40% blast furnace slag.

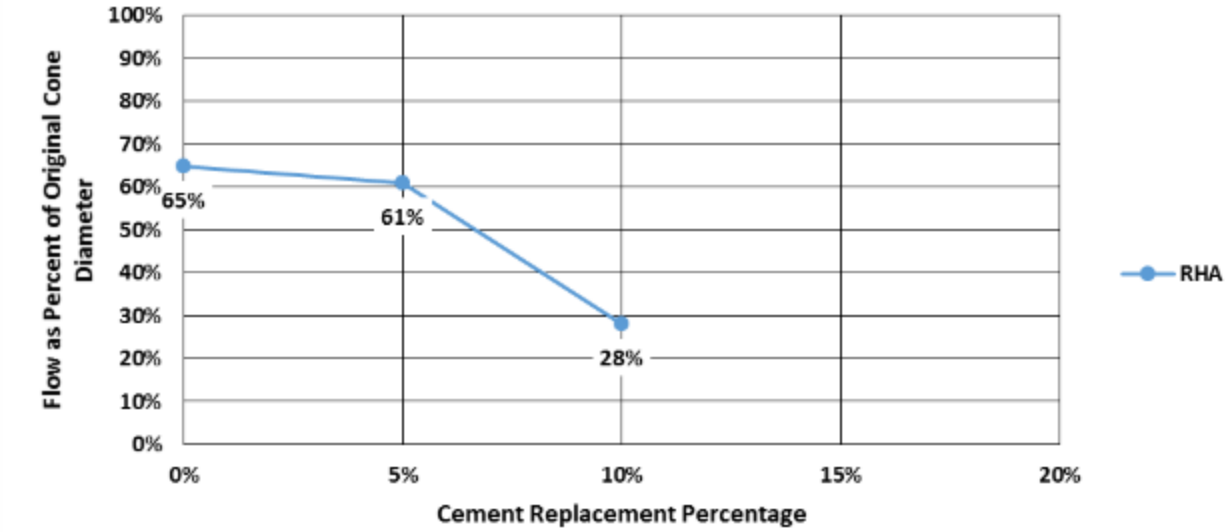

Figure C-141. Mortar flow table results for mortars containing 5% and 10% rice husk ash.

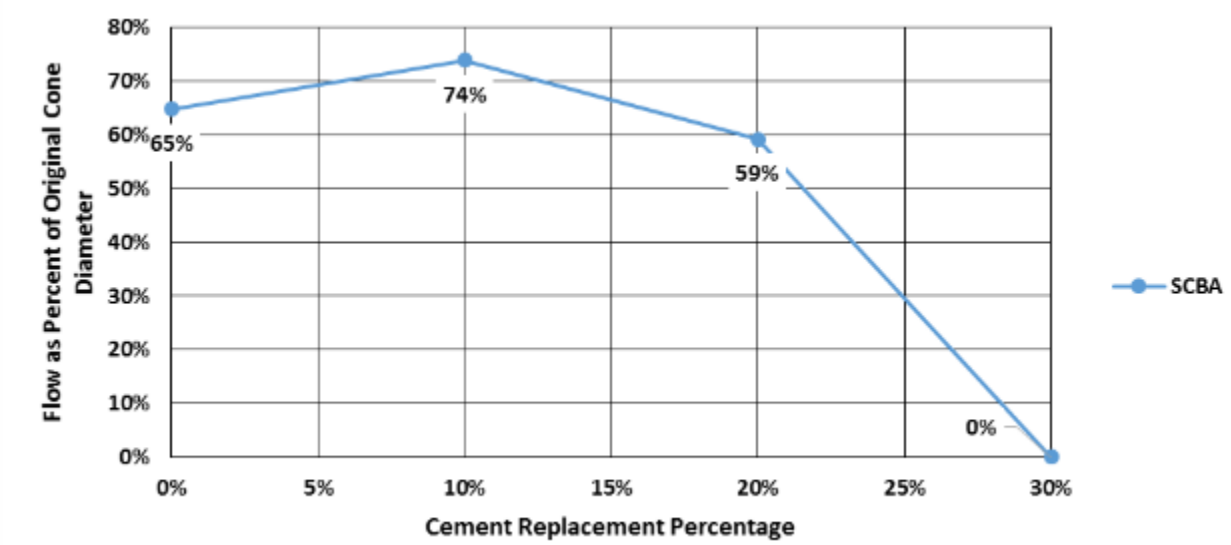

Figure C-142. Mortar flow table results for mortars containing 10% - 30% sugarcane ash.

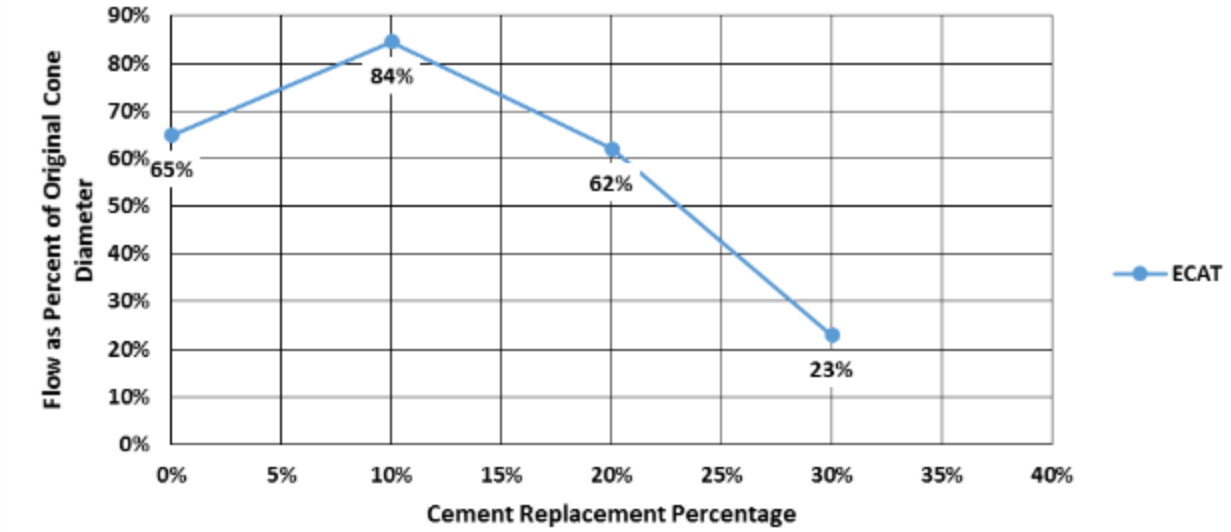

Figure C-143. Mortar flow table results for mortars containing 10% - 30% equilibrium catalyst.

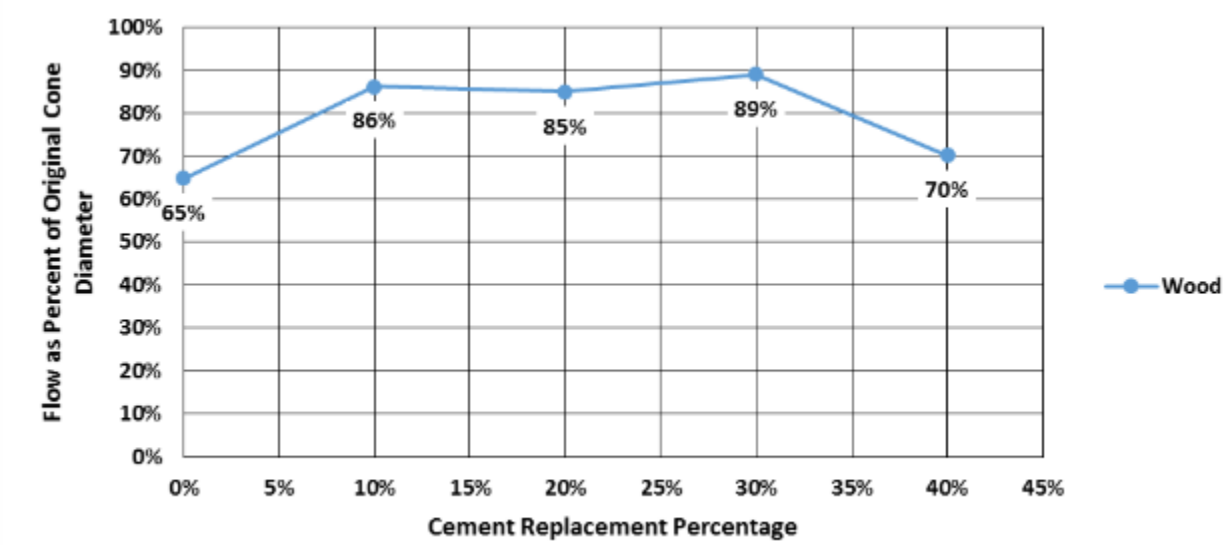

Figure C-144. Mortar flow table results for mortars containing 10% - 40% wood ash.

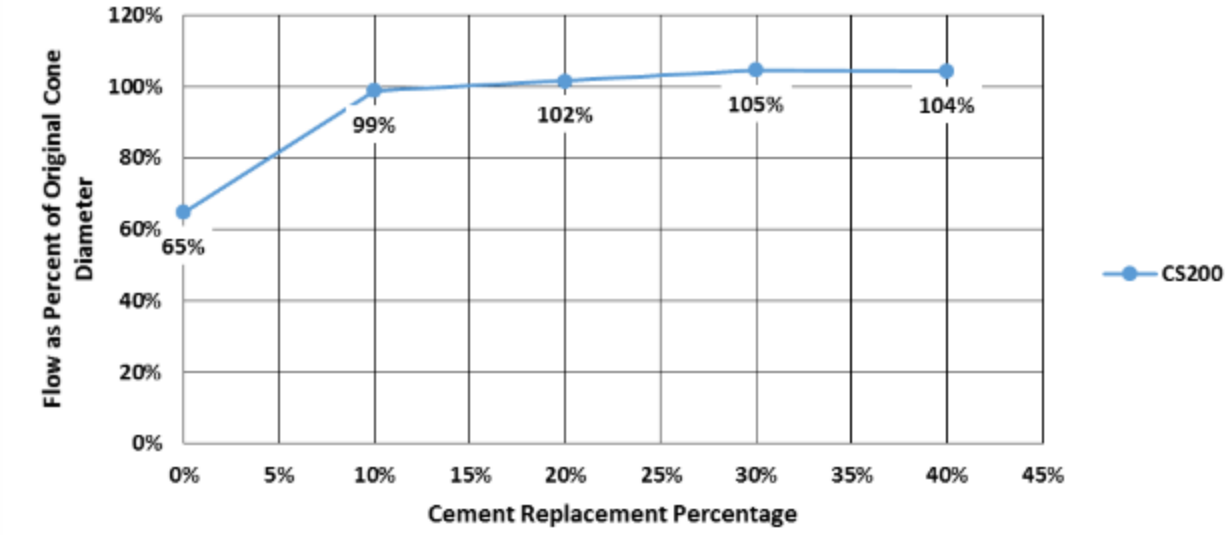

Figure C-145. Mortar flor table results for mortars containing 10% - 40% CS200 glass powder.

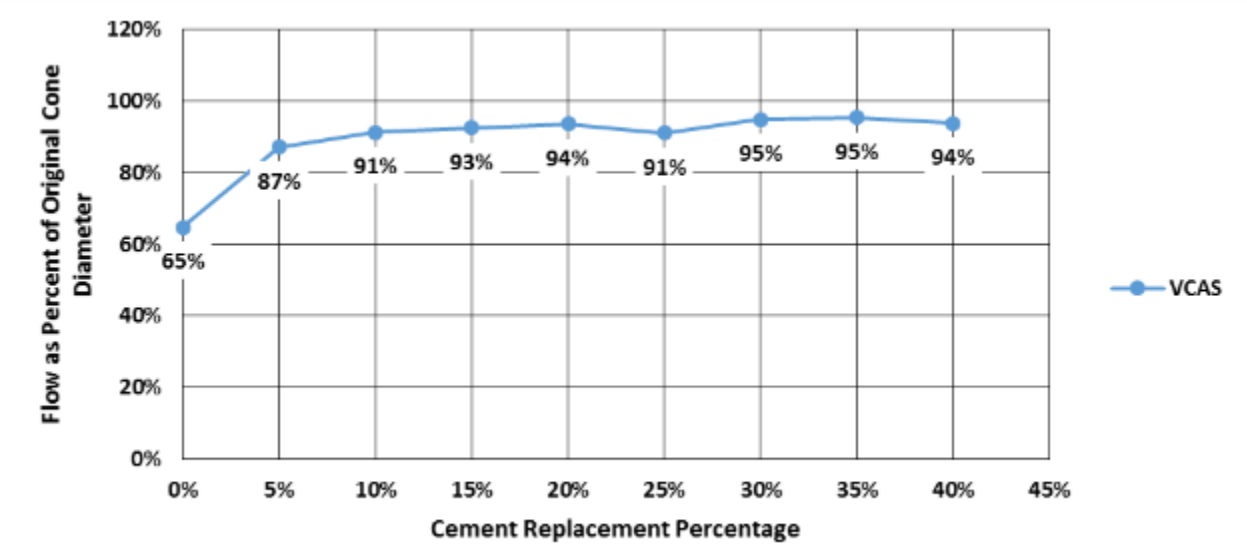

Figure C-146. Mortar flow table results for mortars containing 5% - 40% VCAS 160 glass powder.

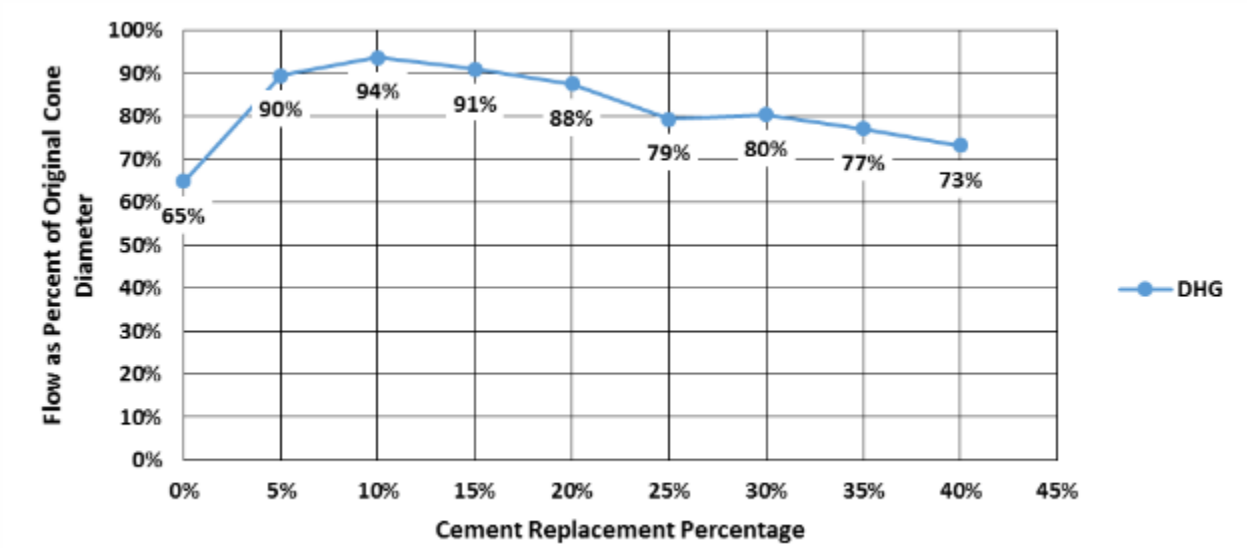

Figure C-147. Mortar flow table results for mortars containing 5% - 40% ground glass powder.

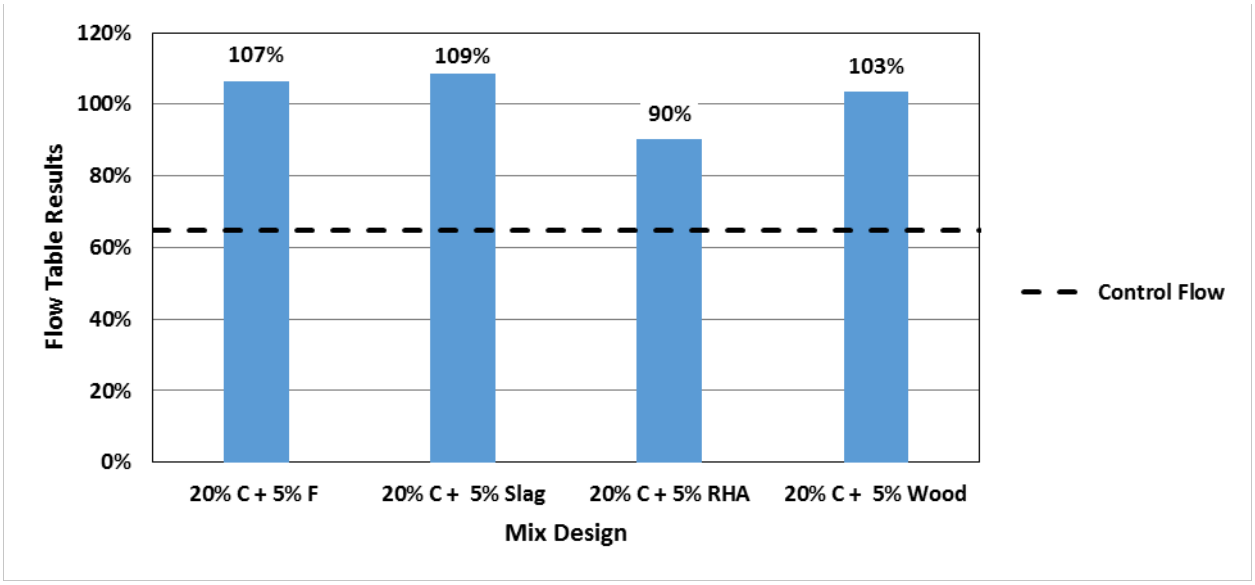

Figure C-148. Mortar flow table results for ternary mortar blends containing 20% class C fly ash and 5% of either class F fly ash, ground blast furnace slag, rice husk ash, or wood ash.

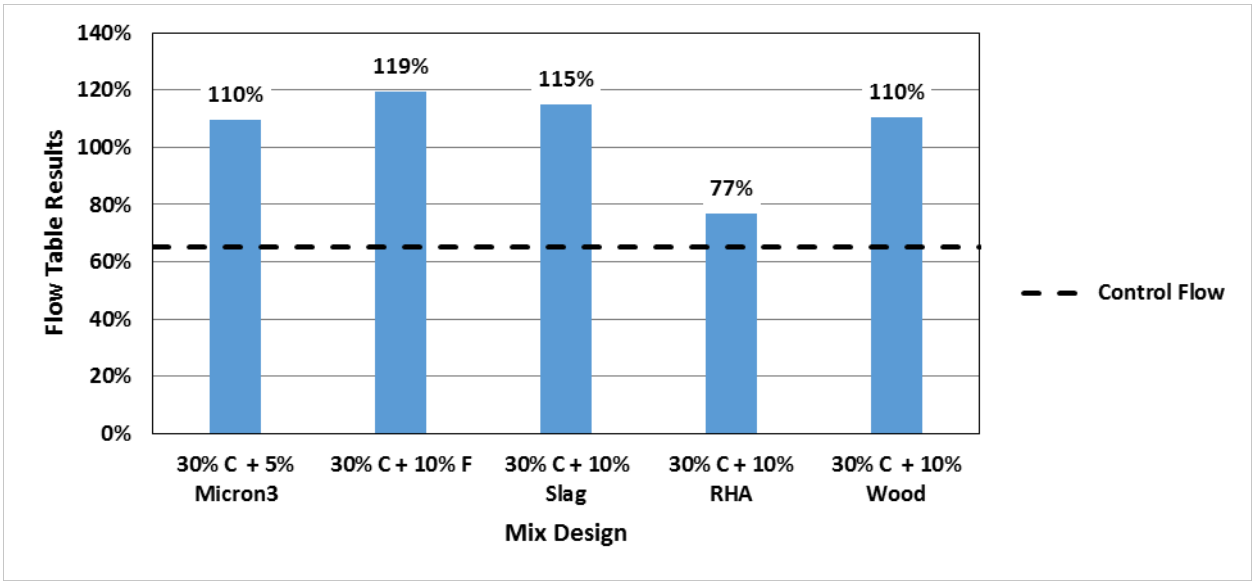

Figure C-149. Mortar flow table results for ternary blended mortars containing 30% class C fly ash and 5% or 10% of either Micron^3 ultrafine fly ash, class F fly ash, ground blast furnace slag, rice husk ash, or wood ash.

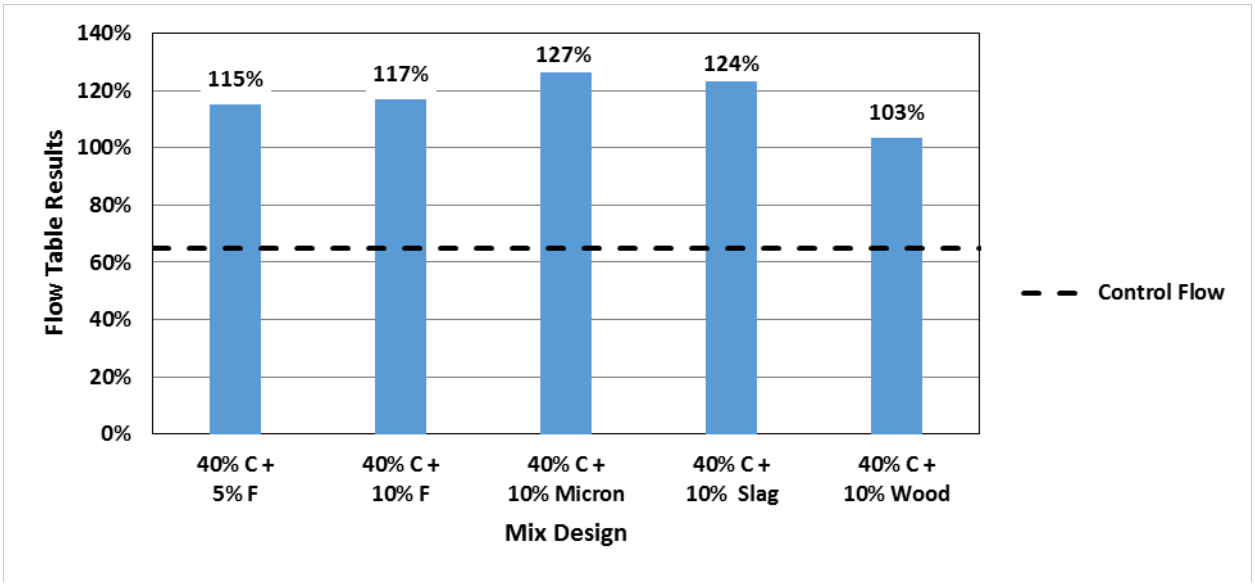

Figure C-150. Mortar flow table results for ternary blended mortars containing 40% class C fly ash and 5% or 10% class F fly ash, Micron[3] ultrafine fly ash, ground blast furnace slag, or wood ash.

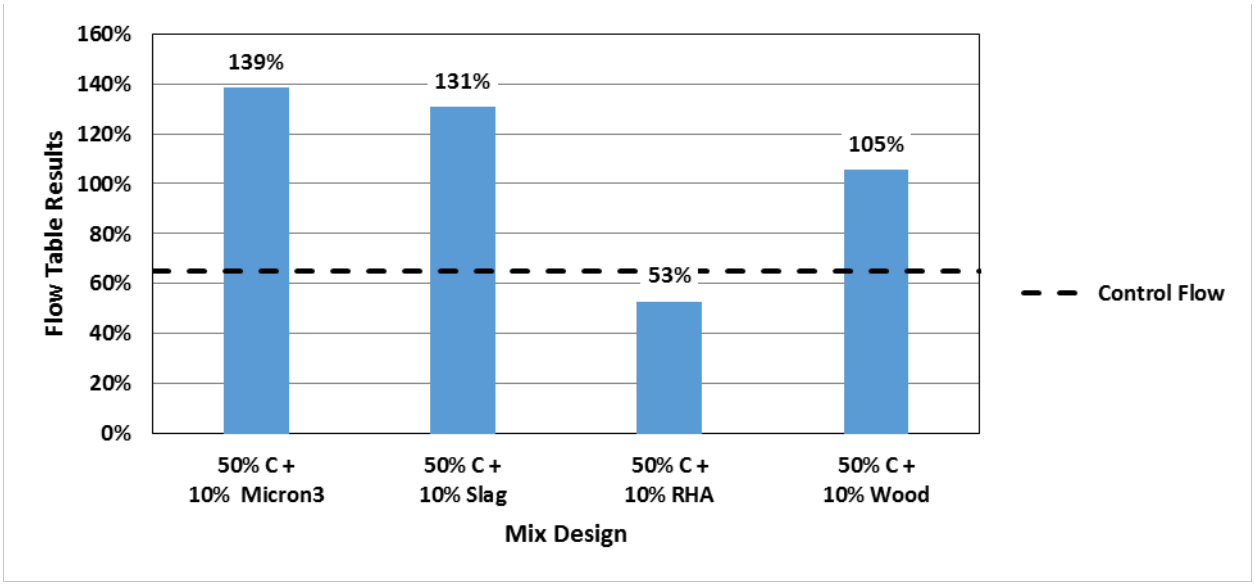

Figure C-151. Mortar flow table results for ternary blended mortars containing 50% class C fly ash and 10% of either Micron[3] ultrafine fly ash, ground blast furnace slag, rice husk ash, or wood ash.

C.5. Time of Set of Mortar Results

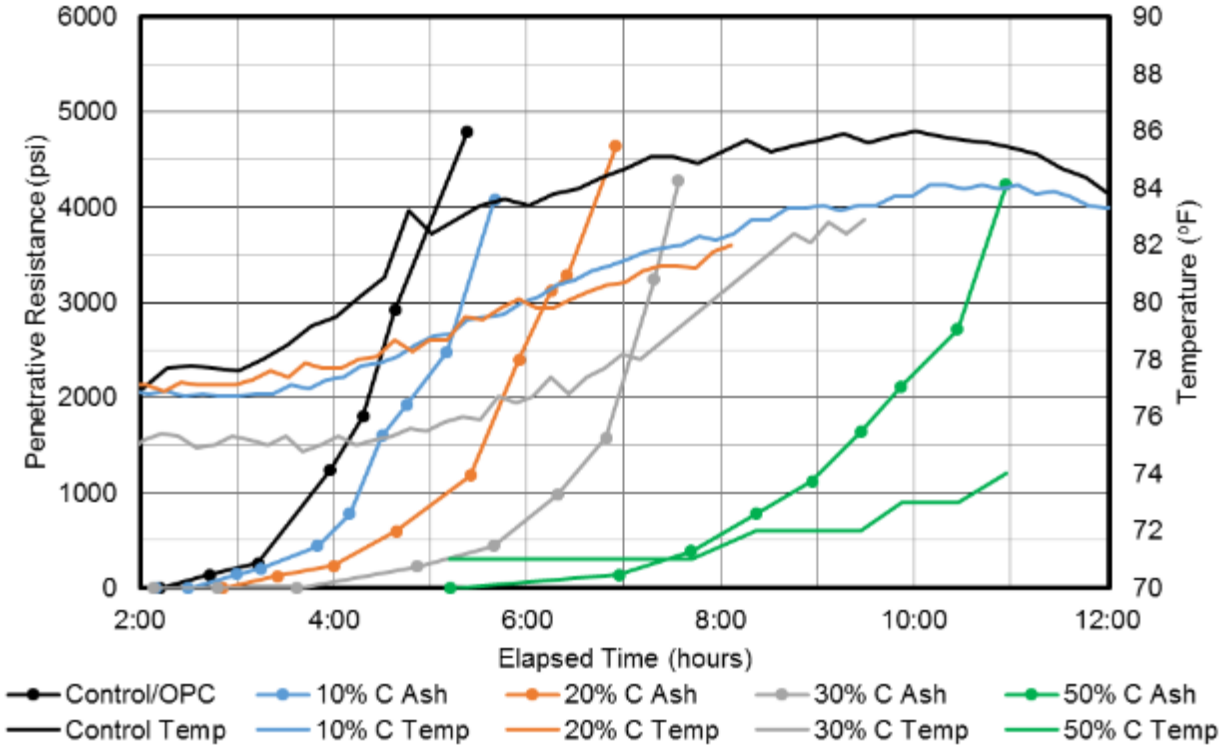

Figure C-152. Time of set for binary mortars containing class C fly ash.

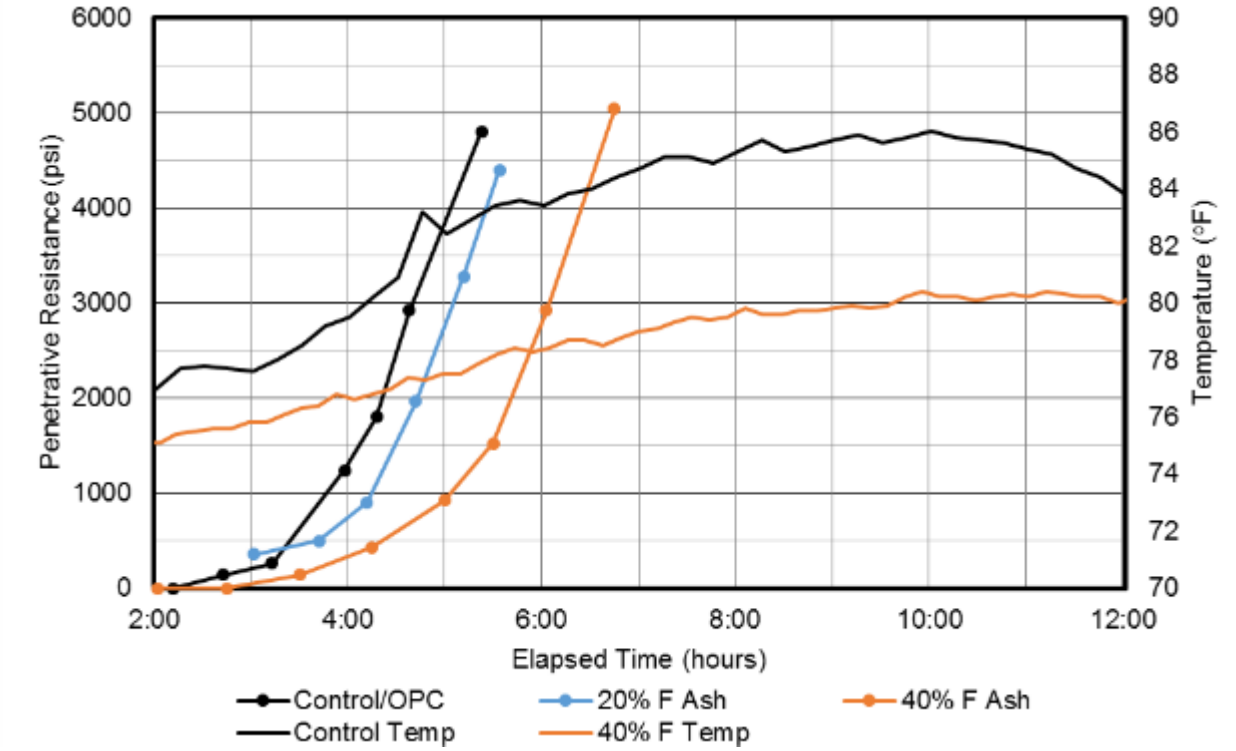

Figure C-153. Time of set for binary mortars containing class F fly ash.

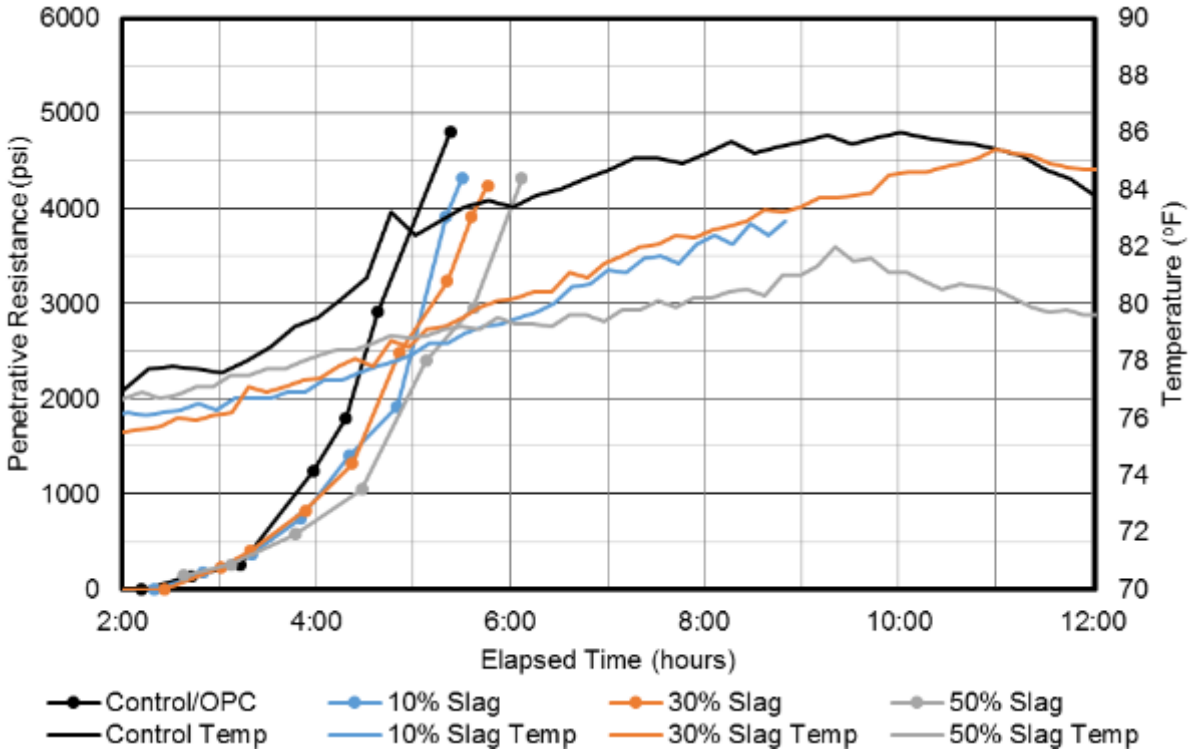

Figure C-154. Time of set for binary mortars containing slag.

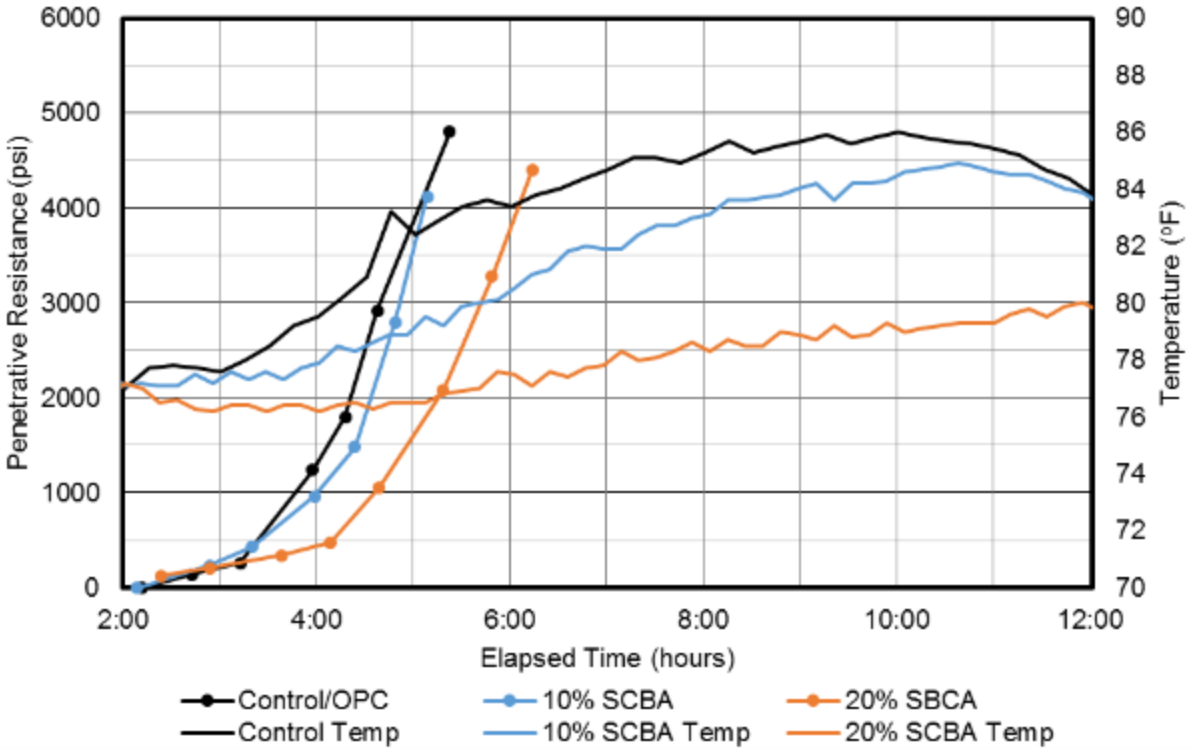

Figure C-155. Time of set for binary mortars containing sugarcane bagasse ash.

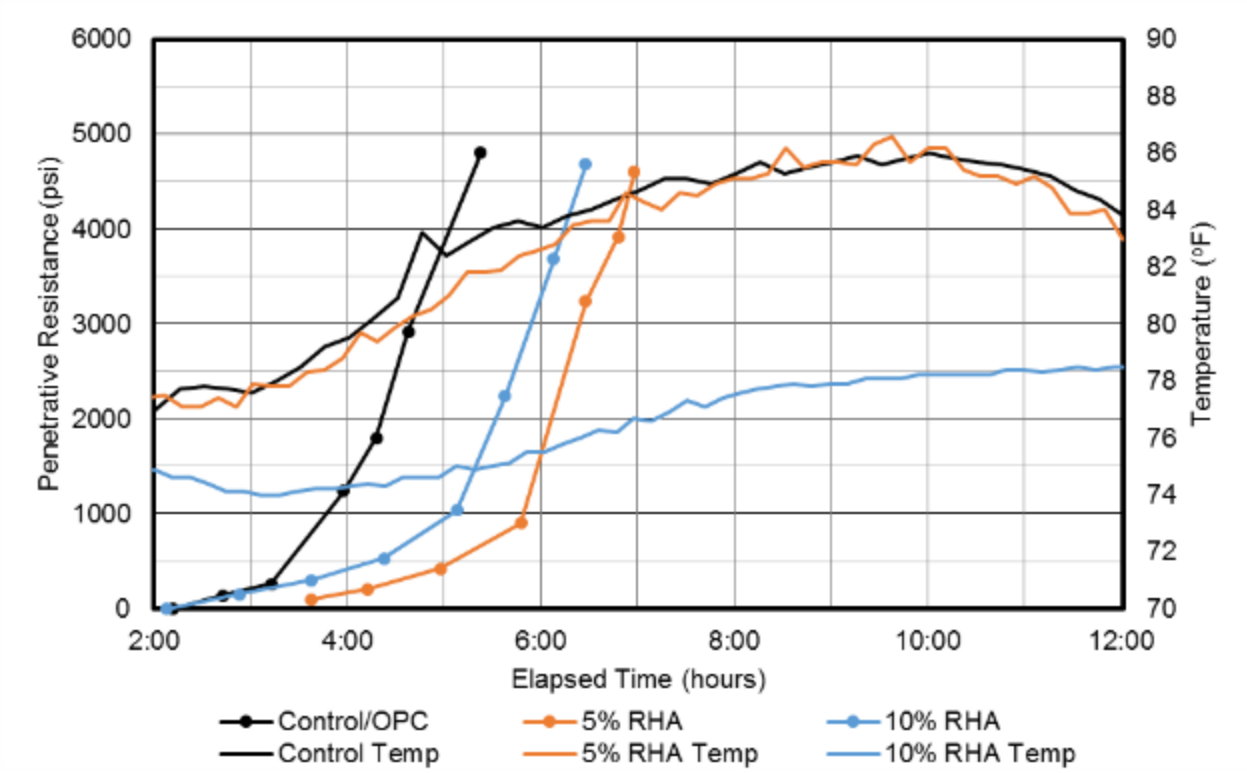

Figure C-156. Time of set for binary mortars containing rice husk ash.

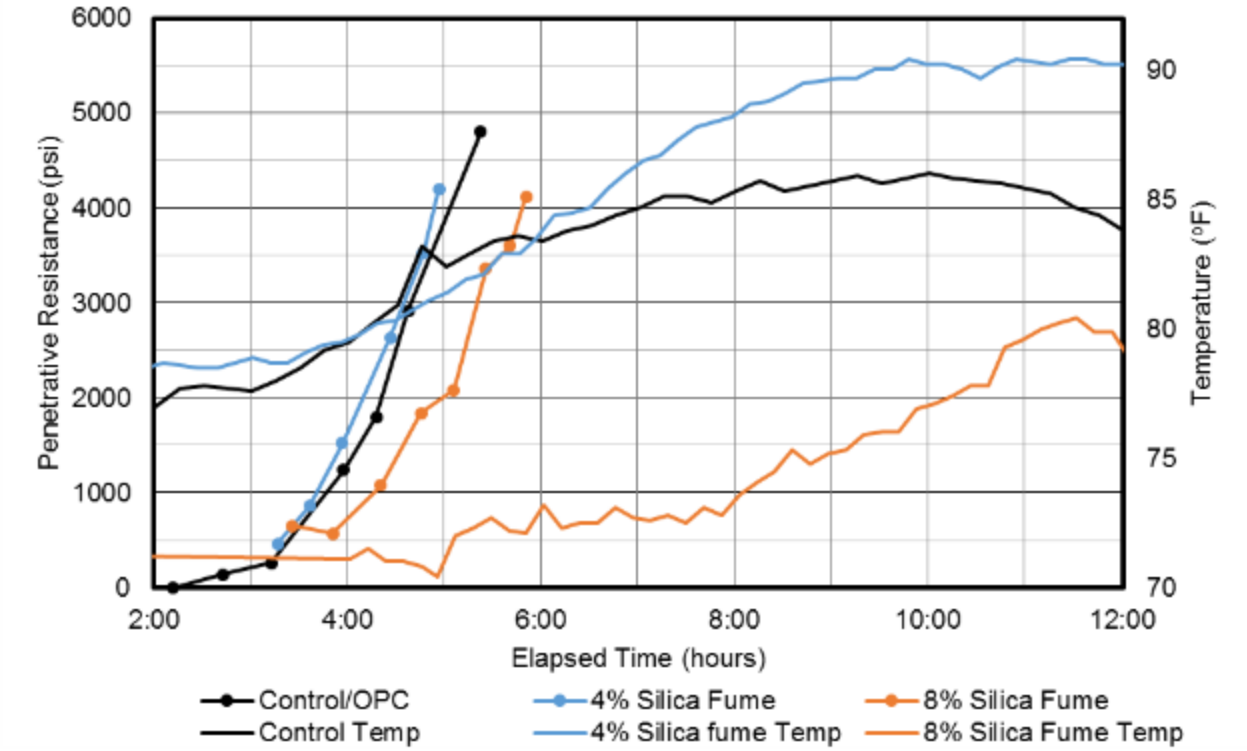

Figure C-157. Time of set for binary mortars containing silica fume.

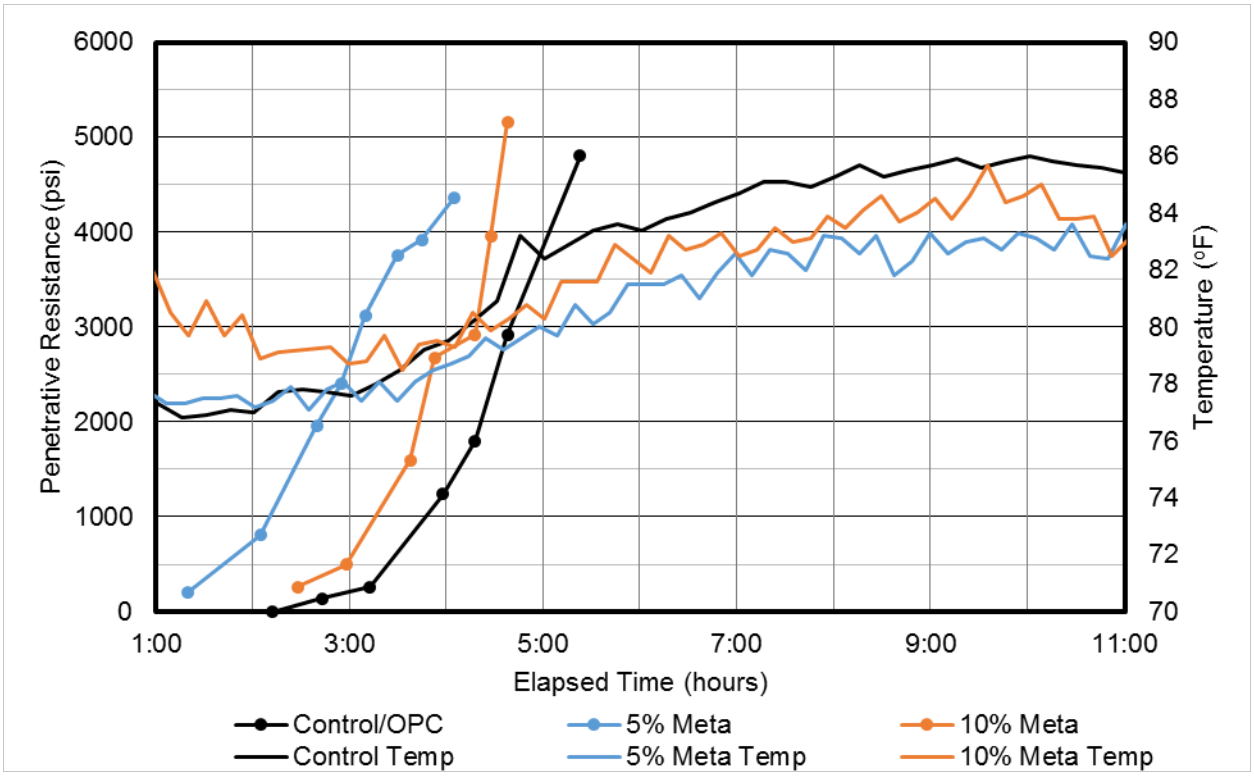

Figure C-158. Time of set of mortars containing metakaolin.

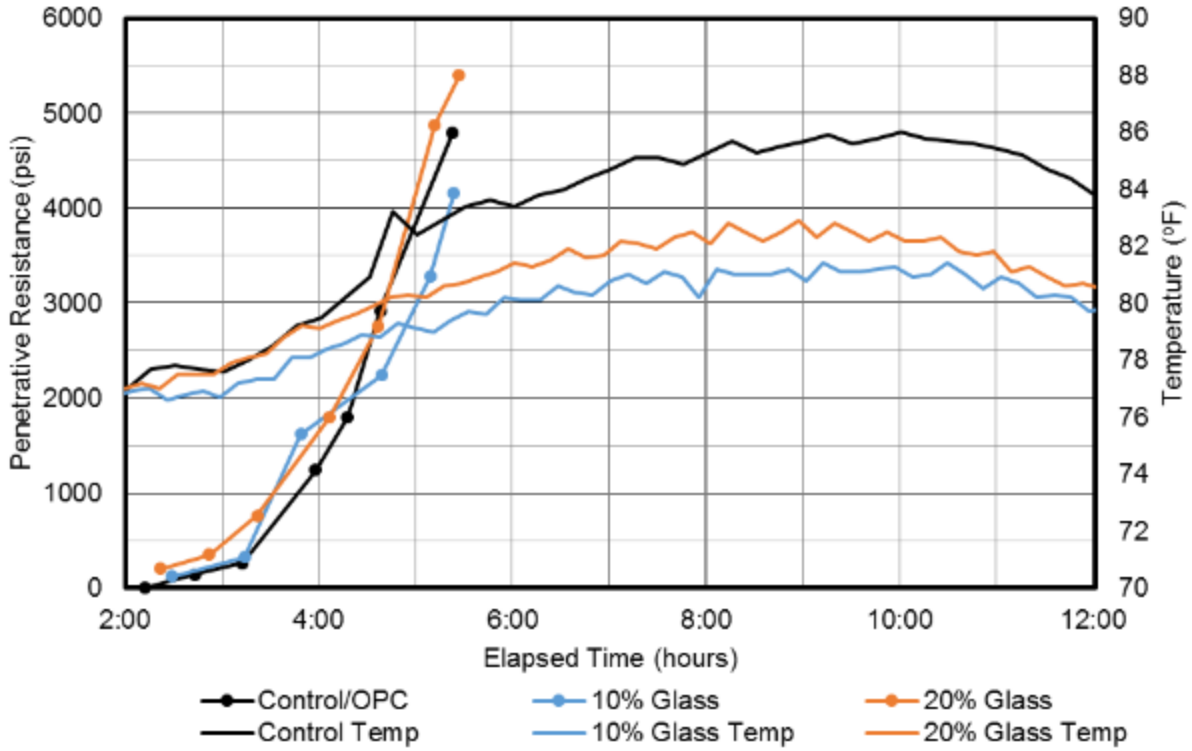

Figure C-159. Time of set for binary mortars containing ground glass.

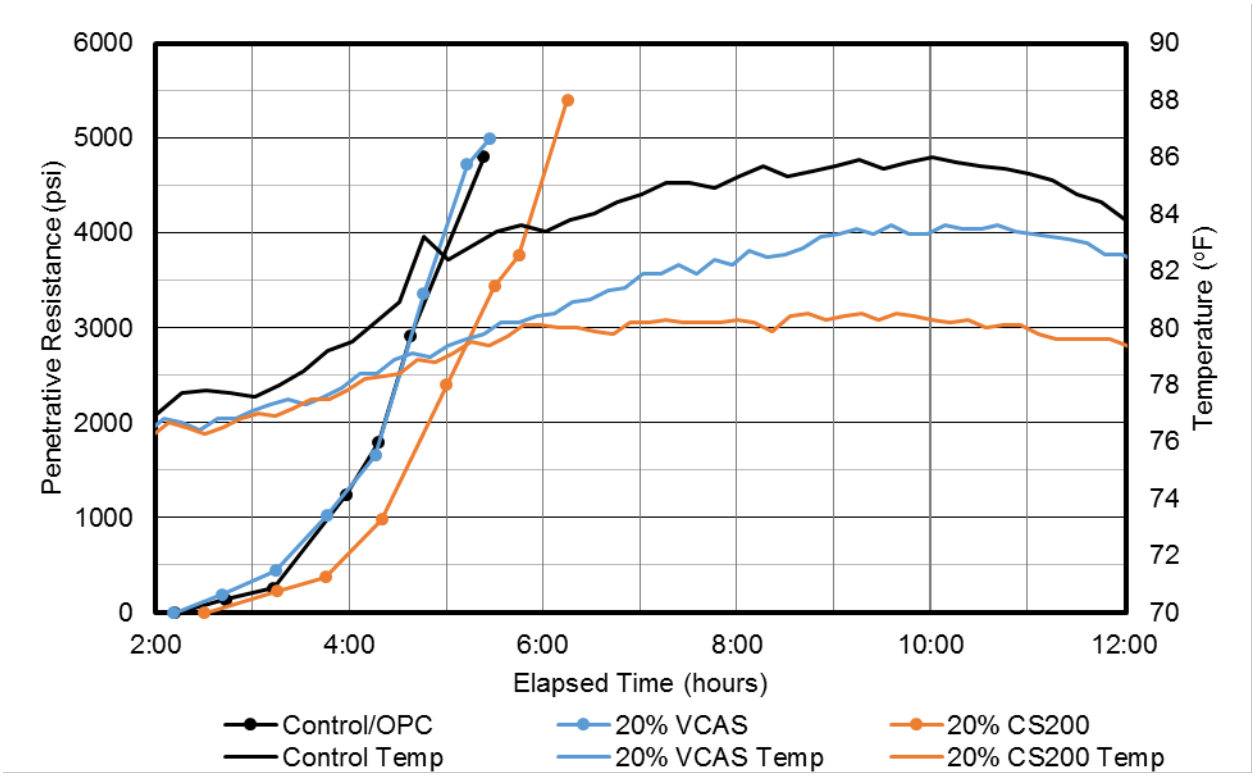

Figure C-160. Time of set for binary mortars containing VCAS160 or CS200 glass.

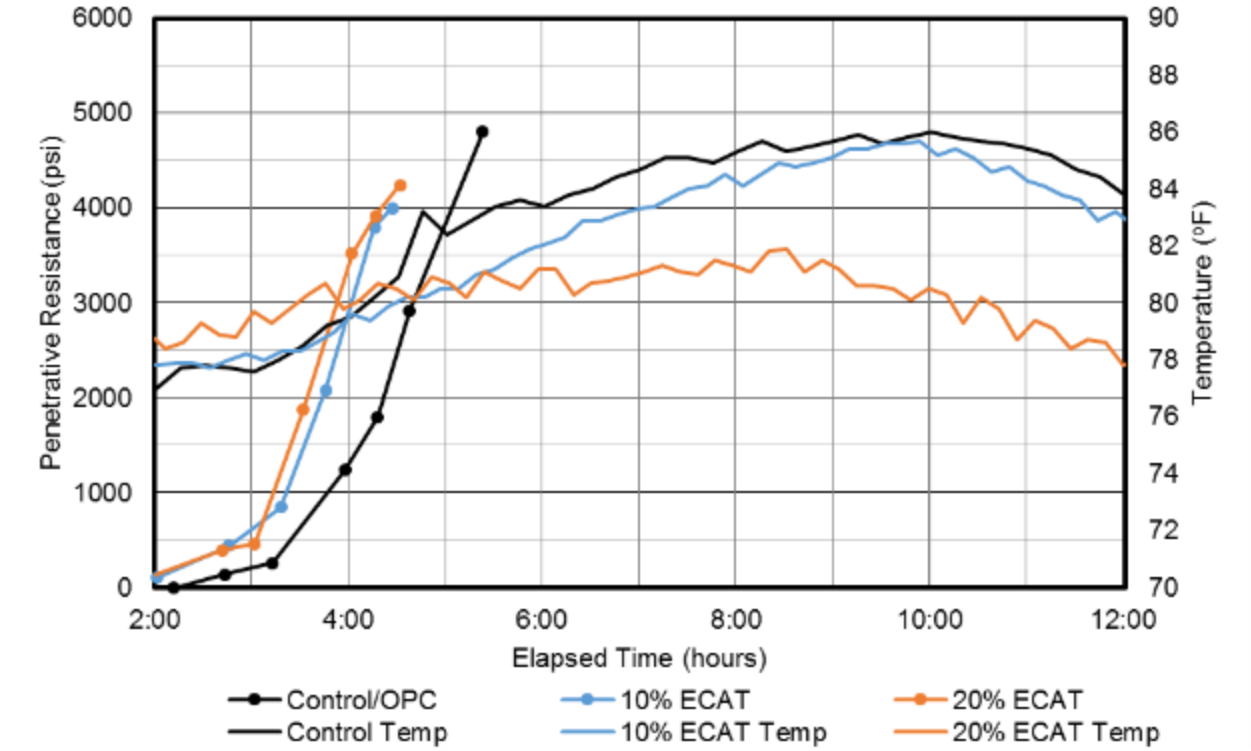

Figure C-161. Time of set for binary mortars containing equilibrium catalyst.

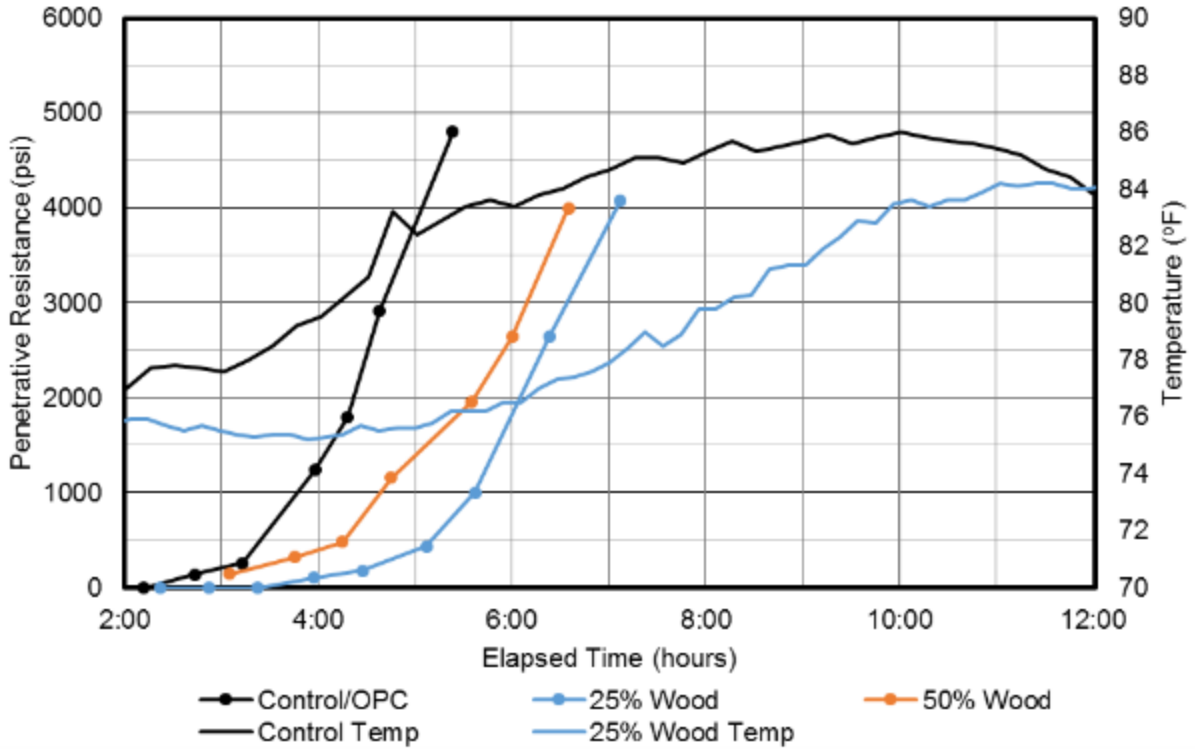

Figure C-162. Time of set for binary mortars containing wood ash.

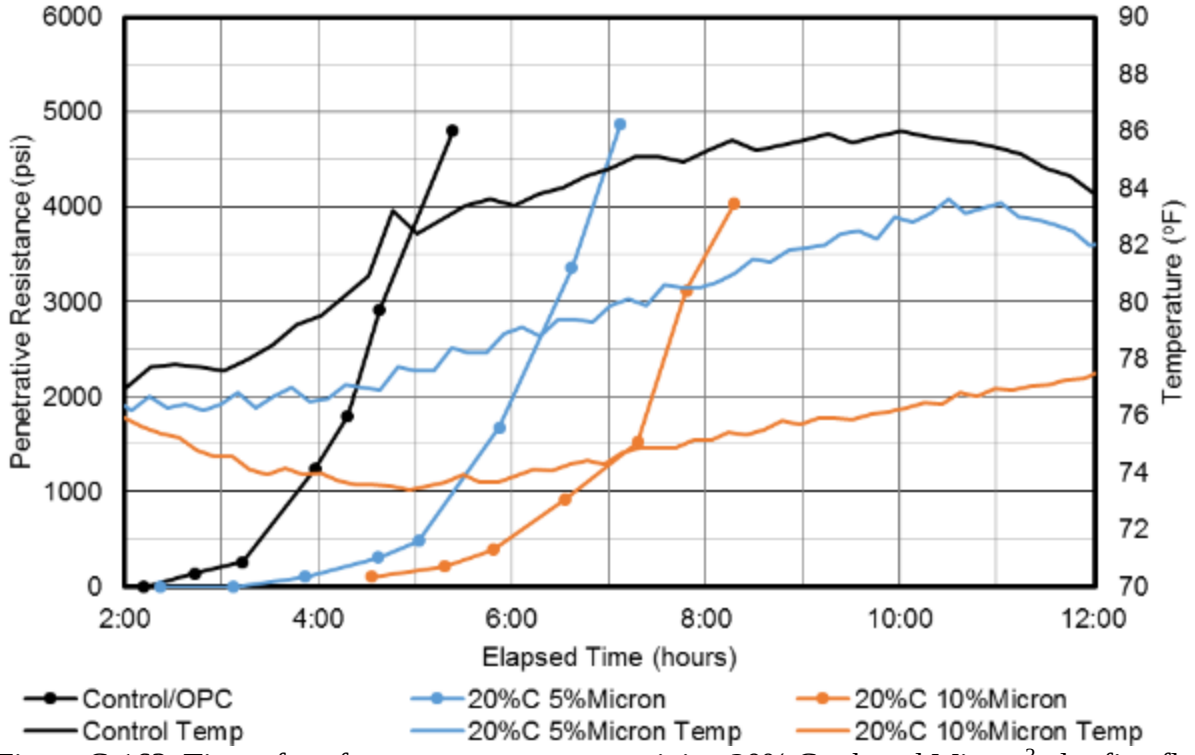

Figure C-163. Time of set for ternary mortars containing 20% C ash and Micron[3] ultrafine fly ash.

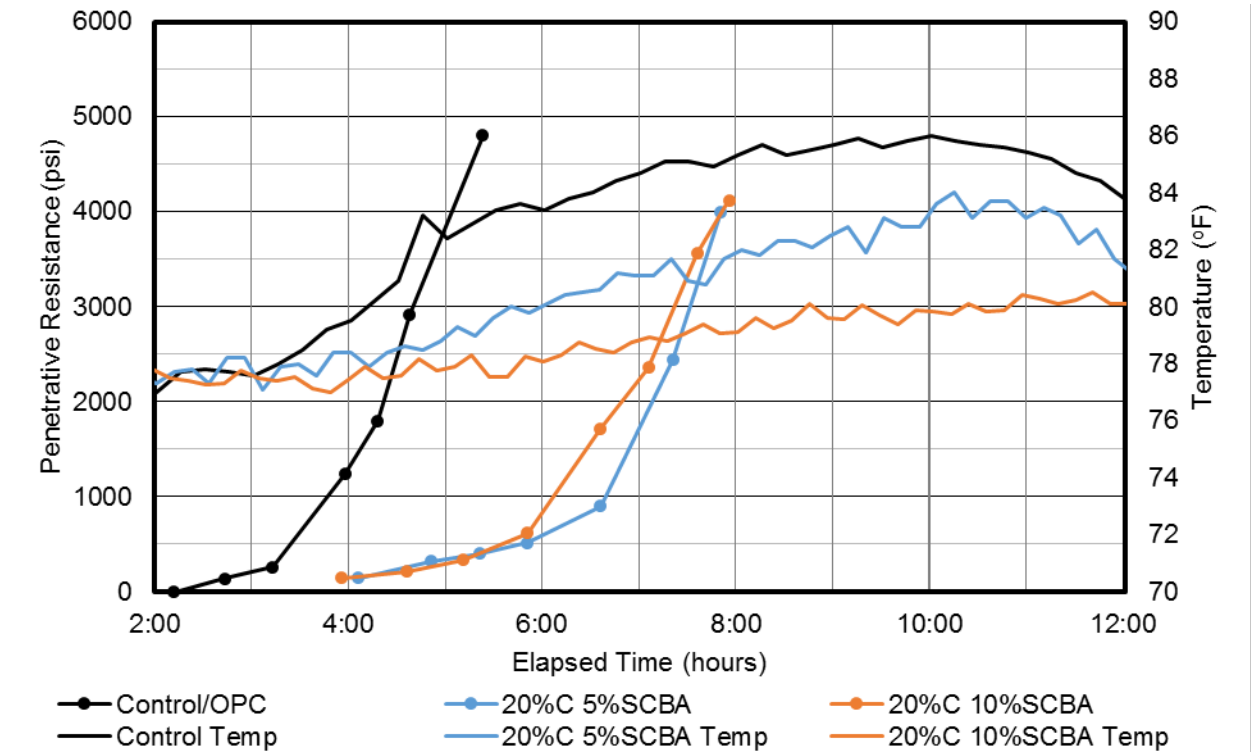

Figure C-164. Time of set of ternary mortars containing 20% C ash and sugarcane bagasse ash.

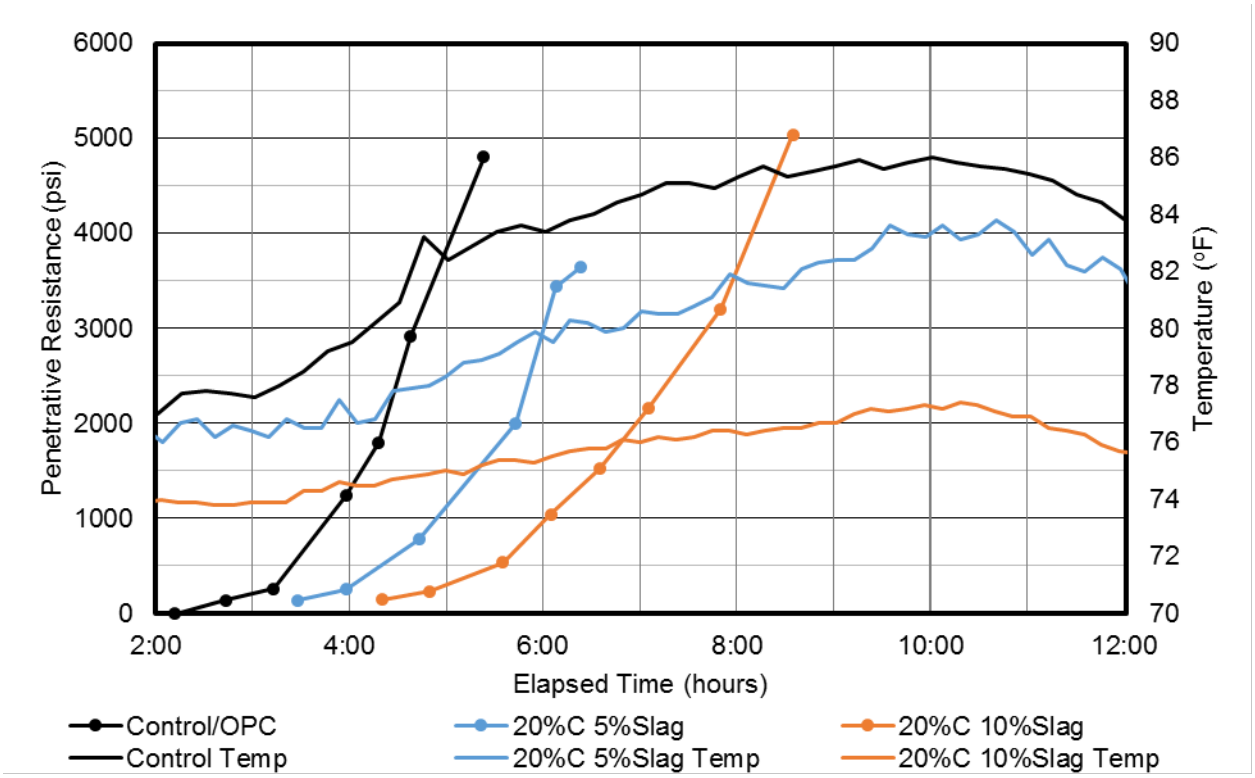

Figure C-165. Time of set of ternary mortars containing 20% C ash and slag.

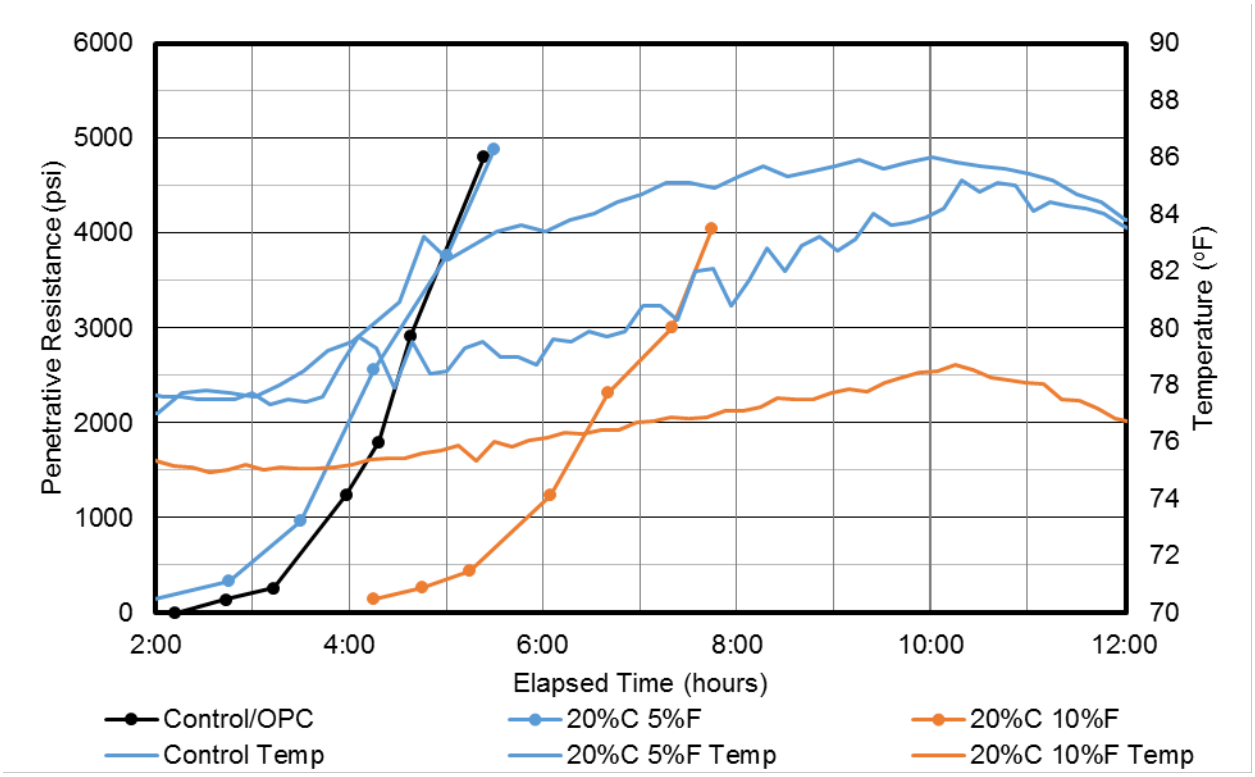

Figure C-166. Time of set of ternary mortars containing 20% C ash.

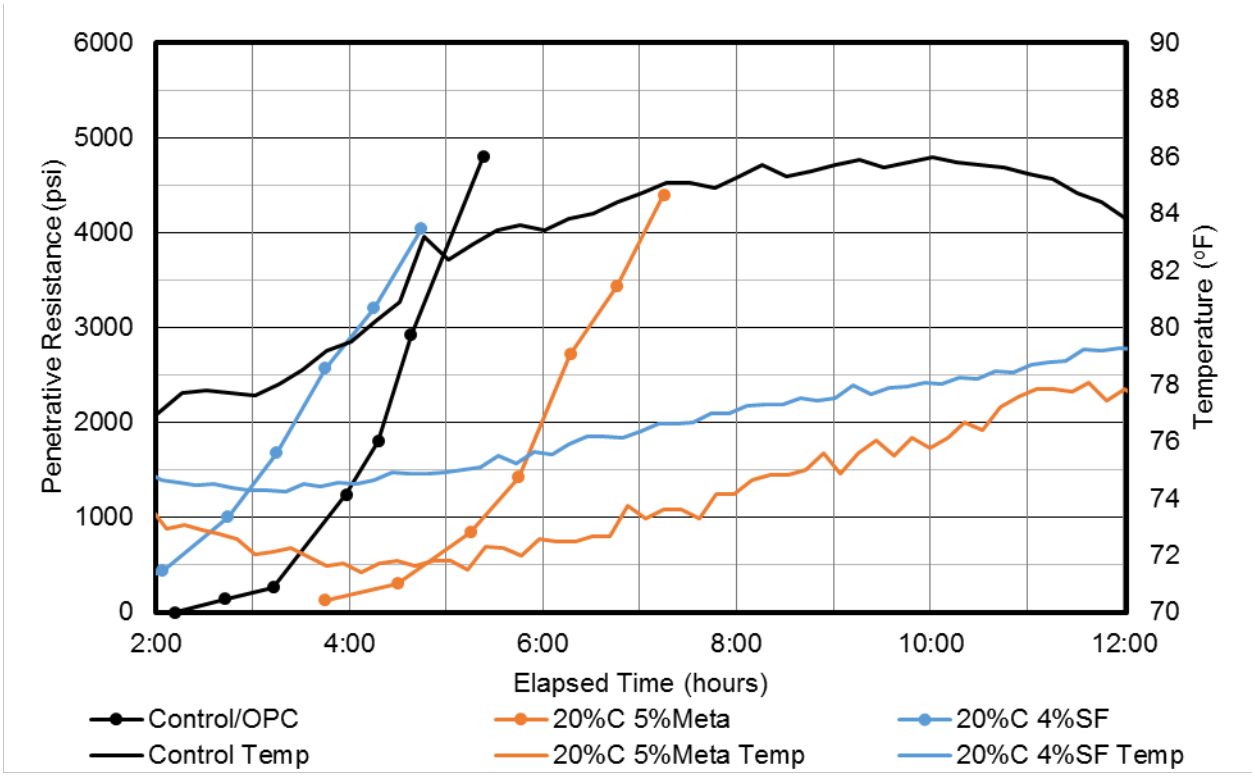

Figure C-167. Time of set of ternary mortars containing 20% C ash.

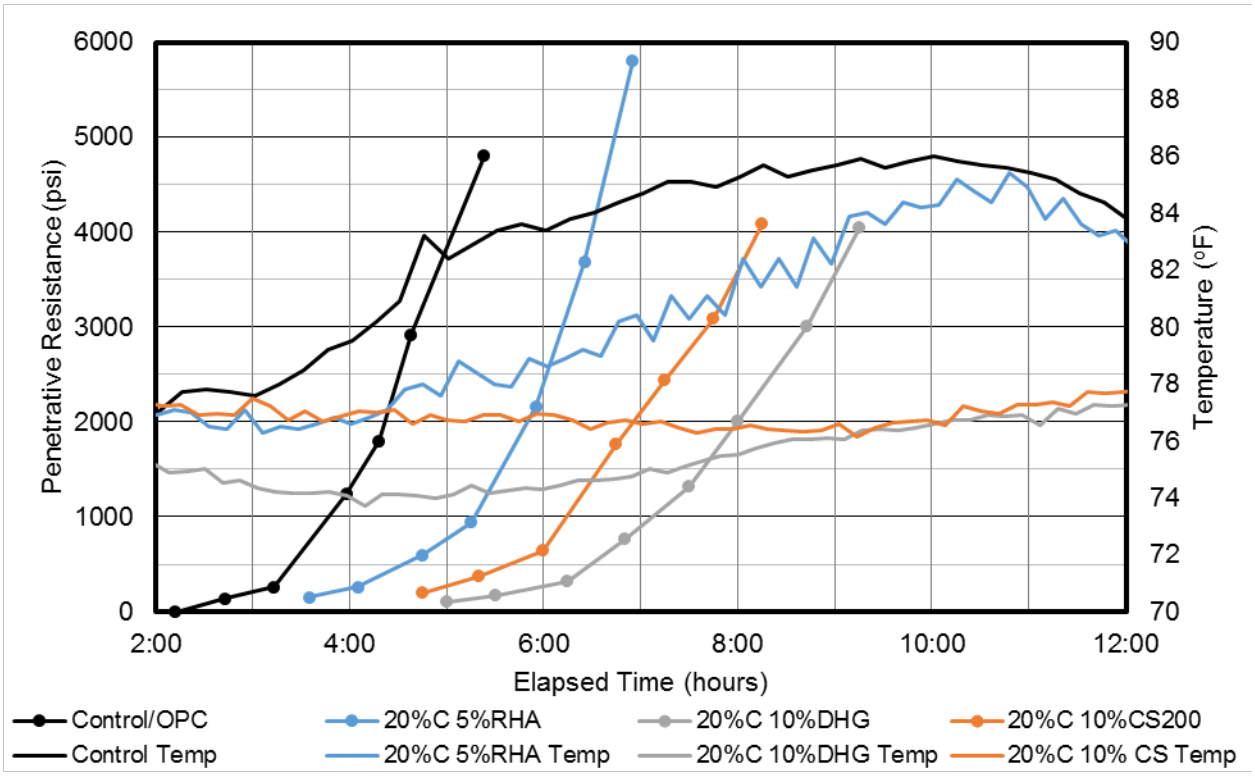

Figure C-168. Time of set of ternary blended mortar containing 20% C ash.

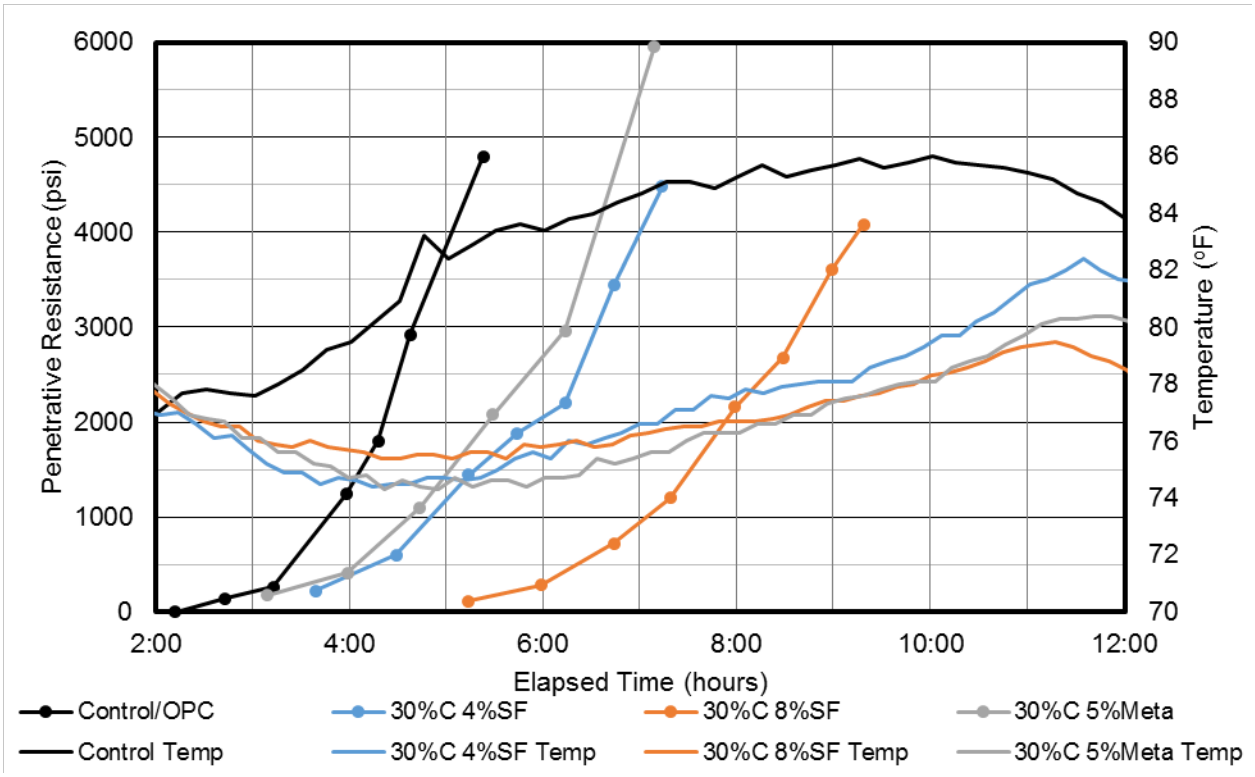

Figure C-169. Time of set of ternary blended mortar containing 30% C ash.

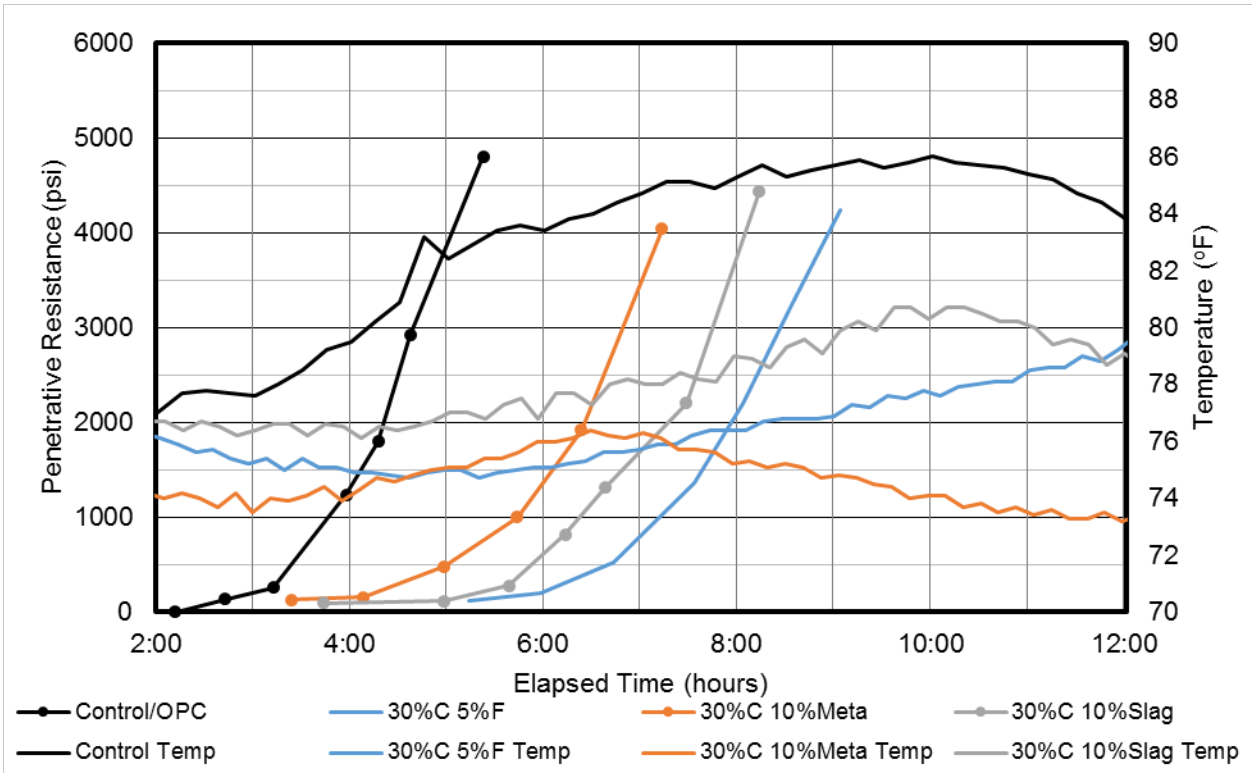

Figure C-170. Time of set of ternary blended mortar containing 30% C ash.

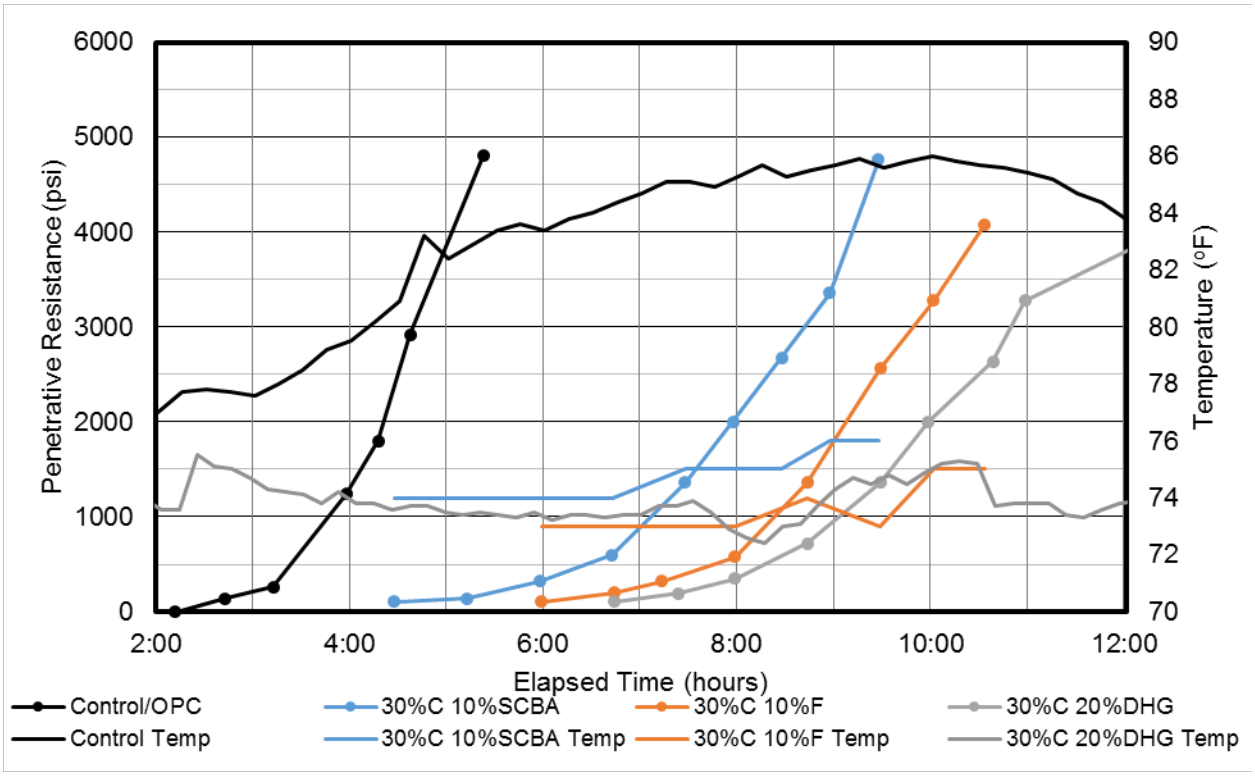

Figure C-171. Time of set of ternary blended mortar containing 30% C ash.

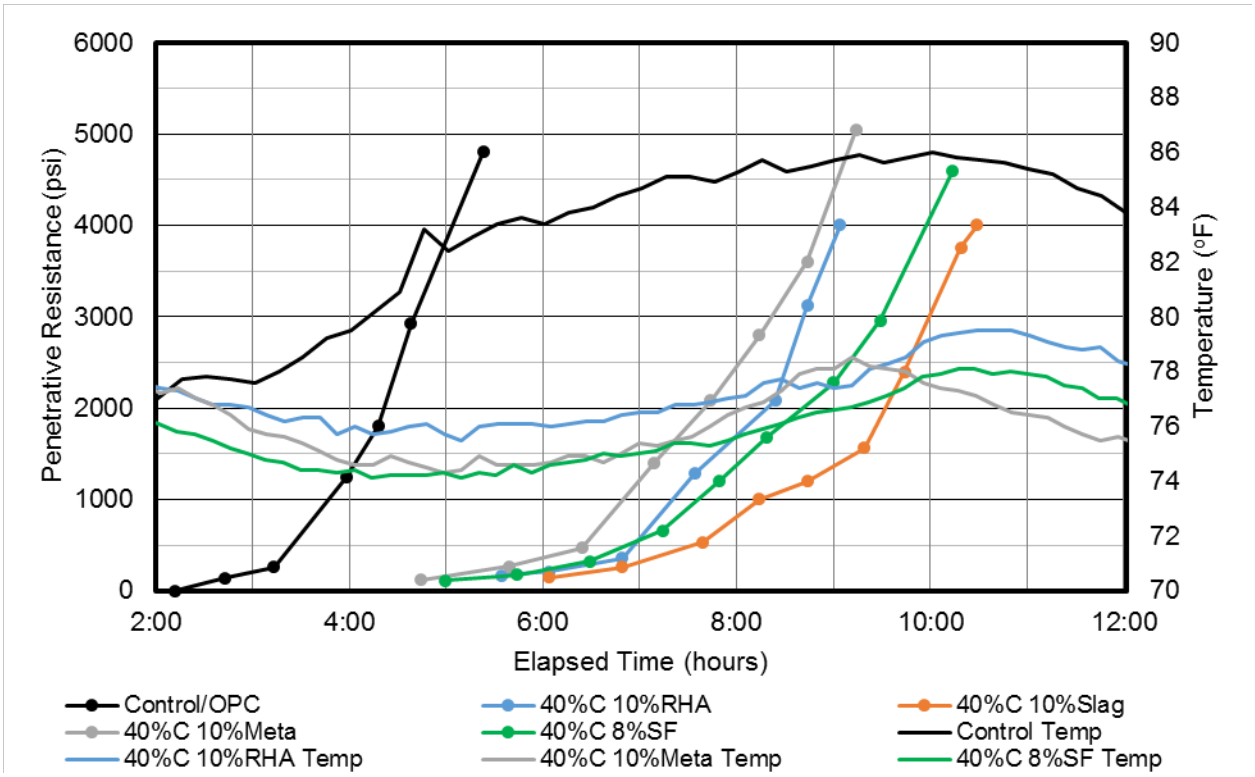

Figure C-172. Time of set of ternary blended mortar containing 40% C ash.

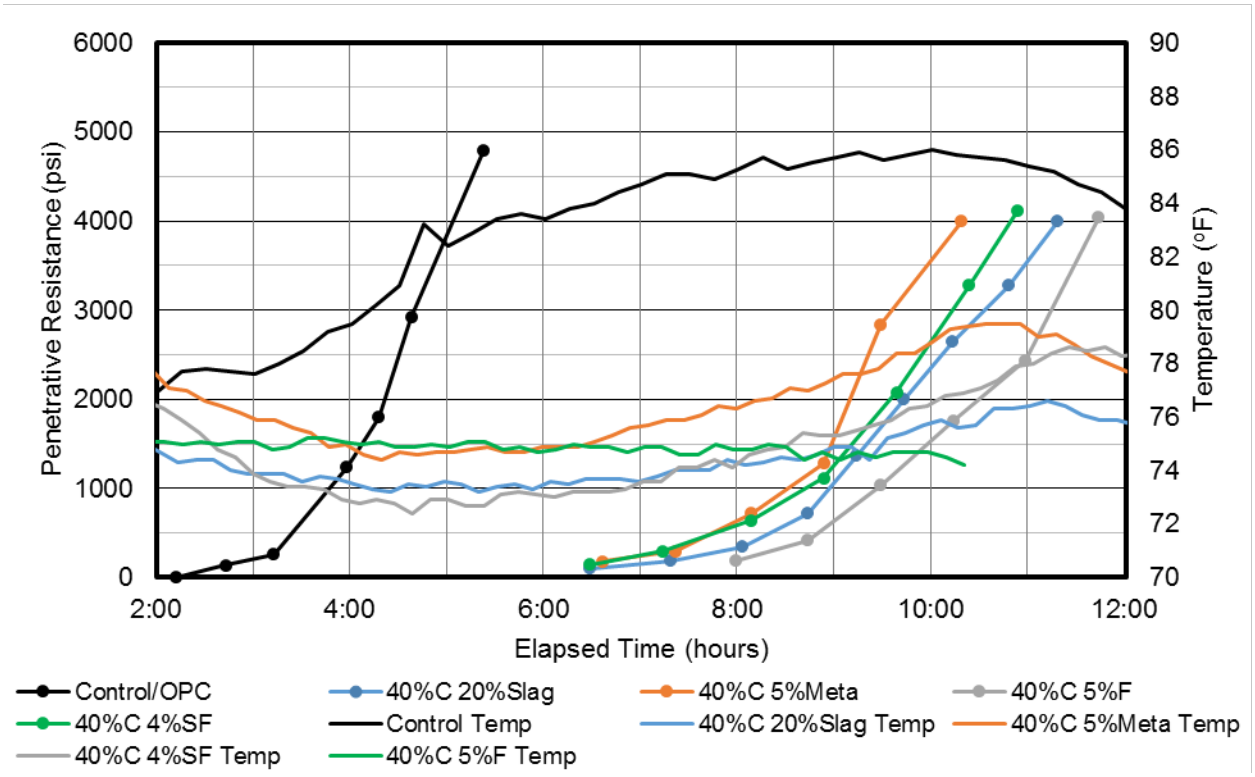

Figure C-173. Time of set of ternary blended mortar containing 40% C ash.

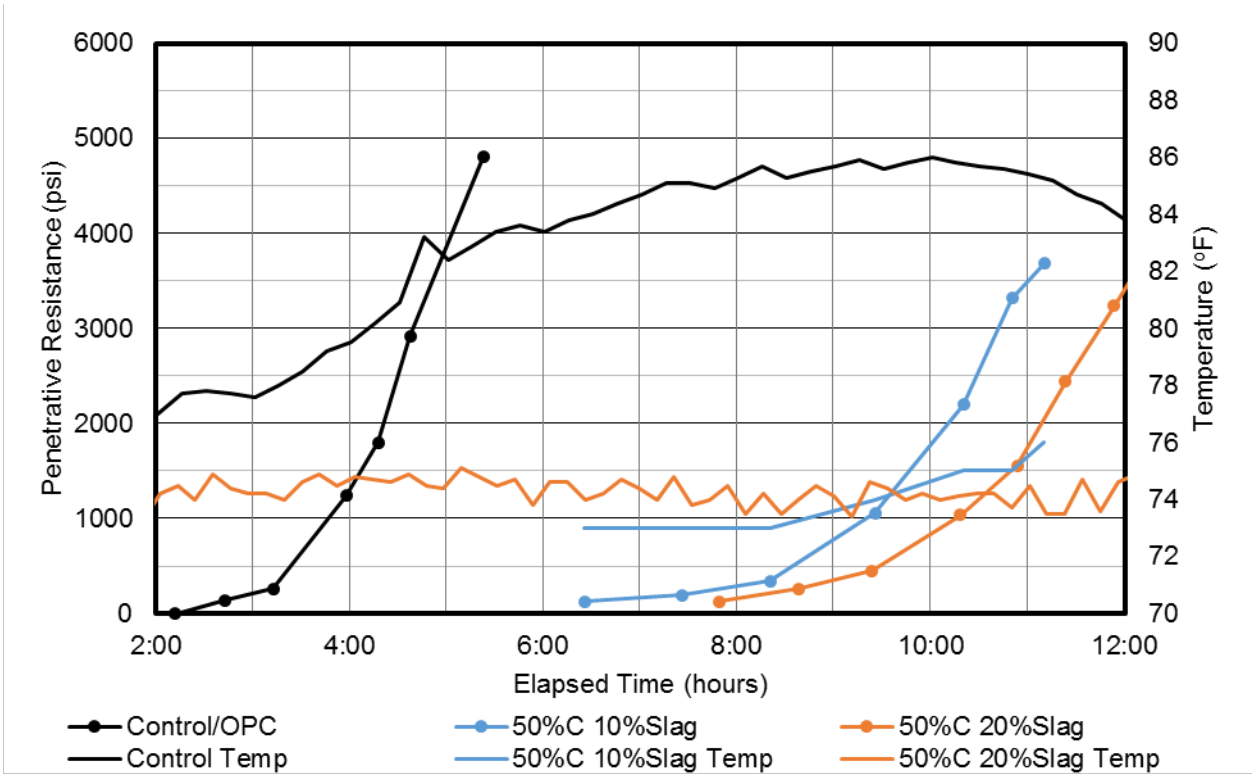

Figure C-174. Time of set of ternary blended mortar containing 50% C ash.

C.6. Length Change of Mortar Results

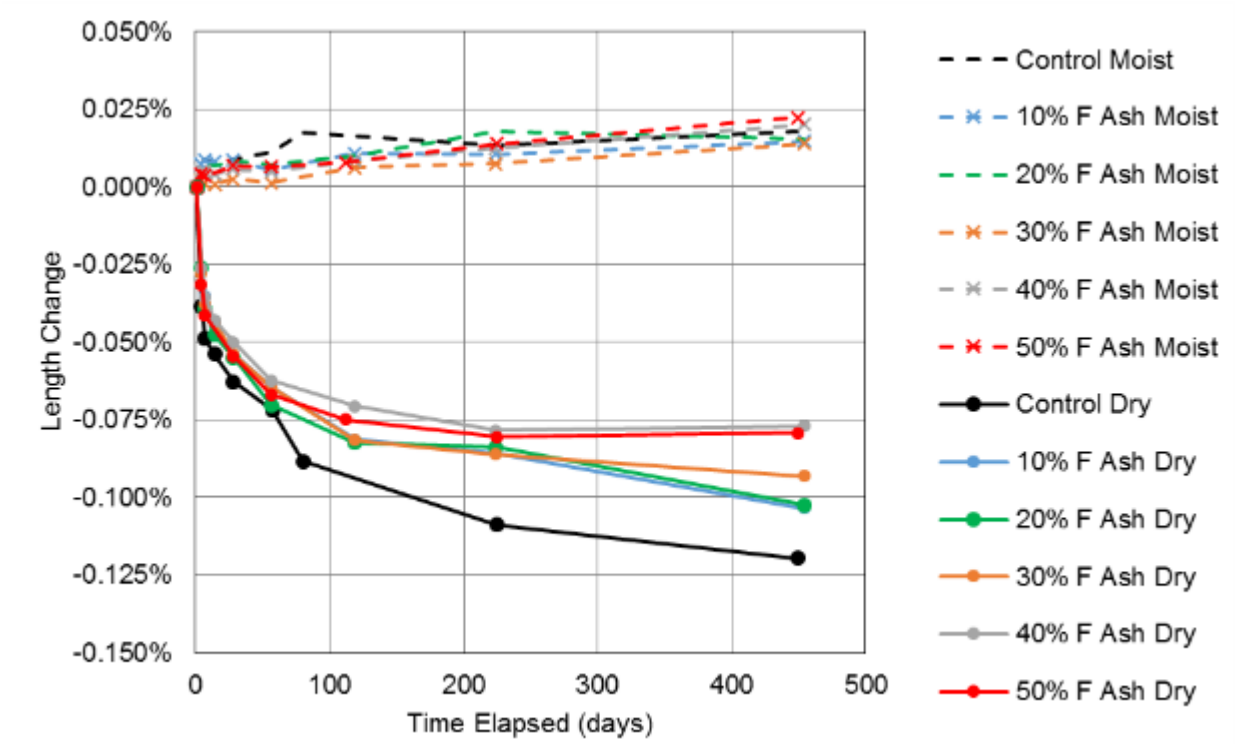

Figure C-175. Length change of mortars containing 10 - 50% class F fly ash.

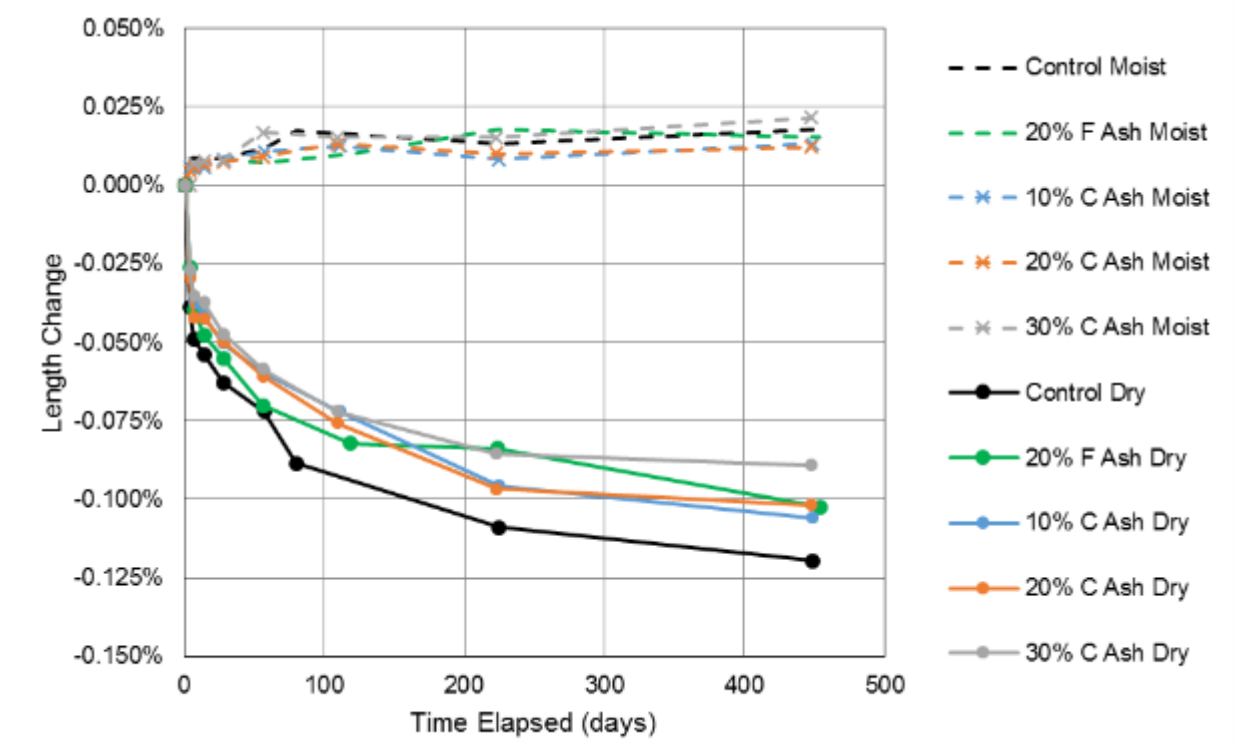

Figure C-176. Length change of mortars containing 10 - 30% class C fly ash.

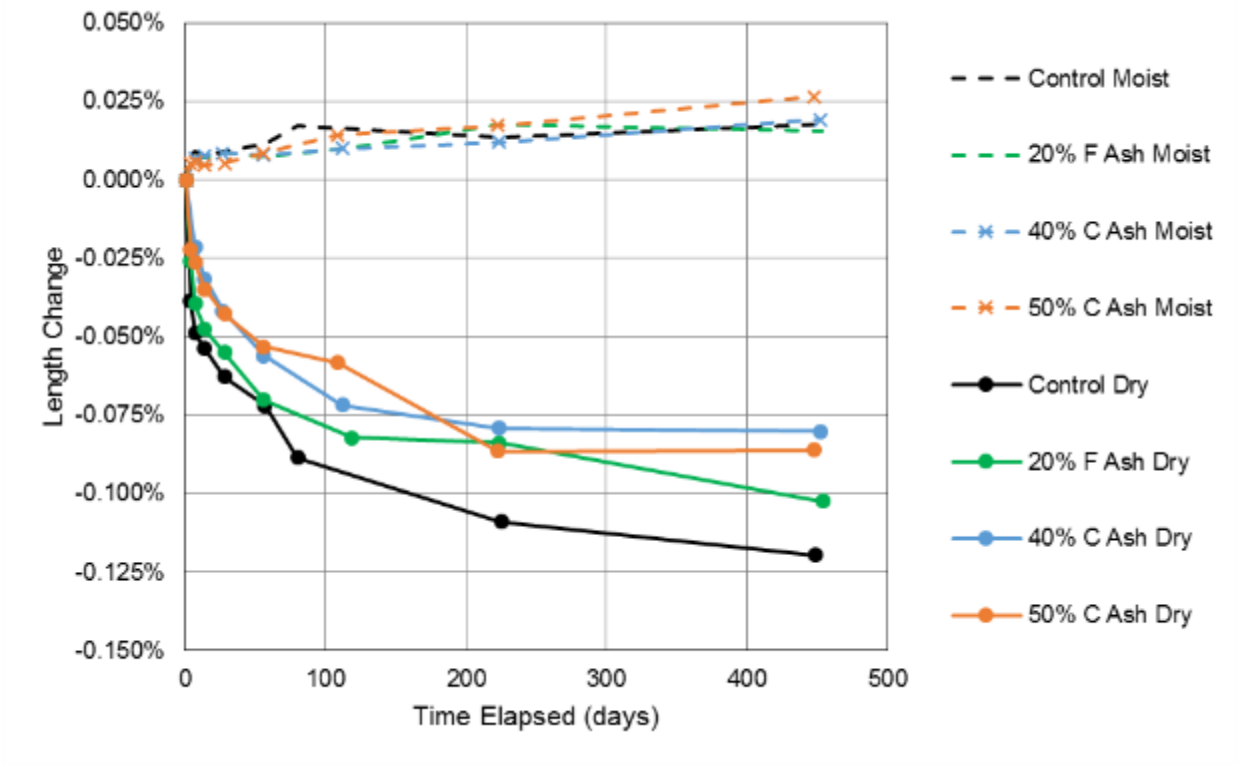

Figure C-177. Length change of mortars containing 40 - 50% class C fly ash.

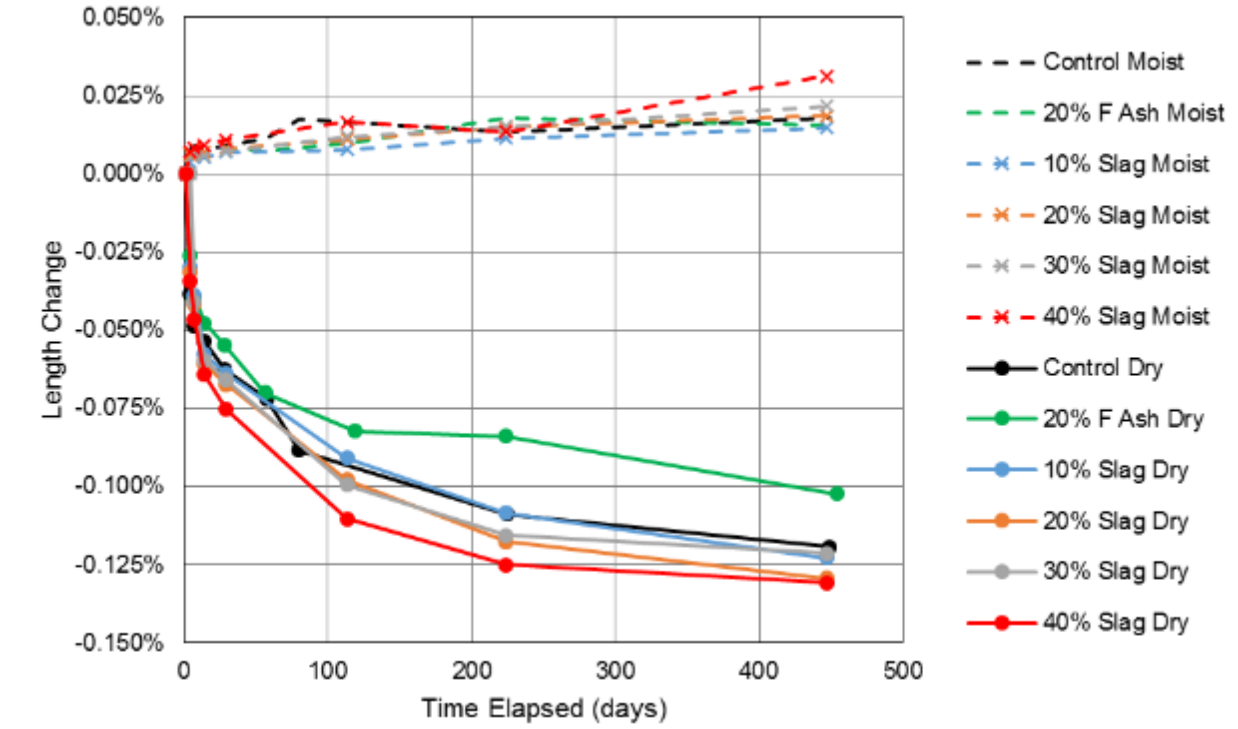

Figure C-178. Length change of mortars containing 10 - 40% ground blast furnace slag.

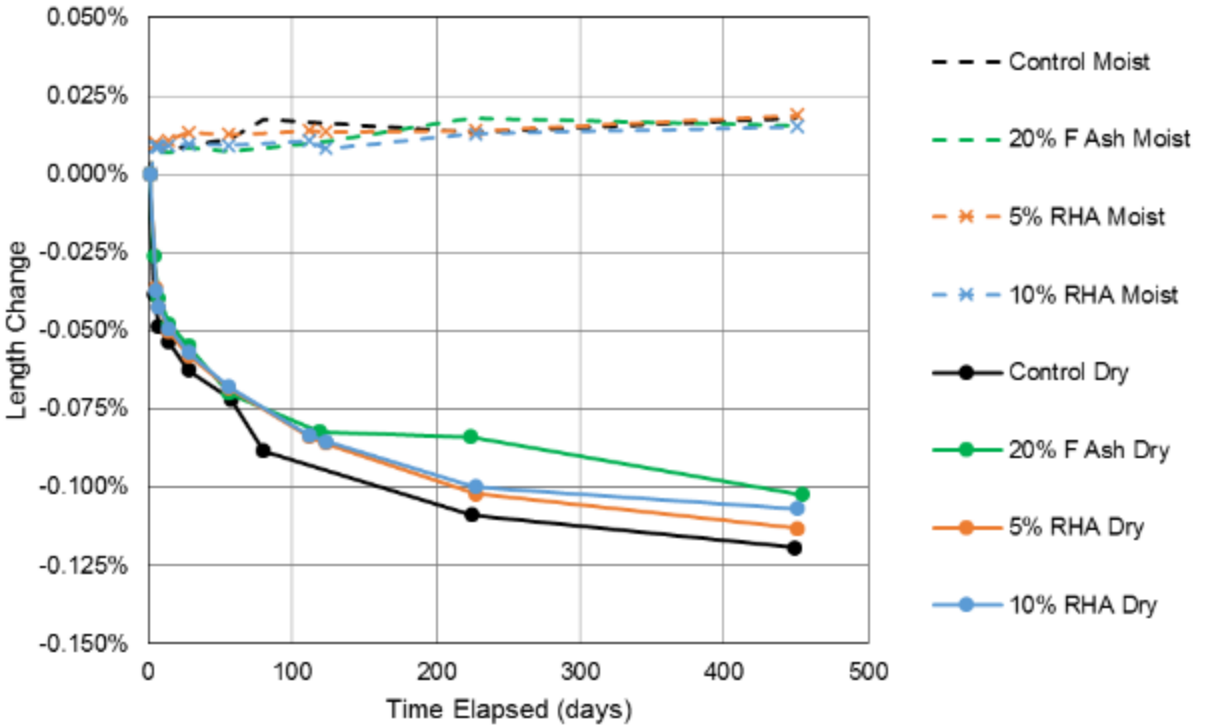

Figure C-179. Length change of mortars containing 5 - 10% rice husk ash.

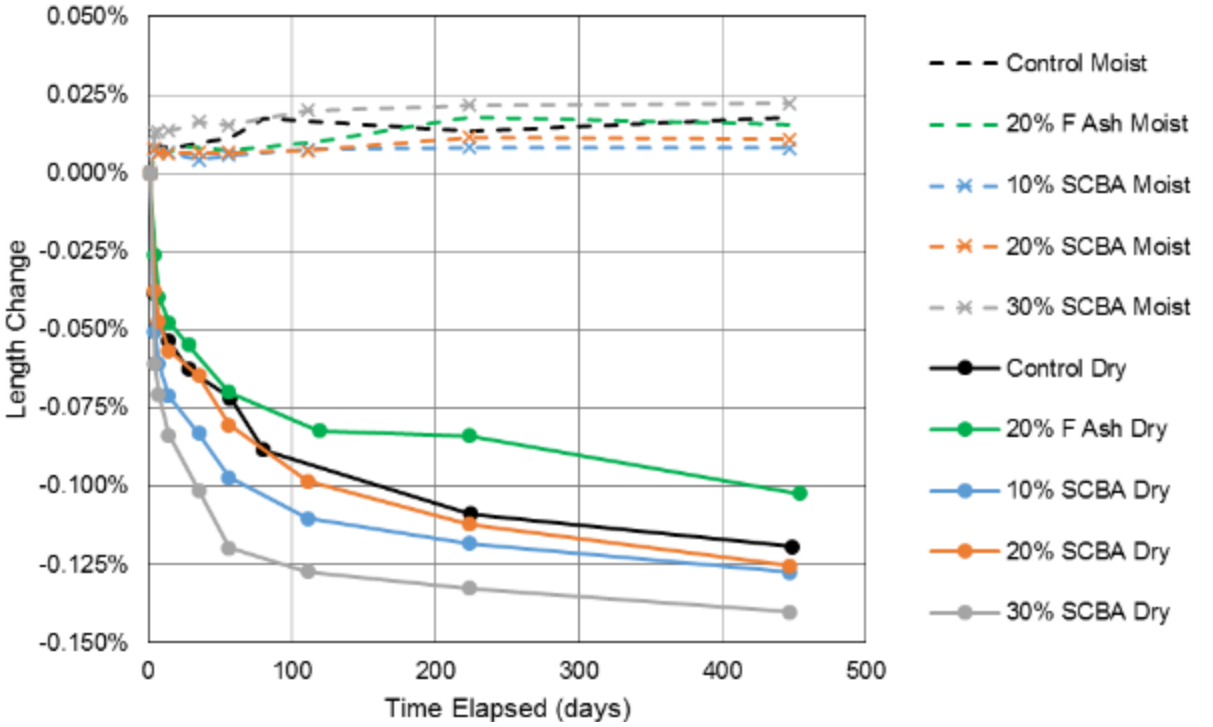

Figure C-180. Length change of mortars containing 10 - 30% sugarcane bagasse ash.

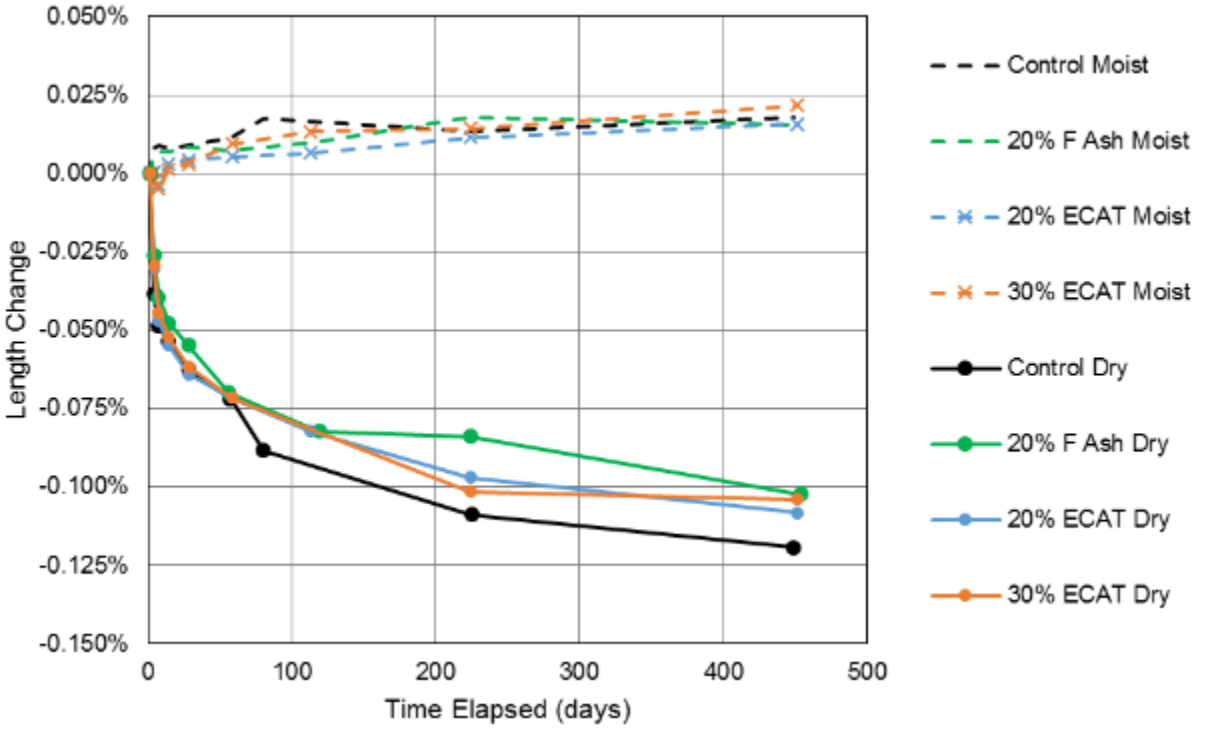

Figure C-181. Length change of mortars containing 20 - 30% equilibrium catalyst.

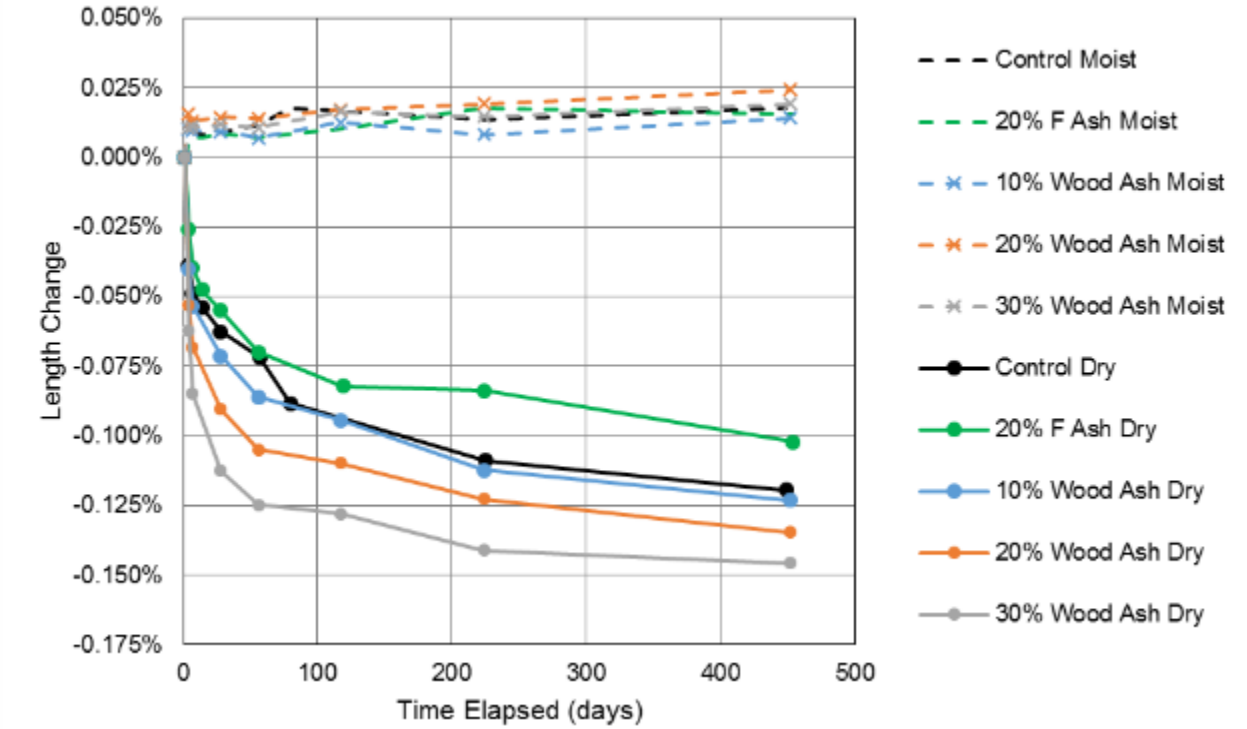

Figure C-182. Length change of mortars containing 10 - 30% wood ash.

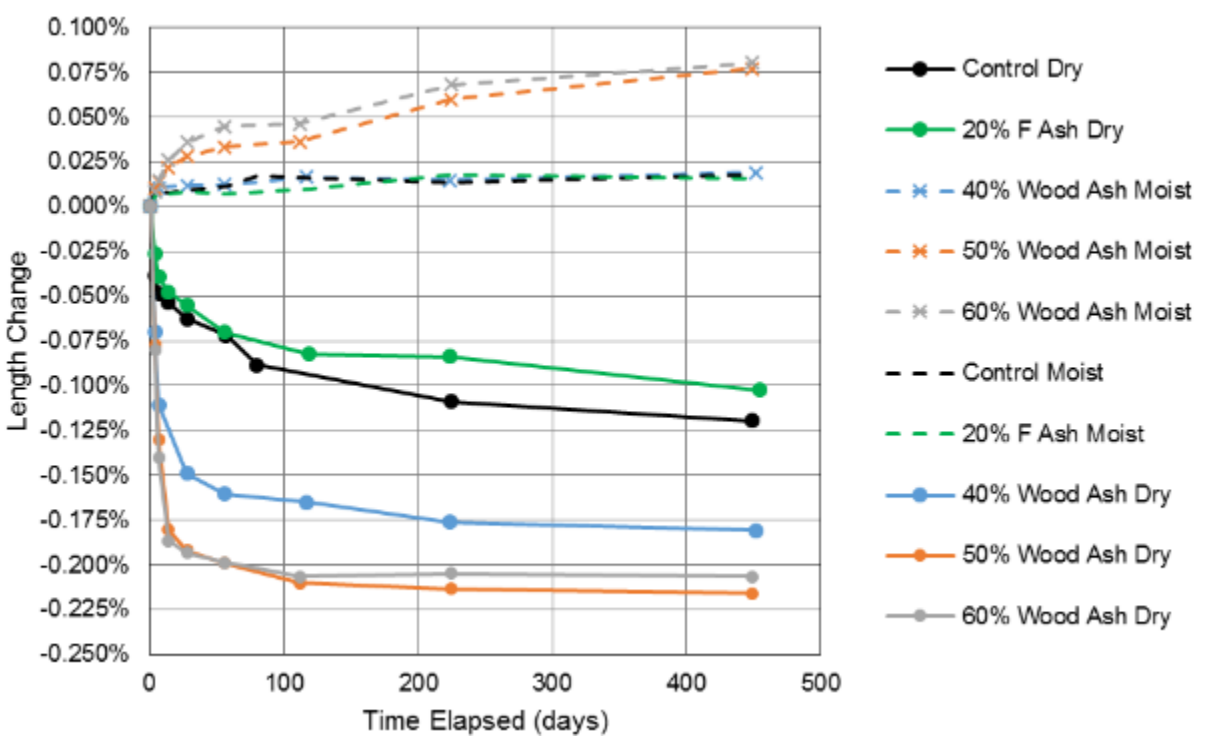

Figure C-183. Length change of mortars containing 40 - 60% wood ash.

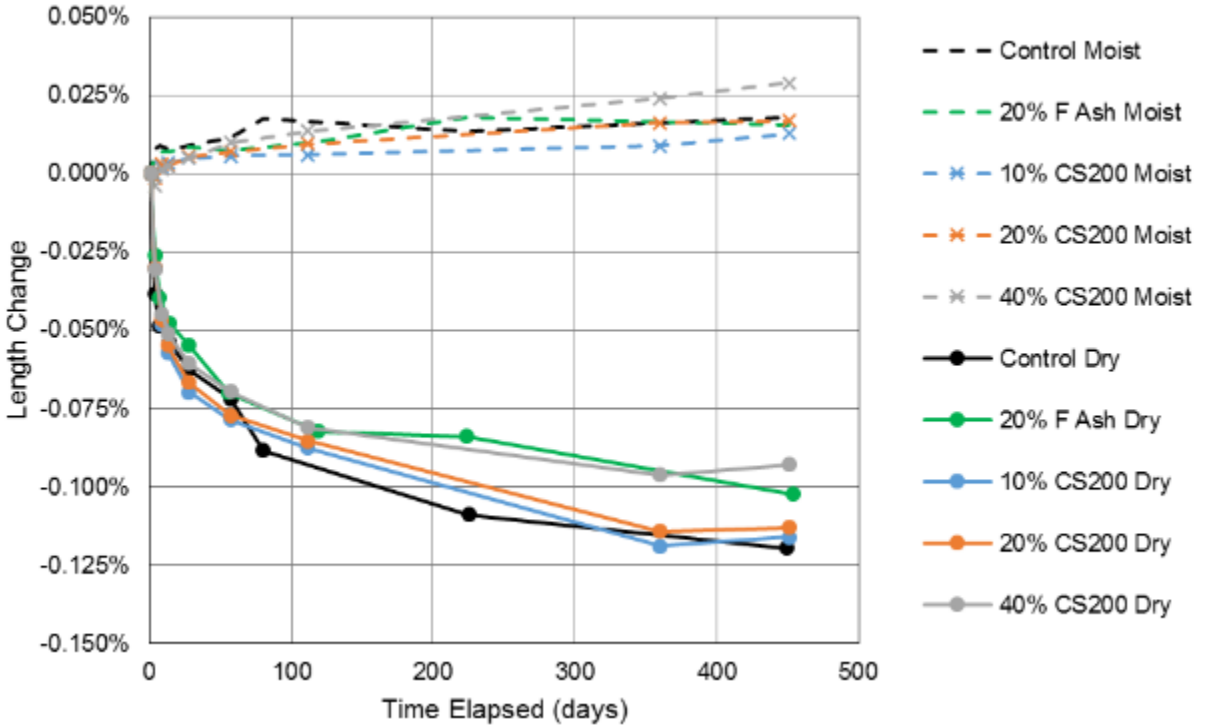

Figure C-184. Length change of mortars containing 10 - 40% CS200 glass powder.

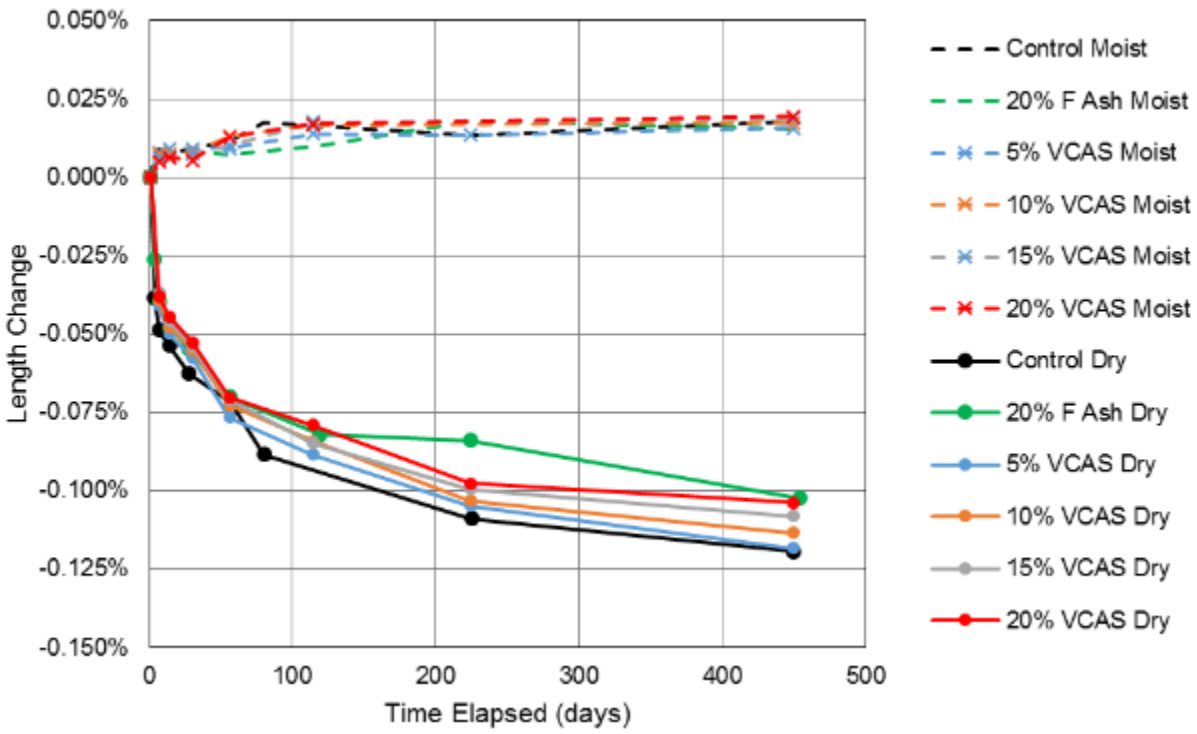

Figure C-185. Length change of mortars containing 5 - 20% VCAS160 glass powder.

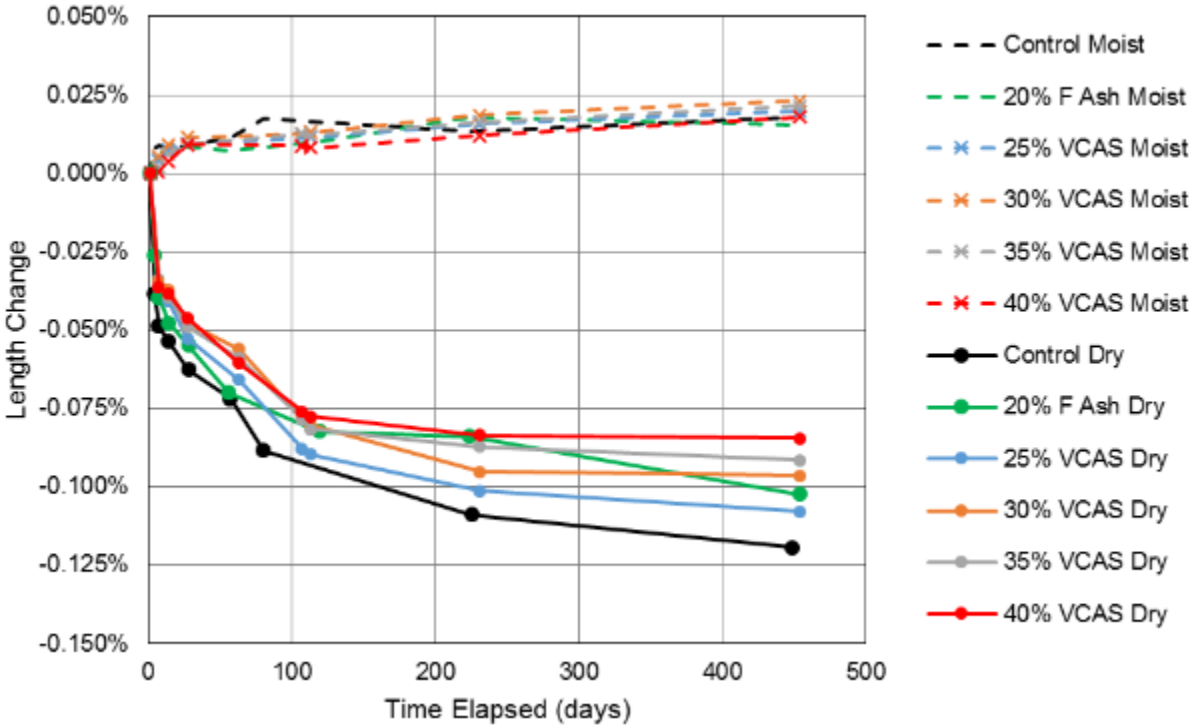

Figure C-186. Length change of mortars containing 25 0 40% VCAS160 glass powder.

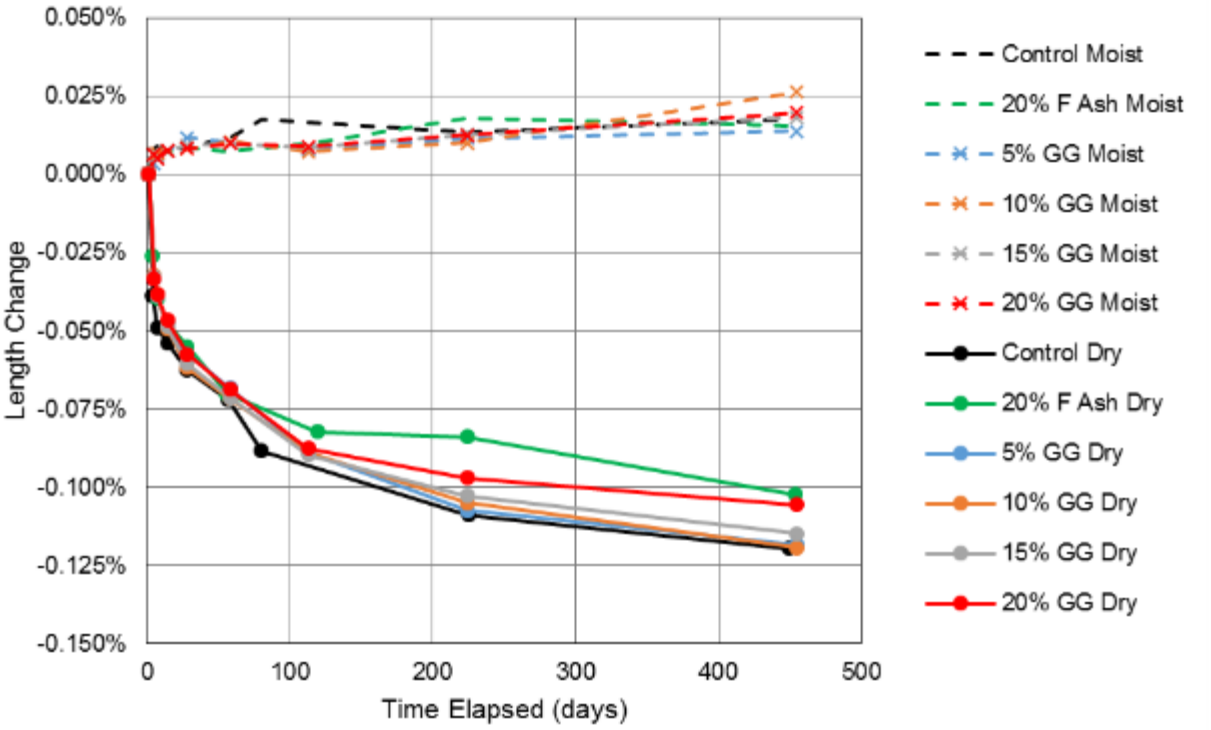

Figure C-187. Length change of mortars containing 5 - 20% ground glass powder.

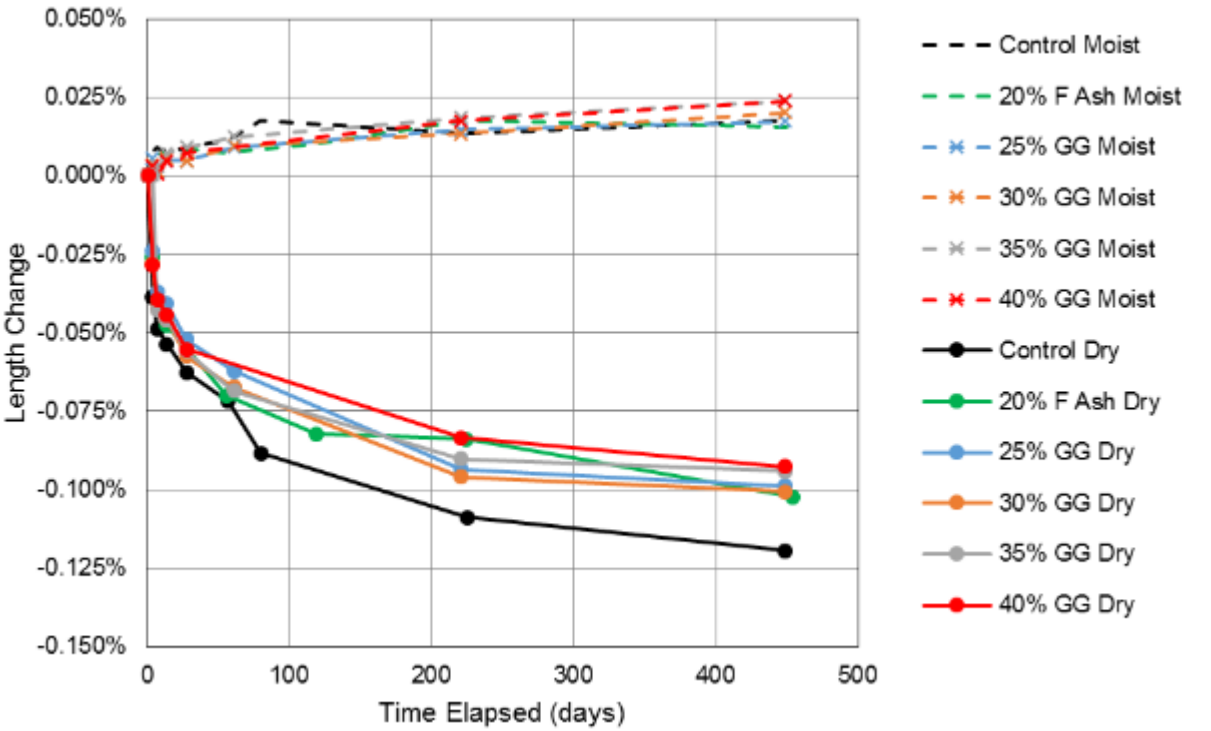

Figure C-188. Length change of mortars containing 25 - 40% ground glass powder.

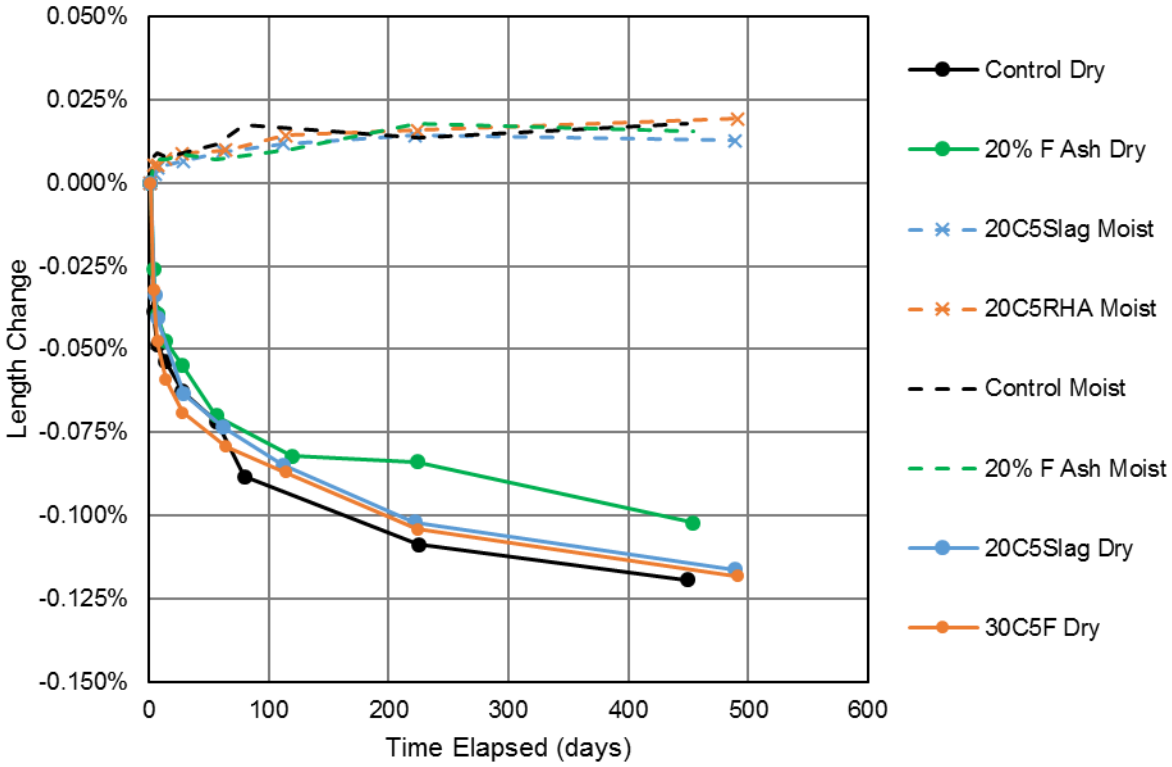

Figure C-189. Length change of mortars containing 20% class C fly ash and 5% of either slag or rice husk ash.

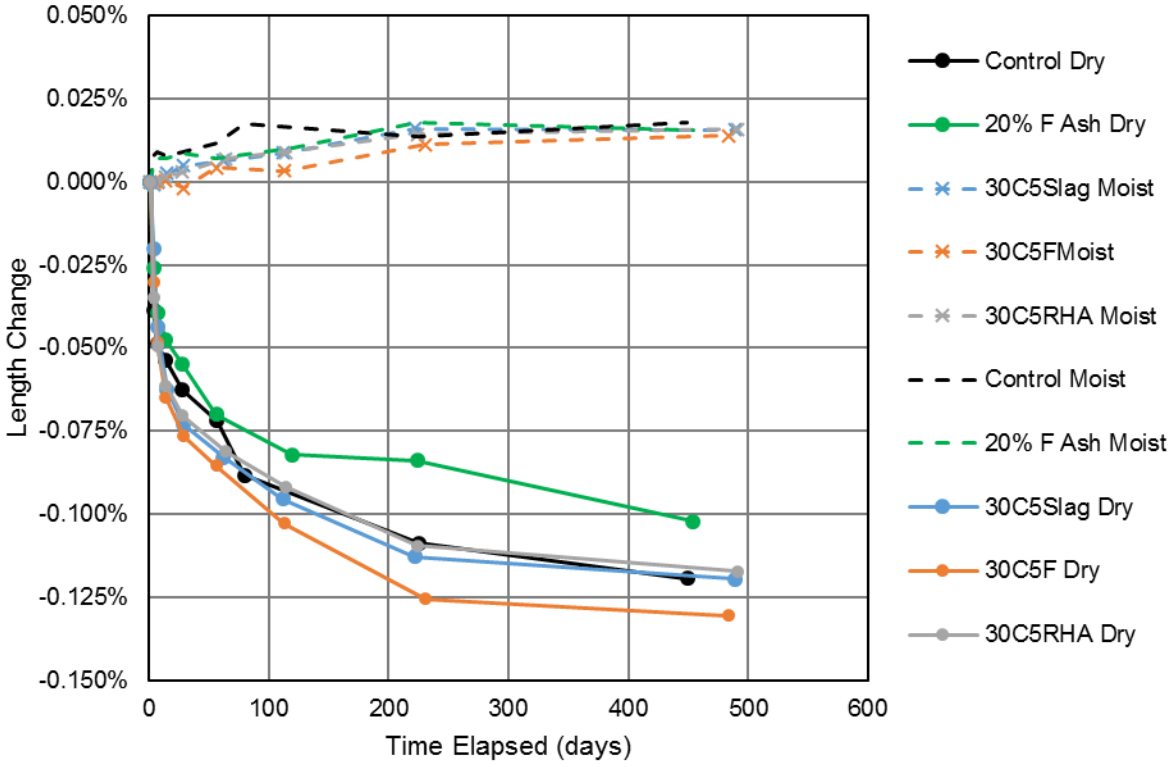

Figure C-190. Length change of mortars containing 30% class C fly ash and 5% of either slag, class F fly ash, or rice husk ash.

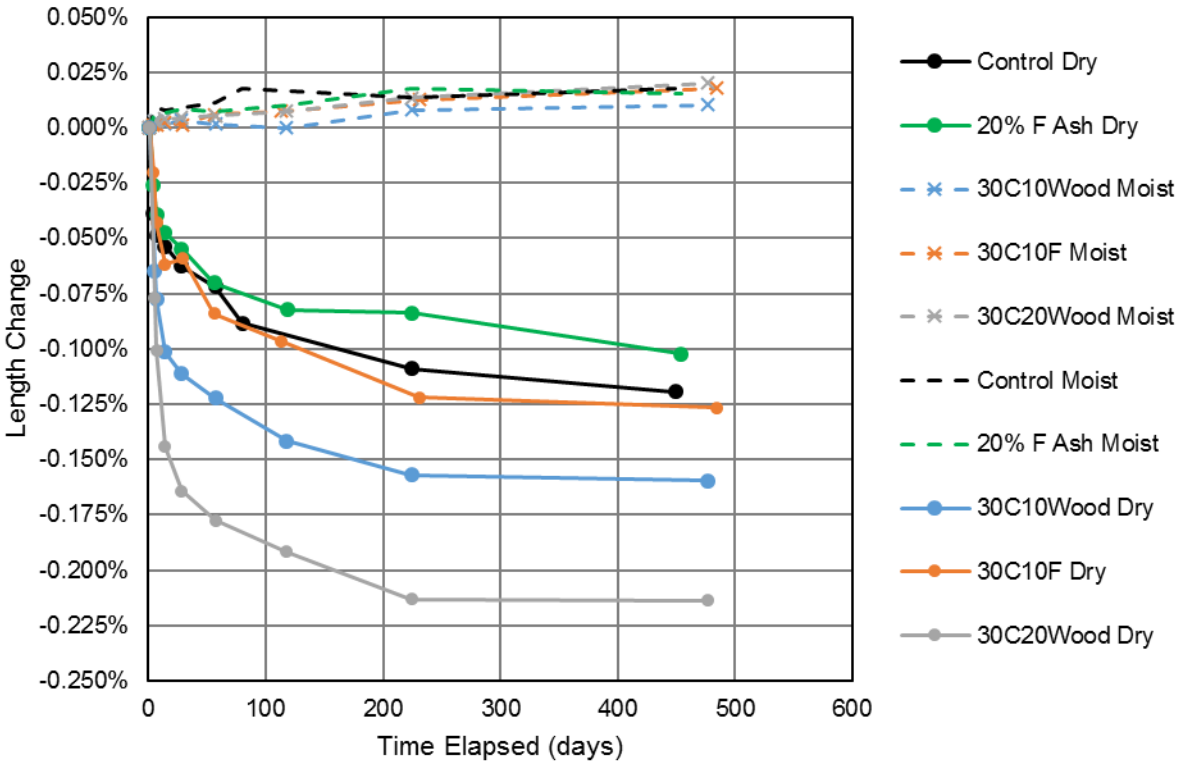

Figure C-191. Length change of mortars containing 30% class C fly ash and 10% - 20% class F fly ash or wood ash.

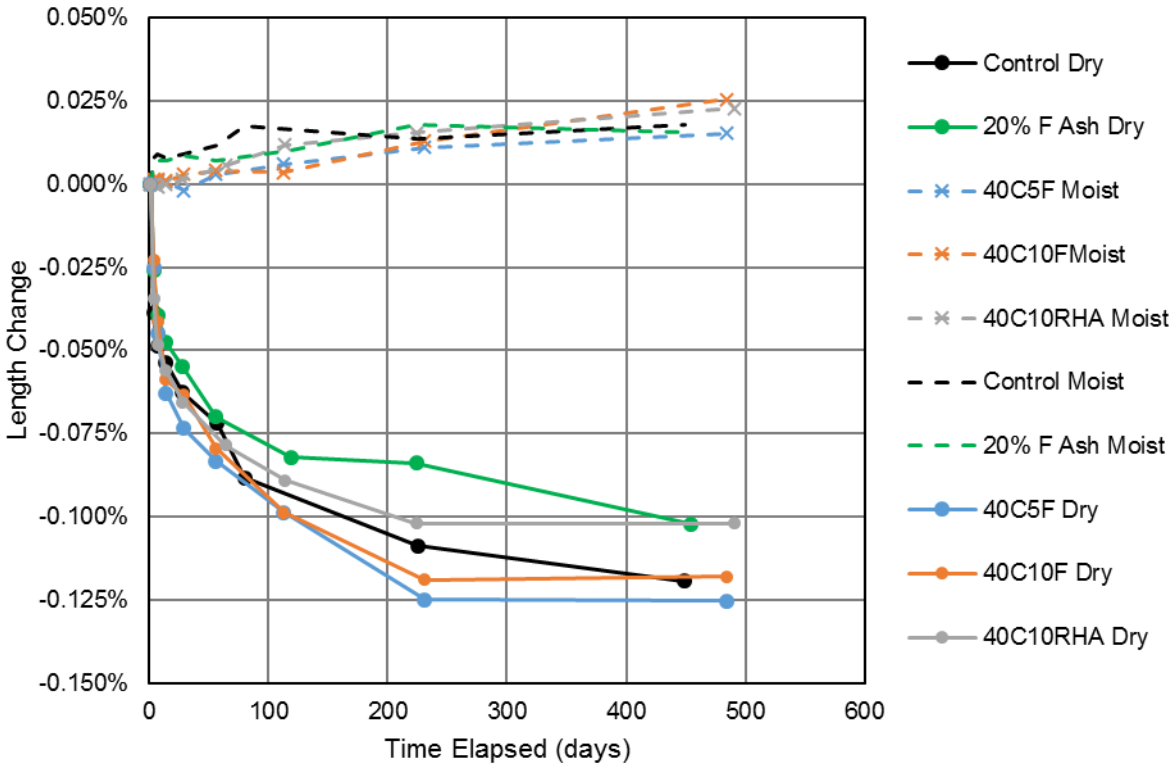

Figure C-192. Length change of mortars containing 40% class C fly ash and 5% - 10% of either class F fly ash or rice husk ash.

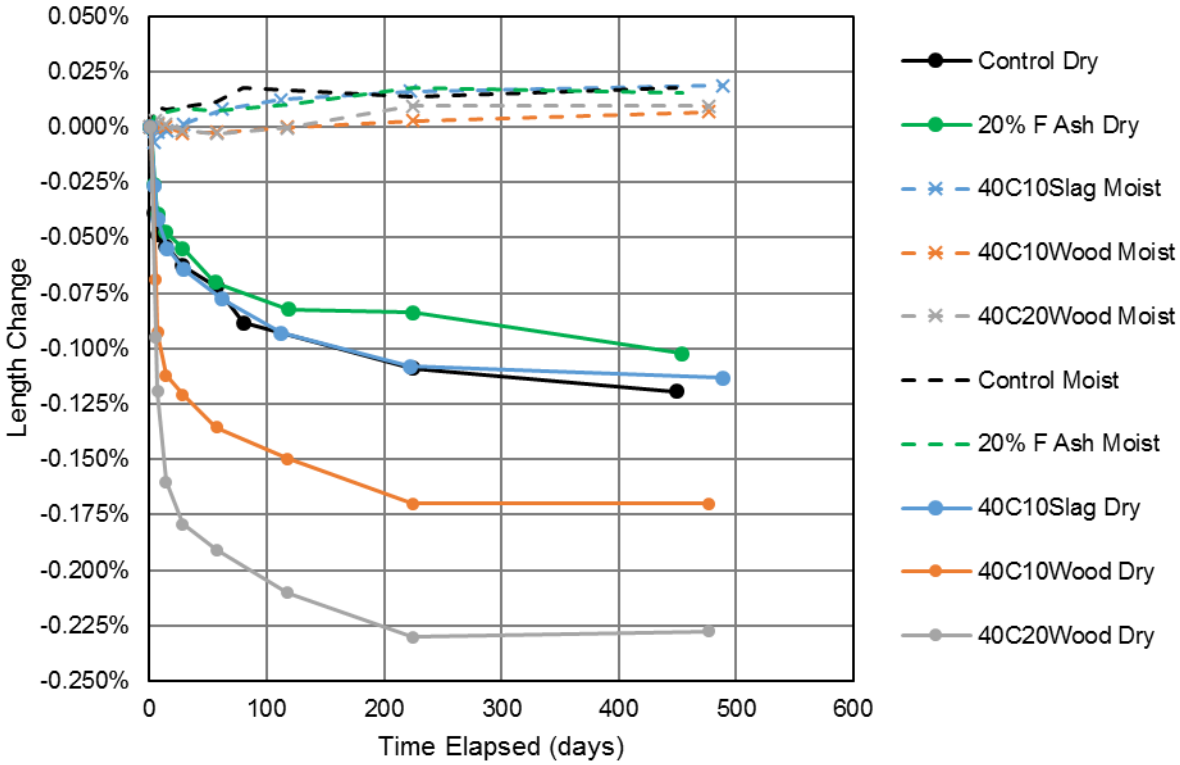

Figure C-193. Length change of mortars containing 40% class C fly ash and 10% - 20% of either slag or wood ash.

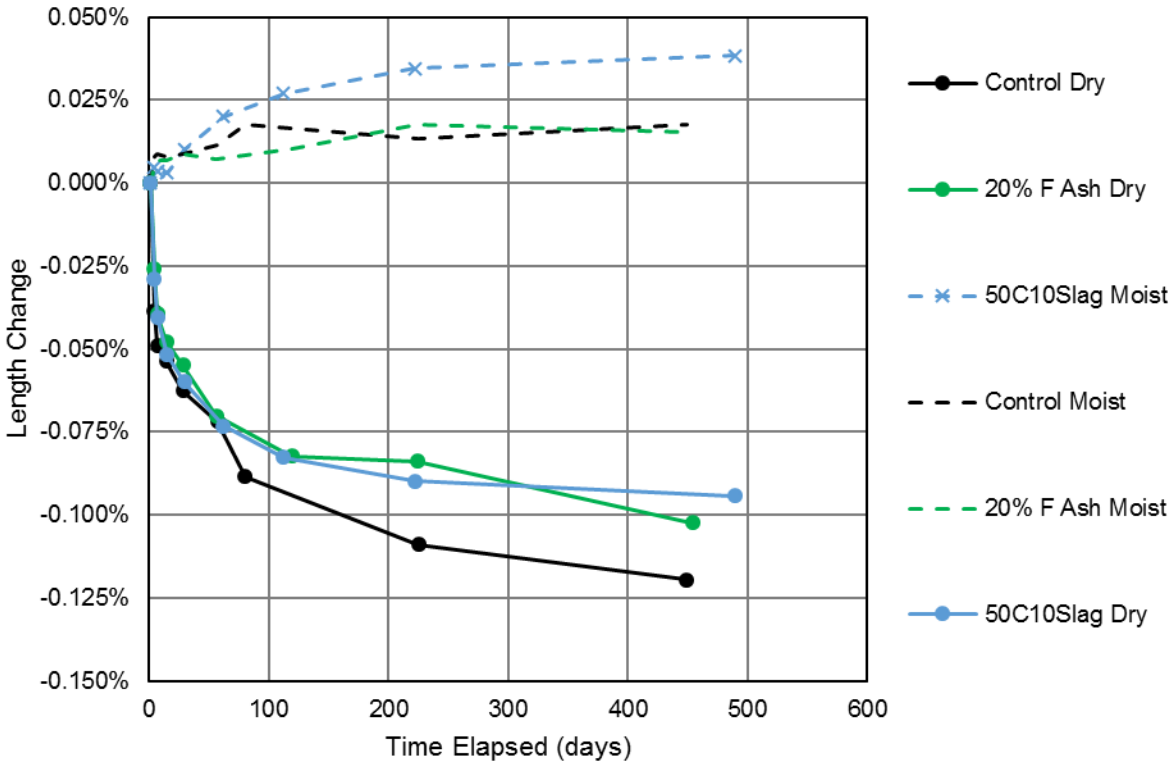

Figure C-194. Length change of mortars containing 50% class C fly ash and 10% slag.

C.7. Accelerated Length Change (ASR Reactivity) of Mortars Results

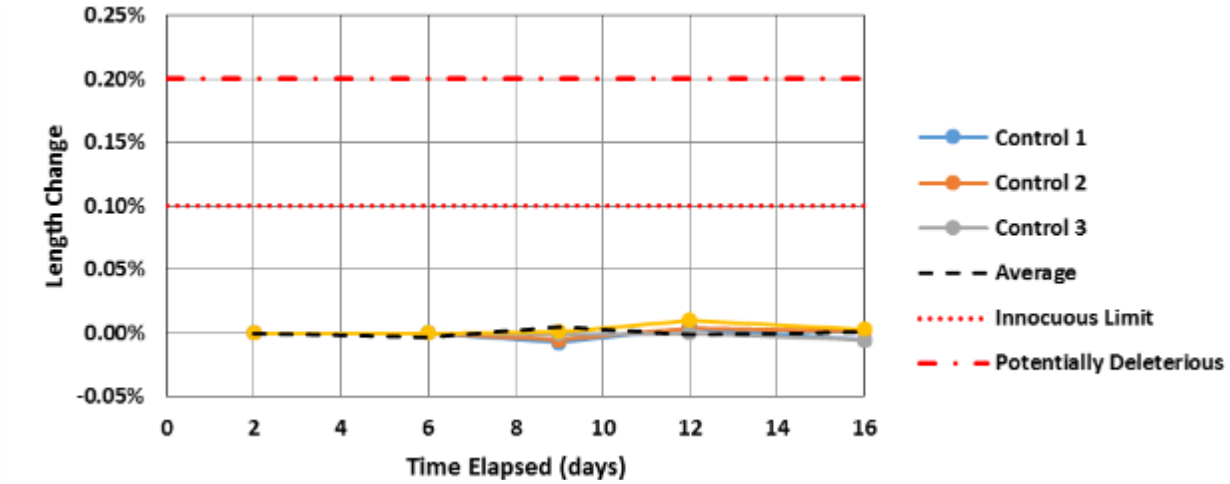

Figure C-195. Accelerated length change of the control mortar specimens.

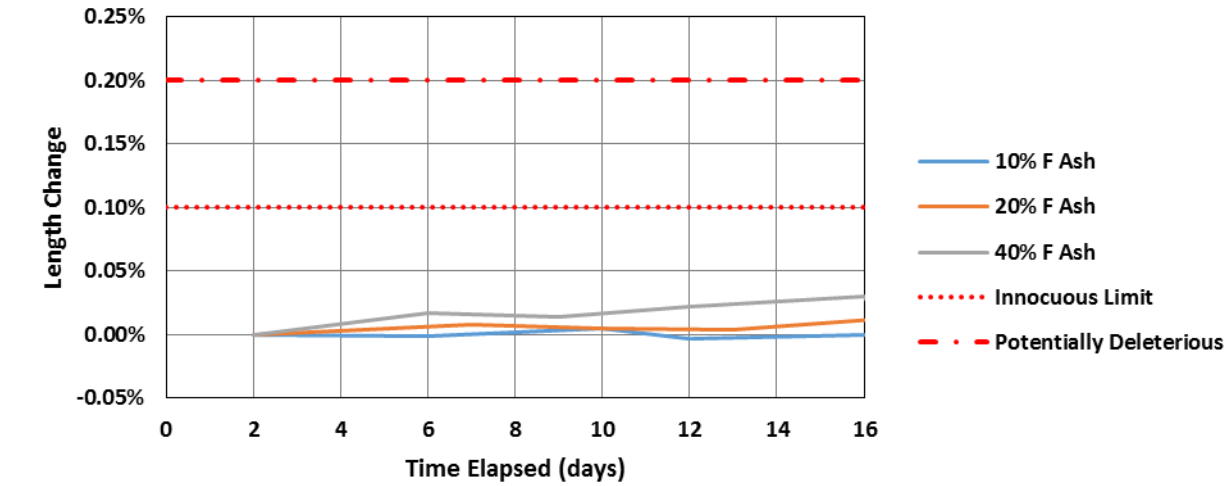

Figure C-196. Accelerated length change of mortars containing 10 - 40% class F fly ash.

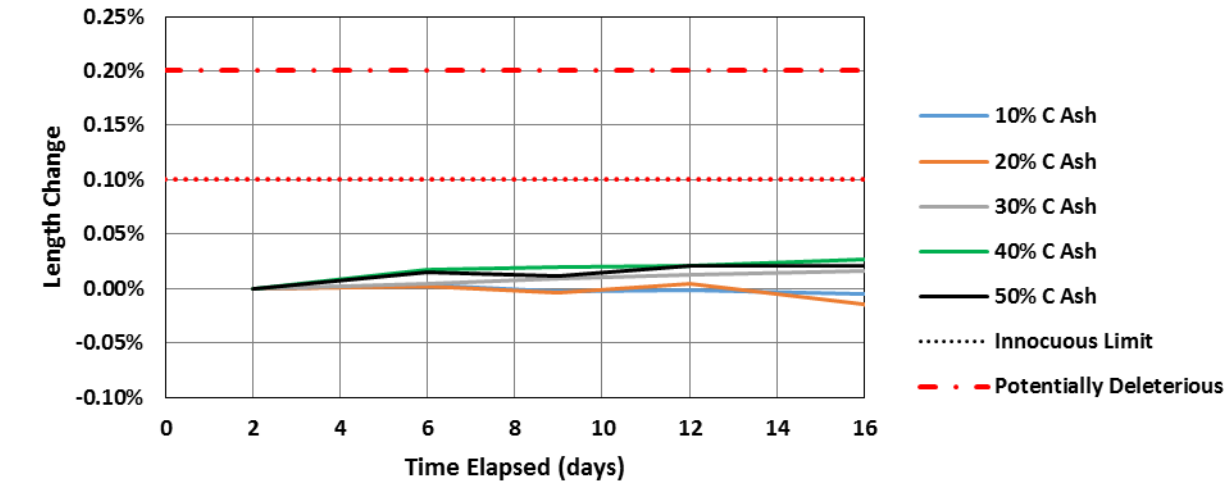

Figure C-197. Accelerated length change of mortars containing 10 - 50% class C fly ash.

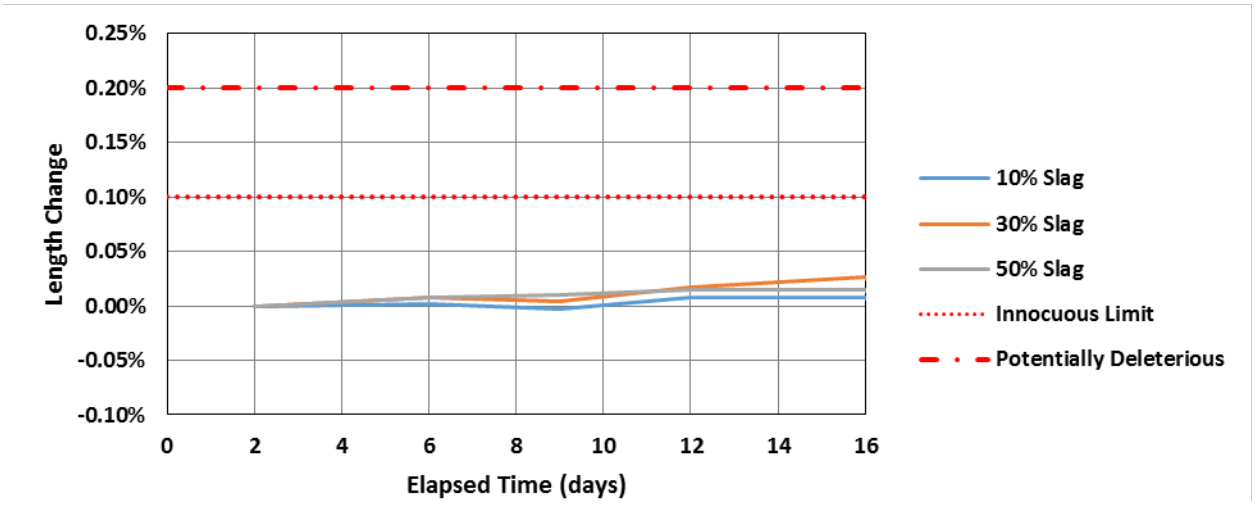

Figure C-198. Accelerated length change of mortars containing 10 - 50% ground blast furnace slag.

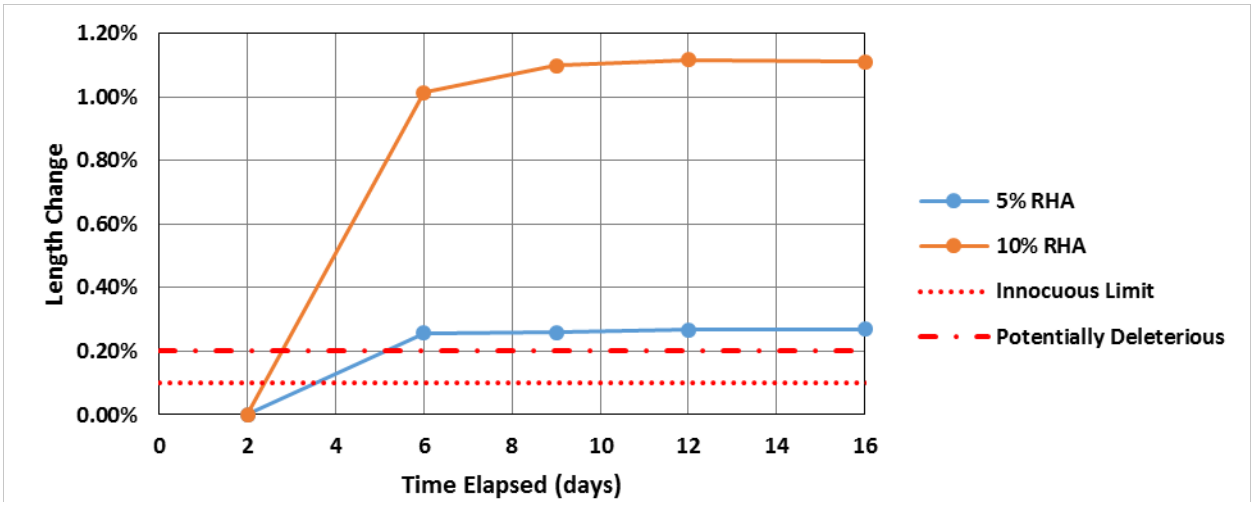

Figure C-199. Length change of mortars containing 5 and 10% rice husk ash.

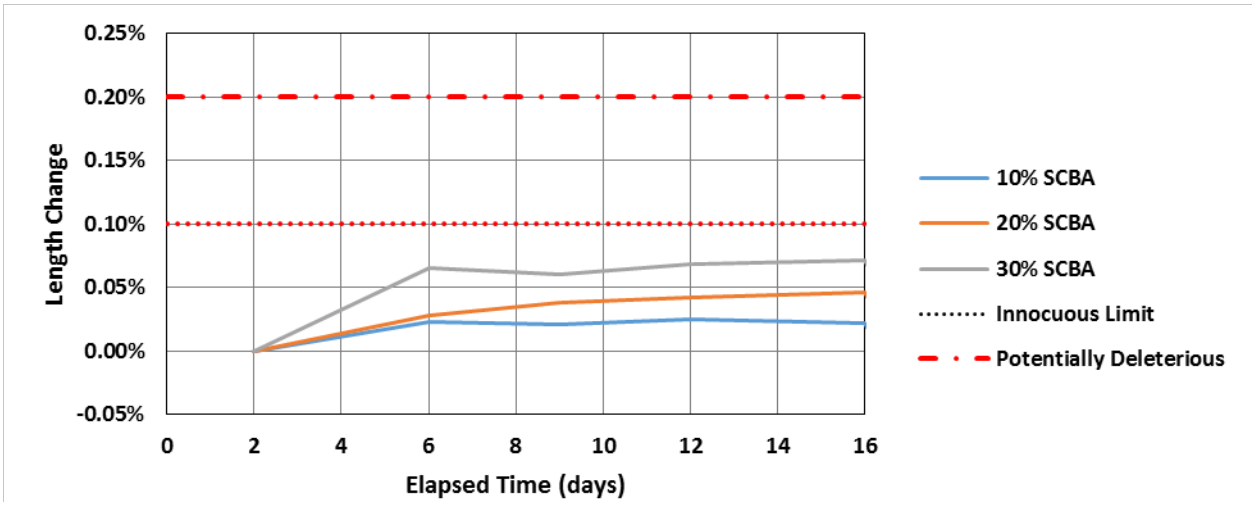

Figure C-200. Length change of mortars containing 10 - 30% sugarcane bagasse ash.

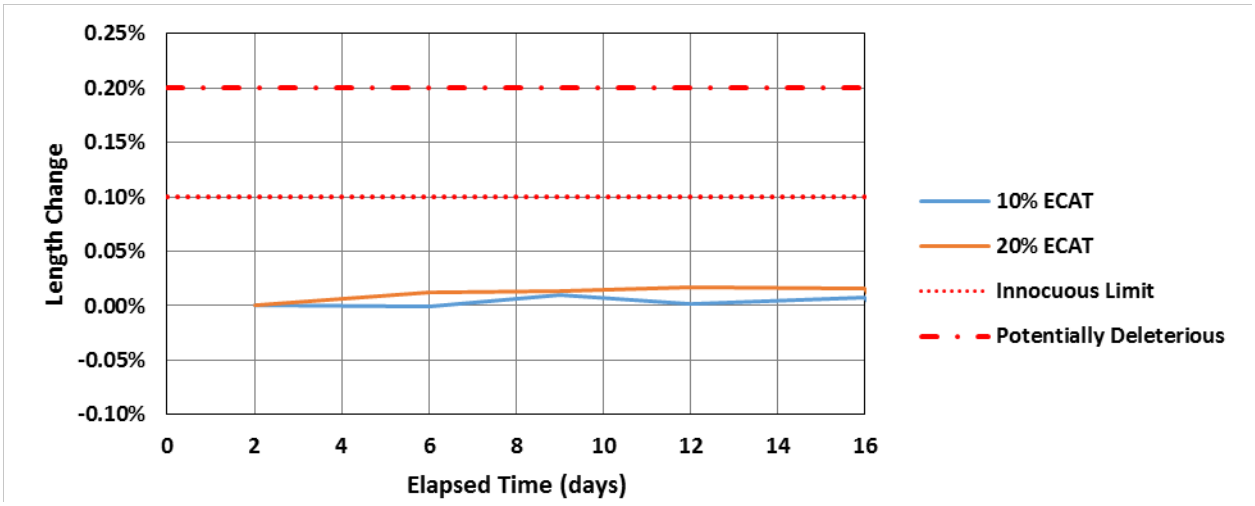

Figure C-201. Length change of mortars containing 10 and 20% equilibrium catalyst.

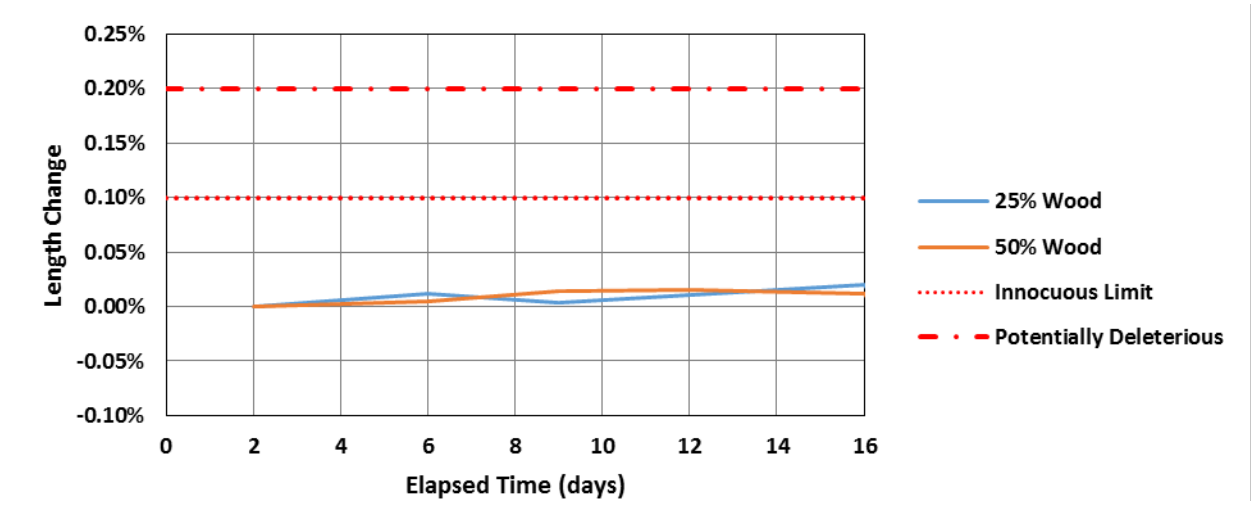

Figure C-202. Length change of mortars containing 25 and 50% wood ash.

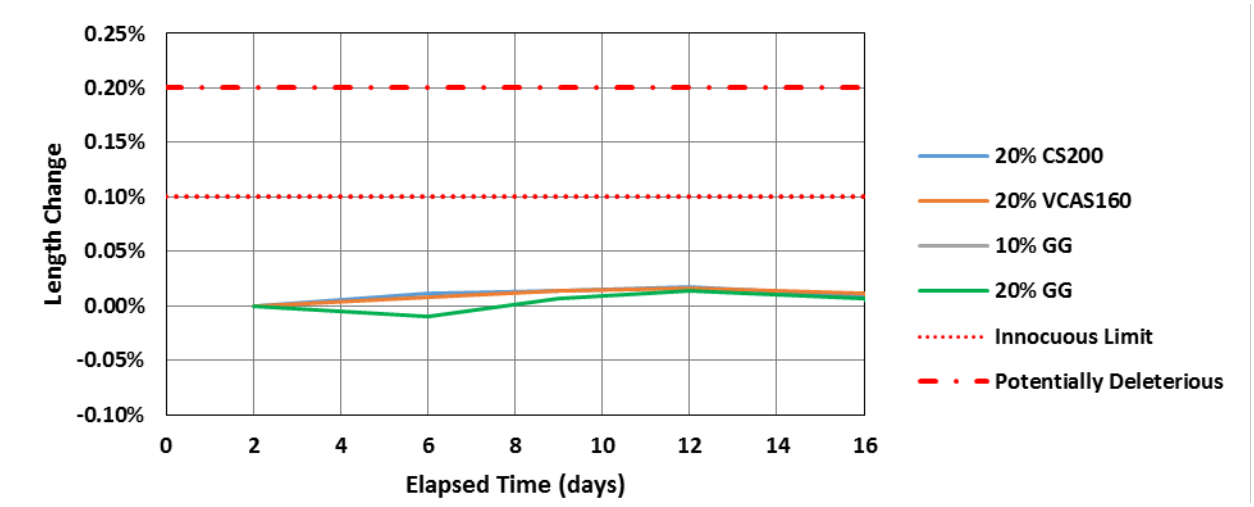

Figure C-203. Length change of mortars containing 20% CS200, 20% VCAS160, and 10 - 20%

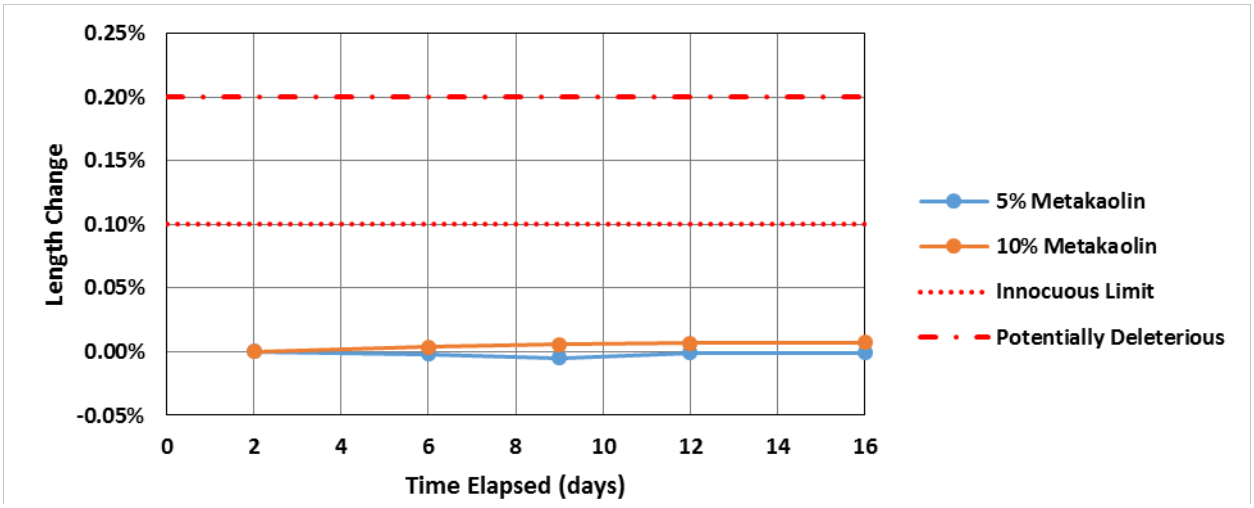

Figure C-204. Accelerated length change of mortars containing 5% and 10% metakaolin.

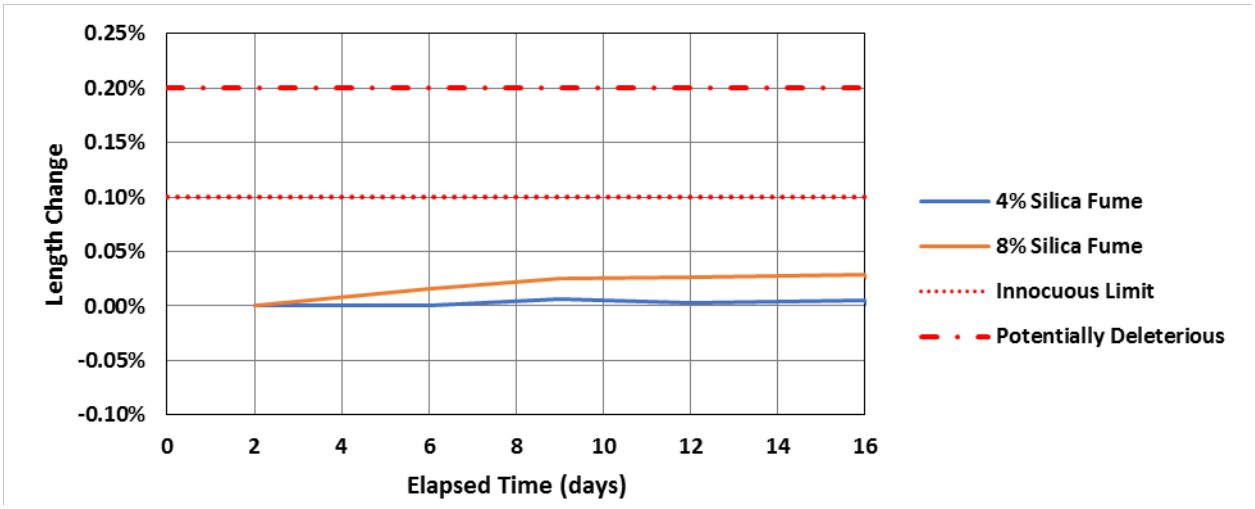

Figure C-205. Accelerated length change of mortars containing 4% and 8% silica fume.

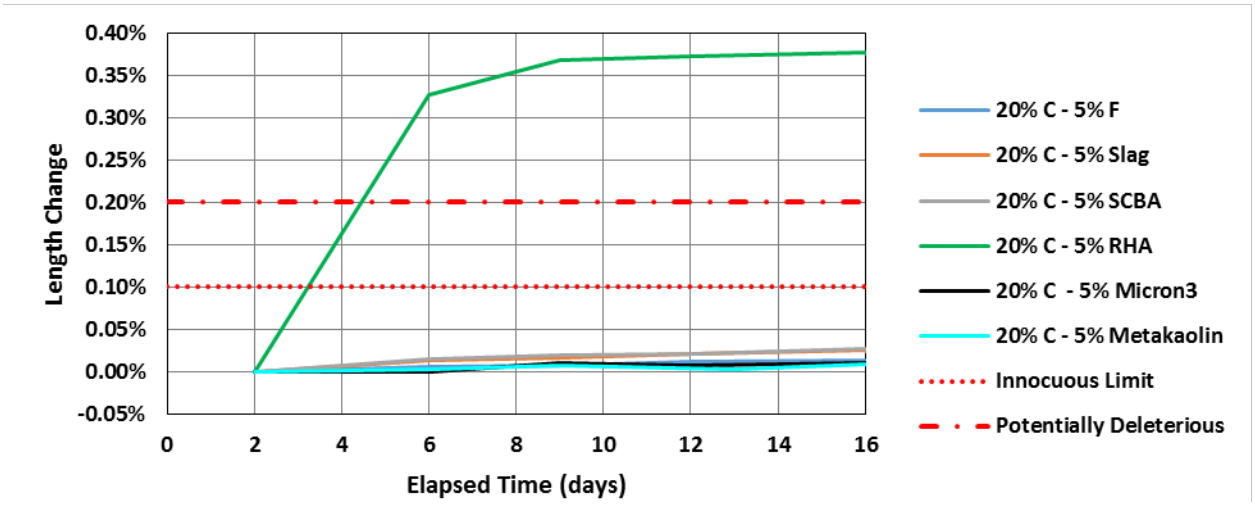

Figure C-206. Length change of ternary blended mortars containing 20% class C fly ash and 5% of either class F fly ash, ground blast furnace slag, sugarcane bagasse ash, rice husk ash, Micron[3], or metakaolin.

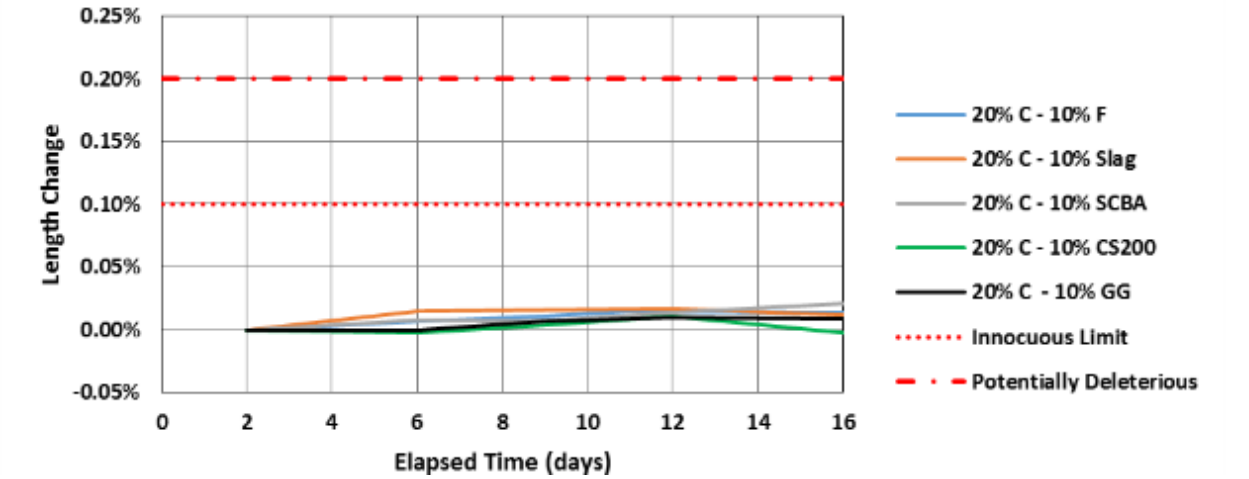

Figure C-207. Length change of ternary blended mortars containing 20% class C fly ash and 10% of either class F fly ash, blast furnace slag, sugarcane bagasse ash, CS200, or glass powder.

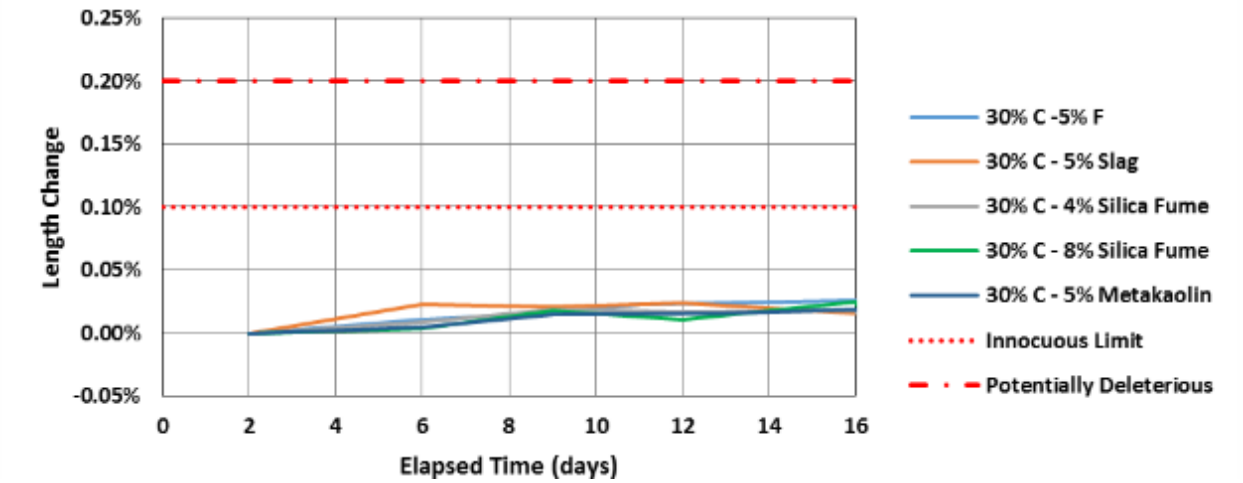

Figure C-208. Length change of ternary blended mortars containing 30% class C fly ash and less than 10% of either class F fly ash, ground blast furnace slag, silica fume, or metakaolin.

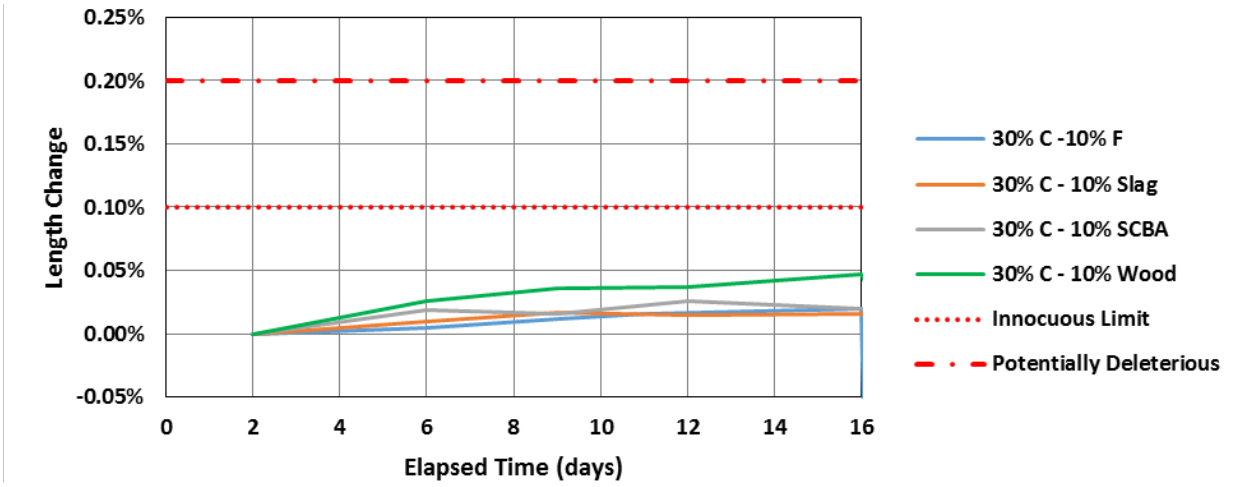

Figure C-209. Length change of ternary blended mortars containing 30% class C fly ash and 10% of either class F fly ash, ground blast furnace slag, sugarcane bagasse ash, or wood ash and 30% class C fly ash with 20% wood ash.

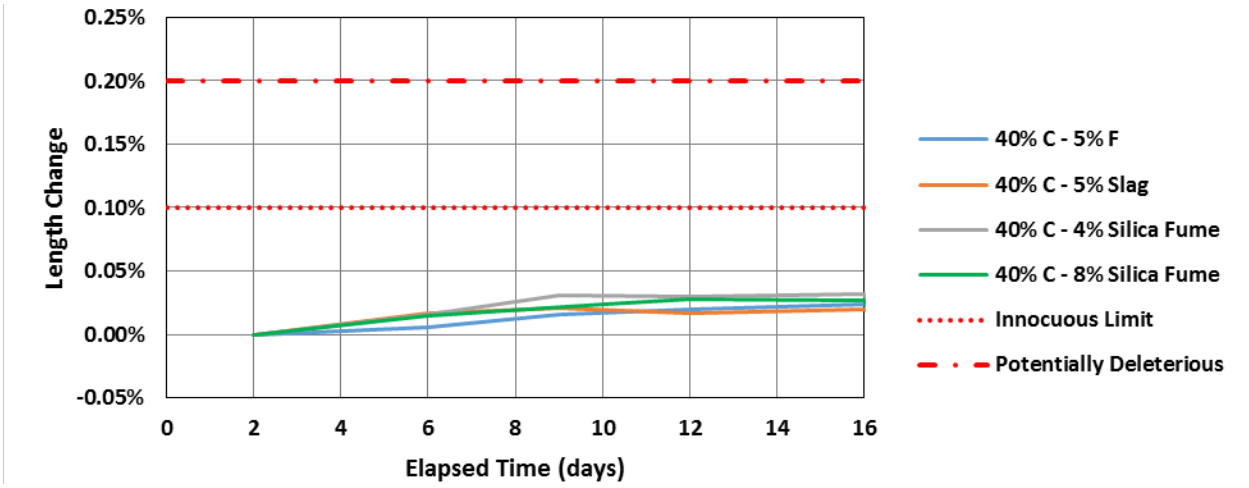

Figure C-210. Length change of ternary blended mortars containing 40% class C fly ash and less than 10% of either class F fly ash, blast furnace slag, or silica fume.

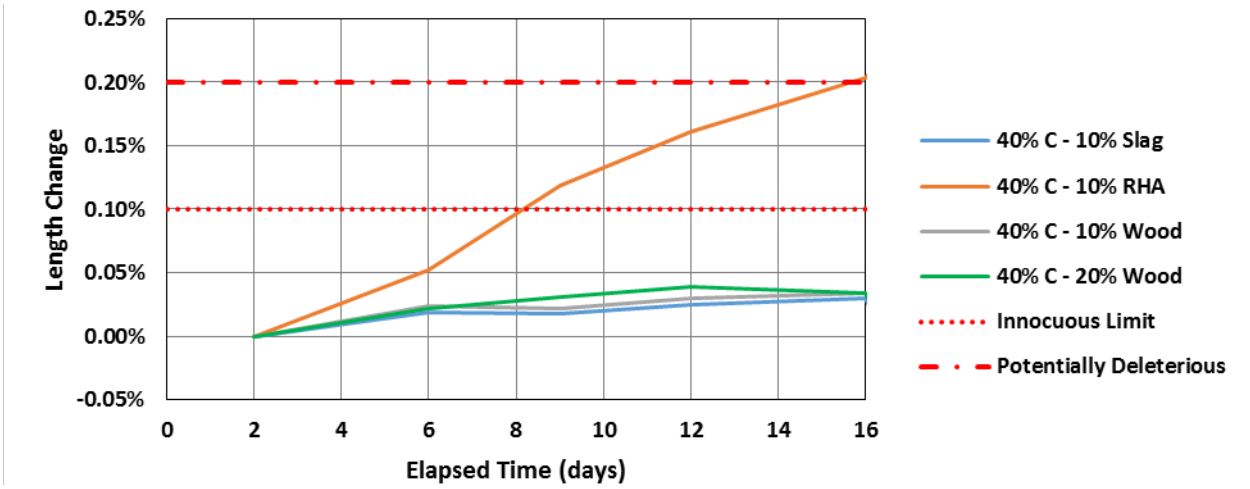

Figure C-211. Length change of ternary blended mortars containing 40% class C fly ash and at least 10% of either ground blast furnace slag, rice husk ash, or wood ash.

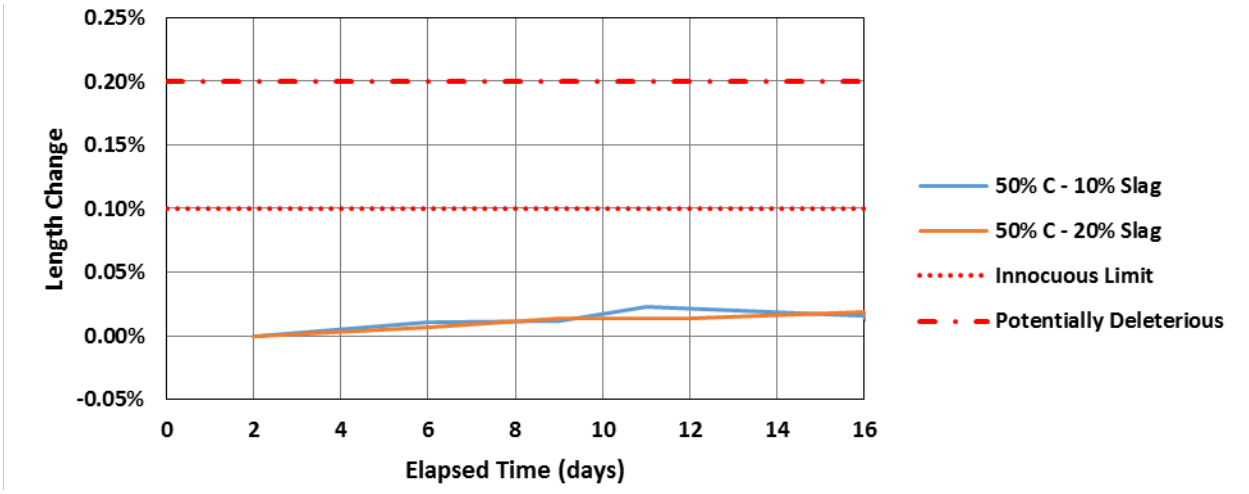

Figure C-212. Length change of ternary blended mortars containing 50% class C fly ash and 10% or 20% ground blast furnace slag.

D. APPENDIX D – CONCRETE RESULTS

D.1. Compressive Strength of Concrete Results

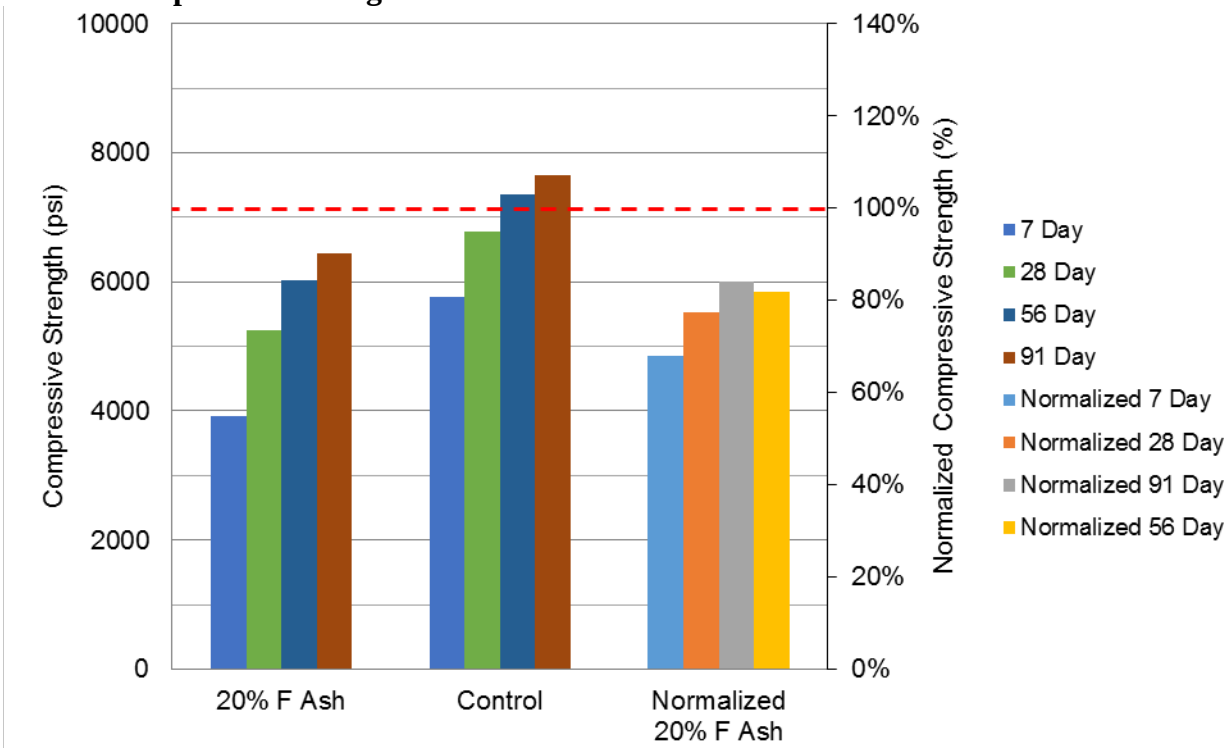

Figure D-1. Compressive strength of concrete containing 20% class F fly ash.

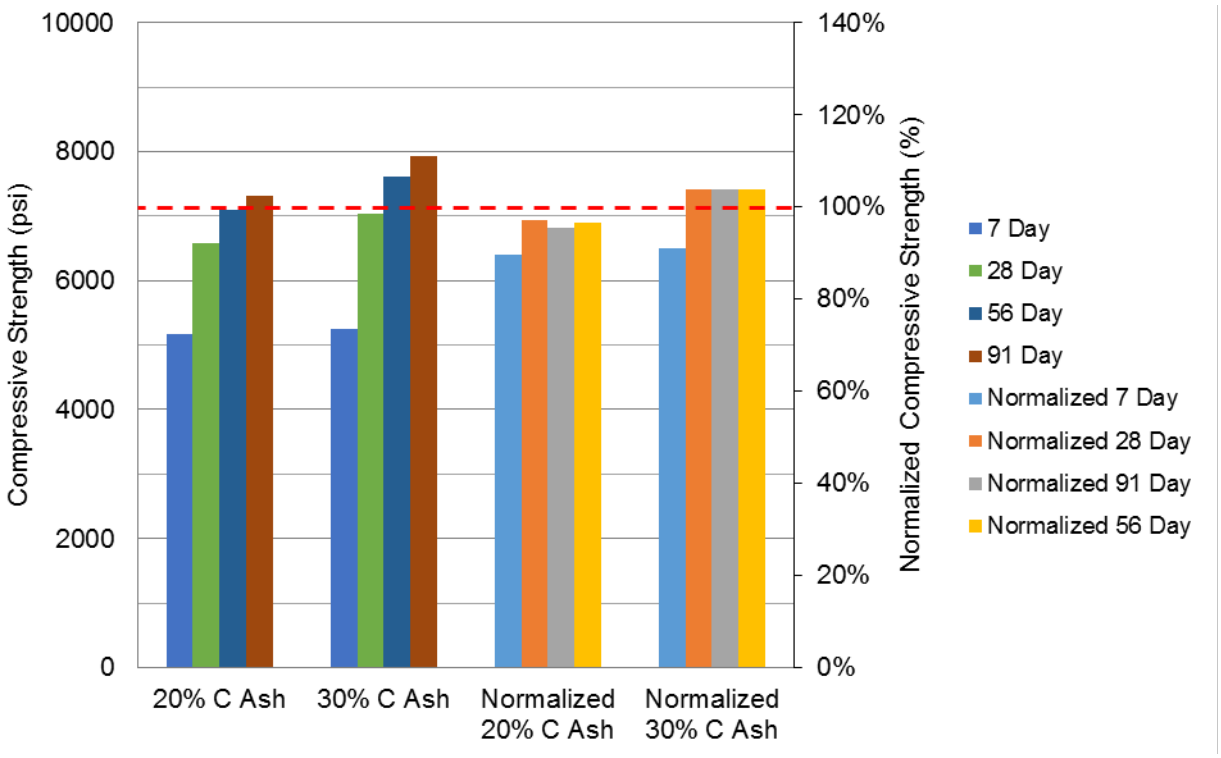

Figure D-2. Compressive strength of binary blended concretes containing 20 and 30% class C fly ash.

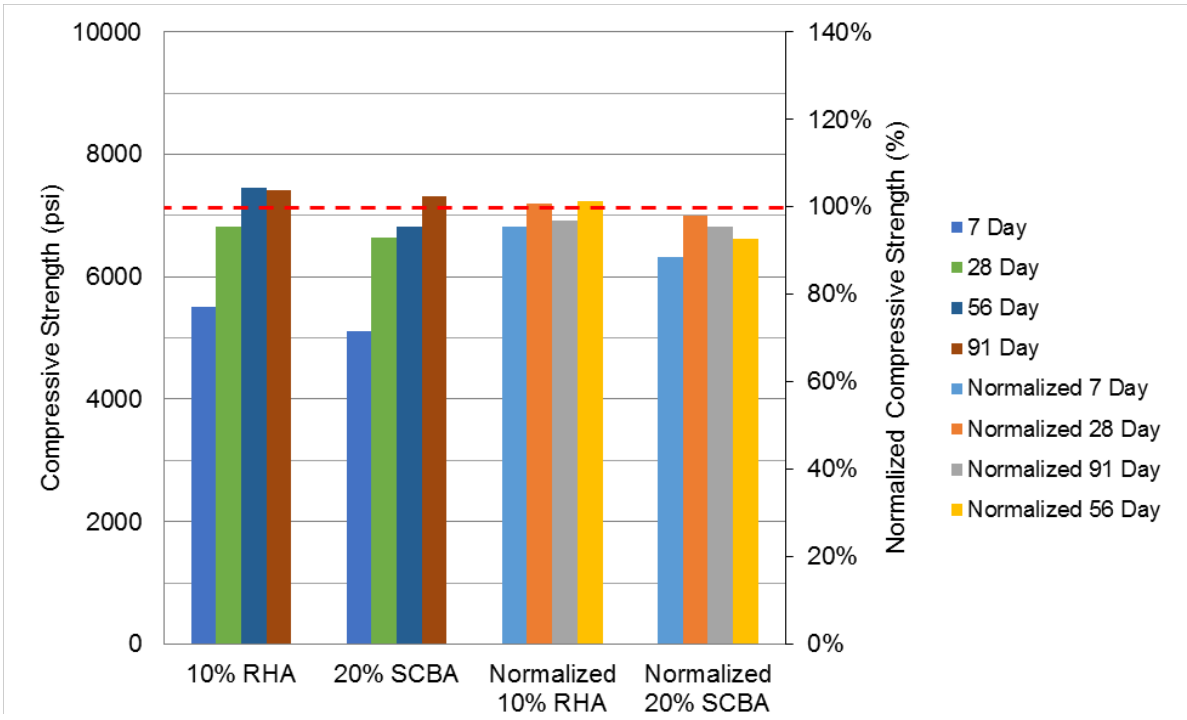

Figure D-3. Compressive strength of binary blended concrete containing RHA and SCBA.

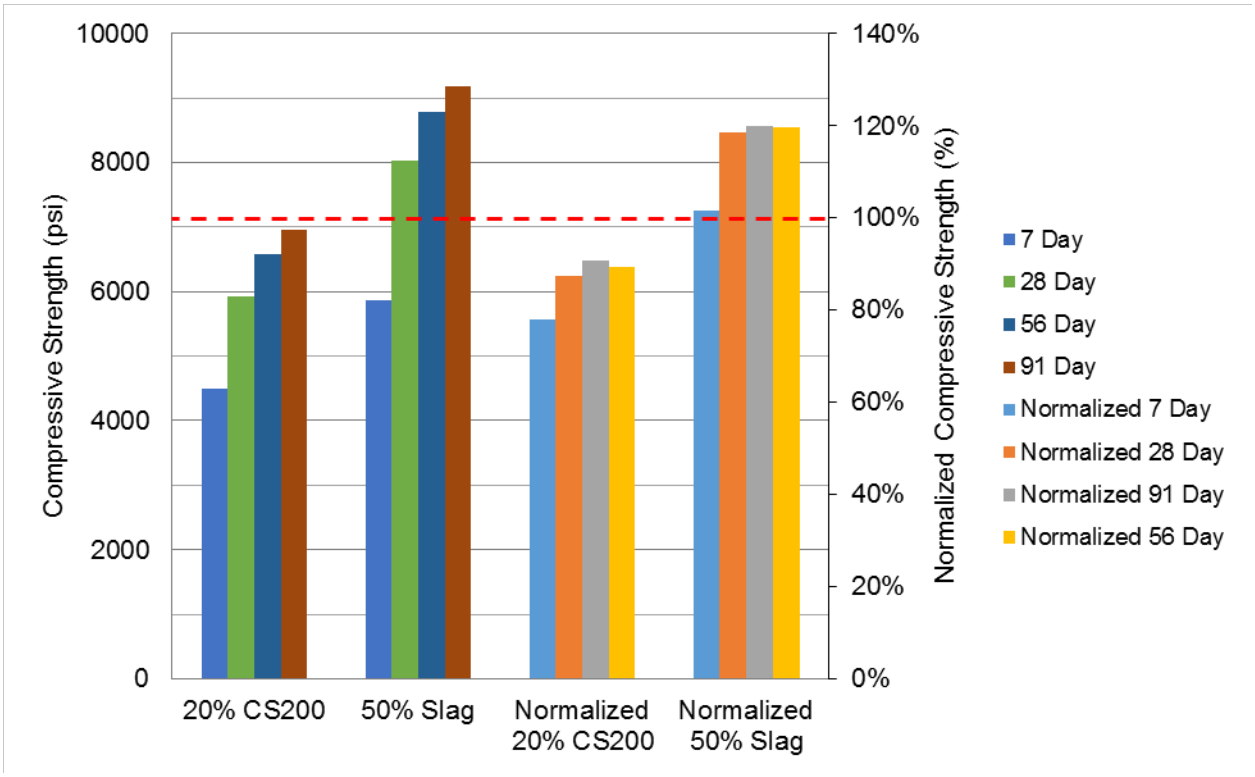

Figure D-4. Compressive strength of binary blended concrete containing CS200 glass and slag.

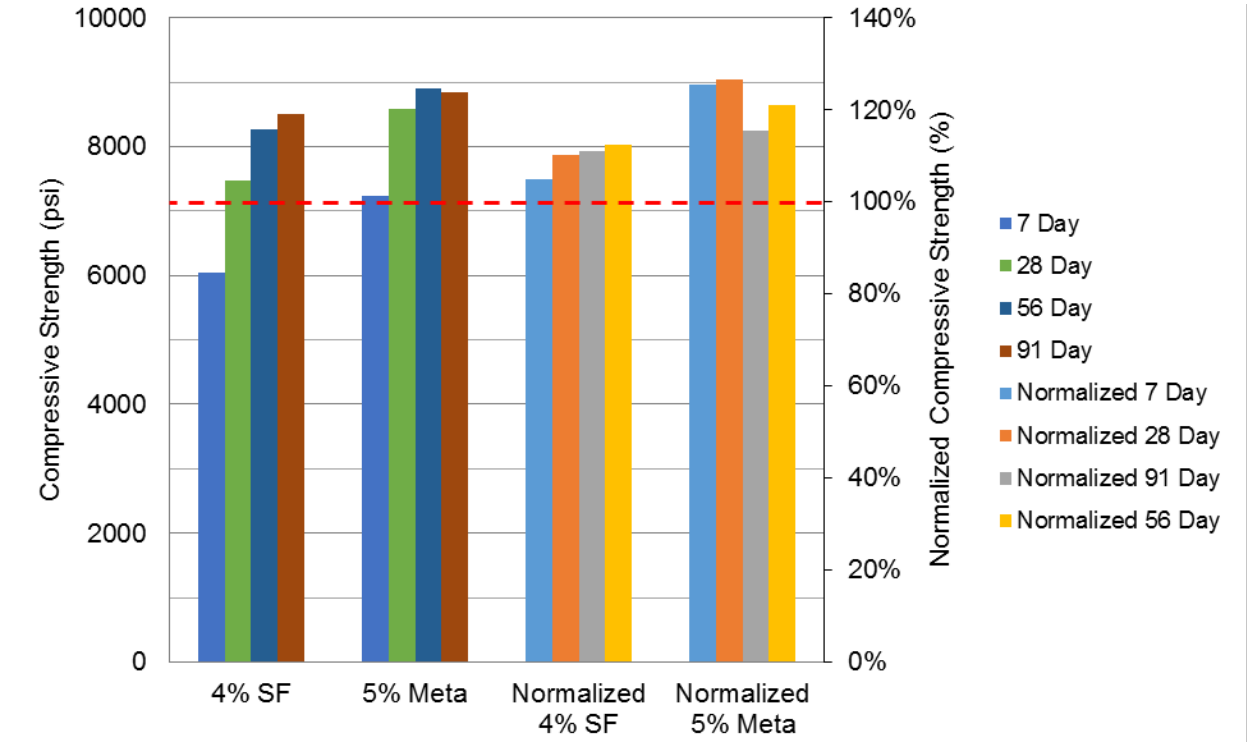

Figure D-5. Compressive strength of binary blended concrete containing silica fume and metakaolin.

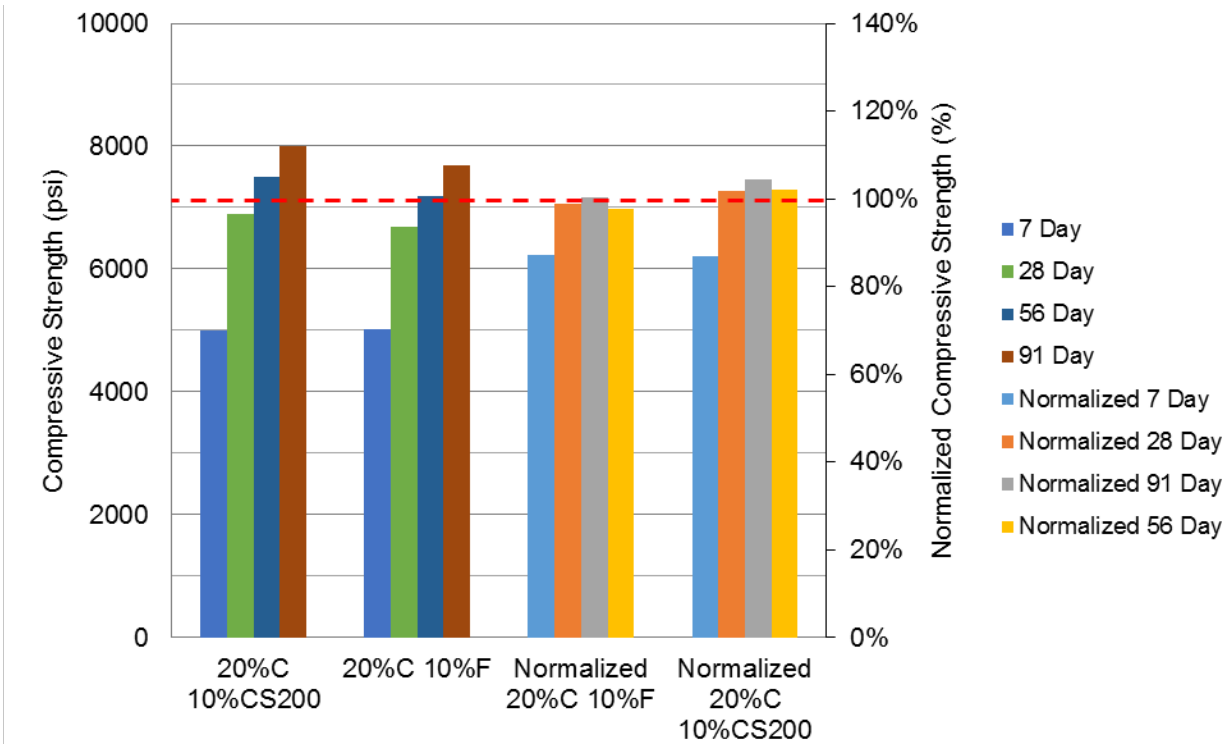

Figure D-6. Compressive strength of ternary blended concretes containing 20% class C fly ash and 10% class F fly ash or CS200 ground glass.

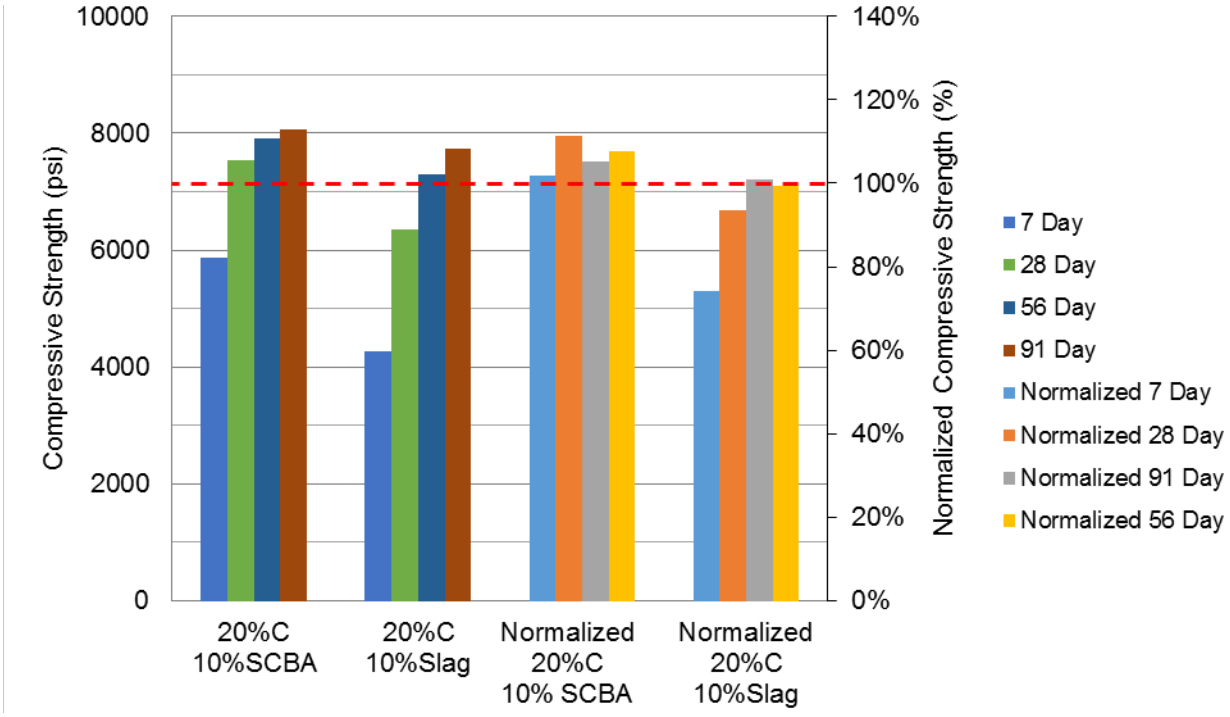

Figure D-7. Compressive strength of ternary blended concretes containing 20% class C fly ash and 10% sugarcane bagasse ash or slag.

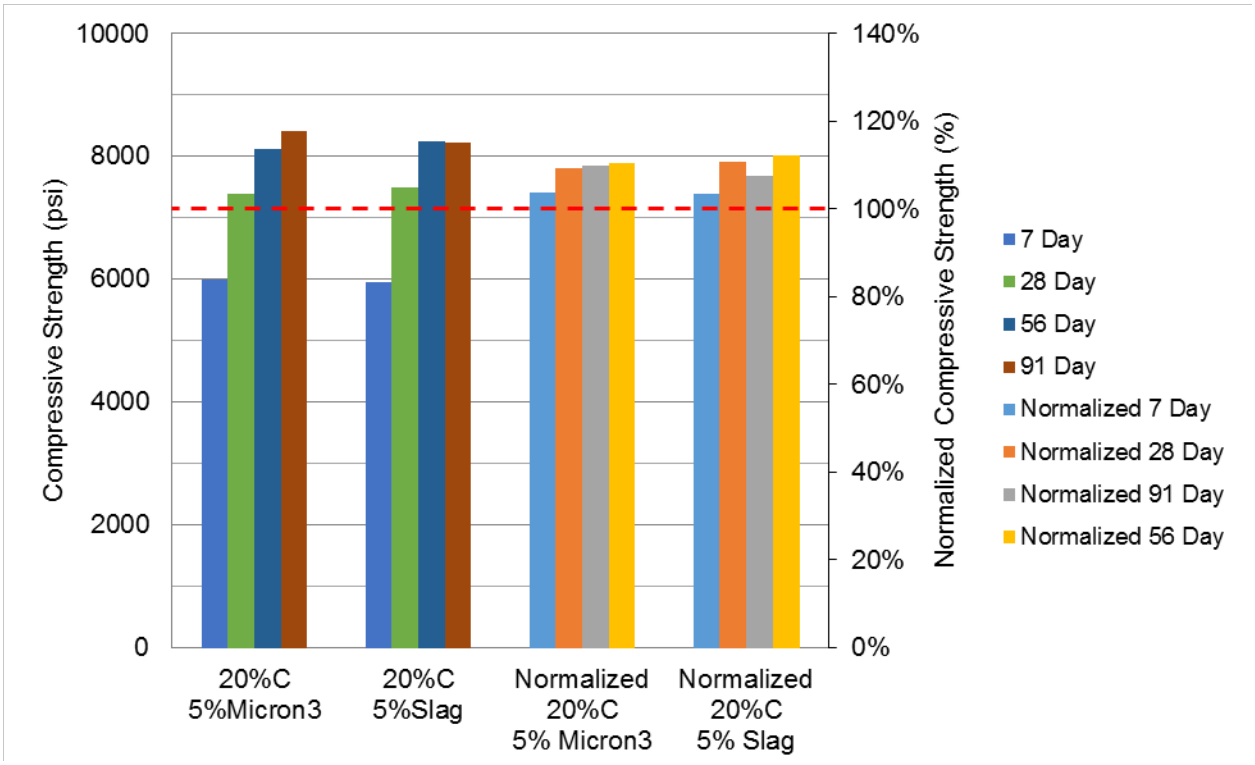

Figure D-8. Compressive strength of ternary blended concrete containing 20% class C fly ash and 5% Micron^3 or slag.

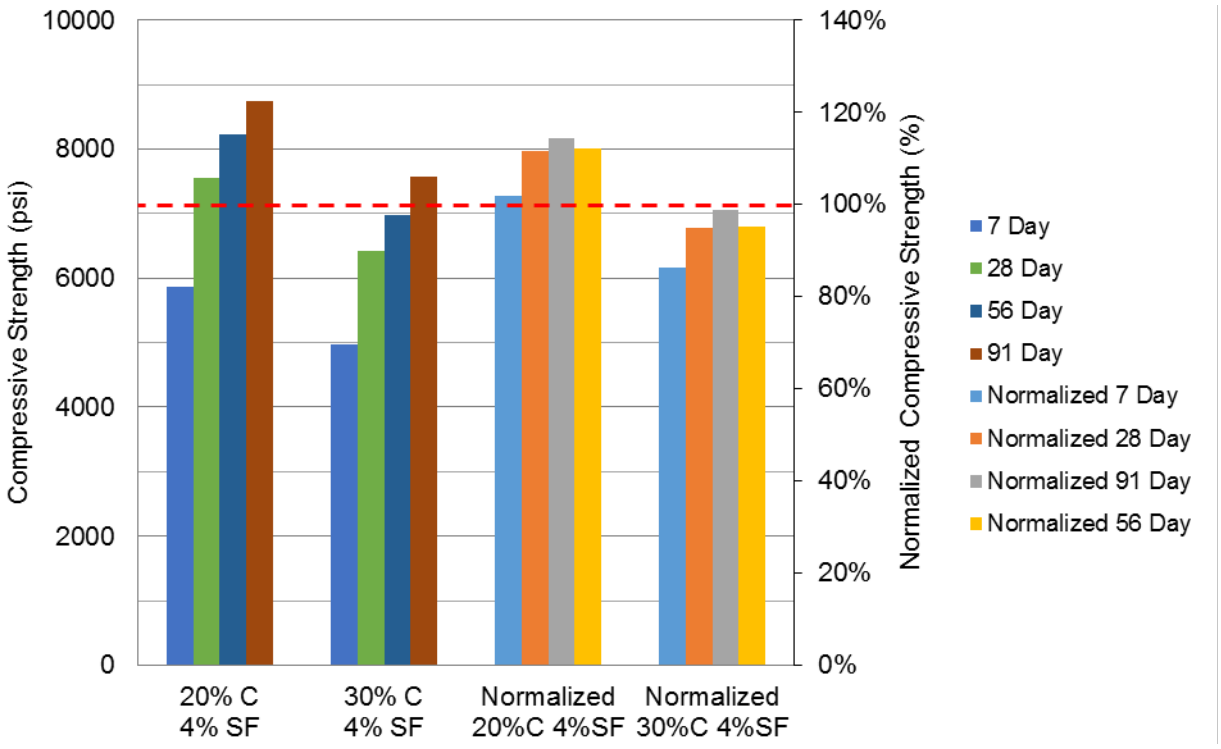

Figure D-9. Compressive strength of ternary blended concrete containing 20% or 30% class C fly ash and 4% silica fume.

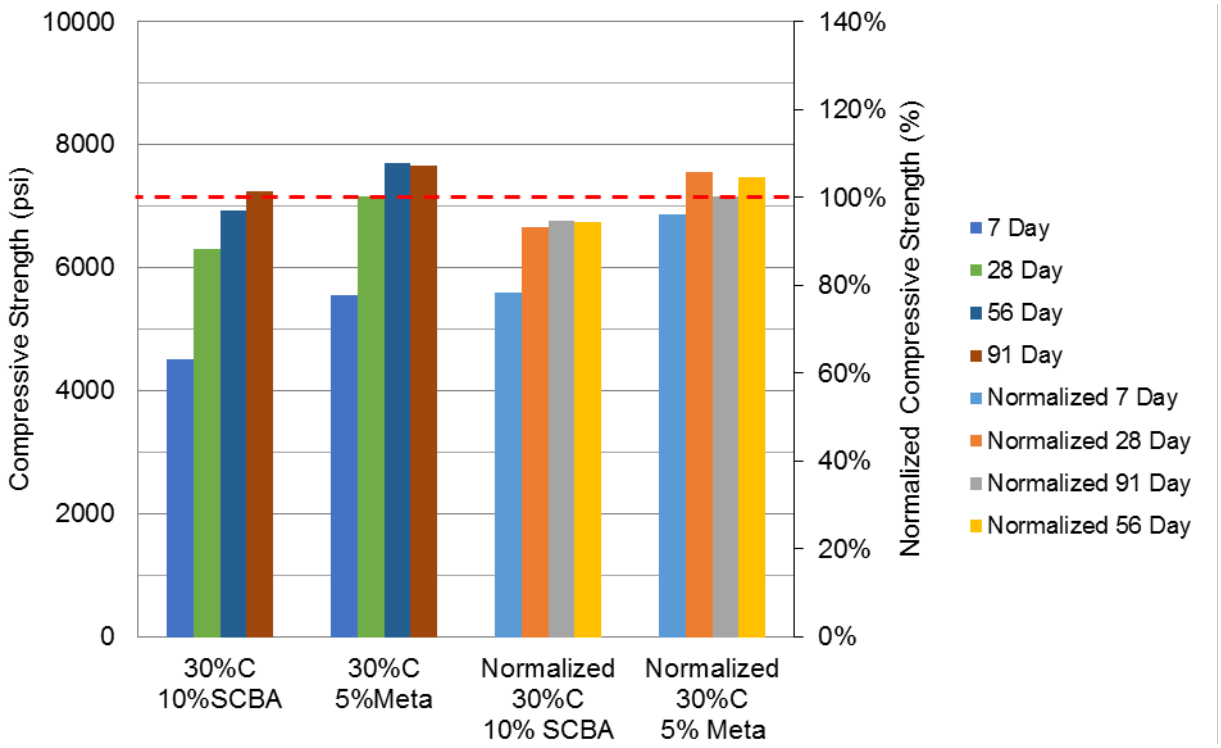

Figure D-10. Compressive strength of ternary blended concrete containing 30% class C fly ash and 5% metakaolin or 10% sugarcane bagasse ash.

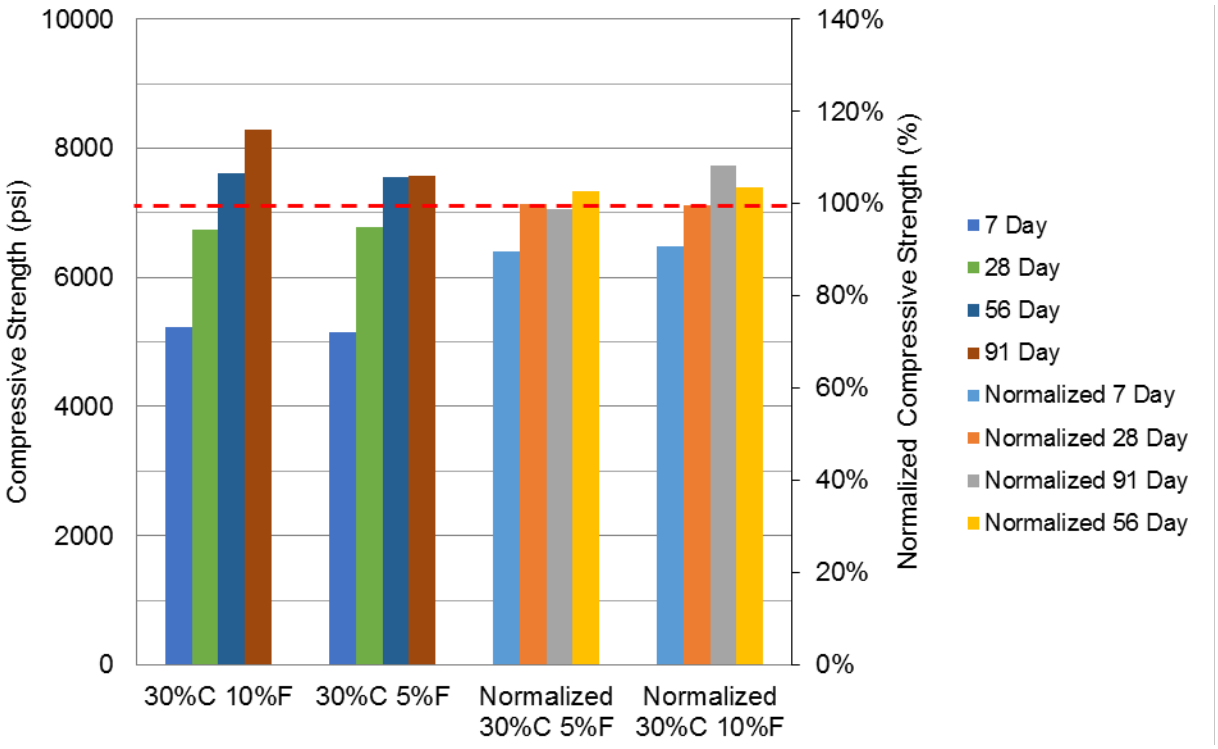

Figure D-11. Compressive strength of ternary blended concrete containing 30% class C fly ash and 5% or 10% class F fly ash.

D.2. Semi-Adiabatic Temperature Rise of Concrete Results

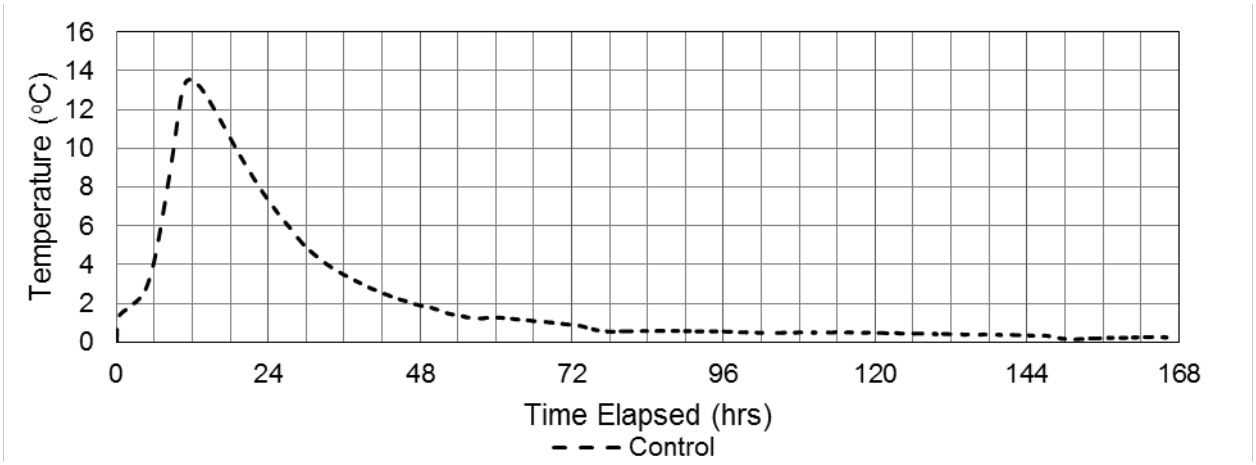

Figure D-12. Semi-adiabatic temperature rise of control concrete.

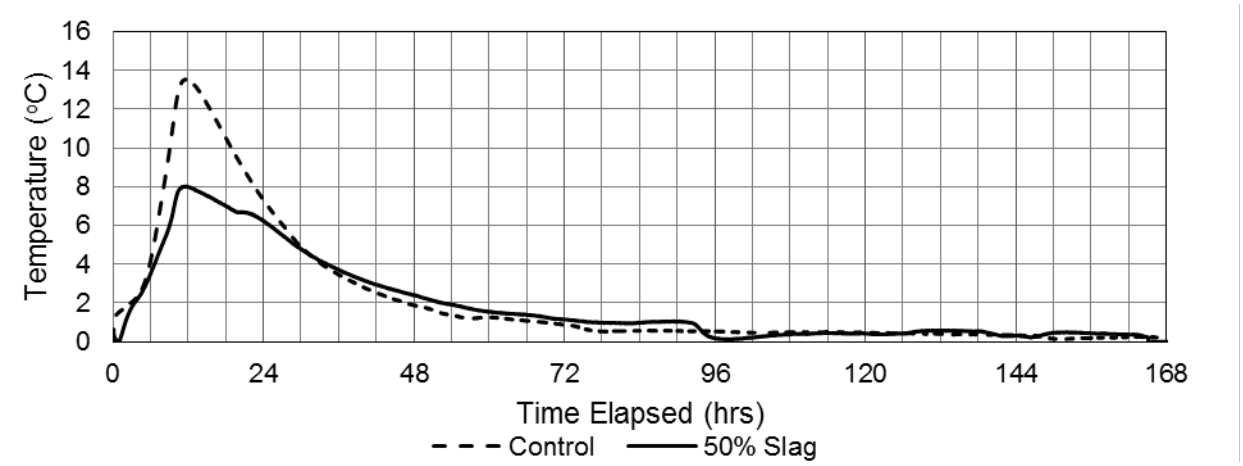

Figure D-13. Semi-adiabatic temperature rise of 50% Slag concrete.

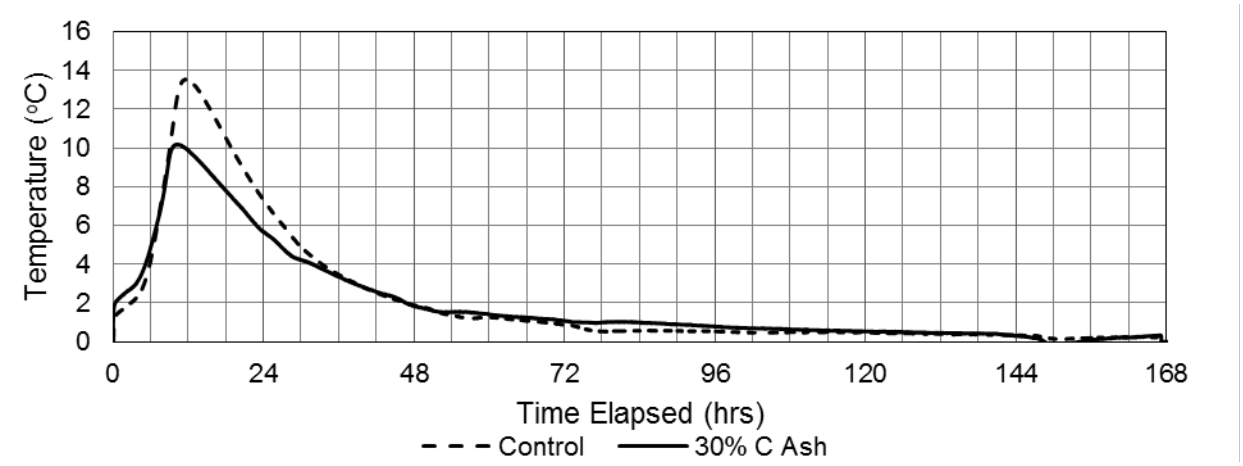

Figure D-14. Semi-adiabatic temperature rise of 30% C Ash concrete.

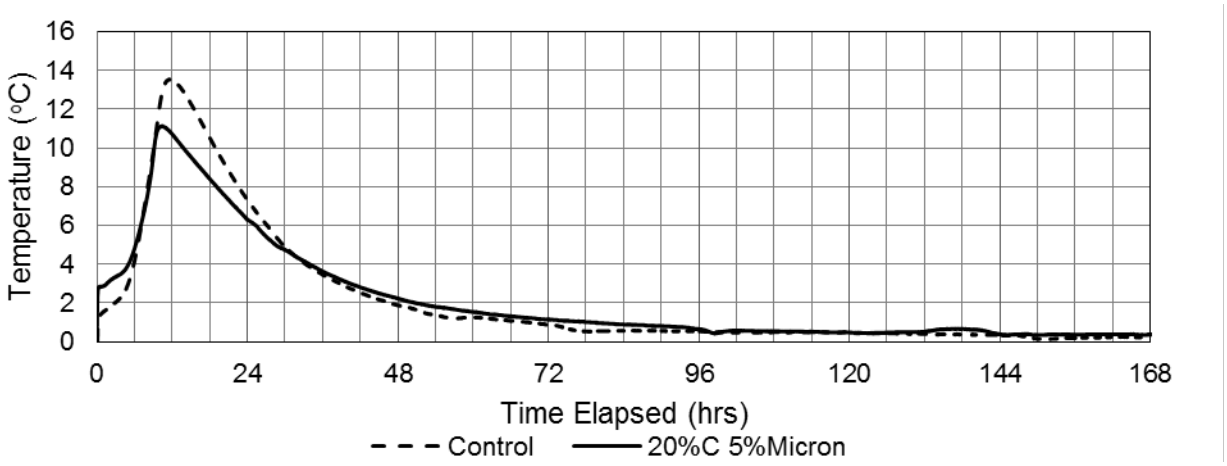

Figure D-15. Semi-adiabatic temperature rise of 20%C 5%Micron[3] concrete.

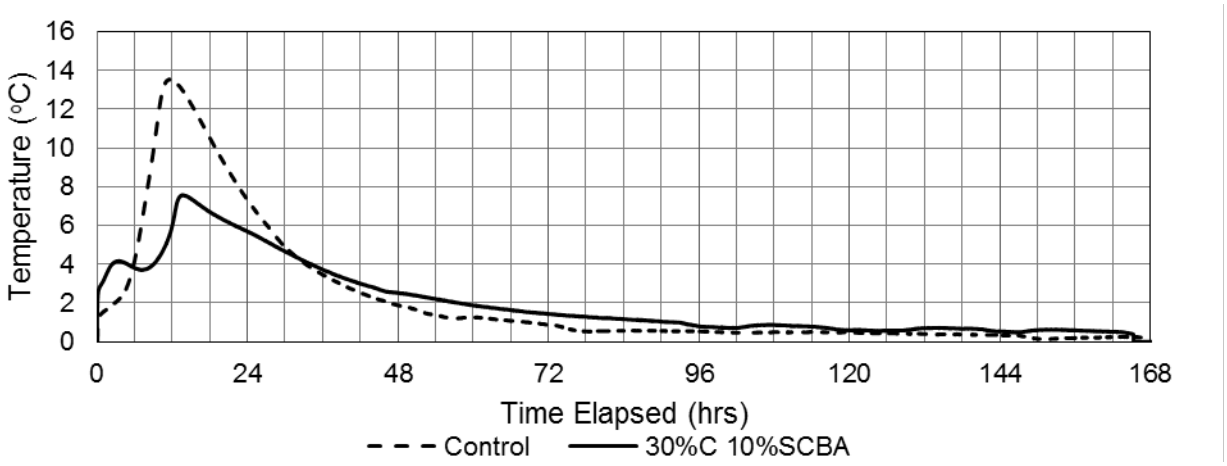

Figure D-16. Semi-adiabatic temperature rise of 30%C 10%SCBA concrete.

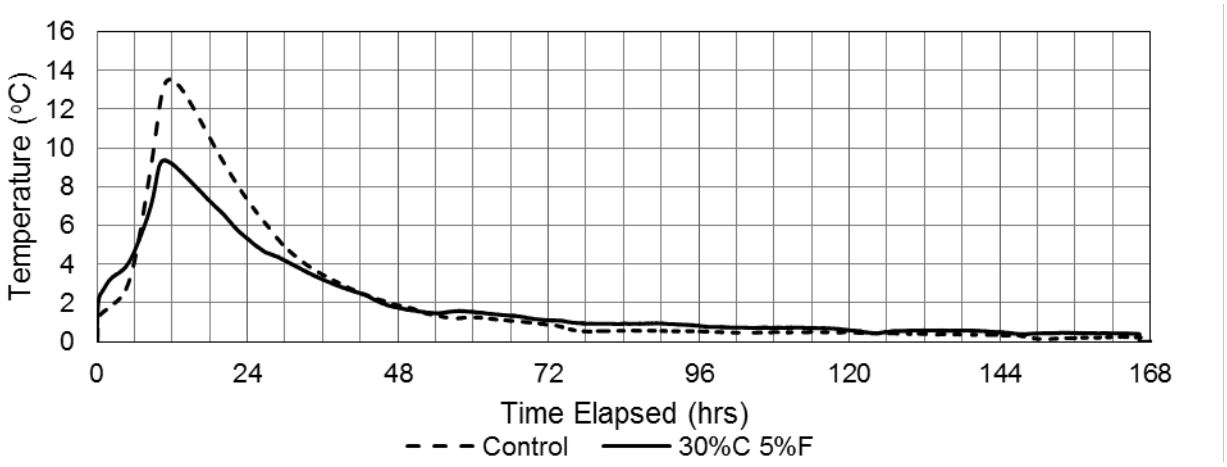

Figure D-17. Semi-adiabatic temperature rise of 30%C 5%F concrete.

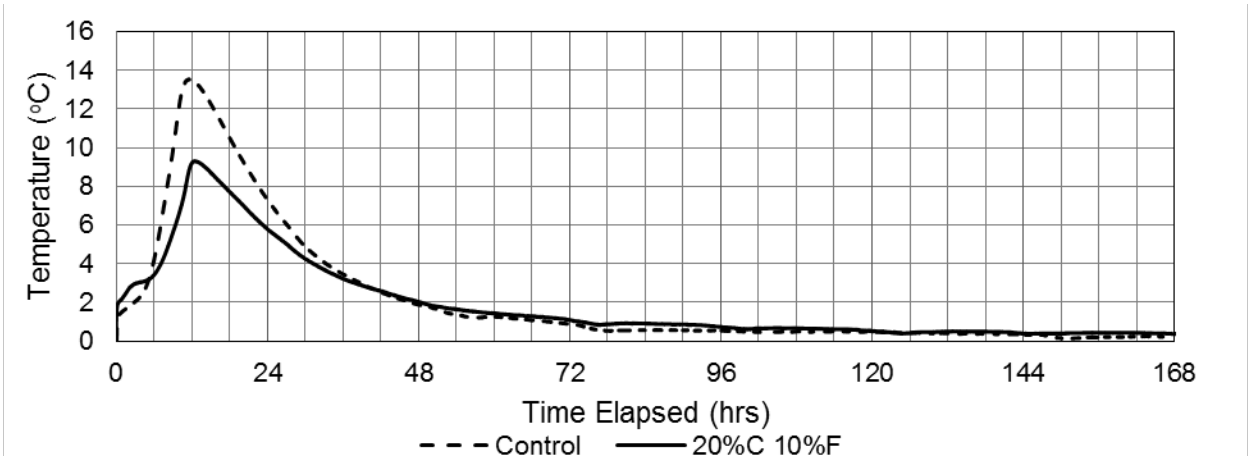

Figure D-18. Semi-adiabatic temperature rise of 20%C 10%F concrete.

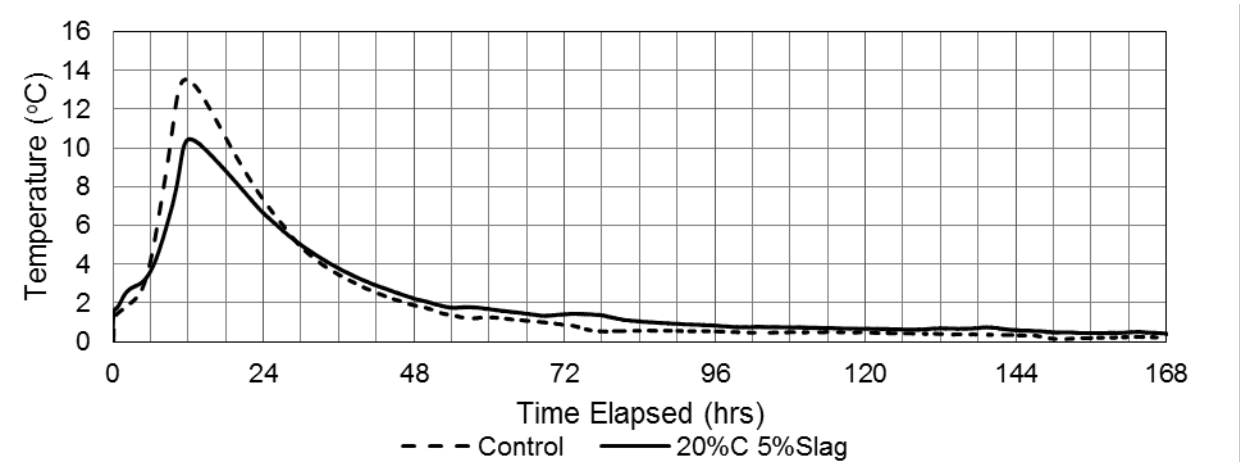

Figure D-19. Semi-adiabatic temperature rise of 20%C 5% slag concrete.

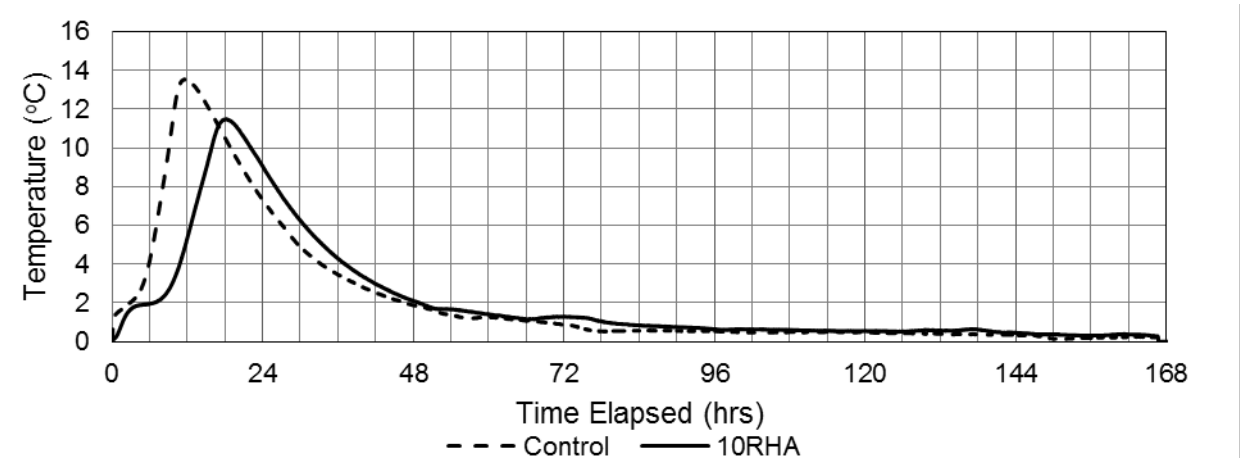

Figure D-20. Semi-adiabatic temperature rise of 10% RHA concrete.

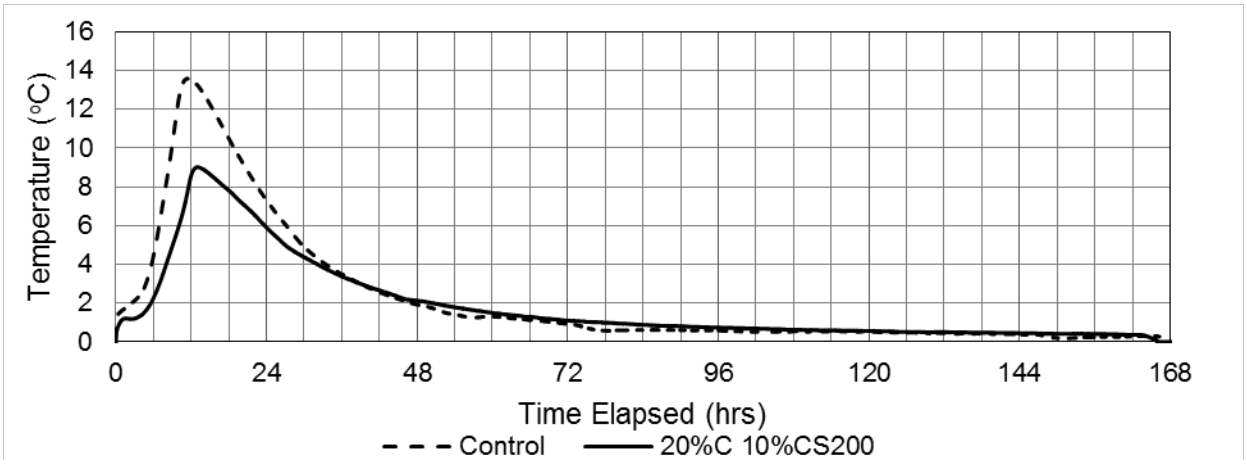

Figure D-21. Semi-adiabatic temperature rise of 20%C 10%CS200 glass concrete.

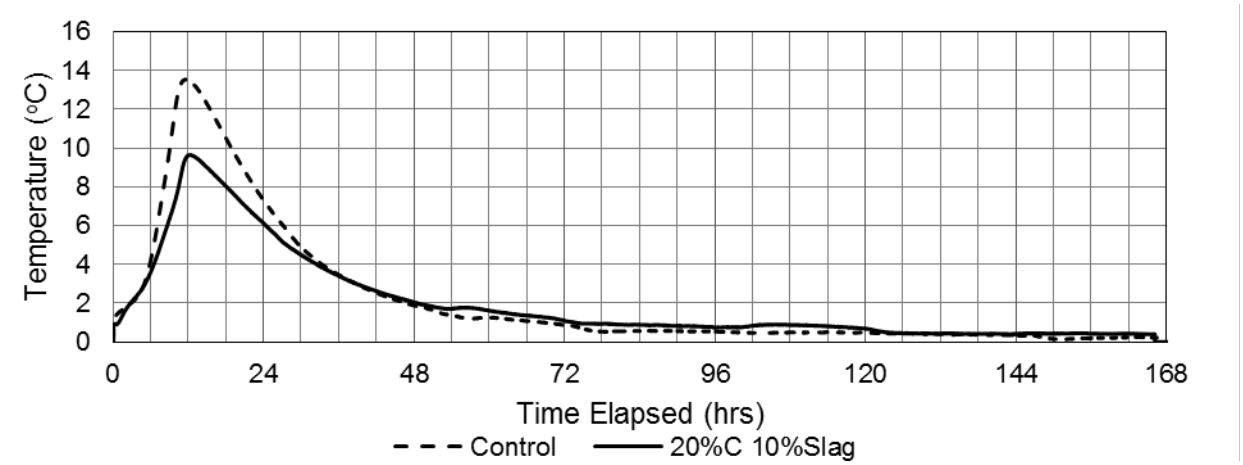

Figure D-22. Semi-adiabatic temperature rise of 20%C 10%Slag concrete.

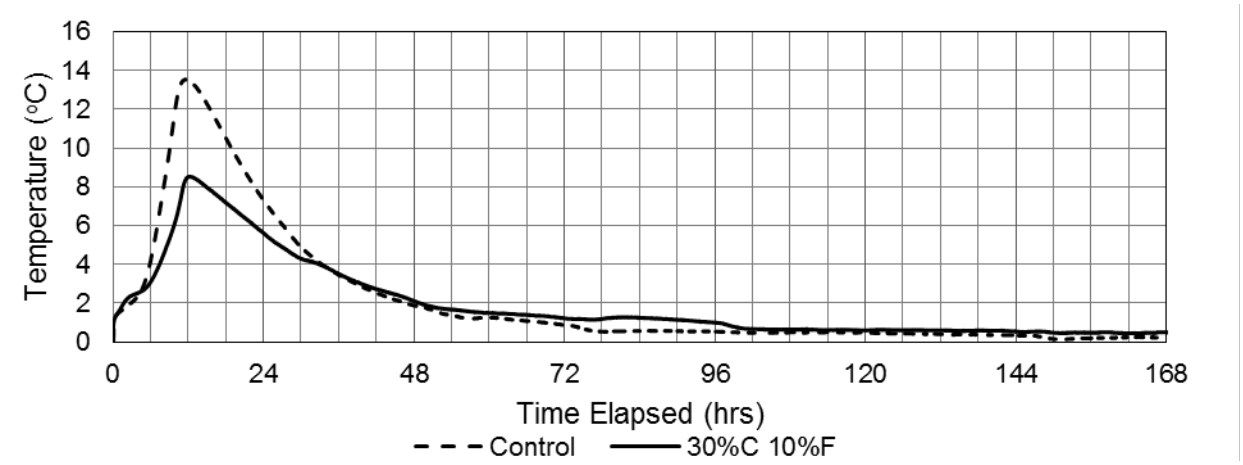

Figure D-23. Semi-adiabatic temperature rise of 30%C 10%F concrete.

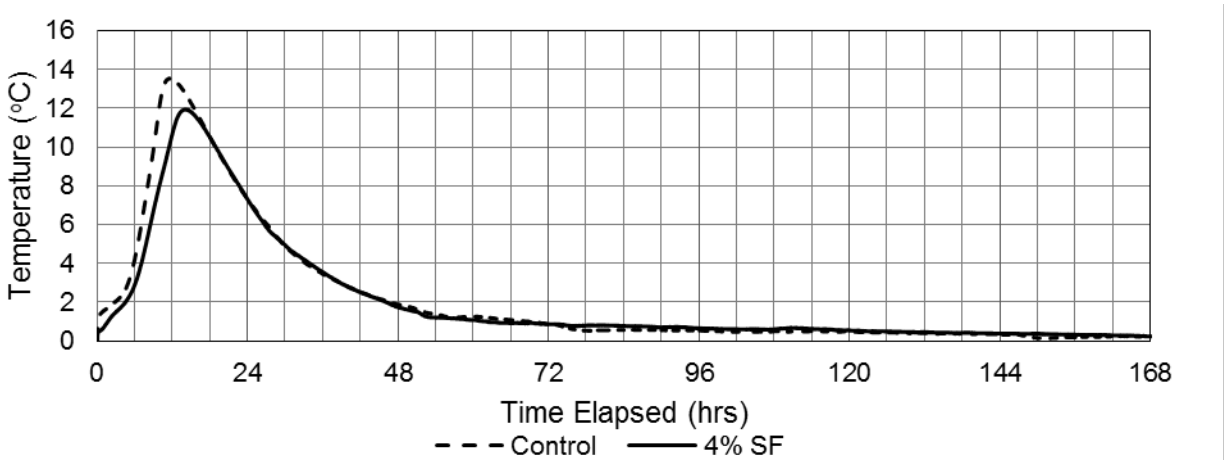

Figure D-24. Semi-adiabatic temperature rise of 4% SF concrete.

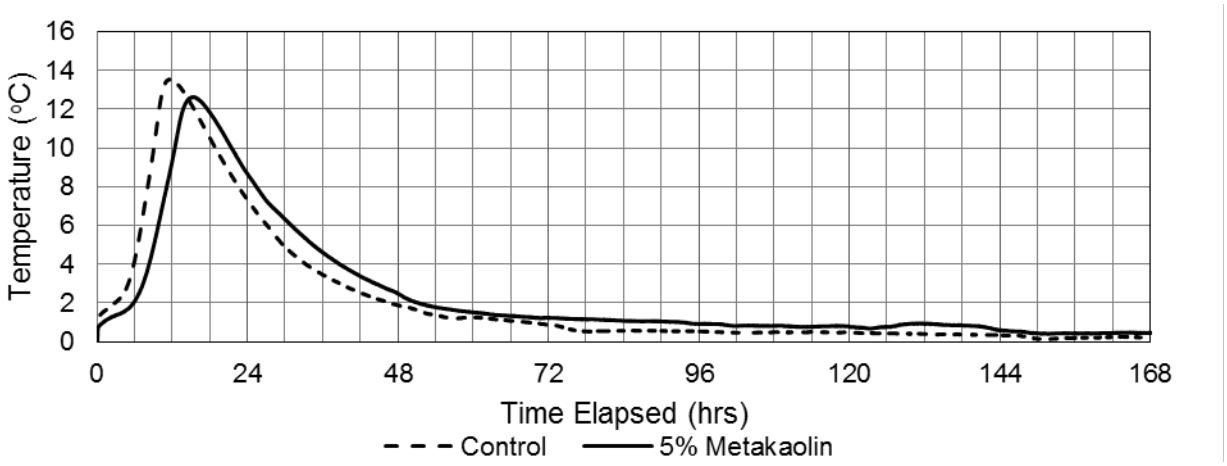

Figure D-25. Semi-adiabatic temperature rise of 5% metakaolin concrete.

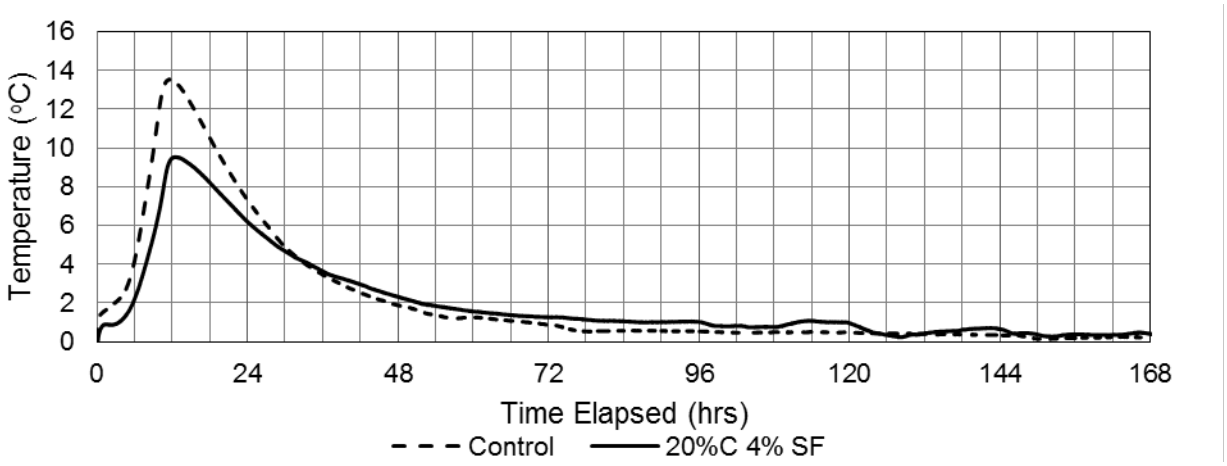

Figure D-26. Semi-adiabatic temperature rise of 20%C 4%SF concrete.

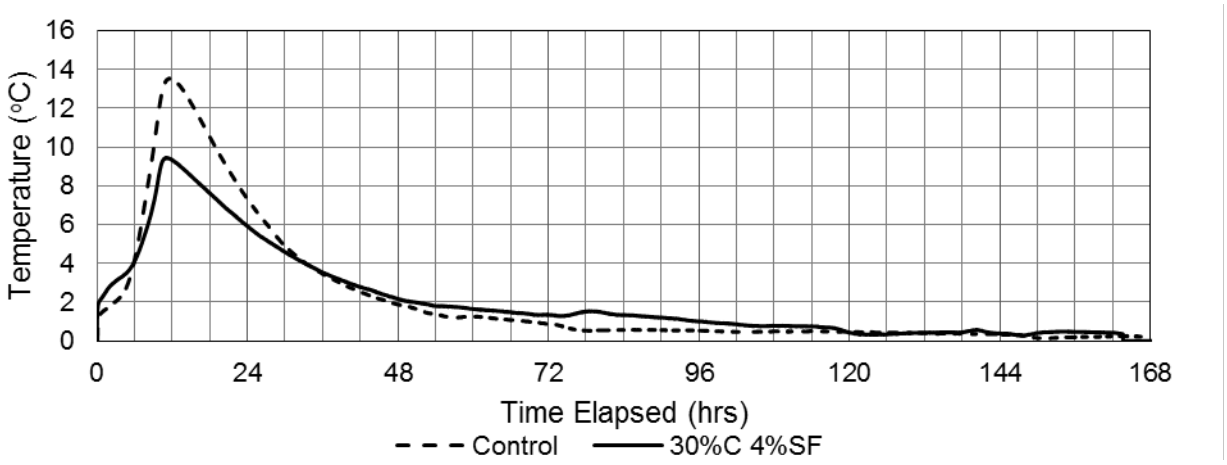

Figure D-27. Semi-adiabatic temperature rise of 30%C 4%SF concrete.

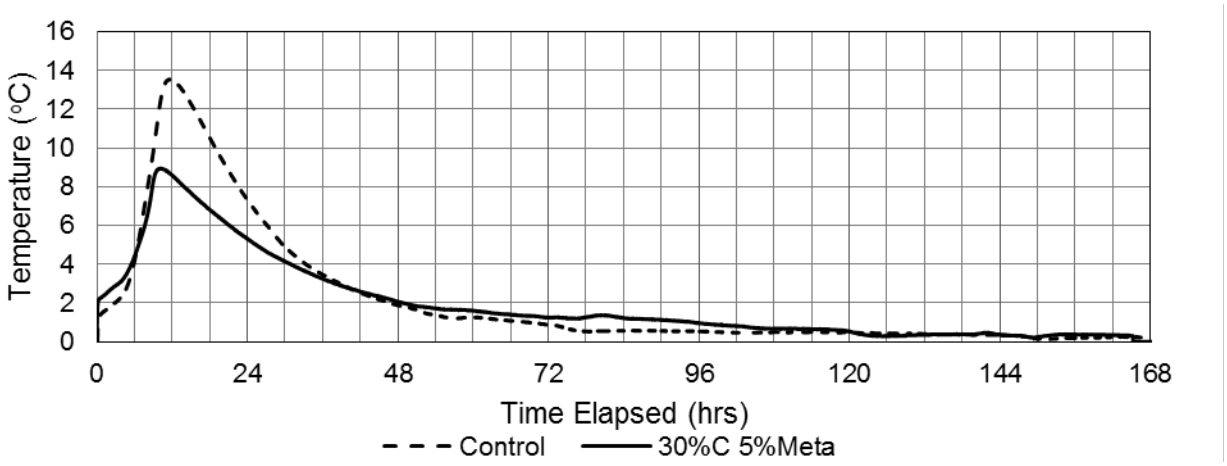

Figure D-28. Semi-adiabatic temperature rise of 30%C 5%Metakaolin concrete.

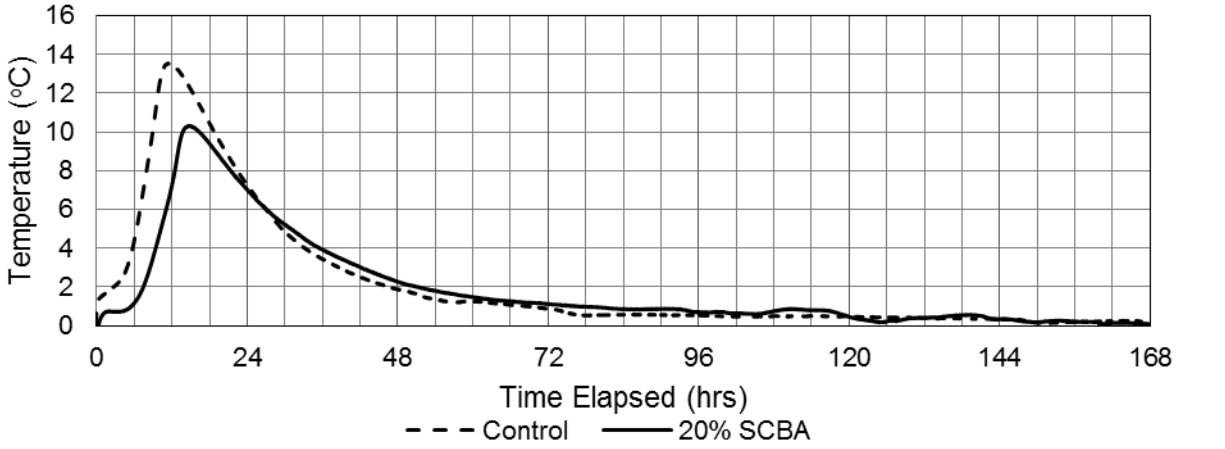

Figure D-29. Semi-adiabatic temperature rise of 20% SCBA concrete.

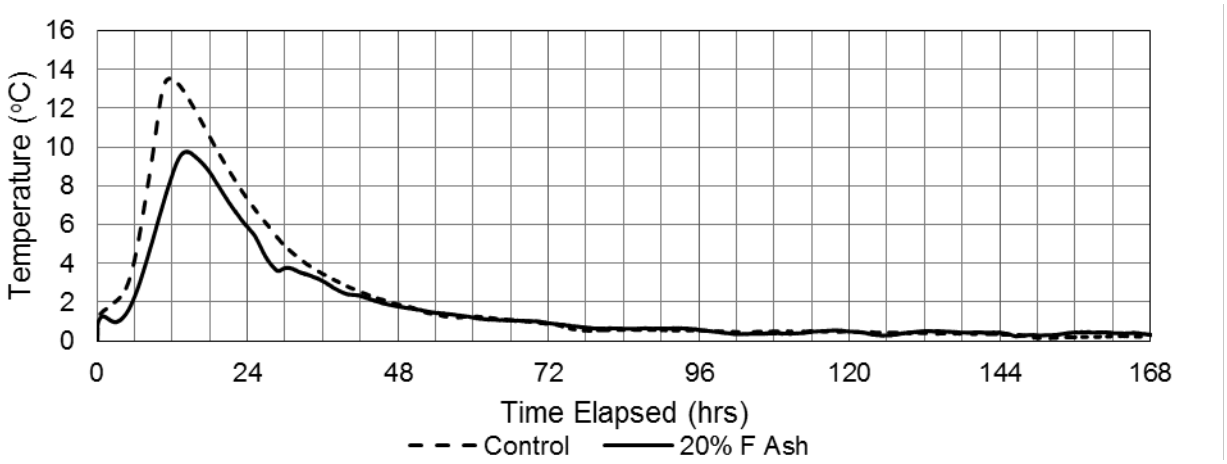

Figure D-30. Semi-adiabatic temperature rise of 20% F Ash concrete.

D.3. Concrete Surface Resistivity Results

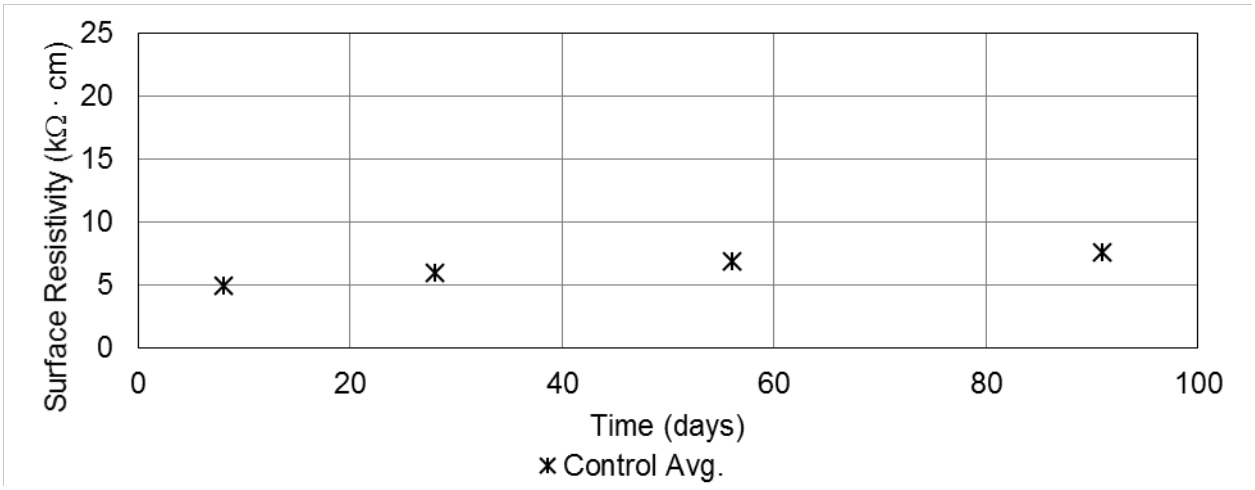

Figure D-31. Surface resistivity of the control concrete mix.

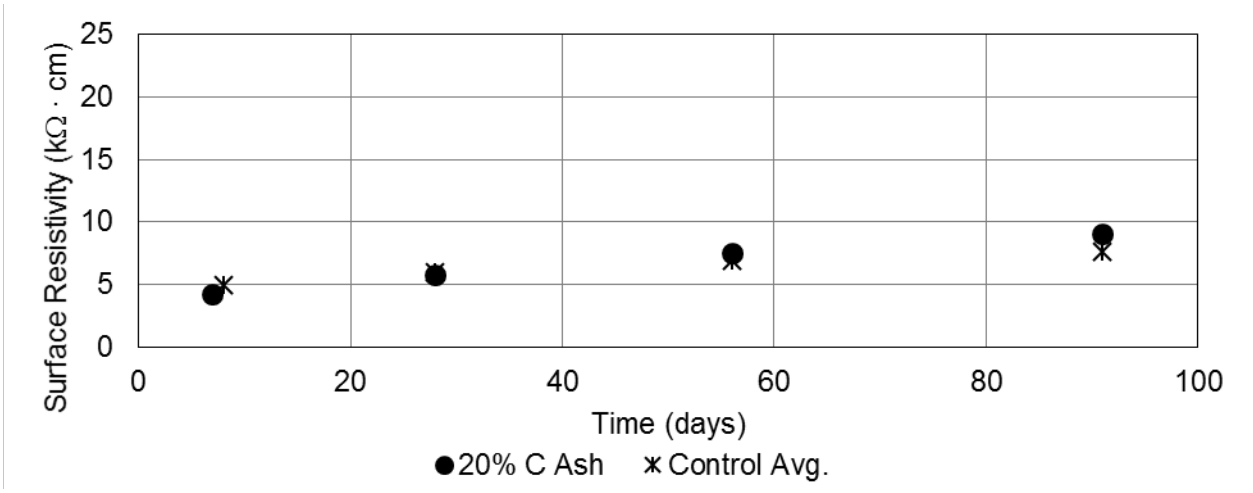

Figure D-32. Surface resistivity of concrete containing 20% class C fly ash.

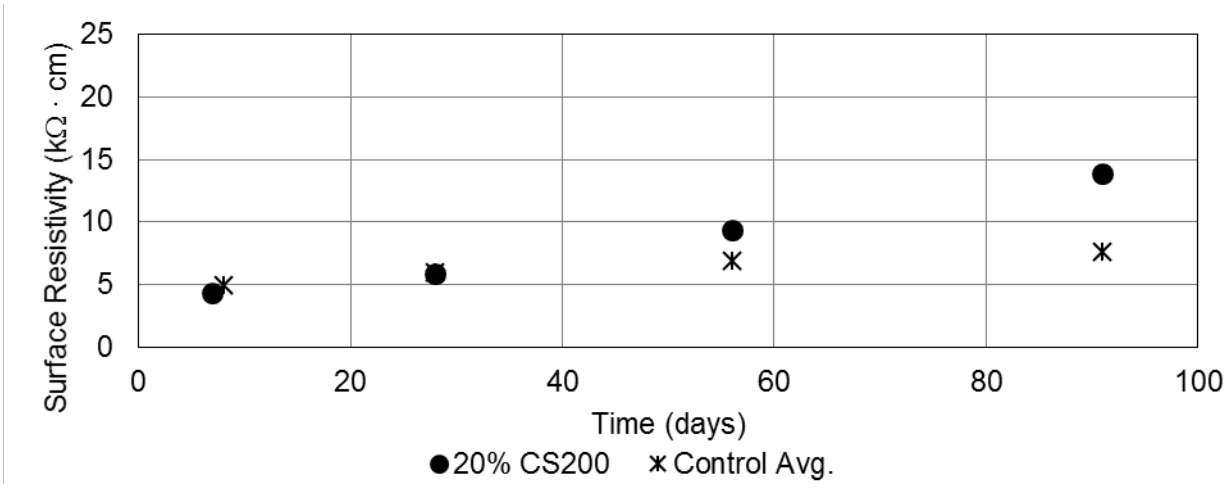

Figure D-33. Surface resistivity of concrete containing 20% CS200 ground glass.

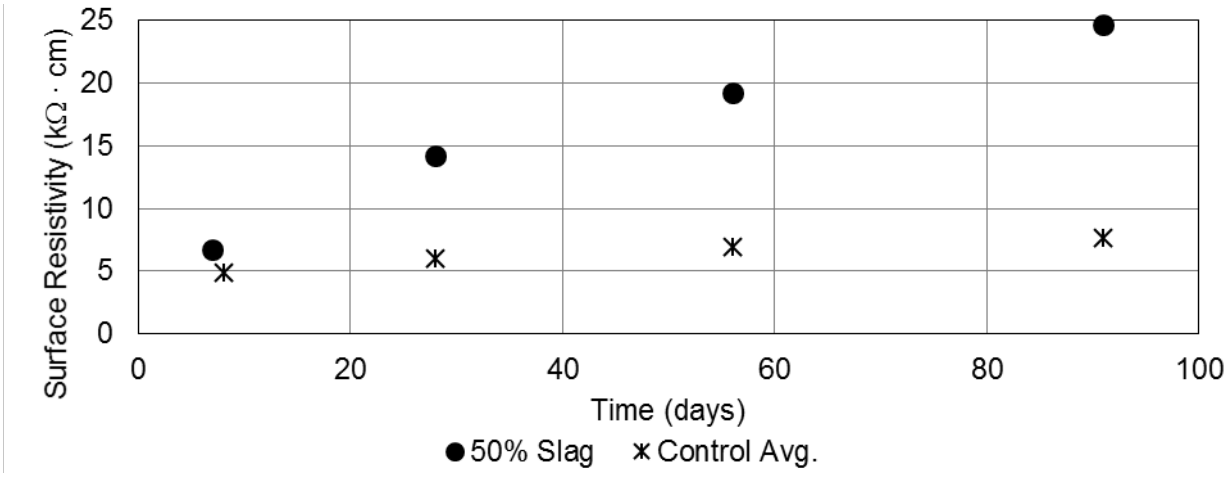

Figure D-34. Surface resistivity of concrete containing 50% slag.

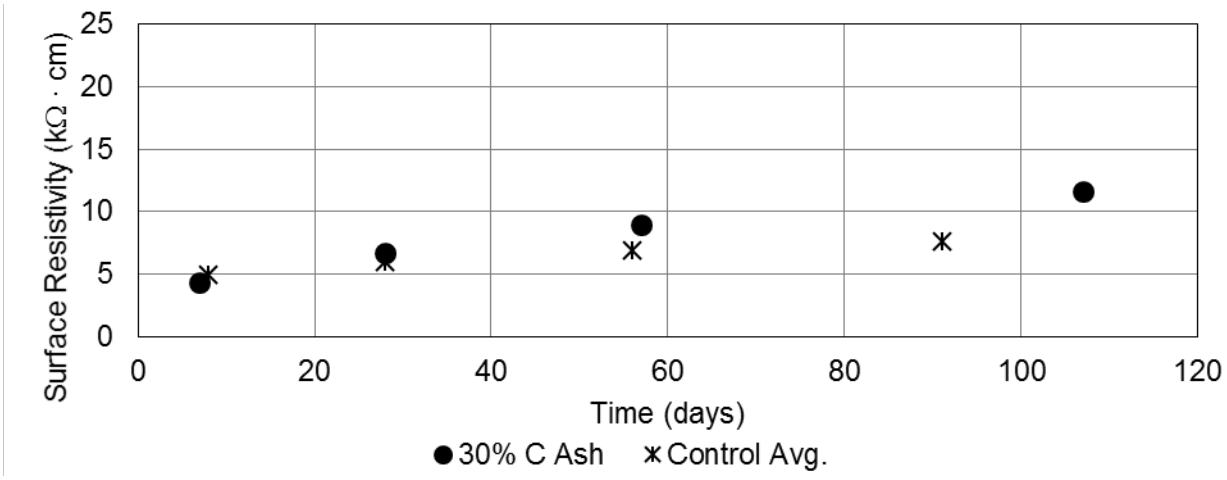

Figure D-35. Surface resistivity of concrete containing 30% class C fly ash.

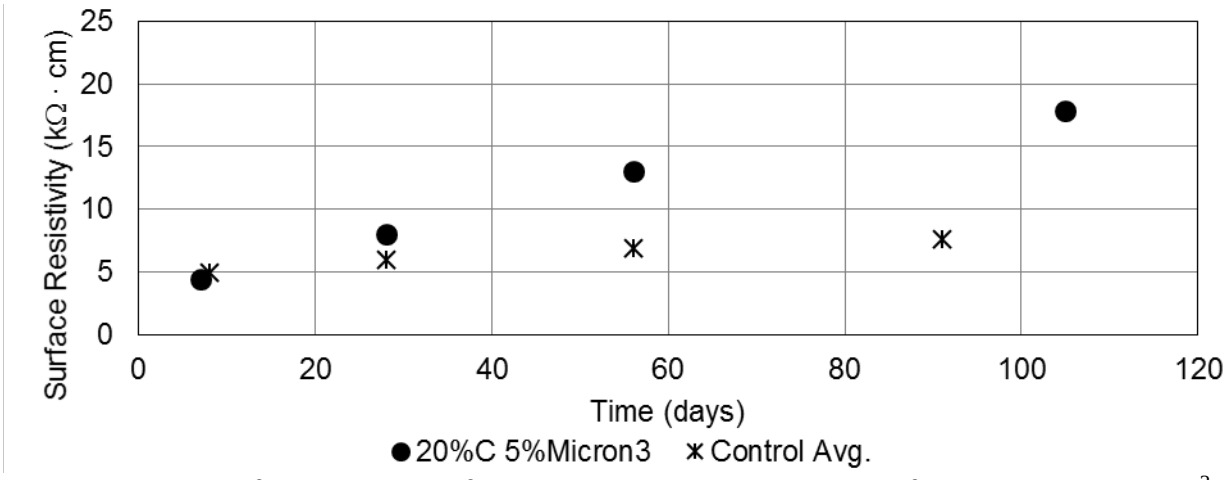

Figure D-36. Surface resistivity of concrete containing 20% class C fly ash and 5% Micron[3].

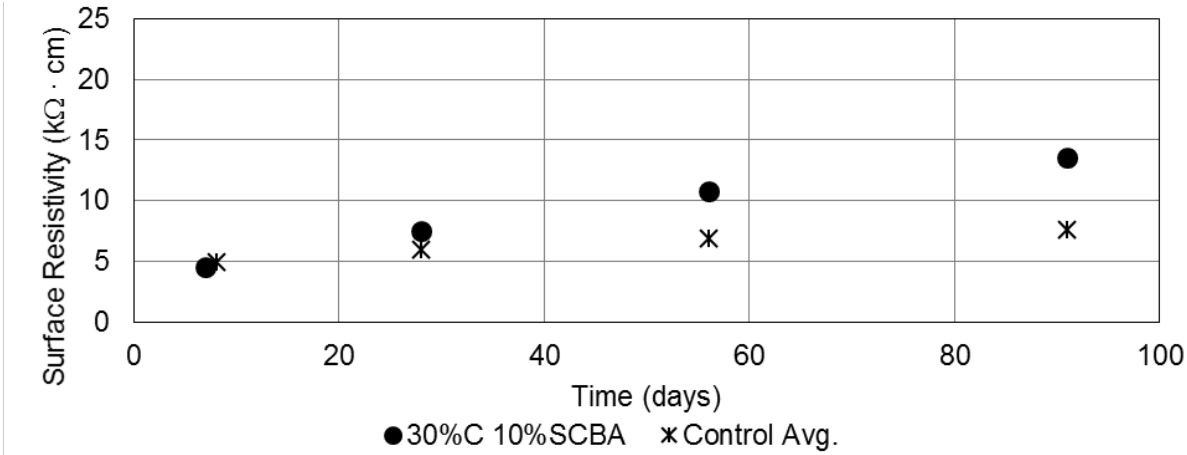

Figure D-37. Surface resistivity of concrete containing 30% class C fly ash and 10% SCBA.

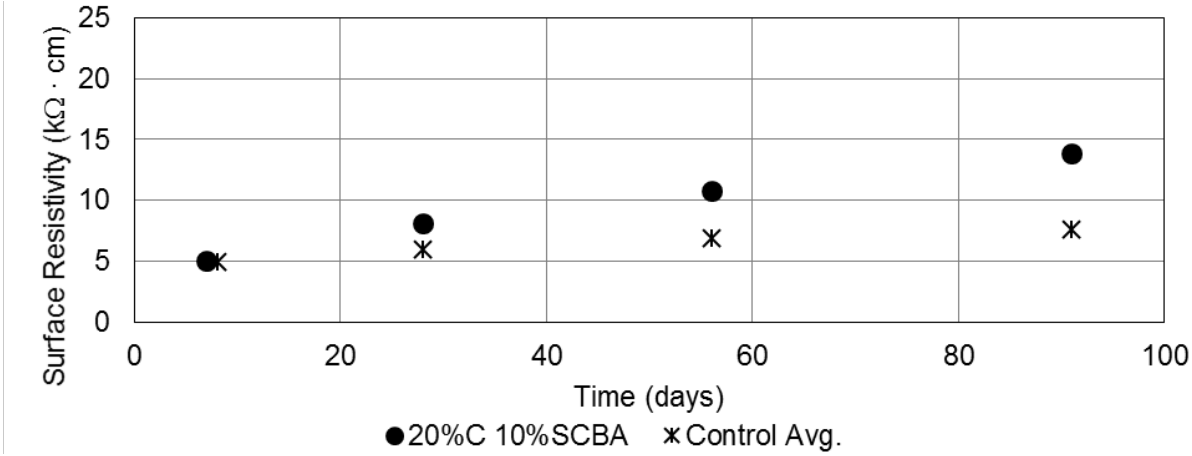

Figure D-38. Surface resistivity of concrete containing 20% class C fly ash and 10% SCBA.

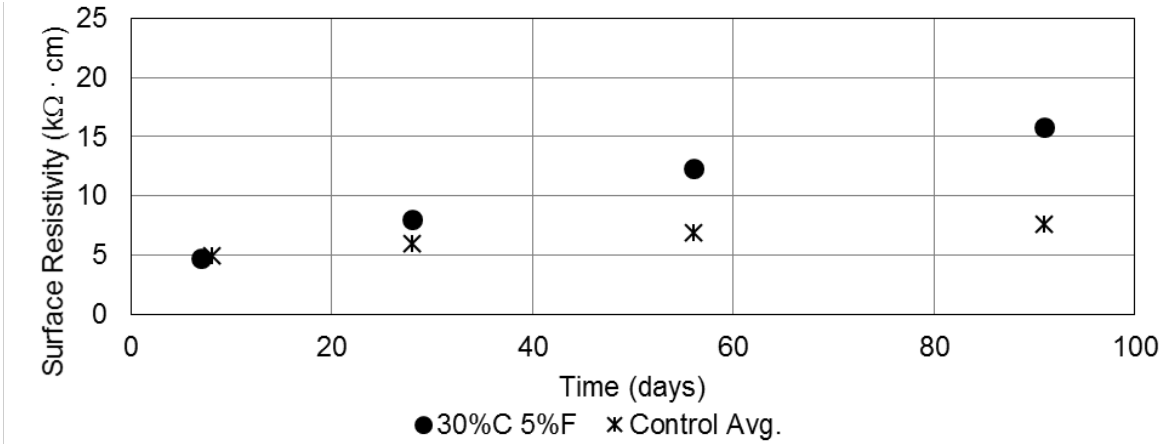

Figure D-39. Surface resistivity of concrete containing 30% class C fly ash and 20% class F fly ash.

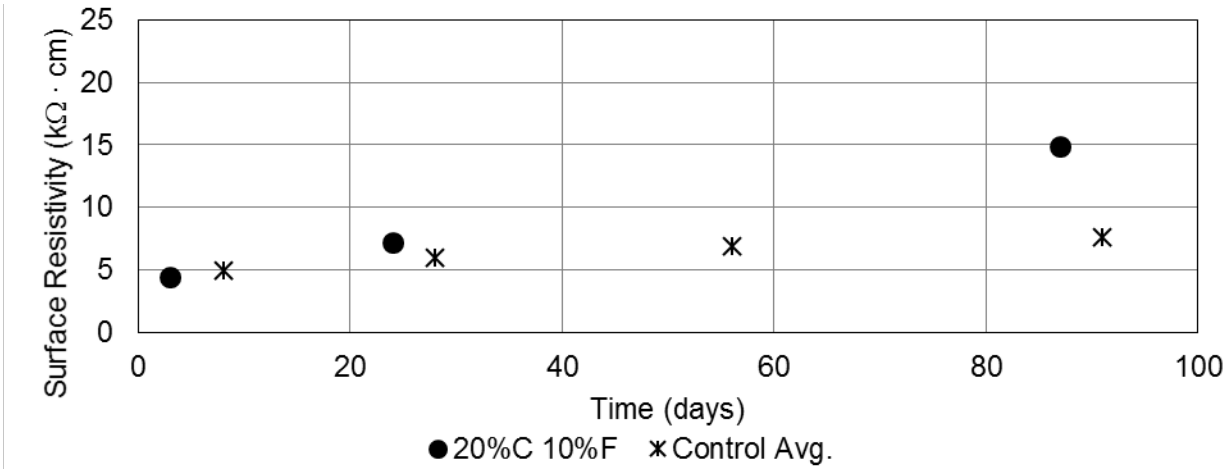

Figure D-40. Surface resistivity of concrete containing 20% class C fly ash and 10% class F fly ash.

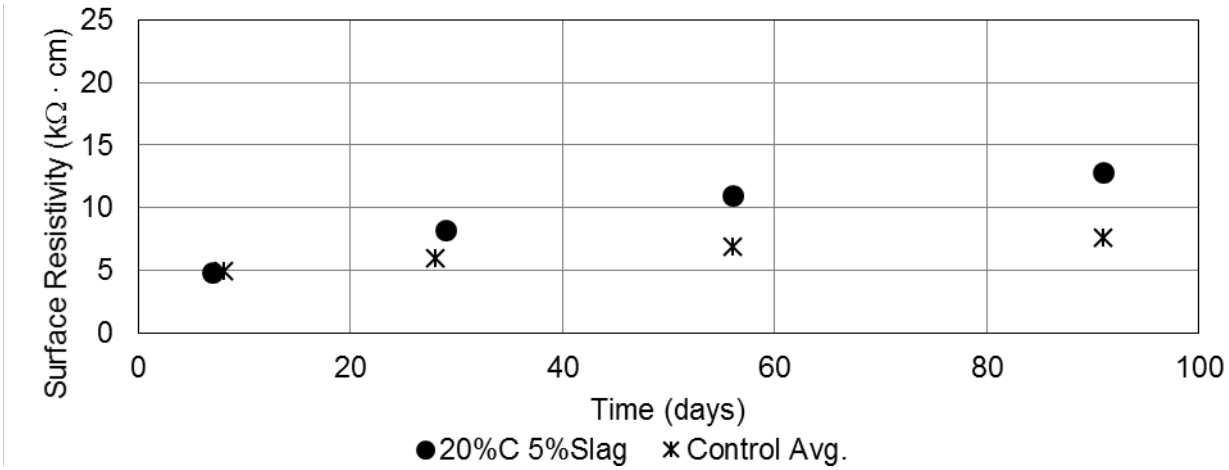

Figure D-41. Surface resistivity of concrete containing 20% class C fly ash and 5% slag.

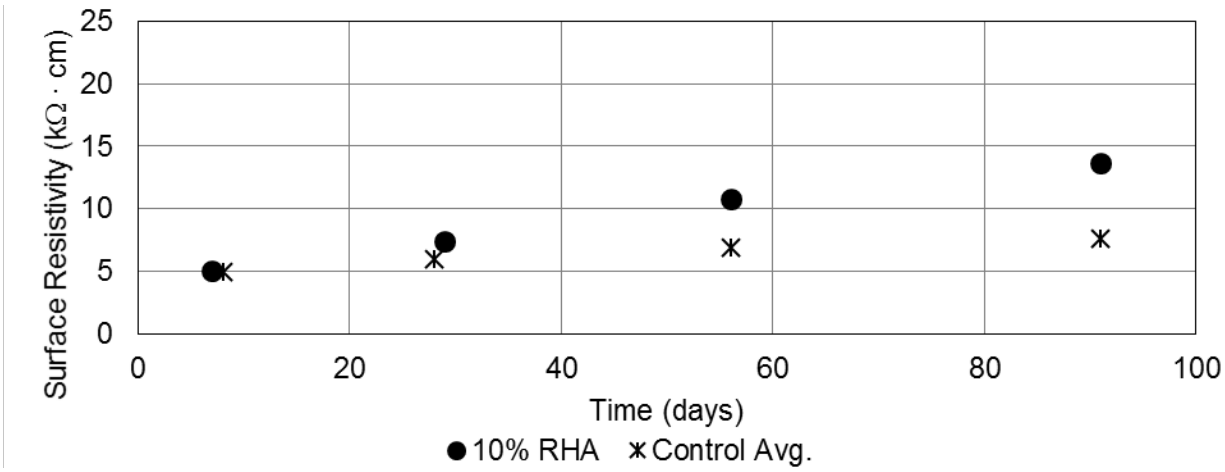

Figure D-42. Surface resistivity of concrete containing 10% RHA.

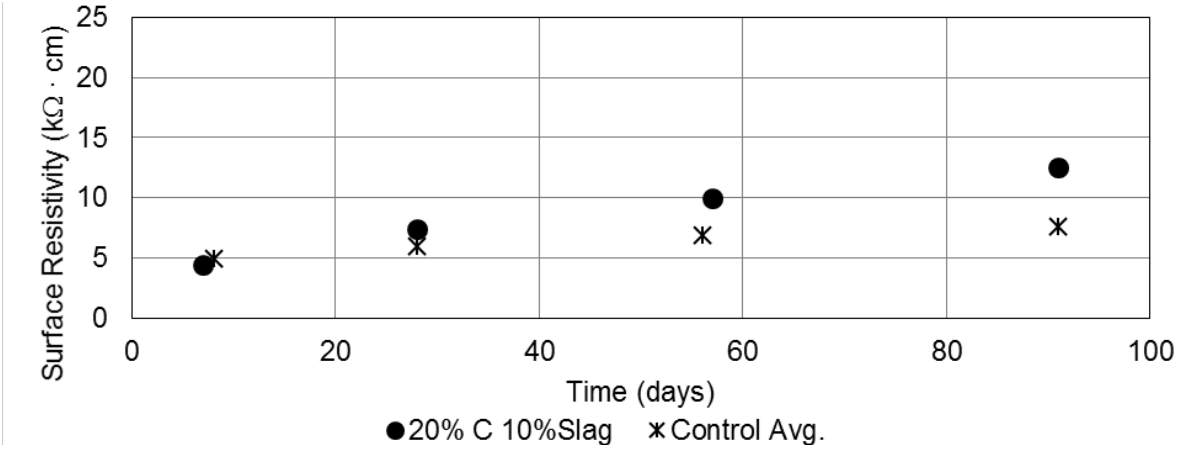

Figure D-43. Surface resistivity of concrete containing 20% class C fly ash and 10% slag.

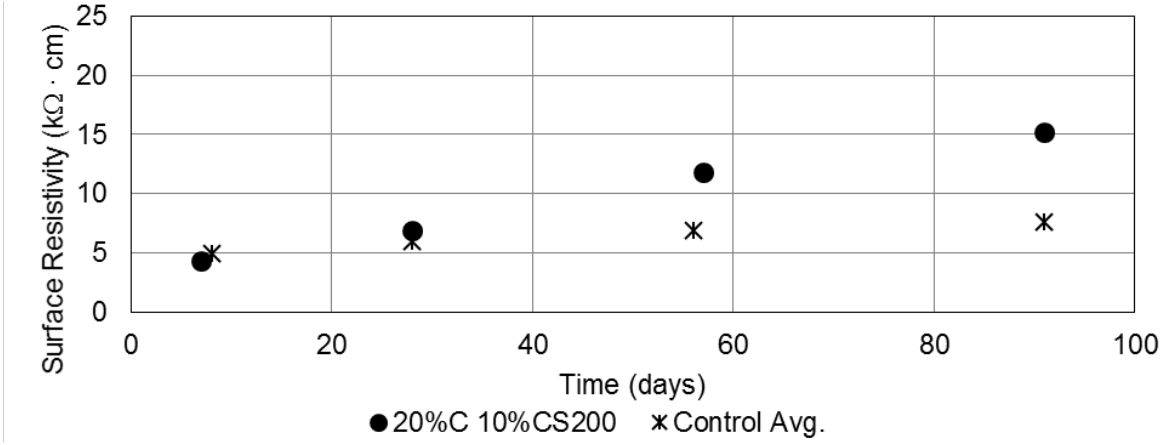

Figure D-44. Surface resistivity of concrete containing 20% class C fly ash and 10% CS200.

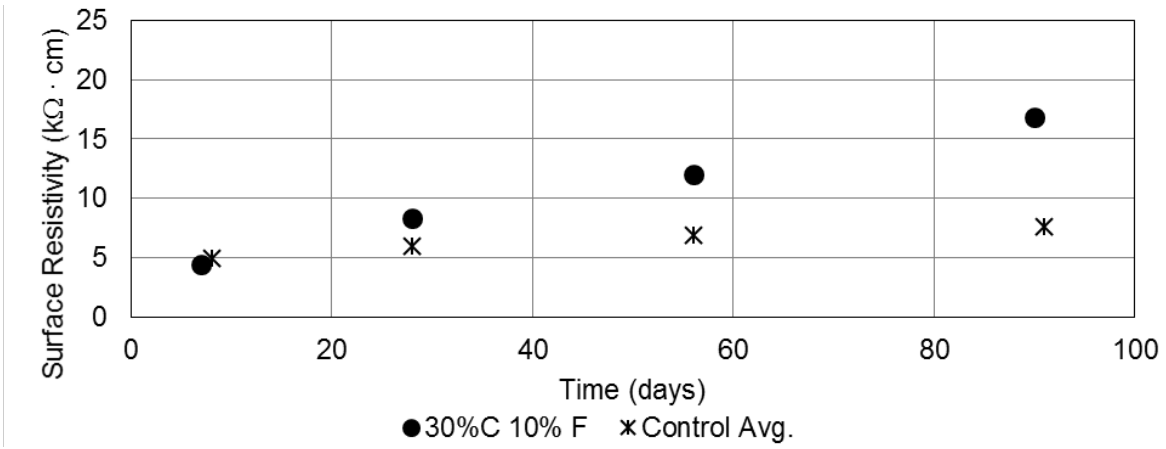

Figure D-45. Surface resistivity of concrete containing 30% class C fly ash and 10% class F fly ash.

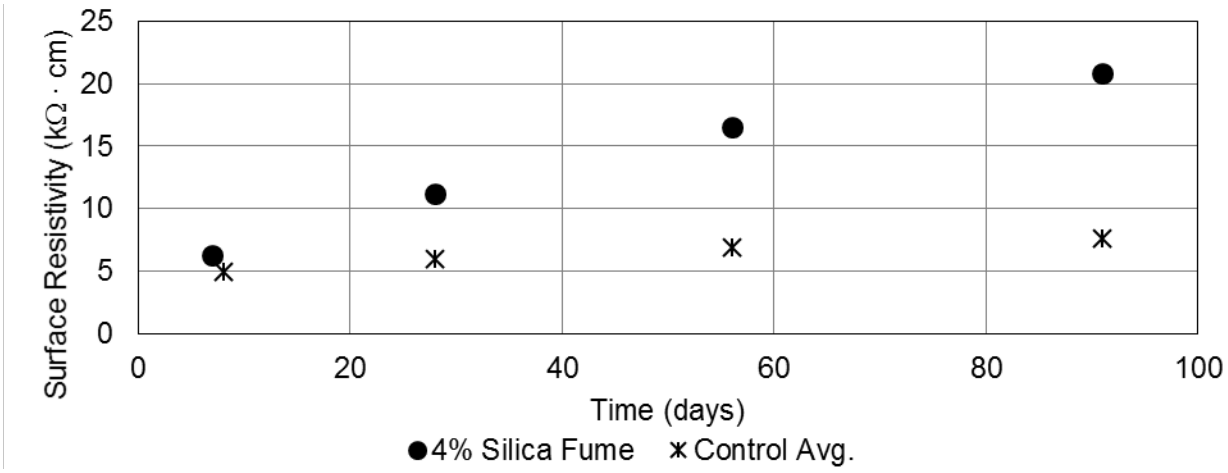

Figure D-46. Surface resistivity of concrete containing 4% silica fume.

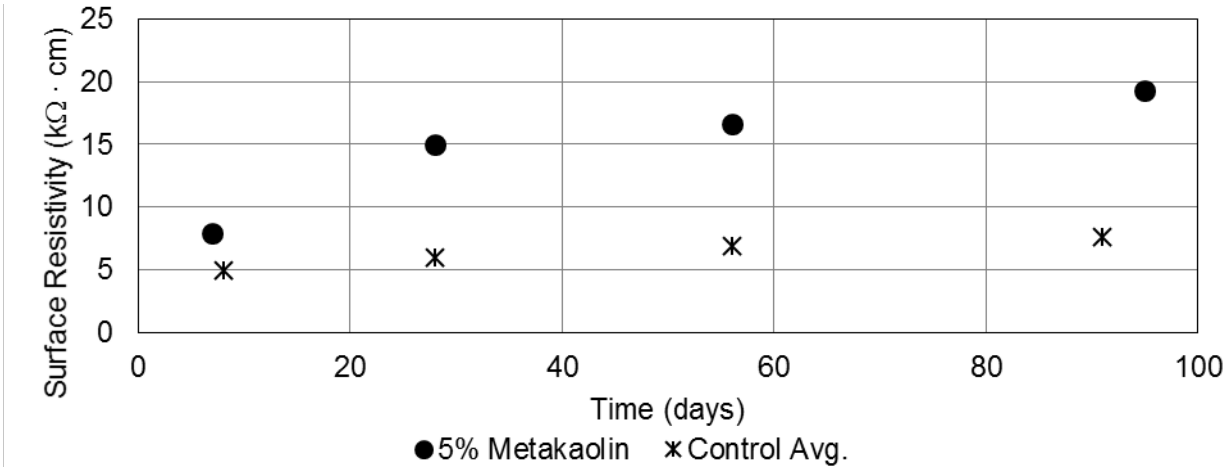

Figure D-47. Surface resistivity of concrete containing 5% metakaolin.

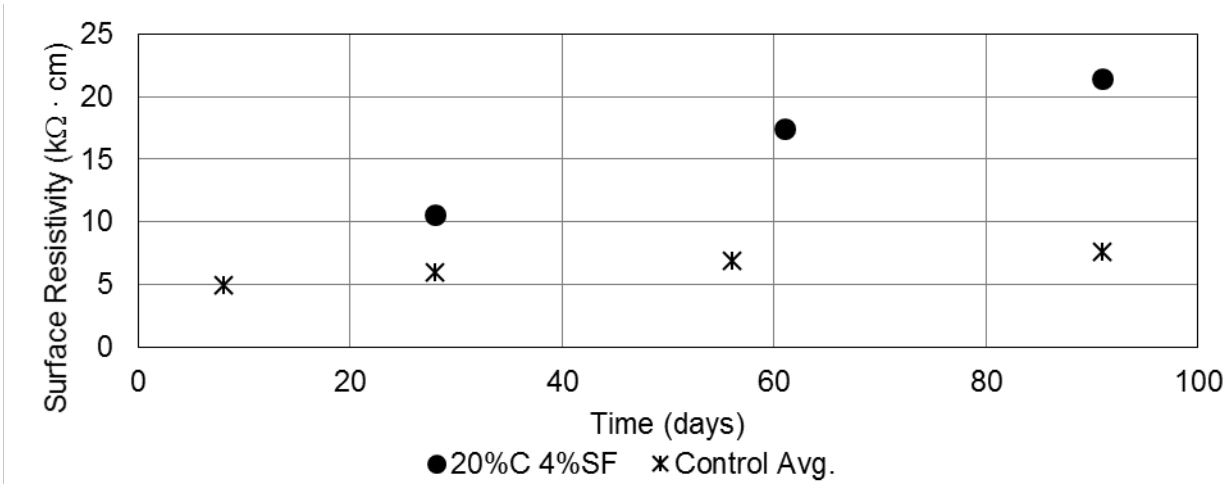

Figure D-48. Surface resistivity of concrete containing 20% class C fly ash and 4% silica fume.

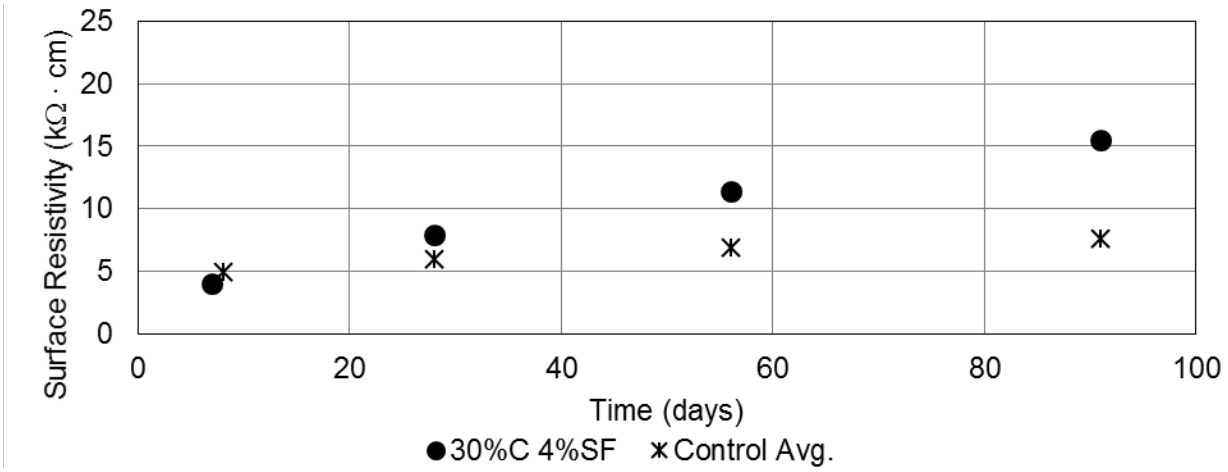

Figure D-49. Surface resistivity of concrete containing 30% class C fly ash and 4% silica fume.

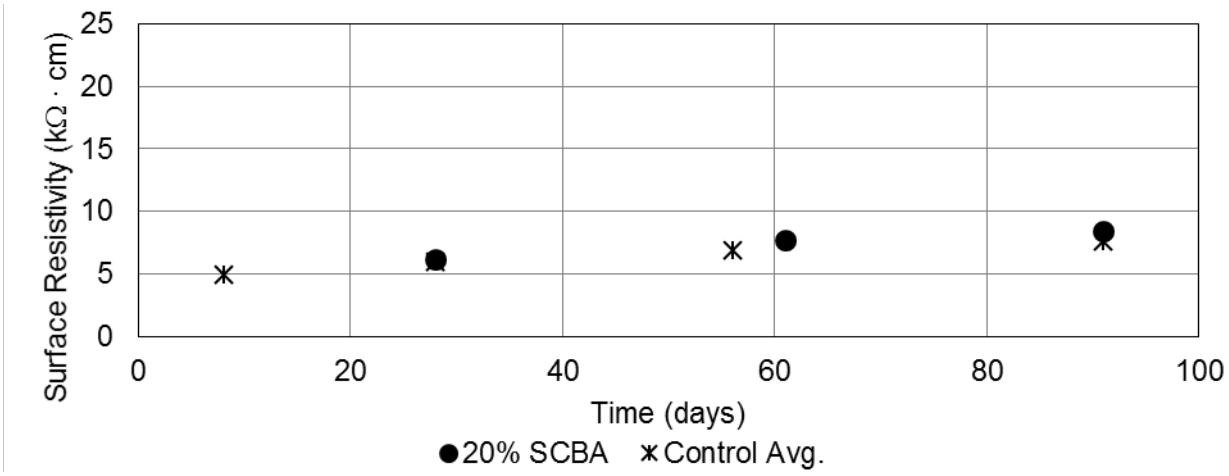

Figure D-50. Surface resistivity of concrete containing 20% sugarcane bagasse ash.

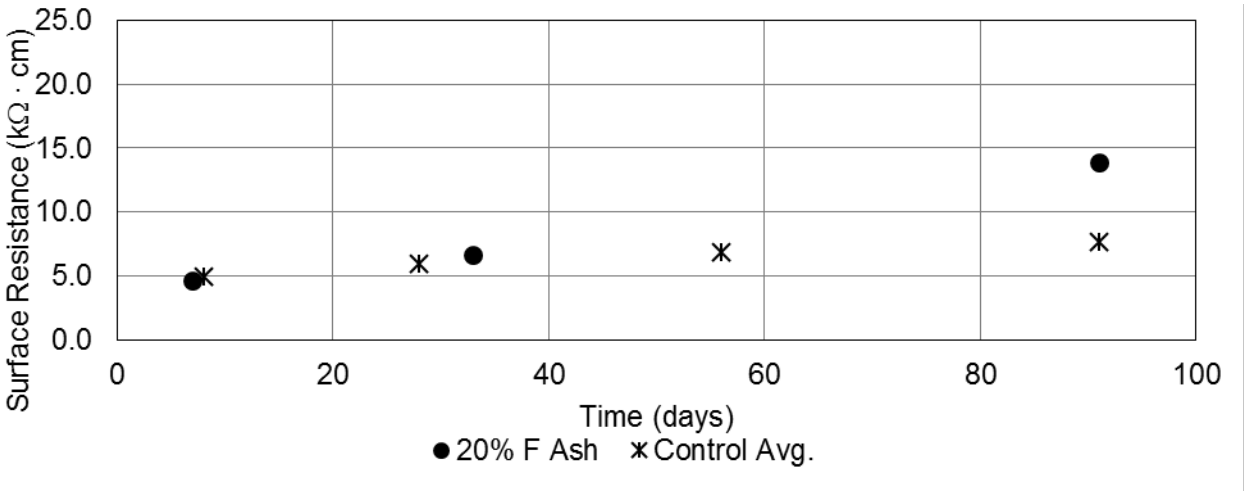

Figure D-51. Surface resistivity of concrete containing 20% class F fly ash.

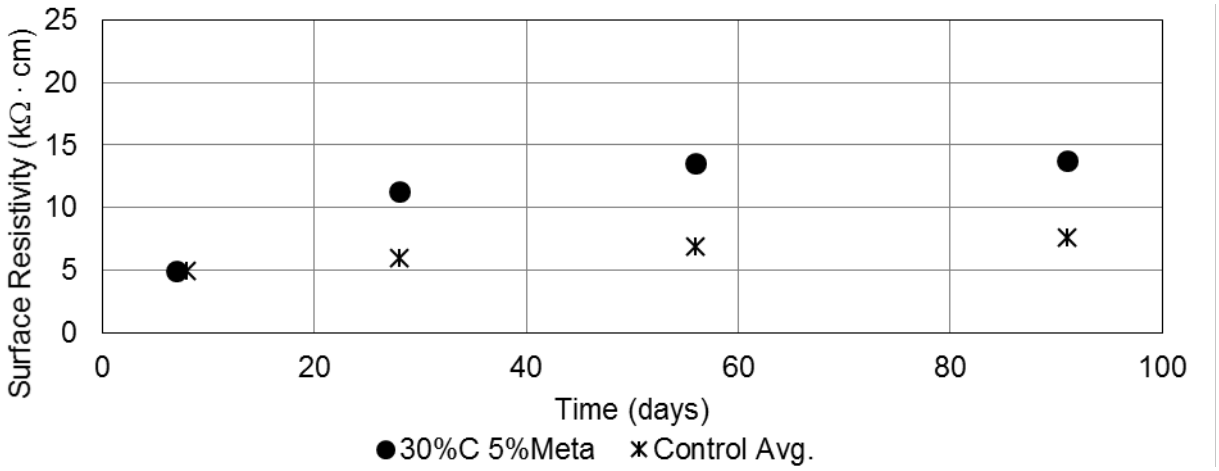

Figure D-52. Surface resistivity of concrete containing 30% class C fly ash and 5% metakaolin.

D.4. Bulk Resistivity of Concrete Results

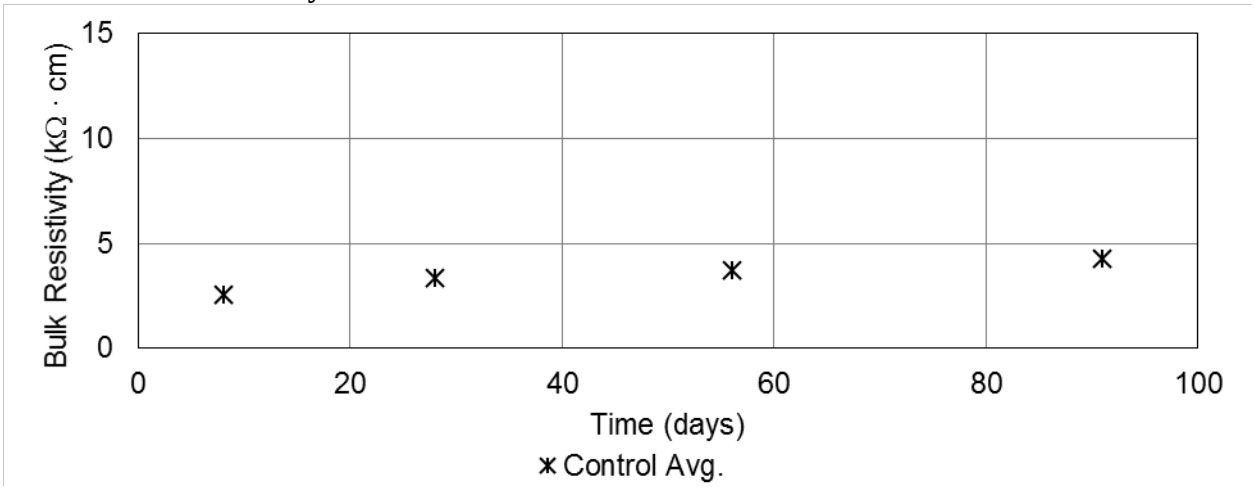

Figure D-53. Bulk resistivity of the control concrete mix.

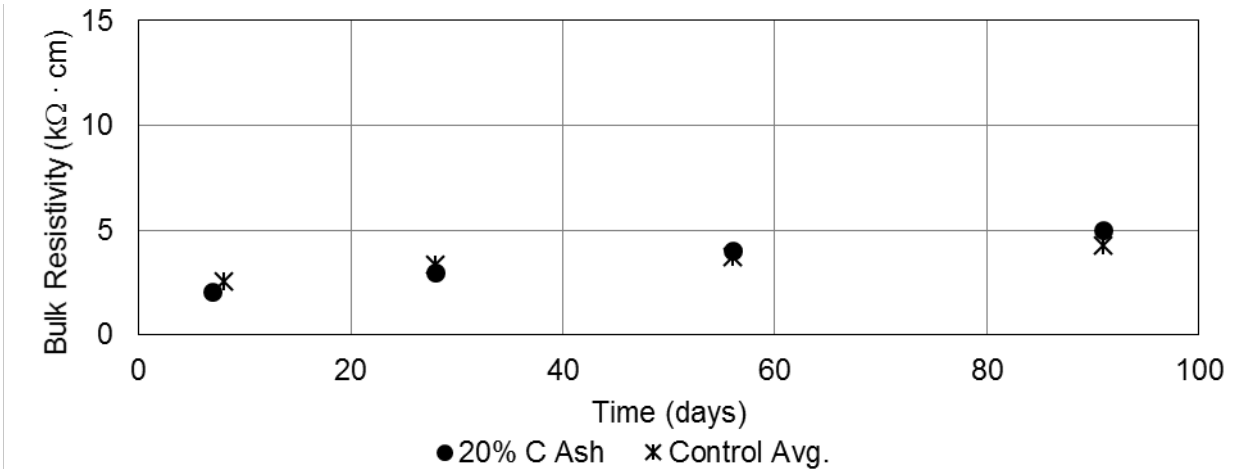

Figure D-54. Bulk resistivity of concrete containing 20% class C fly ash.

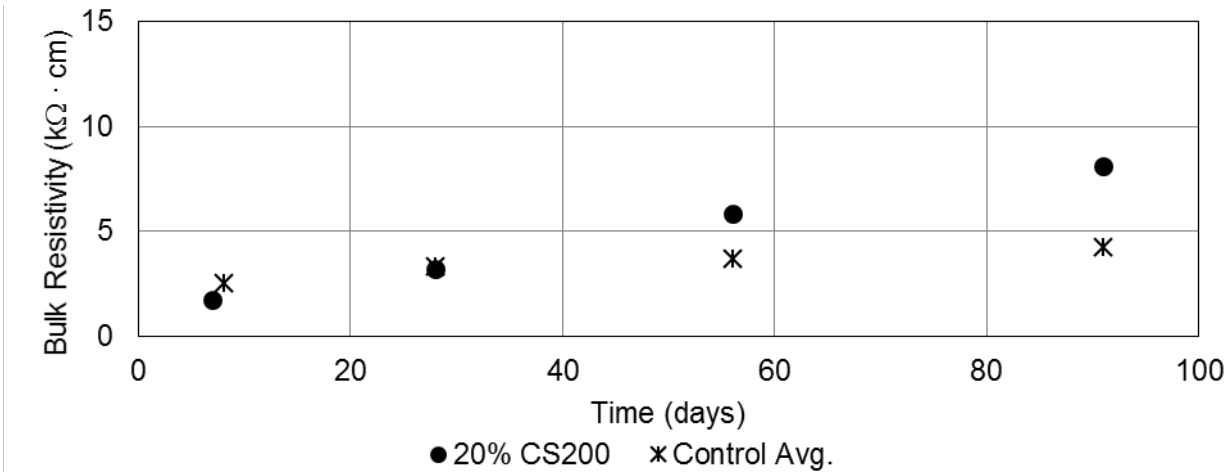

Figure D-55. Bulk resistivity of concrete containing 20% CS200 ground glass.

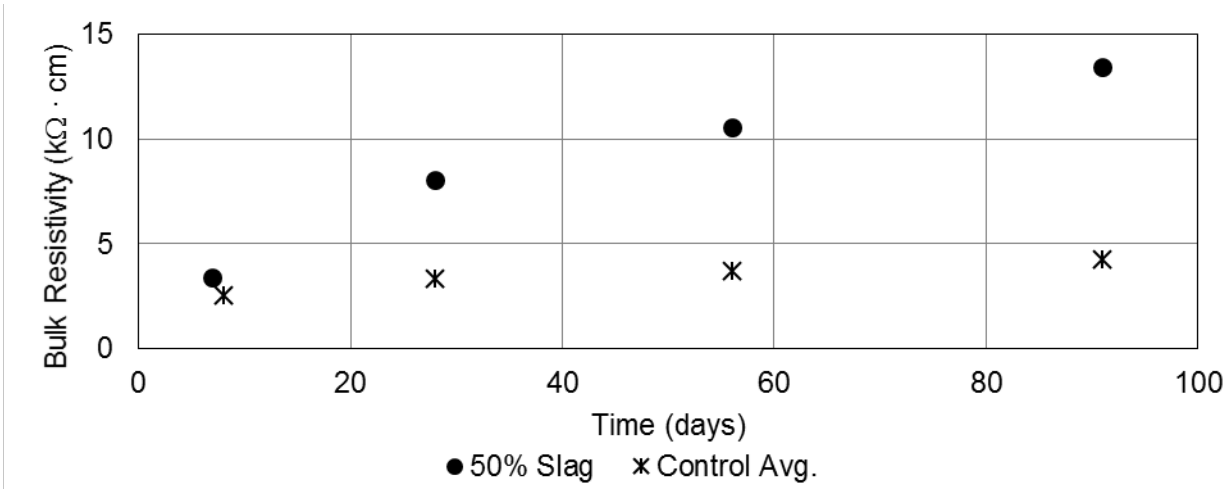

Figure D-56. Bulk resistivity of concrete containing 50% slag.

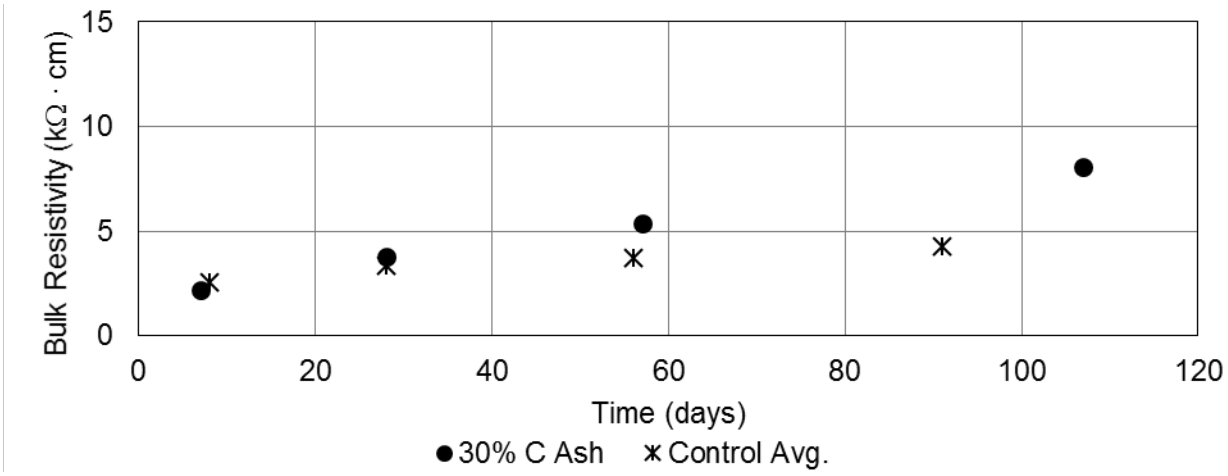

Figure D-57. Bulk resistivity of concrete containing 30% class C fly ash.

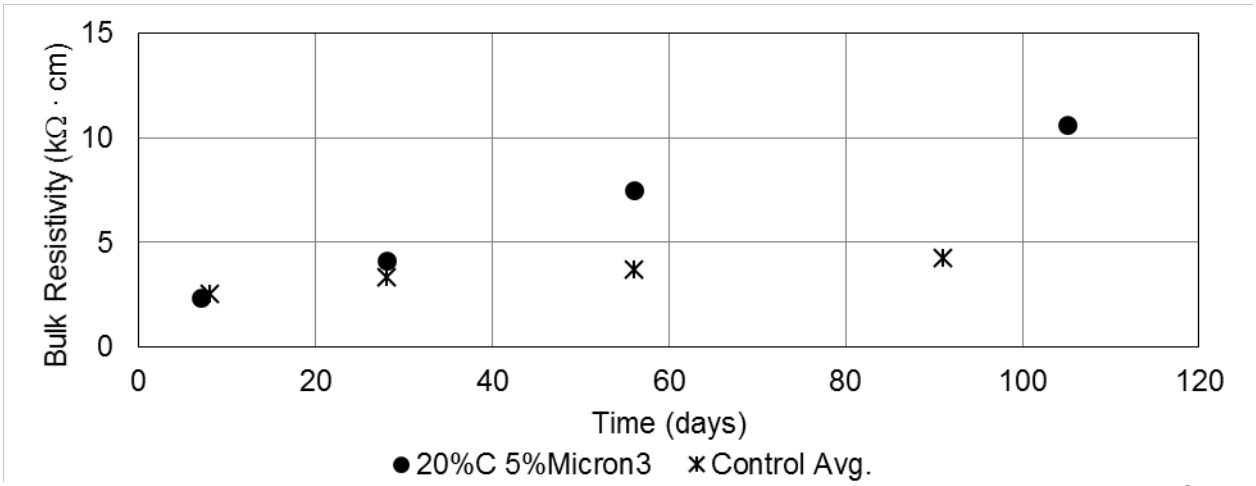

Figure D-58. Bulk resistivity of concrete containing 20% class C fly ash and 5% Micron[3].

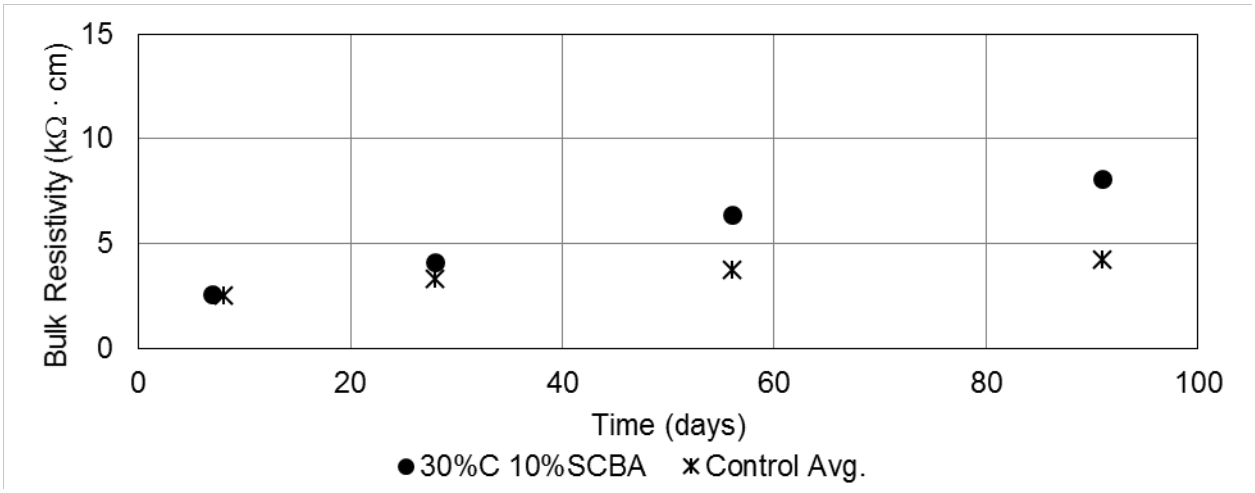

Figure D-59. Bulk resistivity of concrete containing 30% class C fly ash and 10% SCBA.

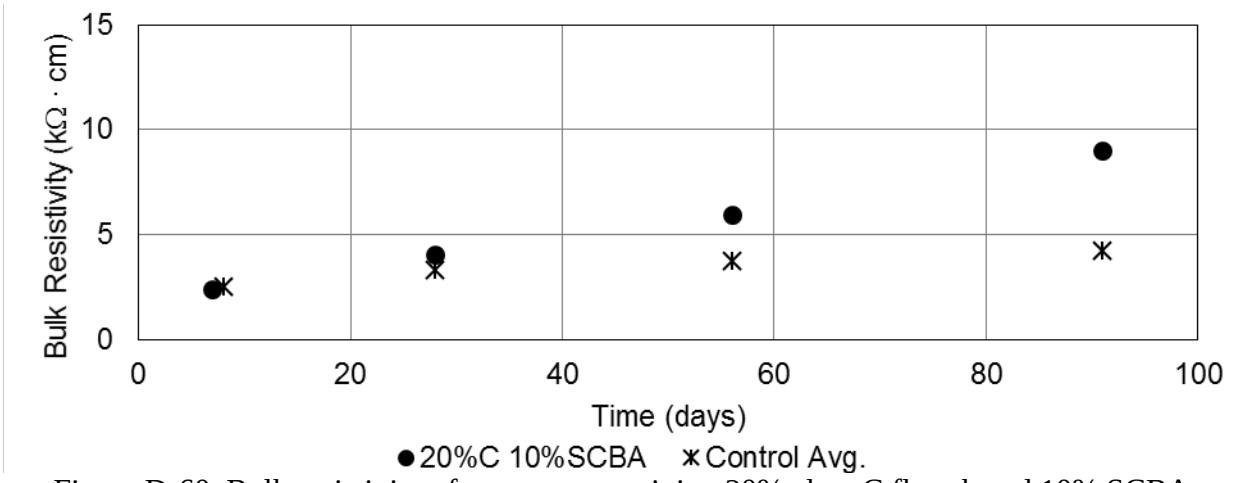

Figure D-60. Bulk resistivity of concrete containing 20% class C fly ash and 10% SCBA.

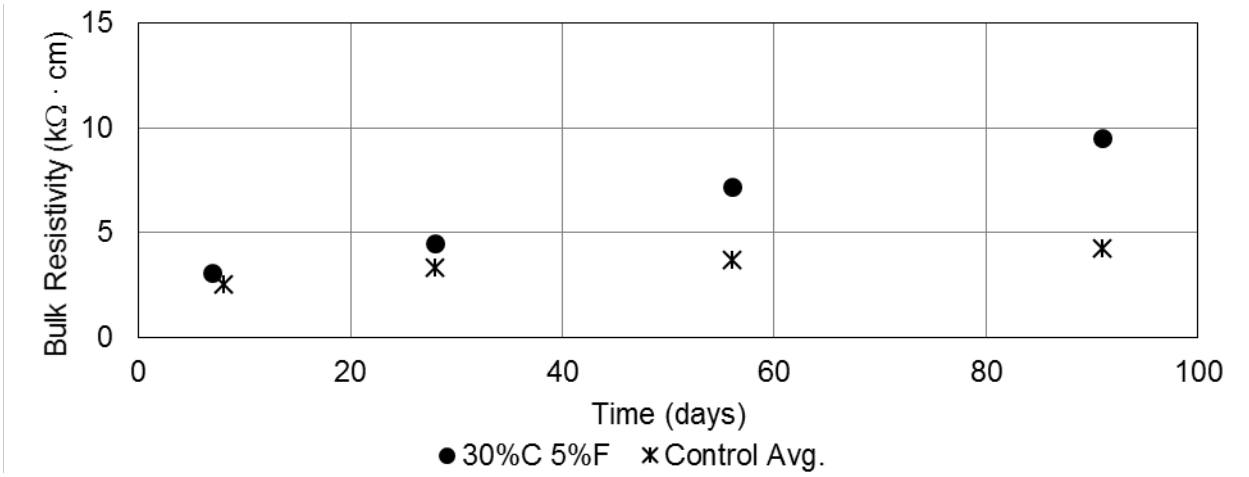

Figure D-61. Bulk resistivity of concrete containing 30% class C fly ash and 20% class F fly ash.

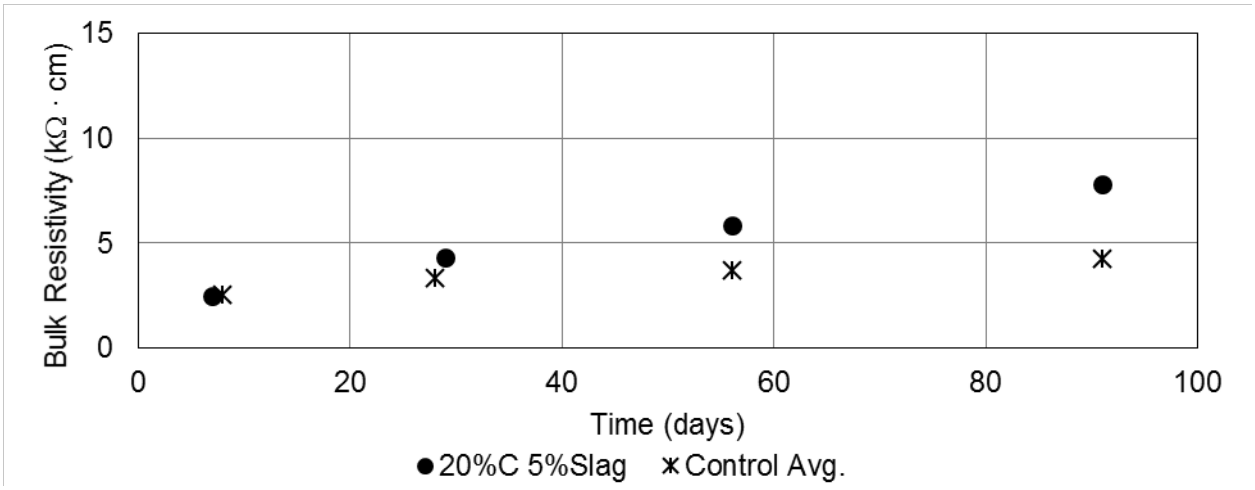

Figure D-62. Bulk resistivity of concrete containing 20% class C fly ash and 5% slag.

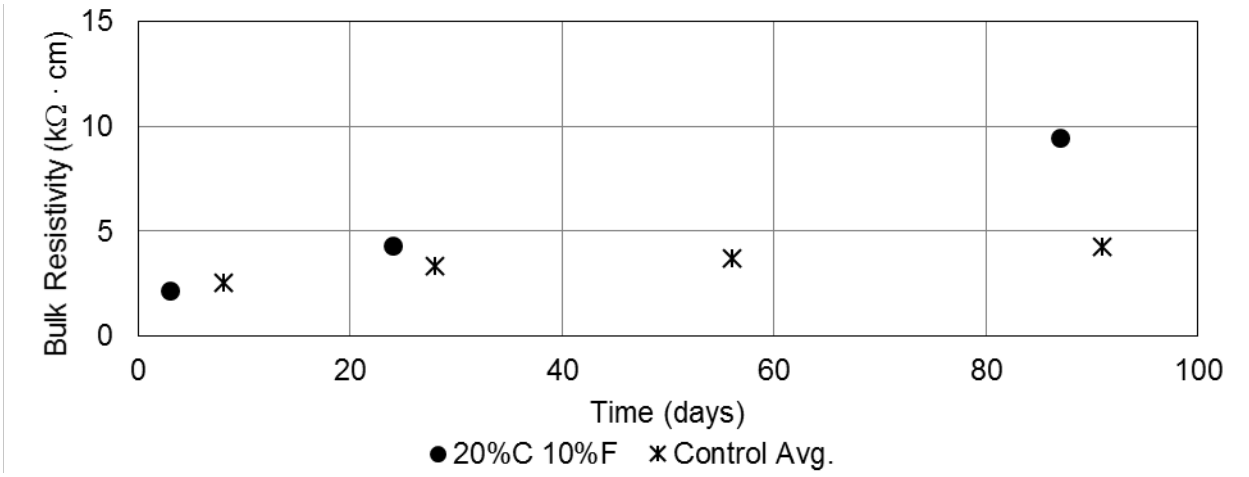

Figure D-63. Bulk resistivity of concrete containing 20% class C fly ash and 10% class F fly ash.

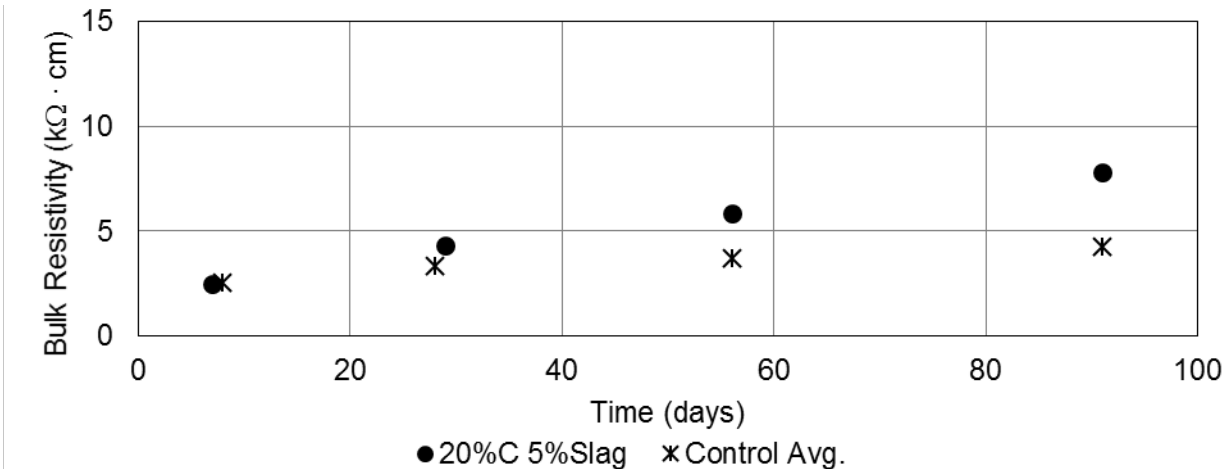

Figure D-64. Bulk resistivity of concrete containing 20% class C fly ash and 5% slag.

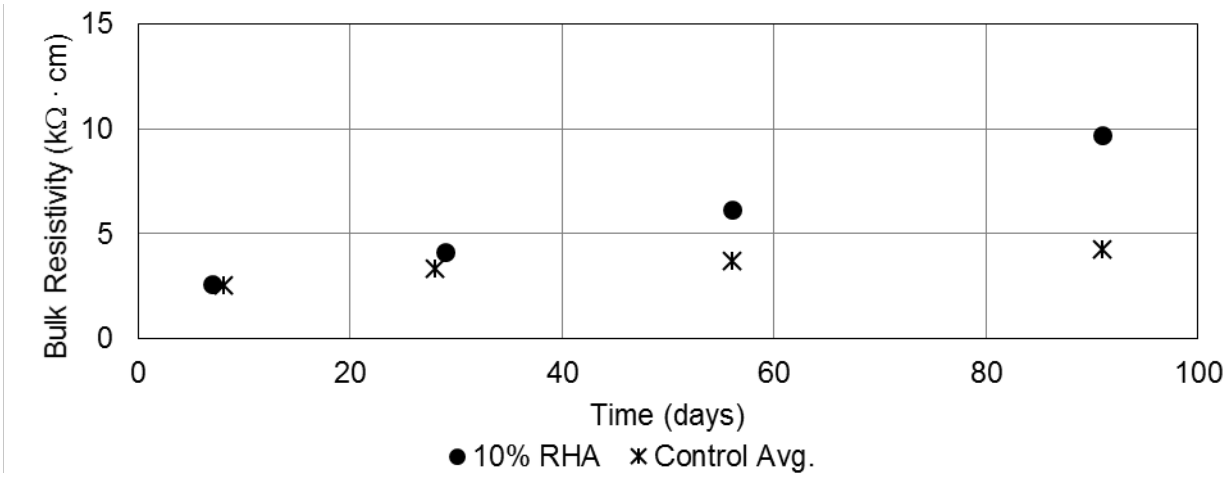

Figure D-65. Bulk resistivity of concrete containing 10% RHA.

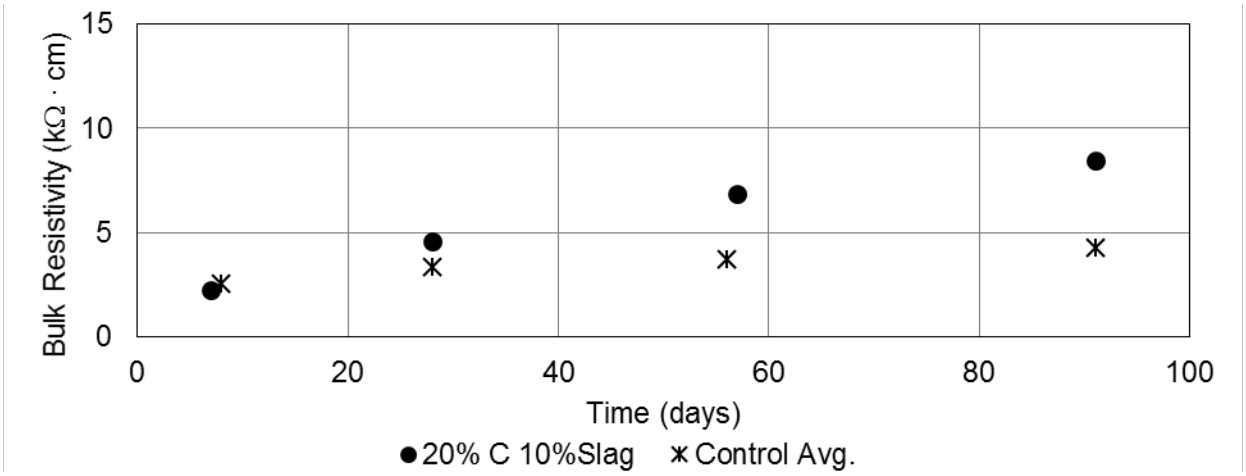

Figure D-66. Bulk resistivity of concrete containing 20% class C fly ash and 10% slag.

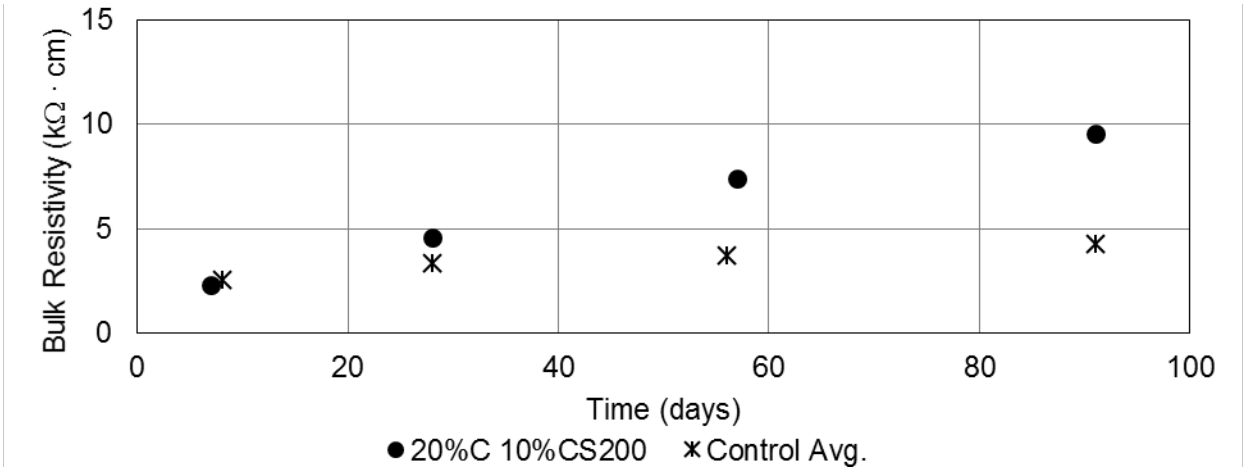

Figure D-67. Bulk resistivity of concrete containing 20% class C fly ash and 10% CS200.

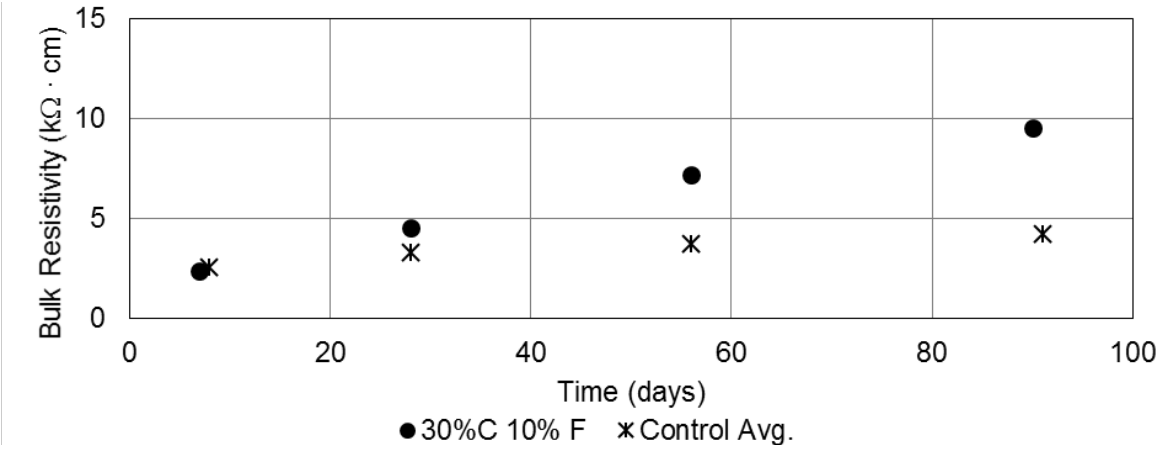

Figure D-68. Bulk resistivity of concrete containing 30% class C fly ash and 10% class F fly ash.

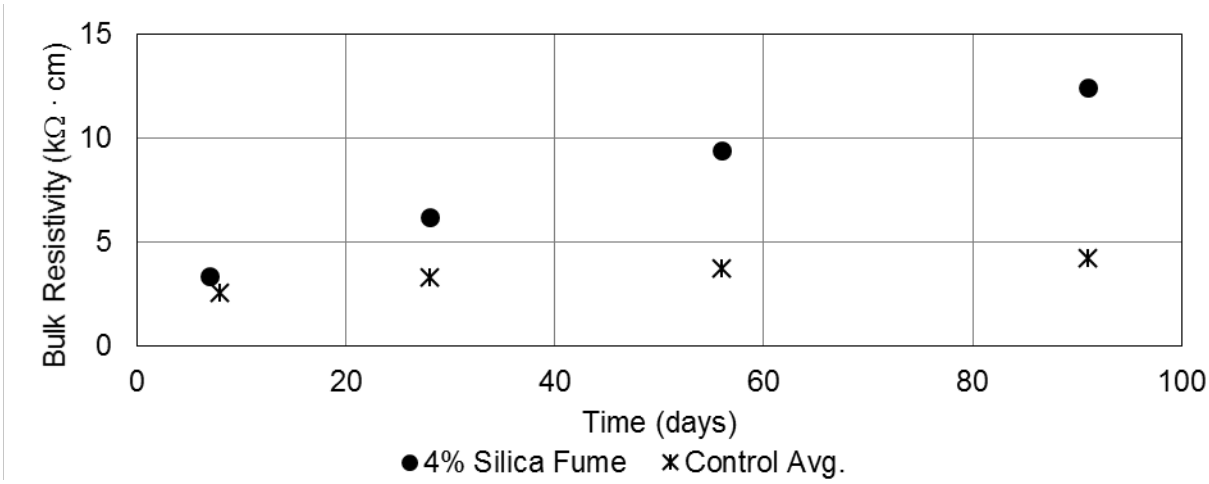

Figure D-69. Bulk resistivity of concrete containing 4% silica fume.

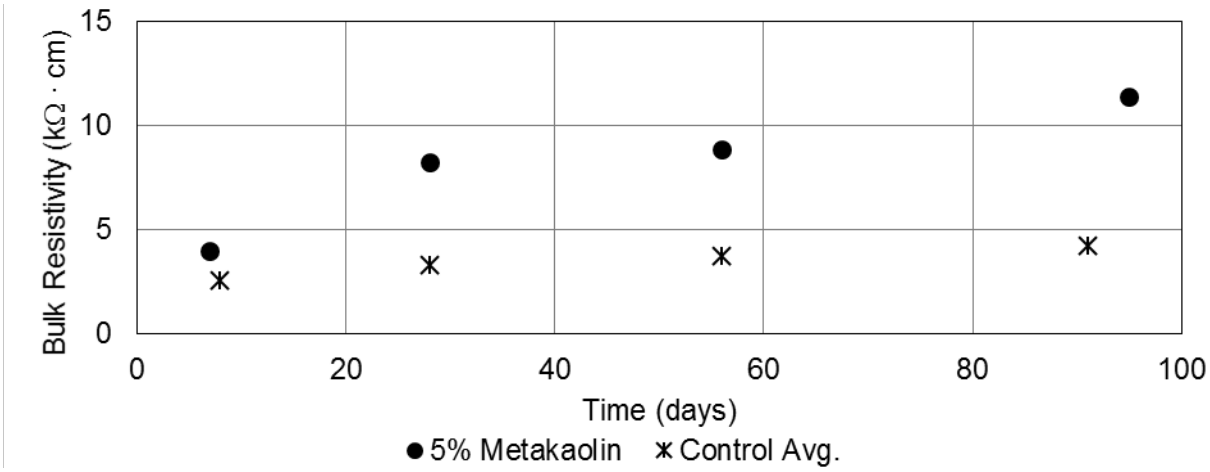

Figure D-70. Bulk resistivity of concrete containing 5% metakaolin.

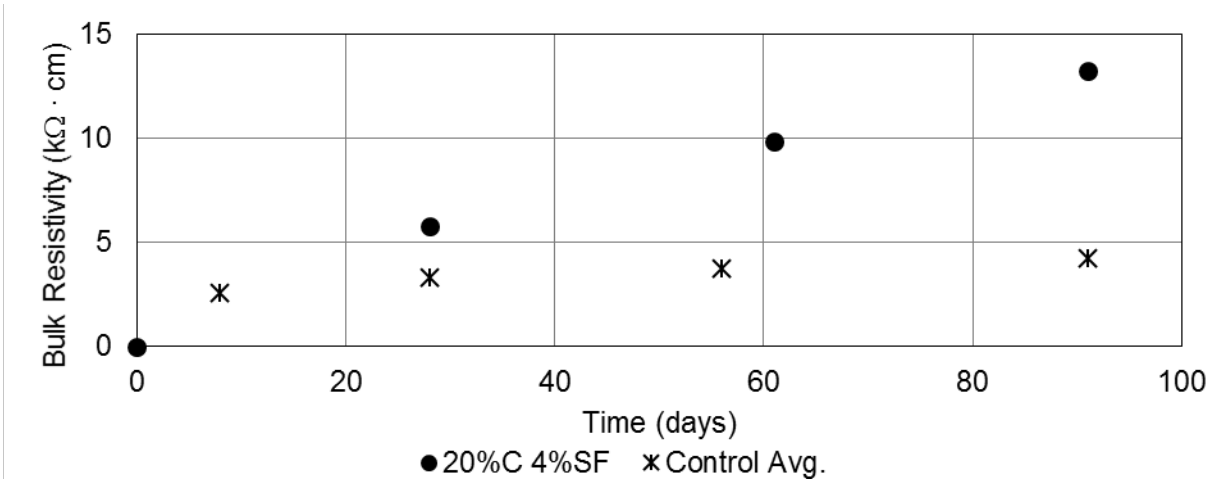

Figure D-71. Bulk resistivity of concrete containing 20% class C fly ash and 4% silica fume.

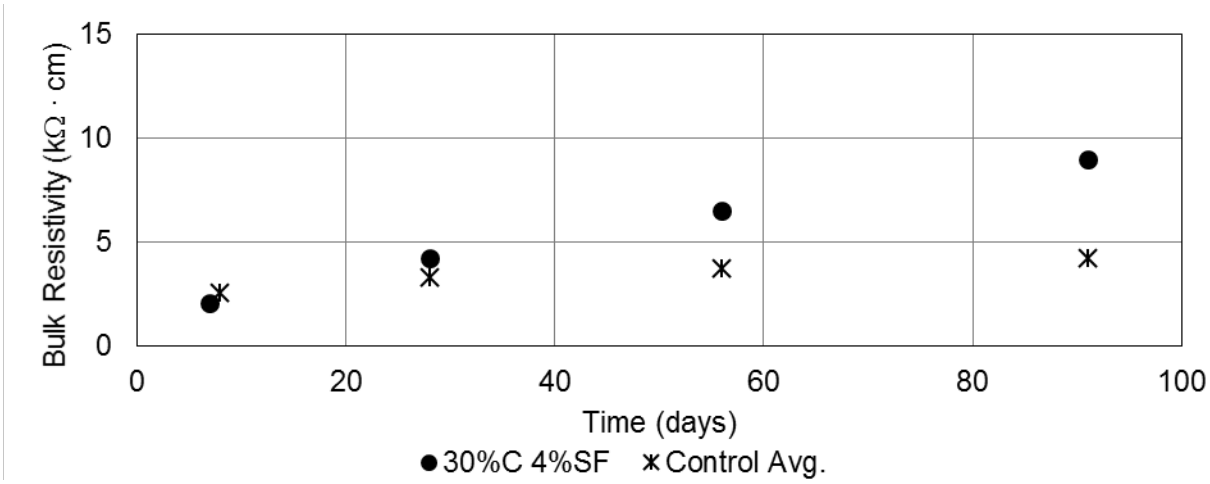

Figure D-72. Bulk resistivity of concrete containing 30% class C fly ash and 4% silica fume.

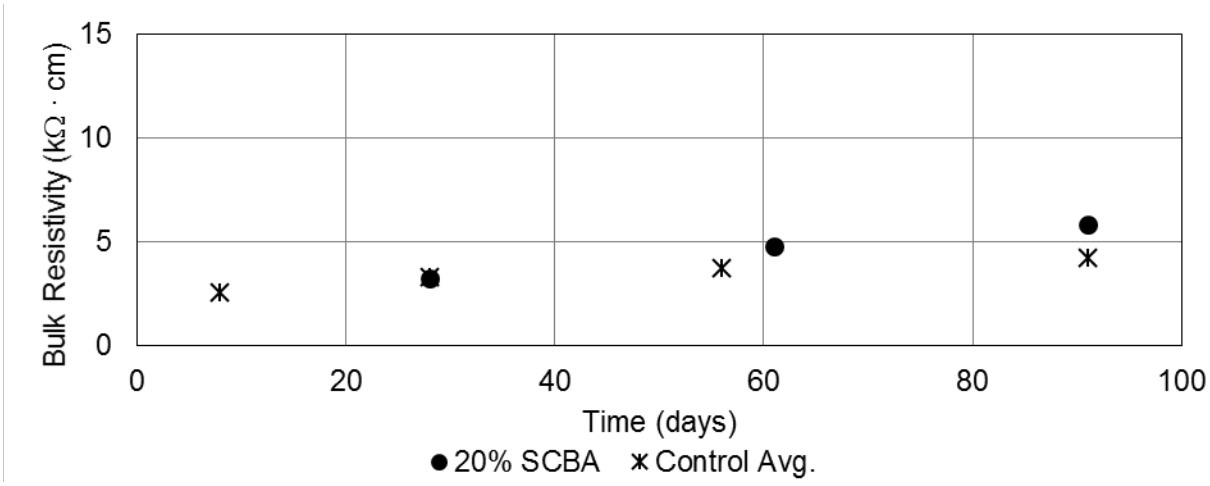

Figure D-73. Bulk resistivity of concrete containing 20% sugarcane bagasse ash.

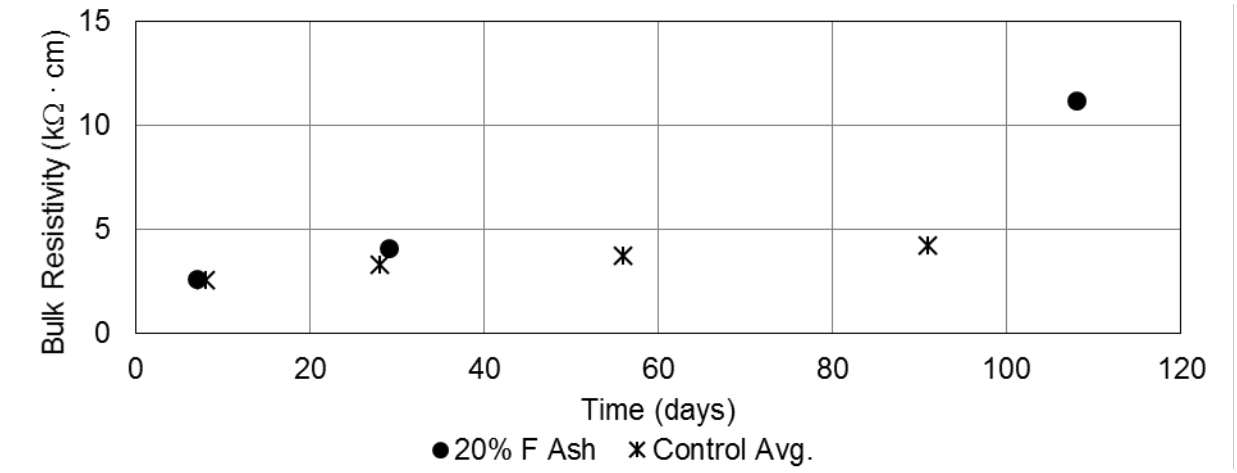

Figure D-74. Bulk resistivity of concrete containing 20% class F fly ash.

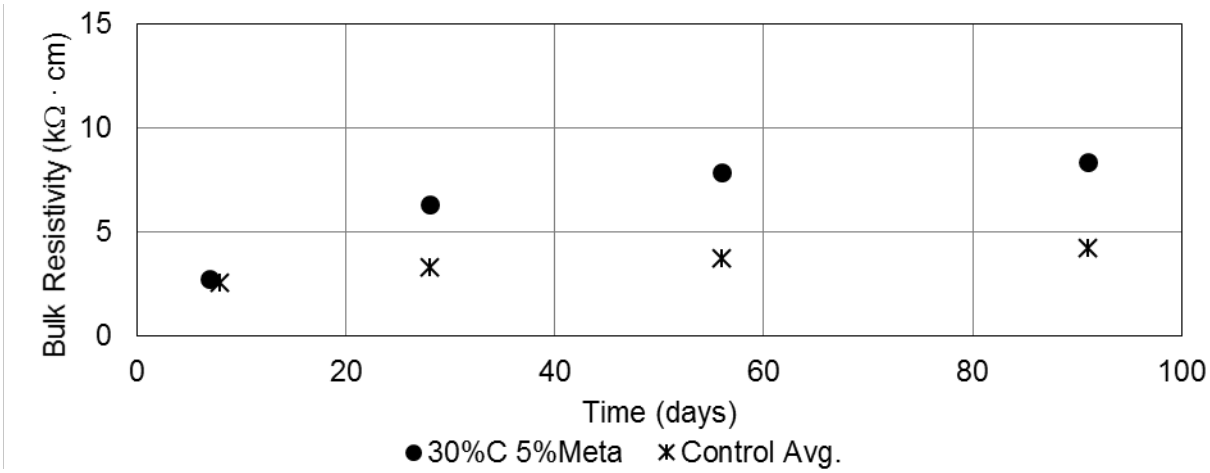

Figure D-75. Bulk resistivity of concrete containing 30% class C fly ash and 5% metakaolin.